Probabilistic TSUnami Hazard MAPS
for the NEAM Region (TSUMAPS-NEAM)
ECHO/SUB/2015/718568/PREV26

NEAMTHM18 Documentation: the making of the TSUMAPS-NEAM Tsunami Hazard Model 2018

Author: **TSUMAPS-NEAM Technical Integrators (TI) team**
Date: **11 September 2019**
Version: **1.0**

Basili, R., Brizuela, B., Herrero, A., Iqbal, S., Lorito, S., Maesano, F.E., Murphy, S., Perfetti, P., Romano, F., Scala, A., Selva, J., Taroni, M., Thio, H.K., Tiberti, M.M., Tonini, R., Volpe, M., Glimsdal, S., Harbitz, C.B., Løvholt, F., Baptista, M.A., Carrilho, F., Matias, L.M., Omira, R., Babeyko, A., Hoechner, A., Gurbuz, M., Pekcan, O., Yalçıner, A., Canals, M., Lastras, G., Agalos, A., Papadopoulos, G., Triantafyllou, I., Benchekroun, S., Agrebi Jaouadi, H., Attafi, K., Ben Abdallah, S., Bouallegue, A., Hamdi, H., Oueslati, F. (2019). NEAMTHM18 Documentation: the making of the TSUMAPS-NEAM Tsunami Hazard Model 2018. Istituto Nazionale di Geofisica e Vulcanologia (INGV); DOI: http://doi.org/10.5281/zenodo.3406625.

The TSUMAPS-NEAM project was co-financed by the European-Union Civil Protection Mechanism through the Agreement Number: ECHO/SUB/2015/718568/PREV26.

Acknowledgments

The TSUMAPS-NEAM Technical Integrator team members thank the EDANYA Group, Universidad de Málaga, Spain for making the HySEA code available, CINECA for providing access to computing facilities. Our warm thanks go to F. Romano, R. Omira, F. Lovholt, A. Babeyko, A. Yalciner, G. Papadopoulos, M. Canals, A. Bouallegue, A. Armigliato, M. Sorensen, C. Ozer, G. Davies, W. Power, J. Polet, and C. Meletti for participating in the elicitation experiment and to J. Behrens, M. Dolce, D. Di Bucci, E. Geist, M. Pagani, A. Amato, A. Zaytsev, M. Gonzalez, and J. M. Gonzalez Vida for reviewing the documentation presented here. Special thanks go to T. Parsons for coordinating the two review stages. We also thank all the scientists, observers, and stakeholders who participated in our project meetings openly sharing their views and invaluable feedback with us.

Contacts

INGV
Istituto Nazionale di Geofisica e Vulcanologia
Via di Vigna Murata, 605, 00143, Roma, Italy

http://www.tsumaps-neam.eu

Detailed list of authors and their affiliations

Full name	Affiliation	ORCID	e-mail
Basili, Roberto	1	0000-0002-1213-0828	roberto.basili@ingv.it
Brizuela, Beatriz	1	0000-0002-0851-3543	beatriz.brizuela@ingv.it
Herrero, André	1	0000-0001-5633-5852	andre.herrero@ingv.it
Iqbal, Sarfraz	1	0000-0003-2442-9963	sarfraz.iqbal@gmail.com
Lorito, Stefano	1	0000-0002-1458-2131	stefano.lorito@ingv.it
Maesano, Francesco Emanuele	1	0000-0002-5652-1548	francesco.maesano@ingv.it
Murphy, Shane	1	0000-0003-2795-0463	shane.murphy@ifremer.fr
Perfetti, Paolo	1	0000-0002-0584-6879	
Romano, Fabrizio	1	0000-0003-2725-3596	fabrizio.romano@ingv.it
Scala, Antonio	1, 12	0000-0003-4584-463X	scala@fisica.unina.it
Selva, Jacopo	1	0000-0001-6263-6934	jacopo.selva@ingv.it
Taroni, Matteo	1	0000-0001-6999-4590	matteo.taroni@ingv.it
Tiberti, Mara Monica	1	0000-0003-2504-853X	mara.tiberti@ingv.it
Thio, Hong Kie	2	0000-0002-9051-9601	hong.kie.thio@aecom.com
Tonini, Roberto	1	0000-0001-7617-7206	roberto.tonini@ingv.it
Volpe, Manuela	1	0000-0003-4551-3339	manuela.volpe@ingv.it
Glimsdal, Sylfest	3	0000-0001-6654-2994	sylfest.glimsdal@ngi.no
Harbitz, Carl B.	3	0000-0003-4280-7497	carl.bonnevie.harbitz@ngi.no
Løvholt, Finn	3	0000-0003-1019-7321	finn.lovholt@ngi.no
Baptista, Maria Ana	4, 13	0000-0002-6381-703X	mavbaptista@gmail.com
Carrilho, Fernando	4	0000-0003-3287-6800	carrilho.fernando@ipma.pt
Matias, Luis Manuel	5	0000-0002-8086-4874	lmatias@fc.ul.pt
Omira, Rachid	4, 5	0000-0002-6198-7588	raomira@fc.ul.pt
Babeyko, Andrey	6	0000-0002-5725-1113	babeyko@gfz-potsdam.de
Hoechner, Andreas	6	0000-0002-3494-5200	
Gurbuz, Mucahit	7	0000-0003-2954-3300	gurbuz@metu.edu.tr
Pekcan, Onur	7	0000-0003-3603-5929	opekcan@metu.edu.tr
Yalçıner, Ahmet	7	0000-0001-8947-7523	yalciner@metu.edu.tr
Canals, Miquel	8	0000-0001-5267-7601	miquelcanals@ub.edu
Lastras, Galderic	8	0000-0002-8756-3855	glastras@ub.edu
Agalos, Apostolos	9	0000-0001-7395-6431	agalos@noa.gr
Papadopoulos, Gerassimos	9	0000-0003-1982-8214	papadop@noa.gr
Triantafyllou, Ioanna	9	0000-0002-8920-5322	ioannatriantafyllou@yahoo.gr
Benchekroun, Sabah	10	0000-0002-1414-4238	sabahbenchekroun@gmail.com
Agrebi Jaouadi, Hedi	11		direction.generale.inm@gmail.com
Attafi, Kheireddine	11		attafi@meteo.tn
Ben Abdallah, Samir	11		ben_abdallah@meteo.tn
Bouallegue, Atef	11		atef.bouallegue@gmail.com
Hamdi, Hassene	11		hassenehamdi@meteo.tn
Oueslati, Foued	11		foued@meteo.tn

1. Istituto Nazionale di Geofisica e Vulcanologia (INGV), Italy
2. AECOM Technical Services, USA
3. Norwegian Geotechnical Institute (NGI), Norway
4. Instituto Português do Mar e da Atmosfera (IPMA), Portugal
5. Instituto Dom Luiz, Faculdade de Ciências da Universidade de Lisboa, Portugal
6. Helmholtz-Zentrum Potsdam - Deutsches GeoForschungsZentrum (GFZ), Germany
7. Middle East Technical University (METU), Turkey
8. GRC Geociències Marines, Departament de Dinàmica de la Terra I de l'Oceà, Facultat de Ciències de la Terra, Universitat de Barcelona (UB), Spain
9. National Observatory of Athens (NOA), Greece
10. Centre National pour la Recherche Scientifique et Technique (CNRST), Morocco
11. National Institute of Meteorology (INM), Tunisia
12. Dipartimento di Fisica "Ettore Pancini", University of Naples Federico II, Italy
13. Instituto Superior de Engenharia de Lisboa, Instituto Politécnico de Lisboa (IPL), Portugal

Table of Contents

PRELIMINARY IMPLEMENTATION: Phase 1, Pre-assessment (June 2017)

PHASE 1 – STAGE 1: Shaping the Project

Author: **PM & TI team**

Date: **31 May 2017**

Version: 1.0

Table of Contents

This page is intentionally left blank.

Executive Summary

In this document (Doc_P1_S1_ProjectSummary), we present a synthesis of the project proposal and its updates done during the Pre-Assessment Phase until the 1st review round.

Some background information is also given to help understanding decisions made and methods adopted in the current context; such as:

- the funding agency type – the European Civil Protection;
- their expectations;
- the general purpose of this effort – a first region-wide long-term assessment;
- the feedback received from End-Users (both at the Project Kick-Off Meeting, Rome, and at the Technical Review Meeting, Athens).

We then report about the "proposal execution decisions and specifications" concerning both technical and dissemination aspects, made by the Project Manager (PM) and by the Technical Integrator (TI) before the implementation of the PTHA.

We focus, in particular, on those aspects that are not entirely standard practice in S-PTHA and / or approaches to specific issues that have been developed on purpose within the EU Project ASTARTE (http://www.astarte-project.eu/) or TSUMAPS-NEAM.

The full documentation regarding the project, and some technical documents on specific topics are provided as Appendices to this document. They are:

- T1 and T2 forms (documents containing the technical descriptions of the project) + updated GANTT: 'T1_2017-01-24.pdf' and 'T2_2017-01-24.pdf'; 'Gantt_2017-01-24.pdf'.
- The relevant sections of ASTARTE D8.39 (ASTARTE_D839_Excerpt_w/References.pdf).
- A. Herrero et al. EGU 2017 'Poster_Non_PlanarV2.pdf'; Molinari et al. (2016) NHESS paper, Selva et al. (2016) GJI paper.

This page is intentionally left blank.

1 Proposal Summary

1.1 The Project

The TSUMAPS-NEAM project aims to develop the **first homogeneous region-wide long-term Probabilistic earthquake-induced Tsunami Hazard Assessment** (Seismic PTHA, S-PTHA) for the coastlines of the North East Atlantic, the Mediterranean, and connected seas (NEAM), and trigger a common tsunami-risk management strategy in the region.

These results will be achieved through:

1) realization of state-of-the-art SPTHA with full uncertainty treatment;

2) review process with international experts;

3) production of the PTHA database and maps;

4) publicity of results through an awareness raising and education phase, and a capacity building phase.

The PTHA products can serve as a **basis for future local and national PTHA efforts** and be the first step to include tsunamis in **multi-hazard risk assessments**.

The project is funded by the European Commission under the auspices of the Directorate General of the European Civil Protection and Humanitarian Aid Operations (DG-ECHO) set forth in 2015 with a call for proposals for prevention and preparedness projects in the field of civil protection and marine pollution (http://ec.europa.eu/echo/funding-evaluations/financing-civil-protection/calls-for-proposal/2015-prevention-and-preparedness_en). After evaluation, 25 projects were funded under this call (http://ec.europa.eu/echo/search/site/2015_en?f[0]=im_field_year_2%3A2015).

The duration of the project was initially set to 18 months and then extended to 21 months; it started on 01/01/2016 and will end on 30/09/2017. The project extension was required to meet the opportunity of having the project final meeting together with IOC/UNESCO and thereby creating an excellent occasion for the publicity scopes of the project. Some internal deadlines and milestones have also changed accordingly to the extension and review of the project tasks. The current detailed version of the project can be found in the attached official project documentation: 'T1_2017-01-24.pdf' and 'T2_2017-01-24.pdf'. The updated timeline can be found in the attached file 'Gantt_2017-01-24.pdf'.

The project development and activities can be followed through the project website http://www.tsumaps-neam.eu/.

1.2 Understanding the framework of the Project under the EU DG-ECHO

TSUMAPS-NEAM is a **Prevention Project**, **Priority 3**, **External Budget item**. These terms reflect the DG-ECHO funding scheme.

The DG-ECHO funds two types of projects: 1) Prevention Projects and 2) Preparedness Projects.

1) **PREVENTION PROJECTS:** *Prevention means any action aimed at reducing risks or mitigating adverse consequences of disasters for people, the environment and property, including cultural heritage.*
2) **PREPAREDNESS PROJECTS:** *Preparedness means a state of readiness and capability of human and material means, structures, communities and organisations enabling them to ensure an effective rapid response to a disaster, obtained as a result of action taken in advance.*

Within the Prevention projects the following priorities exist:

1) Action-oriented projects focusing on “risk-proofing" of public and/or private investments and development and testing of tools and methodologies for tracking of resilient investments.
2) Pilot and demonstration projects with replication capacity focusing on urban resilience to disasters. Projects should build upon existing knowledge and good practices (e.g. resilient cities scoreboard and campaign, local resilience forums, local climate change adaptation strategies).
3) Technical cooperation projects with the objective of implementing at all levels of government methodologies aiming at developing multi-hazard assessments of risks and risk management capabilities and risk management planning, including cross border dimension.

For all projects, there exist the following two types of budgeting:

1) **Internal Budget item**: projects covering the Participating States in the EU Civil Protection Mechanism.
2) **External Budget item**: projects covering the Enlargement countries and the European Neighbourhood Policy countries.

The DG-ECHO specifies that "...funds from the external budget item can be allocated to projects addressing the needs in European Neighbourhood Policy countries and enlargement countries“ and that "the results of the project shall be mainly for the benefit of the enlargement countries and the European Neighbourhood Policy countries and relevant for the EU."

1.3 Project partnership, roles, and tasks

The project partnership is reported in the table below.

Institution	Country	EU status	Role
INGV	Italy	Member State	Coordinator
NGI	Norway	Participating State	Partner
IPMA	Portugal	Member State	Partner
GFZ	Germany	Member State	Partner
METU	Turkey	Enlargement	Partner
UB	Spain	Member State	Partner
NOA	Greece	Member State	Partner
CNRST	Morocco	Neighbourhood Policy	Partner
INM	Tunisia	Neighbourhood Policy	Partner

The responsibilities for the project main tasks, and actions within them, are distributed as shown in the table below.

Task ID	Task Title	Actions	Task leader institutions
A	Management and Reporting to the Commission	A.1 Coordination A.2 Management and Reporting	INGV
B	Hazard Assessment	B.1 Earthquake Model B.2 Tsunami Modelling B.3 Probabilistic Model B.4 Hazard Analysis	INGV + IPMA
C	Review and Sanity Check	C.1 Best Practices C.2 Expert's Review and Sanity Check C.3 Documentation	GFZ + NOA
D	Publicity	D.1 Awareness and Education D.2 Capacity Building	METU

1.4 Project deliverables

The list below summarizes the project deliverables per task. The deadline for each deliverable is indicated as month number from the start of the project.

Task A

- D1. First Progress Report (M7)
- D2. Second Progress Report (M14)
- D3. Final Report (M21)

Task B

- D4. Online Tsunami Hazard Database (M14)
- D5. Tsunami Hazard and Probability Maps (M14)

Task C

- D6. Experts' Review and Sanity Check (M18)
- D7. Methods and data Documentation (M18)

Task D

- D8. Project Website (M4)
- D9. Awareness and Education Materials (M16)
- D10. Guidelines and Training Tools (M19)
- D11. Layman's Report (M21)

At the time of writing this document, D1, D2, D4 (Preliminary version), D5 (Preliminary version), and D8 are completed. D9 is under completion and will be transmitted in one-two weeks.

More specifically, D4 (Online Tsunami Hazard Database) and D5 (Tsunami Hazard and Probability Maps) can be accessed, in protected mode, through an interactive tool, the TSUMAPS-NEAM Interactive Hazard Curve Tool, via the temporary link http://ai2lab.org/tsumapsneam/interactive-hazard-curve-tool/ (password made available upon request).

This website demonstrates that the preliminary hazard curve database and the corresponding tool to visualize it are all in place and working. The most important missing features is the switch to visualize the probability maps, but it will be implemented soon. Moreover, several versions of the

probability and hazard maps will be provided for different intensities and average return periods. However, the data uploaded so far do not reflect values and coverage described in the actual content of the project hazard assessment. We thus make the access credential (link and password) to this website available only within the project partnership and the Commission.

Please also note that the entire hazard tool will be migrated to the official project website (http://www.tsumaps-neam.eu/) at the end of the project and then made accessible to the public.

2. Proposal execution decisions and specifications

This section is about the main, yet in some cases preliminary, decisions on some technical aspects, and some result dissemination policy aspects, which were only qualitatively described in the project proposal.

The decisions were made by the Project Manager (PM) and by the Technical Integrator (TI) during several meetings, workshops and remote conversations.

Overall, these decisions concern: the selection of the Points of Interest (POIs) along the coastlines of the NEAM region; the treatment of the different source regions potentially affecting these POIs; the approach to include earthquake slip distribution and tsunami numerical modelling, and the approximations made therein; the uncertainty treatment from source to site; the hazard intensity metric; the ranges and discretization of the hazard curves; the exposure window for probability maps and the average return period for hazard maps.

We present here only a brief description of these topics; further necessary details and actual datasets will be presented in the more extended specifications in the preliminary implementation plan (Doc_P1_S4_Prel_Impl_Plan), describing the models (with alternatives) to be actually implemented.

Some decisions may change in due course; some aspects of the models may be not implemented due to limited resources. However, in case of any updates, we'll document them accurately in the documentation for the second review round.

2.1 Points of Interest (POIs)

The POIs are the locations where the output of the tsunami simulations is stored for subsequent hazard calculations. They nominally lie on the 50 meters isobaths of the NEAM region (see figure 2.1 below), and they are approximately regularly spaced at 20 km from each other.

The choice of the 50 m isobaths is motivated by the need of a compromise between preserving linearity of the tsunami propagation, on one hand, and being close enough to a coastline, on the other hand. Linearity is needed because, in current approach, individual tsunami propagation scenarios are obtained by linear superposition of virtual tsunamis generated either by unit Gaussian-shape sources distributed along the sea surface, or by unit sub-faults (see section 2.2).

We make this approximation since the probabilistic earthquake models include tens of millions of scenarios, and thus it is mandatory to reduce computational costs. Still, millions of linear combinations together with accompanying post-processing (e.g., calculation of coastal amplification) are time consuming. Hence, our strategy is to start with a reduced set of POIs, e.g. 200 km from each other and calculate the hazard curves with this coarser step along the coasts. We'll then progressively "densify" the results down to the desired resolution.

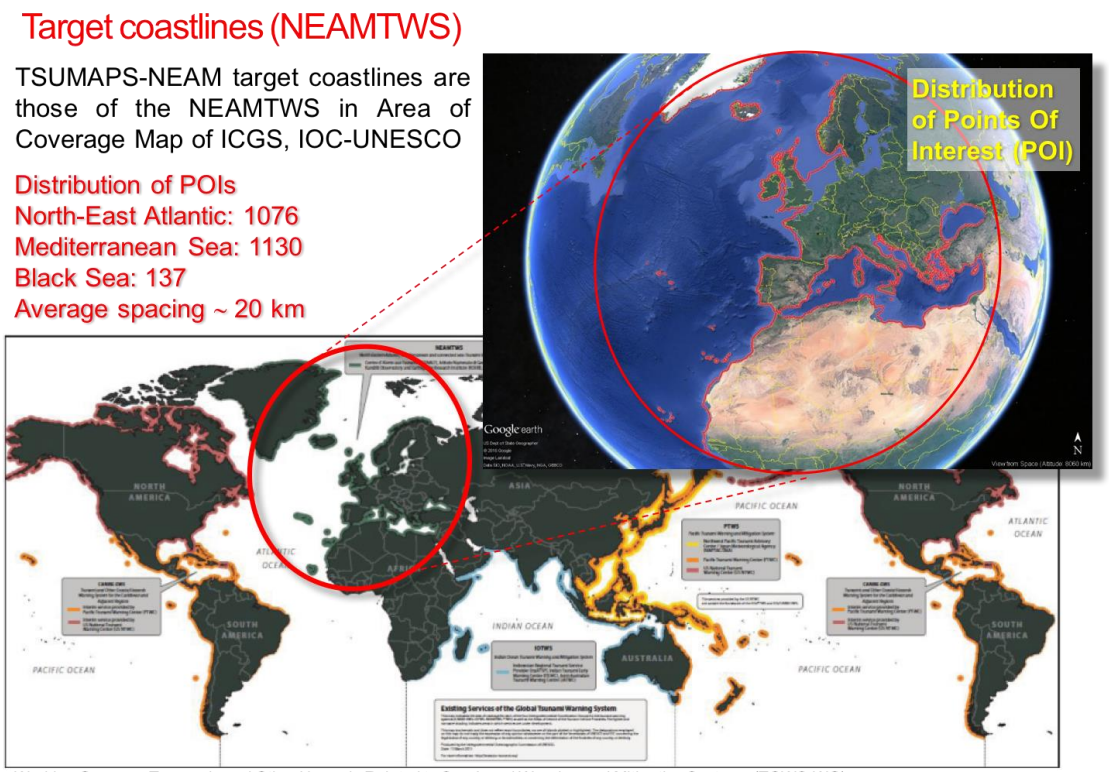

FIGURE 2.1.1 Distribution of Points of Interest (POIs) in the NEAM region.

2.2 Treatment of earthquake sources and tsunami modelling

To deal with epistemic uncertainty concerning earthquake sources, seismicity is treated with two different modelling approaches: Predominant Seismicity (PS) and Background Seismicity (BS).

Generally speaking, PS is meant to capture the (generally larger) earthquakes generated by rather well known faults (e.g. plate boundaries in general, and subduction zones in particular), thus constraining the epistemic uncertainty, while BS takes into account all other earthquakes, including those at unknown or unmapped faults (see Figure below). This seismicity-splitting approach was first introduced for SPTHA by Selva et al. (2016). In the probabilistic calculations, PS and BS probabilities are balanced to represent actual seismicity.

Predominant Seismicity (PS) source definition: Several individual well-known fault structures may be of particular relevance for tsunami generation (i.e., they are deemed to generate larger magnitude earthquakes as, for example, subduction interfaces). Since such structures are well known (e.g., in their 3D geometric fault properties), earthquakes generated by them can be treated separately from the rest of the seismicity (the BS) in order to maximize the use of all the available information. This approach will significantly constrain the epistemic uncertainty related to the source parameters.

Background Seismicity (BS) source definition: Since earthquakes also occur outside the well-known faults, and not all tsunamigenic faults are mapped well enough, we introduce so-called background seismicity (BS). BS exists in addition to PS and accounts for earthquakes occurring everywhere within a crustal volume with a certain variability of the faulting mechanism. The presence of known faults

(not those already treated as PS), historical seismicity (focal mechanisms), and dominant stress regime can be used to constrain probabilities of distribution of various faulting mechanisms.

In each region defined by the tectonic regionalization (see Figure 2.2.1), three different situations may occur:

1) a region is treated as a mix of PS and BS (e.g. a subduction zone and crustal earthquakes above it);
2) a region is treated as pure BS region (similarly to usual PSHA approaches) if there are no well mapped major structures;
3) a region is treated as pure PS region; this generally applies to source zones located far away from the target POIs, in this case modelling a subset of the largest earthquakes is sufficient (e.g. the Caribbean subduction zone with respect to the target POIs in the North-East Atlantic); a region can also be simplified to a pure PS because the allotted project resources do not allow tsunami simulations for numerous BS sources (e.g. the spreading ridge and transform faults in the mid-Atlantic Sea); future updates of the SPTHA will possibly integrate the BS approach on the closest or intermediate distance source regions not considered here.

The PS sources and the ensuing tsunamis are modelled following two different strategies, depending on the location of the sources with respect to the POIs.

The PS sources in the Mediterranean are always close to the coastlines. Hence, sufficiently 'short-wavelength' slip heterogeneity needs to be modelled. For Hellenic, Cyprus and Calabrian Arcs, in the Mediterranean Sea (see Figure 2.2.2), the PS ruptures are modelled using non-planar triangular meshes (with typical edge length of about 15 km) implying heterogeneous stochastic slip distribution (see section). Resulting sea-surface deformation is then projected onto the tsunami unit sources as described in section .

For several seismic sources, such as Gloria fault zone, normal and transform faults along the Mid-Atlantic Ridge, and the Caribbean subduction (Figure 2.2.2), PS is modelled using planar rectangular faults divided into subfaults. Here, tsunami unit sources are directly related to the unit slip at the subfaults and the slip distribution is assumed to be uniform with its value obtained from a scaling law. This approach is used also for the parts of the fault segments of the Mid-Atlantic Ridge and the Gloria fault covered by Gaussians (the light-blue area in Figure 2.2.2). These quite common simplifications, made to save computation time, are considered appropriate because these structures are very distant from the target coast lines. Due to the large uncertainty on available models, the approach for the Cadiz subduction (Figure 2.2.2) is still under discussion, and the decision is pending on whether it should be treated as PS or incorporated into the BS.

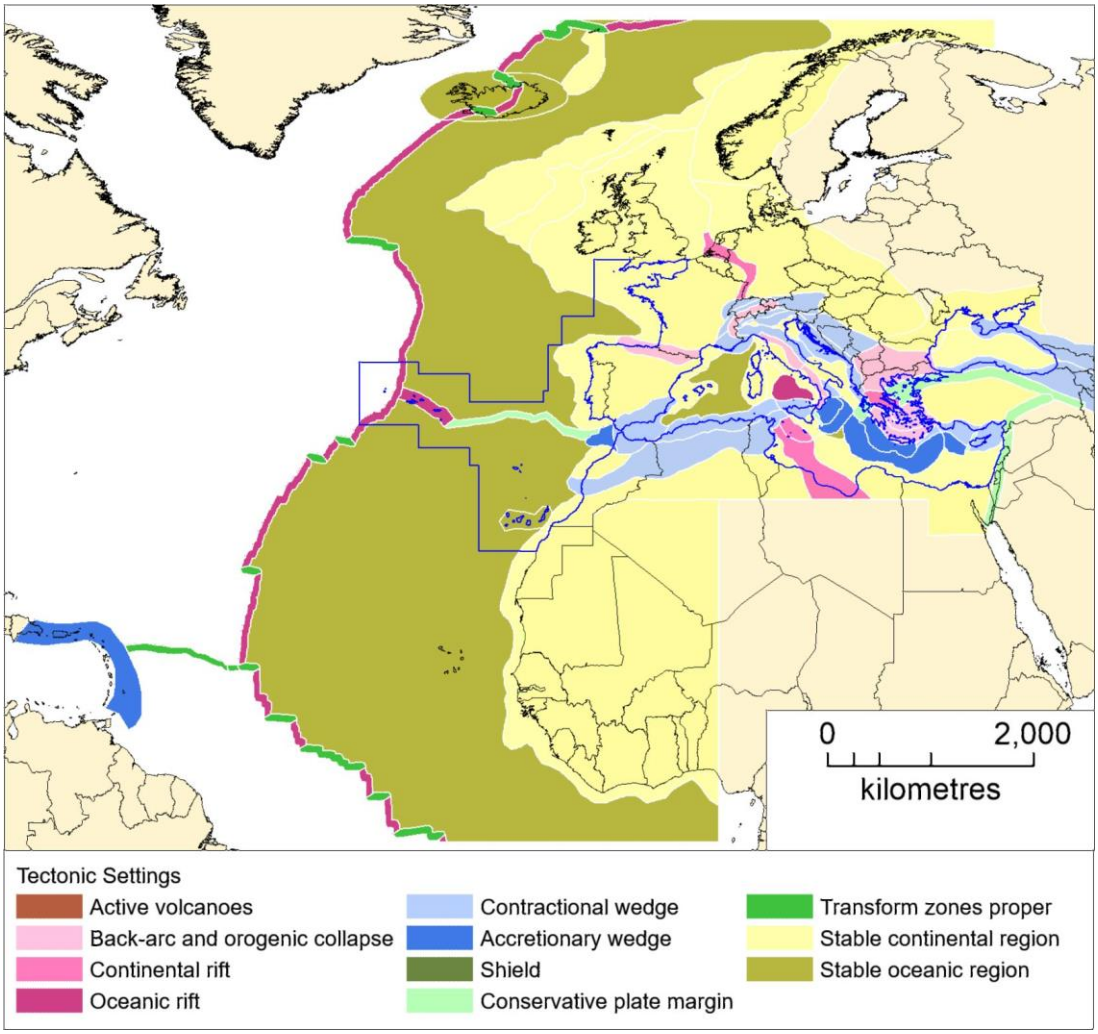

FIGURE 2.2.1 Tectonic regionalization. The blue outline marks the area where the tsunami unit sources are pre-calculated (see also Figure 2.2.2).

Virtual tsunamis for the elementary Gaussian-shape unit sources are routinely computed at a fine resolution, 30 arc seconds, bathymetric grid. Spatial and temporal extensions of the simulation domain depend on the maximum earthquake magnitude that needs to be simulated at each location. Moreover, Gaussians needs to be quite small to approximate relatively small earthquake displacements. Hence, the number of simulations is on the order of hundreds of thousands. Therefore, to limit the computational cost, very large simulation domains have been used only for Gaussians around the SWIM source zone (at the Atlantic side of the Gibraltar Strait, which includes the 1755 Lisbon earthquake and tsunami source zone), where the faults are too uncertain to be treated as PS. Anywhere else in the Atlantic, Gaussians are used only to treat smaller events in the BS (up to M7.5), whereas the bigger earthquakes (up to M9) are included as PS simulated with subfaults. Figure 2.2.3 shows the NEA Gaussian source zones together with the extent of the corresponding associated simulation domains. The largest domain enclosed in the dashed-line rectangle is the one used for the Gaussians used to cover the SWIM source zone.

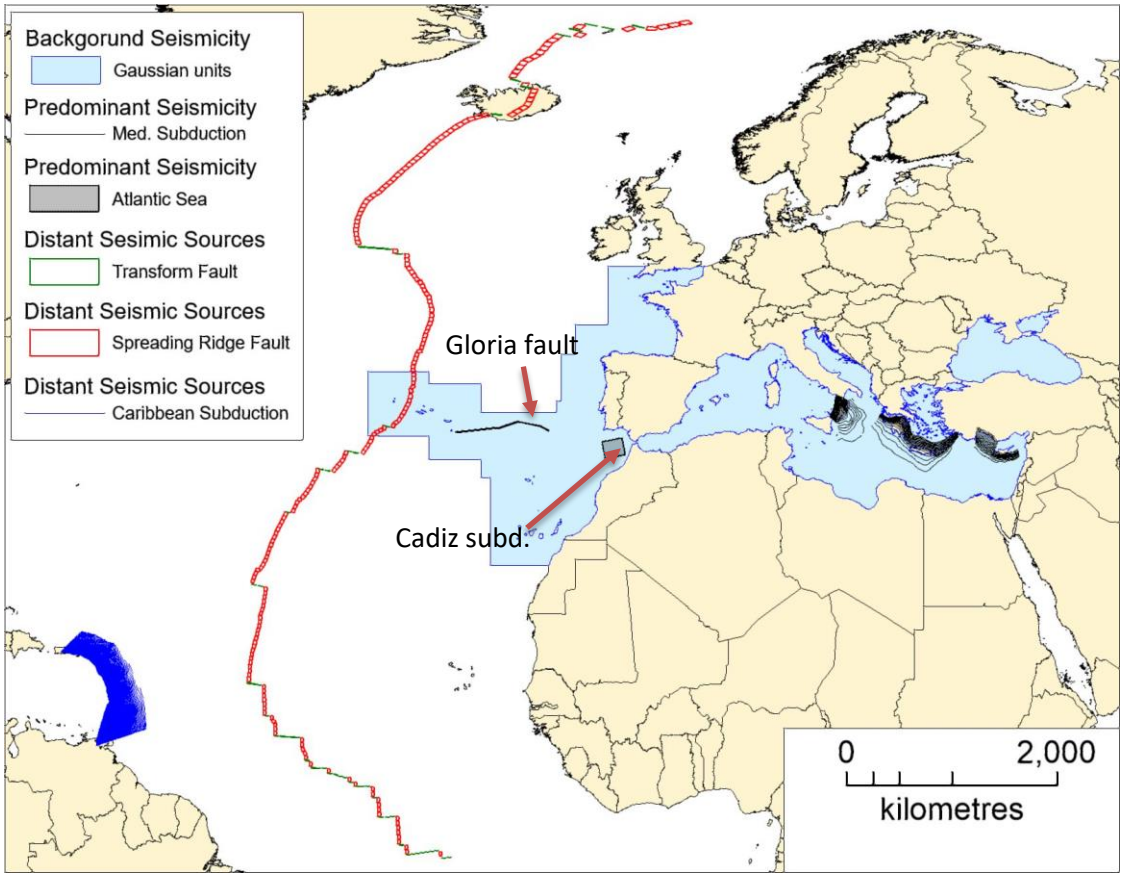

FIGURE 2.2.2 Predominant seismicity (PS) and background seismicity (BS) sources.

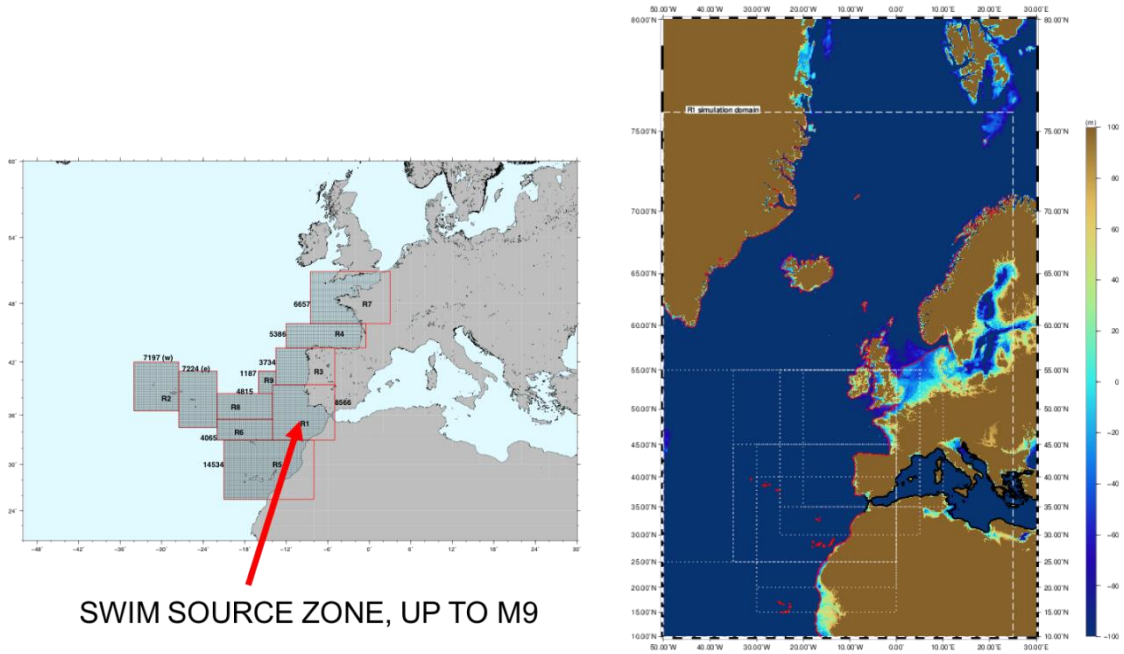

FIGURE 2.2.3 NEA Gaussian source zones (left) and the associated simulation domains (right).

In order to capture the full epistemic uncertainty of seismic sources, earthquakes envisaged to occur outside the PS, or those that have focal mechanisms different from the PS-dominant, are taken into

account by the BS. The light-blue area in Figure 2.2.2 illustrates the coverage of the BS zones with Gaussian unit sources (Section) in the Mediterranean region, including the Black Sea, and in part of the Atlantic Sea. This coverage includes a number of tsunami scenarios in the order of many millions. The BS are spatially treated through a regular grid composed by non-conformal equal-area cells of 25x25 km (Figure 2.2.4). The grid origin coordinates are 24°N - 3°E. In each cell, probability density function of faulting mechanisms at each node of the regular grid is constrained by (1) earthquake catalogues and (2) by the geometry of mapped crustal faults not treated as PS (Figure 2.2.5).

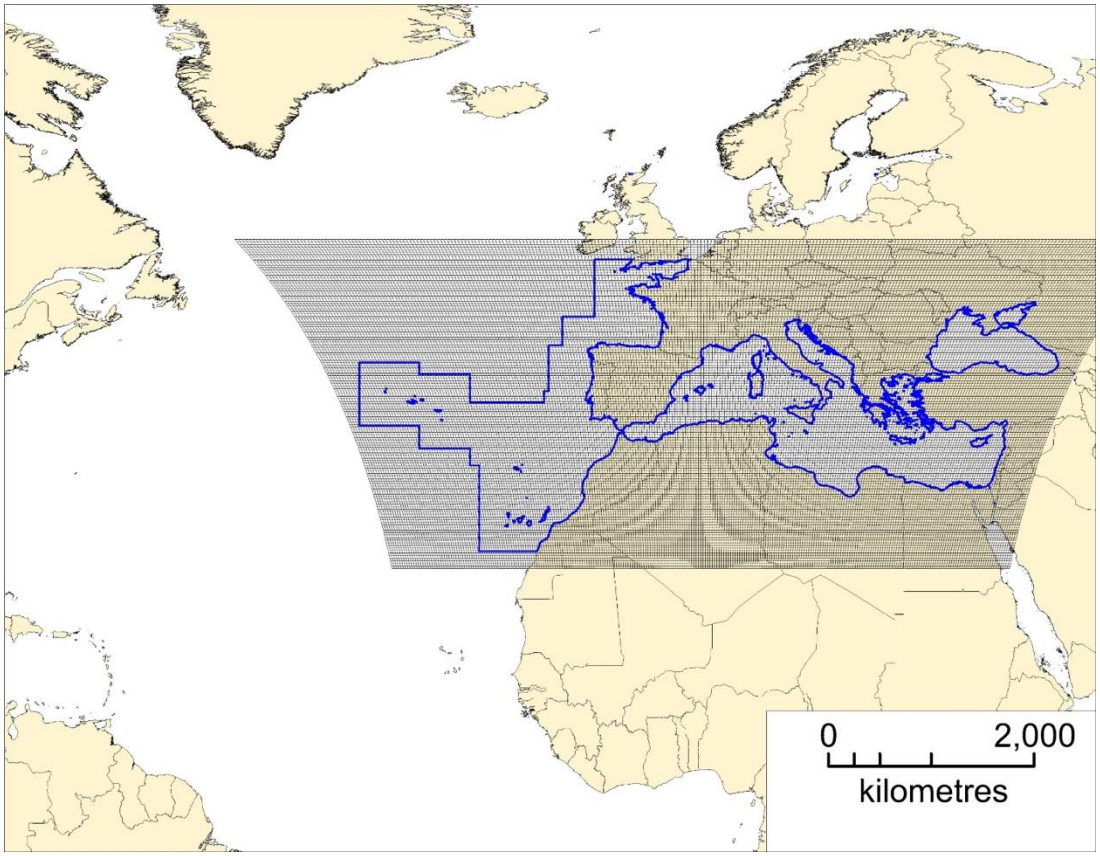

FIGURE 2.2.4 Regular grid (grey quadrangles) for the background seismicity (BS) sources covering the entire domain of Gaussian units (blue outline).

At each node (x,y) of the grid, different focal depths (z) and focal mechanisms (strike, dip, rake), with different magnitudes, are allowed (see e.g. the Event Tree table in Section 2.5.1 of this document). The discrete parameter space covered by this single-fault homogeneous slip events will be described in another document (Doc_P1_S4_Prel_Impl_Plan.docx). It is in dealing with this large amount of events that the sea surface tsunami unit source approach described in Section reveals its full potential. In particular, unit Gaussian-shaped sources at the sea surface do not constrain any faulting mechanism, which is instead the case of the classical subfaults approach.

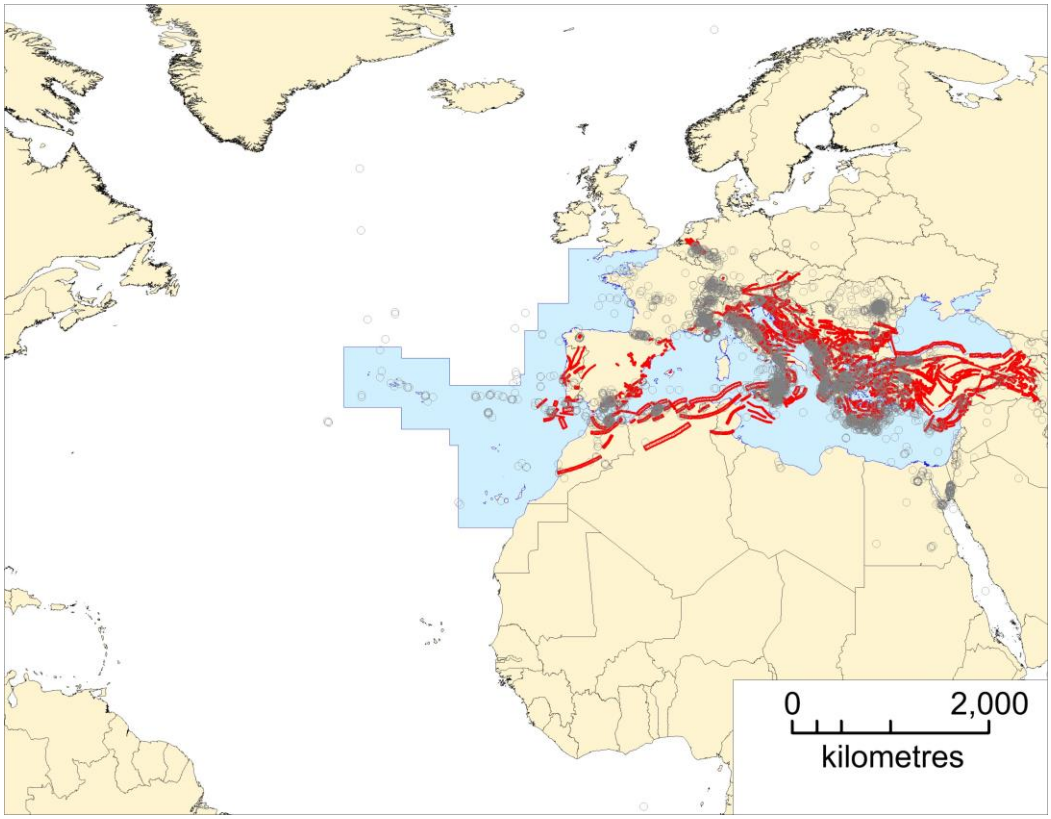

FIGURE 2.2.5 Crustal faults and location of earthquake focal mechanisms used to constrain the faulting mechanisms of the background seismicity (BS). Light blue area as in Figure 2.2.2.

Potential BS sources within the stable oceanic regions of the Atlantic Sea, to the north and to the south of the area covered by Gaussian unit sources and to the west of the mid-Atlantic spreading ridge, are ignored. This choice is supported by the observation that the seismicity of plate interiors, including both oceanic and continental stable regions, accounts for less than 4% of all global seismicity (Kagan et al., 2010).

More in general, BS occurring within all far-distant areas in relation to the Atlantic coasts is neglected, assuming that it has a very little impact on hazard. One exception is around Iceland, this region will be covered by Gaussian sources as soon as Project resources make it possible.

By modeling of PS and BS sources, the initial sea level elevation field is obtained from the co-seismic sea floor displacement using a rough implementation of the low-pass Kajiura filter (Kajiura, 1963). Present implementation is rough as it assumes a constant water depth within the source area. This depth is averaged along the four corners of the rupture surface projection. Recall that the efficiency of the Kajiura filter against smaller wavelength increases with water depth.

2.2.1 Uniform vs Heterogeneous slip

Heterogeneity of the slip distribution is well known to influence the tsunami impact particularly in the near-field of the source. The extent of the near-field region increases with the size of the fault rupture, which in turn increases with the earthquake magnitude.

Ideally, a very big number of different heterogeneous slip scenarios should be used, but this might be practically unfeasible. It was thus decided to use uniform slip for the BS, and heterogeneous

stochastic slip distributions only for PS within the Mediterranean, that is for the subduction zones, starting from a given lowest magnitude value, likely from 7.5-8 depending on the zone. The exact minimum magnitude will be decided on the basis of the results of ongoing sanity checks and sensitivity analysis of the preliminary hazard results. It is also still under discussion the decision on the use of heterogeneous slip for the closest source zones in the North East Atlantic (the SWIM BS source zone; the Gloria PS source zone).

A recently developed algorithm for putting a composite stochastic slip distribution on 3D (non-planar) faults is used (Herrero et. al. EGU 2017 poster included as appendix contains some further details). Figure 2.2.6 shows two examples for slip distributions with one and two "asperities" and a k^{-2} spectrum.

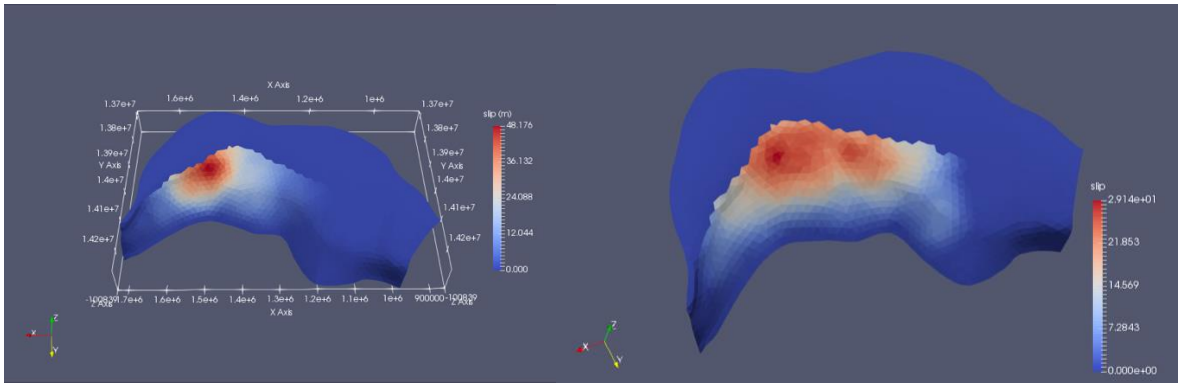

FIGURE 2.2.6 Examples of slip distributions on non-planar faults with one asperity (left) or two asperities (right).

Another issue yet to be addressed is depth-dependence of the spatial slip probability; for example, as the result of depth-dependent rigidity and / or shallow slip amplification. Its implementation is not trivial. Nevertheless, this aspect is expected to have a significant influence on hazard and must be considered as a future update of the assessment: the point will be clearly documented for the next revision round.

2.2.2 Tsunami unit sources for modelling deep sea tsunami propagation

We use a database of pre-calculated tsunami waveforms at the POIs, obtained by numerical propagation triggered by uniformly spaced Gaussian-shaped elementary sources at the sea surface. It is important that, in contrast to the common tectonic unit-sources technique, present surface unit sources are fully independent of any presumed earthquake focal mechanism. Based on arbitrary initial sea surface displacement, the database allows the fast calculation of full waveforms at POIs (distributed along the 50 m isobaths) by means of linear superposition. A computationally inexpensive procedure is set to estimate the weights for the linear superposition based on the preservation of potential energy of the initial elevation field. The size (~20 km base width) and spacing (~7 km) of elementary sources (Figure 2.2.7) is fine enough to satisfactorily reproduce the effects of $M \geq 6.0$ earthquakes.

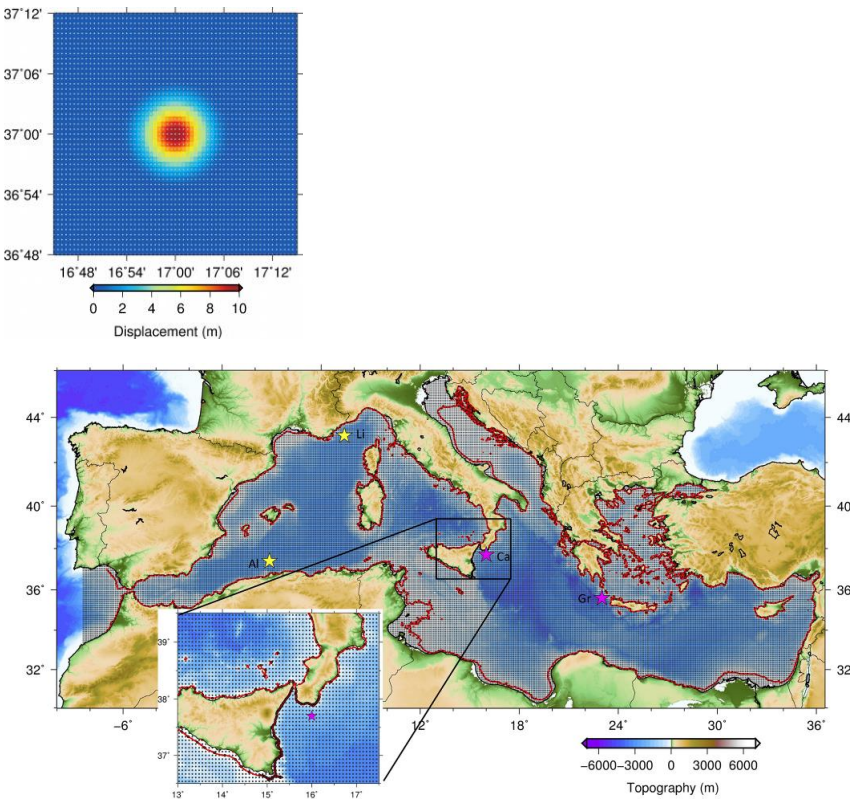

FIGURE 2.2.7 Unit source size and spacing.

Tsunami propagation from Gaussian sources to POIs is modelled by using the Tsunami-HySEA code (e.g. de la Asunción et al., 2013), a GPU finite volume solver for the non-linear shallow water (NLSW) equations developed by the EDANYA Group of the Applied Mathematics Department of University of Malaga, Spain (https://edanya.uma.es/). As said, the database is independent on the faulting geometry and mechanism, which makes it applicable in any tectonic environment; hence, it can be used to "propagate" both the PS and the BS sources.

We have tested that weak non-linearity of tsunami evolution affects the reconstruction of the waveforms and of their maxima by introducing an almost unbiased (centered at zero) error distribution of relatively modest extent. Depending on the project resources, this uncertainty can be propagated onto the final hazard estimates. In Figure 2.2.8 (from Molinari et al., 2016) the maximum amplitudes from linear combinations are plotted versus those by direct simulations showing limited scatter; the histogram of the percentage errors is also shown. More details on the database of Gaussian unit sources can be found in Molinari et al. (2016), which is provided as appendix to this document. At the time of writing the paper, the database covered only the Mediterranean Sea. For TSUMAPS-NEAM, the coverage of the different source zones with the unit sources was extended to the Black Sea and to some regions of the North East Atlantic, as shown in Figures 2.2.2 and 2.2.3.

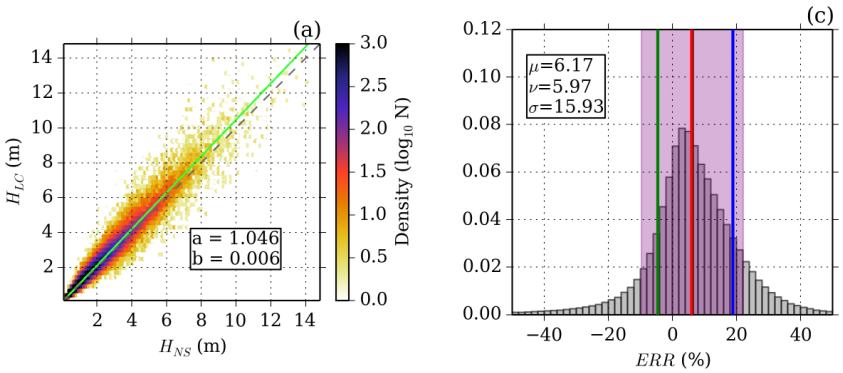

FIGURE 2.2.8 Maximum amplitudes from linear combinations versus those by direct simulations (left), and histogram of the percentage errors (right).

2.3 Tsunami Hazard Intensity metrics

We'll provide the final results using three different hazard intensity metrics.

We propose to use as principal quantity the Maximum Inundation Height (MIH), that is the estimated maximum flow depth from the envelope of the tsunami wave at all times (see Figure 2.3.1). We briefly report in the next sections how this quantity is approximated starting from offshore (50 m isobath) tsunami wave amplitudes and how the estimated uncertainty is combined with other uncertainty sources.

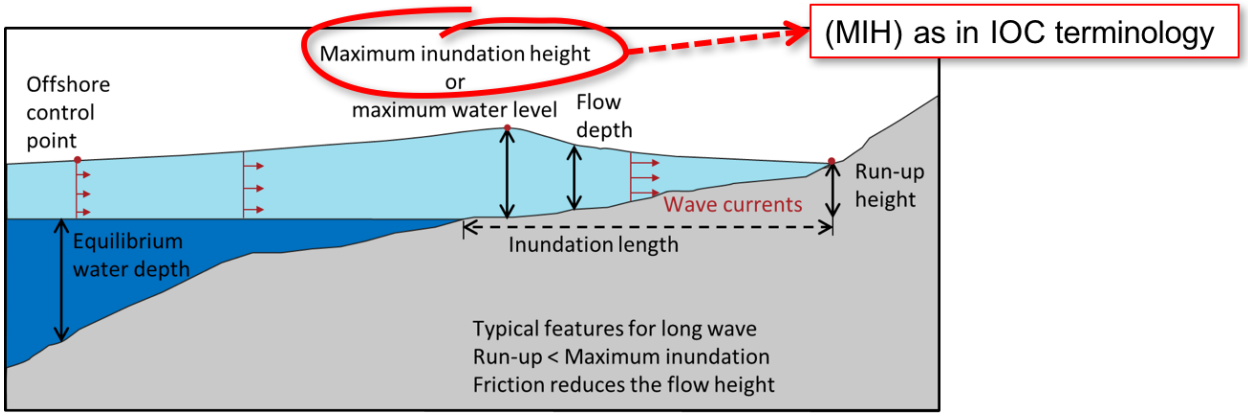

FIGURE 2.3.1 Graphical representation of the Maximum Inundation Height.

MIH is suitable for a regional, initial screening assessment type such as the objective of TSUMAPS-NEAM. Computing of full probabilistic inundation maps for the whole region is not a feasible task within the current Project. Moreover, reliable inundation maps would require high-resolution DEMs which are not available with the exception of a few locations. The TSUMAPS-NEAM results must be considered only as input reference study for further site-specific assessments, and this will be clearly stated when presenting the results.

Converting the MIH into expected inundation distances / runups by means of an approximate treatment of inland dissipation is still under discussion, and the outcomes of this discussion will be reported for the next review round.

Nevertheless, two other quantities will be provided as alternative hazard intensity measures: the 'raw' tsunami heights obtained at the 50 m isobaths as well as wave heights evaluated at 1 m depth by application of the common Green's law.

2.3.1 Approximation of MIH with local amplification factors

The standard way of estimating the tsunami run-up and producing inundation maps is to apply depth averaged nonlinear shallow water (NLSW) models that include drying-wetting schemes. However, these detailed numerical inundation simulations are computationally too intensive for the project objectives because we need (i) to estimate tsunami run-up height for millions of scenarios, and (ii) to reach the resolution of the local costal complexity while covering large stretches of coastlines at the scale of the whole NEAM region. Therefore, we approximate the maximum inundation height (MIH) at any location of a coastline using the method of amplification factors. This is a computationally inexpensive approach suitable for establishing the MIH for large regions. The amplification factors method can be used to produce tsunami hazard maps starting form regional tsunami simulations.

The regional approach is primarily meant as an initial screening needed for comparing different areas and / or locating areas that are particularly hazardous. We stress that locally, e.g. for a given harbor or city, this approach would not be suitable, and high-resolution numerical inundation models should be used.

The amplification factors method relates the near-shore surface elevations at the offshore POIs to the maximum shoreline water levels. The surface elevation at the shoreline then acts as an approximation for the maximum inundation height or run-up height along the shoreline.

The basic principles of method are described by Løvholt et al. (2012) and Løvholt et al. (2015). It makes use of linear wave theory, and for non-breaking plane waves the amplification factor method should then theoretically yield the exact run-up. Wave propagation is simulated along bathymetric transects, using 1D LSW model all the way to the shoreline. The incident wave is a sinusoidal pulse, with leading peak or leading trough. Combined with results from offshore tsunami simulations, it can be used to estimate the mean or median tsunami run-up or maximum inundation height at a coastal location. However, the Løvholt et al. (2012) and Løvholt et al. (2015) version of the method used amplification factors determined for a set of idealized coastal profiles; then, the profile best matching the real profile was searched and the corresponding amplification factor used for hazard calculations.

We here employ a new and improved version of the amplification method originally proposed by Løvholt et al. (2012). The new amplification factor method takes into account shoaling on the local bathymetry. The new method uses a set of local transects normal to the coastline. The amplification factor applied to the specific stretch of coast is the median of those obtained for each transect within that stretch. The local amplification factor method is expected to replicate the median tsunami inundation height more accurately than the previous method using idealized profiles. However, as the method is intrinsically deterministic, we need to compare the method with local inundation models to quantify its associated bias and uncertainty. Quantifying this uncertainty is also necessary for the general uncertainty quantification of tsunami hazards in TSUMAPS-NEAM.

This new version of the method was partly developed within the ASTARTE EU project (http://www.astarte-project.eu/). Some details are then described in the ASTARTE Deliverable D8.39, Section 3.2. An excerpt from D8.39 with relevant information is reported as an Appendix (ASTARTE_D839_Excerpt_w/References.pdf).

The full set of transects for the whole NEAM region, and the full set of amplification factors, have been developed within the TSUMAPS-NEAM project. Figure 2.3.2 shows all transects that we analyzed within the Mediterranean, the Black Sea, and the North East Atlantic.

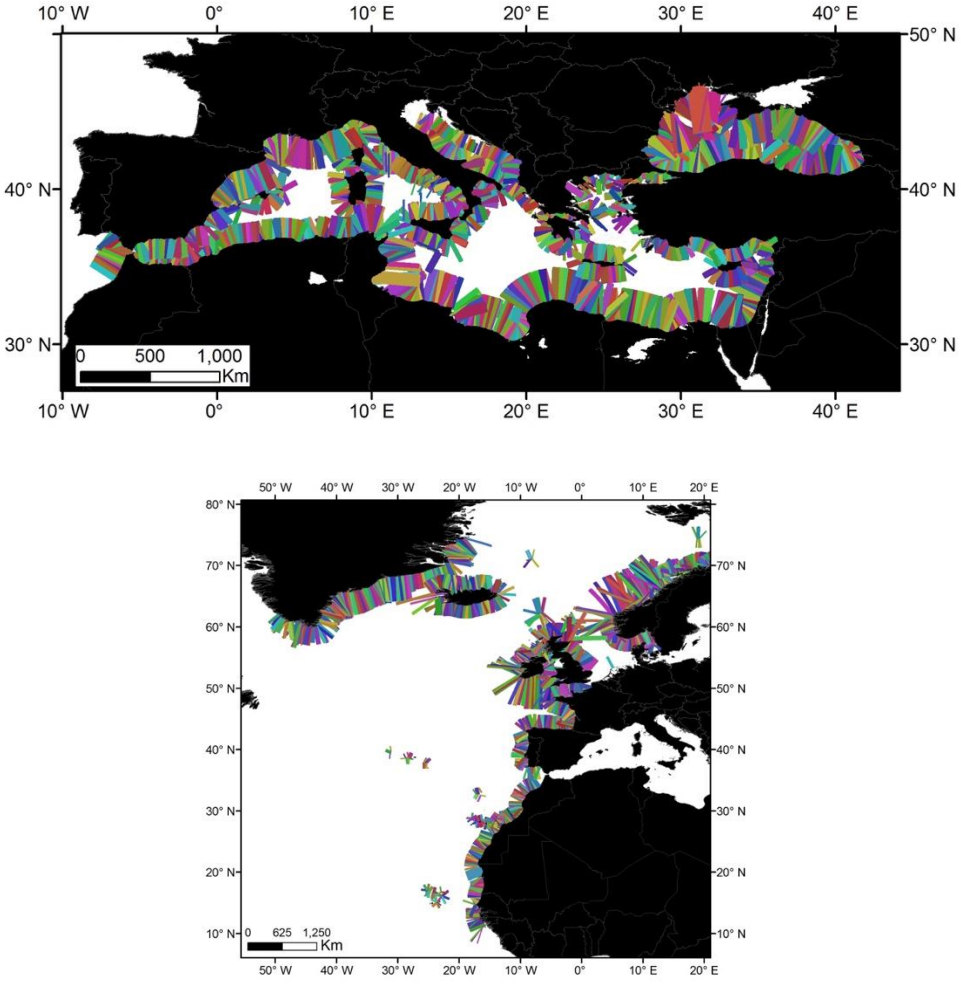

FIGURE 2.3.2 Map of transects for the analysis of the amplification factors in the NEAM region.

The amplification factors have been calculated for incident wave with both leading peak (positive) and leading trough (negative), and for wave periods ranging from 120-3600s. Some examples of the results are reported in Figure 2.3.3.

To apply the results for hazard calculations, an algorithm which extracts the period and the polarity of the leading wave was developed and applied to each single tsunami scenario of the SPTHA.

The method used to determine the bias and the dispersion with respect to MIHs through detailed inundation numerical simulations, assuming that the MIH should be log-normally distributed, is explained in the excerpt from ASTARTE D8.39 provided as an Appendix to this document.

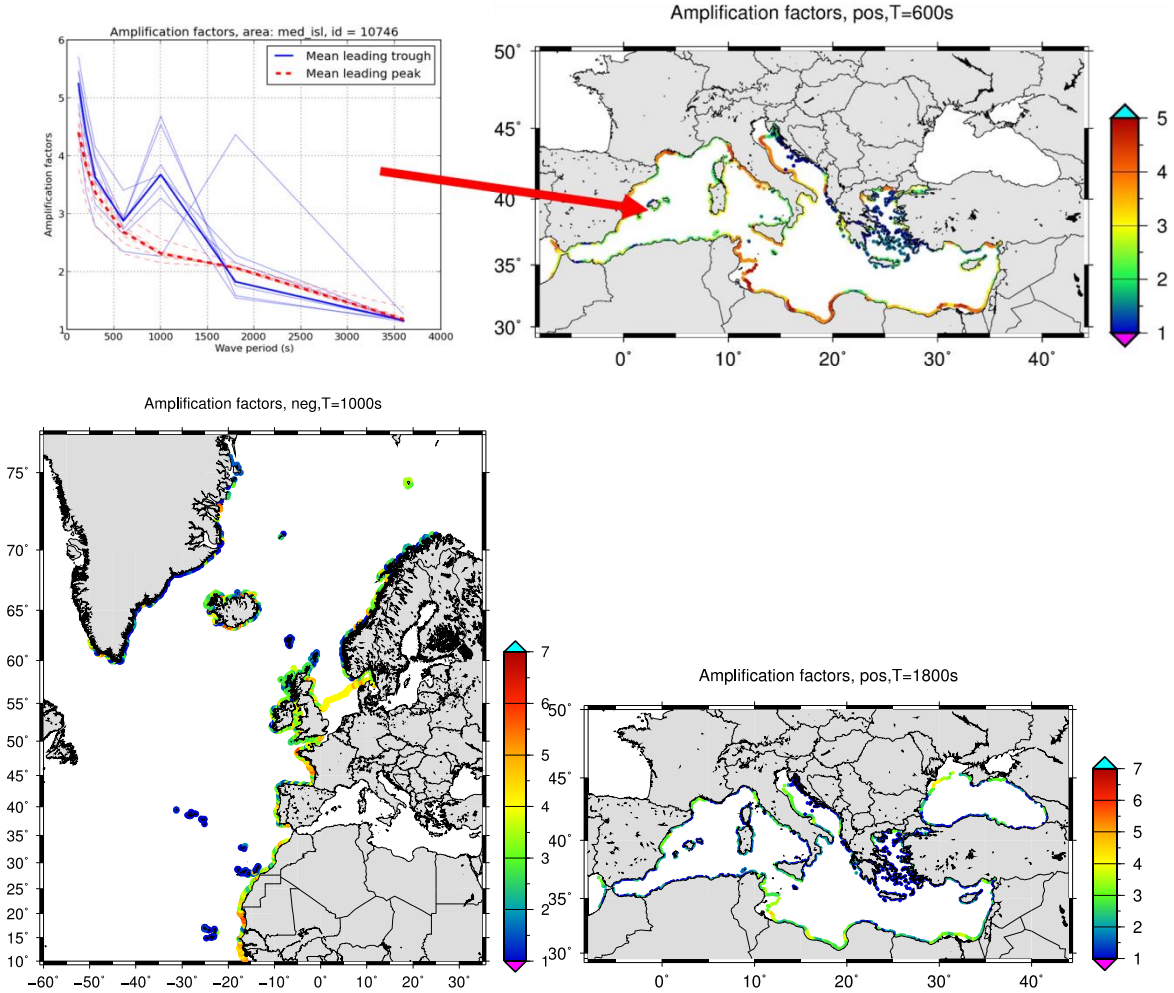

FIGURE 2.3.3 Sample maps of amplification factors in the NEAM region.

With respect to that deliverable, we extended the simulations to five sites (see Figure 2.3.4) and used four different earthquake moment magnitudes (M_w 7.0, 7.5, 8.0, and 8.5) to reproduce different dominant wave periods. The simulations are performed for some sites also with different tsunami numerical codes, i.e. HySEA, which is the code used for all TSUMAPS-NEAM simulations, but also the NSWING code (Miranda et al., 2014), which is in turn largely based on the Cornell Multi-grid Coupled Tsunami model (COMCOT; Wang and Power, 2011) and the MOST code through the COMMIT interface (http://nctr.pmel.noaa.gov/ComMIT/). We'll keep adding numerical simulations to better constrain the uncertainty. Some results are provided as an example in Figure 2.3.4.

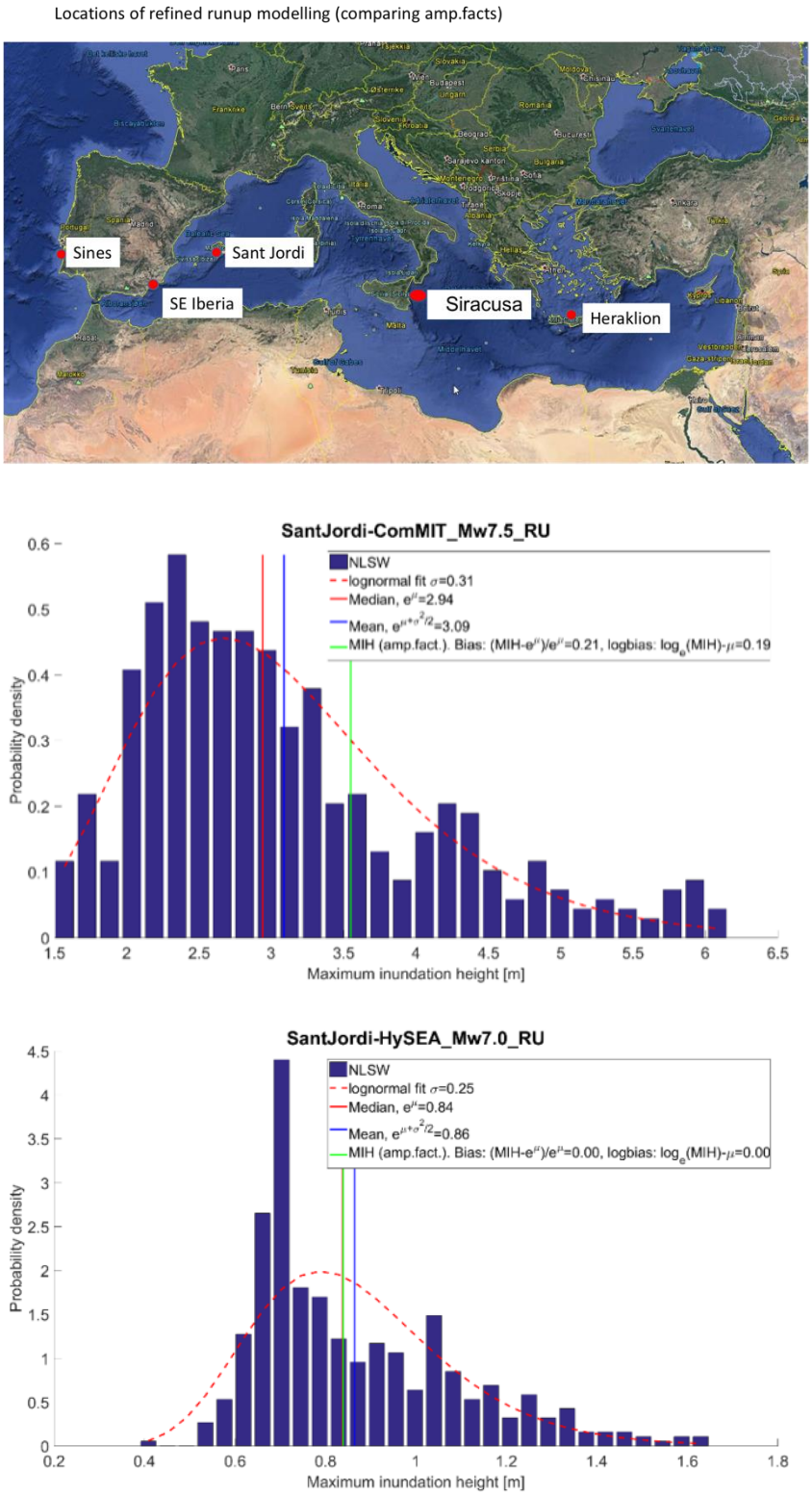

FIGURE 2.3.4 Map of the sites were detailed numerical simulations were performed (upper panel), and two diagrams showing the distribution of MIH and fitted lognormal distribution for two sample sites (lower two panels).

2.4 Modelling of tides in the Atlantic Ocean

The tide prediction is accomplished with the Tide Model Driver (TMD) developed by Egbert and Erofeeva (2002; https://www.esr.org/ptm_index.html).

The original Atlantic Ocean inverse tide model presents a grid resolution of 1/12º. In our study, we used a bathymetry grid of higher resolution (1/120º) that was compiled by the TSUMAPS-NEAM team from different sources. This bathymetry grid file was then converted to OTIS file (the format required for the TMD model).
At each POI of the NE Atlantic, the tidal signal was predicted for a 10-year period, starting from 2017/01/01 at 00h00min00sec, and considering a sampling interval of 10 min.

As an output of the TMD model, each POI has its corresponding predicted tide time series. Using these outputs, the probability density function (PDF), the cumulative density function (CDF) and the probability of exceedance were derived at each POI of the NE Atlantic.

Below we show examples of calculations for 10 selected POIs (Figure 2.4.1) and the corresponding prediction of tide signal, PDF, CDF, and probability of exceedance (Figure 2.4.2).

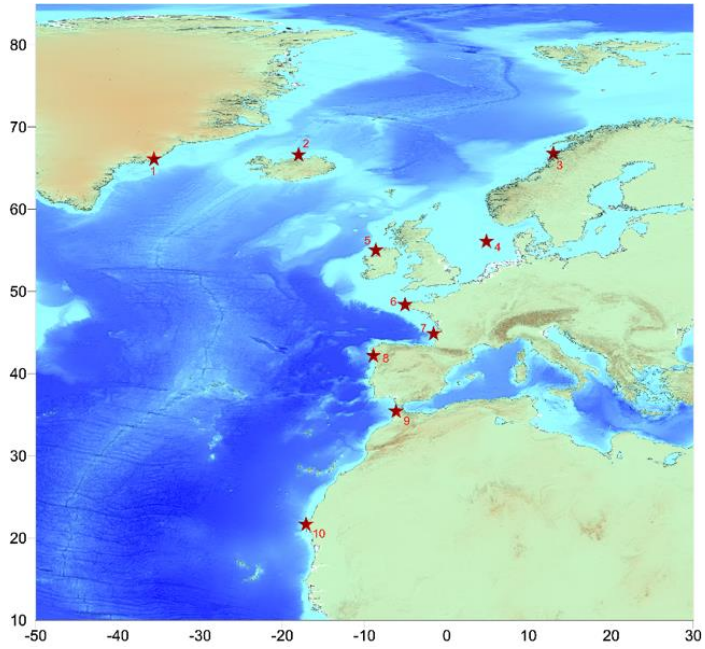

PoI	Longitude	Latitude
1	-35.6259	66.0833
2	-18.0250	66.60074
3	12.97358	66.78333
4	4.833330	56.06250
5	-8.63833	54.98333
6	-5.07500	48.36754
7	-1.59417	44.84167
8	-8.92257	42.16667
9	-6.16249	35.39167
10	-17.1280	21.65000

FIGURE 2.4.1 Example for 10 POIs (red stars).

	Tide	PDF	CDF	Prob. of exceedance
1	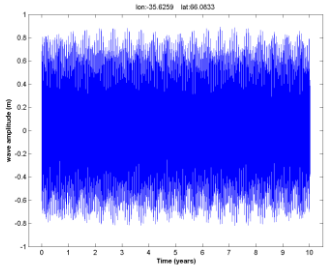	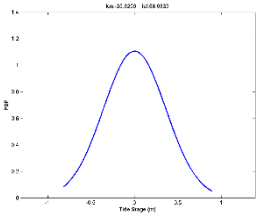	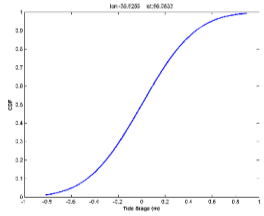	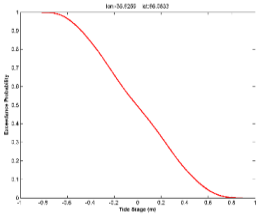
2	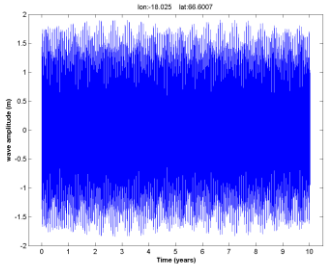	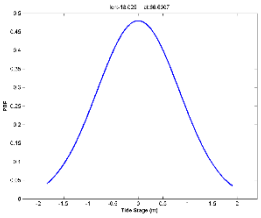	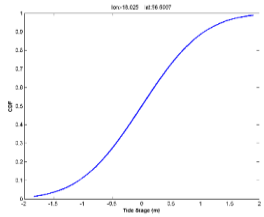	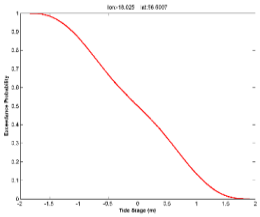
3	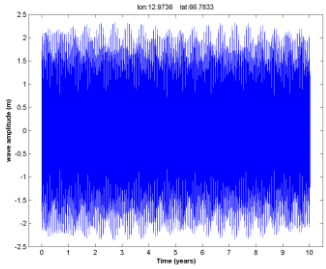	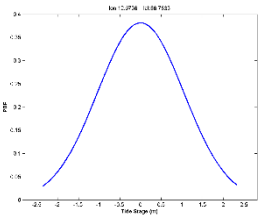	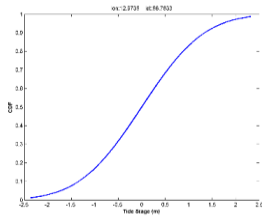	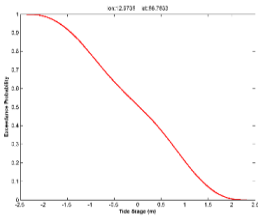
4	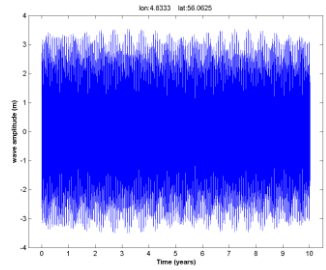	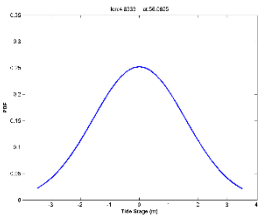	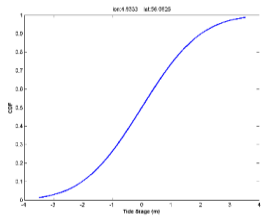	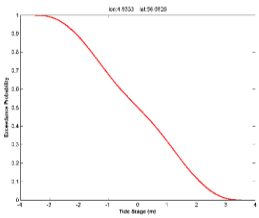
5	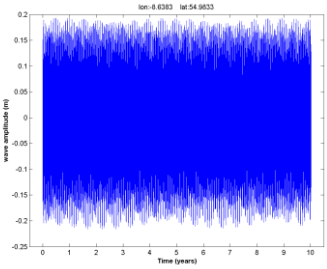	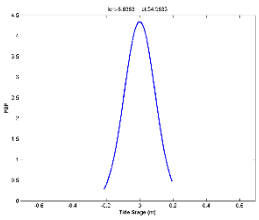	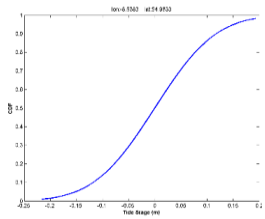	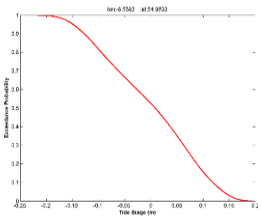
6	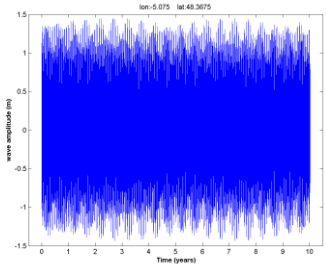	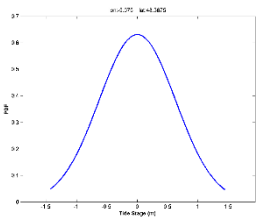	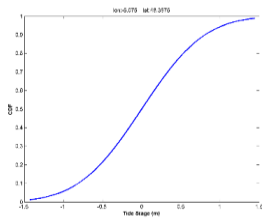	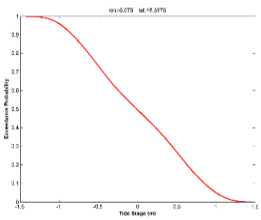

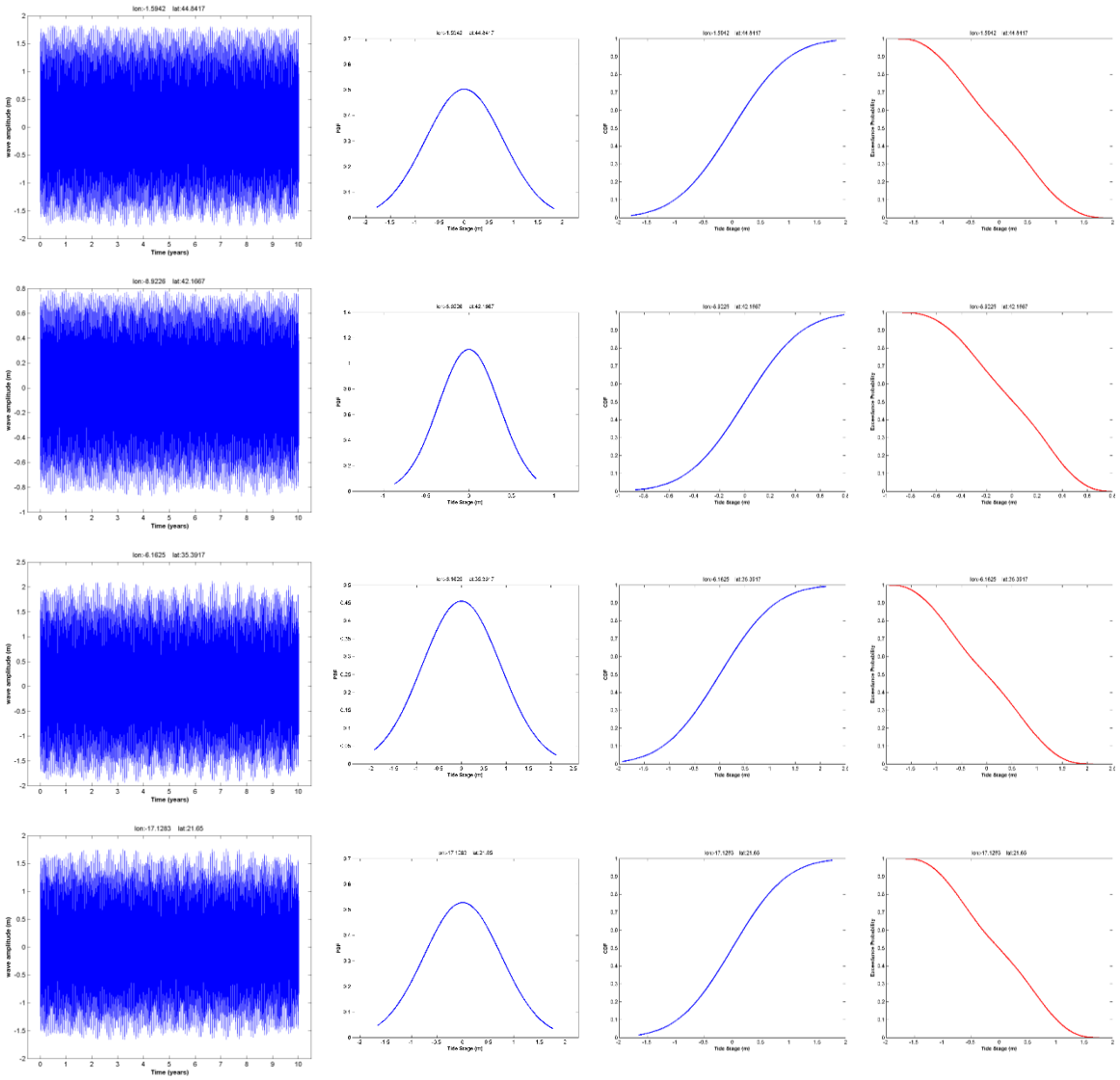

FIGURE 2.4.2 Results from the TMD model. At left the predicted tide for a period of 10 years, and the corresponding PDF, CDF, and the probability of exceedance.

2.5 STEPS and Levels, ensemble modelling and uncertainty quantification

The workflow for SPTHA adopted in TSUMAPS-NEAM is organized into the following 4 STEPS:

- STEP 1: PROBABILISTIC EARTHQUAKE MODEL
- STEP 2: TSUNAMI GENERATION & MODELING IN DEEP WATER
- STEP 3: SHOALING AND INUNDATION
- STEP 4: HAZARD AGGREGATION & UNCERTAINTY QUANTIFICATION

Each of these steps is further subdivided into several Levels (see Figure 2.5.1). These Levels constitute the finer grain of the analysis workflow within each STEP. Note that Level 0 at each STEP is a peculiar one as it contains the definition of the datasets onto which the analyses at all subsequent Levels rely.

Sanity checks are being performed at all STEPS; the results of the sanity checks will be reported at the next review round. All the STEPS and Levels are briefly described in what follows. A more detailed description and the alternative models implemented at each level, are instead documented in the Preliminary Implementation Plan (Doc_P1_S4_Prel_Impl_Plan), as a result of the elicitation described in Doc_P1_S2_ PoEkickoff and Doc_P1_S3_Elicitation.

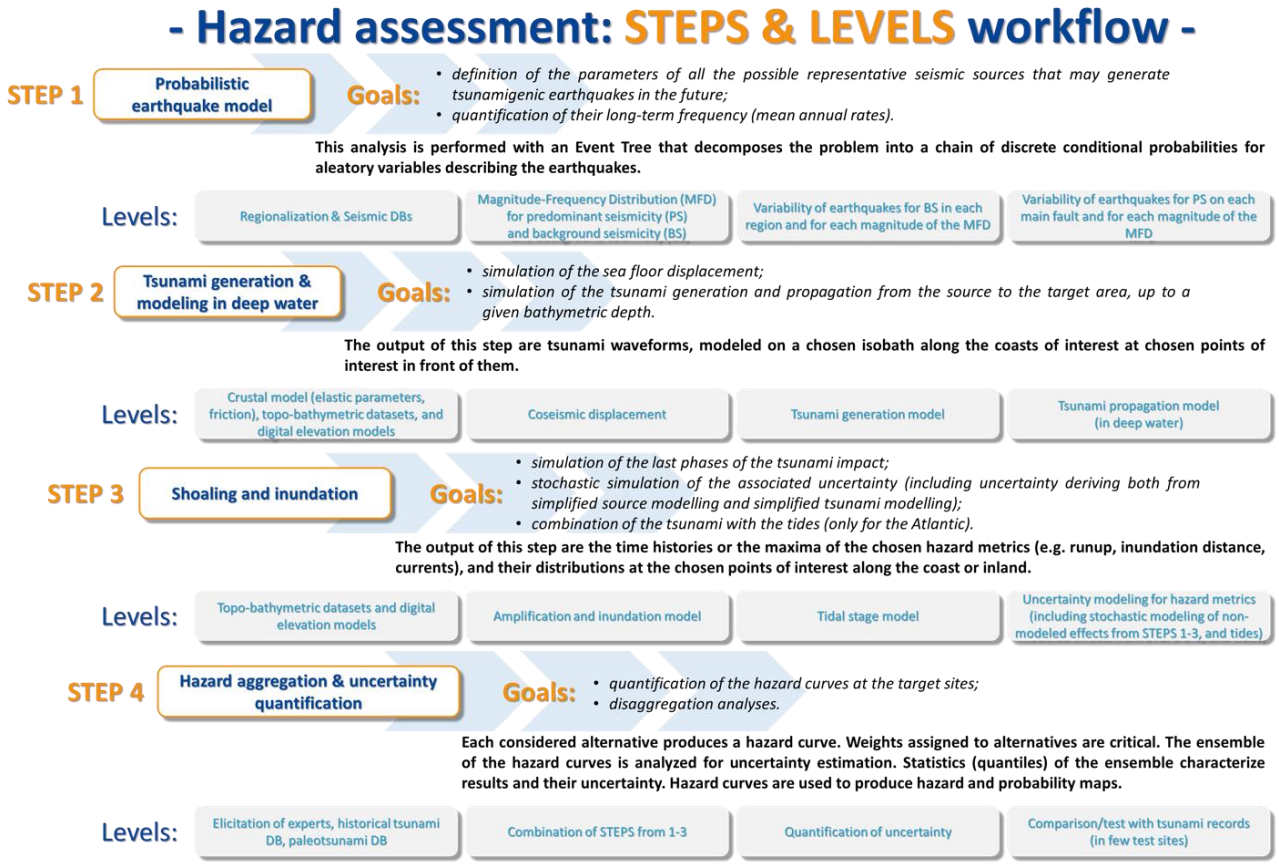

FIGURE 2.5.1 Sketch of the workflow.

2.5.1 STEP 1 - PROBABILISTIC EARTHQUAKE MODEL.

The goals of STEP 1 are:

1) the definition of the set of seismic sources which are considered representative of all the seismic sources that may generate tsunamigenic earthquakes in the future;
2) the quantification of their frequency (mean annual rates) ;
3) the definition of their parameterisation and of the probabilities associated to their parameters.

This analysis, i.e. the treatment of the aleatory (natural) variability of the seismic sources, is conducted through the definition of an Event Tree (ET). An ET is a branching graph representation of events in which individual branches are possible alternative steps from a general prior event, state, or condition, and which evolve into increasingly specific subsequent events. Examples of the use of an ET for SPTHA can be found in Lorito et al. (2015) and in Selva et al. (2016). This type of approach is an alternative to more classical approaches for the discretization of the total probability in SPTHA (e.g. Geist and Parsons, 2006).

STEP 1 defines the ET used in TSUMAPS-NEAM for the treatment of the seismic sources aleatory variability. All Levels in STEP 1 except for Level 0, which only defines the used datasets) coincide with the nodes of this ET. At each Level (i.e. at the ET nodes), discrete probabilities are evaluated for the parameters under investigation. The Levels are organized in a logical sequence, and probabilities at each Level are conditioned to the events at the previous Level.

STEP 1 (the TSUMAPS-NEAM ET, see Figure 2.5.2) is organized in the following Levels:

- Level 0: Regionalization, Definition of the Predominant Seismicity (PS) sources, Seismic DBs.
- Level 1: Magnitude-frequency distribution for each region, defined through the contribution to it of Predominant Seismicity (PS) and Background Seismicity (BS).
- Level 2a: Variability (position on hosting fault and finite fault dimensions, average slip and slip distribution) of earthquakes of the Predominant Seismicity in each region, given each magnitude. PS sources (from Level 0) are 3D, potentially curved.
- Level 2b: Variability (location, depth, faulting mechanism, finite fault dimensions, average slip) of earthquakes of the Background Seismicity in each region, given each magnitude. BS sources are assumed planar.

2.5.2 STEP 2 - TSUNAMI GENERATION & MODELING IN DEEP WATER.

The goals of STEP 2 are:

1) the numerical simulation of the sea floor displacement;
2) the numerical simulation of the tsunami generation and propagation from the source up to a given bathymetric depth offshore of the target area.

This is the STEP in which the numerical simulation of the tsunamis produced by the full set of earthquake scenarios defined by STEP 1 is performed. This analysis is then undertaken in TSUMAPS-NEAM in a completely deterministic fashion.

As described in the previous sections, some common simplifications are here adopted, which are a source of uncertainty in the final results. They are: Okada-like faults in homogeneous half space; Kaijura-type filtering of the sea floor displacement; tsunami propagation up to the POIs distributed

along the 50m isobaths and Green's functions approach (linear combinations) to limit the computational burden (see Section 2.3).

However, the Levels are separated in a way that makes simulation 'modular' allowing more complex approaches for each Level in future updates. Uncertainties introduced by these simplifications are addressed later at STEP 3.

STEP 2 is organized in the following levels:

- Level 0: Crustal model (e.g., elastic parameters); Topo-Bathymetric datasets and digital elevation models
- Level 1: Co-seismic displacement model
- Level 2: Tsunami generation model
- Level 3: Tsunami propagation (in deep water) model

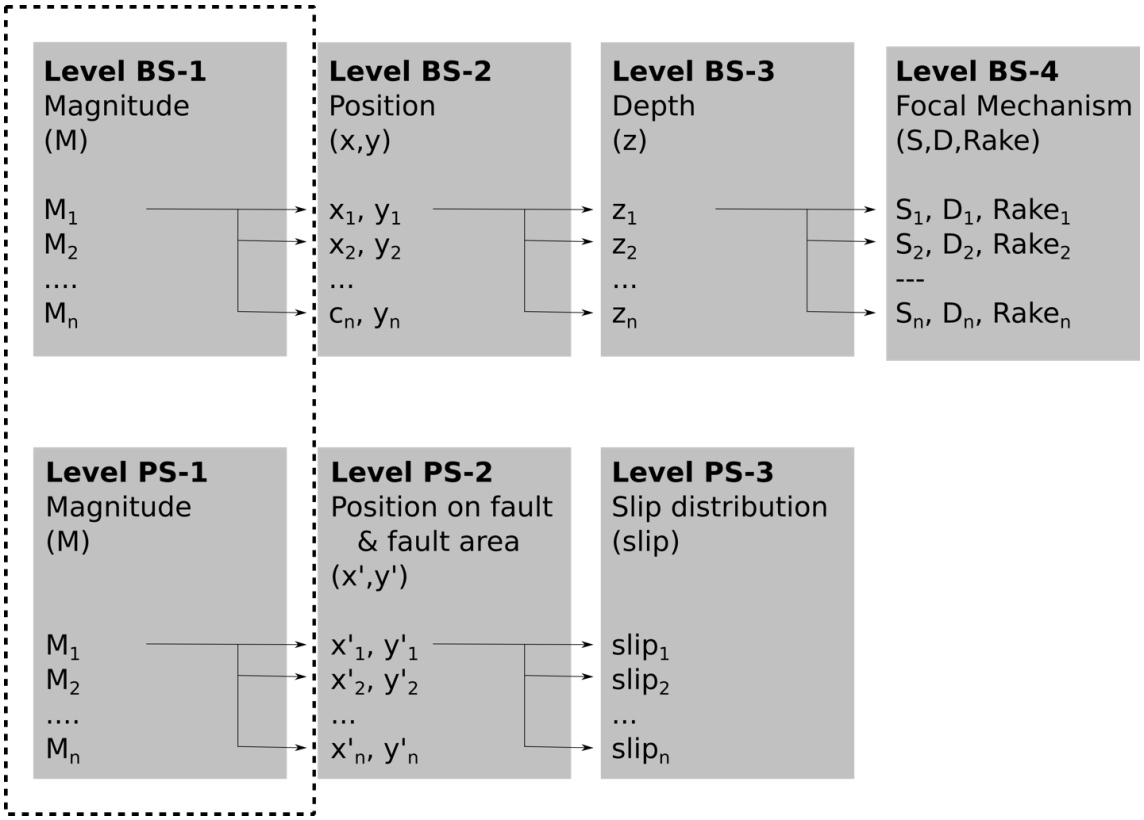

FIGURE 2.5.2 Schematic of the Event Tree.

2.5.3 STEP 3 - SHOALING AND INUNDATION.

The goals of STEP 3 are:

1) simulation of the coastal tsunami impact;
2) assessment of the associated uncertainties (including uncertainties originated from simplified source and tsunami models);
3) combination of tsunamis with tides.

This is the STEP in which the approximations described in Sections 2.2.2 and 2.3.1 are implemented. STEP 3 also involves the combination of tides and tsunamis at coastal locations with relevant tide amplitudes (Section 2.4).

STEP 3 is organized in the following levels:

- Level 0: Topo-bathymetric datasets and digital elevation models
- Level 1: Amplification and inundation model
- Level 2: Tidal stage model
- Level 3: Uncertainty modelling for tsunami hazard metrics (including uncertainties of unmodelled effects from STEPS 1-3, and tides)

Modularity of Levels leaves open possibilities for future improvements. For example, for more sophisticated inundation calculations in case enough computational resources and high-resolution topo-bathymetric models become available. Another extension can be re-use of the regional results for subsequent local studies with cluster analysis for important scenario selection (e.g. Lorito et al., 2015). The modular structure can also be useful for all kinds of sensitivity studies.

Uncertainty associated with the amplification factors method needs to be estimated here (see Section 2.3). Moreover, uncertainties introduced by various model approximations at STEP 2 (Sections 2.2 and 2.5.2) should be also modeled at this STEP. Hence, analysis at STEP 3 is partly deterministic and partly probabilistic.

The exact way to model the aforementioned uncertainties is still under discussion. A preliminary assessment has been made and the following points identified:

1. The uncertainty associated with the linear combinations (Section 2.2) should be propagated within the uncertainty framework established for the MIH due to the amplification factors method (Section 2.3); it is probably reasonable to assume that the two are not correlated;
2. At both levels, the uncertainties have been directly estimated by comparison to the much more accurate numerical simulations in which the specific approximations were removed (linear combinations and amplification factors);
3. Yet, the more accurate numerical simulation are done in the 2D NLSW approximation (i.e. the equations solved numerically are an approximation with respect to, for example, 3D free surface Navier-Stokes models, which in terms of computational cost are clearly out of reach for a region-wide approach and maybe even for a site-specific approach);
4. It is probably feasible to assess ‘global’ uncertainties, that is combining all together the results from comparison over a large number of simulations spanning the source parameter space (location, size, mechanism, etc. of the earthquakes) and different locations (different POIs and test sites for inundation) and to have enough simulations to obtain quite robust estimations;
5. It is instead more difficult to achieve enough numerical simulations to estimate ‘local’ uncertainties (i.e. for a given earthquake magnitude / wave periods / etc. at a given site). Hence, it is likely that we will get to an upper limit only for the epistemic uncertainty arising from tsunami modelling; we are considering the possibility and robustness of intermediate solutions (e.g. separating the scenarios basing on wave periods, etc.);

6. The uncertainty stemming from a simplified modelling of the earthquake source and the tsunami generation process have not yet been addressed; they could be addressed following Davies et al. (2017); note that in this case the source effect is not separated from the propagation and inundation effects and this is to be taken into account;
7. Although not feasible with the project resources, to assess the uncertainty introduced by simplified source modelling, further simulations and comparisons might be done by modelling the source / generation complexity with more sophisticated – and again more time consuming – techniques, by replacing Okada static initial conditions with 3D-FEM, time-dependent, 3D potential theory (e.g. Nosov and Kolesov, 2011), etc. approaches;
8. An approach for assessing PDFs for the bias and dispersion of lognormal PDFs is being drafted starting from the above elements and reasoning; qualitative 'safety' factors could be discussed for other effects not considered, such as the various discretizations used at all levels; then, these PDFs can be sampled, the results combined with the tides, and the exceedance probability assessed.

The outcome of this discussion will be reported in the second review stage.

2.5.4 STEP 4 - HAZARD AGGREGATION & UNCERTAINTY QUANTIFICATION

The goals of STEP 4 are:

1) quantification of hazard curves at target sites, that is of the exceedance probability of a chosen hazard metric within given time window including treatment of epistemic uncertainty;
2) comparison with observations and disaggregation analysis.

This STEP merges the results of STEP 1, namely the probability associated to each considered scenario, with the tsunami impact due to each scenario (STEP 2 + STEP 3) to calculate the hazard curves at chosen points of interest.

The workflow of STEPS 1-3 is repeated for each alternative model that is adopted at any Level within these STEPS. The whole process of alternative selection (trimming) and weighting through multi-step expert elicitation is considered at Level 0 of STEP 4.

A very important and critical point of STEP 4 is the way in which the different alternatives are weighted, and how these weights are computed. The weights will be produced as a result of a second elicitation of the PoE, not yet performed.

Within TSUMAPS-NEAM, the alternatives are aggregated through an ensemble modelling technique (see Selva et al., 2016, provided as an Appendix, for details). The ensemble of the hazard curves is produced from these curves and the above-mentioned weights, quantifying the inherent uncertainty. In this way, aleatory and epistemic uncertainty are simultaneously quantified and propagated in all the results. Different statistics (quantiles) of the ensemble are then used to describe the results and the uncertainty.

Further analysis of the results (disaggregation, comparison with local observations) is also performed at this STEP.

This analysis is mainly probabilistic, and it is organized in the following levels:

- Level 0: Elicitation of experts, historical tsunami DB, paleotsunami DB
- Level 1: Combination of STEPS from 1-3
- Level 2: Quantification of uncertainty
- Level 3: Comparison/test with tsunami records; disaggregation.

Note that the comparison with observations will be likely possible only for a few sites in the Mediterranean where frequency of past events and in some cases minimum inundation extent have been studied, as reported by tsunami catalogues and by compilations of paleotsunamis (e.g., Maramai et al., 2014; Papadopoulos et al., 2014).

2.5.5 Specifications for hazard curves, probability and hazard maps

The outputs of TSUMAPS-NEAM will be:

- Hazard Curves:(annual probability/rate vs MIH (Maximum Inundation Height)
- Hazard maps for different return periods
- Probability maps for different Intensity thresholds
- The above for different quantiles of the epistemic uncertainty

Preliminary choices have been made for thresholds, ranges, and other quantities concerning the hazard curves, and their vertical and horizontal 'cuts', that is, respectively: the probability corresponding to a given hazard intensity (the probability maps); and the hazard intensity corresponding to a fixed probability level or average return period (the hazard maps).

The first decision concerns the range (and thresholds) for the MIH. These will be calculated in the range [0.5 – 50] meters. The lowest threshold is generally considered as the limit between the marine and coastal risk, for example by the NEAMTWS. The upper limit is reasonably that for which higher earthquake-generated tsunamis have never been observed. If the calculations show that a larger value is needed, the upper limit will be changed.

The lowest annual probability level of interest is fixed at 10^{-5}, which seems to be a reasonable choice for non-critical, non-nuclear regulatory concerns. Moreover, under this threshold, the contribution of non-seismic sources becomes likely to be more and more important for some locations. This choice will be further discussed with the end-users and stakeholders.

Preliminary lists of intensity values and return periods to be used for probability and hazard maps have been chosen as follows:

- 0.5 – 1 – 5 – 10 – 20 m (more depending on the results)
- 100 – 1000 – 10000 years;

Quantiles for the epistemic uncertainty (again, preliminary), are:

- Median;
- Mean;
- 2^{nd}, 16^{th}, 84^{th}, 98^{th} percentile.

Until the end of the project, the dissemination of results through the Interactive Hazard Curve Tool will be limited to the European Commission, and to the interested reviewers only. The preliminary documentation of the tool is available upon request.

More in general, it has been discussed in several meetings that particular care should be taken in producing specific documentation and/or clear disclaimers to clarify what the results are and what they aren't; what are their possible uses or misuses; and to clearly communicate uncertainties. These, and other related issues also related to capacity building in the NEAM region, will be documented for the second review round.

References

Davies G, Griffin J, Løvholt F, Glymsdal S, Harbitz C, Thio HK, Lorito S, Basili R, Selva J, Geist E, Baptista MA (2017). A global probabilistic tsunami hazard assessment from earthquake sources. From: Scourse, E. M., Chapman, N. A., Tappin, D. R. & Wallis, S. R. (eds) Tsunamis: Geology, Hazards and Risks. Geological Society, London, Special Publications, 456, https://doi.org/10.1144/SP456.5.

de la Asunción, M., Castro, M. J., Fernández-Nieto, E. D., Man- tas, J. M., Ortega Acosta, S., and González Vida, J. M.: Efficient GPU implementation of a two waves TVD-WAF method for the two-dimensional one layer shallow water system on structured meshes, Comput. Fluids, 80, 441–452, 2013.

Egbert, G.D., and S.Y. Erofeeva, 2002: Efficient inverse modeling of barotropic ocean tides, J. Atmos. Oceanic Technol., 19(2), 183-204.

Geist, E. L. and Parsons, T. (2006). Probabilistic Analysis of Tsunami Hazards, Nat. Hazards, 37, 277–314.

Kajiura, K. (1963). The leading wave of a tsunami, Bull. Earthquake Res. Inst. Univ., Tokyo, 41, 535–571.

Kagan, Y.Y., Bird, P., Jackson, D.D., 2010. Earthquake Patterns in Diverse Tectonic Zones of the Globe. Pure and Applied Geophysics 167, 721-741, doi: 10.1007/s00024-010-0075-3.

Lorito, S.,Selva J., Basili R., Romano, F., Tiberti, M. M., and Piatanesi, A (2015). Probabilistic Hazard for Seismically-Induced Tsunamis: Accuracy and Feasibility of Inundation Maps, Geophys. J. Int., 200, 574–588.

Løvholt F, Glimsdal S, Harbitz CB, Nadim F, Zamora N, Peduzzi P, Dao HI, Smebye H (2012). Tsunami hazard and exposure on the global scale, Earth-Science Reviews, Volume 110, Issues 1–4, Pages 5873, ISSN 0012-8252, 10.1016/j.earscirev.2011.10.002.

Løvholt F, Griffin J, Salgado-Galvez M (2015). Tsunami Hazard and Risk Assessment on the Global Scale, R.A. Meyers (ed.), Encyclopedia of Complexity and Systems Science, Springer, DOI 10.1007/978-3-642-27737-5_642-1.

Maramai A., Brizuela B., Graziani L. (2014) The Euro-Mediterranean Tsunami Catalogue, Annals of Geophysics, 57, 4, S0435; doi:10.4401/ag-6437.

Miranda, J. M., Luis, J. F., Reis, C., Omira, R., and Baptista, M. A.: Validation of NSWING, a multi-core finite difference code for tsunami propagation and run-up, Paper Number S21A-4390, Session Number and Title S21A, Natural Hazards, American Geophysical Union (AGU) Fall Meeting, San Francisco, 2014.

Molinari I, Tonini R, Lorito S, Piatanesi A, Romano F, Melini D, Hoechner A, Gonzàlez Vida JM, Maciás J, Castro MJ, de la Asunción M (2016). Fast evaluation of tsunami scenarios: uncertainty assessment for a Mediterranean Sea database, Nat. Hazards Earth Syst. Sci., 16, 2593-2602, doi:10.5194/nhess16-2593-2016.

Nosov, M.A. & Kolesov, S.V. (2011). Optimal Initial Conditions for Simulation of Seismotectonic Tsunamis, Pure Appl. Geophys. 168: 1223. doi:10.1007/s00024-010-0226-6.

Papadopoulos G. A., E. Gràcia, R. Urgeles, V. Sallares, P.M. De Martini, D. Pantosti, M. González, A. C. Yalciner, J. Mascle, D. Sakellariou, A. Salamon, S. Tinti, V. Karastathis, A. Fokaefs, A. Camerlenghi, T. Novikova and A. Papageorgiou, 2014. Historical and pre-historical tsunamis in the Mediterranean and its connected seas: Geological signatures, generation mechanisms and coastal impacts. Marine Geology, 2014, DOI: 10.1016/ j.margeo.2014.04.014.

Selva J., Tonini R., Molinari I., Tiberti M.M., Romano F., Grezio A., Melini D., Piatanesi A., Basili R., Lorito S. (2016). Quantification of source uncertainties in Seismic Probabilistic Tsunami Hazard Analysis (SPTHA). Geophys. J. Int., 205, 1780-1803, doi:10.1093/gji/ggw107.

Wang, X.; Power, W.L. 2011. COMCOT: A Tsunami Generation Propagation and Run-up Model. *GNS Science Report 2011/43*.

Probabilistic TSUnami Hazard MAPS
for the NEAM Region (TSUMAPS-NEAM)
ECHO/SUB/2015/718568/PREV26

PHASE I – STAGE 2: Pool of Expert Kick-off

Author: TSUMAPS-NEAM Technical Integrator (TI) team

Date: 2 June 2017

Version: 1.0

Table of Contents

This page is intentionally left blank.

Executive Summary

In this document we report the initialization of the activity of the Pool of Experts (PoE) in the TSUMAPS-NEAM project.

In ***Section 1***, we shortly describe the PoE and its goal within the project, summarizing the information reported in the document ***Doc_P1_S1_Project_Summary***.

In ***Section 2***, we describe the PoE kick-off meeting, held in Athens on 30 June 2016. The goal of this meeting was to introduce the project to the members of the PoE, and to initialize the experts' weights to be adopted in all the elicitations of the project.

In ***Section 3***, we discuss the evaluation of the experts' weights, as computed from their answers to a seed questionnaire. We evaluated group's answers by adopting the different experts' weights. This analysis has been presented in its preliminary version at the end of the Athens meeting, and it is reported in more details in Section 3.3.

To complete the information of the present document, we attach the following Appendixes:

- ***Appendix A***: Minutes of the Athens meeting;
- ***Appendix B***: Presentations of the PoE kick-off meeting;
- ***Appendix C***: Questionnaire used for the elicitation experiment.

This page is intentionally left blank.

1. Pool of Experts in the TSUMAPS-NEAM project

Fifteen experts were invited to join the Pool of Experts (PoE) of the TSUMAPS-NEAM project. Following the EU project STREST protocol (Selva et al., *in prep*), the PoE assists the Technical Integrator (TI) in taking the critical decisions required for implementing the Seismic Probabilistic Tsunami Hazard Analysis (S-PTHA) for the NEAM region.

The members of the PoE have been selected from inside and outside the project, based on their competences and known field of expertise. The experts from within the project which are members of the PoE are not participating in any activity related to the coordination of the multiple-expert process, that is, they are not part of the Technical Integrator (TI) and Project Manager (PM) teams. The fifteen experts of the PoE are listed in **Table 1**.

Table 1: List of experts of the PoE along with their affiliations.

Expert	Affiliation
F. Romano	INGV
R. Omira	IPMA
F. Lovholt	NGI
A. Babeyko	GFZ
A. Yalciner	METU
G. Papadopoulos	NOA
M. Canals	UB
A. Bouallegue	INM
A. Armigliato	UNIBO
M. Sorensen	UIB
C. Ozer	KOERI
G. Davies	GA
W. Power	GNS
J. Polet	CALTECH
C. Meletti	INGV

The members of the PoE participate in the expert elicitation procedure that the Technical Integrator (TI) organizes during the TSUMAPS-NEAM project. Two elicitations are scheduled, the first one did already take place:

- **Elicitation 1 (conducted during Phase 1, pre-assessment)** Prioritization of the levels at which the analysis of epistemic uncertainty has to be deepened during the pre-assessment phase.
- **Elicitation 2 (conducted during Phase 2, assessment):** Quantification of the weights to be assigned to alternative models for the ensemble model of the SPTHA uncertainty during the assessment phase.

Further elicitation experiments may be organized if required by the TI and the PM teams. More details can be found in ***Doc_P1_S1_Project_Summary.***

2. PoE Kick-off Meeting

The general scheme of the hazard assessment in the TSUMAPS-NEAM project was presented and discussed during the first day of the technical meeting held in Athens (Greece) from 29 June to 1 July, 2016. The members of the PoE were invited to participate to the whole meeting, during which they had the opportunity to start familiarizing with the TSUMAPS-NEAM project approach, goals, and partners.

A half-day PoE kick-off session was then organized in the morning of the second day of the meeting. In this kick-off session, the TI presented the role of the PoE and the whole process of interaction with the TI and the PM teams. This enabled an effective discussion to clarify the scope of the tasks of experts in the elicitation and their specific role.

After the discussion, the fifteen members of the PoE were invited to answer a seed questionnaire in order to assign weights to the experts themselves. In particular, the questionnaire consisted of two parts. In the first part each expert was asked to answer a set of seed questions prepared by the TI. In the second part each expert was asked to acknowledge two other experts of her/his own choice within the PoE. These activities are propaedeutic to the application of two different weighting schemes which are discussed in **Section 3**.

The minutes of the Athens meeting are reported in ***Appendix A***. The PoE participated in the whole meeting (Appendix A, Sections 1.3 and 1.4), but the PoE kick-off took place on 30 June: Morning session (Appendix A, section 2.3). In this session, we specifically discussed i) the overall multiple-expert process followed within the TSUMAPS-NEAM project, the different actors foreseen, and the specific role of the PoE; ii) the elicitation process and the potential techniques to be applied; iii) the goals of the weighting experts and the weighting schemes to be adopted; iv) the seed questionnaire and its use to quantify experts' weights. Three presentations were given, each followed by questions and discussion. These presentations are reported in ***Appendix B***. Note that these presentations were prepared on the basis of an earlier version of the EU project STREST protocol (Selva et al. 2015), whereas the protocol shortly discussed in ***Doc_P1_S1_Project_Summary*** is based on a review of that experimental process in light of the TSUMAPS-NEAM application (Selva et al., *in prep*). After this preliminary part, the experts answered to the seed questionnaire reported in ***Appendix C***.

To complete the explanations regarding the use of experts' weights and their importance to the PoE, the preliminary version of the results reported in **Section 3** were presented at the end of the Athens meeting (see **Section 2.5.3**. Additional presentations of ***Appendix A***).

3. Experts' weights

The aggregation of experts' judgements is often supported by the use of different weighting schemes for the experts themselves. Many different schemes were proposed and adopted in previous analyses, such as equal weighting, self-weighting, peer weighting, performance weighting, acknowledgement weighting, and many others (e.g., Selva et al. 2012; Aspinall and Cooke, 2013). The rationale for adopting experts' weights in the aggregation phase is to favor rational consensus, based on reproducibility, accountability, empirical control, neutrality, and fairness (Cooke 1991; Cooke & Goossens 2000).

In TSUMAPS-NEAM, the idea is to compare the impact on the elicitation results of three alternative schemes that depend on the expertise and acknowledgement of the experts within the tsunami science community. These comparisons also allow for evaluating the impact of the selection of the PoE members, and thus enable a more aware decision making.

3.1. Alternative weighting schemes

Three alternative weighting schemes are taken into account in the elicitation process and their respective results are compared one to another, in order to check their consistency, and all together will provide the input for final decision-making.

In order to assign weights to the PoE members, we consider the following alternative schemes:

- Equal Weighting (EW) scheme,
- Acknowledge-based Weighting (AW) scheme,
- Performance-based Weighting (PW) scheme.

Equal weighting scheme: this weighting scheme is straightforward. Every expert gets the same weight which is obtained by W=1/N, where N is the number of involved experts. In our case, fifteen experts were involved in the PoE, so each expert was assigned a weight of 1/15.

Acknowledgement-based weighting scheme: a weight is assigned to each expert on the basis of mutual recognition among the experts themselves, expressed through a blind procedure (Selva et al. 2012). To quantify such weights, each expert is asked to vote for other members of the PoE.

During the PoE kick-off meeting, the following activity was performed. The list with the names of the 15 experts was distributed. The experts were requested to assign a weight of 1 (one) to themselves and a weight of 1 and 3 to other two colleagues. The weight of 1 and 3 indicates the different levels of confidence that one expert put on his/her colleagues. The weight of each expert is then evaluated by 1) summing the weights that each expert received, and 2) renormalizing to 1 the sum of the weights of all experts.

The resulting weights are presented in anonymized form in **Figure 1**. Note that to preserve the anonymity of experts, **Table 1** and **Figure 1** are intentionally sorted in different ways. The graph in **Figure 1** shows that the experts E6, E8, and E13 received higher acknowledgment from their colleagues, thus obtaining the highest weights. The experts E1, E3, and E4 received the lowest weight.

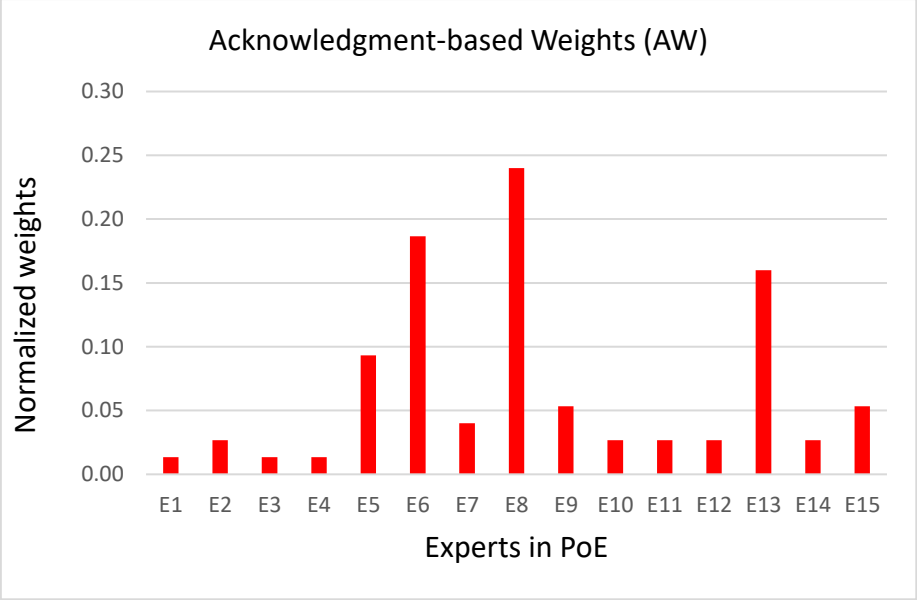

Figure 1: The weights assigned to experts according to the Acknowledgement-based Weighting (AW) scheme. Note that the experts' numbers are assigned by randomly shuffling the list in **Table 1**.

Performance-based weighting scheme: This scheme is based on a classical method developed by Cooke (1991), in which the weights on experts' opinion are assigned through experts' relative performance in answering a set of seed questions.

During the PoE kick-off meeting, a questionnaire related to tsunami hazard was given to the experts and they were asked to express their best guess (numerical value) and related confidence intervals (5^{th}, 50^{th}, and 95^{th} percentiles) to each question. Their assessments were used to obtain weights using Excalibur, a software package for structured expert judgement elicitation using Cooke's (1991) model.

The questionnaire was prepared observing a balance between questions belonging to various aspects:

- 2 main categories: Earthquake (E) and Tsunami (T) science;
- 3 sub-categories: Phenomenology (Phe, observations from past events), Probability (Prb, hazard analysis), Modelling (Mod, physical or numerical);
- 2 typologies for Phe and Prb: Local (L, target area) or Global (G, any area in the world).

The questionnaire comprised 14 questions, in order to have enough (> 5) seed questions in each category, as reported in **Table 2**.

Table 2: Balance of expertise in preparing the seed questions.

Q	DESCRIPTION	E	T	Phe	Prb	Mod
1	Displacement of one historical earthquake in the Atlantic	x		L		
2	Length of fault of Chile 1960 earthquakes	x		G		
3	M > 6.0 earthquakes in Europe (from ANSS)	x			L	
4	Change in Mc of tapered Pareto, worldwide	x			G	

5	Vertical displacement, Java earthquake	x				x
6	Tsunami wave-height, Greece		x	L		
7	Tsunami inundation height, Japan		x	G		
8	Messina Strait Area, percentage of seismic tsunamis in the last 500 yr		x		L	
9	NOAA/WDS worldwide, n of tsunamis > 10 m in 1970-2005		x		G	
10	Run-up along inundation with MOST		x			x
11	Amplification Synolakis		x			x
12	Mmax close to Gibraltar	x	x		L	
13	Return period Cascadia	x	x		G	
14	ARP for 2% in 50 yr	x	x		G	

The resulting normalized weights are presented in anonymized form in **Figure 2**. Note that the expert ordering in **Figure 1** and **Figure 2** is the same, but it does not correspond to the ordering in **Table 1**. Most of the weight on experts' opinions is assigned to four experts (E1, E4, E9, and E13). Among those, E9 received the highest weight. This shows that the relative performance of four experts in answering the questions was significantly better than that of all other members of the PoE.

Note that the weights assigned to the experts using the PW scheme are here estimated based on all fourteen questions, but they can also be estimated category-wise and sub-category-wise. This was used to check the stability of the results.

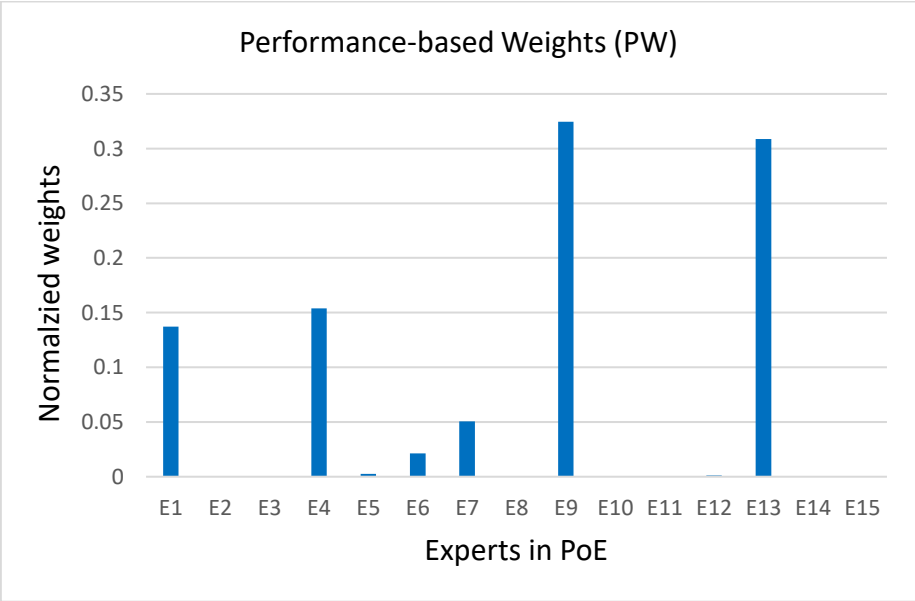

Figure 2: The weights assigned to experts according to the Performance-based Weighting (PW) scheme. Note that the experts' numbers are assigned by randomly shuffling the list in **Table 1** (but same ordering as in Figure 1).

3.2 Comparison of expert weights under alternative weighting schemes

Experts were assigned different weights based on alternative weighting schemes. The comparison for each expert is shown in **Figure 3**.

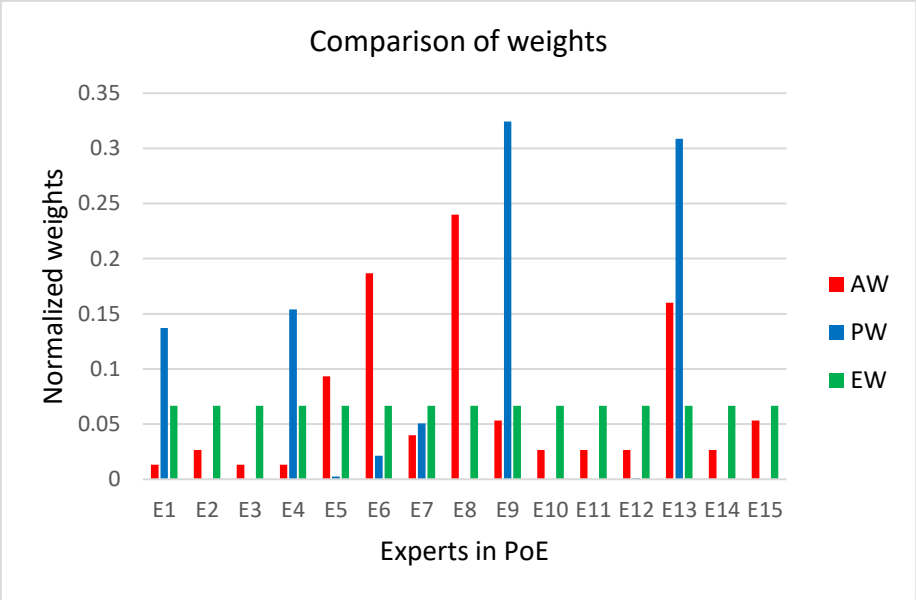

Figure 3: Comparison of weights assigned to experts based on alternative weighting schemes.

The comparison shows that the variability under the different schemes is rather large. The resulting weights are indeed often inconsistent, with some extreme case where highly acknowledged experts have very small performance weights (e.g., expert E8) and vice versa (e.g., expert E4). One exception is expert E13 who performed very well (second best) in answering the questions and was also significantly acknowledged by other colleagues.

3.3. Performance of the PoE on seed questions

Here we present how weights would have performed, if applied in aggregating the answers of experts on the 14 seed questions used for the PW scheme. We note that, since the PW are obtained by maximizing the performance on exactly these 14 questions, the results are automatically biased in favor of this weighting scheme. Conversely, EW and AW are computed independently from these 14 questions. For this reason, the effective performance of the three weighting schemes cannot be judged by these results only.

To each of the 14 seed questions, the experts provided their assessment in terms of best guesses and associated confidence intervals. What would be the best estimate and uncertainty ranges for each question that takes into account weighted assessments from all experts? This solution is presented in **Tables 3**, **4,** and **5,** based on each weighting scheme along with the real value of the answer. In these tables, the columns with headers 5%, 50%, and 95% represent, as a suggested solution, the minimum, the best, and the maximum value, respectively. The column named "realization" provides all the real values, i.e. the expected correct answer. The same results are

reported in **Figure 4** normalized to 1 by dividing each value (5th, 50th and 95th percentiles of the group result) by the realization (correct answer) to the same question. The results show a good agreement between best guess and true answers, with uncertainty bounds very variable but in general within the 10% relative variation bounds. This demonstrate that the group collectively perform well over the seed questions.

Table 3: Results for Equal Weighting (EW) scheme.

Solution for : EW

Resulting solution (combined DM distribution of values assessed by experts)
Bayesian Updates: no Weights: equal DM Optimisation: no
Significance Level: 0.0000 Calibration Power: 1.0000

Nr.	Id	Scale	5%	50%	95%	Realization	Full Name
1	Q1	UNI	0.7519	9.928	34.01	11	Displacement of one historical earthquake in the Atlantic (Earthquake)
2	Q2	UNI	295.4	797.4	2353	920	Length of fault of Chile 1960 earthquakes (Earthquake)
3	Q3	UNI	8.64	69.55	295	75	M > 6.0 earthquakes in Europe (from ANSS) (Earthquake)
4	Q4	UNI	7.32	8.418	19.5	8.76	Change in Mc of tapered Pareto, worldwide (Earthquake)
5	Q5	UNI	0.05969	0.2662	0.7032	0.43	Vertical displacement, Java earthquake (Earthquake)
6	Q6	UNI	2.95	10.87	31.97	20	Tsunami wave-height, Greece (Tsunami)
7	Q7	UNI	4.117	16.14	45.4	19.5	Tsunami inundation height, Japan (Tsunami)
8	Q8	UNI	2.755	12.28	18.91	13	Messina Strait Area, percentage of seismic tsunamis in the last 500 yr (tsunami)
9	Q9	UNI	1.418	9.162	60.82	15	NOAA/WDS worldwide, n of tsunamis > 10 m in 1970-2005 (Tsunami)
10	Q10	UNI	1.055	2.689	14.4	3.01	Run-up along inundation with MOST (Tsunami)
11	Q11	UNI	0.2968	3.015	59.83	4	Amplification Synolakis (Tsunami)
12	Q12	UNI	5.083	5.968	8.223	6.4	Mmax close to Gibiltar (Earthquake)
13	Q13	UNI	218.9	672.3	1.331E004	512	Return period Cascadia (Earthquake)
14	Q14	UNI	28.12	2438	2708	2475	ARP for 2% in 50 yr (Earthquake)

Table 4: Results for Acknowledgement-based Weighting (AW) scheme.

Solution for : DMaker 1

Resulting solution (combined DM distribution of values assessed by experts)
Bayesian Updates: no Weights: user DM Optimisation: no
Significance Level: 0.0000 Calibration Power: 1.0000

Nr.	Id	Scale	5%	50%	95%	Realization	Full Name
1	Q1	UNI	0.6548	8.66	29.55	11	Displacement of one historical earthquake in the Atlantic (Earthquake)
2	Q2	UNI	303	754.2	1954	920	Length of fault of Chile 1960 earthquakes (Earthquake)
3	Q3	UNI	18.31	75.61	240.3	75	M > 6.0 earthquakes in Europe (from ANSS) (Earthquake)
4	Q4	UNI	7.486	8.418	17.89	8.76	Change in Mc of tapered Pareto, worldwide (Earthquake)
5	Q5	UNI	0.03961	0.2257	0.6551	0.43	Vertical displacement, Java earthquake (Earthquake)
6	Q6	UNI	2.43	9.735	28.84	20	Tsunami wave-height, Greece (Tsunami)
7	Q7	UNI	2.65	14.73	46.17	19.5	Tsunami inundation height, Japan (Tsunami)
8	Q8	UNI	3.973	13.56	18.94	13	Messina Strait Area, percentage of seismic tsunamis in the last 500 yr (tsunami)
9	Q9	UNI	2.318	11.75	49.39	15	NOAA/WDS worldwide, n of tsunamis > 10 m in 1970-2005 (Tsunami)
10	Q10	UNI	1.166	2.639	11.02	3.01	Run-up along inundation with MOST (Tsunami)
11	Q11	UNI	0.2702	3.198	41.1	4	Amplification Synolakis (Tsunami)
12	Q12	UNI	5.059	5.797	7.626	6.4	Mmax close to Gibiltar (Earthquake)
13	Q13	UNI	222.7	660	3899	512	Return period Cascadia (Earthquake)
14	Q14	UNI	36.96	2468	2687	2475	ARP for 2% in 50 yr (Earthquake)

Table 5: Results for Performance-based Weighting (PW) scheme.

Solution for : PW

Resulting solution (combined DM distribution of values assessed by experts)
Bayesian Updates: no Weights: global DM Optimisation: no
Significance Level: 0.0000 Calibration Power: 1.0000

Nr.	Id	Scale	5%	50%	95%	Realization	Full Name
1	Q1	UNI	1.224	11.96	35.35	11	Displacement of one historical earthquake in the Atlantic (Earthquake)
2	Q2	UNI	221.4	827	3003	920	Length of fault of Chile 1960 earthquakes (Earthquake)
3	Q3	UNI	22.69	72.49	170.9	75	M > 6.0 earthquakes in Europe (from ANSS) (Earthquake)
4	Q4	UNI	5.912	9.094	27.31	8.76	Change in Mc of tapered Pareto, worldwide (Earthquake)
5	Q5	UNI	0.02973	0.2515	0.7012	0.43	Vertical displacement, Java earthquake (Earthquake)
6	Q6	UNI	3.025	19.65	35.81	20	Tsunami wave-height, Greece (Tsunami)
7	Q7	UNI	5.521	20.43	40.82	19.5	Tsunami inundation height, Japan (Tsunami)
8	Q8	UNI	7.989	15.28	19.23	13	Messina Strait Area, percentage of seismic tsunamis in the last 500 yr (tsunami)
9	Q9	UNI	2.093	11.42	36.35	15	NOAA/WDS worldwide, n of tsunamis > 10 m in 1970-2005 (Tsunami)
10	Q10	UNI	0.5977	2.748	12.71	3.01	Run-up along inundation with MOST (Tsunami)
11	Q11	UNI	1.414	3.814	14.65	4	Amplification Synolakis (Tsunami)
12	Q12	UNI	5.083	5.985	8.237	6.4	Mmax close to Gibiltar (Earthquake)
13	Q13	UNI	203	687	1.993E004	512	Return period Cascadia (Earthquake)
14	Q14	UNI	26.13	2445	2578	2475	ARP for 2% in 50 yr (Earthquake)

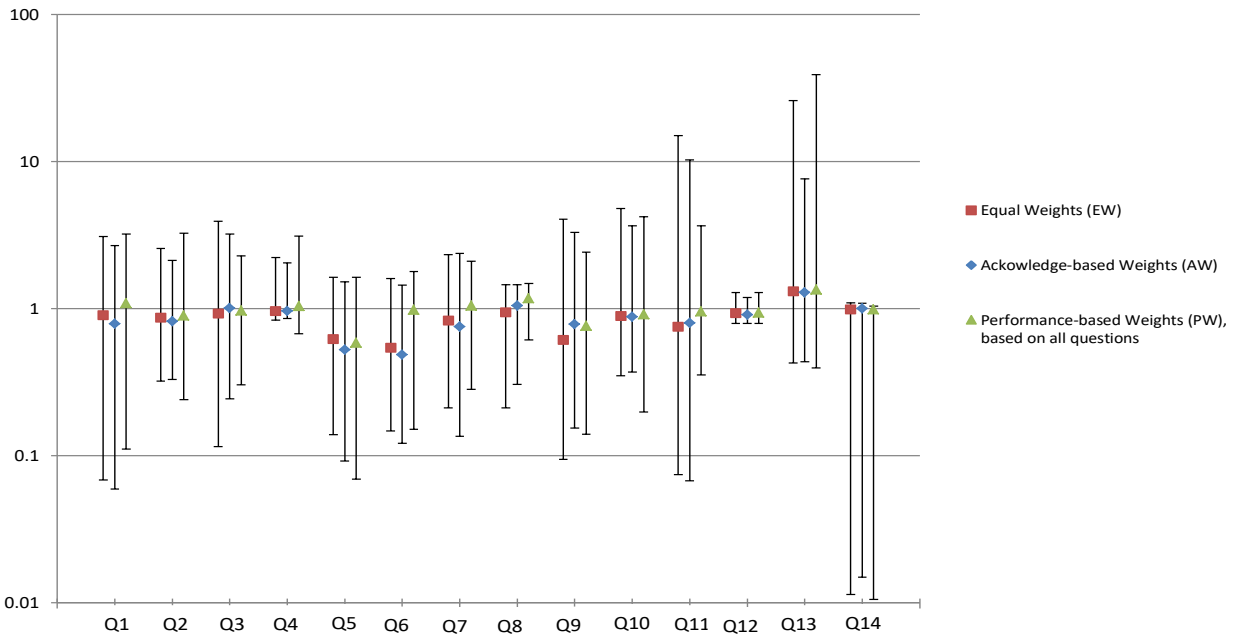

Figure 4: Comparison of normalized solutions for the three weighting schemes. The position of the symbols represent the median, and the bars the interval between the 5th and 95th percentiles.

References

Aspinall, W.P., Cooke, R.M., 2013. Quantifying scientific uncertainty from expert judgement elicitation, in “Risk and Uncertainty Assessment for Natural Hazards” (Eds J. Rougier, L. Hill, R.S.J. Sparks), Cambridge University Press, Cambridge, UK, ISBN 978-1-107-00619-5.

Cooke, R. M. (1991). Experts in Uncertainty: Opinion and Subjective Probability in Science,” Oxford University Press, Oxford.

Cooke, R.M. and Goossens, L.H.J. (2000), “A Procedures Guide for Structured Expert Judgment,” EUR 18820, European Commission Report.

Selva, J., Marzocchi, W., Papale, P., & Sandri, L. (2012). Operational eruption forecasting at high-risk volcanoes: the case of Campi Flegrei, Naples. Journal of Applied Volcanology, 1(1), 1.

Selva, J. et al. (2015). Report on the effects of epistemic uncertainties on the definition of LP-HC events. Deliverable 3.1 STREST Project.

Selva J., S. Iqbal, F. Cotton, D. Giardini, S. Esposito, B. Stojadinovic, S. Argyroudis, K. Pitilakis, A. Mignan, and S. Lorito (in prep). Management of subjectivity in probabilistic single/multi-hazard/risk assessments: a Multiple-Expert Management Protocol (MEM-Pr).

Probabilistic TSUnami Hazard MAPS
for the NEAM Region (TSUMAPS-NEAM)
ECHO/SUB/2015/718568/PREV26

PHASE I – STAGE 3: Elicitation Experiment

Author: TSUMAPS-NEAM Technical Integrator (TI) team

Date: 2 June 2017

Version: 1.0

Table of Contents

This page is intentionally left blank.

Executive Summary

In this document, we report the first elicitation experiment of the Pool of Experts (PoE), in which the experts are asked to trim the alternative implementations for the epistemic uncertainty quantification. Many potential alternative implementations were initially proposed at all the STEPs and levels of the analysis (as discussed in ***Doc_P1_S4_Prel_Impl_Plan***, sections 1 and 2). In order to reduce the total number of alternatives to be actually implemented without decreasing the quality of the model, a PoE elicitation is performed to specifically prioritize the STEPs/levels in terms of their potential impact on the total epistemic uncertainty. The quantitative results of the elicitations will support the decisions on which STEPs and levels the Technical Integrator (TI) team should focus the development of alternative implementations.

In ***Section 1***, we introduce the rationale and the selected method for the elicitation.

In ***Section 2***, we discuss the elicitation results.

To complete the information of the present document, we attach the following Appendixes:

- ***Appendix A***: Minutes of the Athens meeting;
- ***Appendix B***: Questionnaire used for the elicitation experiment.

This page is intentionally left blank.

1. Elicitation

1.1 Elicitation preparation

Once the overall framework for the Seismic Probabilistic Tsunami Hazard Analysis (SPTHA) is defined, many alternative implementations of the framework are possible. Alternative formulations are possible depending on alternative parameterizations of a given model, as well as alternative models and assumptions (e.g., Bommer and Scherbaum, 2008; Rougier et al., 2013). If one does not have (enough) data to falsify alternative models, they should be all considered as being *scientifically acceptable*. The quantification of the epistemic uncertainty mainly relies on quantifying the potential variability of the results that depends on the use of scientifically acceptable alternative models in the form of the community distribution (e.g., SSHAC 1997; Bommer 2012; Marzocchi et al. 2015).

In order to constrain the community distribution, it is not necessarily required to implement a huge number of alternative models. Instead, it is required to define and implement a sufficient number of alternative models (and weights) that allow for capturing simultaneously the best estimates that the evaluators can develop and the range of alternatives that should be implemented in view of the limitations of the data and the currently available knowledge (Bommer 2012). The selection of these models should theoretically depend on an extensive sensitivity analysis of the results based on the alternative implementations (Bommer and Scherbaum 2008). However, this is not possible in many cases, due for example to limitations in budget and time (Musson 2012). In case of the TSUMAPS-NEAM project, we notice the additional difficulty of dealing with a relatively young science such as the SPTHA.

In order to define a list of alternative models to be effectively implemented in this project, we first established a reference framework for the SPTHA, in which we identified a finite list of steps and levels to be followed to reach the final results. The framework proposed in Selva et al. (2016) was presented as reference model in the project kick-off meeting. Then, we widely reviewed the framework first through online discussions (Google Group of Task B), and then during the Athens meeting (see ***Appendix A***, in dedicated sessions in Day 1 - afternoon and Day 2 - afternoon). After this meeting, the general framework was finalized (an extensive description of this framework is available in ***Doc_P1_S4_Prel_Impl_Plan***).

Once the SPTHA steps and levels had been established, we could define an elicitation experiment to prioritize them. A STEP/Level is considered more important than another STEP/Level if the epistemic uncertainty associated to that specific STEP/Level is expected to be larger than that for the other STEP/Level or because its influence on the results is larger than the one of the other STEP/Level). Hence, more alternative models should be developed to carefully explore and quantify this epistemic uncertainty for the STEP/Level that is judged to be more important. Such alternative models will either be implemented, if this is feasible within the resources allocated to the project, or the need for their implementation in a future assessment will be clearly reported.

1.2 Elicitation method

There are several structured elicitation processes that are described in pertinent literature with prioritization purpose. We use one procedure that is named Analytic Hierarchy Process (AHP). AHP was originally developed by Saaty (1980); it is a multi-criteria decision-making method that is useful

for making decisions when facing complex problems. The hierarchy process breaks down the complex decisions into a series of pairwise comparisons, synthesizes the results, and then helps to take into account both subjective and objective aspects of the decision. Additionally, the process incorporates a useful technique for checking the consistency of the expert judgments, thus reducing the bias in the process of decision making.

The process works by decomposing the decision-making problem into a hierarchy of evaluation criteria and alternative options among which the best decision is to be made. The best decision refers to the goal of the analysis. In general, the structure of the method consists of an overall goal, a group of options or alternatives for reaching the goal, and a group of factors or criteria that relate the alternatives to the goal.

In the first round of the elicitation, we have a simplified scheme with only one criterion. Specifically, we calculate a score for each alternative through the experts' pairwise comparisons of the models with respect to the criterion under consideration. The relative importance of one model over the others is usually expressed with numeric rating from one (equally important) to nine (extremely important) (Saaty 1980) and can be collected into a matrix; the scores are the components of the normalized principal eigenvector of this matrix (Saaty and Hu 1998). Here, we adopted the numeric translation reported in **Table 1 – Column 4 ("Weights of models")**, which was presented to the experts and reported in the introduction of the questionnaire. However, the results are tested for robustness against the classical linear rating 1 to 9 of Saaty (1980), as reported in **Table 1 – Column 5 ("Standard AHP weights")**. The test showed that the variability introduced by these different scales is negligible, as compared to the inter-expert uncertainty, in terms of both final results and consistency of the experts' answers.

Some inconsistencies may arise when many pairwise comparisons are performed (Harker and Vargas 1987), which is typically measured by the Consistency Ratio (CR) (Saaty 1980). A perfectly consistent judgement by experts should always be zero, i.e. CR = 0, but, inconsistencies are tolerated if CR < 0.1 (Saaty 1980). However, it has been suggested to relax this cutoff value up to 0.3 depending on the number of criteria and the kind of project (Goepel 2013).

One important issue in AHP is aggregation of judgements when many experts are involved. Different approaches can be employed to aggregate their individual or group opinions (Forman and Peniwati, 1998), depending on the level of the aggregation and mathematical method used for the aggregation. As for the level of aggregation, the most popular methods consist of either aggregating individual judgments regarding each set of pairwise comparisons to produce an aggregate hierarchy (aggregation of individual judgments - AIJ) or synthesizing each of the individual hierarchies and aggregating the resulting priorities (aggregation of individual priorities – AIP). As for the mathematics of the aggregation, both weighted geometric and arithmetic means are commonly used as aggregation method, considering equal or subjective weights on experts (Goepel, 2013; Forman and Peniwati, 1998; Zio, 1996). Here, we select the aggregation of individual judgments (AIJ), in order to analyze and visualize both individual and group prioritizations. We consider as equal three weighting schemes for the experts (equal (EW), performance-based (PW) and acknowledgement-based weights (AW); see ***Doc_P1_S2_PoEkickoff***). To analyze the results, we take the ensemble distribution of individual priorities of all experts as the main result and, to estimate the group central tendency, we consider both (weighted) arithmetic and geometric means.

1.3 Questionnaire

The questionnaire sent to the experts can be found in ***Appendix B***. The questionnaire is structured into a short introduction followed by 5 questions. Question #1 is focused on prioritizing the 4 STEPs foreseen for the SPTHA framework. Questions #2 through #5 are then dedicated to prioritize the levels and sub-levels inside each one of these STEPS. In appendix to the questionnaire, we also reported a list of the potential alternative implementations at each of the steps and levels. The goal of this appendix was twofold: 1) to help clarifying the meaning of levels, and 2) to specify what kind of alternatives were actually under consideration for the TSUMAPS-NEAM project.

Table 1: Fundamental scale of absolute numbers.

Intensity of Importance	**Definition**	**Explanation**	**Weights of models**	***Standard AHP weights***
1	Equal importance	Two steps/levels/sublevels contribute equally to the objective	0.5-0.5	*0.5-0.5 (x1)*
3	Moderate preference	Experience and judgment slightly favor one step/level/sublevel over another	0.6-0.4 (x1.5)	*0.75-0.25 (x3)*
5	Strong preference	Experience and judgment strongly favor one step/level/sublevel over another	0.75-0.25 (x3)	*0.83-0.17 (x5)*
7	Very strong preference	A step/level/sublevel is favored very strongly over another; its dominance demonstrated in practice	0.95-0.05 (x19)	*0.86-0.14 (x7)*
9	Extreme preference	Overwhelming evidence favoring one step/level/sublevel over another	0.99-0.01 (x99)	*0.90-0.10 (x9)*

2. Results

2.1 Analysis of the results

The questionnaire was sent to the Pool of Experts (PoE) members (15 experts). We received 14 answers, that is, all the experts with only one exception answered the questionnaire. Out of the 14 filled-in questionnaires, each including five questions, we found at least one inconsistency larger than 0.3 only for three experts. We then sent back the questionnaire to these experts, explaining the meaning of the found inconsistencies and asked to review the questionnaire only for the questions for which a high inconsistency was found. The revised answers were received only from one of them. However, since the number of experts with consistent answers is considered sufficient (12 out of 15), we report below the analysis of results considering only these answers. The results are stable with respect to this choice.

The results are used to set the priorities in developing model alternatives. For each question, we report the following plots:

- The empirical CDF of the scores of the proposed alternatives, obtained by considering the prioritization of the different experts as weighted samples; we report one plot for each weighting scheme.
- The parametric variability of the scores of the proposed alternatives, considering arithmetic and geometric means and percentiles 16^{th}, 50^{th} (median) and 84^{th}; we report one plot for each weighting scheme.
- The CR of all the experts, compared with thresholds of 0.1 and 0.3. If one expert had CR > 0.3 for at least one question, the questionnaire was sent back for review of that question.
- The weights of the experts, adopting the different weighting schemes.

The prioritizations obtained by the different weighting schemes are compared, both in terms of central values and of inter-expert distributions. Based on this comparison, the steps and levels of the SPTHA are ranked into three groups:

- **High priority (red):** steps/levels with clear high priority in all weighting schemes. For these steps/levels, alternative implementations are strongly recommended by the PoE. In this case, the alternatives should be carefully selected to represent a range of models that cover the full range of scientifically acceptable modeling alternatives (following SSHAC 2012, “the center, body, and range of technically defensible interpretations”).
- **Medium priority (orange):** steps/levels with either high priority in one (but not all) the weighting schemes, or intermediate priority in all weighting schemes. For these steps/levels an evaluation of the potential consequence of alternative implementations is recommended by the PoE. In this case, some alternative implementations should be considered and/or some sensitivity test should be planned.
- **Low priority (green):** steps/levels with low priority in all weighting schemes. For these steps/levels the PoE suggests a relatively low potential impact of epistemic uncertainty and a single preferred implementation can be considered.

2.2 Specific results

The results show that:

Question #1: Alternatives are strongly encouraged for STEP 1 and STEP 3 only. The potential influence of alternatives in STEP 4 should be tested (Q5 below). Alternatives can be avoided in STEP 2 (Q3 below). The analytic results for Question #1 are reported in ***Section 2.2.1***.

Question #2: Within STEP 1, alternatives are strongly encouraged (Q1 above). From Q2, alternatives are strongly encouraged for 1) the selection of the PS interfaces to be modelled separately, and 2) the quantification of the frequency-magnitude distribution. Alternatives are recommended for 1) the seismic catalog considered, 2) the models for spatial distribution on PS, and 3) the models for slip distribution on PS. The analytic results for Question #2 are reported in ***Section 2.2.2***.

Question #3: Within STEP 2 (if alternatives were to be considered), alternatives are strongly encouraged for 1) Topo-bathymetric datasets and digital elevation models. Alternatives are recommended for 1) coseismic displacement models, 2) tsunami generation models, and 3) tsunami propagation (in deep water) models. The analytic results for Question #3 are reported in ***Section 2.2.3***.

Question #4: For STEP 3, alternatives are strongly encouraged for 1) Topo-bathymetric datasets and digital elevation models, 2) Amplification and inundation models at the points of interest along the coast, and inland, corresponding to the offshore points of STEP 2, and 3) Models of the uncertainty on the tsunami metrics. The analytic results for Question #4 are reported in ***Section 2.2.4***.

Question #5: For STEP 4, alternatives are recommended for 1) the quantification of weights of the experts, and 2) the quantification of the weights of alternative models. The analytic results for Question #5 are reported in ***Section 2.2.5***.

Any choice different from PoE suggestions requires specific justification in the selection of the alternatives actually implemented in the TSUMAPS-NEAM project (see ***Doc_P1_S4_Prel_Impl_Plan***).

2.2.1 Question #1: Prioritization of STEPs

Each of the STEPs contains a number of quantitative assessments that may potentially introduce epistemic uncertainty on the SPTHA results, as summarized in the following table:

No.	Model code	Description
1	STEP1	Definition of the seismic source variability and quantification of the long-run frequencies of all the seismic sources
2	STEP2	Tsunami generation and off-shore propagation
3	STEP3	Near-shore tsunami propagation and inundation
4	STEP4	Computation of the weights of the alternative models developed in STEPs 1 to 3 to measure their credibility, and construction of the "ensemble" model

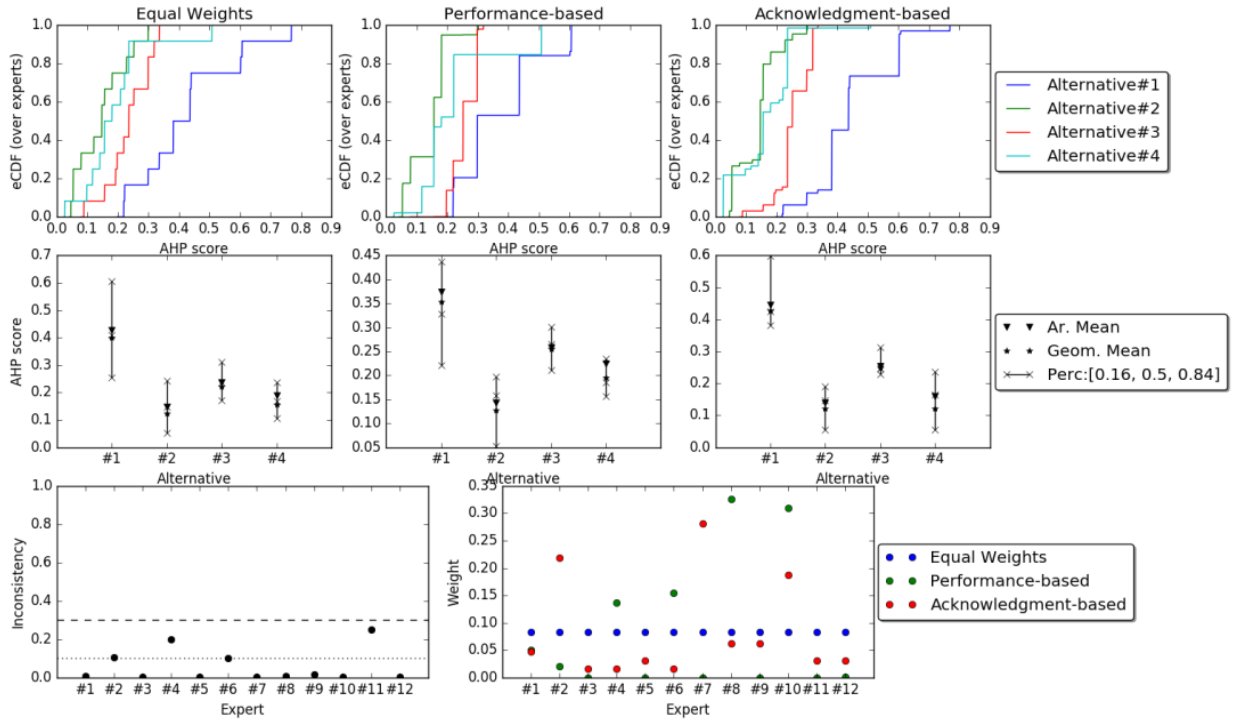

Figure: AHP results, removing highly inconsistent experts (2).

2.2.2 Question #2: Prioritization of Levels in STEP 1

Within the described levels and sublevels, we enumerated a total of 10 groups of quantitative decisions/assessments that may potentially introduce epistemic uncertainty on the STEP 1 results, as reported in the following table:

No.	Model code	Description
1	Region	Level 0 - Regionalization
2	PSDef	Level 0 - Selection of interfaces to be modeled separately
3	SeismicCat	Level 0 - Seismic catalogues
4	FreqMag	Level 1 - Quantification of the Magnitude-frequency (of PS and BS, separately)
5	PS-Pos	Level 2a - Sublevel PS-1: spatial distribution (position and area) and average slip of earthquakes over PS
6	PS-Slip	Level 2a - Sublevel PS-2: slip distribution of PS
7	BS-Pos	Level 2b - Sublevel BS-1/2: hypocentral distribution of BS
8	BS-Mech	Level 2b - Sublevel BS-3: focal mechanism of BS
9	BS-Size	Level 2b - Sublevel BS-4: size of finite faults of BS (scaling laws)
10	BS-Slip	Level 2b - Sublevel BS-5: slip distribution of BS

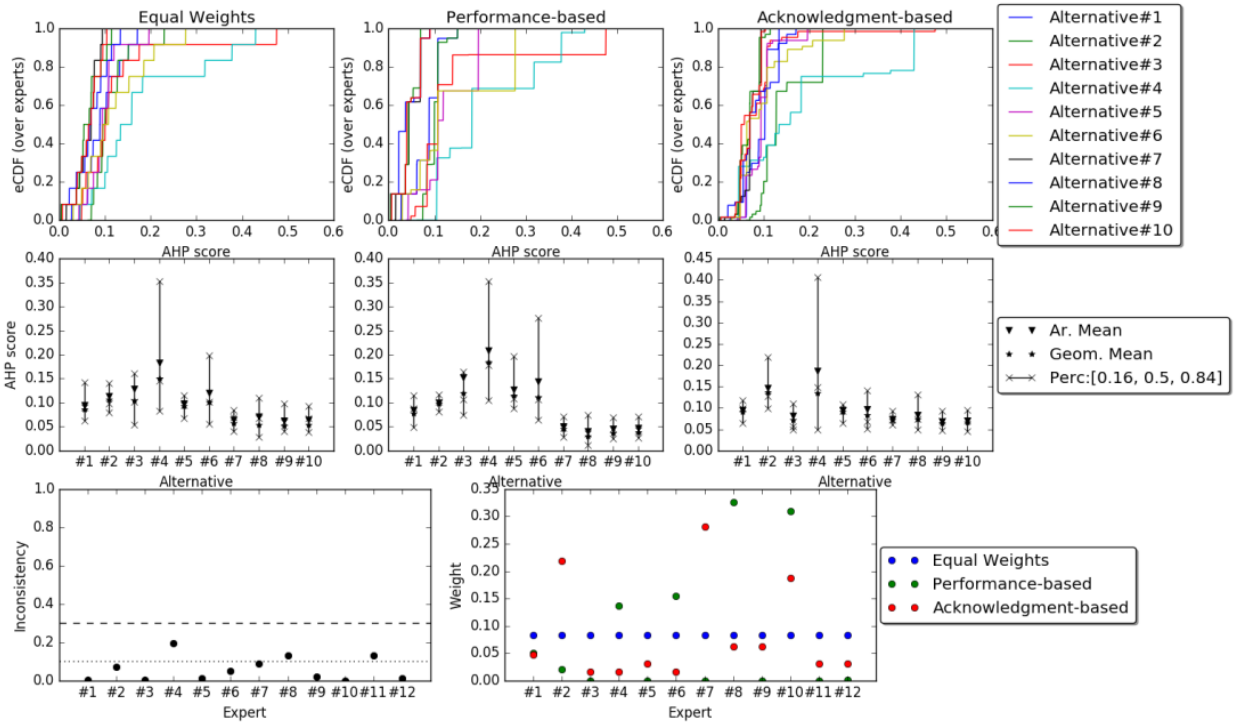

Figure: AHP results, removing highly inconsistent experts (2).

2.2.3 Question #3: Prioritization of Levels in STEP 2

Within the described levels, we enumerated a total of 5 groups of quantitative decisions/assessments that may potentially introduce epistemic uncertainty on the STEP 2 results, as reported in the following table.

No.	Model code	Description
1	Crust	Level 0 - Crustal models (elastic parameters)
2	TopoBath	Level 0 - Topo-bathymetric datasets and digital elevation models
3	CoSeis	Level 1 - Coseismic displacement model
4	TsuGen	Level 2 - Tsunami generation model
5	TsuProp	Level 3 - Tsunami propagation (in deep water) model

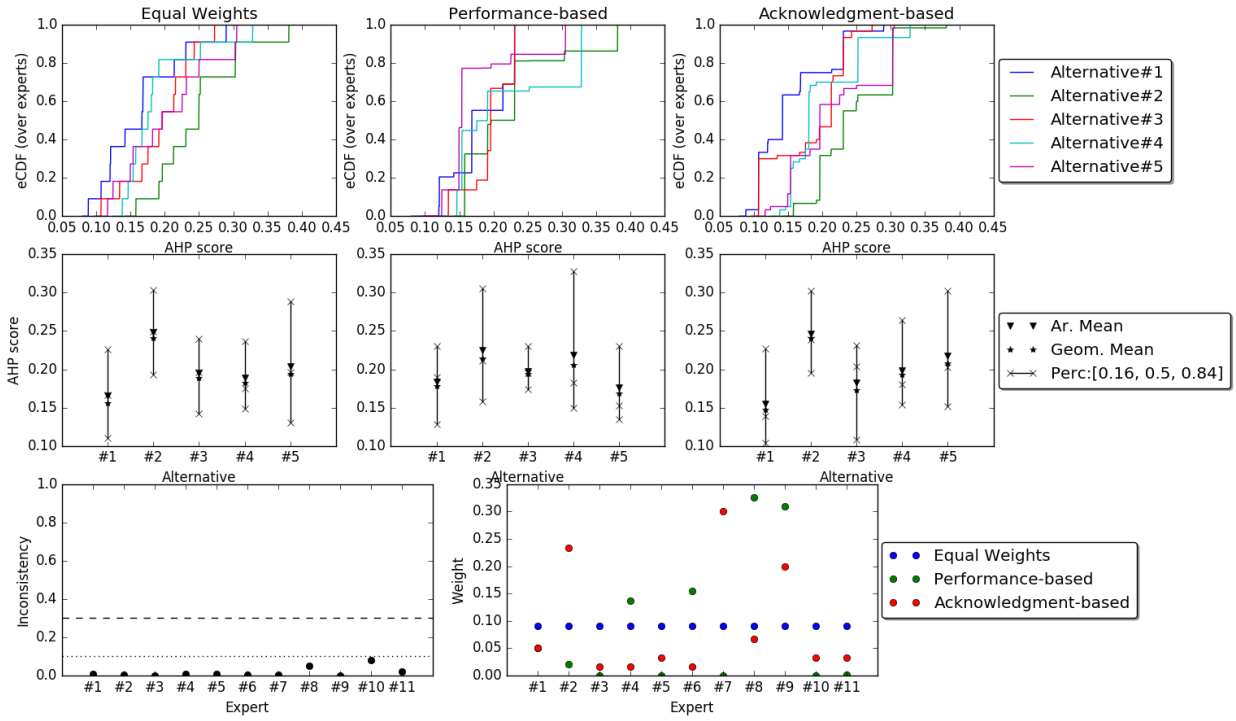

Figure: AHP results, removing highly inconsistent experts (3).

2.2.4 Question #4: Prioritization of Levels in STEP 3

Within the described levels, we enumerated a total of 4 groups of quantitative decisions/assessments that may potentially introduce epistemic uncertainty on the STEP 3 results, as reported in the following table

No.	Model code	Description
1	TopoBath	Level 0 - Topo-bathymetric datasets and digital elevation models
2	Inund	Level 1 - Amplification and inundation models at the points of interest along the coast, and inland, corresponding to the offshore points of STEP 2
3	Tide	Level 2 – Evaluation of the probability of tidal stage at the points of interest
4	Uncertainty	Level 3 - Model the uncertainty on the tsunami metrics

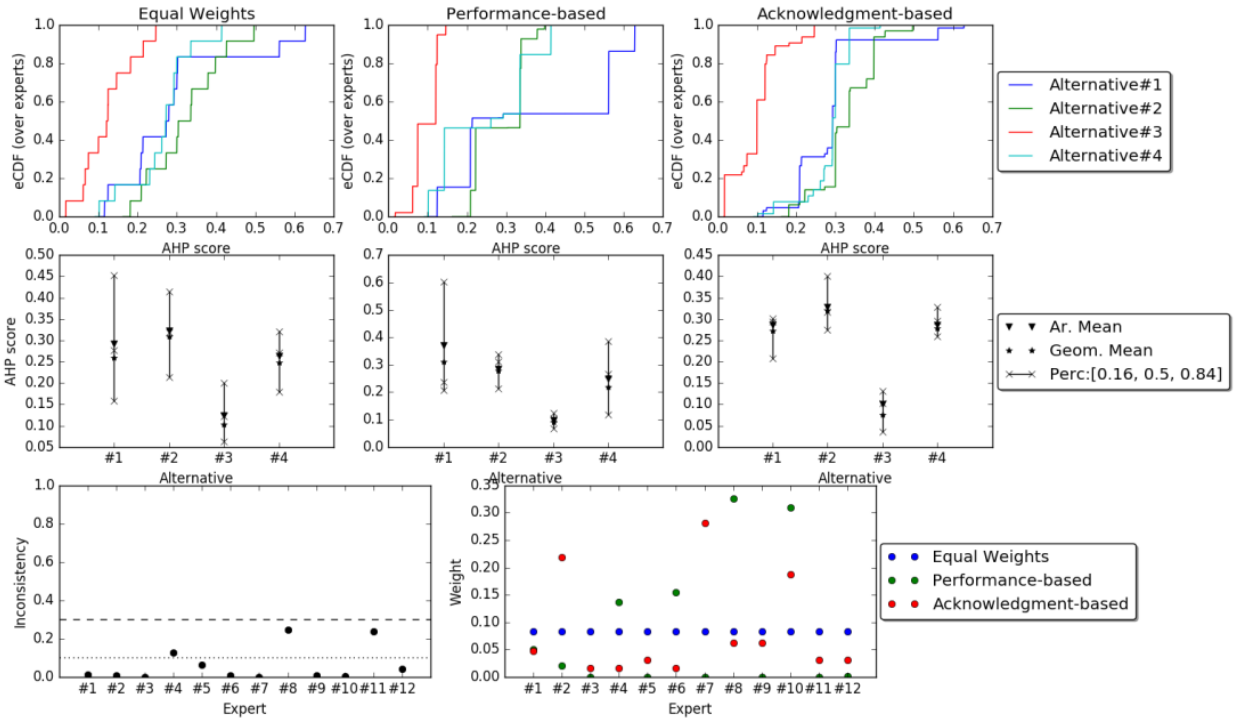

Figure: AHP results, removing highly inconsistent experts (2).

2.2.5 Question #5: Prioritization of Levels in STEP 4

Within the described levels, we enumerated a total of 2 groups of quantitative decisions/assessments that may potentially introduce epistemic uncertainty on the STEP 4 results, as reported in the following table:

No.	Model code	Description
1	WeightsExperts	Level 0 – Quantification of weights of the experts
2	Aggregation	Level 1 – Method for aggregating hazard results within each model
3	WeightsModels	Level 2 – Quantification of the weights of alternative models
4	EpisIntegration	Level 2 – Method for integrating the alternative models into a single model that quantifies also the epistemic uncertainty (e.g., Logic Tree, Ensemble models)

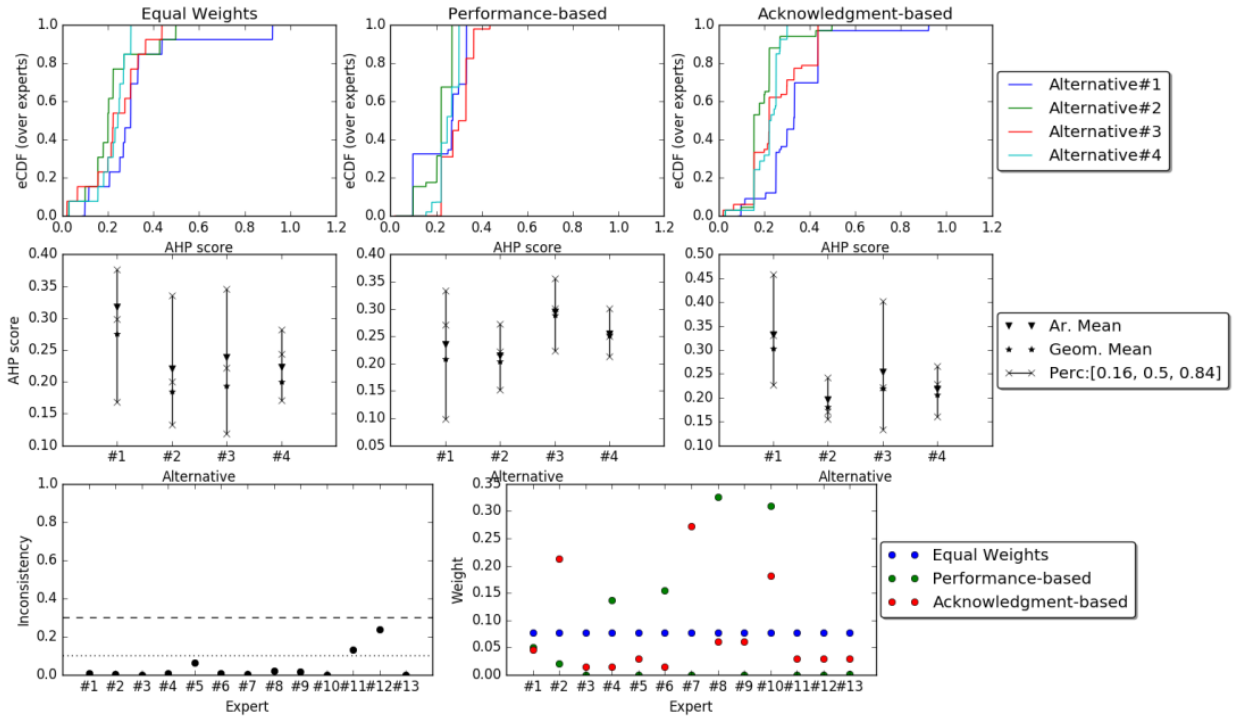

Figure: AHP results, removing highly inconsistent experts (1).

References

Bommer, J.J., Scherbaum, F., 2008. The use and misuse of logic-trees in PSHA. Earthquake Spectra 24 (4), 997–1009.

Bommer JJ (2012). Challenges of Building Logic Trees for Probabilistic Seismic Hazard Analysis, EARTHQUAKE SPECTRA, Vol: 28, 1723-1735, ISSN: 8755-2930.

Forman, E. & Peniwati, K. (1998). Aggregating individual judgments and priorities with the analytic hierarchy process. European Journal of Operational Research, 108(1), 165-169.

Goepel, K.D., 2013, IMPLEMENTING THE ANALYTIC HIERARCHY PROCESS AS A STANDARD METHOD FOR MULTI-CRITERIA DECISION MAKING IN CORPORATE ENTERPRISES – A NEW AHP EXCEL TEMPLATE WITH MULTIPLE INPUTS, Proceedings of the International Symposium on the Analytic Hierarchy Process 2013.

Harker, P., Vargas, L. 1987. The Theory of Ratio Scale Estimation: Saaty's Analytic Hierarchy Process. Management Science. 33(11), 1383–1403.

Marzocchi, W., Taroni, M., Selva, J., 2015. Accounting for epistemic uncertainty in PSHA: logic tree and ensemble modeling. Bulletin of the Seismological Society of America, 105(4), 2151-2159.

Musson, R. M. W. (2012). On the nature of logic trees in probabilistic seismic hazard assessment, Earthq. Spectra 28, 1291–1296.

Rougier, J., R. Sparks, and L. J. Hill (2013), Risk assessment and uncertainty in natural hazards, in Risk and Uncertainty Assessment for Natural Hazards, edited by J. C. Rougier, R. S. J. Sparks, and L. J. Hill, pp. 1–18, Cambridge Univ. Press, Cambridge, U. K.

Saaty, T.L., 1980. The Analytic Hierarchy Process: Planning, Priority Setting, Resource Allocation, ISBN 0-07-054371-2, McGraw-Hill

Saaty, T.L., Hu, G., 1998, Ranking by Eigenvector Versus Other Methods in the Analytic Hierarchy Process, Appl. Math. Lett. Vol. 11, No. 4, pp. 121-125, 1998

Selva, J., Tonini, R., Molinari, I., Tiberti, M.M., Romano, F., Grezio, A., Melini, D., Piatanesi, A., Basili, R., Lorito, S., 2016. Quantification of source uncertainties in Seismic Probabilistic Tsunami Hazard Analysis (SPTHA), Geophys. J. Int., 205: 1780-1803, DOI: 10.1093/gji/ggw107.

SSHAC (Senior Seismic Hazard Analysis Committe), 1997. Recommendations for probabilistic seismic hazard analysis: Guidance on uncertainty and use of experts, U.S. Nuclear Regulatory Commission Report NUREG/CR-6372.

SSHAC 2012: USNRC (U.S. Nuclear Regulatory Commission), 2012. Practical Implementation Guidelines for SSHAC Level 3 and 4 Hazard Studies, Prepared by AM Kammerer & JP Ake, NRC Project Manager: R Rivera-Lugo, NUREG-2117.

Zio E., 1996. On the use of the analytic hierarchy process in the aggregation of expert judgments, Reliability Engineering & System Safety, Volume 53 (2), 127-138, ISSN 0951-8320

Probabilistic TSUnami Hazard MAPS
for the NEAM Region (TSUMAPS-NEAM)
ECHO/SUB/2015/718568/PREV26

PHASE I – STAGE 4: Preliminary Implementation Plan (Workflow)

Author: **TSUMAPS-NEAM Technical Integrator (TI) team**

Date: **19 June 2017**

Version: **1.0**

Table of Contents

Executive Summary

This document describes the details of the planned implementation at all STEPS.

This is the final result of the pre-assessment PHASE in which a larger number of alternatives have been 'trimmed' as a result of the first elicitation STAGE.

The Levels within each of the four STEPS which compose the SPTHA have already been introduced in Section 2.5 of DOC_P1_S1.

This document is organized into two parts.

The first part reports a more detailed explanation of the Levels, specifically defining the assessment to be performed at each of the Levels. That is, in this part we specify what we want to do.

The second part presents the alternatives selected for implementation at each Level, with some technical detail. That is, in this part we specify how we want to do it.

Altogether, the two parts of this document constitute the Preliminary Implementation Plan of TSUMAPS-NEAM SPTHA.

This page is intentionally left blank.

1. Detailed explanation of the Levels for STEPs

From document *Doc_P1_S1_ProjectSummary*, we recall that the four STEPs of the assessment in TSUMAPS-NEAM are:

- STEP 1: PROBABILISTIC EARTHQUAKE MODEL
- STEP 2: TSUNAMI GENERATION & MODELING IN DEEP WATER
- STEP 3: SHOALING AND INUNDATION
- STEP 4: HAZARD AGGREGATION & UNCERTAINTY QUANTIFICATION

In this section, we describe in more details with respect to the *Doc_P1_S1_ProjectSummary* the different Levels composing these four STEPs. At each Level, we specifically define what needs to be quantified. The methods with alternatives used for these quantifications will be described in *Section 2*.

At each STEP, Level 0 defines data and definitions required for the assessment. Levels starting from 1 define actual actions undertaken within the assessment.

1.1 STEP 1 - PROBABILISTIC EARTHQUAKE MODEL

At STEP 1 we have defined three Levels (0-2). A branching exists for Level 2 that is split into Level 2a and 2b.

The general aim of STEP 1 is definition of a list of scenarios $\{\sigma_k\}$ for all potential earthquakes in all source regions and quantification of their mean annual rates $\lambda(\sigma_k)$.

From document *Doc_P1_S1_ProjectSummary*, we recall that the Levels for STEP 1 are:

- Level 0: Regionalization, Definition of the Predominant Seismicity (PS) sources, Seismic datasets.
- Level 1: Magnitude-frequency distribution for each region including splitting of seismic activity into Predominant Seismicity (PS) and Background Seismicity (BS).
- Level 2a: Variability of PS earthquakes of given magnitude including: position along the hosting 3D-curved fault and finite fault dimensions, average slip, and slip distribution.
- Level 2b: Variability of BS earthquakes of given magnitude including: location, depth, faulting mechanism, finite fault dimensions, average slip. BS sources are assumed to be planar.

Level 0, as for the next STEPs, is used for treating the databases (including possible alternatives) which are relevant for the STEP.

Next Levels at STEP 1 coincide with the Levels of an Event Tree (ET). Hence, Levels 1-2 with their branches decompose the problem into a chain of discrete conditional probabilities for aleatory variables describing the earthquakes. Each path (or branch) through the ET represents one specific combination of all the parameters and, thus, completely defines a particular scenario to be modelled in STEPs 2 and 3. The corresponding mean annual rate of this scenario can be obtained by multiplying the mean annual rate evaluated at Level 1 with conditional probabilities along the path.

The quantifications required at these Levels are described in details below.

1.1.1 Level 0 - Regionalization & Seismic Datasets

At this Level, we discuss the regionalization, the employed/available seismicity and fault datasets, and their basic processing techniques (e.g., de-clustering, determination of completeness).

The regionalization is a subdivision of the entire NEAM seismic source area into discrete regions that are as homogeneous as possible from the standpoint of dominant tectonics. Quantification of each of the STEP 1 Levels will be performed separately for each of the regions defined by the regionalization.

Rationale for splitting seismicity into PS (Predominant Seismicity) and BS (Background Seismicity) has been presented in Section 2.2 of *Doc_P1_S1_ProjectSummary.*

Seismic datasets include:

- earthquake catalogues and their seismicity attributes (including completeness levels);
- focal mechanism catalogues;
- crustal fault catalogues for BS, including geometry, mechanism, and slip rate;
- detailed fault description for PS only, including 3D geometry, mechanism, slip rate or convergence rate, seismogenic depth and seismic efficiency (coupling, defined as a mean value over the fault surface).

Earthquake catalogues are accompanied by completeness analyses compatible with the regionalization, and both complete and de-clustered versions of these catalogues are made available.

1.1.2 Level 1 - Magnitude-frequency distribution for each region

At this Level, the frequency of the different magnitudes in each region is quantified as the sum of the contribution of Predominant Seismicity (PS) and Background Seismicity (BS). *An* earthquake belongs to a region if the geometrical centre of its fault lies within this region.

The assessment consists of quantifying mean annual rates for a set of discrete magnitude intervals M_j, with reference to the defined exposure time window (50 yr), for both Predominant and Background Seismicity in region R_i, that is $\lambda_i^{(PS)}(M_j)$ and $\lambda_i^{(BS)}(M_j)$, respectively. These two quantifications correspond to the first Level of the ET (PS-1 and BS-1, respectively) as described in Section 2.5 of document *Doc_P1_S1_Project_Summary*.

1.1.3 Level 2a - Variability of PS earthquakes of given magnitude within given region

This Level is the Predominant Seismicity (PS) branch; we here consider only earthquakes modelled as occurring along major seismogenic interfaces, e.g., subduction zones. All the parameters identifying individual sources on the 3D PS structures geometry defined at Level 0 are analysed.

The PS analysis is subdivided into the 2 sub-Levels that stack on Level PS-1, that are:

- sub-level PS-2 – Positioning along the PS hosting structure and rupture area
- sub-level PS-3 – Slip distribution

At the sub-level PS-2, position and size of the rupture area are treated simultaneously. Earthquake positions on each PS hosting fault are discretized by defining a set of coordinates $\{x_c, y_c\}$ along the 3D fault geometry. Assessment consists of quantifying the probability $\Pr_i(x_c, y_c, A|M_j)$, that is, the joint probability of a fault centre x_c, y_c and a maximum rupture area A for an earthquake of magnitude M_j in the region R_i. We simplify this quantification by computing the A as a function of

magnitude M_j from scaling laws, so that $\Pr_i(x_c, y_c, A|M_j) = \Pr_i(x_c, y_c|M_j)$, since no aleatory uncertainty is modelled for A. Average effective slip can also be estimated from the same scaling law.

At the sub-Level PS-3, we model the aleatory variability of the heterogeneous slip distribution within the rupture area A. We quantify the joint probability of a slip vector field conditioned to the occurrence of an earthquake centred at $\{x_c, y_c\}$ and having rupture area A and magnitude M_j, that is, $\Pr_i(\vec{s}\,|x_c y_c, A, M_j)$. This joint probability distribution should take into account many different constrains, such as total slip, spatial correlation of slip, etc. To simplify this quantification, instead of discretizing the slip vector space and quantifying the joint probability distribution, at this Level, we adopt a Monte-Carlo approach. We build a sampling of slip distributions, propagating each equally-probable sample with conditional probability $\Pr_i(\vec{s}\,|x_c y_c, A, M_j) = 1/n$, where n is the sample size.

The total set of scenarios to be modelled for Predominant Seismicity, $\{\sigma_k\}^{(PS)}$, is composed by all combinations of regions R_i, magnitudes M_j, centers $\{x_c, y_c\}$ and all the sampled slip distributions $\vec{s}$. The corresponding mean annual rate is computed then as:

$$\lambda\left(\sigma_k^{(PS)}\right) = \lambda^{(PS)}(R_i, M_j, x_c, y_c, \vec{s}) = \lambda_i^{(PS)}(M_j)\ \Pr_i(x_c, y_c|M_j)\ \Pr_i(\vec{s}\,|x_c y_c, A, M_j)\ .$$

1.1.4 Level 2b - Variability of earthquakes of the Background Seismicity

This Level is the Background Seismicity (BS) branch; we here consider only the earthquakes modelled as occurring outside the Predominant Seismicity faults. For BS, the dominant faulting mechanism is, hence, not pre-determined as well as the spatial distribution of earthquakes. They both vary within the volume defined by a set of cells on a regular 3D grid (see Figure 2.2.4 in of *Doc_P1_S1_ProjectSummary*). Ruptures of the Background Seismicity are modelled as single rectangular planar faults with uniform slip distribution. We analyse all the corresponding parameters: location, depth, strike, dip, rake, and slip, identifying all individual sources. Coordinates of the fault centres are distributed along the nodes of the regular grid. Similarly to the PS case, correspondence of a BS earthquake to a particular region is controlled by the position of its geometrical centre.

The BS analysis is subdivided into the 3 sub-Levels that stack on Level BS-1, that are:

- sub-level BS-2 - spatial distribution of earthquakes
- sub-level BS-3 - depth distribution of earthquakes
- sub-level BS-4 - focal mechanisms

Note that, in order to reduce the computational effort, the aleatory variability of finite fault dimensions and slip distribution are not modelled. Instead, the average values from scaling laws are adopted

At sub-level BS-2 - spatial distribution of earthquakes - given an earthquake of a given magnitude in a given region, the geometrical centre of a fault may be at different positions. The area covered by the region is thus discretised by a regular 2D grid. The assessment consists of quantifying the conditional probability $\Pr_i(x, y)$ for each potential rupture centre $\{x, y\}$ (that are, essentially, longitude and latitude) within region R_i. Note that, differently from PS, this quantification is

assumed to be independent from the magnitude value, which is consequently omitted from the notation.

At sub-level BS-3 - depth distribution -, given an earthquake of a given magnitude in a given region at a given grid cell, the geometrical centre of a fault may be at different depth. The column of crust identified by $\{x, y\}$ is thus discretised by depth levels. The assessment consists of quantifying in each region R_i the conditional probability of these different depth levels $\Pr_i(d|M_j, x, y)$ conditioned to magnitude M_j and geographical position $\{x, y\}$.

At sub-level BS-4 - focal mechanisms -, given an earthquake of a given magnitude in a given region at a given cell and depth, various faulting mechanisms are possible. Here we analyse probabilities of different strike/dip/rake combinations for each cell. Note that these probabilities are not random but, instead, their expected PDF's are derived according to past seismicity and presence of known faults. The joint conditional probability $\Pr_i(strike, dip, rake|x, y)$ in each cell $\{x, y\}$ is quantified. Note that this quantification is assumed to be independent from magnitude and depth, which are consequently omitted from the notation.

The total set of scenarios to be modelled for Background Seismicity $\{\sigma_k\}^{(BS)}$ is composed by all combinations of regions R_i, magnitudes M_j, positions $\{x, y\}$, depths d and focal mechanisms $\{strike, dip, rake\}$. The corresponding mean annual rate is then computed as:

$$\lambda\left(\sigma_k^{(BS)}\right) = \lambda^{(BS)}\left(R_i, M_j, x, y, d, strike, dip, rake\right) = \lambda_i^{(BS)}\left(M_j\right) \Pr_i(x, y) \Pr_i(d|M_j, x, y) \Pr_i(strike, dip, rake|x, y).$$

1.2 STEP 2 - TSUNAMI GENERATION & MODELING IN DEEP WATER

At STEP 2 we have defined 4 Levels (0-3).

The general aim of STEP 2 is calculation of tsunami wave time series (mareograms) at each offshore Point of Interest (POI) corresponding to the earthquake scenarios $\{\sigma_k\}$ defined at STEP 1. The logical sequence of Levels in STEP 2 is straightforward, and there is no any branching at this step.

From document *Doc_P1_S1_ProjectSummary*, we recall that the Levels for STEP 2 are:

- Level 0: Crustal elastic model; Topo-bathymetric datasets and digital elevation models
- Level 1: Co-seismic displacement model
- Level 2: Tsunami generation model
- Level 3: Tsunami propagation (in deep water) model

Level 0 is used for treating the databases (with also possible alternatives) which are relevant for this STEP.

Levels 1-3 in STEP 2 is the sequence composing the tsunami modelling from generation to propagation in deep water, up to the offshore POIs distributed along the 50 m isobaths.

The quantifications required at these Levels are described in details below.

1.2.1 Level 0 - Crustal elastic model; Topo-bathymetric datasets and digital elevation models

At this Level, we treat the choice of the: crustal models employed for calculation of the co-seismic surface displacement; topo-bathymetric databases, and the preparation of the digital elevation model on a grid (the topo-bathymetric grid) used for subsequent tsunami numerical modelling.

1.2.2 Level 1 – Co-seismic displacement model

The seafloor displacement is here modelled for each earthquake scenario $\{\sigma_k\}$ defined by the sampling at STEP1.

1.2.3 Level 2 - Tsunami generation model

This is the step where the tsunami initial condition are derived starting from the seafloor deformation obtained at the previous Level.

1.2.4 Level 3 - Tsunami propagation (in deep water) model

Here, the tsunami simulations are performed, according to the initial condition from the previous Level. The tsunami waveforms (mareograms) at the offshore POIs (Points Of Interest) corresponding to each scenario $\{\sigma_k\}$ are computed. Principle wave parameters necessary for the application of the amplification factors method (Section 2.3 *Doc_P1_S1_ProjectSummary)* including maxima, period and polarity are also extracted and stored for subsequent usage in STEP 3.

1.3 STEP 3 - SHOALING AND INUNDATION

At STEP 3 we have defined 4 Levels (0-3).

The general aim of STEP 3 is calculation, starting from the mareograms of STEP 2, of probabilities of exceedance for different hazard thresholds, conditioned to the occurrence of the scenarios $\{\sigma_k\}$ defined at STEP 1. This includes the aleatory variability introduced by the tides and the uncertainty on the hazard metric.

From document *Doc_P1_S1_ProjectSummary*, we recall that the Levels for STEP 3 are:

- Level 0: Topo-bathymetric datasets and digital elevation models
- Level 1: Amplification and inundation model
- Level 2: Tidal stage model
- Level 3: Uncertainty modelling for tsunami hazard metrics (including uncertainties from modelling approximations at STEPS 1-3, and tides).

Level 0 is used for treating the databases which are relevant for the STEP.

Level 1 deals with the estimation of coastal and / or inland tsunami hazard intensity from offshore numerical simulations at STEP 2.

Level 2 deals with the calculation of tidal stages.

Level 3 deals with uncertainty modelling and propagation at STEPs 1-3: from source to the hazard intensity metric. It can be done through the construction of PDF's for various uncertainty sources, and combination with tides. As anticipated in *Doc_P1_S1_ProjectSummary*, this part of the analysis is still under discussion.

The quantifications required at these Levels are described in details below.

1.3.1 Level 0 - Topo-bathymetric datasets and digital elevation models

Here we treat the choice of the: digital elevation model on a grid (the topo-bathymetric grid), or along 1D profiles, used for the subsequent estimation of the coastal / inland hazard intensities.

1.3.2 Level 1 - Amplification and inundation model

At this Level accepted tsunami hazard intensity metrics are computed by extrapolation of the offshore tsunami intensities stored at the end of STEP 2 (maxima, periods, polarities) to the coast / inland.

1.3.3 Level 2 - Tidal stage model,

The tidal stage time series, and their probability distributions, are evaluated at the respective POIs.

1.3.4 Level 3 - Uncertainty modelling for tsunami hazard metrics (including stochastic modelling of unmodelled effects from STEPS 1-3, and tides)

Here we model the probability of exceedance of predefined thresholds for the accepted hazard intensity metric, for each scenario and each possible combination with tidal stages. By doing this, we also need to account for uncertainties which may arise at the previous STEPs due to different model approximations and non-modelled effects. To do this, we need to quantify and sample the distributions describing the epistemic uncertainty associated with tsunami modelling.

1.4 STEP 4 - HAZARD AGGREGATION & UNCERTAINTY QUANTIFICATION

At STEP 4 we have defined 4 Levels (0-3).

The general aim of STEP 4 is quantification of hazard curves at POIs that is the exceedance probability of a chosen hazard metric within a given time window. This is done by the aggregation of the probabilities of STEP 3 according to the mean annual rates $\lambda(\sigma_k)$ of the individual scenarios $\{\sigma_k\}$ from STEP 1, and according to the weights of the alternatives models, within an ensemble modelling treatment of uncertainties. This STEP includes also comparison with observations and disaggregation analysis.

From document *Doc_P1_S1_ProjectSummary*, we recall that the Levels for STEP 4 are:

- Level 0: Elicitation of experts, historical tsunami DB, paleo-tsunami DB
- Level 1: Combination of STEPS 1-3
- Level 2: Quantification of uncertainty
- Level 3: Comparison/test with tsunami records; disaggregation

Level 0 is generally used at all STEPS for treating the databases which are relevant for the STEP. In this specific case it deals with definition of weights for the alternative models (via expert elicitation).

Level 1 deals with hazard aggregation from the previous STEPS.

Level 2 deals with concrete uncertainty estimation.

Level 3 deals with comparison with observations and disaggregation of the results.

The quantifications required at these Levels are described in details below.

1.4.1 Level 0 - Elicitation of experts

The relative credibility of alternative implementations is quantified by means of weights. The assessment consists of the quantification of w_{mnl} where m represents a given alternative model of STEP n and Level l. These weights are subjective and will be quantified through a structured elicitation experiment by the Pool of Experts (PoE). This experiment will be performed considering all the alternatives planned at all the STEPs and Levels, keeping STEPs and Levels separated (whenever possible).

1.4.2 Level 1 - Combination of STEPS 1 to 3

The contributions of all sources to the hazard at each POI are aggregated, considering the mean annual rate of each source (STEP 1), the generation and propagation in deep water of the consequent tsunami (STEP 2) and its inundation (STEP 3). The assessment consists of quantifying the hazard curves in terms of mean annual rates of exceedance of a hazard threshold for the accepted tsunami intensity metric H $\lambda_{mn}(H \geq H_k; POI, \Delta T)$ at each POI (as defined in STEP 2) for all predefined threshold values (as defined in STEP 3).

1.4.3 Level 2 - Quantification of uncertainty

All the alternative implementations at Level 1 are used on input to the Ensemble Modelling procedure to produce, for each target point, an ensemble distribution that quantifies both aleatory and epistemic uncertainty. In particular, all the annual rates $\lambda_{mn}(H \geq H_k; POI, \Delta T)$ are first transformed into $\Pr_{mn}(H \geq H_k; POI, \Delta T)$ and then they form an input to produce an ensemble distribution that quantifies simultaneously all uncertainties and represents the community distribution of the resulting hazard curves (SSHAC 1997; Bommer 2012; Marzocchi et al. 2015).

1.4.4 Level 3 - Comparison/test with tsunami records; disaggregation

The results of Level 1 are used for production of secondary results. Since TSUMAPS-NEAM Project has a regional scope, the main purpose of this Level is to test the compatibility of results with available data as well as to provide general indications to be used as input and/or comparison for future analyses.

2. Alternative modeling and critical choices

In this section, we detail the implementation plan regarding alternative modelling of all the STEPs and their Levels for epistemic uncertainty quantification in TSUMAPS-NEAM.

To trim the potentially huge number of alternatives in order to focus on the most significant uncertainty-drivers, we performed the elicitation described in document *Doc_P1_S3_Elicitation*. Here, we present our implementation plan that accounts for the requests of the Pool of Experts (PoE) emerging from the elicitation and also respects practical constrains imposed by the project.

In each STEP and each Level, we summarize the PoE suggestions, our choices in response, and an overview of the alternative models to be implemented. Further technical details will be reported in the next review round. Some details need in fact to be still addressed; and some likely minor changes may be expected to happen during actual implementation.

2.1 STEP 1 - PROBABILISTIC EARTHQUAKE MODEL

The PoE elicitation recommended to implement alternatives at STEP 1 (question Q1 in Doc_P1_S3_Elicitation).

According to the question Q2 (*Doc_P1_S3_Elicitation*), alternative models are recommended for:

- Level 0: selection of the PS interfaces to be modelled separately
- Level 1: quantification of the magnitude-frequency relation

Alternatives or sensitivity tests are also suggested for:

- Level 0: tectonic regionalization
- Level 0: seismic catalogue(s) considered
- Level 2a: models for spatial distribution on PS-interfaces
- Level 2a: models for slip distribution on PS-interfaces

Alternatives and sensitivity tests can be avoided for all Level 2b sublevels.

In the next sub-sections, we discuss the implementation plan for all STEP1 levels and sublevels.

2.1.1 Level 0 - Regionalization & Seismic DBs

The PoE elicitation recommended alternatives for the selection of the PS interfaces. Additionally, alternatives or sensitivity tests were suggested for the regionalization and seismic catalogue.

As far as the PS interfaces are concerned, we opted for a different strategy. Instead of using alternatives for the selection, we added as much as possible further well-known PS sources, compatibly with the project resources available for them (creating further meshes, calculating the displacements, performing linear combinations, etc.). That is, we increased their total number with respect to those presented to the PoE at the Kick-off meeting. Additionally, we plan sensitivity tests with respect to inclusion / exclusion of PS sources. If feasible, we will perform also sensitivity tests to the PS geometry and mechanism.

The introduction of an alternative regionalization model seems instead very difficult to be accomplished within the project resources. Most likely, the second regionalization will be left for a future update of the TSUMAPS-NEAM assessment.

Finally, we plan a total of two alternative methods to assign the observed seismicity either to PS or BS sources, for discriminating the relative proportion of seismic rates and the PDFs of the faulting mechanism in a region.

The rationale behind all these choices is explained below together with a more detailed description of the implementation.

Regionalization

TSUMAPS-NEAM will adopt the regionalization specifically realized for the project, which is presented in Figure 2.1.

A second, suitable regionalization could be instead obtained by extending the EU SHARE project (http://www.share-eu.org/) zonation to the whole TSUMAPS-NEAM source region. The SHARE regionalization was specifically designed for seismic hazard in Europe, so it does not include several offshore tectonic regions, particularly along the coasts of northern Africa and in the Black Sea (see, e.g., http://portal.share-eu.org:8080/opencms/opencms/share/model/Area-Source-Model.html).

The TSUMAPS-NEAM regionalization is a subdivision of the entire source space relevant for the NEAM region into as homogeneous as possible regions, based on the dominant tectonic process acting within them. Following basic principles of plate tectonics and building on previous experience of the SHARE project (Delavaud et al., 2012), the following eleven tectonic settings are defined:

1 Active volcanoes;
2 Back-arc and orogenic collapse;
3 Continental rift;
4 Oceanic rift;
5 Contractional wedge;
6 Accretionary wedge;
7 Conservative plate boundary;
8 Transform faults s.s.;
9 Shield;
10 Stable continental region;
11 Stable oceanic region.

Region type #1 is not considered and region type #9 is not encountered. See map on Figure 2.1 (top) for the distribution of the tectonic settings defined for the NEAM region, already presented in *Doc_P1_S1_Project_Summary*, Section 2.2.

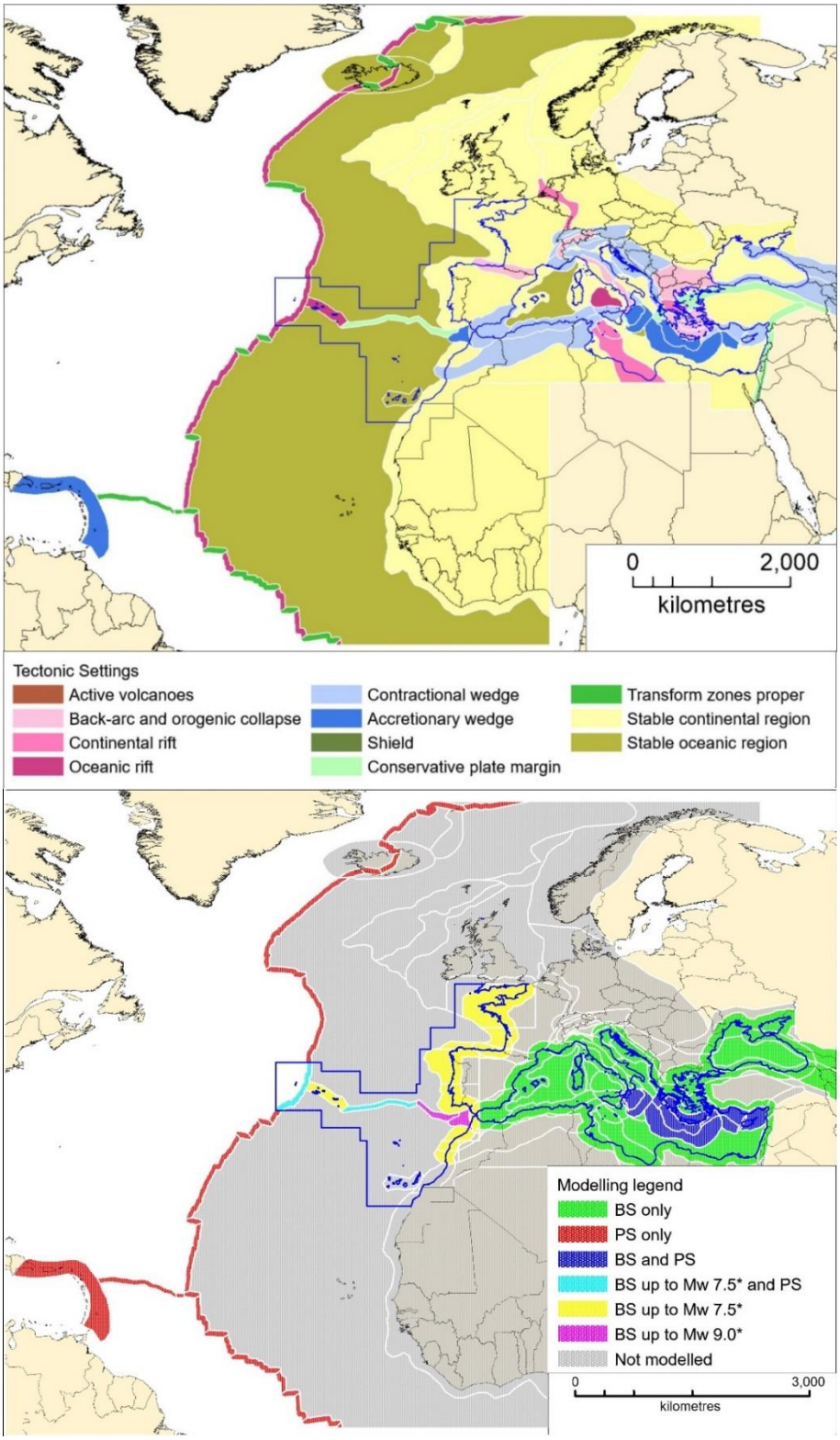

Figure 2.1 Map of the regions, colour coded depending on the tectonic setting (top) and colour coded depending on the modelling type (bottom) in the whole source area. The domain of Gaussian unit sources (blue outline) is also indicated in both maps. Asterisks '*' indicate that in some regions the computational cost of tsunami simulation imposes a hard threshold to the upper magnitude value that can be modelled, as explained in *Doc_P1_S1_Project_Summary* and later on in this document.

Seismic DBs

TSUMAPS-NEAM will adopt only one seismicity catalogue. This is obtained by merging two existing catalogues. After scrutiny of the time and geographic coverage of the largest and most authoritative catalogues available in the recent literature, we decided to adopt the ISC (ISC, 2014) catalogue for the area of the Atlantic Sea (time span 1900-2015) and the SHEEC-EMEC catalogue (Stucchi et al., 2012; Grünthal & Wahlström, 2012) for the area of the Mediterranean and connected seas (time span 1000-2006).

A statistical completeness analysis of these catalogues was performed by considering macro-regions, resulting from combinations of the individual regions in the regionalization (Figure 2.2). Other alternative seismicity catalogues will be used only for consistency checking, such as the catalogue for Mw≥7 recently compiled by NOA and the ISC-GEM historical catalogues (Storchak et al., 2013) for large magnitude earthquakes. If feasible, other sources of information will be collected.

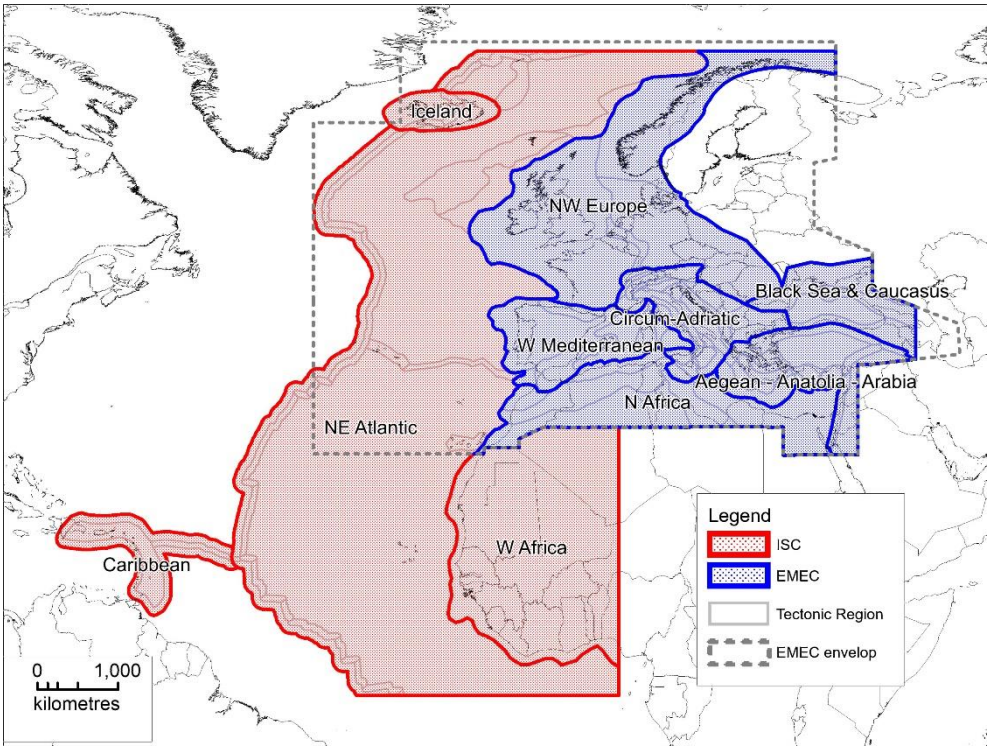

Figure 2.2. Map showing the regions used for the completeness analysis in relation with the adopted earthquake catalogues. Notice the outline of the availability of the EMEC catalogue.

TSUMAPS-NEAM will adopt only one catalogue of focal mechanisms. Considering the geographic coverage, we will adopt the global CMT catalogue (Dziewonski et al., 1981; Ekström et al., 2012) for the area of the Atlantic Sea and the RCMT catalogue (Pondrelli & Salimbeni, 2015) for the area of the Mediterranean and connected seas.

All these catalogues will be separated in two parts: PS-only and BS-only catalogues. This will be done by adopting two alternative procedures, by using two different cut-off distances of 5 and 10 km.

These two alternatives will affect all the levels of STEP 1 where data from these catalogues are used. In addition, this imposes that once a cut-off is selected at level 0, the alternatives at the following levels will be forced to be compatible (see discussion in Section 1.4, above).

We prefer to use this hard-threshold cut-off method over methods using a softer cut-off (e.g., a weighting function), for two main reasons: first, the definition of a weighting function would contain a weight-with-distance rule, which would add a further subjective choice; second, and more importantly, the Boolean separation induced by the cut-off distance allows for a smoother implementation of all models at the following levels, since it provides alternative but clearly separated catalogues of PS and BS events, instead of one single catalogue with uncertain attribution to PS/BS. The latter would have required the development of specific methods that we prefer to avoid, in order to reference (when possible) to standard and tested methodologies.

All the catalogues are also declustered adopting the Gardner and Knopoff (1974) method. The adoption of the declustered or not-declustered catalogue version will be commented in what follows at each implementation.

Fault catalogue and Predominant Seismicity (PS) selection

Fault catalogues are used as information source in combination with the CMT catalogue in two ways: for assigning the PDFs for the BS fault geometries (at sub-level BS-4 of Level BS-1, see Section 1.1.4); and for constraining the PS sources.

TSUMAPS-NEAM will adopt the European Database of Seismogenic Faults (EDSF; Basili et. al, 2013) compiled in the framework of the EU project SHARE. EDSF covers mainly the Mediterranean, the Gulf of Cadiz, and the southern part of the Black Sea. Outside these regions, i.e. most of the North Atlantic, we resorted to additional data and developed our own fault models. We used the plate boundary model by Bird (2003) as the starting reference for the Gloria fault and of the Mid Atlantic Ridge. We also used some additional information for some PS sources, such as Maesano et al. (2017) for the Calabrian Arc, and Hayes et al. (2012) for the Caribbean Arc.

According to our PS fault selection criteria (*Doc_P1_S1_Project_Summary*), we selected the following tectonic structures to be treated as PS (see also Figure 2.1):

- In the Mediterranean:
    - Calabrian Arc (subduction interface)
    - Hellenic Arc (subduction interface)
    - Cyprus Arc (subduction interface)
- In the Atlantic:
    - Gloria fault (crustal fault)
    - Mid-Atlantic Ridge (crustal faults)
    - Caribbean Subduction (subduction interface)

Project resources do not allow for considering further PS sources, such as for example the North Algerian thrust margin, neither allow for considering alternative descriptions of the selected sources. Selected PS faults are divided into the two classes (subduction interfaces / crustal faults) since the assignment of seismicity distribution between PS and BS will be treated slightly differently, as discussed later.

As said at the beginning of this Section, we prefer not to consider any alternative in the selection of PS faults. Provided that the knowledge of the modelled fault is good enough, its inclusion decreases potential significant biases in the hazard. Hence, rather than considering alternative sets of PS sources, we maximise their number.

Indeed, inclusion of one fault allows for considering much more information limiting the presence of modelled seismicity which is incompatible with the local geological and structural setting, given the sensitivity of tsunamis to the fault position, 3D fault geometry and mechanism.

Spurious sources may indeed alter the overall PSHA results (Selva et al., 2016, Selva et al., 2017). We have anyway performed some testing of the sensitivity of individual tsunami scenarios to these fault parameters (Basili et al., 2017), and to the modelling of heterogeneous slip distributions on 3D versus planar faults (Herrero et al., 2017).

Although we cannot maintain that we have a perfect knowledge of the faults that we treat as PS, adding alternative models for the fault geometry (e.g. varying the dip) would have an unaffordable computational cost for this project.

Nevertheless, we plan sensitivity tests on this issue, based on artificially reducing (or set to 0) the seismicity rate on selected PS sources. If allowed by the resources, we will also perform some further sensitivity analyses concerning how the PS geometry influences the PTHA (not only the individual tsunami scenarios). This should be anyway planned for any project update or follow up.

Convergence rate of Predominant Seismicity (PS)

In some alternative implementations described at Level 1 (next Section), to constrain the rate of activity of PS we will derive the moment rate from coupling (or seismic efficiency), rigidity (or shear modulus), fault area, and convergence rate for subduction or slip rate for other faults.

The area of each subduction zone is that of the nucleation polygon (see Sublevel PS 2). All parameters for subduction zones are derived from Davies et al. (2017) and Berryman et al. (2015). The parameters for the Gloria Fault are preliminary and those for the Mid Atlantic Ridge are yet to be defined. According to the values used for scaling laws at Levels 2a and 2b, rigidity is set to an average value of 30 GPa for subduction zones, and to 33 GPa for crustal faults (e.g. the Gloria fault) for consistency with the adopted fault scaling laws. Whether implementing depth-dependent rigidity models for subduction zones is under discussion.

2.1.2 Level 1 - Magnitude-frequency (MF) distribution

The PoE elicitation recommended alternatives for the quantification of the magnitude-frequency relation.

We describe in what follows all the implementations with their numerous alternatives occurring at Level 1.

We plan a total of 44 (8 Bayesian + 36) alternative implementations for quantifying epistemic uncertainty of MF distribution, especially on seismic rates and tails. Alternatives are planned for the shape of the distributions and their parameters, the sources of information for rates (geodetic vs seismicity), and the independence of PS and BS events.

We also plan sensitivity tests i) to check the consistency of Bayesian models with more classical MF estimation models, and ii) to quantify the probability of high magnitudes emerging from unbounded MF, for which conversely a geological limit imposed by the fault size is assumed and / or the tsunami propagation simulations would become unfeasible (modelling of a huge number of high magnitude earthquakes in the BS and their tsunamis).

Table 2.1. Tectonic data for modelling PS.

	Calabrian Arc	Hellenic Arc	Cyprus Arc	Caribbean Arc	Gloria Fault*
Nucleation area (km^2)	16008	87312	37243	TBD	17062
Convergence rate (mm/y)	1.75	10.00	6.77	11.00	4.00
b-value 1	0.70	0.70	0.70	0.70	0.70
b-value 2	0.95	0.95	0.95	0.95	0.95
b-value 3	1.20	1.20	1.20	1.20	1.20
Coupling 1	0.30	0.20	0.30	0.30	0.50
Coupling 2	0.50	0.60	0.50	0.50	0.75
Coupling 3	0.70	1.00	0.70	0.70	1.00
Mmax 1	7.60	8.00	7.70	8.00	8.30
Mmax 2	8.10	8.60	8.30	8.80	8.60
Mmax 3	9.00	9.10	9.00	9.60	8.80

* Preliminary values.

Magnitude discretization and range

As already mentioned in document *doc_P1_S1_Project_Summary*, we set M=6 as minimum tsunamigenic magnitude, meaning that in no case we model tsunamis generated by earthquakes of magnitude smaller than 6. Hence, we do not include these small magnitudes in the discretization scheme below. However, seismicity of earthquakes smaller than magnitude 6 in the catalogues contributes to the seismic rate quantification.

Magnitude discretization is performed according to Table 2.2 below. Actual intervals used for rate determination are those in the right-hand column. Tsunami modelling is performed once for each interval using the minimum value, which is the most probable (the mode) in the interval itself. In principle, if the intervals are narrow enough, these choices should not affect the results.

The sampling step gets (roughly exponentially) finer as earthquake magnitude increases; this should allow an approximately even sampling of the corresponding tsunami intensity increase, which should turn out to be approximately linear (e.g., Lorito et al., 2015).

Table 2.2. Magnitude discretization.

Nominal Magnitude	Interval represented
M_1: 6.0	[6.0000, 6.5000[
M_2: 6.5	[6.5000, 6.8012[
M_3: 6.8	[6.8012, 7.0737[
M_4: 7.1	[7.0737, 7.3203[
M_5: 7.3	[7.3203, 7.5435[
M_6: 7.5	[7.5435, 7.7453[
M_7: 7.7	[7.7453, 7.9280[
M_8: 7.9	[7.9280, 8.0933[
M_9: 8.1	[8.0933, 8.2429[
M_{10}: 8.2	[8.2429, 8.3782[
M_{11}: 8.4	[8.3782, 8.5007[
M_{12}: 8.5	[8.5007, 8.6115[
M_{13}: 8.6	[8.6115, 8.7118[
M_{14}: 8.7	[8.7118, 8.8025[
M_{15}: 8.8	[8.8025, 8.8846[
M_{16}: 8.9	[8.8846, 8.9588[
M_{17}: 8.95	[8.9588, 9.0260[
M_{18}: 9.0	[9.0260, ∞[

The maximum earthquake magnitude modelled for each BS and PS source has been chosen as follows (see also Figure 2.1).

- For all PS sources, the maximum earthquake allowed by the fault geometry and adopted scaling laws;
- for BS sources:
    - M=8.0933, corresponding to magnitude interval M_9, for the Mediterranean and connected seas;M=7.5435, corresponding to magnitude interval M_6, for all the Atlantic regions where BS has been modelled; except
    - M=9.0260, corresponding to magnitude interval M_{18}, for the Cadiz Gulf and SWIM zone.

The rationale for these limits are based on the MF global analogues proposed by Kagan et al. (2010). Most of the Mediterranean and Atlantic regions correspond to the “Active continent” and “Slow spreading ridges”, respectively, defined by Kagan et al. (2010). We thus adopt magnitude values beyond the corner magnitude obtained from the MF global estimates, which is where the rates of occurrence of higher magnitude decreases very rapidly. In the Cadiz Gulf and SWIM zone the maximum magnitude is higher because of the presence of several major faults not modelled as PS and because a subduction zone may also be present. As regards the Euro-Mediterranean region,

these magnitude values are also consistent with the annual rate decrease of the overall MF calculated by Woessner et al. (2015) for the PSHA of the project SHARE.

We thus assume that the annual rates of the higher magnitudes not modelled for tsunami propagation is negligible.

To test this, we will quantify the annual rate of all these magnitudes, as emerging from all the quantification models described below, in order to check that these values are actually negligible in terms of their influence on hazard.

Quantification of $\boldsymbol{\lambda_i^{(PS)}(M_j)}$ and $\boldsymbol{\lambda_i^{(BS)}(M_j)}$:

Two main alternatives are considered in quantifying the MF distributions for PS and BS in each region: either PS/BS distributions are quantified jointly, or independently.

For the joint PS/BS quantification, the MF distribution is quantified in two stages: in stage 1, a common MF for the region is quantified; in stage 2, the MF is split into PS and BS seismicity as a function of the magnitude (Selva et al. 2016), that is:

$$\begin{cases} \boldsymbol{\lambda_i^{(PS)}}(M_j) = \lambda_i(M_j)\,\Pr(PS|M_j, R_i) \\ \boldsymbol{\lambda_i^{(BS)}}(M_j) = \lambda_i(M_j)\,\Pr(BS|M_j, R_i), = \ \lambda_i(M_j)\left[1 - \Pr(PS|M_j R_i)\right] \end{cases}$$

where $\lambda_i(M_j)$ is the total mean annual rate of earthquakes within the region R_i having a magnitude within the interval range M_j, and $\Pr(PS|M_{j,Ri})$ represents the probability that a randomly selected event within region R_i and interval M_j belongs to the PS. Both these quantifications are based on a Bayesian formulation, with data coming from the non-declustered seismic catalogue.

For the quantification of $\lambda_i(M_j)$, we select the procedure based on the Bayesian formulation by Campbell (1982). This procedure was first suggested for the unbounded Gutenberg-Richter (GR) distribution and later refined by Keller et al. (2014) for the truncated GR distribution. The novelty of our work consists a) in extending the methodology of Keller et al. (2014) to any magnitude distribution and b) in the simultaneous estimation of all parameters. Following Keller et al. (2014), we include the temporal variability of the completeness period with magnitude, as proposed by Weichert (1980).

Both Truncated and Tapered Pareto functional forms will be considered as two alternatives. The prior distributions will be set as non-informative or slightly informative for λ_0 and Mmax/Mc (the upper limit for magnitude in the truncated Pareto and the corner magnitude of the tapered Pareto, respectively), considering all the known constraints (for example, maximum magnitude observed in the region).

Two further alternatives are planned for the parameter β (2/3 of the b-value), considering two informative priors based either on worldwide tectonic analogue estimations of Kagan et al. (2010) and a subjective "applicability index" of the worldwide analogue and the specific region, or forcing the b-value to 1. Sanity checks against more classical methods and independent databases are planned.

$\Pr(PS|M_j, R_i)$ is set as a function of magnitude, assuming that all high magnitude events must occur on PS, while events are randomly dispersed between PS and BS for low magnitudes (Selva et al. 2016). In particular, we set:

$$\Pr(PS|M_j, R_i) = \begin{cases} a(M_f) & \text{for } M \le M_f \\ a(M_f) + \left(1 - a(M_f)\right) f(M_j; M_f, M_u) & \text{for } M_f < M < M_u \\ 1 & \text{for } M \ge M_u \end{cases}$$

where M_u and M_f are the lower and upper magnitude limits for this transition, $a(M_f)$ represents the fraction of the total number of events being PS for magnitudes $M \le M_f$, and $f(M_j; M_f, M_u)$ represents a transition function. Here, we select a sigmoidal polynomial function $\mathrm{f}(M; M_f, M_u) = 3x^2 - 2x^3$ with $x = [M - M_f]/[M_u - M_f]$. Following this formulation, $\Pr(PS|M_j)$ depends on 3 parameters: M_u, M_f and a, that will be quantified as it follows separately in each region R_i.

For coherence with the MF model above, a Bayesian procedure is planned also for quantifying $\Pr(PS|M_j, R_i)$.

- For M_f, we plan to use a uniform distribution between magnitude 5 and 6.
- For M_u,, we plan to use a uniform distribution between 6 and 7 for PS relative to crustal faults, and between 7 and 8 for PS relative to subduction interfaces.
- For the parameter $a(M_f)$, we plan to set a non-informative prior (uniform between 0 and 1) updated by the measured fraction of PS events in the region in the seismicity catalogue. Given that at Level 0 we defined two alternative PS-only seismicity catalogues (different cut-off distances), two alternative implementations emerge for the fraction of PS events below magnitude M_f.

These choices produce a total of 2x4 = 8 Bayesian alternative implementations for the joint PS-BS quantification of the FM distribution, with 2 alternative shapes (tapered vs truncated Pareto), 2 b-values (from data or set to 1), and 2 PS fractions (from the different cut-off distances of Level 0). All of them are Bayesian, so that they automatically include the epistemic uncertainty emerging from parameter estimations.

For the separate PS-BS quantification, the FM distribution for PS is set as in Davies et al. (2016). This means that for constraining the rate of activity of PS we will use the classical formulation for seismic moment rate $\dot{m}_s$ as given by

$$\dot{m}_s = \chi \dot{m}_g = \chi \mu A \dot{D}$$

where $\dot{m}_g$ is the geologic moment rate, χ is a coefficient that determines how much of the geologic rate is converted into the seismic rate (so called coupling or seismic efficiency), μ is the rigidity or shear modulus, A is the fault area, and $\dot{D}$ is either convergence rate for subduction or slip rate for other faults. The area of each subduction zone is that of the nucleation polygon (see Sublevel PS 2).

Following Davies et al. (2016), and using the data reported in Table 2.1 at Level 0, we define several alternative implementations. They are: the average geodetic rate (from Berryman et al., 2015), 3 alternatives for maximum magnitudes, 3 alternative estimations for the b-value (0.7, 0.95 and 1.2) on all source zones, and 3 alternative estimations for the seismic coupling (from Berryman et al.,

2015 + coupling 0), resulting with a total of 3x3x4=36 alternatives. For BS, one of the models above is randomly sampled, independently from the PS model.

These models come with two main sensitivity tests, regarding the consistence with more classical methods. In addition, considering the upper limits in the magnitudes that may be simulated, the probability of non-simulated magnitudes will be quantified, reported and discussed, in the form of a sensitivity test.

2.1.3 Level 2a - Variability of earthquakes in Predominant Seismicity – PS

The PoE elicitation (document Doc_P1_S3_Elicitation) suggested alternatives or sensitivity tests for both sub-levels of this Level 2a (sublevels PS-2 and PS-3). Sublevel PS-2 deals with the spatial distribution of individual rupture scenarios along PS faults; sublevel PS-3 deals with slip distribution models.

We plan a total of 12 alternative implementations to explore the corresponding epistemic uncertainty. The alternatives arise from 6 different ways of distributing the seismicity on the PS sources, and from 2 alternative scaling laws. Sensitivity tests are planned for the definition of the stochastic slip distribution sampling size. Only one implementation is considered but with a variable number of asperities for each stochastic slip distribution (1 to 4 asperities), and a sensitivity test against uniform slip is performed.

We are presently also discussing (as already mentioned in *doc_P1_S1_Project_Summary*) how and whether implementing an alternative model with depth-dependent rigidity in subduction zones. This would perhaps mimic the possibility of enhanced slip towards the trench, as observed in some tsunami earthquakes and in some great megathrust earthquakes. Note that other peculiar types of tsunamigenic earthquakes, such as the outer-rise events, are allowed for occurring around the PS sources within the BS, even if they are not explicitly treated.

We first describe the discretization of the PS interfaces. Then we describe the planned implementations for both the *PS-2 and PS-3* sublevels of Level 2a.

Discretization of PS interfaces

PS faults are present only in a limited subset of regions, as reported in Figure 2.1. Note that PS coexists with BS in most of these regions, with the exception of the distant source regions, such as the Caribbean and most of the Mid-Atlantic Ridge.

3D triangular meshes have been built up for the subduction interfaces of the Hellenic, the Calabrian and the Cyprus arcs (Figure 2.3). The element size was set at about 16 km, resulting in meshes containing 3104, 1072 and 722 triangular elements, respectively. The models have been produced using the Cubit mesh generator (http://cubit.sandia.org).

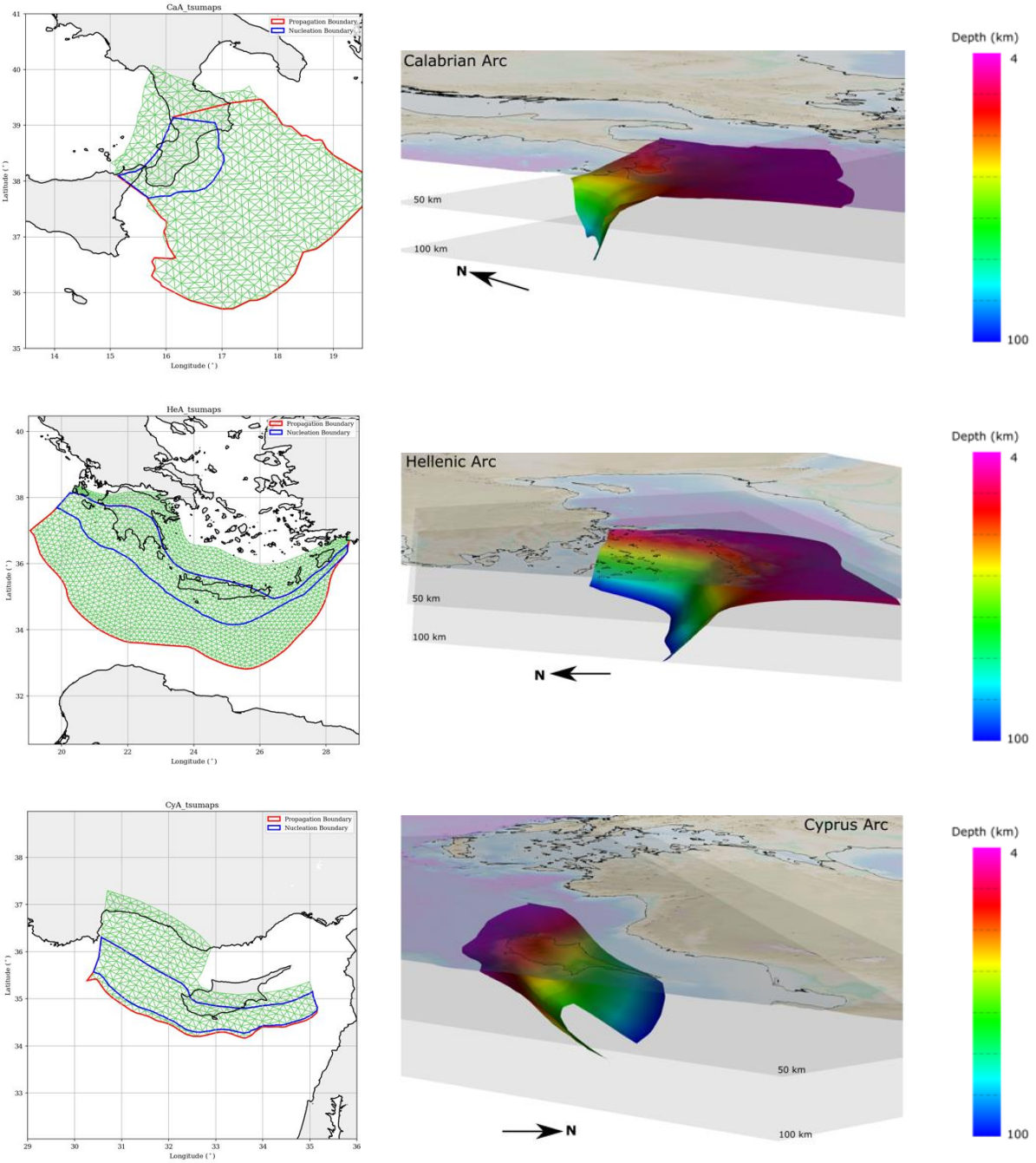

Figure 2.3 Map views of the meshes used to discretize the subduction interface in the Mediterranean region, from top to bottom (left panels) they are: Calabrian Arc, Hellenic Arc, and Cyprus Arc. The polygons which include the centres of rupture nucleation (blue) and the limits of rupture propagation (red) are also shown. 3D views of the subduction interfaces displayed with color-coded depths (right panels).

Following Selva et al. (2016) we use two alternatives for the seismogenic depth interval in the subduction zones treated as PS sources. The first alternative forces the whole earthquake slip to occur within the classic seismogenic depth interval, which we here name “nucleation zone” of each PS hosting fault. This is the zone likely dominated by unstable frictional sliding areas, mixed with relatively smaller areas of conditional stability (similar to the Domain B and C in Lay et al., 2012). The

second alternative allows for slip occurring into the “propagation zone”, the shallowest part of the PS hosting faults, where ruptures propagating updip from the nucleation zone can enter the otherwise aseismic zone due to dynamic frictional conditions controlled by sediments and fluids. The nucleation and propagation zones are those shown in Figure 2.3, enclosed by blue and red polylines, respectively.

Centres of potential earthquakes are defined inside the nucleation zone only, with the aim of uniformly covering the whole area (see Figure 2.3). Average distance between centres roughly corresponds to the size of the smallest considered earthquake with magnitude M=6.

The Mid Atlantic Ridge (Figure 2.4) was discretized into 270 rectangular subfaults; 214 of them with normal faulting mechanism, constant dip angle=45° and size 40x45 km; 56 with pure strike slip mechanism, constant dip angle=90° and size 55x20 km. The earthquake magnitude sampling can be honoured by combining a different number of subfaults (Table 2.3), since the subfault sizes are determined to make this possible according to the Leonard (2014) scaling laws.

The size of the subfaults is chosen in order to use one or more subfaults for spanning over the magnitude values of Table 2.1, starting from the minimum tsunamigenic magnitude defined for each PS zone.

For the Mid-Atlantic Ridge, earthquakes smaller than 7.3 have been tested to create negligible tsunamis along the POIs defined by TSUMAPS-NEAM along the NEAM coastlines. The only exception is where the Ridge is close enough to the POIs, such as the zone around the Azores Islands shown in close-up view in Figure 2.4, which also roughly corresponds to the cyan segment of the Mid-Atlantic Ridge in Figure 2.1. In these zone, the small PS zone earthquakes are modelled by combination of the Gaussian sources instead of using subfaults. The segment crossing Iceland will be treated in the same way.

The Gloria fault (Figure 2.5) is discretized in the same way as the Mid-Atlantic transform faults.

The discretization for the Caribbean subduction (Figure 2.6) uses the same principles, i.e. it is discretised with subfaults, but with the subfault size determined according the scaling laws for the subduction interface (Table 2.4). The magnitude range to be used for the Caribbean subduction is yet to be decided and will determine the actual discretization to be achieved that depends also on the minimum magnitude to be simulated.

Two alternative scaling laws will be adopted for the subduction interfaces treated as PS, that is those in Strasser et al. (2010) and in Murotani et al. (2013). Table 2.4 lists discretization of the relevant parameters for modelling the individual ruptures on subduction interfaces adopting the fault scaling law by Strasser et al. (2010). Figure 2.7 shows a comparison of the values listed in Table 2.4 with the values that would results by adopting other scaling laws.

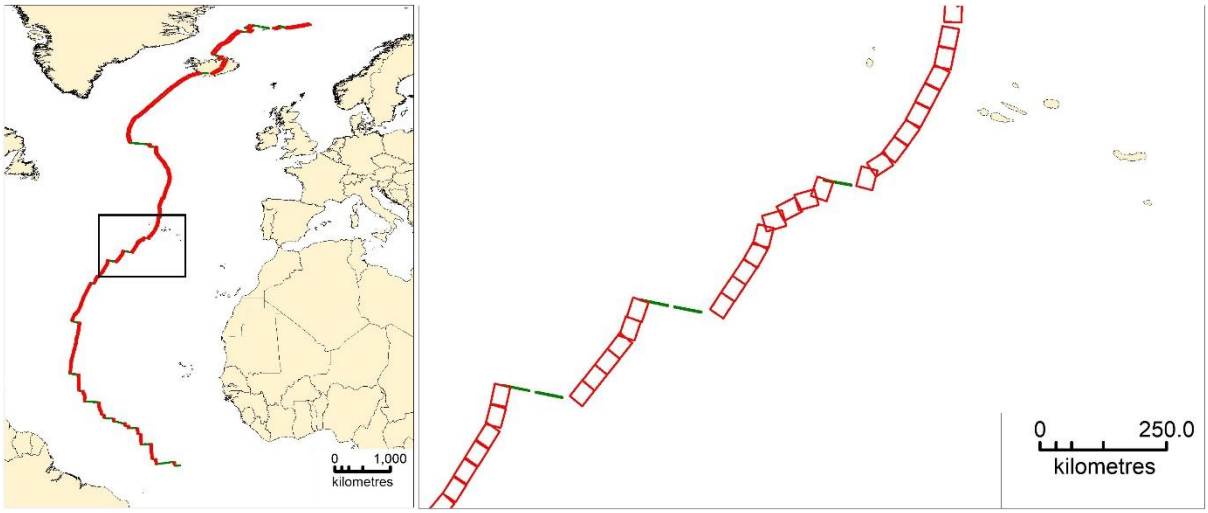

Figure 2.4 PS discretization of the Mid Atlantic Ridge (red = normal; green = transform). Right panel: distribution of all subfaults in the NEA; left panel: close-up view in the Azores (see right panel for location).

Table 2.3. Parameters of subfaults in the Mid-Atlantic Ridge zone.

A) Normal faults (spreading ridges): fixed patch size: L = 40, W = 45; total number of patches = 214

M_w	M_0 (Nm)	L (km)	W (km)	A (km^2)	D (m)	N. subfaults	L* (km)	A* (km)	ΔA (km^2)	D* (m)	ΔD (m)
7.3203	1.22E+20	70	30	2091	1.94	1	40	1800	-291	2.25	0.31
7.5435	2.63E+20	96	37	3495	2.51	2	80	3600	105	2.44	-0.07
7.7453	5.28E+20	127	44	5563	3.17	3	120	5400	-163	3.26	0.10
7.9280	9.93E+20	163	52	8472	3.91	5	200	9000	528	3.68	-0.23

B) Strike-slip faults (transforms): fixed patch size: L = 55, W = 20; total number of patches = 56

M_w	M_0 (Nm)	L (km)	W (km)	A (km^2)	D (m)	N. subfaults	L* (km)	A* (km)	ΔA (km^2)	D* (m)	ΔD (m)
7.3203	1.22E+20	112	19	2139	1.90	2	110	2200	61	1.84	-0.05
7.5435	2.63E+20	188	19	3577	2.45	3	165	3300	-277	2.66	0.21
7.7453	5.28E+20	299	19	5692	3.09	5	275	5500	-192	3.20	0.11
7.9280	9.93E+20	455	19	8670	3.82	8	440	8800	130	3.76	-0.06

* recalculated parameter after combining subfaults

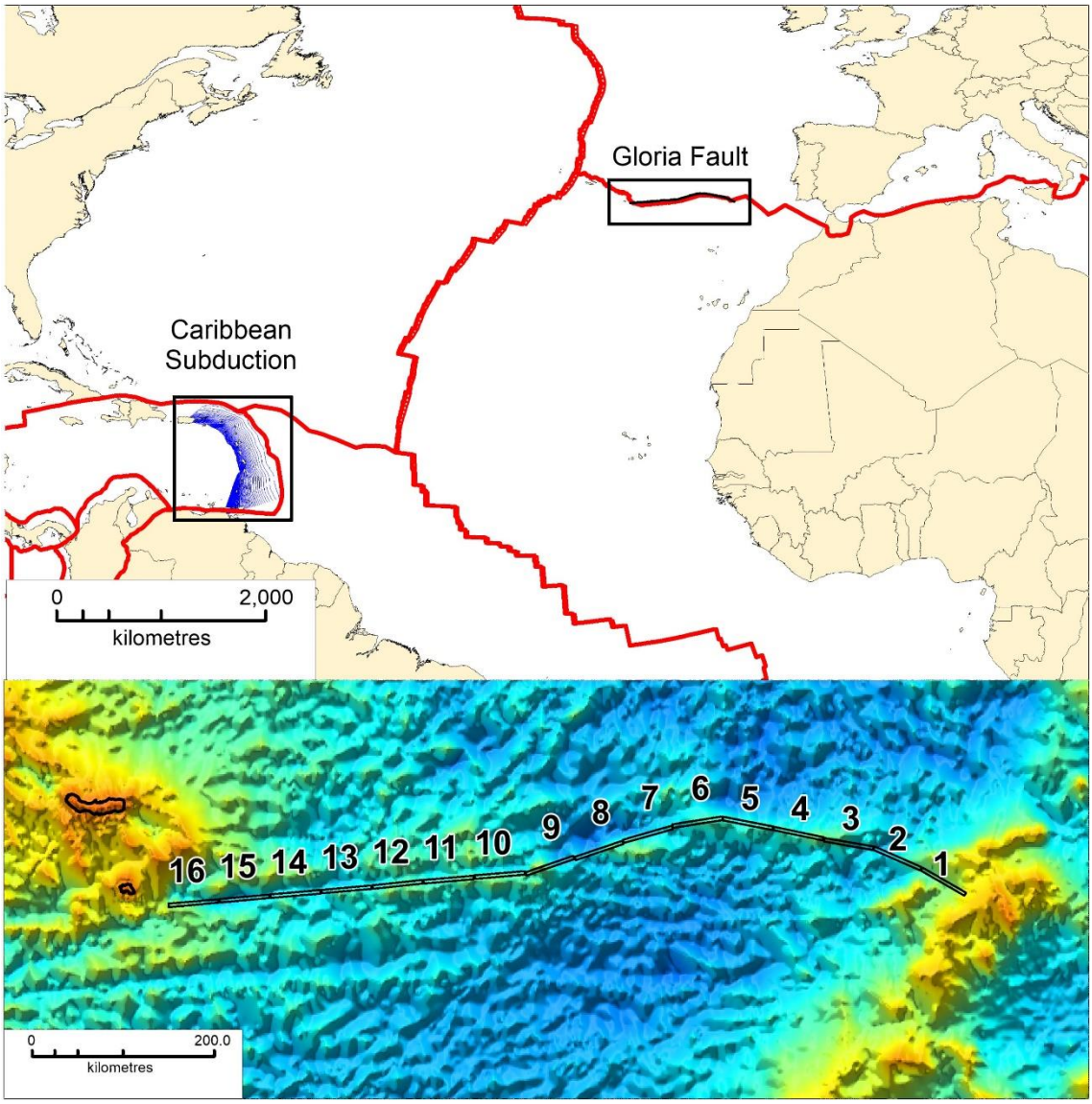

Figure 2.5 Discretization of the Gloria Fault in 16 subfaults (lower panel) whose parameters are shown in Table 2.3B. Location of the Gloria Fault (upper panel) in the Atlantic Sea context and the plate boundaries after Bird (2003).

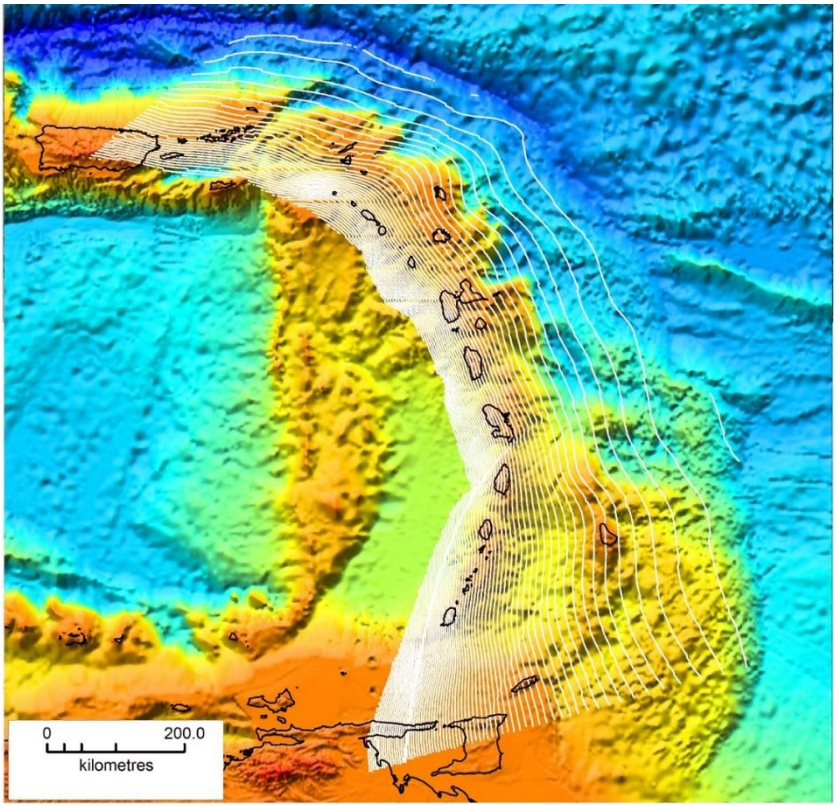

Figure 2.6 Map showing the subduction interface (white lines are contours starting at 5 km depth at the trench, with 5 km interval) from the Slab 1.0 model by Hayes et al (2012). Location shown in Figure 2.5.

Table 2.4. Slab Interface: predictions of L, W, and A by Strasser et al. (2010), as well as D derived from seismic moment and A adopting a rigidity of 33 GPa.

Mw	M_0 (Nm)	L (km)	W (km)	A (km^2)	D (m)
6.0000	1.27E+18	11	17	172	0.22
6.5000	7.16E+18	21	25	515	0.42
6.8012	2.03E+19	32	32	997	0.62
7.0737	5.19E+19	46	40	1812	0.87
7.3203	1.22E+20	64	49	3111	1.19
7.5435	2.63E+20	86	58	5075	1.57
7.7453	5.28E+20	113	69	7898	2.03
7.9280	9.93E+20	145	80	11788	2.55
8.0933	1.76E+21	181	91	16936	3.14
8.2429	2.95E+21	221	103	23509	3.80
8.3782	4.70E+21	266	114	31626	4.51
8.5007	7.18E+21	313	126	41368	5.26
8.6115	1.05E+22	364	138	52741	6.05
8.7118	1.49E+22	416	150	65710	6.86
8.8025	2.04E+22	470	161	80164	7.70
8.8846	2.70E+22	525	172	95971	8.54
8.9588	3.49E+22	581	183	112922	9.37
9.0260	4.41E+22	636	193	130843	10.20

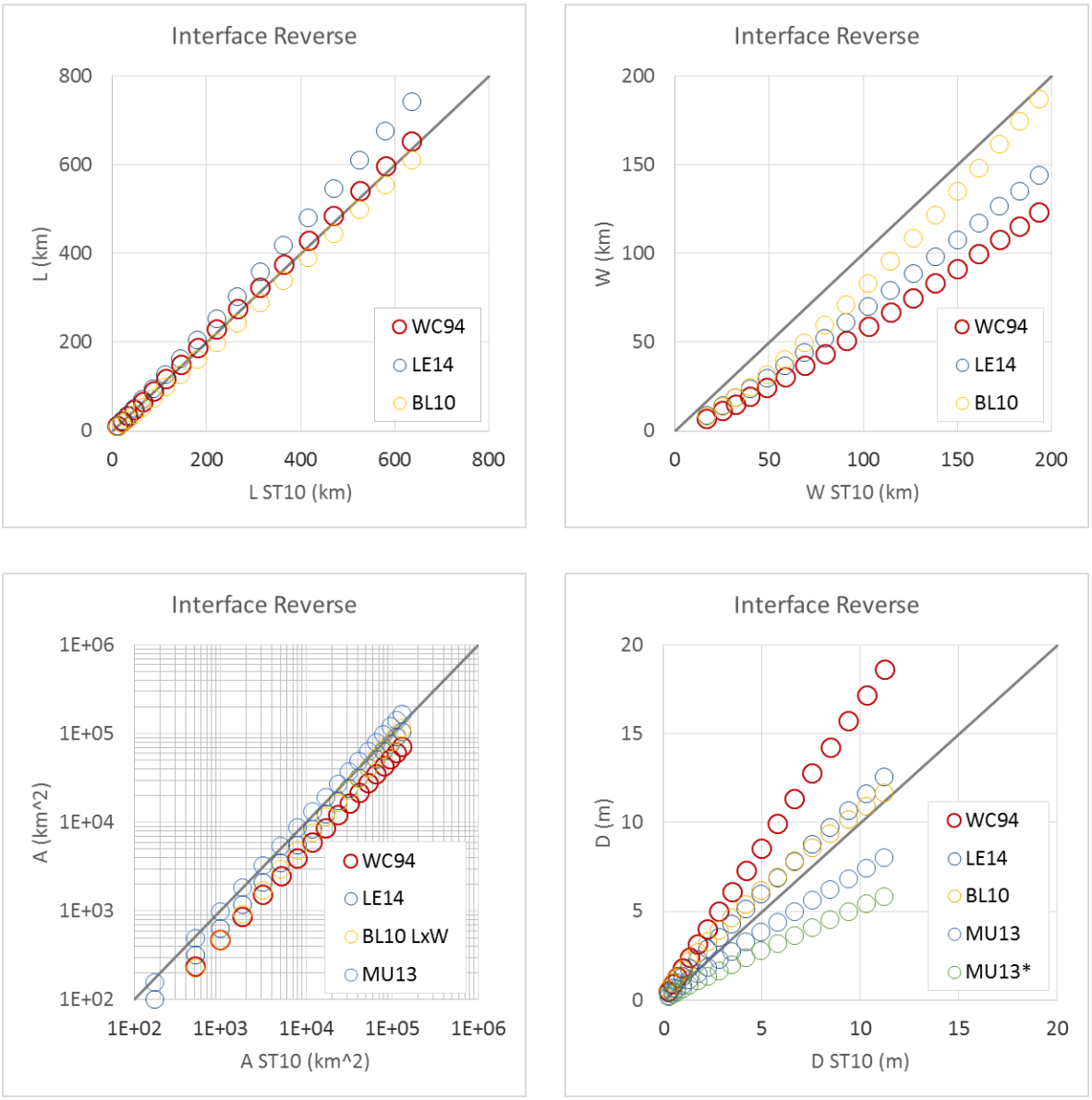

Figure 2.7. Comparison of relations by Strasser et al. (2010) (ST10) with relations by Wells and Coppersmith (1994) (WC94), Leonard (2014) (LE14), Blaser et al. (2010) (BL10), and Murotani et al. (2013) (MU13) in predicting fault length (L), width (W), area (A), and average displacement (D) in the case of dip-slip earthquakes on subduction interfaces for all Mw samples in Table 2.4. Displacement in MU13* is directly derived from the relationship, in all other cases it is derived from seismic moment, using an average shear modulus of 30 GPa and the area predicted by the relationship.

Sublevel PS-2

Quantification of: $\mathbf{Pr}_{\mathbf{i}}\,(x_c, y_c, A|M_j)$

The assessment consists of quantifying simultaneously position and size of the rupture area for each $\{x_c, y_c\}$ indicating the rupture centres.

For sublevel PS-2, the spatial distribution of events along the PS faults is modelled either uniformly, or it can vary along the strike proportional to the observed seismic rate. For the latter option, we will use an *ad hoc* procedure similar to the smoothed seismicity (for coherence with Level 2b – sublevel BS-2, described below). The declustered catalogue will be used, considering PS-only catalogue, as emerging from the 2 alternative cut-off distances considered at Level 0. This leads to 3 alternatives (uniform + 2 PS-only catalogues).

In all the cases, centres of ruptures are allowed only if the corresponding fault area A can be embedded into the boundaries of the PS hosting structure, that is, the distance from the edges should be larger or equal to $L/2$ laterally, and W/2 along dip, with L and W being the length and width provided by the scaling laws. From these latter relationships and for each magnitude bin the size of the mesh area actually involved in the rupture is also computed.

Two alternatives are considered in defining such boundaries, that is the "nucleation" and "propagation" zones defined above (in "***Discretization of PS interfaces***") for all PS sources. In both of the cases the centres however fall only inside the nucleation zone. However, when the model using both the nucleation and the propagation zones is used, the centres are allowed to lie closer to the shallow nucleation zone boundary, since more space is allowed updip for the rupture area. Rupture in the propagation zone is not assumed to contribute to the seismic moment balance, which is in both cases evaluated by considering only the nucleation zone area.

Since the two alternative scaling laws of Strasser et al. (2010) and Murotani et al. (2013) are used, the above procedure is repeated twice.

All these choices lead to 12 alternative implementations for computing $\Pr_{\mathrm{i}}(x_c, y_c | M_j)$.

Sublevel PS-3

Quantification of: $\boldsymbol{\Pr_i(\vec{s}\,|x_c y_c, A, M_j)}$

To build the heterogeneous slip on non-planar faults using the above-mentioned triangular mesh, the following scheme is implemented.

For each event defined by $\{x_c y_c, A\}$, the area A is iteratively covered extracting nearby cells starting from the geometric center and over this area a Probability Density Function (PDF) for the slip distribution is defined as the sum of a random number N of Gaussian functions, with $1 \leq N \leq 4$, such that the slip can represent either single or multiple asperities distributions.

Each Gaussian is defined by randomly extracting the position of the maximum from a uniform distribution and setting the standard deviation as one fifth of the square root of the rupture area, so that, when the centre is quite far from the edges the probability goes to zero well-within the rupture zone. When the centre of the Gaussian is closer to the edge, the slip has to be *a-posteriori* re-distributed accordingly with the imposed seismic moment.

Within the fault area, the slip value is assigned to each triangle using a hierarchical set of overlapping circular sub-events on the fault surface; the number of sub-events is a decreasing power-law of their radii as in the following law:

$$n(R) = pR^{-D-1}$$

R is defined in the interval $[R_{min}\ R_{max}]$ where R_{min} is fixed such that the circle covers at least five elements to ensure that the slip is everywhere well resolved by the mesh; R_{max} is fixed at 35% of the rupture width derived from the pre-computed magnitude and length. Only one asperity of maximum radius is placed, whereas the total number of cracks is fixed at 1000. D, the fractal dimension and it is set to 2 to ensure the self-similarity of the slip distributions (Herrero & Bernard, 1994), whereas the constant p is set accordingly to the moment, equal to the fractal dimension of the expected stress drop (Zheng *et al.*, 1994, Murphy *et al.*, 2016).

The precision of the circular asperities on the non-planar mesh is ensured by a double-lateration algorithm (Herrero & Murphy, SSA meeting, 2017; Herrero *et al.*, EGU meeting, 2017) derived from a multi-lateration scheme proposed by Novotni & Klein (2002). Finally, the slip distribution across the single sub-events is assigned by an Eshelby function (Eshelby, 1957; Ruiz *et al.* 2011), based on the above-described probability density function.

To mimic the smooth end of the seismogenic fault zone the centre of each single sub-event must lie at least at a distance from the edge larger than their radius. This constraint is released close to the shallower boundary: this may allow to model the shallow slip amplification due to the free surface effect. The algorithm is efficiently implemented in a Fortran code and produce a slip distribution approximately every ten seconds.

As discussed in Section 1 and in the document *doc_P1_S1_Project_Summary*, at this level we adopt a Monte-Carlo sampling procedure. The size of the sample will be defined at later stages, based on temporal feasibility and sensitivity tests. Additionally, this sampling will be limited to large magnitudes ($M > 7.5$ or $M > 8.0$, depending on the region) and to a subset of PS faults. Specific sensitivity tests will be implemented to support decisions.

As said, we are also considering the feasibility of another approach based on depth-dependent rigidity, and as a consequence a depth-dependence of slip. Heterogeneous stochastic slip on curved interfaces will be superimposed according to the average slip value.

As said at the beginning of this Section 2.1.3, only one implementation is considered but with a variable number of asperities for each stochastic slip distribution (1 to 4 asperities), and a sensitivity test against uniform slip is performed.

2.1.4 Level 2b - Variability of earthquakes in Background Seismicity – BS

The PoE elicitation (document Doc_P1_S3_Elicitation) did not recommend nor suggest alternatives for Level 2b and its sublevels.

We plan a total of 2 alternatives (with 1 Bayesian model for strike-dip-rake), exploring the epistemic uncertainty induced by BS catalogue definitions. These alternatives cannot be trimmed since they are inherited from Level 0. We do not plan any specific sensitivity tests at this level.

Since for BS we use uniform slip and the best guess for spatial dimensions from a single scaling law, we can foresee testing of this simplification in a future update of the assessment.

BS is present in most of the regions, as reported in Figure 2.1, bottom panel. The only exception is the distant source regions of the Atlantic (in red in Figure 2.1). In most of the cases, it is the only seismicity class present, and in some cases, it coexists with PS.

In the following we describe the planned implementations for both Level 2b sublevels BS-2 and BS-3.

Scaling laws for (crustal) BS sources.

As discussed in Section 1 and recalled above, fault size and average slip are set as the central value (mean) of the scaling laws and a uniform slip distribution on planar rectangular faults is assumed.

The adopted fault scaling law for the BS are those by Leonard (2014), which are based on the largest dataset of earthquake ruptures from around the world and, with respect to older scaling laws, allow for considering not only the faulting mechanism (dip slip and strike slip) but also the tectonic setting (interplate and stable continental regions). Note that these scaling laws are used also for the crustal faults treated as PS (Mid-Atlantic Ridge, Gloria fault).

Tables 2.5 and 2.6 show the earthquake magnitude sampling for crustal faults for interplate and stable continental regions (SCR), respectively. For each magnitude, the rupture area A is derived from scaling laws, and average slip <D> from the seismic moment, as $<D>=M_0/\mu A$, assuming a shear modulus μ=33 GPa.

Table 2.5. Interplate: predictions (rounded) of L, W, A, and D by Leonard (2014).

				Dip Slip				Strike Slip	
Mw	M_0 (Nm)	L (km)	W (km)	A (km^2)	D (m)	L (km)	W (km)	A (km^2)	D (m)
6.0000	1.27E+18	11	9	100	0.38	13	7	102	0.38
6.5000	7.16E+18	23	14	316	0.68	25	11	324	0.67
6.8012	2.03E+19	34	19	633	0.96	38	15	647	0.95
7.0737	5.19E+19	50	24	1185	1.31	64	19	1213	1.29
7.3203	1.22E+20	70	30	2091	1.74	112	19	2139	1.72
7.5435	2.63E+20	96	37	3495	2.25	188	19	3577	2.22
7.7453	5.28E+20	127	44	5563	2.84	299	19	5692	2.80
7.9280	9.93E+20	163	52	8472	3.50	455	19	8670	3.46

Table 2.6. SCR: predictions (rounded) of L, W, A, and D by Leonard (2014).

				Dip Slip				Strike Slip	
Mw	M_0 (Nm)	L (km)	W (km)	A (km^2)	D (m)	L (km)	W (km)	A (km^2)	D (m)
6.0000	1.27E+18	10	6	65	0.59	11	5	66	0.58
6.5000	7.16E+18	20	9	204	1.05	22	8	209	1.04
6.8012	2.03E+19	31	12	409	1.48	34	11	418	1.47
7.0737	5.19E+19	45	15	765	2.03	49	14	783	2.01
7.3203	1.22E+20	63	19	1350	2.69	76	17	1381	2.67
7.5435	2.63E+20	86	23	2257	3.48	127	20	2309	3.45
7.7453	5.28E+20	113	28	3592	4.39	202	20	3675	4.36
7.9280	9.93E+20	146	33	5470	5.42	308	20	5598	5.38

The comparison of the fault area and displacement predicted by Leonard (2014) in interplate setting and SCR setting (Figure 2.7) shows the importance of using different scaling laws in different tectonic settings. From Leonard (2014) it appears that faults in SCR are relatively smaller and have relatively higher average slip for any given earthquake magnitude.

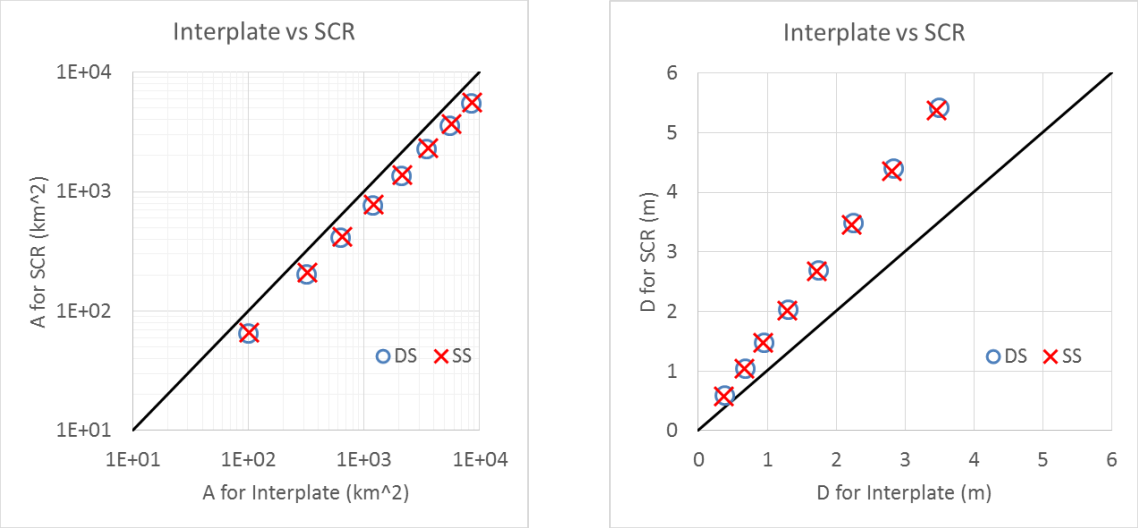

Figure 2.7. Predictions for fault area (A) and fault displacement (D) in the case of dip-slip (DS) and strike-slip (SS) earthquakes in interplate setting compared with those in stable continental region (SCR) setting using the relationship by Leonard (2014). The earthquake magnitude samples are as in Table 2.5 and Table 2.6.

Sub-level BS-2

Discretization: As shown in Section 2.2 of *Doc_P1_S1_Project_Summary*, the discretization of the spatial domain is based on a regular grid composed by non-conformal equal-area cells of 25x25 km. The centres of each grid points inside the regions in which BS is modelled represent the discretization for each region.

Quantification of $Pr_i(x, y)$:

A spatial smoothed seismicity model will be adopted, using the Nearest Neighbour (adaptive kernel) method. The declustered seismicity catalogue will be adopted, considering the BS-only catalogue, leading to the 2 alternatives arising from Level 0.

Sub-level BS-3

Discretization: The discretization of the depth domain is defined by considering different depth levels for the top of the fault. To achieve a good sampling of the volume in each cell, a different discretization of the depth is considered for each of the different magnitude levels Mj (Figure 2.8), that is:

M_1: 1.0, 3.53, 6.06, 8.59, 11.13, 13.66, 16.19, 18.72, 21.25 km
M_2: 1.0, 4.54, 8.08, 11.62, 15.15, 18.69 km
M_3: 1.0, 4.91, 8.81, 12.72, 16.63 km
M_4: 1.0, 5.44, 9.88, 14.32 km
M_5: 1.0, 6.4, 11.8 km
M_6: 1.0, 9.08 km
M_7: 1.0, 6.2 km
M_8: 1.0 km
M_9: 1.0 km

The discretization of the hypocentral depth depends on the earthquake's magnitude; we assume an average thickness of the seismogenic layer equal to 27 km.

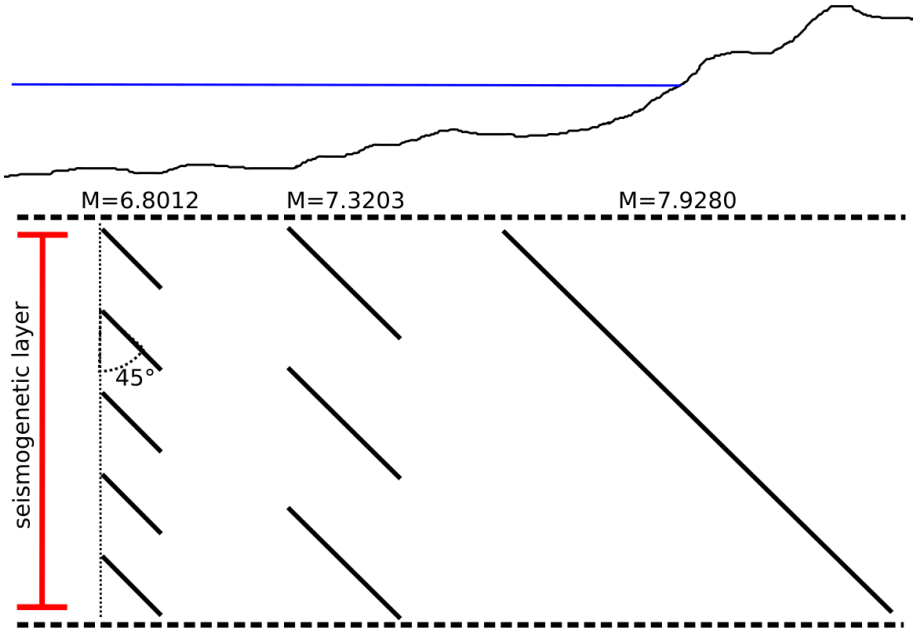

Figure 2.8 Scheme for the earthquake magnitude-dependent depth discretization for BS fault sources.

Quantification of $\underset{i}{\boldsymbol{Pr}}(\boldsymbol{d}|\boldsymbol{M_j}, \boldsymbol{x}, \boldsymbol{y})$ ***:*** A uniform distribution for depths is assumed.

Sub-level BS-3

Discretization: The discretization is made separately for strike, dip and rake. To manage the toroidal properties of angles, the strike and dip transformed as it follows:

$$S = \begin{cases} strike, strike < 180 \\ strike - 180, strike > 180 \end{cases}$$
$$D = \begin{cases} dip, \ strike < 180 \\ 180 - dip, strike > 180 \end{cases}$$

With this 1-1 reversible transformation, both strike and dip range between 0 and 180, and two sub-vertical fault planes with opposite strike and dip close to 90 will have equal S and close D values. Adopting this transformation, the following discretization is adopted:

- S: 22.5, 67.5, 112.5, 157.5 (each representing intervals of 45 degrees, starting from 0 up to 180)
- D: 10, 30, 50, 70, 90, 110, 130, 150, 170 (each representing 20 degree intervals around the central values, starting from 0 up to 180).
- Rake: -90, 0, 90, 180 (each representing 90 degree intervals around the central values)

This makes a total of 4x9x4=144 combinations.

Quantification of $\boldsymbol{Pr_i(strike, dip, rake|x, y)}$ ***:***

A Bayesian method similar to the one adopted in Selva et al. (2016) is implemented. In particular, in each region an informative prior model based on worldwide data is used that is updated with the focal mechanism catalogue available. We will consider the BS-only not declustered catalogue, and both focal planes are assumed equiprobable and included into the uncertainty quantification. The obtained regional posterior is then used as prior in each cell. If faults are present in the fault catalogue in each cell, this prior is combined to a strongly informative prior distribution based on local faults.

In all these assessments, the BS-only catalogues are considered as emerging from the 2 alternative cut-off distances considered at Level 0.

2.2 STEP2 - TSUNAMI GENERATION & MODELING IN DEEP WATER

The PoE elicitation (document Doc_P1_S3_Elicitation) did not recommend nor suggest alternatives for STEP 2 (question Q1).

Even if STEP 2 is not considered overall critical by the PoE, they pointed out that some Levels within the STEP contain some elements that are more critical than others. For example, at Level 0, the importance of the digital elevation model used for tsunami simulations has been pointed out. Similarly to other cases, repeating the tsunami simulations would be unaffordable though. Conversely, we focussed on implementing alternatives for STEPS that are considered overall more critical.

Implementation of all the levels of STEP 2 was already described in some details in document Doc_P1_S1_Project_Summary. We here add some further information on specific aspects.

Level 0 - Crustal model (elastic parameters, friction); Topo-Bathymetric datasets and digital elevation models

Crustal model: Poisson solid; elastically homogeneous crustal models.

Topo-bathymetry: SRTM30+, improved in the NE region with local data in Portugal, and in the Black Sea with SRTM15+ resampled at 30 arcsec. Both SRTM datasets are available at http://topex.ucsd.edu/WWW_html/srtm30_plus.html.

Level 1 - Coseismic displacement model

Sea-bottom co-seismic displacement associated to each scenario is computed for the BS sources and for the individual PS subfaults in the Atlantic Sea with an algorithm which solves for the static displacement due to a planar rectangular fault buried in a homogeneous Poisson's solid (Okada, 1992). A special version of this algorithm (Meade, 2007) has been used for the triangular subfaults forming the meshes for the 3D PS structures (Calabrian, Hellenic, and Cyprus Arcs).

Heterogeneous slip values are imparted to the triangles of the meshes to implement the slip distributions defined at STEP 1.

The vertical component of the displacement used as input for tsunami simulations is sampled at 30 arcsec, which is the spatial resolution of the grids used for tsunami modelling. Since Okada's analytical solution is prone to produce very long 'tails' of low-amplitude surface displacements, for practical reasons, we restrict the deformation area to vertical displacements larger than 1 cm.

Due to the extremely large number of simulated scenarios in TSUMAPS-NEAM, we do not consider any alternatives for this Level 1. Potential alternatives for this step could include, e.g., 1D layered crustal model or 3D FEM with realistic crustal structure (especially in the vicinity of the subduction zones).

Level 2 - Tsunami generation model

Since water column effectively acts as a low-pass filter when transferring sea-bottom displacements to the sea-surface, this effect also has to be modelled in order to obtain consistent initial conditions for the subsequent tsunami wave modelling.

As anticipated in *Doc_P1_S1_Project_Summary*, in order to account for the attenuation of the short wavelengths through the water column, we apply a two-dimensional filter of the form 1/cosh(kH) (Kajiura, 1963) to the static vertical seafloor deformation field calculated at Level 1. Here *k* is the wavenumber and *H* is the effective water depth taken as the average above the 4 fault corners. The filter is applied using a spatial 2D Fast Fourier Transform algorithm.

One possible alternative at this Level 2 could be a more sophisticated filtering algorithm by Nosov and Kolesov (2011) which is not restricted to the effective uniform depth but, instead, can be applied above arbitrary complex bathymetry. This algorithm, however, is much more time consuming, so we have no possibility to employ it within the limited time of the TSUMAPS-NEAM project.

Level 3 - Tsunami propagation (in deep water) model

In this Project we simulate around 50 000 000 tsunami propagation scenarios. To accomplish this task, we employ the approach of Green's functions. Two types of Green's functions are used: to model PS scenarios in the Atlantic Ocean we use the usual approach of virtual tsunamis pre-computed for a unit slip at buried elementary faults; whereas for the rest of scenarios (BS and PS) we use a new approach with Gaussian-shaped elementary sources distributed directly at the sea surface (Molinari et al., 2016). In both cases, virtual mareograms are precomputed and stored for all possible combinations of elementary sources and POIs.

We made some exceptions though, as already discussed in Section 2.2 of *Doc_P1_S1_Project_Summary*, to limit the computational cost associated with the whole project. These exceptions are based on geophysical constraints discussed at STEP 1 in this document (Section 2.1). We recall that they are: we didn't cover stable oceanic regions with Gaussians, assuming that the seismicity is low enough; for most of the Gaussians in the Atlantic, we didn't extend enough the computational domains to allow distant propagation of the magnitudes higher than 7.5, assuming that their probability is low out of the PS sources; for several PS sources, we didn't use small enough subfaults to simulate the lower magnitudes, assuming that the tsunamis associated with these

magnitudes would not significantly affect distant NEAM coastlines; for some PS sources in the Atlantic, we used subfaults instead of triangular meshes on a 3D geometry, assuming that detailed geometry of distant sources was less important; we considered everywhere M6 as the lowest tsunamigenic magnitude. As discussed at STEP 1 (Section 2.1), we plan to test the sensitivity of the hazard to some of these choices.

Final scenario mareograms are then assembled by linear combination of the virtual tsunami Green's functions using the weights calculated from the seismic source model. In the case of "slip Green's functions", these weights correspond to the scenario slip distribution, whereas in case of "Gaussian Green's functions", weights are directly computed from the initial sea surface deformation by 'filling' the initial wave profile with the Gaussians.

Pre-computed tsunami Green's functions were simulated in all cases with the Tsunami-HySEA non-linear shallow water (NLSW) GPU-optimised code (e.g., de la Asunción et al., 2013). The code has been benchmarked during several NTHMP (http://nws.weather.gov/nthmp/) benchmarking workshops. Some details of the simulation setup can be found in Molinari et al. (2016). In all cases the spatial resolution of the simulation grid is 30 arcsec; the time series are saved each 30 s. Open boundary and drying-wetting schemes at the coast are used as boundary conditions. The time-step is automatically adapted by Tsunami-HySEA to match the Courant–Friedrichs–Lewy (CFL) condition for the deepest point in the simulation grid. The duration of the simulations depends on the specific case. For the Gaussians: in the Mediterranean, 8 hours; in the Black Sea, 4 hours; in the Atlantic, 15 hours for the larger grid (SWIM source zone Gaussians, see *Doc_P1_S1_Project_Summary*), and 8 hours for the smaller grids (all the others); for individual sources simulated up to now, i.e. those on the Mid-Atlantic Ridge, 16 hours.

Scenario mareograms obtained by linear combinations exist at the POIs located offshore: at about 50 m depth. At STEP 3, offshore wave characteristics will be used for the estimation of the coastal hazard intensity metric. Our "offshore-to-onshore" transformation (see next STEP) requires an advanced set of wave parameters including wave maximum, dominant period and polarity. At the end of the present Level 2, we perform mareogram analysis to derive the necessary wave characteristics. This analysis has following steps (see also Figure 2.9):

1. find the tsunami first arrival (by variance analysis or threshold);
2. (optionally) restrict the time window to account for the 2-3 leading waves;
3. find the maximum wave amplitude and store the value (the maximum is the hazard intensity);
4. select a 2 hours' time window W centred around the maximum;
5. remove the high-frequency component of the signal by a robust LOWESS (locally weighted scatterplot smoothing; this roughly preserves the maximum);
6. find the neighbouring relative minima on the filtered waveform;
7. estimate the period of the signal from the time distance between these minima;
8. estimate the polarity of the leading wave from the trough-to-peak ratio (R), where the trough is the first relative minimum preceding in time the (positive) maximum; and the peak is the maximum itself; polarity is assumed negative if R>25%, positive otherwise.

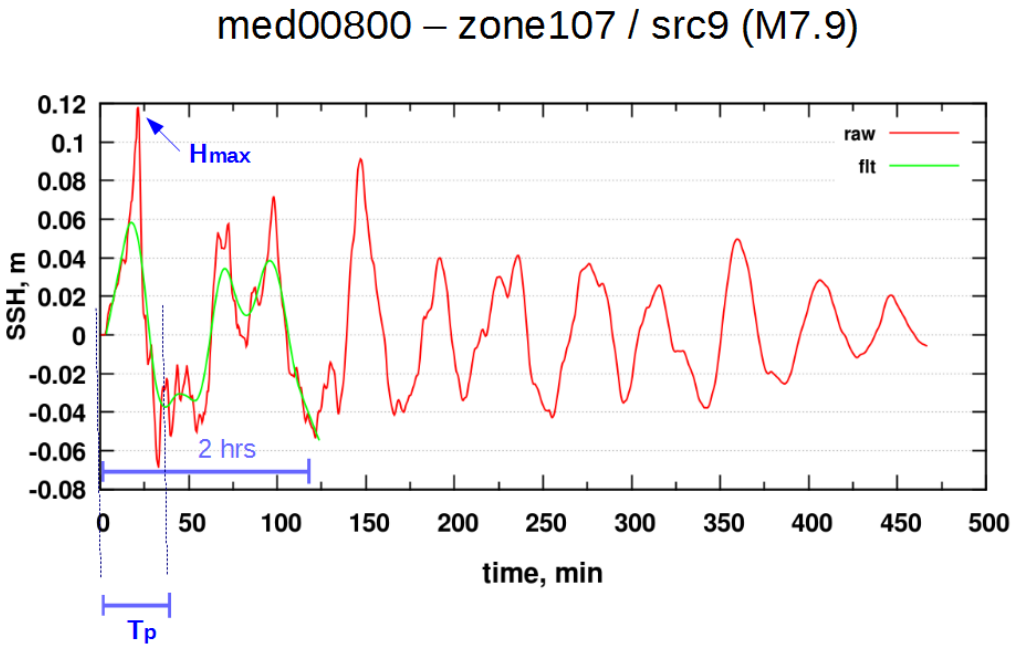

Figure 2.9 – Principles of the mareogram analysis for derivation of main wave characteristics required for the "offshore-to-onshore" transformation at STEP 3: maximum wave height, dominant wave period and polarity.

2.3 STEP 3 - SHOALING AND INUNDATION

The PoE elicitation (document Doc_P1_S3_Elicitation) recommended alternatives for STEP 3 (Question Q1).

For STEP 3 levels (question Q4), alternatives are recommended for:

- *Level 0: Topo-bathymetric datasets and digital elevation models;*
- *Level 1: Amplification and inundation model at the points of interest along the coast, and inland, corresponding to the offshore points of STEP 2;*
- *Level 3: Model the uncertainty on the tsunami metrics.*

Alternatives and sensitivity tests can instead be avoided for Level 2 (quantification of the probability for tidal stages at the points of interest).

We share the view of the PoE but unfortunately some of these alternatives are unaffordable within the project resources. We then devise a different strategy. As said in Section 2.3 of *Doc_P1_S1_Project_Summary*, along with the MIH, we will consider two alternative hazard metrics, i.e. the 'raw' offshore amplitudes at the offshore POIs, and the Green's law amplification. We will present the three types of results.

Considering that the scope of the assessment is regional, we don't need to address probabilities for local (high-resolution) inundation quantities. The above metrics are probably sufficient for regional screening of the coasts and for prioritization of local studies.

We will also estimate at this STEP the uncertainty associated with our amplification factors approach (Section 2.3 of *Doc_P1_S1_Project_Summary*).

A specific effort will be devoted to uncertainty communication to end-users.

Details of the Levels with alternatives are presented below.

Level 0: Topo-bathymetric datasets and digital elevation models

As for STEP 2, as topo-bathymetric model we use the SRTM30+ dataset improved in the NE region with local data, and in the Black Sea SRTM15+ resampled at 30 arcsec. Currently, we do not plan any alternative topo-bathymetric datasets due to the limited time and resources available to TSUMAPS-NEAM. At Level 1 of this STEP, offshore wave parameters derived at STEP 2 must be transferred into the tsunami intensity metric at the nearby coast.

As our main approach, we employ the method of local amplification factors. We then prepare here the database of coastal profiles and amplification factors as described in Section 2.3 of Doc_P1_S1_Project_Summary at all POIs, for different periods and polarities of the incident wave.

Level 1: Amplification and inundation model

The PoE elicitation (document Doc_P1_S3_Elicitation) did recommend alternatives for Level 1.

We define the Maximum Inundation Height (MIH) as our main hazard intensity metric at the coast. To estimate this metric from the offshore positions, here we employ the locally defined amplification factors obtained at Level 0. To convert the offshore quantities into MIH values, a table of pre-computed local amplification factors is used as a lookup table, according to the main wave characteristics derived at the end of STEP 2.

As an alternative metric of the coastal tsunami impact, we use Green's Law to extrapolate the maximum wave height values from 50 to 1 m depth in front of the coast.

We also provide offshore wave amplitudes as a reference.

Please note that these are not alternatives in the strict sense, since they are estimation of different tsunami metrics, not alternative approaches to the same metric approximation. Moreover, uncertainty estimation based on detailed inundation simulations presented in Section 2.3 of *Doc_P1_S1_Project_Summary* will be performed for MIH only.

Optional, inundation distance: Combine topography, empirical coastal dissipation factors, and maximum shoreline water elevation to compute a local inundation distance. Alternatively, produce maps by employing GIS inverse distance weighting extrapolation combining the above information with the STRM30+ topographical map. These possibilities are subject to consideration. Two main issues are foreseen: the difficulty of communicating the limitations inherent in such an approximated inundation distance estimation; and availability of project resources.

Level 2: Tidal stage model

The PoE elicitation (document Doc_P1_S3_Elicitation) did not recommend alternatives nor sensitivity tests for Level 2.

Tide model: we use the TPXO tool to predict tidal signal at corresponding POIs. We also calculate PDF's of the predicted tidal signal for corresponding POIs. Some details of the actual implementations have been reported in Section 2.4 of Doc_P1_S1_Project_Summary.

Level 3: Model the uncertainty on the tsunami metrics

The PoE elicitation (document Doc_P1_S3_Elicitation) recommended alternatives for Level 3 - Uncertainty modelling for tsunami hazard metrics (including uncertainties of modelling approximations from STEPS 1-3, and tides).

As discussed in the document Doc_P1_S1_Project_Summary (section 2.5.3) a new approach for dealing with the various sources of uncertainties is still under discussion in TSUMAPS-NEAM.

In alternative to this innovative approach, we plan to implement a method largely based on the log-normal sampling procedure described in Davies et al. (2016).

The results will also be tested against not including this uncertainty quantification as a sensitivity test to check the impact on the final results of choices about this level.

The details of the actual implementations of the selected models will be reported for the next review round. We also plan

2.4 STEP 4 - HAZARD AGGREGATION & UNCERTAINTY QUANTIFICATION

The PoE elicitation (document Doc_P1_S3) suggested alternatives or sensitivity tests for STEP 4 (question Q1).

For STEP 4 levels, alternatives or sensitivity tests are suggested for:

- *Level 0: Quantification of weights of the experts*
- *Level 2: Quantification of the weights of alternative models*

Alternatives and sensitivity tests can be avoided for all the other considered alternatives, that is, for the method for aggregating hazard results within each model (level 1) and for the method for integrating the alternative models into a single model (level 2).

For coherence with the other levels, the quantification of the weights of the alternative models should be considered at Level 0, instead of Level 2 as reported for the elicitation. This is also consistent with the fact that the weight values are used in the quantification of level 1. We stress that this inconsistency is only formal, and it has no impact on the results. Therefore, in the following we discuss the issue of models weights directly in Level 0.

The alternatives implemented at Levels 0 and 2 are described in what follows.

Level 0: Elicitation of experts, historical tsunami DB, paleotsunami DB

At Level 0, the PoE elicitation suggested alternatives or sensitivity tests for the quantification of weights of the experts and of models (question Q5).

In the elicitation process of PHASE 1, we weighted the experts in three different ways, that is, equal weights, performance-based weights and acknowledgement-based weights (see Doc_P1_S2 and Doc_P1_S3).

The second elicitation of the Panel of Experts (PoE) in PHASE 2 will be focused on quantifying the credibility of the different models through a weight.

In agreement with what we have done analysing the first round of elicitation of the PoE (see Doc_P1_S3), we plan to consider performance-based and acknowledgement-based weights as 2 alternative weighting schemes for experts also for the second elicitation. As a sensitivity test, we will also check the consistency of the results against the equal weights assumption.

As in PHASE 1, the elicitation will be based on a structured questionnaire provided to the TSUMAPS-NEAM Pool of Experts (PoE). The same elicitation scheme will be performed at all the levels of all the STEPs for which alternatives are available, including STEP 4 alternatives (also at this level 0).

The quantification will be based on an Analytical Hierarchical Process (AHP) procedure (Saaty 1980), which is the same method adopted in PHASE 1 (pre-assessment) – STAGE 3, as described in details in *DOC_P1_S3_Elicitation*. However, a slightly more sophisticated approach will be probably adopted in PHASE 2. In particular, the plan is to implement AHP adopting multiple criteria (yet to be defined in details), instead of using just one single criterion (personal preference) as in PHASE 1.

The model weights will be quantified directly considering the normalized scores in output from the AHP analysis of the answers of the experts. Given that 2 alternative expert weights will be implemented, we will have also two alternative quantifications of model weights.

If it will be judged feasible within TSUMAPS-NEAM, an additional quantification method will be adopted. In particular, a second quantification method can be considered by combining the expert judgements with other quantitative criteria, again adopting the AHP method. Different potential quantitative criteria may be defined, as for example the performance of models in sanity-checks, statistical tests, etc. In case, several options will be considered, leading to at least to 2 alternative methods for quantifying the weights of the alternative models. Considering the 2 alternative weights for experts and these 2 alternative procedures to quantify the weights of the models, we will reach a total of at least 4 alternative quantifications of models' weights.

This expert elicitation will be fully documented for the next review round.

As for the tsunamis datasets, we will consider the ASTARTE paleotsunami catalogue (Deliverable D2.44, http://www.astarte-project.eu/) and the Euro-Mediterranean Tsunami Catalogue, (Maramai et al. 2014). If other relevant databases will be made available, they will be considered as well.

Level 1 (combination of STEPS from 1-3)

At Level 1, the PoE elicitation did not recommend nor suggest alternatives for level 1 (question Q5).

As a consequence, we did not plan alternative, nor did sensitivity tests.

The quantification of $\lambda_{mn}(\geq H_k; POI, \Delta T)$ in each POI (as defined in STEP 2) at all the discrete tsunami intensity value H_k (as defined in STEP 3) should be in theory repeated for all the combinations of potential alternative models of STEPs 1 to 3 (identified by the indexes *m* and *n*).

Given the large number of considered alternatives. To reduce the computational effort, a Monte Carlo sampling procedure is here adopted (similarly to Selva et al., 2016). At each STEP and level, potential alternatives are sampled proportionally to their weights (the larger the weight, the higher the chance to sample for the corresponding model). Models weights emerge from Level 0. The sampling process starts from sampling the sets of weights to be used, among the alternatives

quantifications considered at STEP 4 Level 0. The corresponding set of weights will be then used for sampling the weights at all the Levels of STEPs 1 to 3.

In doing this, potential incompatibility among models will be accounted for. For example, if a 5 km cut-off for the PS/BS-only catalogue is sampled at one level, for coherence only this option should be considered in all the following levels. To allow for that, weights are sampled starting from STEP 1 – Level 1 through STEP 3 – Level 3, running first levels and then STEPs. At each sampling, only the alternative implementations which are compatible with the already sampled models will be considered, with weights re-normalized to 1. Once one model is sampled at all levels and STEPs, they are combined as in Selva et al. (2016), to produce one sample of hazard curves in each target point.

The described procedure will be performed at least 1000 times, in order to have a reasonable quantification of 16th and 84th percentiles of the epistemic uncertainty.

Level 2: Quantification of uncertainty

At Level 2, the PoE did not suggest alternative implementations nor sensitivity tests for the model for integrating the alternative models into a single ensemble model (alternative models' weights are considered at Level 0, instead of here).

As a consequence, we do not plan alternatives. Nevertheless, we plan a sensitivity test to check the unimodality of the community ensemble distribution.

The transformation of mean the annual rates $\underset{mn}{\lambda}(\geq H_k; POI, \Delta T)$ in probability will be performed by assuming a Poisson process. Given that the size of the sample of alternative models is rather large (1000 samples), we plan to produce the ensemble distribution as the empirical distribution emerging from the sample.

However, we plan to test the potential non unimodality of this distribution, in order to highlight choices that may potential lead to a separation in families of hazard curves. If distributions significantly multimodal are found, we plan to investigate which are the main alternatives that cause such separations.

The ensemble distribution will be evaluated at discrete levels of tsunami intensity, as well as, considering limits in probability values. Also, maps will be produced at predefined hazard levels, probability levels and percentiles of the epistemic uncertainty. Note that some preliminary decisions about this discretization have been reported in Section 2.5.5 of *Doc_P1_S1_Project_Summary*.

Level 3: Comparison/test with tsunami records; disaggregation

Level 3 deals with secondary results of the assessment. For this reason, it was not originally planned and thus not included into the elicitation of PHASE 1. As for level 1, we did not plan alternatives, nor sensitivity tests at this level.

For testing the results against the available tsunami records, the "community distribution" (e.g. SSHAC 1997; see also Doc_P1_S3_Elicitation) is compared with historical and paleotsunami data, in locations where enough data are available. The comparison consists of checking the compatibility of hazard curves with the observed frequency of exceedance of predefined hazard levels. An example of this comparison is reported in figure 2.10, in which we show two example of comparison, with incompatible and incompatible results (modified from ASTARTE D8.39).

Disaggregation analyses will be also performed in several key POIs. Disaggregation against magnitudes and regions are foreseen (e.g., like in Selva et al., 2016). The details of disaggregation within TSUMAPS are still under discussion, since they depend on the availability of resources.

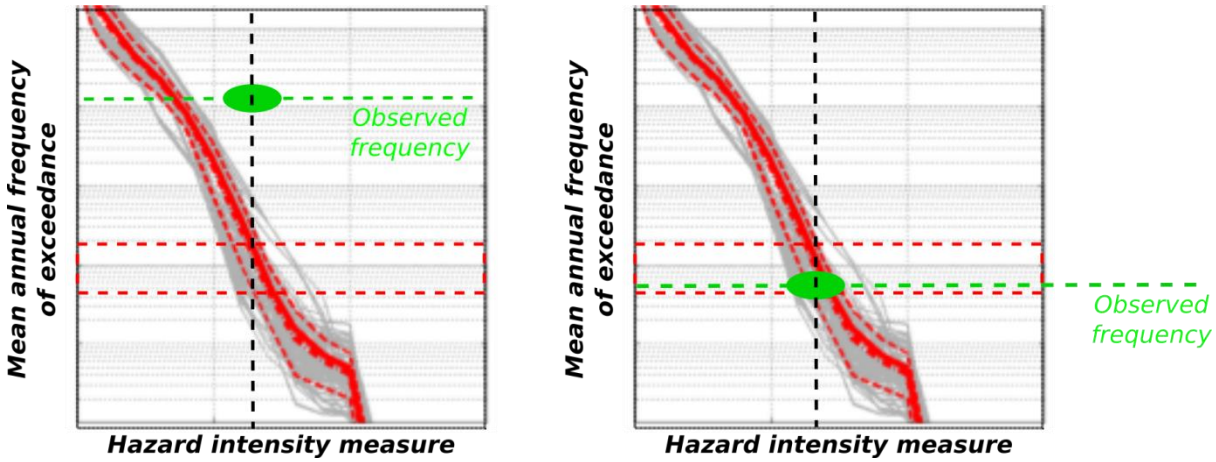

Figure 2.10: comparison scheme between the hazard curve and its epistemic uncertainty (red lines) and the observation from historical or paleotsunami records, modified from ASTARTE D8.39). Given one hazard intensity level (black dashed line), the observed frequency is computed by counting the number of non-overlapping ΔT in the past with exceedance of a given hazard threshold, divided by the total number of ΔT for which the information (exceedance / non exceedance) exists. The observation dots are plotted considering the potentially large uncertainty in measuring MIH in past observation over rather large areas. The acceptability bounds (horizontal red dashed lines) are set considering both the epistemic uncertainty on the hazard curves (red dotted lines) for the same intensity level of the observation point.

References

Basili R., Kastelic V., Demircioglu M. B., Garcia Moreno D., Nemser E. S., Petricca P., Sboras S. P., Besana-Ostman G. M., Cabral J., Camelbeeck T., Caputo R., Danciu L., Domac H., Fonseca J., García-Mayordomo J., Giardini D., Glavatovic B., Gulen L., Ince Y., Pavlides S., Sesetyan K., Tarabusi G., Tiberti M. M., Utkucu M., Valensise G., Vanneste K., Vilanova S., Wössner J. (2013). The European Database of Seismogenic Faults (EDSF) compiled in the framework of the Project SHARE. *http://diss.rm.ingv.it/share-edsf/*, doi: 10.6092/INGV.IT-SHARE-EDSF.

Basili R, Volpe M, Maesano FE, Tiberti MM, Lorito S, Romano F, Tonini R (2017). Influence of seismogenic source geometrical accuracy on PTHA: a test case for the Calabrian subduction interface, Geophysical Research Abstracts, Vol. 19, EGU2017-18872-1, EGU General Assembly 2017.

Berryman K., Wallace L., Hayes G., Bird P., Wang K., Basili R., Lay T., Pagani M., Stein R., Sagiya T., Rubin C., Barreintos S., Kreemer C., Litchfield N., Stirling M., Gledhill K., Haller K., Costa C. (2015). The GEM Faulted Earth Subduction Interface Characterisation Project, Version 2.0, April 2015, GEM Faulted Earth Project, available from http://www.nexus.globalquakemodel.org/gem-faulted-earth/posts.

Bird, P. (2003) An updated digital model of plate boundaries, Geochem Geophys Geosys 4(3), 1027, doi:10.1029/2001GC000252.

Blaser, L., Krüger, F., Ohrnberger, M., Scherbaum, F., 2010. Scaling relations of earthquake source parameter estimates with special focus on subduction environment. Bulletin of the Seismological Society of America 100, 2914-2926, doi: 10.1785/0120100111.

Bommer JJ (2012). Challenges of Building Logic Trees for Probabilistic Seismic Hazard Analysis, EARTHQUAKE SPECTRA, Vol: 28, 1723-1735, ISSN: 8755-2930.

Davies G, Griffin J, Løvholt F, Glymsdal S, Harbitz C, Thio HK, Lorito S, Basili R, Selva J, Geist E, Baptista MA (2017). A global probabilistic tsunami hazard assessment from earthquake sources. From: Scourse, E. M., Chapman, N. A., Tappin, D. R. & Wallis, S. R. (eds) Tsunamis: Geology, Hazards and Risks. Geological Society, London, Special Publications, 456, https://doi.org/10.1144/SP456.5.

de la Asunción, M., Castro, M. J., Fernández-Nieto, E. D., Man- tas, J. M., Ortega Acosta, S., and González Vida, J. M.: Efficient GPU implementation of a two waves TVD-WAF method for the two-dimensional one layer shallow water system on structured meshes, Comput. Fluids, 80, 441–452, 2013.

Delavaud E., Cotton F., Akkar S., Scherbaum F., Danciu L., Beauval C., Drouet S., Douglas J., Basili R., Sandikkaya M., Segou M., Faccioli E., Theodoulidis N. (2012). Toward a ground-motion logic tree for probabilistic seismic hazard assessment in Europe. Journal of Seismology, 16(3), 451-473, doi: 10.1007/s10950-012-9281-z.

Dziewonski, A.M., T.A. Chou, and J.H. Woodhouse (1981). Determination of earthquake source parameters from waveform data for studies of global and regional seismicity, Journal of Geophysical Research, 86(B4), 2825, doi: 10.1029/JB086iB04p02825.

Ekström, G., M. Nettles, and A.M. Dziewoński (2012). The global CMT project 2004–2010: Centroid-moment tensors for 13,017 earthquakes, Physics of the Earth and Planetary Interiors, 200-201, 1-9, doi:10.1016/j.pepi.2012.04.002.Geist, E. & Parsons, T., 2006. Probabilistic analysis of tsunami hazards, *Nat. Hazards,* 37, 277–314.

Eshelby, J. The determination of the elastic field of an ellipsoidal inclusion and related problems. Proc. Roy. Soc. London, Series A 241, 376–396. doi: 10.1098/rspa.1957.0133 (1957).

Grünthal G. and R. Wahlström (2012). The European-Mediterranean Earthquake Catalogue (EMEC) for the last millennium. Journal of Seismology, 16, 535-570, doi 10.1007/s10950-012-9302-y.

Hanks, T.C., Bakun, W.H., 2008. M-logA Observations for Recent Large Earthquakes. Bulletin of the Seismological Society of America 98, 490-494, doi: 10.1785/0120070174.

Hayes, G. P., Wald, D. J. & Johnson, R. L. (2012) Slab1.0: A three-dimensional model of global subduction zone geometries. Journal of Geophysical Research: Solid Earth 117, n/a-n/a, doi: 10.1029/2011jb008524.

Herrero, A. & Bernard, P. A Kinematic Self-Similar Rupture Process for Earthquakes. Bull. Seismol. Soc. Am. 84(No. 4), 1216–1228 (1994).

Herrero A., Murphy S., Complex slip distributions on complex fault geometries. SSA meeting, Denver 17-21 april. (2017).

Herrero A, Murphy S, Lorito S, Romano F, Volpe M (2017). The influence of complex fault geometry and slip of large subduction earthquakes on tsunami generation, Geophysical Research Abstracts Vol. 19, EGU2017-14724-1, EGU General Assembly 2017.

ISC - International Seismological Centre (2014), On-line Bulletin, http://www.isc.ac.uk, Internatl. Seismol. Cent., Thatcham, United Kingdom.

Kagan, Y.Y., Bird, P., Jackson, D.D. (2010) Earthquake Patterns in Diverse Tectonic Zones of the Globe, Pure Appl. Geophys., 167(6), 721-741, doi:10.1007/s00024-010-0075-3.

Keller M., Pasanisi A., Marcilhac M., Yalamas T., Secanell R., and Senfaute G. (2014), A Bayesian Methodology Applied to the Estimation of Earthquake Recurrence Parameters for Seismic Hazard Assessment, Qual. Reliab. Engng. Int., 30, 921–933, doi: 10.1002/qre.1735

Kajiura, K. (1963). The leading wave of a tsunami, Bull. Earthquake Res. Inst. Univ., Tokyo, 41, 535–571.

Lay, T., Kanamori, H., Ammon, C.J., Koper, K.D., Hutko, A.R., Ye, L., Yue, H., Rushing, T.M., 2012. Depth-varying rupture properties of subduction zone megathrust faults. J. Geophys. Res. 117, B04311. http://dx.doi.org/10.1029/2011JB009133.

Leonard, M., 2014. Self-Consistent Earthquake Fault-Scaling Relations: Update and Extension to Stable Continental Strike-Slip Faults. Bulletin of the Seismological Society of America, doi: 10.1785/0120140087.

Lorito, S.,Selva J., Basili R., Romano, F., Tiberti, M. M.,and Piatanesi, A (2015). Probabilistic Hazard for Seismically-Induced Tsunamis: Accuracy and Feasibility of Inundation Maps, Geophys. J. Int., 200, 574–588.

Maramai A., Brizuela B., Graziani L. (2014). The Euro-Mediterranean Tsunami Catalogue, Annals of Geophysics, 57, 4, S0435; doi:10.4401/ag-6437.

Maesano F.E., Tiberti M.M., Basili R., (2017). The Calabrian Arc: three-dimensional modelling of the subduction interface. Sci. Rep., under review.

Marzocchi, W., Taroni, M., Selva, J., 2015. Accounting for epistemic uncertainty in PSHA: logic tree and ensemble modeling. Bulletin of the Seismological Society of America, 105(4), 2151-2159.

Meade, B. J. (2007), Algorithms for the calculation of exact displacements, strains, and stresses for triangular dislocation elements in a uniform elastic half space, Comput. Geosci., 33, 1064–1075, doi:10.1016/j.cageo.2006.12.00.

Molinari I, Tonini R, Lorito S, Piatanesi A, Romano F, Melini D, Hoechner A, Gonzàlez Vida JM, Maciás J, Castro MJ, de la Asunción M (2016). Fast evaluation of tsunami scenarios: uncertainty assessment for a Mediterranean Sea database, Nat. Hazards Earth Syst. Sci., 16, 2593-2602, doi: 10.5194/nhess16-2593-2016.

Murotani, S., Miyake, H., Koketsu, K., 2008. Scaling of characterized slip models for plate-boundary earthquakes. Earth Planets Space 60, 987-991, doi.

Murotani, S., Satake, K., Fujii, Y., 2013. Scaling relations of seismic moment, rupture area, average slip, and asperity size forM~9 subduction-zone earthquakes. Geophysical Research Letters 40, 5070-5074, doi: 10.1002/grl.50976.

Murphy, S. et al. Shallow slip amplification and enhanced tsunami hazard unravelled by dynamic simulations of mega-thrust earthquakes. Sci. Rep. 6, 35007; doi: 10.1038/srep35007 (2016).

Nosov, M.A. & Kolesov, S.V. (2011). Optimal Initial Conditions for Simulation of Seismotectonic Tsunamis, Pure Appl. Geophys. 168: 1223, doi: 10.1007/s00024-010-0226-6.

Novotni, M. & Klein, R. Computing geodesic distances on triangular meshes. The 10-th International Conference in Central Europe on Computer Graphics, Visualization and Computer Vision 2002 (WSCG 2002).

Okada, Y. (1992). Internal deformation due to shear and tensile faults in a half-space, Bull. Seismol. Soc. Am., 82, 1018–1040.

Pondrelli S. and Salimbeni S. (2015). Regional Moment Tensor Review: An Example from the European Mediterranean Region. In Encyclopedia of Earthquake Engineering (pp. 1-15), http://link.springer.com/referenceworkentry/10.1007/978-3-642-36197-5_301-1, Springer Berlin Heidelberg.

Ruiz, J. A., Baumont, D., Bernard, P. & Berge-Thierry, C. Modelling directivity of strong ground motion with a fractal, k− 2, kinematic source model. Geophys. J. Int. 186, 226–244, doi: 10.1111/j.1365- 246X.2011.05000.x (2011).

Saaty, T.L., 1980. The Analytic Hierarchy Process: Planning, Priority Setting, Resource Allocation, ISBN 0-07-054371-2, McGraw-Hill.

Selva J., Tonini R., Molinari I., Tiberti M.M., Romano F., Grezio A., Melini D., Piatanesi A., Basili R., Lorito S. (2016). Quantification of source uncertainties in Seismic Probabilistic Tsunami Hazard Analysis (SPTHA). Geophys. J. Int., 205, 1780-1803, doi:10.1093/gji/ggw107.

Selva J, Lorito S, Basili R, Tonini R, Tiberti MM, Romano F, Perfetti P, Volpe M (2017). On the use of faults and background seismicity in Seismic Probabilistic Tsunami Hazard Analysis (SPTHA), Geophysical Research Abstracts Vol. 19, EGU2017-17395-1, EGU General Assembly 2017.

Stucchi, M., A. Rovida, A.A. Gomez Capera, P. Alexandre, T. Camelbeeck, M.B. Demircioglu, P. Gasperini , V. Kouskouna, R.M.W. Musson, M. Radulian, K. Sesetyan, S. Vilanova, D. Baumont, H. Bungum, D. Faeh, W. Lenhardt, K. Makropoulos, J.M. Martinez Solares, O. Scotti, M. Zivcic, P. Albini, J. Batllo, C. Papaioannou, R. Tatevossian, M. Locati, C. Meletti, D. Viganò and D. Giardini (2012). The SHARE European Earthquake Catalogue (SHEEC) 1000-1899. Journal of Seismology, doi 10.1007/s10950-012-9335-2.

SSHAC (Senior Seismic Hazard Analysis Committe), 1997. Recommendations for probabilistic seismic hazard analysis: Guidance on uncertainty and use of experts, U.S. Nuclear Regulatory Commission Report NUREG/CR-6372.

Storchak, D.A., D. Di Giacomo, I. Bondár, E. R. Engdahl, J. Harris, W.H.K. Lee, A. Villaseñor and P. Bormann, 2013. Public Release of the ISC-GEM Global Instrumental Earthquake Catalogue (1900-2009). Seism. Res. Lett., 84, 5, 810-815, doi: 10.1785/0220130034.

Strasser, F.O., Arango, M.C., Bommer, J.J., 2010. Scaling of the source dimensions of interface and intraslab subduction-zone earthquakes with moment magnitude. Seismological Research Letters 81, 941-950, doi: 10.1785/gssrl.81.6.941.

Weichert DH. (1980) Estimation of the earthquake recurrence parameters for unequal observation periods for different magnitudes. Bulletin of the Seismological Society of America; 70:1337–1356.

Wells, D.L., Coppersmith, K.J., 1994. New empirical relationships among magnitude, rupture length, rupture width, rupture area, and surface displacement. Bull. Seismol. Soc. Am. 84, 974-1002, doi.

Woessner J., Danciu L., Giardini D., Crowley H., Cotton F., Grünthal G., Valensise G., Arvidsson R., Basili R., Demircioglu M., Hiemer S., Meletti C., Musson R.W., Rovida A., Sesetyan K., Stucchi M., and the SHARE consortium. (2015). The 2013 European Seismic Hazard Model - Key Components and Results. Bulletin of Earthquake Engineering, 13, 3553-3596, doi: 10.1007/s10518-015-9795-1.

Zheng, Y. H., Anderson, J. G. & Yu, G. A Composite Source Model for Computing Realistic Synthetic Strong Ground Motions. Geophys. Res. Lett 21, 725–728, doi: 10.1029/94GL00367 (1994).

Summary of the Internal Review Process Phase 1: TSUMAPS-NEAM Project

The TSUMAPS-NEAM project has implemented a voluntary internal review process that consists of two stages. This report summarizes the first stage, where reviewers were asked to express opinions regarding the project processes and methods, as described in the Preliminary Assessment Plan documents and its appendices. The second review stage will be on the final implementation and results.

Reviewers were asked to submit a numerical rating from 0-5 (5 being the highest rating) on the following questions:

RQ1. Using a scale of 0-5, how do you rate the clarity of the provided documentation for judging the planned implementation of the method?

RQ2. Using a scale of 0-5, how do you rate the capability of the proposed methodology to fulfill the needs of end-users, as described in the project proposal?

RQ3. Using a scale of 0-5, how do you rate the capability of the proposed methodology to fulfill the requests of the Pool of Experts, as quantitatively expressed in the elicitation?

RQ4. Using a scale of 0-5, how do you rate the capability of the used datasets to perform a satisfactory quantification of the hazard?

RQ5. Using a scale of 0-5, how do you rate the representativeness of the proposed alternative models for capturing the "community distribution" of state-of-the-art SPTHA?

RQ6. Using a scale of 0-5, how do you rate the robustness of the overall proposed methodology for providing a quantification of the SPTHA for the NEAM region?

Reviewers were given the opportunity to add specific suggestions and comments to accompany their responses, and also to give unlimited general comments. The internal review panel and review status is listed in the table below:

Name	Affiliation	
Jörn Behrens	Universität Hamburg (UHAM), Department of Mathematics and CliSAP, Germany	Y
Mauro Dolce & Daniela Di Bucci	Italian Civil Protection Department (DPC), Italy	Y[1]
Tom Parsons	United States Geological Survey (USGS), Pacific Coastal and Marine Science Center, USA	Y
Eric Geist	United States Geological Survey (USGS), Pacific Coastal and Marine Science Center, USA	N[2]
Marco Pagani	Global Earthquake Model (GEM) Foundation, Italy	Y
Alessandro Amato	Istituto Nazionale di Geofisica e Vulcanologia, INGV, National Earthquake Centre, Italy	Y
Andrey Zaytsev	Russian Academy of Sciences (RAS), Special Research Bureau for Automation of Marine Researches, Russia	Y
Mauricio Gonzalez	Universidad de Cantabria (UNICAN), Instituto de Hidráulica Ambiental "IH Cantabria", Spain	Y
Jose Manuel Gonzalez Vida	Universidad de Málaga (UMA), Dpto. Matemática Aplicada, Spain	Y

1 Provided review together.

2 Will participate in Phase 2.

The numerical scoring was generally very positive with most frequent scores assessed at 4 (of 5), and with scores of 5 being more common than 3. No clear trend is identified across the six questions. From 8 scorers, the mean values for each question were:

RQ1	4.3
RG2	4.3
RQ3	4.1
RQ4	4.1
RQ5	4.2
RQ6	4.2

This scoring is interpreted as support for the basic framework of the TSUMAPS-NEAM project and documentation. However there were a number of specific comments raised that required a response from the implementation group as detailed below.

RQ1: Documentation

Some reviewers found the initial documents confusing, with several parallel tracks, and varying levels of detail. The response to these complaints will be a single document that follows a timeline of all the steps, and workflows. Additionally explicit langue will be added to emphasize that the TSUMAPS results are regional in nature, and that additional computation will be necessary for site specific results.

RQ2: End Users

There were not many issues raised about how well the project will fulfill needs of the end users. One idea was to prepare a questionnaire that could be submitted to potential end users to find out what their needs are. At the meeting in Tunis, the Italian Civil Protection made presentations about their needs that were taken under advisement. The response will also be to prepare a questionnaire for the second review, and also to post end use scenarios on the project web site.

RQ3: Fulfillment of Pool of Expert requests

There were only a few comments raised on this issue, in part because of strong reviewer support for the weighting schemes designed to implement expert opinion. There was one comment suggesting that there may have been some confusion introduced by the number of expert rating questions that will be noted in the final documentation. According to the implementation team, this concern is mitigated in part by the overlapping reviewer rating modes.

RQ4: Quality and capability of the input data

The reviewers demonstrated some consensus on two points: (1) a desire to see the sensitivity of the hazard results to the data and choices made about their interpretations, and (2) use of more detailed and/or high quality bathymetric data sets. Generally the response to

the first point by the implementation team has been to introduce more logic tree branches, particularly with regard to the primary seismic source distribution uncertainty, and applying the quantification scheme on expert weighting to assess expert opinion influence. The reviewer team agrees that exploration of a wide array of logic tree branches is a reasonable way to assess sensitivity.

For the most part, while additional bathymetry data are known, the best application of these data is most likely for detailed regional hazard/risk studies that are based on the broader TSUMAPS-NEAM results. However, additional bathymetry data (such as EMODNET) will be applied where it is reasonable to do so.

Other data-related reviewer comments have been addressed such as initial use of a too-thick 27-km average crustal thickness in tsunami source zones, and moment balancing the seismic source rates against plate motion rates.

A few reviewers noted that the paleotsunami databases can be controversial, and urged caution in using them for rate calculation verification.

RQ5: Quality and capability of the proposed methods

Mostly the reviewers requested further documentation and justification of alternative methods that were not planned to be adopted. Some suggestions, while potentially interesting would be impossible to incorporate uniformly given uneven data, or time constraints, such as time-dependent source rates and 3D tsunami generation calculations everywhere.

A comment was made regarding linear superposition of tsunami height with tidal data that may not be accurate as this can be dependent on stage and locality effects, and another about tidal effects on flood height vs. inundation distance.

Additional methodological points that may require documentation/consideration include:

• Proposed application of the alternative filtering algorithm by Nosov and Koselov (2011).

•Explanation on why no characteristic magnitude frequency distyribution (MFD) was considered, but only the Gutenberg-Richter MFD.

•Impact of the smoothness of Gaussian background seismic sources on hazard.

RQ6: Overall robustness of the proposed methods

Specific reviewer comments with regard to the robustness of the proposed methods have been listed above. Perhaps the most important factors remaining will be the ability to quantify the impact that each methodological choice or data limitation will have on hazard estimates. In most cases, it will not be possible to quantify the effect of methods that were not adopted, but clear documentation of these is planned. A planned verification step to compare results with empirical data will also yield information on the robustness.

Based on some reviewer comments it is clear that the exact goals and resulting products of the TSUMAPS-NEAM project were not entirely understood. A challenge thus remains to provide a very clear definition of what the reported hazard values mean, and the possible site-specific variability that remains. There isn't time before the final reports are completed, but some examples (a sort of 'how-to' manual) of carrying a few TSUMAPS results all the way to inundation distance probability, and/or flood height at specific points would probably be very helpful to end users. This was noted as a planned activity for the TSUMAPS website at the Tunis meeting.

An important result of TSUMAPS-NEAM, that should be highlighted, will be a unified representation of the *relative* hazard across a very broad region. Even though there is significant uncertainty, it will be possible to identify broad areas of concern, and to take necessary mitigation steps.

FINAL IMPLEMENTATION: Phase 2, Assessment

Probabilistic TSUnami Hazard MAPS
for the NEAM Region (TSUMAPS-NEAM)
ECHO/SUB/2015/718568/PREV26

PHASE II – STAGE 1: Hazard Model Implementation (Workflow)

Author: **TSUMAPS-NEAM Technical Integrator (TI) team**

Date: **12 September 2019**

Version: **2.1**

Table of Contents

Executive Summary

This document describes the execution of Stage 1 (implementation) in PHASE 2 of the TSUMAPS-NEAM Project.

In this Stage the hazard model is finally defined, and its outcome is the NEAM Tsunami Hazard Model 2018 (hereinafter "NEAMTHM18") whose results are presented in Doc_P2_S5.

The decisions made during the realization of the NEAMTHM18 resulted from a complex interaction among three groups of experts: the project's development team (including a Project Manager, a Technical Integrator, and an Evaluation Team), a Pool of Experts, and a team of Internal Reviewers. Interactions of the TSUMAPS-NEAM Team with the Experts and with the Reviewers (which includes this Review) occur twice, once per each PHASE. The decision-making and project execution workflow are briefly described in the Introduction (Section "Project structure"). The hazard model implementation (Stage 1) is structured in four STEPS and several Levels within each STEP. The STEPS and Levels are also briefly and schematically presented in the Introduction (Section "NEAMTHM18 workflow structure").

CHAPTERS from 1-4 describe all the STEPS and the Levels within each STEP. These descriptions are given in greater detail, including alternative modelling choices where they occur. The purpose of these descriptions is to document the data used, the adopted methods and the obtained results.

This page is intentionally left blank.

Introduction

The TSUMAPS-NEAM project produced the first region-wide long-term homogenous Seismic Probabilistic Tsunami Hazard Assessment (SPTHA), that is PTHA from earthquake sources only, with the aim of triggering a renewed and common tsunami risk management strategy in the NEAM region. NEAM stands for North-eastern Atlantic, the Mediterranean, and connected Seas, which is one of the four regions of the UNESCO-IOC subdivision of the World's Oceans.

We specify that this SPTHA is time-independent and based on a Poissonian model for the earthquake occurrence.

This document describes the details of the **NEAM Tsunami Hazard Model 2018 (hereinafter "NEAMTHM18")** implementation.

The NEAMTHM18 results are described in the document named "Doc_P2_S5_Results.docx" and are available online for visualization and download at http://www.tsumaps-neam.eu/ (under the "PTHA" menu).

Project structure

A formalized decision-making process was implemented for building the NEAMTHM18, following a multiple-expert protocol recently introduced within the European project STREST (2013-2016, http://www.strest-eu.org/), and further adapted to TSUMAPS-NEAM needs. This protocol was inspired by similar protocols developed for seismic hazard (USNRC 1997; 2012; 2018) and establishes the existence of several teams of experts (internal and external to the project's development team) who play different roles within the model development.

The NEAMTHM18 was achieved through two project PHASES (FIGURE I.1), in which three main groups interacted with each other: the project's development team (including a Project Manager, a Technical Integrator, and an Evaluation Team), a Pool of Experts, and a team of Internal Reviewers. Interactions of the TSUMAPS-NEAM Team with the Experts and with the Reviewers (which includes this Review) occur twice, once per each PHASE.

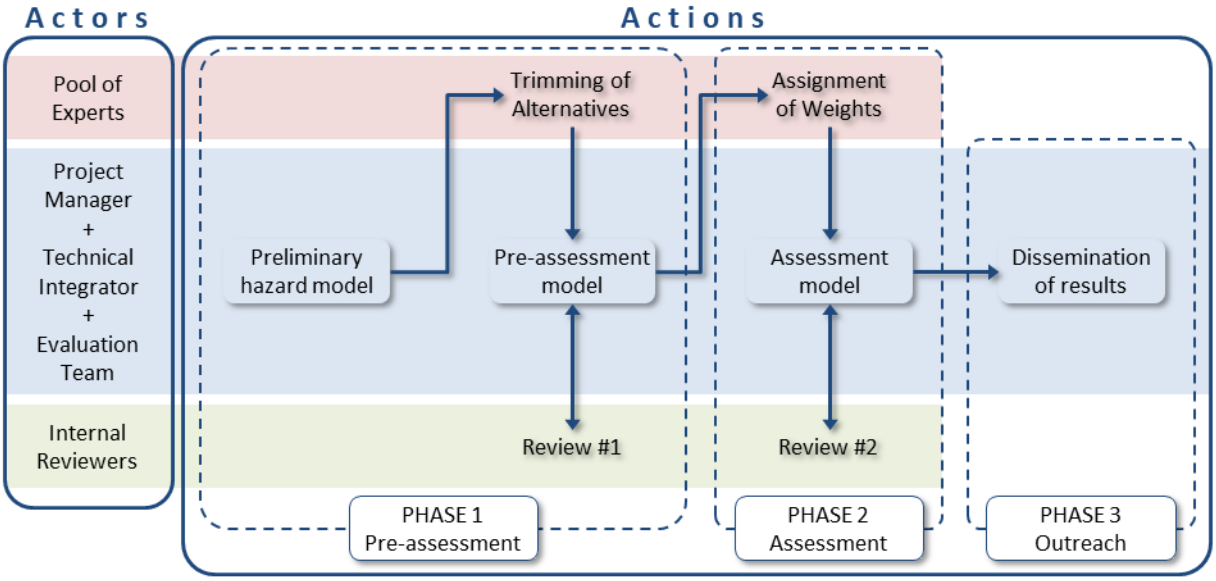

FIGURE I.1. Schematic illustration of PHASES 1 and 2, each of them including one elicitation experiment and one revision stage.

Both phases include the production of a detailed Documentation. This document belongs to the documentation of PHASE 2 that overall includes four documents:

- Doc_P2_S1_Implementation (this document), containing the detailed description of the implementation of the hazard model;
- Doc_P2_S3_Data&Codes, including a detailed description of the data used and of the codes written or used to produce the results;
- Doc_P2_S4_Elicitation, describing the results of the 2nd elicitation experiment devoted to the quantification of the weights expressing the "degree of credibility" to be assigned to the alternative models of the adopted alternative tree (equivalent of the Logic Tree in the Ensemble model context; see Marzocchi et al., 2015);
- Doc_P2_S5_Results, containing a general description of the hazard model results and of the different tests and post-processing analyses (including sanity checks, sensitivity analyses and disaggregation) made to check the consistency of the results.

More details regarding the process and the roles of the different Actors (Internal Reviewers, Pool of Experts, TSUMAPS-NEAM Team) were already given in the Guidelines_for_Reviewers document provided to the Reviewers during PHASE 1. We describe below only some basic concepts concerning the three PHASES of the Project Actions.

PHASE 1 concerned the selection of methods, data, and modelling alternatives, as well as the first review round.

- Hazard analysis is almost never completely well constrained by observations, nor the physics of the hazardous phenomenon always totally understood. Different alternative scientifically acceptable models, including different datasets, may then be generally used at the various steps of a hazard assessment, which reflect the inherent uncertainty.
- Here, after defining the basic methodology for hazard analysis, a variety of possible modeling alternatives and datasets, to be possibly used at the different STEPS of the analysis, were presented to the Pool of Experts (PoE). The PoE guided the selection of the data and models to be implemented in the NEAMTHM18, by means of the Elicitation STAGE 1, while some of the proposed alternatives where discarded ("trimmed").
- The resulting PRE-ASSESSMENT model (a preliminary implementation plan) was then presented to the Internal Reviewers (IR). Most of the comments made by the IR were addressed and implemented in PHASE 2, while some suggestions could not be implemented for practical reasons. A "rebuttal presentation" was given during the TSUMAPS-NEAM final meeting in Tunis, Tunisia (11-12 September 2017), and a summary of Review STAGE 1 was sent by Tom Parsons (USGS) on behalf of the IR.

PHASE 2 concerned the implementation of the hazard workflow, including weighting of the alternatives, building the final NEAMTHM18, and checking the sanity of results, as well as the second review round.

- Different implemented alternative models – e.g. two different earthquake magnitude-frequency distributions or two different tsunami coastal amplification relationships – may have different "degrees of credibility" within the reference scientific community.
- The model credibility should in principle coincide with the accuracy of its output; however, this is not always quantifiable because of the general lack of independent data for rare phenomena such as tsunamis, and the weighting was then here achieved through a further elicitation of the experts' judgement. Elicitation STAGE 2 of the PoE was then performed to assign the relative weights of the selected alternative models.
- The Project Team finalized the TSUMAPS-NEAM Model accordingly, and the NEAMTHM18 was eventually presented to the Internal Reviewers (IR), along with its results. Note that the

NEAMTHM18 results have now been online for about one year for community feedback. Moreover, the NEAMTHM18 has been presented in many scientific and professional contexts in search for further feedbacks. Hence, unless gross mistakes are revealed with this second review round, the NEAMTHM18 won't be further modified. Nevertheless, the IR comments will be included in the documentation, and will guide possible future versions of the NEAMTHM18.

PHASE 3 concern the dissemination of results. Dissemination has actually started at the very beginning of the project with the publication of several preliminary, intermediate, and final results, in the project website (http://www.tsumaps-neam.eu/). This website fully illustrates the project development and provides links to access the project documentation. Most relevant webpages are:

- http://www.tsumaps-neam.eu/documentation/ that already provides access, project progression technical reports along with other dissemination material, and all the documents of the PHASE 1. The documents of PHASE 2 will also be added at the end of this review.
- http://www.tsumaps-neam.eu/publications/ lists the relevant articles already published in peer-review journals, and presentations at scientific meetings. Future publications will be added here.
- http://www.tsumaps-neam.eu/neamthm18/ is the landing page associated with the Digital Object Identifier to be minted by INGV through DataCite (https://datacite.org/). This page includes: 1) links to the interactive mapper where the hazard and probability maps (see Doc_P2_S5_Results) can be navigated, interrogated, and hazard data be downloaded; 2) links to hazard data distributed through the Open Geospatial Consortium standard protocols via the INGV platform http://www.tsunamidata.org/index.php/services/tsumaps-neam-ows-services; 3) the license terms of use (CC BY 4.0); 4) citation and abstract. All these elements guarantee that the project results remain persistently findable, accessible, interoperable, and reusable (FAIR).

The project also produced several by-products that will be distributed in the future depending on availability of resources to finalize them. Doc_P2_S5_Results provides a brief description of them.

NEAMTHM18 workflow structure

The NEAMTHM18 workflow is structured in "STEPs" and "Levels" (FIGURE I.2).

The four STEPs are:

- STEP 1: PROBABILISTIC EARTHQUAKE MODEL
- STEP 2: TSUNAMI GENERATION & MODELING IN DEEP WATER
- STEP 3: SHOALING AND INUNDATION
- STEP 4: HAZARD AGGREGATION & UNCERTAINTY QUANTIFICATION

STEP 1 provides (FIGURE I.3):

1. a list of scenarios $\{\sigma_k\}$ for all potential earthquakes in all considered source regions, and
2. their mean annual rates $\{\lambda(\sigma_k)\}$ according to their Magnitude-Frequency Distribution (MFD) and the scenario parameters (earthquake magnitude, fault rupture position, strike, dip, rake, size, and slip);
3. Alternative modelling of both $\{\sigma_k\}$ and $\{\lambda(\sigma_k)\}$.

STEP 2 provides:

1. the numerical (deterministic) simulation of the sea floor displacement corresponding to each of the individual earthquake scenarios $\{\sigma_k\}$ defined at STEP 1;

2. the numerical (deterministic) simulation of the tsunami generation from these displacements and their propagation from the source up to each offshore Point of Interest (POI), resulting in the mareograms $\{M(\sigma_k, POI)\}$; the parametric lookup tables $\{(max_t, T, \mp)[M(\sigma_k, POI)]\}$ of maximum positive amplitude max_t, periods T, and polarities $\mp$ for all mareograms.

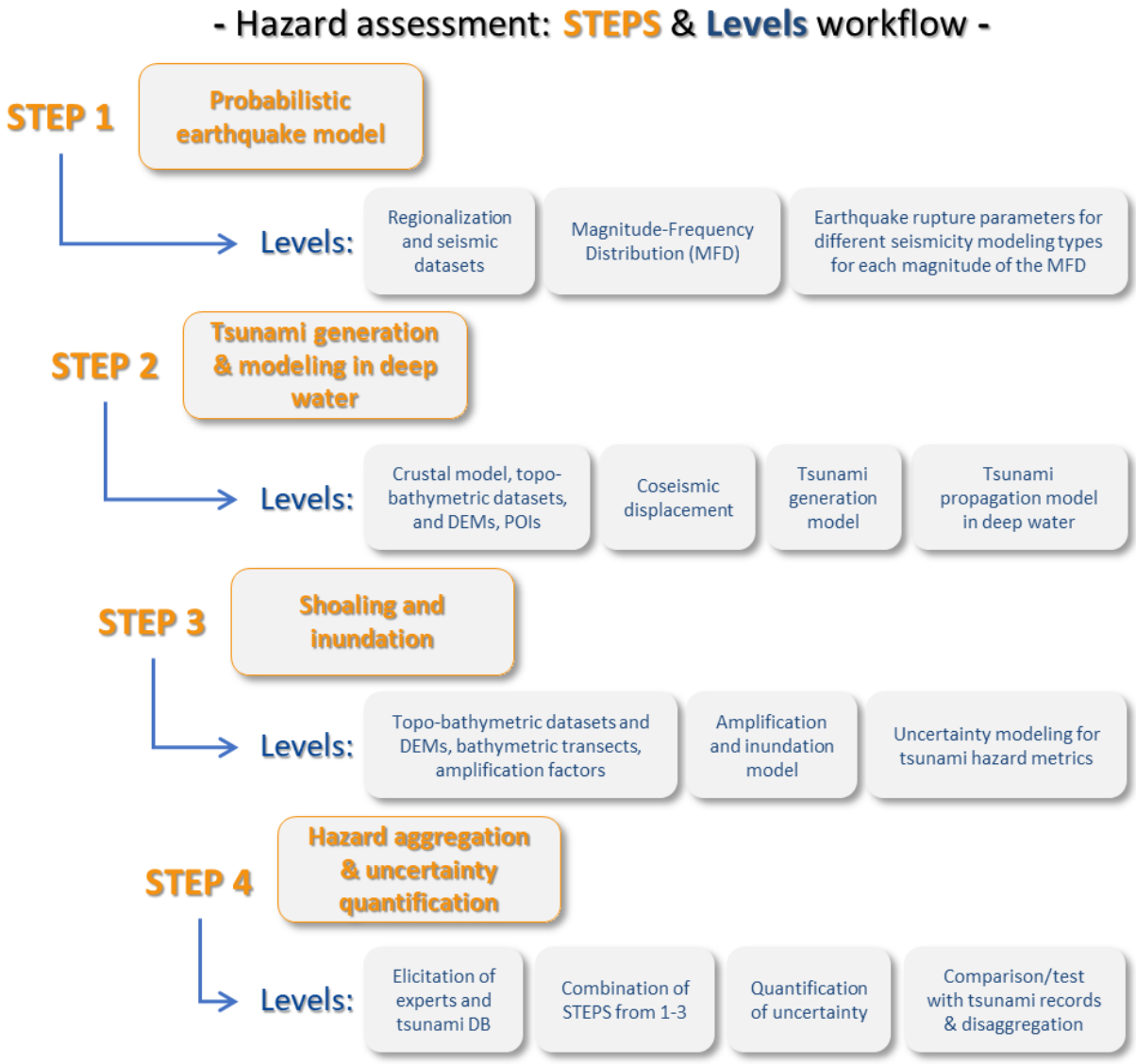

FIGURE I.2. Sketch of the NEAMTHM18 workflow.

STEP 3 provides:

1. deterministic modelling of the coastal tsunami impact at all the POIs defined at STEP 2 for all the scenarios $\{\sigma_k\}$ defined at STEP 1

    a. expressed by a Maximum Inundation Height (MIH) as calculated from the offshore results (STEP 2) employing local amplification factors $AF(T, \mp, POI)$ lookup tables;

b. and, alternatively, through Green's law;

2. assessment of the variability along the coast of the tsunami intensity in the form of conditional hazard curves $P(> MIH_{th}|\sigma_k)_{POI}$, where MIH_{th} indicates a threshold value for MIH;

3. assessment of the associated uncertainties (including uncertainties originated from linear combinations at STEP 2), estimated through sampling alternative implementations of the conditional hazard curves $\{P(> MIH_{th}|\sigma_k)_{POI}\}$.

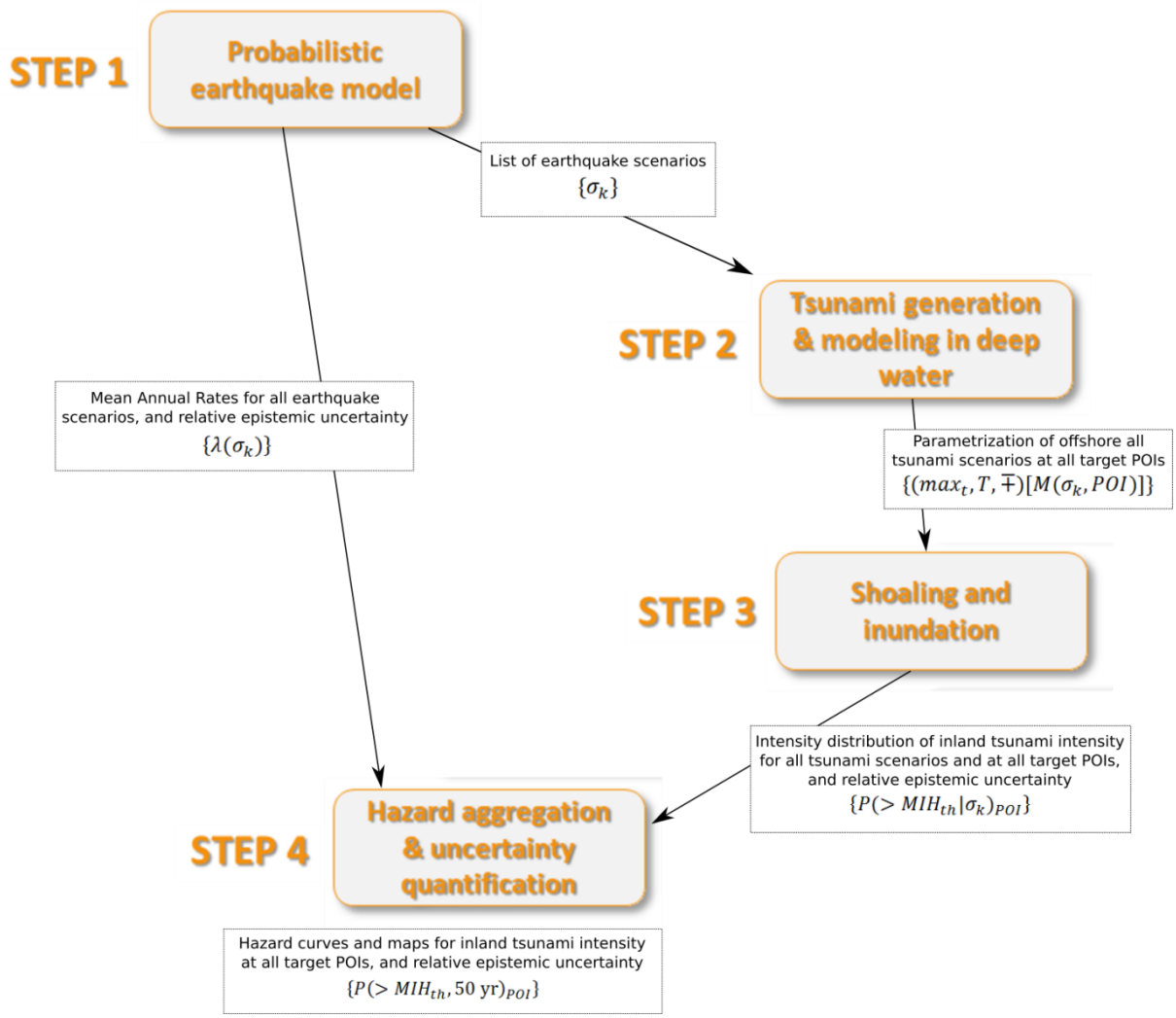

Figure I.3: Sketch of the information flux of the NEAMTHM18. This procedure is repeated for each considered alternative model.

STEP 4 provides:

1. probabilistic hazard model of the coastal tsunami impact expressed through the exceedance probability in $50\ yr$ $\{P(> MIH_{th}, 50\ \mathrm{yr})_{POI}\}$ versus different MIH intensity thresholds MIH_{th}; this is obtained by aggregating all scenario annual rates $\{\lambda(\sigma_k)\}$ from STEP 1 with the conditional PoE $\{P(> MIH_{th}|\sigma_k)\}$ from STEP 3;

2. assessment of the model uncertainties expressed through distributions of hazard curves $\{P(> MIH_{th}, 50\ \mathrm{yr})_{POI}\}$ and their statistics; hazard and probability maps; disaggregation products.

The workflow within of each of these STEPS is subdivided into several Levels. Level 0 at each STEP is a peculiar one as it contains the definition of the datasets used at all subsequent Levels. The other Levels constitute the finer grain of the hazard analysis workflow within each STEP. At each Level within each STEP, mainly depending on the indications of the PoE, several alternative approaches, datasets, or models are implemented to explore the epistemic uncertainty.

In the next four CHAPTERS, we describe the four STEPs and the different Levels within them. This includes the description of alternative implementations at each STEP and each Level.

1 STEP 1 - PROBABILISTIC EARTHQUAKE MODEL

The general aim of STEP 1 is the definition of the two basic elements of the probabilistic earthquake model:

1. a list of scenarios $\{\sigma_k\}$ for all potential earthquakes in all considered source regions, and
2. their mean annual rates $\{\lambda(\sigma_k)\}$ according to their Magnitude-Frequency Distribution (MFD) and the scenario parameters (earthquake magnitude, fault rupture position, strike, dip, rake, size, and slip);
3. Alternative modelling of both $\{\sigma_k\}$ and $\{\lambda(\sigma_k)\}$.

For each k, the notation σ_k indicates all the parameters that describe a specific earthquake as used in this model (e.g. location, fault size, focal mechanism and slip distribution), and that are needed to define the tsunami initial condition through the computed sea floor displacement.

The mean annual rates $\lambda(\sigma_k)$ are used here for a time-independent SPTHA. As later specified in more detail, this occurs under the assumption that for the earthquakes follow a temporal stationary Poisson process (e.g. Grezio et al., 2017; Selva et al., 2016; Geist and Parsons, 2006).

In addition, the seismicity is subdivided into several "seismicity modeling types", and thus will be parameterized in several different ways, accordingly. The rationale and the details for this approach are explained in the next SUBSECTION.

1.1 Seismicity modeling types: different ways to parameterize earthquake occurrence

The basic principle applied here is that knowledge of the potential earthquake sources is somehow limited and then we acknowledge that earthquakes are possible everywhere. However, certain sources (faults) can be known better than others (e.g. Basili et al., 2013a). To optimally deal with this heterogeneous uncertainty while maximizing the use of all the available information, the seismicity is subdivided into several categories, each one adopting a different modeling approach for one or more parameters. Some values of the earthquake parameters can be even fixed when their uncertainty is considered negligible with respect to other parameters and to other source zones. This approach to seismicity types in probabilistic calculations was first introduced for SPTHA by Selva et al. (2016), as well as in previous earthquake probability studies (Field et al., 2014; Woessner et al., 2015).

It must be made clear since the beginning that seismicity types have little or nothing to do with any seismicity classification based on tectonic considerations and distinctions, such as intra- and inter-plate seismicity, crustal or subduction interface seismicity. The seismicity types in this model are rather defined in terms of different modeling/parameterization approaches, which may occasionally coincide with some seismotectonic classification. The chosen approach, and thus the seismicity type, depends on how well the different parameters are constrained relative to each other, for a given fault or source zone. For example, if the 3D geometry of a subduction zone may be considered as sufficiently well constrained, subduction earthquakes can be assumed to occur on the subduction interface with a dominantly thrusting mechanism. Thus, some parameters such as the depth at a given location and the rake will be fixed. The subduction earthquakes on this relatively well-known subduction zone can be treated separately from the rest of the crustal seismicity around it, whose

mechanism can be characterized by a relatively higher variability. In other words, and more in general, relatively larger uncertainty will characterize the focal mechanism of "background" seismicity around a well-known major fault or fault system. The latter does not necessarily need to be a subduction zone; for example, the same reasoning may apply as well for the San Andreas Fault or the North Anatolian Fault. The parameters describing the background or diffuse seismicity around these faults or within a generic volume where no major faults are well identified, are all modeled as aleatory variables; conversely, some of those describing the earthquakes on major faults will be fixed.

Two main seismicity modeling types are defined and used in the probabilistic earthquake model: Background Seismicity (BS) and Predominant Seismicity (PS). The BS is meant to capture all the seismicity in a tectonically defined region and for which there is a low level of knowledge, especially the earthquakes at the lower end of the magnitude values of interest. Because of this, fault sources in the BS category are characterized by the largest variability. The PS is meant to capture the larger earthquakes generated by rather well-known major faults. Fault sources in the PS category are characterized by limited variability.

Depending on the level of available knowledge, compared with the level of knowledge required for the quantification, and depending on the distance between the source and the closest target coast, the above described categories may be modified to accommodate special situations. In this respect, we defined two additional categories: Special PS (SPS), and Special BS (SBS). While PS and BS are two "end-members" featuring the maximum and the minimum number of fixed parameters, respectively, SBS and SPS are intermediate cases in which the number of fixed and variable parameters is modulated case by case. In any case, only one or two categories may be modelled in any given region. The following SECTIONS will present the seismicity modeling types one by one. The assignment to the considered fault sources will be presented in SECTION 1.3.4.

1.1.1 Background Seismicity (BS)

The BS seismicity modeling type is meant to capture all the seismicity for which there is a low level of knowledge, including the smaller earthquakes of interest and deals with faults characterized by the largest variability. It resembles a large class of seismic sources commonly adopted for Probabilistic Seismic Hazard Analysis (from Cornell, 1968). An example of application in tsunami hazard is the case of Sørensen et al. (2012).

Most of BS earthquake parameters are treated as aleatory variables. That is, BS accounts for earthquakes occurring everywhere within a crustal volume according to a spatial probability distribution, and with a certain variability of the faulting mechanism. We introduce this category because earthquakes often occur outside the well-known major faults treated as PS, and moreover not all tsunamigenic faults are necessarily mapped well enough. Still, both these "background" earthquakes around mapped faults, possibly including outer-rise earthquakes proximal to subduction zones, or those occurring on unknown or un-mapped faults, may contribute to tsunami hazard. The probability distribution of the faulting mechanism (strike, dip and rake) may be non-uniform, as it can be constrained by: the possible presence of known mapped faults (except for those already treated as PS); and by the focal mechanisms within the considered volume. The spatial probability of the earthquakes is instead constrained by the seismicity only.

Variable BS parameters, treated as aleatory variables, are magnitude, map position of geometrical center, depth, rupture mechanism. Nominal rupture length and width, and average slip are instead taken from empirical scaling relations (see SECTION 1.3.6). BS sources are all assumed to be single planar faults. Uniform slip distribution is used here, since the maximum modeled magnitudes are in the range of those adopting uniform slip (also for the PS), but in principle heterogeneous slip could be used. Extending heterogeneous slip to lower magnitudes would be computationally very expensive.

1.1.2 Predominant Seismicity (PS)

The PS seismicity modeling type is meant to capture the larger earthquakes generated by rather well-known major faults, e.g. plate boundaries and, particularly, subduction zones. We note that this is the most frequent approach to tsunamigenic seismicity in PTHA (e.g., González et al., 2009; Power et al., 2013), under the assumption that this type of earthquakes (e.g. mega-thrust earthquakes on known subduction zones) dominate the tsunami hazard. As before noted, merging PS with BS in an assessment was first proposed by Selva et al. (2016), although with a slightly different terminology ("interface seismicity, IS" was used instead of predominant seismicity).

The PS family is formed by 3 sub-categories: proper PS, SPS and SBS, depending on the state of knowledge about the fault and the distance between the fault and the closest target area. The PS sub-categories are alternative in all source regions, meaning that they are never considered simultaneously in the same source region.

PS is the seismicity modeling type dealing with major faults characterized by the smallest uncertainty; therefore, some of the parameters describing earthquakes belonging to PS are assumed as known. Specifically, the earthquakes are assumed to occur on a fault of known geometry; the rupture mechanism is inherited from the hosting fault according to the dominant strain direction, e.g. convergence for subduction zones.

Variable PS earthquake parameters, treated as aleatory variables, are earthquake magnitude, position along the planar or 3D-curved hosting fault, nominal rupture length and width, average slip, and slip distribution. A non-uniform slip distribution within the rupture area is applied only to some selected PS. This depends upon their distance from the target coastlines and it is used for earthquakes larger than a minimum magnitude. This circumstance follows the principle that tsunami hazard is more sensitive to slip heterogeneity of faults that are nearer to the target coast or that generate larger earthquakes.

1.1.3 Special PS (SPS)

This special seismicity modeling type was devised to more efficiently treat the lower magnitude range of faults included in the PS category. The reason is an exquisitely practical and technical one. SPS is used as a loophole for reducing the computational cost associated with the relatively more numerous lower magnitude scenarios.

The smaller magnitude earthquakes generated by a SPS structure are modeled with the same approach used for BS. We then renounce to some accuracy; for this reason, we recur to the SPS only for sources not too close to the coastline. The geometry and centers of the ruptures instead remain the same as those adopted for the PS.

Conversely, for higher magnitudes, the same approach as for PS is used. In this way, the size of the subfaults of a given PS can be also kept relatively large, comparable to that of a M7 earthquake. Recall that a M<7 earthquake may in some cases produce a sizable tsunami in the near field, as it was for example the case of the Zemmouri-Boumerdes, Algeria, Mw 6.8 earthquake in 2003 (Alasset et al., 2006).

Variable SPS parameters are magnitude, position of geometrical center, nominal rupture length and width, and average slip. SPS sources are all assumed to be planar faults with uniform slip distribution. The fault geometry and rupture mechanism are predefined as for PS.

1.1.4 Special BS (SBS)

This special seismicity modeling type is used to treat the higher magnitude range of faults deemed to generate large earthquakes, which would suggest a treatment as PS, but whose position and geometry are not well-enough known which would suggest a treatment as BS. SBS may be used in the case of relatively unconstrained faults, for which it would be excessive to allow for a random parameter variability as large as that used for BS. For example, in a subduction zone the range of the dip angle variability may be known to be quite limited, tending to almost sub-horizontal at shallow depths, although it cannot be very well constrained.

The modeling approach for SBS is thus borrowed from the BS with the following modifications:

- The magnitude range is extended to generally higher magnitudes than that considered for BS;
- The seismogenic depth limit adopted from the crustal model for the BS can be exceeded if the SBS is used for a subduction zone, presuming that the Moho could be not well-enough mapped around it;
- The faulting mechanisms resulting from the strike, dip, and rake have a more limited variability range than for BS, or no variability at all (be fixed);
- The size of the rupture can be determined by different empirical scaling relations, suitable for the case under consideration.

Variable SBS parameters are case specific. We consider magnitude, map position of geometrical center, depth, strike and dip angles, nominal rupture length and width, and average slip. We also assumed SBS to be modeled by planar faults with uniform slip distribution, and fixed rake, although different choices could be applied in other circumstances

1.1.5 Seismicity modeling types in brief

Summarizing, depending on the specific knowledge of a specific source zone and its distance from the target areas, a different seismicity modeling type is adopted, and therefore the most appropriate set of parameters is treated as a set of aleatory variables within a Level of any STEP, as described in the next SUBSECTION. In general, PS treats well-known major faults, while BS treats less energetic diffuse seismicity. BS may be used alone in the regions where PS sources are not present, and PS can be used alone where the seismic source is very distant from the target coasts. The special types may replace PS and be present in combination with BS, when some parameters are less constrained (SBS) and/or to save computational resources where the seismic sources are relatively distant from the target coasts (SPS). It is useful to point out that SPS and SBS are similar in some respects to BS or PS

modeling for several Levels at STEP 1 and other differences may appear only in some Levels at STEP 2.

1.2 Levels at STEP 1

We recall that STEP 1 defines the probabilistic earthquake model. At STEP 1 we have defined three Levels (0-2). A branching exists starting from Level 1, since there is the need to split the workflow into the defined seismicity types.

The Levels at STEP 1 are:

- Level 0 (input data):
    - Tectonic regionalization model.
    - Seismic datasets (earthquake catalogs including de-clustering and completeness).
    - Fault datasets (including focal mechanisms).
    - Assignment of sources to seismicity modeling types; that is to say, which sources have been modeled as Background Seismicity (BS) and Predominant Seismicity (PS), Special PS (SPS), and Special BS (SBS).
    - Earthquake magnitude discretization.
    - Empirical earthquake scaling relations.
    - Discretization of the fault and earthquake parameters for the different sources assigned to the different seismicity modeling types.
    - Attribution ("separation") of the observed seismicity in each region to each seismicity modeling type.
- Level 1. Earthquake Magnitude-frequency distribution (MFD) for each seismicity modeling type defined in each region of the tectonic regionalization of Level 0. In each region, MFDs are quantified for BS and/or for PS, or alternatively for SPS/SBS.
- Level 2a. Variability of parameters within the PS/SPS approach, as described in the previous SECTION and illustrated in FIGURE 1.1a, for each magnitude in the MFD for each region at Level 1.
- Level 2b. Variability of parameters within the BS/SBS, as described in previous SECTIONS and illustrated in FIGURE 1.1a, for each magnitude in the MFD for each region at Level 1.

Note that definitions at Level 0 include which faults will be treated as PS, SPS, or SBS, selecting the most appropriate sub-category in each region, as well as in which region the treatment of BS is required (depending on the distance to the closest target zone). It also includes the analysis of the seismic catalogues.

Levels 1 and 2 coincide with the Levels of an Event Tree (ET). Examples of the use of an ET for SPTHA can be found in Lorito et al. (2015) and in Selva et al. (2016). This type of approach is an alternative to more classical approaches for the discretization of the total probability in SPTHA (e.g. Geist and Parsons, 2006).

The ET decomposes the problem into a chain of discrete conditional probabilities for the aleatory variables that describe the earthquakes (FIGURE 1.1a). Each path through the ET represents one specific combination of all the parameters and defines a scenario σ_k to be modeled in STEP 2 and STEP 3 to obtain the associated tsunami. The mean annual rate $\lambda(\sigma_k)$ of the scenario can be obtained by multiplying the mean annual rate of the MFD evaluated at Level 1 by the conditional

probabilities of all the other parameters evaluated at Level 2. This quantification is made separately for PS and BS, as shown in FIGURE 1.1a.

The actual quantification of all the parameters at all the Levels is subject to epistemic uncertainty. We quantify this uncertainty by means of ensemble modelling (Marzocchi et al., 2015; Selva et al., 2016) at STEP 4. The ensemble of STEP 4 takes as input several alternative implementations defined at each STEP, representing a sample of the epistemic uncertainty.

The alternative implementations of STEP 1 are defined in FIGURE 1.1b. As suggested by the expert panel through the 1st elicitation experiment (see Doc_P1_S3), STEP 1 is the one with the largest number of implemented alternatives, with focus on Levels 1 and 2a. As reported in FIGURE 1.1b, 2 alternatives have been implemented at Level 0 (that propagate at the subsequent levels). At Level 1, we implemented 62 alternatives, considering a rather large range of treatments for quantifying annual rates from seismicity and geodetic data. Among these alternatives, 8 are Bayesian models that include the quantification of the inherent epistemic uncertainty, which should be sampled from the model. At level 2a, 8 alternatives are implemented, considering alternative scaling relations, seismogenic areas and rigidity models. At level 2b, only 2 alternatives have been considered, related to the alternatives in the input catalog.

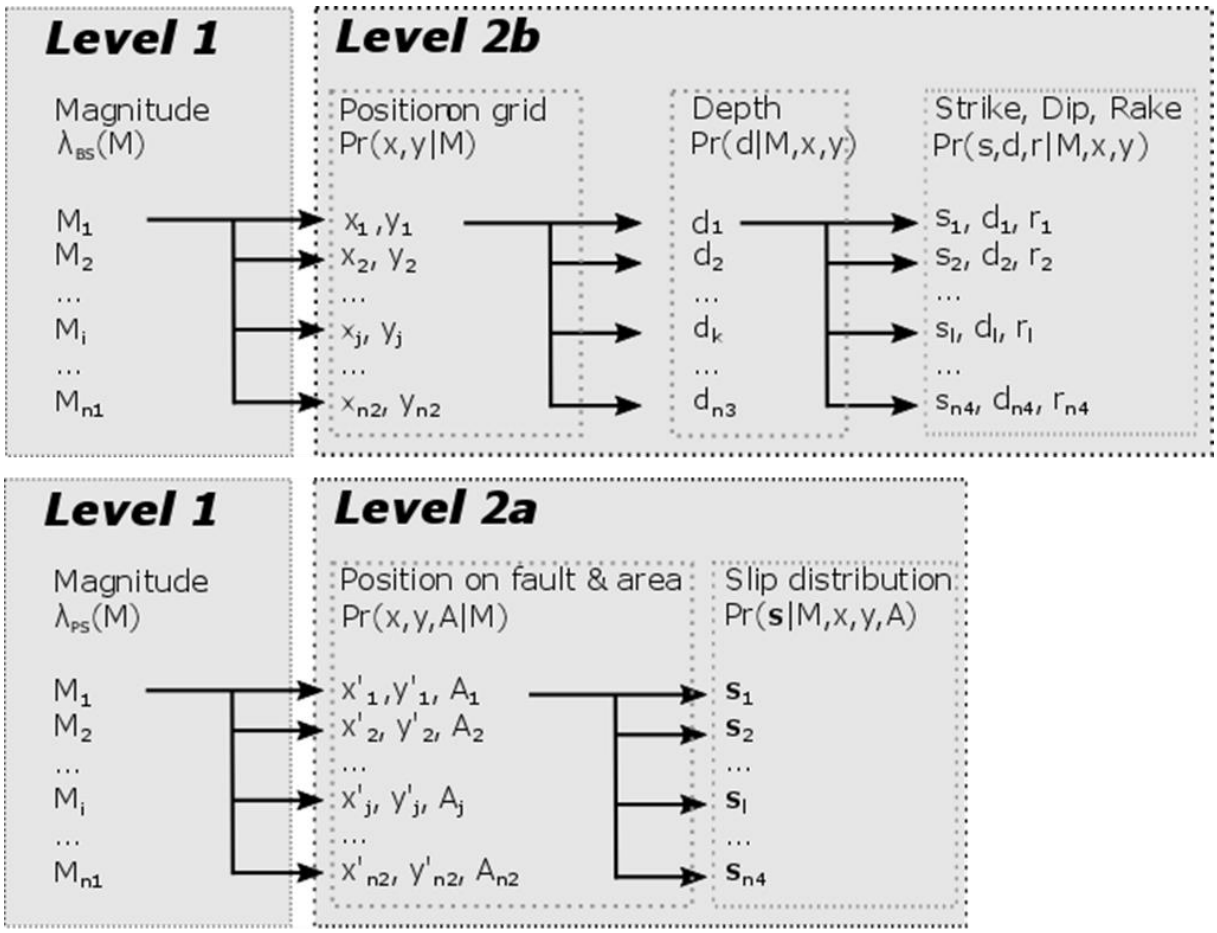

FIGURE 1.1A: Schematic of the Event Tree at STEP 1 for BS and PS. A common magnitude discretization is applied at Level 1 to both PS and BS annual rates.

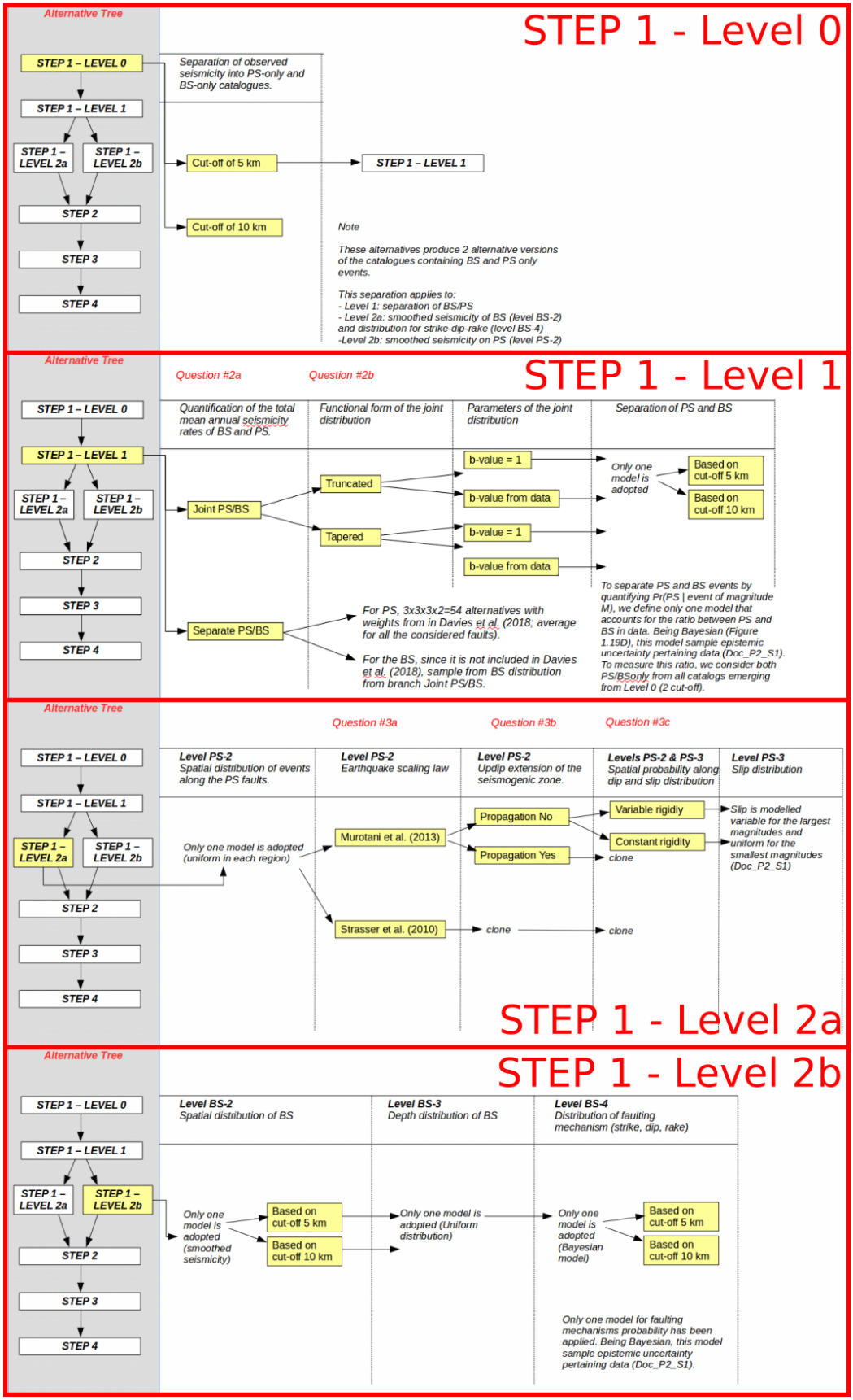

FIGURE 1.1B: Alternative implementations at all levels as described in SECTIONS 1.3, 1.4, 1.5, and 1.6.

1.3 Level 0

The technical specifications, mainly metadata such as data descriptions and formats, for accessing the files containing the datasets described at Level 0, are given in document P2_S3.

1.3.1 Tectonic regionalization model

The regionalization is a subdivision of the entire source space relevant for the NEAM area into discrete regions that are internally as homogeneous as possible from the standpoint of the dominant tectonic process. The seismicity in different regions will be assumed independent.

In the early stages of the project we evaluated possible regionalization model alternatives and then decided to use one single model, specifically developed. The adopted regionalization was built following basic principles of plate tectonics and building on previous experience of the SHARE project (Delavaud et al., 2012).

The following eleven tectonic settings are defined beforehand for the crustal level:

1 Active volcano;
2 Back-arc and orogenic collapse;
3 Continental rift;
4 Oceanic rift;
5 Contractional wedge;
6 Accretionary wedge;
7 Conservative plate boundary (mainly major transcurrent faults);
8 Transform fault s.s.;
9 Shield;
10 Stable continental region;
11 Stable oceanic region.

Region type #1 is not considered and region type #9 is not encountered within the domain of interest.

The geographic distribution of the above-defined tectonic settings forms the regionalization shown in FIGURE 1.2. This regionalization is a 2D subdivision of the crustal volume. In addition, we also consider the 3D geometry of slabs in subduction zones. The cases here considered roughly correspond with the regions classified as accretionary wedges in the map.

Some of the frequency-magnitude models (SECTION 1.4) are based on a truncated Pareto distribution that foresees an externally defined maximum magnitude. The maximum magnitude within each region of the regionalization was determined in three ways using data presented in SECTION 1.3.2:

- From earthquake catalogues, i.e. the maximum magnitude observed values.
- Following, where possible, the results of the SHARE Project (Woessner et al., 2015) which provide estimates of the maximum magnitude from the SHEEC catalog, from faults (SECTION 1.3.3), and a value augmented by a given uncertainty. The SHARE project adopted a subdivision in so-called superzones of the project study area that only partially overlaps the NEAM regionalization.

- By aggregating the maximum values of the two methods above and by aggregating the maximum values according to the tectonic setting each NEAM region belongs to.

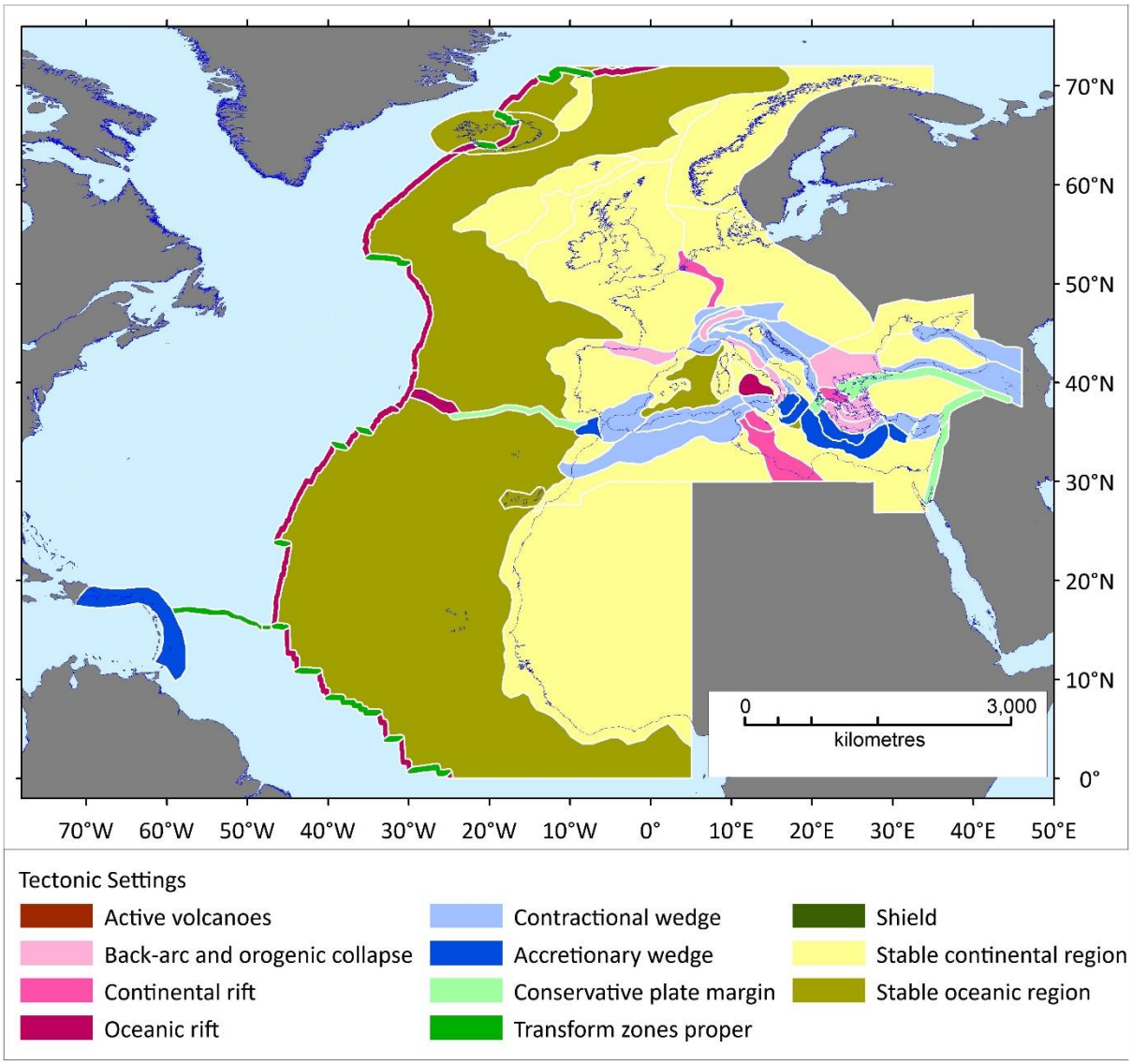

FIGURE 1.2: Map of the regions, color-coded depending on the tectonic setting, covering the whole source area.

Not all the earthquakes falling within a crustal region can be considered in the maximum magnitude determination. Peculiar cases required to be analyzed one by one. Earthquakes located on the subduction interface, determined by the combination of location and depth, and where available, with focal mechanisms consistent with those expected for the subduction plane, were classified as "subduction earthquakes". This category also includes some historical events commonly assumed to be subduction earthquakes. They were not used to assess the maximum magnitude observed within the crustal regions. Earthquakes occurring beyond crustal depths in subduction zones were generally classified as intraslab events, including those occurring at mantle depth in the lower plate in front of a subduction zone. They were not used to assess the maximum magnitude observed within the crustal regions. Earthquakes located near the boundaries of the regions sometimes may not belong to the region they fall in. This could be due to the intrinsic uncertainty of the event location or the

uncertainty of the region boundary definition. Such cases are mainly identified where the focal mechanism of the event is also available. They are used to define the maximum magnitude of the region they are manually associated with, not the region they are located in.

Each crustal region has also been associated to one of the SHARE superzones based on the maximum overlap area between each of them. This association allowed us to apply the maximum magnitude determination from SHARE to the regionalization. Note that the SHARE maximum magnitude includes the consideration of the maximum magnitude associated to seismogenic faults (see SECTION 1.3.3).

1.3.2 Seismic datasets

These seismic datasets will be used to determine the rates of seismicity. To this end, the earthquake catalogues need to geographically cover all the potential seismic sources for the whole NEAM region, cover the longest possible time span, and be to be as homogeneous as possible in terms of parameterization. To meet these conditions, we resorted to two different datasets: 1) the ISC (ISC, 2016) catalogue, which has a global coverage, for the area of the Atlantic Sea (time span 1900-2015) and the SHEEC-EMEC catalogue (Stucchi et al., 2012; Grünthal & Wahlström, 2012), which has a limited extent, for the area of the Mediterranean and connected seas (time span 1000-2006). Their area of application is shown in FIGURE 1.3, which was obtained by merging individual regions of the tectonic regionalization (FIGURE 1.2) into macro-regions and considering the distribution of available data.

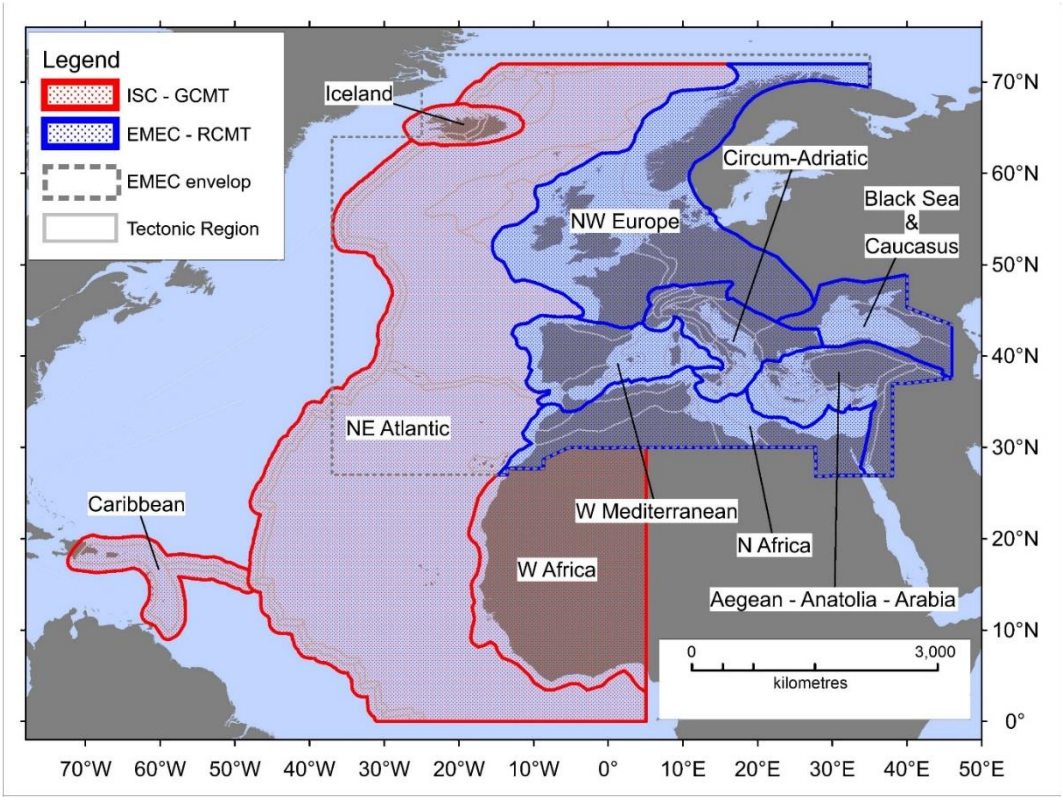

FIGURE 1.3: Map showing the regions used for the completeness analysis in relation with the adopted earthquake catalogues. Notice the outline of the availability of the EMEC catalogue.

For these two earthquake catalogues, we performed the completeness analysis from the statistical viewpoint based on common procedures (e.g. Wiemer 2001; Woessner & Wiemer, 2005), separately for each macro-region (TABLE 1.1), and then adopted the Gardner and Knopoff (1974) method for the declustering (FIGURE 1.4).

TABLE 1.1: Year of completeness for the macro-regions and the relevant earthquake catalog. The value "-1" corresponds to a completeness year not assigned.

Macro-region	Catalog	M 3.5	M 4.0	M 4.5	M 5.0	M 5.5	M 6.0	M 6.5	M 7.0	M 7.5	M 8.0
Iceland	ISC	1996	1996	1980	1980	1972	1972	1944	1944	1944	1944
Caribbean	ISC	2000	2000	1970	1970	1965	1965	1902	1902	1902	1902
NE Atlantic	ISC	1996	1996	1965	1965	1952	1952	1944	1944	1944	1944
W Mediterranean	EMEC	-1	2000	1970	1950	1910	1750	1350	1350	1350	1350
Circum-Adriatic	EMEC	-1	2000	1960	1920	1905	1850	1450	1450	1450	1450
NW Europe	EMEC	2000	1980	1960	1900	1880	1550	1550	1550	1550	1550
Black Sea & Caucasus	EMEC	-1	-1	1950	1920	1900	1850	1550	1550	1550	1550
Aegean - Anatolia - Arabia	EMEC	-1	2000	1965	1911	1905	1750	1550	1100	1050	1050
W Africa	ISC	2009	2009	1975	1975	1940	1940	1940	1940	1940	1940
N Africa	EMEC	-1	-1	1960	1930	1910	1890	1850	1700	1700	1700

We adopted few other seismic datasets, not shown here, at Level 1 to constrain the upper end of magnitude-frequency distributions that will be illustrated in SECTION 1.4. These datasets are the earthquake catalogs ISC-GEM (Storchak et al., 2013; 2015; Di Giacomo et al., 2018) and a catalog of historical earthquakes reviewed by NOA that provide information on the larger earthquakes at global and European (Mediterranean and near Atlantic) scale, respectively. In addition to these, we also considered the zonation developed in the SHARE Project to estimate the larger earthquakes at European scale (Giardini et al., 2013; Woessner et al., 2015).

1.3.3 Fault datasets

The aim of fault datasets is to determine the orientation and sense of movement of future earthquake ruptures. To this end, we compiled two different datasets: catalogues of focal mechanisms, and geological faults. In the same way, as done for earthquake catalogues, we favored geographic coverage over extreme detail.

As regards the catalogues of focal mechanisms we considered the same macro-regions of the earthquake catalogues (FIGURE 1.3). We adopt the global CMT catalogue (Dziewonski et al., 1981; Ekström et al., 2012) for the area of the Atlantic Sea and the RCMT catalogue (Pondrelli & Salimbeni, 2015) for the area of the Mediterranean and connected Seas (FIGURE 1.5). Although these catalogues contain information on date and time and earthquake magnitude, they are shorter in time and less complete at lower magnitudes, and they contain earthquakes already present in the adopted seismicity catalogues. Consequently, they were not used to constrain the seismicity rates. Conversely, they have been used for sanity check the computed annual rates (see *Doc_P2_S5*).

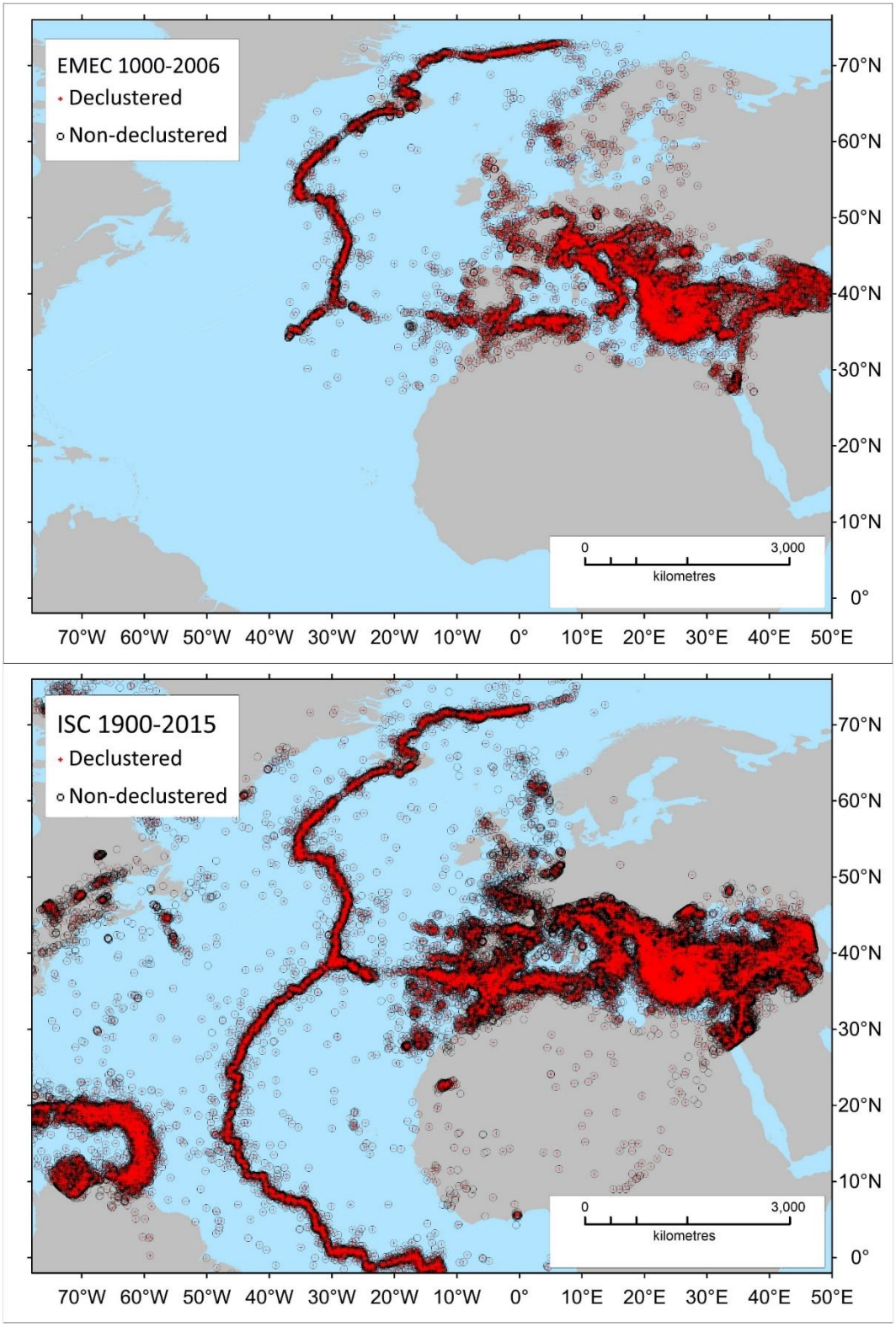

FIGURE 1.4: Earthquake catalogs and their geographic coverage in the NEAM region. For each catalog both the declustered and non-declustered versions are shown.

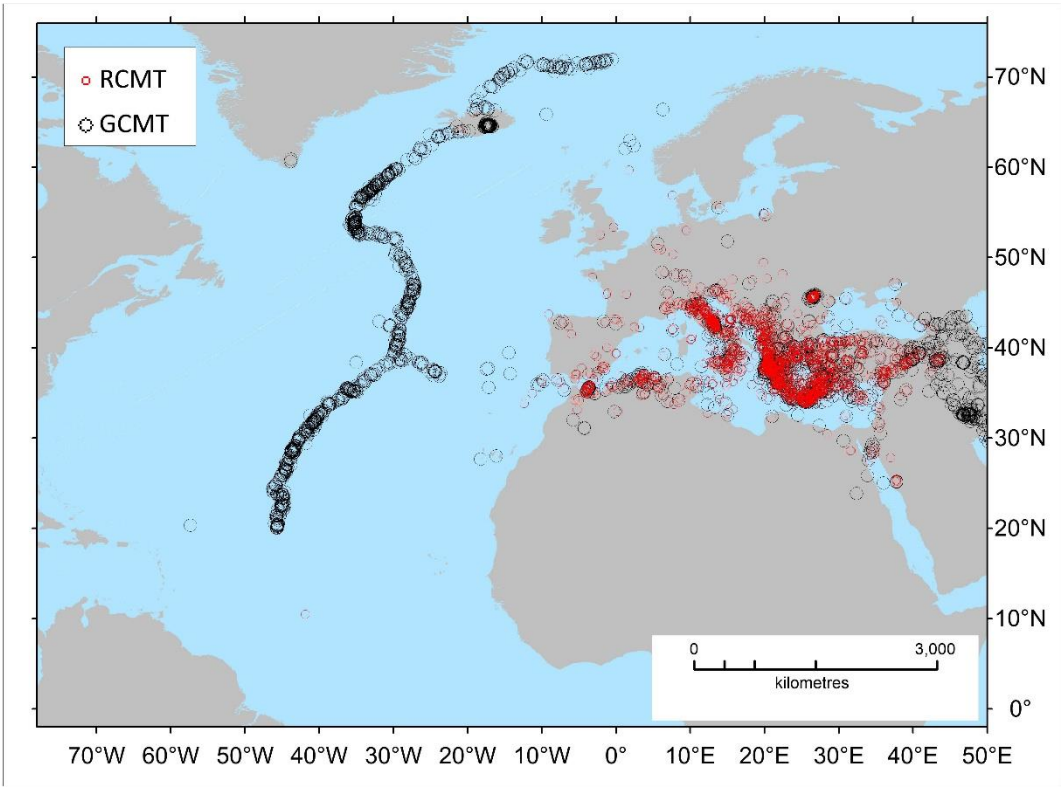

FIGURE 1.5: Map showing the geographic distribution of the catalogues of focal mechanisms (see text for details).

As regards the geological faults, we put together the fault datasets by retrieving data from public large databases of faults, plus some original additions or revisions of specific cases (FIGURE 1.6). In this collection, we considered two main categories of geological structures: crustal faults, particularly on plate boundaries, and subduction zones.

Our main sources of information for the fault geometry and kinematics were the following.

- The European Database of Seismogenic Faults (EDSF; Basili et. al, 2013b) compiled in the framework of the EU project SHARE. EDSF covers mainly the Mediterranean, the Gulf of Cadiz, and the southern part of the Black Sea. It provides information for 1,128 crustal faults and three subduction zones.
- The Database of Individual Seismogenic Sources version 3.2.1 (DISS; DISS Working Group, 2018) which covers the central Mediterranean. It was used to replace EDSF in the central Mediterranean with information for 188 crustal faults.
- The global plate boundary model by Bird (2003) as the starting reference for the Mid Atlantic Ridge, as well as the Gloria fault.
- An early version of the Slab 2.0 model, later published by Hayes et al. (2018) and Hayes (2018), provided as a courtesy by G. Hayes, for the Caribbean Arc subduction.
- A model of the Calabrian Arc subduction, taken from the recent reconstruction of the slab interface by Maesano et al. (2017), replaced the model provided by EDSF and DISS.
- Additional information from recently published papers about the Hellenic and Cyprus Arcs.
- Additional information about the Gloria fault and the Cadiz subduction was derived from the EU project ASTARTE, deliverable D3.12 (http://www.astarte-project.eu/).

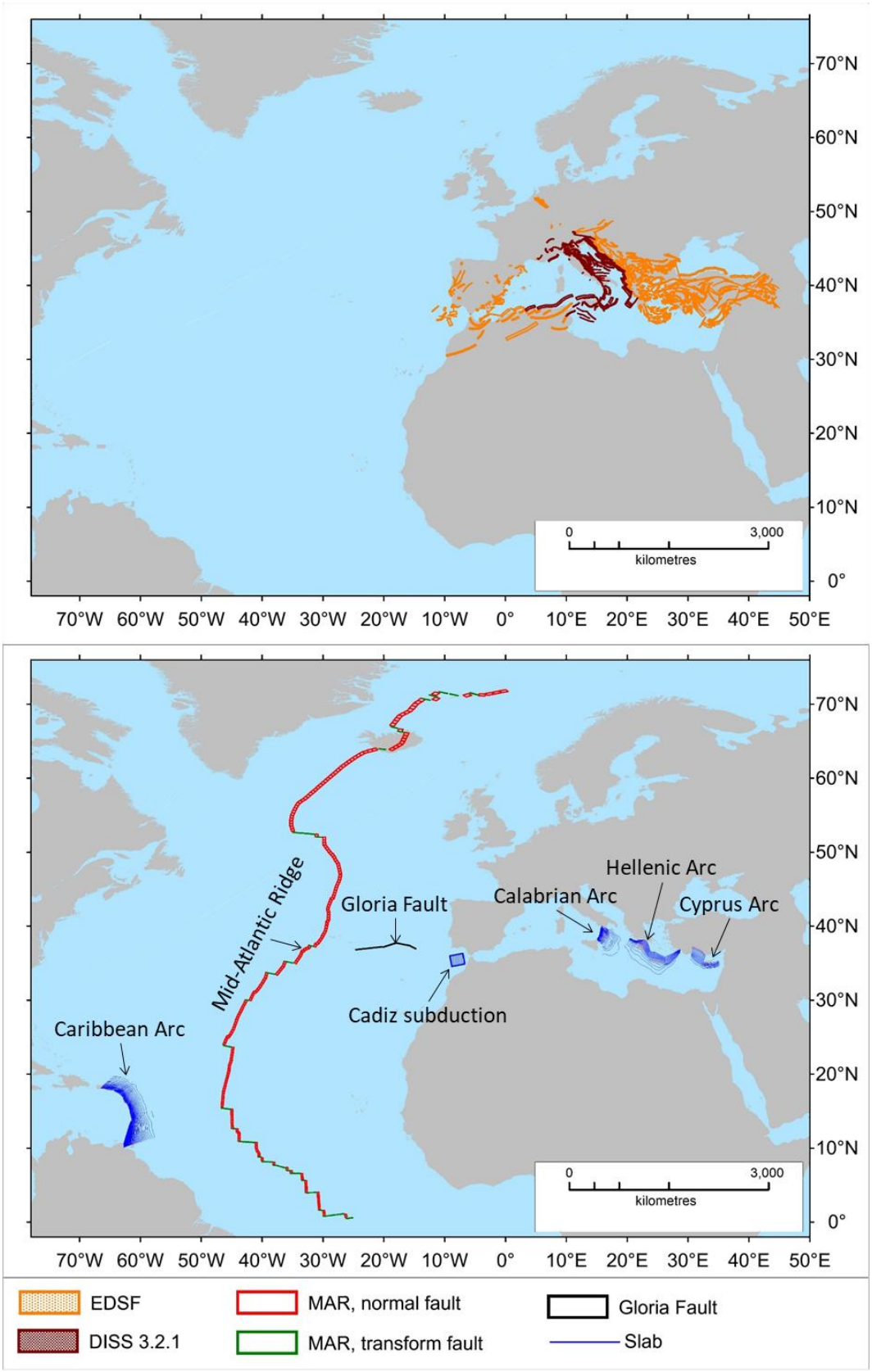

FIGURE 1.6: Fault datasets. EDSF = European Database of Seismogenic Faults; DISS = Database of Individual Seismogenic Sources; MAR = Mid-Atlantic Ridge. See text for description and references.

1.3.4 Assignment of seismicity modeling types to different source zones and faults

The previously introduced four seismicity modeling types (BS, PS, SPS, SBS) are used for different tectonic structures in the probabilistic earthquake model as detailed below. Their geographic distribution is shown in FIGURE 1.7, consistently with the subdivisions of the tectonic regionalization shown in FIGURE 1.2. As previously noted, a maximum of two seismicity modeling types are present in each region, because the special cases (SPS and SBS) are alternative to each other. Faults of FIGURE 1.6 are clearly geographically related to the regions of FIGURE 1.2 in this assignment.

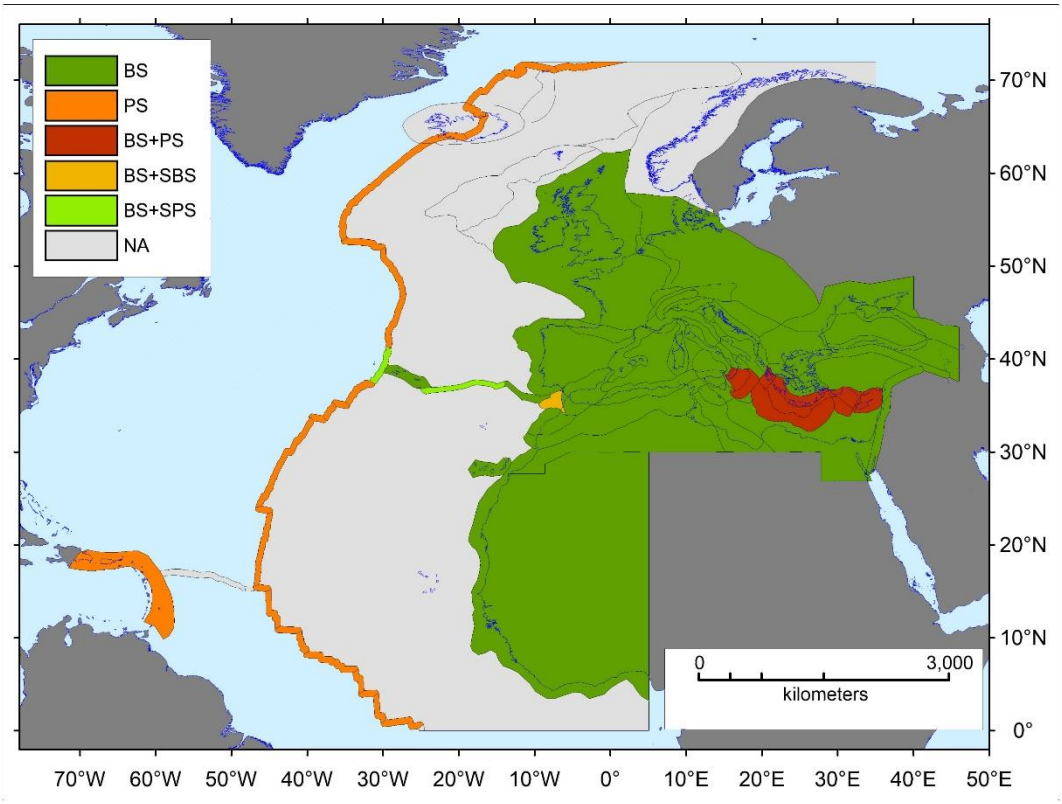

FIGURE 1.7: Map showing the distribution of the seismicity model types assigned to each region of the tectonic regionalization. Compare with FIGURE 1.6 to associate the mapped faults (crustal faults and subduction interfaces) with the classified regions.

Assignment of Background Seismicity (BS)

The BS seismicity modeling type is used everywhere in the Mediterranean and its connected Seas, such as the Aegean and Black Seas (**FIGURE 1.7**). In these basins, BS is also used in the sub-regions including the three subduction zones treated as PS. In the Atlantic Ocean, BS is used in the near-field of most coastlines (**FIGURE 1.7**), including regions where also other seismicity modeling types are used. BS is instead neglected for the source zones considered distant enough from some coastlines, for which the PS is the only seismicity modeling type that significantly contributes to tsunami hazard, such as the Caribbean Arc and the portion of the Mid-Atlantic Ridge distant enough from the Azores Islands. One exception is the region around Iceland, where only PS is used. This is mainly due to the lack of computational resources to calculate tsunami Gaussian-shaped elementary sources (SECTION 2.5), therefore, BS sources should be added in a future update of the NEAMTHM18 for this region. BS is instead neglected in the stable oceanic regions (compare **FIGURE 1.2**), where the seismicity

rates are assumed to be too low to significantly contribute to tsunami hazard, based on global rates in this type of tectonic domain (Kagan et al., 2010).

Assignment of Predominant Seismicity (PS)

The PS seismicity modeling type is used for the following tectonic structures (see **FIGUREs 8 and 9**):

- Mediterranean area:
  - Calabrian Arc (subduction interface, pure thrust)
  - Hellenic Arc (subduction interface, pure thrust)
  - Cyprus Arc (subduction interface, pure thrust)
- Atlantic area:
  - Caribbean Arc (subduction interface, pure thrust)
  - Mid-Atlantic Ridge (crustal fault; normal and transform) except for the zone near the Azores Islands

Hence, PS faults are present only in a limited subset of regions. Note that PS will coexist with BS in most of these regions, except for the distant or relatively distant source regions, such as the Caribbean subduction and the portion of the Mid-Atlantic Ridge relatively far from the Azores islands.

The assignment of seismicity distribution between PS and BS will be treated slightly differently for subduction or crustal PS, since the associated maximum magnitude is generally different. In general, the maximum modeled earthquake magnitudes for subduction zones are higher (up to magnitude 9 in some cases) than for crustal faults.

Although we cannot maintain that we have a perfect knowledge of the faults that we treat as PS, adding alternative models for the fault geometry (e.g. varying the dip) would have an unaffordable computational cost for this project. We have anyway performed some sensitivity tests of individual tsunami scenarios to these fault parameters (Basili et al., 2017), and to the modeling of heterogeneous slip distributions on 3D versus planar faults (Tonini et al., 2017). Further sensitivity analyses concerning how the PS geometry influences the PTHA (not only the individual tsunami scenarios) need to be planned for any project update or follow up. This is described in document Doc_P2_S5.

Project resources neither allowed for considering further PS sources, such as the North Algerian thrust margin, whose geometry is reasonably well constrained. However, the known faults are used for constraining the earthquakes included in the BS, whose focal mechanism and locations is constrained according to known faults and past seismicity. Nevertheless, we performed disaggregation of the SPTHA to evaluate the relative importance of the different PS also in comparison to BS in each region. This is described in document Doc_P2_S5.

Assignment of Special Predominant Seismicity (SPS)

The SPS seismicity modeling type is used for the Gloria fault (crustal fault, transcurrent), a sub-vertical structure trending roughly E-W in the North-eastern Atlantic, and for a portion of the Mid-Atlantic Ridge (crustal fault; normal and transform), that is the portion of the ridge closer to the Azores Islands (see FIGURE 1.6, bottom panel, for the faults, and FIGURE 1.7 for the assignment of

seismicity modeling types). SPS coexists with BS in all cases. This choice allowed us to save some computational resources without significant decrease in modeling accuracy.

Assignment of Special Background Seismicity (SBS)

The SBS seismicity modeling type is used in the Gulf of Cadiz. There, the Cadiz subduction zone is identified (Gutscher et al., 2002; Duarte et al., 2013). Its geometry, according to the available model from the Deliverable 3.16 of the ASTARTE project (http://www.astarte-project.eu/), is quite a crude approximation as it is a planar and almost square interface (FIGURE 1.6, bottom panel). Hence, we decided to impart some variability regarding its position and its dip angle, as later specified when describing the details of the discretization and of the seismicity parameter ranges. The maximum modeled magnitude is that of all other subduction zones. Note that SBS coexists with BS in this region, like PS coexists with BS in several regions as described above.

1.3.5 Magnitude discretization and range

Magnitude discretization is performed according to the values listed in TABLE 1.2. The magnitude values for which a tsunami scenario is numerically modeled are those in the right-hand column. These values are set as the mean moment of the intervals defined by the first two columns, computed assuming a standard Gutenberg and Richter distribution with a b-value equal to 1. The intervals are used for earthquake rate determination. The use of the mean (instead of the mode, that would correspond to the minimum magnitude, Selva et al., 2016) is preferred to avoid any potential bias due to underestimating magnitudes or annual rates of any interval. The sampling step gets (roughly exponentially) finer as earthquake magnitude increases; this should allow for an approximately even sampling of the corresponding tsunami intensity increase, which should turn out to be approximately linear (e.g., Lorito et al., 2015). In principle, if the intervals are narrow enough, these choices should not affect the results.

The one above is the nominal maximum range for the modeled earthquake magnitudes. The range which is then actually implemented for each zone, depends on several factors.

We assume that the interval [5.7,6.34] (corresponding to M=6) is the minimum tsunamigenic earthquake magnitude. Hence, we do not include smaller magnitudes in the discretization.

For source regions located far away from all target coastlines, and modeled as PS only, namely the Caribbean Arc subduction and the sections of the Mid Atlantic Ridge relatively far from the Azores Islands, the four smaller intervals have been omitted, assuming they would have given a negligible contribution to the tsunami hazard in the target coastlines. Therefore, for these PS sources, the minimum modeled magnitude is M=7.3.

Conversely, the maximum earthquake magnitude which is modeled is characterized by larger variability, as it is constrained by:

- the maximum fault size;
- the assumed seismogenic depth interval for a subduction zone (very shallow seismicity allowed or not allowed);
- the crustal thickness;
- the adopted scaling relations.

TABLE 1.2: Magnitude discretization. The interval mean corresponds to the mean moment obtained assuming a truncated Pareto distribution with a b-value equal to 1.

#	Interval lower end	Interval upper end	Interval mean
1	5.7000	6.3383	6.0
2	6.3383	6.6724	6.5
3	6.6724	6.9367	6.8012
4	6.9367	7.2183	7.0737
5	7.2183	7.4265	7.3203
6	7.4265	7.6660	7.5435
7	7.6660	7.8271	7.7453
8	7.8271	8.0330	7.928
9	8.0330	8.1551	8.0933
10	8.1551	8.3338	8.2429
11	8.3338	8.4234	8.3782
12	8.4234	8.5804	8.5007
13	8.5804	8.6430	8.6115
14	8.6430	8.7825	8.7118
15	8.7825	8.8227	8.8025
16	8.8227	8.9481	8.8846
17	8.9481	8.9696	8.9588
18	8.9696	9.0837	9.026

These elements will be provided in the next SECTIONS. Here we anticipated two tables with the implemented earthquake magnitude ranges for each source zone treated as PS, SBS, and SPS, for either crustal or subduction sources (TABLE 1.3 and TABLE 1.4). For all sources, we also report in the tables the (approximate) seismogenic depth intervals. Note that two alternative seismogenic depths are considered for Mediterranean subductions only.

For BS sources, we limited the nominal maximum modeled to M≈7.5 in the Atlantic and M=8.1 in the Mediterranean. These limits are applied to the tsunami modeling possibility, while they may be, in some tectonic regions, further reduced by some of the probabilistic models discussed in SECTION 1.4.

The rationale for these limits is based on the MFD global analogues proposed by Kagan et al. (2010). Most of the Mediterranean and Atlantic regions correspond to the “Active continent” and “Slow spreading ridges”, respectively, defined by Kagan et al. (2010). We thus adopt magnitude values beyond the corner magnitude obtained from the MFD global estimates, which is where the rates of occurrence of higher magnitude decreases very rapidly. As regards the Euro-Mediterranean region, these magnitude values are also consistent with the annual rate decrease of the overall MFD calculated by Woessner et al. (2015) for the PSHA of the project SHARE.

In both basins, maximum magnitudes are generally further limited by thinner crust. The model adopted to constrain crustal sources, and particularly the BS sources, is CRUST 1.0 by Laske et al. (2013), which is shown in FIGURE 1.8. Hence, the spatial distribution of maximum modeled magnitudes for BS sources is quite heterogeneous. Indeed, a thin crust may limit the nominal

maximum magnitude by imposing an upper limit to fault width. This indeed happens at some places, such as in the Tyrrhenian Sea or at many places in the Atlantic (FIGURE 1.9).

TABLE 1.3: Earthquake magnitude and seismogenic depth ranges for Mediterranean PS subduction zones.

	Calabrian Arc (PS)	Hellenic Arc (PS)	Cyprus Arc (PS)
Minimum magnitude	6	6	6
Maximum Magnitude w/ very shallow seismicity not allowed + Strasser et al., 2010 Scaling Relation	8.1	8.9	8.5
Maximum Magnitude w/ very shallow seismicity not allowed + Murotani et al., 2013 Scaling Relation	8.1	8.7	8.4
Seismogenic depth interval (km from the mean sea level) w/ very shallow seismicity not allowed	44-15.5	56.5-14	48.5-5.5
Maximum Magnitude w/ very shallow seismicity allowed + Strasser et al., 2010 Scaling Relation	8.6	9	8.5
Maximum Magnitude w/ very shallow seismicity allowed + Murotani et al., 2013 Scaling Relation	8.6	9	8.4
Seismogenic depth interval (km from the mean sea level) w/ very shallow seismicity allowed +	44-6.8	56.5-8.8	48.5-5.5

TABLE 1.4: Earthquake magnitude and seismogenic depth ranges for Atlantic PS, SPS and SBS subduction zones and crustal faults.

	Caribbean Arc (PS)	Strike-Slip Mid-Atlantic Ridge and Gloria Fault (SPS)	Dip-Slip Mid-Atlantic Ridge (SPS)	Strike-Slip Distant Mid-Atlantic Ridge (PS)	Dip-Slip Distant Mid-Atlantic Ridge (PS)	Cadiz Arc (SBS)
Minimum magnitude	7.3	6	6	7.3	7.3	6
Maximum magnitude	9	8.2	7.9	8.2	7.9	9
Seismogenic depth interval (km from the sea floor)	48-1	20-0	37-0	20-0	37-0	75-0

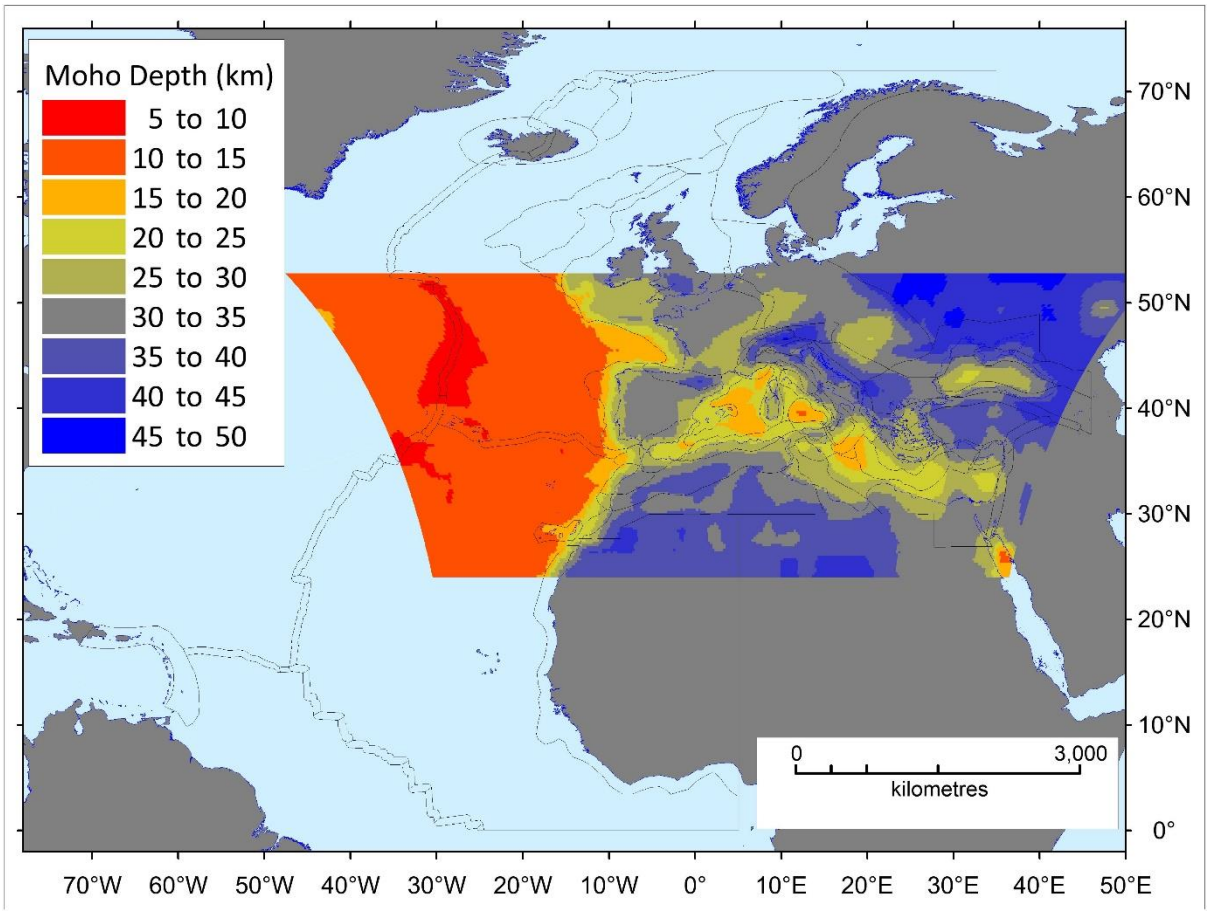

FIGURE 1.8: Map showing the depth of the base of the crust (Moho; Laske et al., 2013), adopted as a proxy for the base of the seismogenic layer, i.e. the depth that cannot be intersected by the modeled earthquake ruptures (see the scheme in FIGURE 1.15).

We assume that the annual rates of the higher-magnitude earthquakes that are not modeled for tsunami propagation due to these limitations are negligible. To test this circumstance, we quantified the annual rate of all these magnitudes, as emerging from all the quantification models described below, in order to check whether these values are negligible in terms of their influence onto the hazard. This sanity check is reported in Doc_P2_S5.

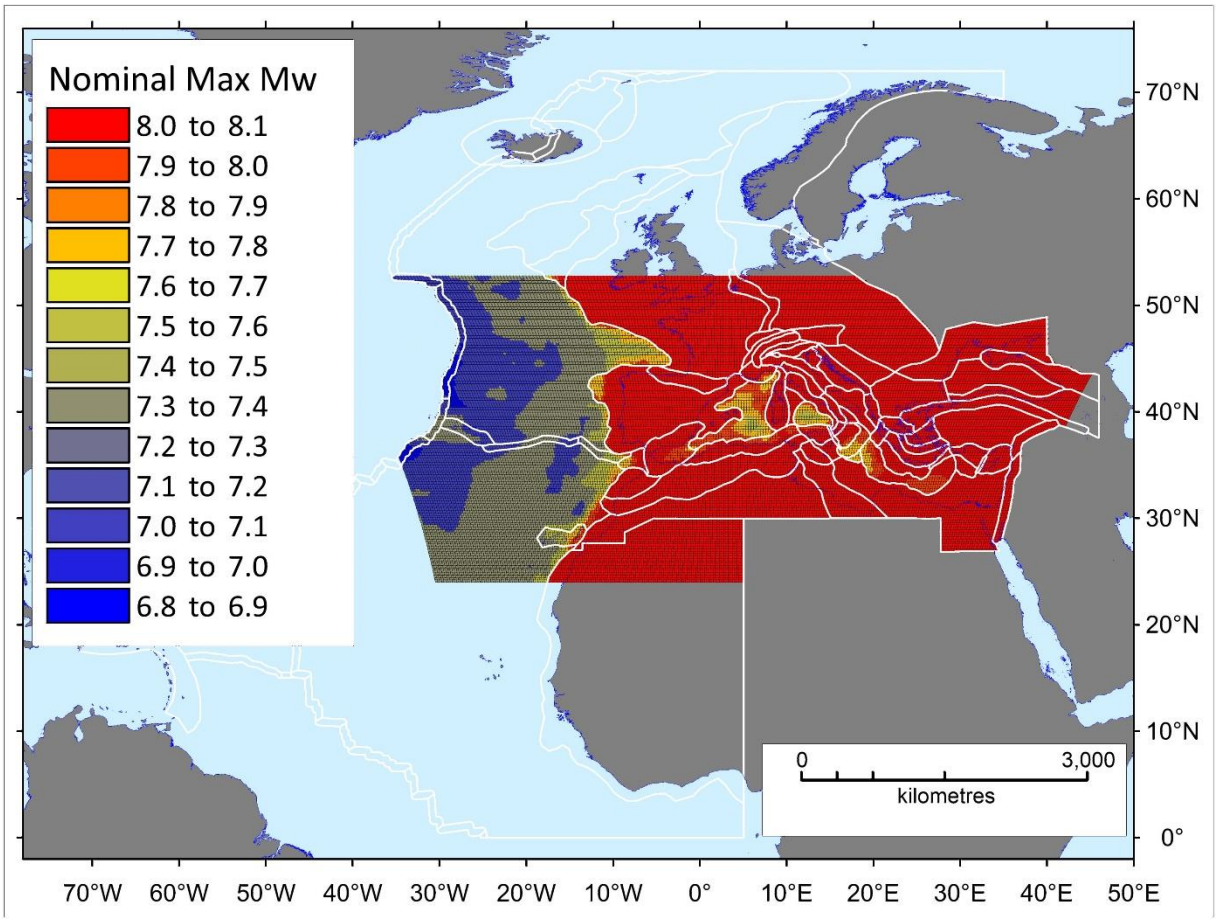

FIGURE 1.9: Map showing the distribution of the nominal maximum modeled moment magnitude in each cell of the crustal discretization (background seismicity model type). As explained in the text, these depths are called nominal as they are applied to all depths in each cell of the BS discretization, but the shallowest depth (top of the fault at 0 km depth).

However, the maximum magnitude of 8.1 and 7.5 in the Mediterranean are in fact allowed everywhere only for the shallowest scenarios in our depth discretization, that is those with the top of the rectangular fault model employed reaching at the surface. Consequently, the maximum magnitude limits imposed by the crust thickness are defined "nominal" in FIGURE 1.9. Conversely, as described in a following SECTION dealing with the discretization of the BS sources, the next deeper depth intervals are all enforced to comply with the maximum magnitudes allowed by the crustal thickness (FIGURE 1.9), according to Moho depth in FIGURE 1.8. The reason for this choice, which is quite a crude approximation indeed, is that we want to avoid missing relatively rare but still possible big crustal earthquakes. The latter are sometimes modelled, for example in PSHA, as thinner aspect ratio earthquakes, so fitting in the available brittle crust depth where the crust is too thin. We instead keep the fault size as imposed by the scaling relations (presented in the next SECTION) even if the fault crosses the Moho.

1.3.6 Empirical fault scaling relations

To determine the size of the earthquake ruptures to model we adopt (empirical) fault scaling relations. The scaling relations are also used for predetermining the geometrical discretization of the seismic sources of all the seismicity model types (PS, BS, SPS, SBS).

In the early stages of the project (Phase 1 and 2) we revised the abundant literature on this subject, analyzed the differences between their predictions, and tested their applicability to our modeling scheme.

TABLE 1.5 lists the association between some common scaling relations and the tectonic settings of the tectonic regionalization. The ones we eventually adopted and their association to the seismicity model types (PS, BS, SPS, SBS) are also indicated. FIGURE 1.10 shows the distribution of the adopted scaling relations in map view.

In summary, we adopt two alternatives – from Strasser et al. (2010) and from Murotani et al. (2013) - for the subduction interfaces (either as PS or SBS), and the set by Leonard (2014) for all crustal faults (either as BS or PS or SPS).

Major features of the Strasser et al. (2010) scaling relations are:

- two tectonic settings: subduction interface and intraslab;
- fitted relations are linear;
- relations provided for moment magnitude vs. length (L), width (W), and area (A);
- relations for the various dimensions are independent from one another;
- a comparison between these relations and previously published relations is given.

Major features of the Murotani et al. (2013), with respect to Strasser et al. (2010), scaling relations are:

- subduction interface only;
- relations provided for seismic moment vs. area (A), and displacement (D);
- include later giant earthquakes in the dataset.

Major features of the Leonard (2014) scaling relations are:

- these are model-driven relations; therefore, they are valid for the range of dimensions that the model is considered valid;
- two tectonic settings: interplate and stable continental region (SCR);
- two faulting mechanisms: dip slip (normal and reverse together) and strike slip;
- relations are consistent with one another depending on length/width ratio and displacement/area ratio;
- fitted relations can either be linear, or bilinear, or trilinear;
- relations provided for seismic moment and moment magnitude vs. length (L), width (W), area (A), and displacement (D);
- uses the largest and most recent earthquake rupture dataset;
- a comparison between these relations and previously published relations is given.

Important differences exist on the predicted size of the rupture for any given moment magnitude in different tectonic settings. These differences can be visually appreciated by analyzing FIGURE 1.11, which shows the expected values for the adopted scaling relations. Note that for dip-slip crustal faults of any given moment magnitude the predicted rupture dimension in SCR is systematically smaller than in interplate regions, and vice versa for the predicted average slip. Note also that the

relations for strike-slip faulting in both interpolate and SCR is bilinear in the range of magnitude explored by our model, indicating that the aspect ratio of the rupture increases for increasing moment magnitude. Ruptures size for the subduction interface is systematically bigger than for crustal faults of any type, and vice versa average slip is smaller, especially in the case of the Murotani et al. (2013) relationship. Note also that each although each scaling relation carries its own stated uncertainty, stemming from the data fitting procedure, we use only best-fitting parameters.

TABLE 1.5: Tectonic settings, associated fault scaling relations, and seismicity model types.

Tectonic setting	Common scaling relations	Adopted	Seismicity model type
Active volcanoes	Not considered.	Not considered.	n.a.
Back-arc and orogenic collapse	Leonard (2010); Leonard (2014), Interplate DS	LE14 INT DS-SS	BS
Continental rift	Leonard (2010); Leonard (2014), Interplate DS	LE14 SCR DS-SS	BS
Oceanic rift	None available.	LE14 INT DS	BS, PS
Contractional wedge	Leonard (2010); Leonard (2014), Interplate DS	LE14 INT DS-SS	BS
Accretionary wedge	Leonard (2010); Leonard (2014), Interplate DS	LE14 INT DS-SS	BS
Conservative plate boundary	Leonard (2014), Interplate SS; Romanowicz and Ruff (2002); Hanks and Bakun (2008); Blaser et al. (2010) strike slip continental or oceanic	LE14 INT SS-DS	BS
Transform faults s.s.	Romanowicz and Ruff (2002); Blaser et al. (2010) strike slip oceanic; Leonard (2014), Interplate SS.	LE14 INT SS	BS, PS, SPS (Gloria)
Shield	Leonard (2010); Leonard (2014), SCR	Not considered.	n.a.
Stable continental region	Leonard (2010); Leonard (2014), SCR; Romanowicz and Ruff (2002) only for SS	LE14 SCR DS-SS	BS
Stable oceanic region	None available.	Not considered.	n.a.
Subduction zone - outer rise	Blaser et al. (2010) normal oceanic, Leonard (2010); Leonard (2014), Interplate DS	LE14 INT DS	BS
Subduction zone - interface	Blaser et al. (2010), reverse oceanic; Strasser et al. (2010) interface; (Murotani et al., 2008; Murotani et al., 2013); Skarlatoudis et al. (2016)	ST10 INF MU13 INF	PS, SBS (Cadiz)
Subduction zone - intraslab	Ichinose (2006); Strasser et al. (2010) intraslab	Not considered.	n.a.

* LE14: Leonard (2014); ST10: Strasser et al. (2010); MU13: Murotani et al. (2013); INT: interplate; INF: interface; SCR: stable continental region; DS: dip slip (normal and reverse); SS: strike-slip.

1.3.7 Discretization and parameterization of the seismic sources

Geometry, spatial discretization and tectonic data for PS subductions

The geometry of the three Mediterranean slabs were initially derived from the European Database of Seismogenic Faults (EDSF; Basili et al., 2013) and then modified according to newer data where available. In particular, the Calabrian Arc is replaced by the more recent model by Maesano et al. (2017) which is derived from the interpretation of a dense network of seismic reflection profiles integrated with the analysis of the seismicity distribution with depth. The Hellenic Arc is the same as that in EDSF, but we verified its consistency with recent works by Soudoudi et al. (2015) or Sachpazi

et al. (2016). The Cyprus Arc was slightly modified in consideration of results from recent works (Bakirci et al., 2012; Salaun al., 2012; Howell et al., 2017; Sellier et al., 2013a; Sellier et al., 2013b) that are based on seismic reflection profiles and tomographic and seismological data and constrain the geometry of the western part of the slab. The geometry of the Caribbean slab was entirely derived from an early version of the Slab 2.0 model, later published by Hayes et al. (2018) and Hayes (2018), provided as a courtesy by G. Hayes.

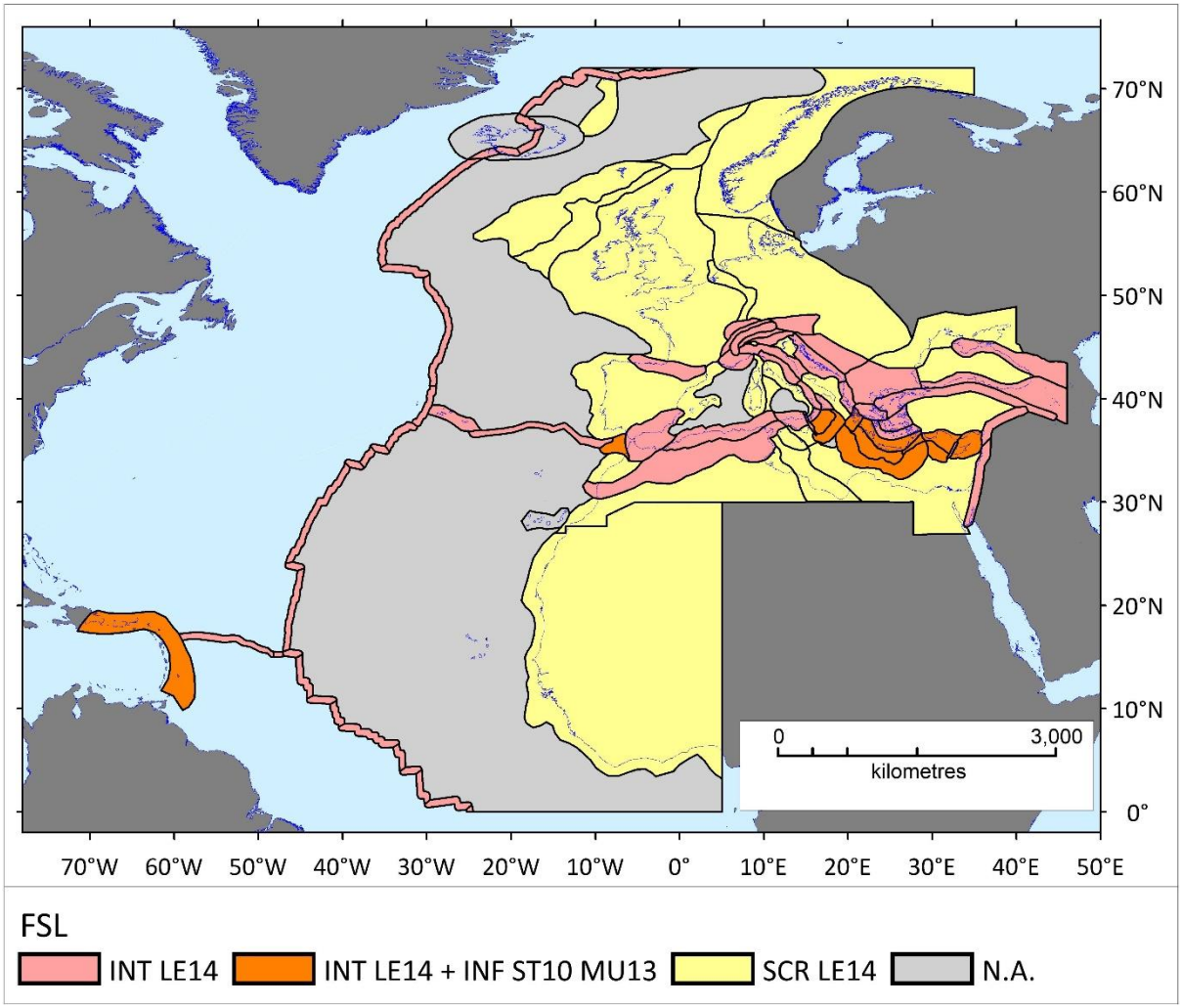

FIGURE 1.10: Map distribution of the relations by Leonard (2014, LE14), Strasser et al. (2010, ST10), and Murotani et al. (2013, MU13) as applied based on the characteristics of the tectonic regionalization. INT = interplate, SCR = stable continental region, INF = slab interface. Faulting mechanisms of crustal faults are assigned based on moment tensors and fault data. Only reverse slip faulting applies to subduction interface.

Starting from these geometries, we built 3D triangular meshes with element size set at ~15 km for the three subduction interfaces in the Mediterranean Sea, and at ~50 km for the subduction interface of the Caribbean Arc, using the Cubit mesh generator (http://cubit.sandia.gov). The triangles are used as elementary sources (subfaults) for setting the coseismic slip (at STEP 1) which determines the displacement used as tsunami initial condition (at STEP 2). The size of the triangles imposes a constraint on the minimum earthquake magnitude that can be modeled and/or on the

allowed maximum wave numbers (the “spatial frequency”) of the slip spatial distribution over the subduction plane.

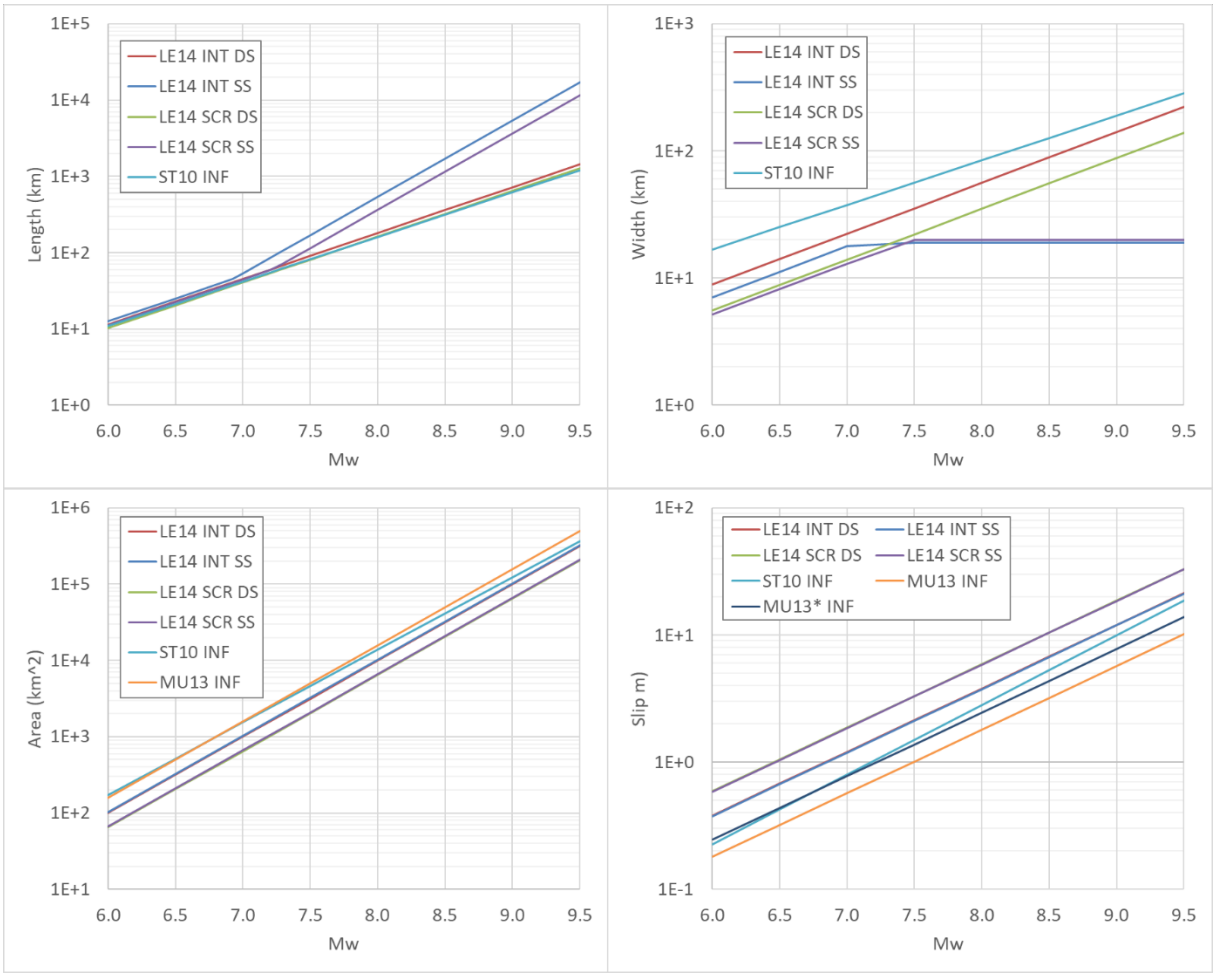

FIGURE 1.11: Comparison of relations by Leonard (2014, LE14), Strasser et al. (2010, ST10), and Murotani et al. (2013, MU13) in predicting fault length (upper left), width (upper right), area (lower left), and average slip (lower right), as applicable, in the cases of earthquake ruptures adopted in the seismicity model (crustal faults and subduction interfaces). INT = interplate, SCR = stable continental region, INF = slab interface (reverse slip only), DS = dip-slip, SS = strike-slip. Slip in ST10 and MU13* it is derived from seismic moment, using an average shear modulus of 33 GPa and the area predicted by the relationship (this also applies to LE14 SCR SS because of errors in the coefficients reported in the paper). In all other cases, slip is directly derived from the relationship.

For all subductions strike and dip are imposed by the discretization (FIGURE 1.12). A pure thrust faulting mechanism (rake 90°) is assumed for Cyprus and Caribbean Arcs. Variable rakes are used for the Calabrian Arc, ranging approximately from 140° to 60° moving from SW to NE, according to an almost S-N aligned overall convergence direction, and for the Hellenic Arc, being around a pure thrust in its western sector until roughly 25°E, where it changes progressively into a strike slip mechanism at the eastern edge.

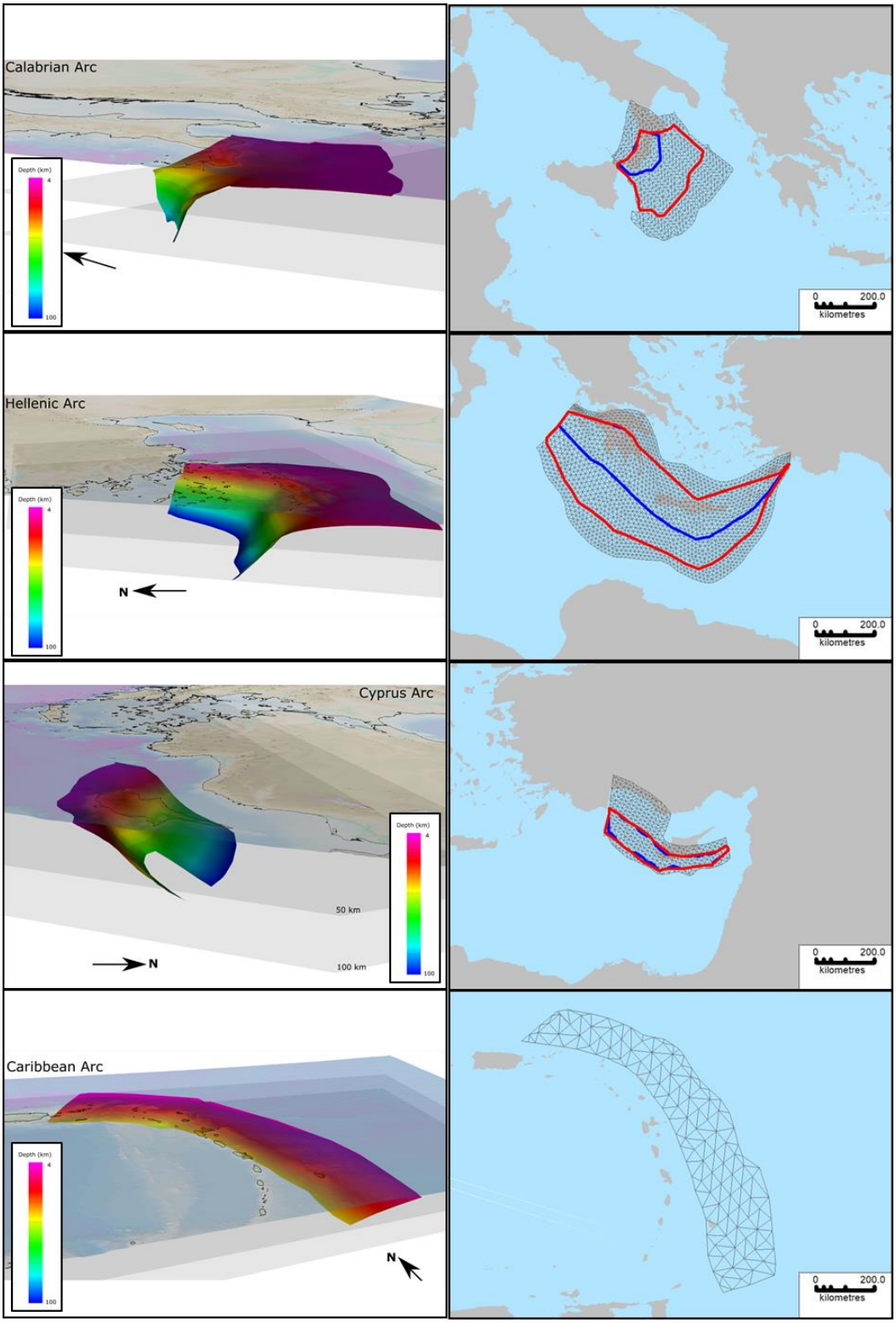

FIGURE 1.12: Map views of the meshes used to discretize the subduction interfaces, from top to bottom (right panels) they are: Calabrian Arc, Hellenic Arc, Cyprus Arc, and Caribbean Arc. 3D views of the subduction interfaces displayed with color-coded depths (left panels). Locations of these slabs are shown in FIGURE 1.6. The discrete meshes are represented with light blue lines; the narrower deeper seismogenic interval by the blue line, while the broader seismogenic depth interval is bounded by the red line (right panels).

As introduced in Selva et al. (2016), for the Mediterranean subduction zones, we use alternative seismogenic depth models (blue and red polygons in FIGURE 1.12). These alternative definitions will be both implemented, as epistemic alternative. Simply speaking, the blue and red zones define two alternative seismogenic depth intervals, with the blue one confining the slip at greater depths. These two alternatives are treated as modeling alternatives in the context of epistemic uncertainty quantification. The effective seismogenic depths for the various subductions treated as PS, anticipated in TABLE 1.3, have been defined coherently with these definitions. For the Caribbean Arc, which is in the far-field, no separation between nucleation and propagation zones has been adopted, hence no epistemic alternatives occur.

Geometry, spatial discretization and tectonic data for PS and SPS crustal faults

The crustal faults treated as PS sources are the transcurrent and normal faults belonging to the distant Mid-Atlantic Ridge (FIGURE 1.13). Where the Ridge is close enough to the POIs, such as the zone around the Azores Islands, and for the transcurrent Gloria fault (the two light-green regions in FIGURE 1.7), the SPS type is used, as already specified in a previous SECTION.

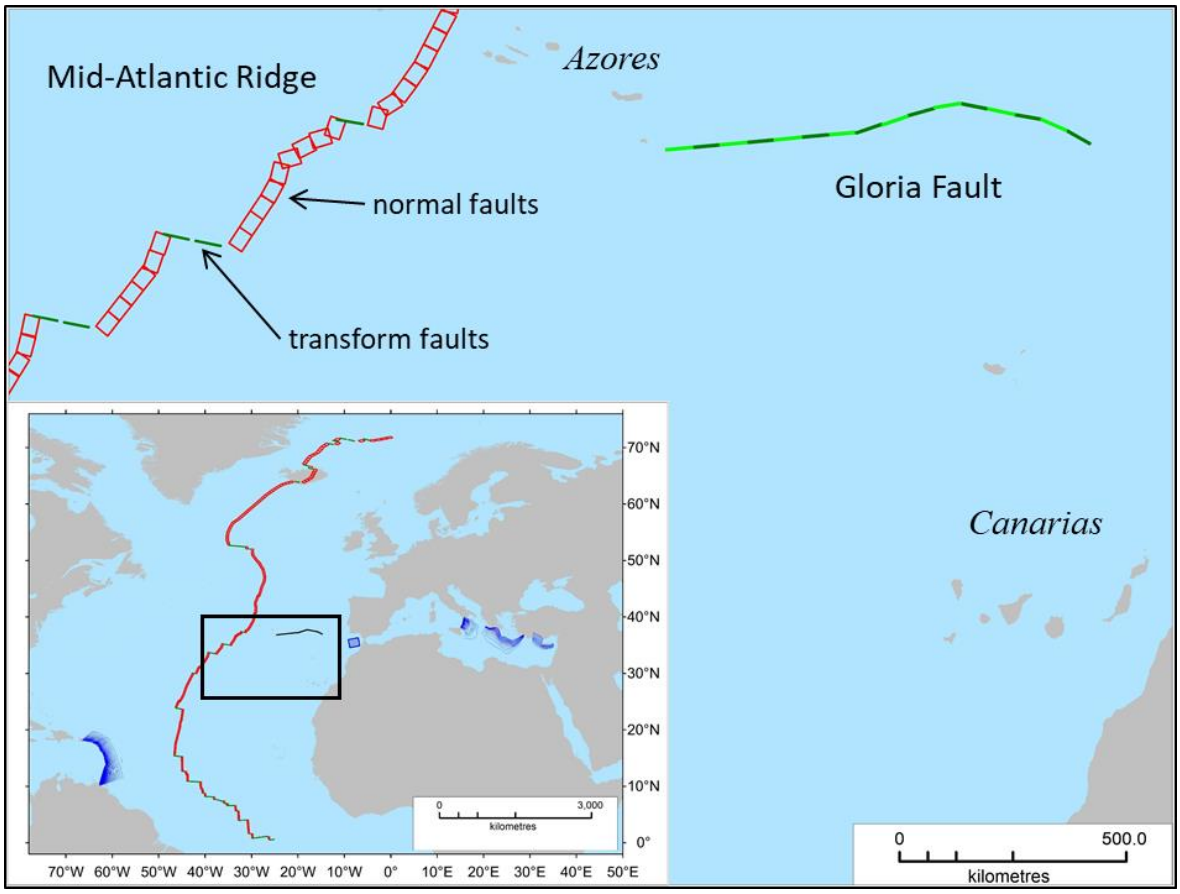

FIGURE 1.13: PS discretization in subfaults of the Mid-Atlantic Ridge (red = normal; green = transform) and the Gloria Fault (alternating light and green). Inset show location of the close-up view. See TABLE 1.6 for the size of subfaults and their combination to make up large ruptures.

The Mid-Atlantic Ridge (FIGURE 1.13) was discretized into 270 rectangular subfaults; 214 of them with normal faulting mechanism, constant dip angle=45° and size 40x45 km; 56 with pure strike slip mechanism, constant dip angle=90° and size 55x20 km. Since subfaults need to be combined to form individual ruptures for different magnitudes, their size was determined to minimize, within the

range of magnitudes considered, deviations with respect to the scaling relations by Leonard (2010, 2014). The Gloria fault (FIGURE 1.13) was discretized in the same way as the Mid-Atlantic transform faults.

So, both PS and SPS crustal faults are discretized in the same way with the same subfaults, down to the same minimum magnitude which depends on the faulting style. However, the only difference is that further smaller magnitudes are modeled for the SPS sources, that is for the sources closer to the Azores Islands. These earthquakes of magnitude down to 6 are approximated with the same technique used for the BS which is presented in the next SECTION.

The values of the geometrical parameters and of the slip for the distant Mid-Atlantic Ridge, both for the normal and strike-slip sections, and for section of the Mid-Atlantic Ridge and for the Gloria fault, the SPS structures described in the next SECTION, are reported in TABLE 1.6. The combinations of 1, 2, 3, or 5 subfaults are used for modeling earthquakes of different magnitudes ranging from 7.3 to 8.2 depending on the cases.

TABLE 1.6: Parameters of subfaults in the Mid-Atlantic Ridge zone (including Gloria fault). Parameters from scaling relations are: M_w=moment magnitude; M_0=seismic moment; L=fault length; W=fault width; A=fault area; D=slip. L*, A*, D* are approximated length, area and slip obtained by combining one or more subfaults; ΔA and ΔD are the deviations from the theoretical values for area and slip respectively.

A) Normal faults (spreading ridges): fixed patch size: L = 40, W = 45; total number of patches = 214

M_w	M_0 (Nm)	L (km)	W (km)	A (km^2)	D (m)	N. subfaults	L* (km)	A* (km)	ΔA (km^2)	D* (m)	ΔD (m)
7.3203	1.22E+20	70	30	2091	1.94	1	40	1800	-291	2.25	0.31
7.5435	2.63E+20	96	37	3495	2.51	2	80	3600	105	2.44	-0.07
7.7453	5.28E+20	127	44	5563	3.17	3	120	5400	-163	3.26	0.10
7.9280	9.93E+20	163	52	8472	3.91	5	200	9000	528	3.68	-0.23

B) Strike-slip faults (transforms): fixed patch size: L = 55, W = 20; total number of patches = 56

M_w	M_0 (Nm)	L (km)	W (km)	A (km^2)	D (m)	N. subfaults	L* (km)	A* (km)	ΔA (km^2)	D* (m)	ΔD (m)
7.3203	1.22E+20	112	19	2139	1.90	2	110	2200	61	1.84	-0.05
7.5435	2.63E+20	188	19	3577	2.45	3	165	3300	-277	2.66	0.21
7.7453	5.28E+20	299	19	5692	3.09	5	275	5500	-192	3.20	0.11
7.9280	9.93E+20	455	19	8670	3.82	8	440	8800	130	3.76	-0.06
8.0933	1.76E+21	666	19	12685	4.20	12	660	13200	515	4.04	-0.16
8.2429	2.95E+21	940	19	17902	4.99	16.	880	17600	-302	5.07	0.09

Geometry, spatial discretization and tectonic data for BS sources

The domain of the BS is uniformly discretized into a grid (FIGURE 1.14) composed by non-conformal equal-area cells of 25x25 km (cell sides depart from right angles with increasing distance from the origin; cell area is preserved everywhere) with origin at 24°N - 3°E.

The grid is trimmed around the area where the BS sources are close to the target coastlines. This implies that, as anticipated, some relatively distant PS do not overlap with BS (see also FIGURE 1.7). This is the case of the Caribbean Arc and most of the Mid-Atlantic Ridge, excluding the portion nearby the Azores Islands.

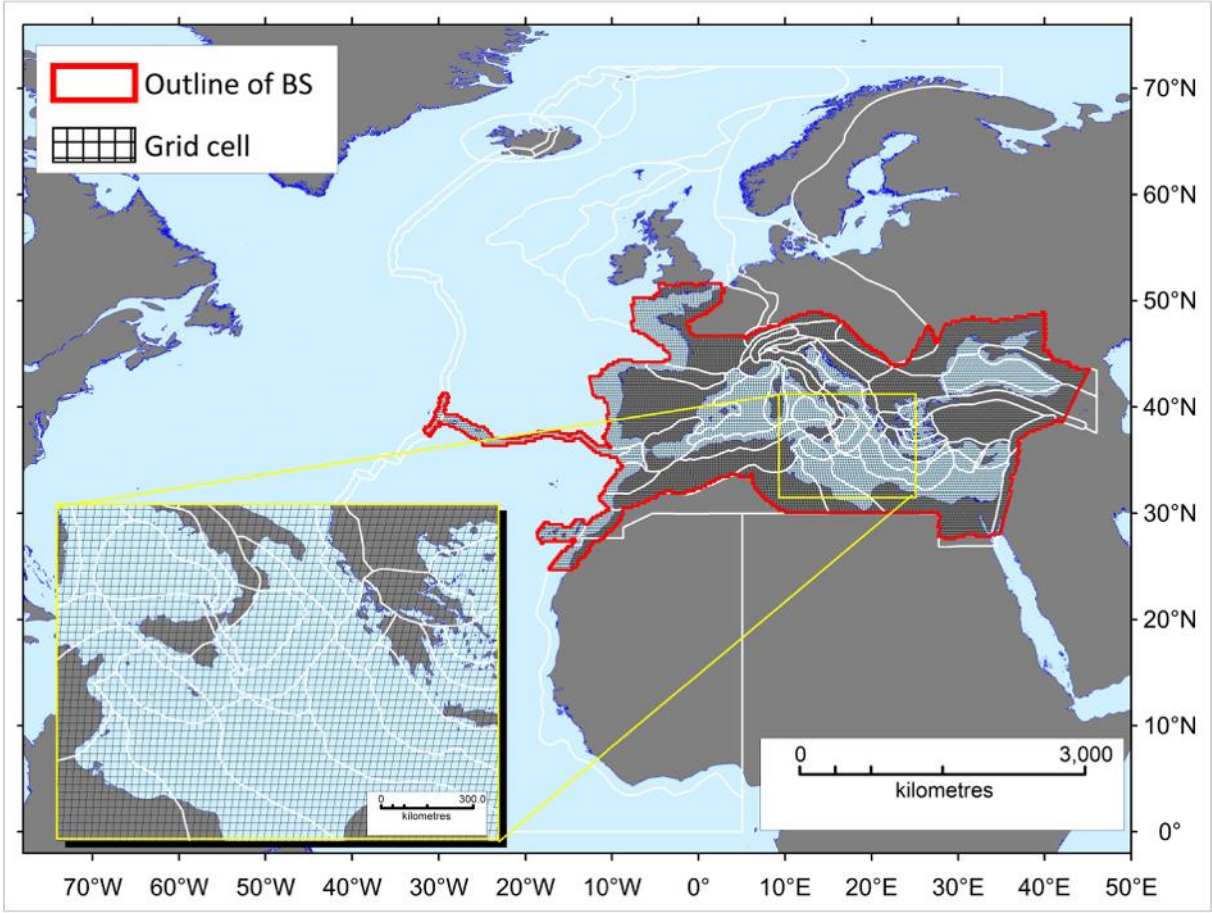

FIGURE 1.14: Regular grid (grey quadrangles, see the zoomed-in inset) for the background seismicity (BS) sources within the domain of calculation (red outline), outside which only predominant seismicity is modeled. Outlines of the individual source zones (regionalization) are shown with white polygons.

At each cell, the depth of the earthquake rupture explores the entire crustal thickness derived from the 1D global crustal model CRUST 1.0 by Laske et al. (2013), already shown in FIGURE 1.8. The discretization of the depth domain at each cell is defined by considering different depth levels for the top of the fault. To achieve a good sampling of the volume in each cell, a different discretization of the depth is considered for each of the different magnitude values as in the example of **FIGURE 1.15**.

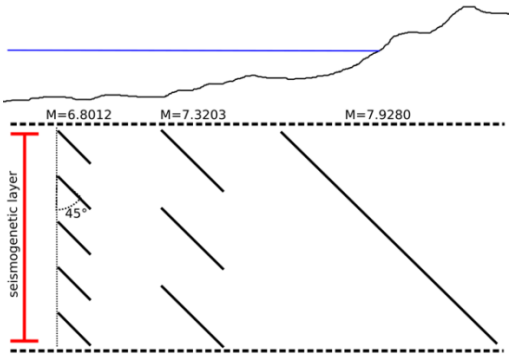

FIGURE 1.15: Scheme for the earthquake magnitude-dependent depth discretization for BS (and SBS) fault sources.

The actual depth values of the top of the fault depths are reported in **TABLE 1.7**, for two tectonic settings, Generic Active Region and Stable Continental Region, where different fault scaling relations apply (**TABLE 1.5**). In the cells where the thickness of the crust is thinner (**FIGURE 1.8**) some of the deeper fault positions may not be used. So, at each grid node of a region where BS is modelled, there are faults centered on the grid node at different depths. Furthermore, at each node and at each depth, different faulting mechanisms, meaning different combinations of strike, dip and rake, are modeled.

TABLE 1.7: Depth of the top of faults in the BS category.

A) Generic Active Region

Mw	Depths (km)
6.0	0, 4.14, 7.27, 10.41, 13.55, 16.68, 19.82, 22.96, 26.09, 29.23, 32.37, 35.50, 38.64, 41.78, 44.91
6.5	0, 5.97, 10.94, 15.91, 20.88, 25.86, 30.83, 35.80, 40.77
6.8012	0, 7.56, 14.12, 20.68, 27.24, 33.80, 40.36
7.0737	0, 9.43, 17.86, 26.30, 34.73
7.3203	0, 11.58, 22.16, 32.75
7.5435	0, 14.00, 26.99
7.7453	0, 16.65, 32.30
7.928	0, 19.52
8.0933	0, 22.57

B) Stable Continental Region

Mw	Depths (km)
6.0	0, 2.96, 4.92, 6.88, 8.84, 10.80, 12.77, 14.73, 16.69, 18.65, 20.61, 22.57, 24.53, 26.49, 28.45, 30.41, 32.37, 34.34, 36.30, 38.26, 40.22, 42.18, 44.14, 46.10
6.5	0, 4.11, 7.22, 10.32, 13.43, 16.54, 19.65, 22.75, 25.86, 28.97, 32.08, 35.19, 38.29, 41.40, 44.51
6.8012	0, 5.10, 9.20, 13.30, 17.41, 21.51, 25.61, 29.71, 33.81, 37.91, 42.01
7.0737	0, 6.27, 11.54, 16.81, 22.09, 27.36, 32.63, 37.90, 43.17
7.3203	0, 7.62, 14.23, 20.85, 27.46, 34.08, 40.69
7.5435	0, 9.13, 17.25, 25.38, 33.50, 41.63
7.7453	0, 10.79, 20.57, 30.36, 40.14
7.928	0, 12.58, 24.16, 35.74
8.0933	0, 14.48, 27.97

The faulting mechanism at each cell is determined based on the available information from focal mechanisms and known faults, excluding those that are part of the PS category. The discretization is made separately for strike, dip and rake. To manage the toroidal properties of angles, the strike and dip transformed as it follows:

$$S = \begin{cases} strike, strike < 180° \\ strike - 180, strike > 180° \end{cases}$$
$$D = \begin{cases} dip,\ strike < 180° \\ 180 - dip, strike > 180° \end{cases}$$

With this 1-1 reversible transformation (Selva and Marzocchi, 2004), both strike and dip range between 0° and 180°, and two sub-vertical fault planes with opposite strike and dip close to 90° will have equal S and close D values.

Adopting this transformation, the following discretization is adopted:

- S: 22.5°, 67.5°, 112.5°, 157.5° (each representing intervals of 45°, starting from 0° up to 180°)
- D: 10°, 30°, 50°, 70°, 90°, 110°, 130°, 150°, 170° (each representing 20° intervals around the central values, starting from 0° up to 180°).
- Rake: -90°, 0°, 90°, 180° (each representing 90° intervals around the central values)

This makes a total of 4x9x4=144 combinations.

Of course, fault size varies too, with the rupture dimension is determined based on the scaling relations by Leonard (2010, 2014), considering the tectonic settings characterization provided by the regionalization and the faulting mechanism, as described in a previous SECTION.

Geometry, spatial discretization and tectonic data for SBS (Cadiz subduction) source

The Cadiz subduction in the SBS type is modelled adopting the same strategy of BS, but with a more limited variability of fault position and source parameters (strike, dip and rake) and allowing for larger magnitudes and depths. More specifically, it has a mechanism whose variability is much more limited, with a total of four combinations: strike 22.5 and 337 (according to the available fault model, see FIGURE 1.6), dip 10° and 30°, the rake fixed to 90°. The centers of the faults occur at a limited number of the grid nodes inside the BS+SBS region of FIGURE 1.16.

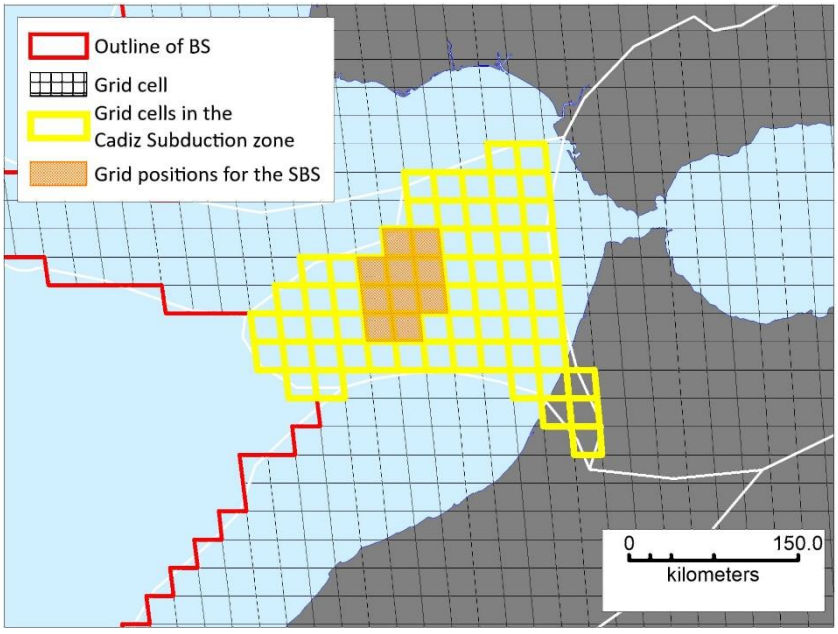

FIGURE 1.16: Cells of the grid (spatial discretization) in the Cadiz region showing the positions occupied by the SBS modeling.

The magnitude range is extended to up to Mw = 9.026 (elementary tsunami source specifically calculated for this case). The size of the rupture is determined by using the scaling relations by Strasser et al. (2010) for the subduction interface. The depth limit from the crustal model is not considered, and the rupture maximum depth is extended to up to 100 km, with a discretization scheme like that of BS but extended to the higher magnitudes as reported in TABLE 1.8.

TABLE 1.8: Depth of the top of faults in the Cadiz Subduction

Magnitude	Depth (km)
6.0	0, 5.19, 9.37, 13.56, 17.75, 21.94, 26.12, 30.31, 34.50, 38.69, 42.87, 47.06, 51.25, 55.44, 59.62, 63.81, 68.00, 72.19, 76.37, 80.56, 84.75, 88.93, 93.12
6.5	0, 7.27, 13.54, 19.82, 26.09, 32.36, 38.63, 44.91, 51.18, 57.45, 63.72, 70.00, 76.27, 82.54, 88.81
6.8	0, 9.00, 17.00, 25.00, 33.01, 41.01, 49.01, 57.01, 65.01, 73.01, 81.01, 89.01
7.07	0, 10.97, 20.95, 30.92, 40.89, 50.86, 60.84, 70.81, 80.78
7.32	0, 13.17, 25.34, 37.52, 49.69, 61.86, 74.03, 86.20
7.54	0, 15.58, 30.16, 44.74, 59.31, 73.89
7.74	0, 18.16, 35.32, 52.48, 69.64
7.92	0, 20.89, 40.78, 60.67
8.09	0, 23.73, 46.47, 69.20
8.2429	0, 26.66, 52.31
8.3782	0, 29.62, 58.24
8.5007	0, 32.60, 64.20
8.6115	0, 35.56
8.7118	0, 38.48
8.8025	0, 41.33
8.8846	0, 44.10
8.9588	0, 46.76
9.026	0, 49.31

1.3.8 Further tectonic data for PS sources

The rate of activity of PS, SPS and SBS sources may depend on several factors, including fault area, rigidity (shear modulus), seismic coupling, convergence rate for subductions or slip rate for crustal faults. Depending on the method implemented for the quantification of the activity rates (Level 1), some or all these parameters are used.

Some parameters (TABLE 1.9) for subduction zones and for crustal faults are derived from Berryman et al. (2015) and Christophersen et al. (2015).

TABLE 1.9: Tectonic data for modeling PS.

	Calabrian Arc	Hellenic Arc	Cyprus Arc	Caribbean Arc	Gloria Fault	Cadiz Arc
Convergence or slip rate (mm/y)	1.75	10.00	6.77	11.00	4.00	3.96
Coupling 1	0.30	0.20	0.30	0.30	0.30	0.30
Coupling 2	0.50	0.60	0.50	0.50	0.50	0.50
Coupling 3	0.70	1.00	0.70	0.70	0.70	0.70

It is worth noting though that the coupling coefficients in the three Mediterranean subduction zones are highly debated and variable. For example, in the Calabrian Arc two competing interpretations ranging from partially-locked to unlocked or inactive were recently proposed (Carafa et al., 2018; Nijholt et al., 2018); whereas in the Hellenic Arc interpretations range from full coupling (Ganas and Parsons, 2009) to low coupling (Shaw and Jackson 2010; Vernant et al., 2014), but also the presence of important along-strike coupling variations has been proposed (Laigle et al., 2004).

Another important parameter for modelling PS faults regards the potential depth-dependence of rigidity. Bilek & Lay (1999) found that, regardless of the geographic zone, the rupture duration normalized by the moment of the event decreases with the depth for most subduction earthquakes. By using the classical scaling relations this feature can be ascribed to either an increasing average rigidity or increasing stress drop with depth or some combination of these two features. They show that considering the end-member case of constant stress drop, an average rigidity profile can be defined according to the following exponential behavior:

$$\boldsymbol{\mu(z) = 10^{a+bz}}$$

with the parameters determined from the average values of the measured rupture duration and assuming an average rupture speed of propagation of $\sim 0.8V_S$ with $V_S = \sqrt{\mu/\rho}$ velocity of the S-wave in the medium. This assumption is well-supported in the framework of theoretical rupture mechanics (Burridge 1973) and by seismological evidence (Mai and Thingbaijam, 2014). For the presented end-member case $a = 0.5631;\ b = 0.0437$ with the rigidity expressed in GPa and the depth in km, being positive and increasing downward.

Due to the strong hypothesis included in the end-member case of Bilek & Lay (1999) the rigidity at shallow depths is very low with respect to the classical reference given by the PREM (Dziewonski & Anderson 1980; Geist & Bilek 2001). As also pointed out by Geist & Bilek (2001) to match the tsunami amplitudes recorded during some tsunami earthquakes, such as Nicaragua 1992 (Satake 1995), Peru 1996 (Heinrich et al. 1998; Tanioka & Satake, 1996) the average rigidity of the shallow portion of the subduction is something in between the one predicted by Bilek & Lay (1999) and the PREM one. Therefore, we define a rigidity variation with depth computed as the average between the two distributions. This contemporary allows to use a larger rigidity than that one expected from the Bilek-Lay end member case (where all the source duration variability is ascribed to the rigidity itself) but even smaller than the PREM, modelling the fault as a weakness region with respect to the global Earth reference. FIGURE 1.17a shows this average (red line) along with the Bilek & Lay (1999) distribution (blue line) and the PREM one (green line). The rigidity profiles as just described are depicted also in map view in FIGURE 1.17b for each subduction zone.

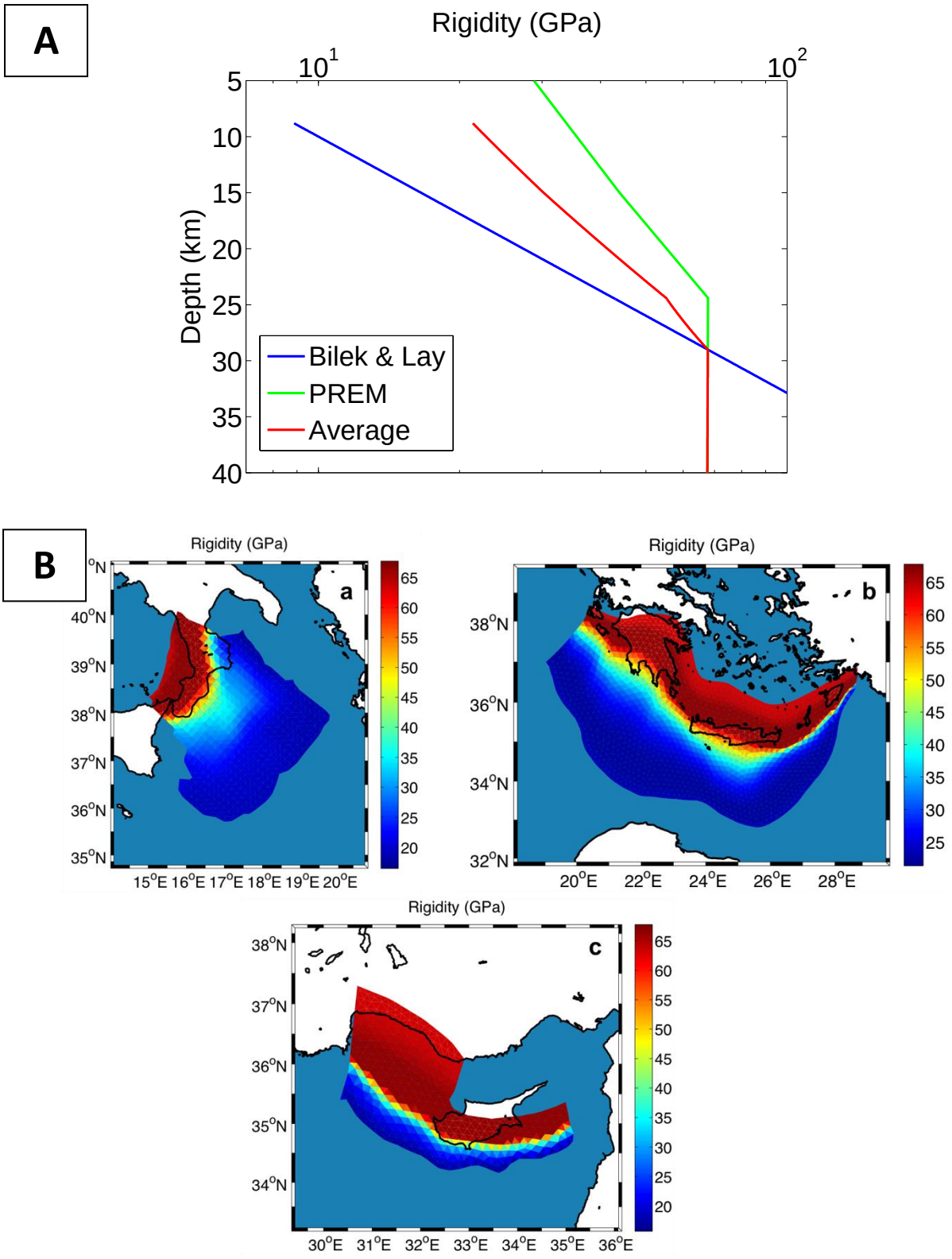

FIGURE 1.17: A) The rigidity variability as inferred from Bilek & Lay (1999) (blue line), from the PREM model (green line) and considering an average between the two profiles. B) Rigidity mapped on Calabrian (panel a), Hellenic (panel b) and Cyprus Arc (panel c).

1.3.9 Further tectonic data for BS sources

The dip angle is one of the fault parameters that most affects the seafloor displacement field. From rock mechanics we know that not all the dip angles are equally likely for normal, reverse, and transcurrent faults. In addition, earthquake focal mechanisms alone, cannot resolve which one of the two nodal planes represent the actual fault plane that ruptured. Therefore, the collections of earthquake fault dip angles are not very rich. In some cases, fault dip angle can be estimated from the aftershock distribution. Otherwise, in several cases only the fault dip direction can be identified. In the last two decades, however, several techniques have been developed which provide realistic earthquake fault plane solutions based on the inversion of GPS and InSar data.

Here we use the G-DIP dataset (Basili and Tiberti, 2016), a collection of 217 earthquakes of Mw > 5, (FIGURE 1.18) with univocally-determined fault plane geometry, paired with uniformly determined moment tensor solutions from the Global CMT catalog (years 1976-2016; Dziewonski et al., 1981, and Ekström et al., 2012). The sources of the G-DIP collection are as follows: 18 from Sibson & Xie (1998); 9 from Collettini & Sibson (2001); 114 from SRCMOD (http://equake-rc.info/SRCMOD/); 76 from a literature search of individual earthquakes. TABLE 1.10 report the dip-angle distribution in bins of 10° for normal, reverse, and transcurrent faults.

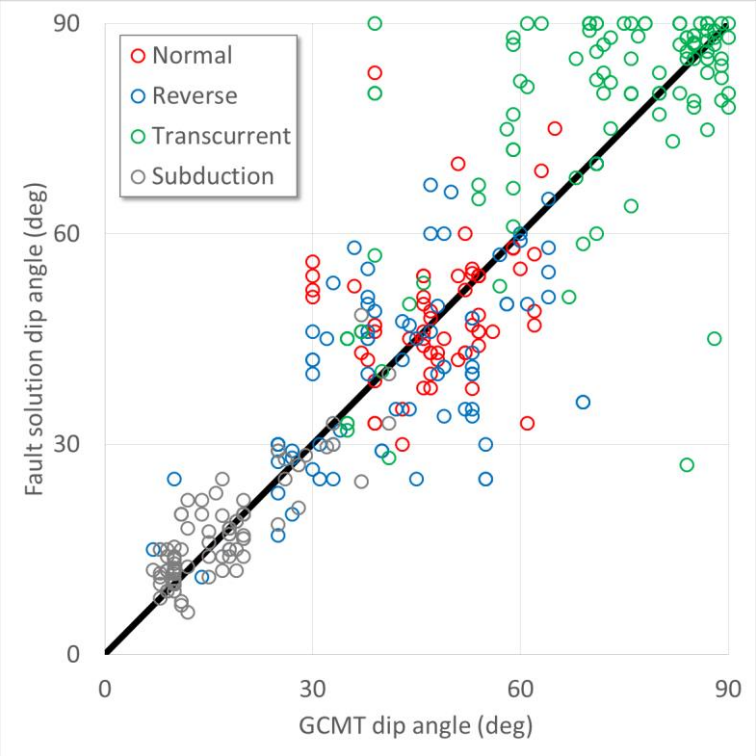

FIGURE 1.18: Dip angles of paired events from the GCMT catalog and from fault solutions obtained through various techniques. No bias appears between the two types of dip-angle solution. Note that reverse faulting earthquakes in subduction zones are excluded from the statistics of reverse crustal faulting.

TABLE 1.10: Global distributions of fault dip angles (from Basili and Tiberti, 2016)

Dip Angle ranges	Normal	Reverse	Transcurrent
]0-10]	0	4	0
]10-20]	0	2	0
]20-30]	3	8	1
]30-40]	7	11	6
]40-50]	14	16	3
]50-60]	10	11	8
]60-70]	5	5	8
]70,80]	0	1	14
[80,90]	1	0	30

1.3.10 Seismicity separation in catalogs

Once the regionalization is set (**FIGURE 1.2**) and all the tectonic sources are assigned to the four seismicity modeling types, and their parameters are defined, the seismic catalogues are analyzed accordingly, to discriminate which earthquakes in each catalogue are assigned to which individual fault of the PS or SPS, and the remaining earthquakes are assigned to BS.

This is done by adopting a procedure that takes the seismicity occurring in a source region, then separates the seismicity falling within a cut-off distance from the faults, and assigns it to the PS and the remaining seismicity to the BS. Two alternative cut-off distances are used: 5 km and 10 km.

We do not apply this procedure to the SBS (in practice for the Cadiz Subduction). In this case, the separation is not performed because of the relatively high uncertainty concerning the subduction interface position and geometry. As it will be discussed in SECTION 1.6, this will lead to adopt the maximum uncertainty (total ignorance) for modelling SBS and BS annual rates in the Cadiz region.

We prefer to use this hard-bound cut-off method over methods using a softer cut-off (e.g., a weighting function), for two reasons: the definition of a weighting function would contain a weight-with-distance rule, which would add a further subjective choice; more importantly, the Boolean separation induced by the cut-off distance allows for a smoother implementation at the following Levels, since it provides two clearly separated catalogues of PS/ SPS and BS/SBS events, instead of one single catalogue with uncertain attribution to either category.

1.4 Level 1 – PS/BS - Magnitude-frequency distribution for each seismicity type in each region

At Level 1, the Magnitude-Frequency Distributions (MFD), that is the mean annual rates $\lambda_i^{(S)}(M_j)$, for a set of discrete magnitude intervals Mj, in each given region R_i, are quantified for the two main seismicity modeling types: BS and PS. The assignment to SPS or SBS impacts only Level 2 (see FIGURE 1.1a). Consequently, the superscript S indicates the seismicity types belonging to the set {PS, BS} and $\lambda_i^{(PS)}(M_j)$ is applied to either PS, SPS or SBS, as indicated in FIGURE 1.2.

The rates are based on the available seismicity data or tectonic data (convergence rates or slip rates) presented in the previous SECTION. The rates, or better their fraction in each region belonging to

either seismicity type, are also influenced by the assumption that the larger the earthquake, the higher the probability that it occurs on major faults possibly treated within the PS/SBS/SPS types.

The rates $\lambda_i^{(S)}(M_j)$ are assigned to the entire volume contained by the 2D borders and the seismogenic depths of a region, as defined in SECTION 1.3.1 (FIGURE 1.2), assigned to the BS, or to a 3D structure, as defined in SECTION 1.3.3 (FIGURE 1.6), assigned to the PS. An earthquake to be modeled belongs to the region in which the causative fault geometrical center lies, and it inherits the annual rate from that region. For example, a subduction zone may exist across different regions; potential earthquakes of a specific magnitude modeled on the subduction interface have finite dimensions (length, and width of the rupture); hence, the rate for that magnitude is taken from the region where the geometrical center of the finite fault defined by these finite dimensions lies.

The quantification of the rates corresponds to Level 1 of the ET for all the seismicity types see FIGURE 1.1a).

As reported in FIGURE 1.1b, we implemented a total of 35 (8 Bayesian + 27) alternatives for quantifying the MFD, to quantify the associated epistemic uncertainty, especially on seismic rates and MFD tails (high-magnitude values with relatively low probability). These alternatives concern: joint or separate quantification of PS and BS rates in each region, which allows for considering different sources of information for earthquake rate estimation (derived either from seismicity or from tectonic rates); functional forms (shape) of the MFDs and their parameters. All these models come with two main sensitivity tests, regarding the consistence with input data and with the simulated maximum magnitudes. More details can be found in Doc_P2_S5.

For the joint PS/BS quantification, the MFD is calculated in two stages (Selva et al. 2016): a total MFD (containing all types of seismicity) is first quantified for each region R_i as a whole; then, the MFD is split into PS and BS:

$$\begin{cases} \boldsymbol{\lambda_i^{(PS)}}(M_j) = \lambda_i(M_j)\,\Pr(PS|M_j, R_i) \\ \boldsymbol{\lambda_i^{(BS)}}(M_j) = \lambda_i(M_j)\,\Pr(BS|M_j, R_i), = \lambda_i(M_j)\left[1 - \Pr(PS|M_j R_i)\right] \end{cases}$$

where $\lambda_i(M_j)$ is the total mean annual rate of earthquakes with magnitude in the interval M_j in the region, and $\Pr(PS|M_j, R_i)$ represents the probability that a randomly selected event within the region R_i and interval M_j belongs to the PS. Both these stages are based on a Bayesian formulation, with data coming from the non-declustered complete seismic catalogue. This choice, also supported from the Review Panel, is made to avoid the significant underestimation of the true hazard that declustering procedure may produce (Boyd, 2012; Iervolino et al., 2012).

For the quantification of $\lambda_i(M_j)$, we selected the procedure based on the Bayesian formulation by Campbell (1982). This procedure was first suggested for the unbounded Gutenberg-Richter (GR) distribution and later refined by Keller et al. (2014) for the truncated GR distribution. The novelty of our work consists a) in extending the methodology of Keller et al. (2014) to any magnitude distribution and b) in the simultaneous estimation of all parameters. Following Keller et al. (2014), we include the temporal variability of the completeness period with magnitude, as proposed by Weichert (1980), so that the observed rate at each magnitude level is computed using all the data

available for that magnitude (thus, the larger the magnitude, the longer the considered period to compute the rates).

We implemented both truncated and tapered Pareto functional forms (Kagan, 2002a,b). As described in Kagan (2002a,b), truncation and tapering are both applied to the probability density functions (PDFs). The parameters to be set are the rate for the smallest considered magnitude (λ_0), the corner or the maximum magnitude (Mc or Mmax, for tapered and truncated distributions, respectively), and the scale parameter β (2/3 of the b-value). As minimum magnitude for the assessment, we set Mw = 5.0, which is smaller than the minimum magnitude considered by the quantification (as defined in the magnitude discretization, the smallest interval for magnitudes starts at 5.7, see SECTION 1.3.5). The prior distributions are set as non-informative for λ_0 and for Mc (for the tapered Pareto). The Mmax for the truncated Pareto is set as discussed in Level 0 (SECTION 1.3), considering all the known constraints (for example, maximum magnitude observed in the region). Two further alternatives are implemented for the parameter β. The first alternative is to compute the b-value from data. To do this, we set a slightly informative Gamma distribution prior centered on the worldwide tectonic analogues from Kagan et al. (2010) with variance corresponding to an equivalent sample size of 10. This means that if there is a large dataset (>>10 data), β is entirely controlled by the data, while in case of very few data the distribution is pushed toward the world-wide value. On the contrary, the second alternative has been to force the b-value to 1, whatever the data say in the region.

For coherence with the MFD model above, a Bayesian procedure is used also for quantifying $\Pr(PS|M_j, R_i)$. The quantification of $\Pr(PS|M_j, R_i)$ is made assuming (following the PS definition) that all high-enough magnitude events must occur on PS, while earthquakes are randomly dispersed between PS and BS for lower magnitudes (Selva et al. 2016). Specifically, we set:

$$\Pr(PS|M_j, R_i) = \begin{cases} a(M_f) & \text{for } M \le M_f \\ a(M_f) + \left(1 - a(M_f)\right) f(M_j; M_f, M_u) & \text{for } M_f < M < M_u \\ 1 & \text{for } M \ge M_u \end{cases}$$

where M_u and M_f are the lower and upper magnitude limits for this transition, $a(M_f)$ represents the fraction of the total number of events being PS for magnitudes $M \le M_f$, and $f(M_j; M_f, M_u)$ represents a transition function. Here, we select a sigmoidal polynomial function $\mathrm{f}(M; M_f, M_u) = 3x^2 - 2x^3$ with $x = [M - M_f]/[M_u - M_f]$. Following this formulation, $\Pr(PS|M_j)$ depends on 3 parameters: M_u, M_f and a, that will be quantified as it follows separately in each region R_i.

- For M_f, we use a uniform distribution between magnitude 5 and 6.
- For M_u, we use a uniform distribution between 6 and 7 for PS relative to crustal faults, and between 7 and 8 for PS relative to subduction interfaces.
- For the parameter $a(M_f)$, we set a non-informative prior (uniform between 0 and 1) updated by a likelihood functions that is the measured fraction of PS events in the region (see separation in seismicity catalogues at Level 0, in SECTION 1.3). Given that at Level 0 we defined two alternative methods to produce the separated catalogues (different cut-off distances), two alternative implementations with potentially different fractions of PS events below magnitude M_f. Note that, in the case of SBS, no separation is performed and a non-

informative (uniform) prior is adopted, in order to represent the poor knowledge of the SBS geometry that do not allow for separating BS from SBS.

As reported in FIGURE 1.1b, these choices produce a total of 2x4 = 8 Bayesian alternative implementations for the joint PS-BS quantification of the MFD, with 2 alternative shapes (tapered vs truncated Pareto), 2 b-values (from data or set to 1), and 2 PS fractions (from the different cut-off distances of Level 0). All of them are Bayesian, so that they automatically include the epistemic uncertainty emerging from parameter estimations. To propagate also this uncertainty to the final results, each of these models is sampled 1000 times, providing 1000 alternative realizations of the Bayesian model.

For the separate PS-BS quantification, the MFD for PS is set as in Davies et al. (2018) starting from convergence/slip rates. Conversely, the MFD for BS cannot be quantified adopting a similar strategy, therefore it is performed independently of the PS, by randomly sampling one of the models available from the joint PS/BS quantification. In this way, the two quantifications are independent, since they are based on different input data.

In Davies et al. (2018), for constraining the rate of activity of PS, we use the classical formulation for seismic moment rate $\dot{m}_s$ as given by

$$\dot{m}_s = \chi \dot{m}_g = \chi \mu A \dot{D}$$

where $\dot{m}_g$ is the tectonic moment rate, χ is a coefficient that determines how much of this rate is converted into the seismic rate (so called coupling or seismic efficiency), μ is the rigidity or shear modulus, A is the fault area, and $\dot{D}$ is either convergence rate for subduction or slip rate for other faults. As described in SECTION 1.3.8 the adopted geodetic rates for all PS sources are derived from Christophersen et al. (2015), as reported in TABLE 1.9.

To derive from these tectonic data the MDF, we follow the approach defined in Davies et al. (2018). Adopting either a characteristic or a truncated Pareto MFD (Kagan 2002), we consider 3 alternatives for maximum magnitudes and three alternative b-values on all source zones, as defined in TABLE 1.11.

TABLE 1.11: Parameters for the MFD from tectonic rates from Davies et al. (2018).

	Calabrian Arc	Hellenic Arc	Cyprus Arc	Caribbean Arc	Gloria Fault	Cadiz Arc
b-value 1	0.70	0.70	0.70	0.70	0.70	0.70
b-value 2	0.95	0.95	0.95	0.95	0.95	0.95
b-value 3	1.20	1.20	1.20	1.20	1.20	1.20
Mmax 1	7.60	8.00	7.70	8.00	8.30	8.20
Mmax 2	8.10	8.60	8.30	8.80	8.60	8.40
Mmax 3	9.00	9.10	9.00	9.60	8.80	8.60

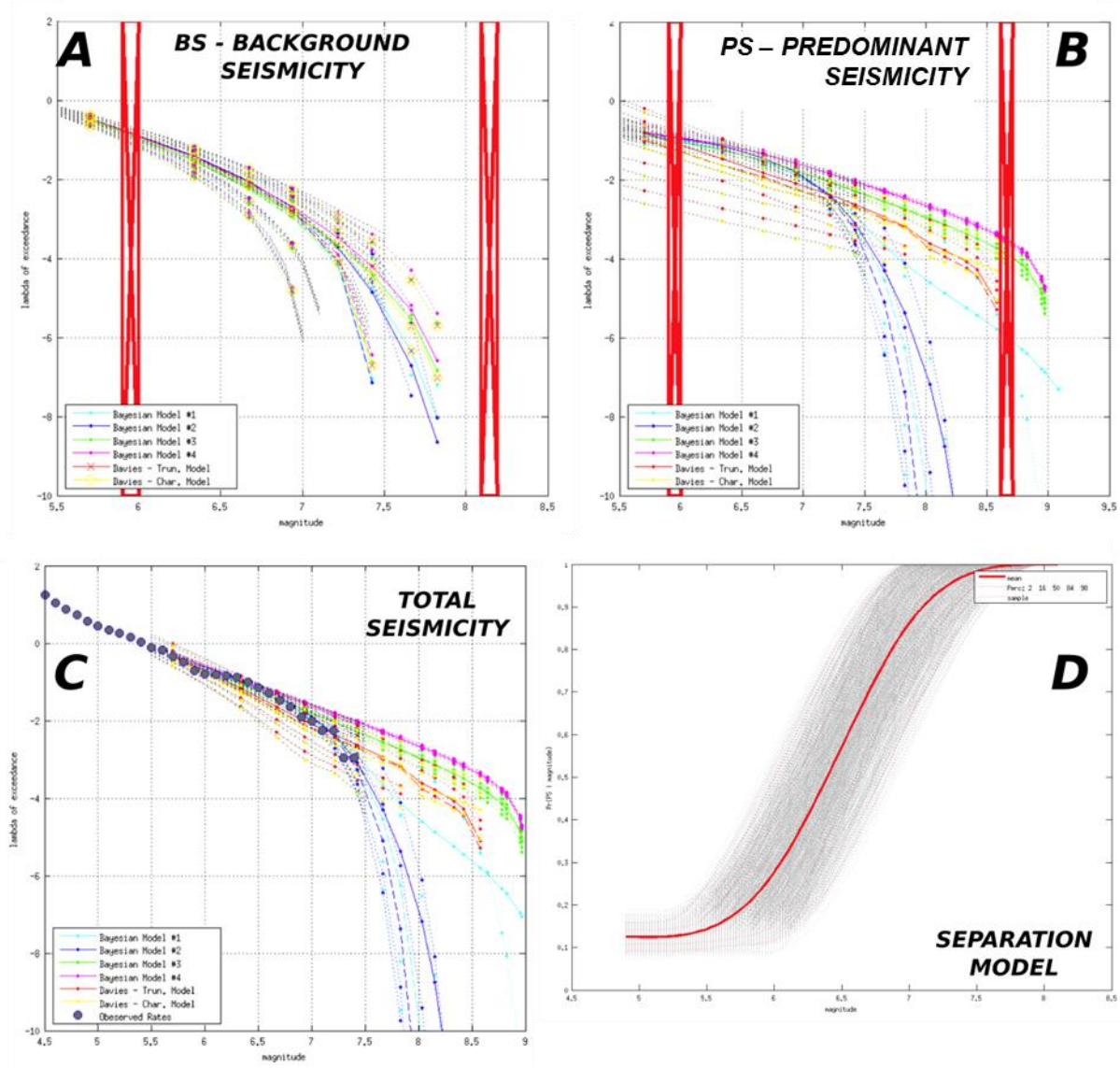

FIGURE 1.19: A) BS seismicity computed by all the alternative models for the 5 km cut-off (4 Bayesian joint models + 27 separated models) for the Kefalonia-Lefkada region. For the Bayesian models, we report the mean, the 10th and 90th percentiles of samples for the epistemic uncertainty. Red vertical lines indicate ranges of magnitudes not modelled in STEP 2, as discussed in SECTIONS 1.1.1 and 1.3.5. B) Same as A), but for PS (the Hellenic Arc). C) the total seismicity (computed as the sum of BS and PPS contributions) compared with the actual input data (gray dots). D) Bayesian separation model for the same region and the 5 km cut-off.

Given that all the subductions in the Mediterranean cover an area including more than one tectonic region, their moment release should be divided into all these regions. In these regions (three for the Calabrian Arc, five for the Hellenic Arc, and four for the Cyprus Arc), we distributed the moment release of each subduction proportionally to the size of the intersection between the subduction area and each given region. This corresponds to the assumption of a uniformly distributed moment release all over the interface. Note that not all the magnitudes are always present in all the regions, given that they are considered in one region only if a fault centered in the region may accommodate the fault size for that magnitude, since the geometrical center cannot be too close to fault

boundaries. The magnitudes will be present only in regions sufficiently large to contain cells with centers enough far away from the borders. To avoid the potential bias induced by attributing to a region the moment release for a magnitude that cannot be hosted, the redistribution is made separately at each magnitude level, renormalizing the fractions accordingly.

Considering also the three alternative estimations for the seismic coupling (from Christophersen et al., 2015), we obtain a total of 3x3x3x2=54 alternatives.

In FIGURE 1.19, we report the implementation in the Kefalonia-Lefkada region of the four joint-BS-PS Bayesian models for the 5-km-wide cut-off, and the separated-BS-PS 54 models. This region includes a part of the Hellenic arc, so it includes PS and BS. The resulting modeled total MFDs (sum of BS and PS contributions) are compared with data. The results for the remaining four Bayesian models, relative to the 10-km-wide cut-off, are equivalent.

1.5 Level 2a - Variability of PS/SPS earthquakes of a given magnitude within a given region

This Level includes the two possible PS-like parameterizations, that is to say PS or SPS branches (FIGURE 1.1a). We here consider only earthquakes along major faults treated either as PS or SPS (see SECTION 1.3.4 for actual assignments to tectonic structures).
The PS analysis is subdivided into the two sub-Levels that stack on Level 1, that are:

- sub-level 2a.1 – Positioning along the PS/SPS hosting structure and rupture area
- sub-level 2a.2 – Slip distribution

We implemented a total of eight alternatives (see FIGURE 1.1b) to explore the corresponding epistemic uncertainty. These alternatives are limited to all subductions in the near-field of target areas, that is the three subduction zones in the Mediterranean: the Calabrian, Hellenic, and Cyprus Arcs (note that the Cadiz subduction zone is discussed in Level 2b, since it is modelled as SBS). The alternatives arise from two alternative scaling relations from two alternative ways of defining the seismogenic area (as defined in SECTION 1.3.7, FIGURE 1.12), and whether the subduction zone parameters have depth-dependent parameters (coupling, rigidity; two alternatives: constant or depth-dependent). This depth-dependent approach to subduction earthquake modelling allows enhanced slip towards the trench (as inversely proportional to rigidity), as observed in some tsunami earthquakes and in some great megathrust earthquakes (e.g. Lay et al., 2012). Note that other peculiar types of tsunamigenic earthquakes, such as the outer-rise events, are allowed for occurring around the PS sources within the BS, even if they are not explicitly treated.

At the sub-level 2a.1, position and size of the rupture area are treated simultaneously. Earthquake positions on each hosting fault are discretized by defining a set of coordinates $\{x_c, y_c\}$ along the 3D fault geometry. Assessment consists of quantifying the probability $Pr_i(\mathrm{x_c}, \mathrm{y_c}, \mathrm{A}|\mathrm{M_j})$, that is, the joint probability of a fault center x_c, y_c and a maximum rupture area A for an earthquake of magnitude M_j in the region R_i. We simplify this quantification by computing A as a function of magnitude $\mathrm{M_j}$ from scaling relations, so that $Pr_i(\mathrm{x_c}, \mathrm{y_c}, \mathrm{A}|\mathrm{M_j}) = Pr_i(\mathrm{x_c}, \mathrm{y_c}|\mathrm{M_j})$, since no aleatory uncertainty is modeled for A. Average effective slip can also be estimated from the same scaling relation. Potential slip distributions within the area A are discussed in this paragraph, below.

The earthquake spatial distribution is assumed uniform in each tectonic region. The only spatial modulation may arise from different rates in the different regions, when the same PS fault is included in multiple regions (see SECTION 1.3.4).

To build all the possible scenarios for a given magnitude, the geometrical properties of the events are determined from the average values of a scaling relation that relates the size of an event to its magnitude. To partially consider the uncertainty deriving from the determination of the scaling relation parameters, only for the subduction zones in the Mediterranean, two different scaling relations were used leading to the creation of two different classes of scenarios covering the entire fault. In these cases, we used the Strasser et al.'s (2010) scaling relations that provide relationships of the earthquake magnitude with area, length and width of the rupture and the Murotani et al.'s (2011) scaling relations that relates the earthquake magnitude with the rupture area and average slip (see discussion on scaling relations in SECTION 1.3.6). For both cases, we use the magnitude-area relationship to determine the size of the event. It is worth noting that, since most of the slip inversions used for the determination of the scaling relations are computed over planar fault surfaces, the areas are generally underestimated with respect to the slip distribution over complex 3D geometries. To consider this feature we systematically round up for excess the area adding mesh cell to the seismic scenario until the expected area is exceeded.

For all the other sources assigned to PS/SPS, we adopted only one scaling relation: the Strasser et al. (2010) relation for the Caribbean Arc (which is more conservative than Murotani et al., 2011), and the Leonard et al. (2014) relation for all crustal PS (Mid-Atlantic Ridge and Gloria fault). Instead, for the Mediterranean subduction interfaces we adopted both scaling relations from Strasser et al. (2010) and Murotani et al. (2011), discussed in SECTION 1.3.6.

Following Selva et al. (2016), we investigated both the hypotheses of the slip confined in the deep part of the subduction interface and the possibility for rupture to extend towards the surface. Indeed, we defined two different seismic active areas which in turn generate two different classes of scenarios covering the entire subduction interface. The first area spans from about 10-15 km depth to the intersection of the slab with the MOHO discontinuity of the upper plate; the second area, which always contains the first one, extends towards the surface. In other words, for each of the previously described classes (deriving from the scaling relation choice) we create two sub-classes with ruptures either confined to the deeper section of the fault (see blue thick lines in FIGURE 1.12) or can extend towards the surface (see red thick lines in FIGURE 1.12). This led to four alternative sets of potential scenarios covering each fault modeled as PS.

It is worth to note that, depending on the geometry of the fault surface, class of propagation, and earthquake area (determined from the scaling relations), each sub-class admits a maximum magnitude that can be modeled (see TABLES 1.3 and 1.4). Furthermore, once the magnitude is fixed within each sub-class, the rupture areas for each scenario are selected according to the following criteria:

1. All the sampled areas (both for deep and shallow propagation case) must cover homogeneously the whole seismogenic area assuming a tapering towards the edges.

2. Only areas for which the original geometrical center is within a fixed distance (a percentage of the expected length, increasing with magnitude) from the real geometrical center of the area are considered.

3. Equal (or nearly equal) areas are considered only once.

Points 2 and 3 ensure a decreasing number of scenarios with increasing magnitude, with centers more and more positioned far from the fault edges.

At the sub-Level 2a.2, we model the aleatory variability of the heterogeneous slip distribution within the rupture area A. This aleatory variability is modelled only for the Mediterranean subduction zones, again because they are the only well-known subduction zones close to target areas. For all the other structures assigned to PS and SPS, the slip is assumed uniform according to the average value prescribed by the adopted scaling relation.

For the Mediterranean subduction zones (FIGURE 1.12), we quantify the probability of a slip vector field conditioned to the occurrence of an earthquake centered at $\{\mathrm{x_c}, \mathrm{y_c}\}$ and having rupture area A, that is, $Pr_i(\vec{\mathrm{s}}|(\mathrm{x_c}, \mathrm{y_c}, \mathrm{A}))$. This probability distribution should consider many different constrains, such as total slip, spatial correlation of slip, etc. To simplify this quantification, we adopt a Monte-Carlo approach. We build an ensemble of n=5 slip distributions, assigning to each equally-probable sample the probability $Pr_i(\vec{\mathrm{s}}|(\mathrm{x_c}, \mathrm{y_c}, \mathrm{A})) = 1/n$.

To build the heterogeneous slip on non-planar faults using the above-mentioned triangular mesh, the following scheme is implemented. This method was further developed and submitted as a scientific paper (Scala et al., 2019).

For each event defined by $\{x_c y_c, A\}$, the area A is iteratively covered extracting nearby cells starting from the geometric center and over this area a Probability Density Function (PDF) for the slip distribution is defined as the sum of a random number N of Gaussian functions, with $1 \leq N \leq 4$, such that the slip can represent either single or multiple asperities distributions.

Each Gaussian is defined by randomly extracting the position of the maximum from a uniform distribution and setting the standard deviation as one fifth of the square root of the rupture area, so that, when the center is quite far from the edges the probability goes to zero well-within the rupture zone. When the center of the Gaussian is closer to the edge, the slip must be *a-posteriori* re-distributed accordingly with the imposed seismic moment.

Within the fault area, the slip value is assigned to each triangle using a hierarchical set of overlapping circular sub-events on the fault surface; the number of sub-events is a decreasing power-law of their radii as in the following equation:

$$n(R) = pR^{-D-1}$$

R is defined in the interval $[R_{min} : R_{max}]$ where R_{min} is fixed such that the circle covers at least five elements to ensure that the slip is everywhere well resolved by the mesh; R_{max} is fixed at 35% of the rupture width derived from the pre-computed magnitude and length. Only one asperity of maximum radius is placed, whereas the total number of cracks is fixed at 1000. D, the fractal dimension and it is set to 2 to ensure the self-similarity of the slip distributions (Herrero & Bernard,

1994), whereas the constant p is set accordingly to the moment, equal to the fractal dimension of the expected stress drop (Zheng *et al.*, 1994, Murphy *et al.*, 2016).

The precision of the circular asperities on the non-planar mesh is ensured by a double-lateration algorithm (Herrero & Murphy, 2018; Herrero et al., 2017) derived from a multi-lateration scheme proposed by Novotni & Klein (2002). Finally, the slip distribution across the single sub-events is assigned by an Eshelby function (Eshelby, 1957; Ruiz et al. 2011), based on the above-described probability density function.

To mimic the smooth end of the seismogenic fault zone the center of each single sub-event must lie at least at a distance from the edge larger than their radius. This constraint is released close to the shallower boundary: this may allow to model the shallow slip amplification due to the free surface effect. The algorithm is efficiently implemented in a Fortran code.

We also defined two further sub-classes: a uniform rigidity class and one for which the rigidity/coupling varies with depth. In the homogeneous case, we use the reference value of 33 GPa, which is widely used for seismological applications. Conversely to impose a depth-dependent rigidity profile we firstly follow the consideration made by Bilek & Lay (1999). To take also into account the effect of less coupled zones at the shallow and deep boundary of the seismogenic zone we define a reference relative coupling function $\boldsymbol{K(z)}$ defined as follows:

$$\begin{cases} \boldsymbol{K(z) = 1 \; if \; z_{seismo\_min} < z < z_{seismo\_max}} \\ \boldsymbol{K(z) \; monotonically \; decreasing \; to \; 0 \; if \; z > z_{seismo\_max} \; \vee \; z < z_{seismo\_min}} \end{cases}$$

The subscripts $\boldsymbol{seismo\_max}$ and $\boldsymbol{seismo\_min}$ respectively refer to the depth at which the MOHO discontinuity begins and to the depth at which the dip angle decreases generating an almost flat sedimentary wedge.

Once variable rigidity and coupling with depth are defined, we would expect a larger slip where the rigidity is smaller and the coupling larger. A second PDF must be imposed following the variability of the rheology. Indeed, this variability of rigidity and coupling is used, to the first order, to modulate the shallow slip amplification. Therefore, we define for each cell $\boldsymbol{n}$ a Slip Weight Function ($\boldsymbol{SWF_n}$):

$$\boldsymbol{SWF_n = C \frac{K_n}{\mu_n}}$$

where $\boldsymbol{C}$ is a normalization factor whereas $\boldsymbol{K_n}$ and $\boldsymbol{\mu_n}$ are respectively the coupling and the rigidity at the average depth of the $\boldsymbol{n}$-th cell. Basically, once a specific scenario is extracted, the restricted $\boldsymbol{SWF_n}$ to the ruptured area represents an estimate of the expected spatial variability of the slip on the fault. In FIGURE 1.20 the $\boldsymbol{SWF_n}$ is shown for the three subduction zones. The re-normalized restriction of the $\boldsymbol{SWF_n}$ to the selected scenario represents the rheology dependent PDF to be used in the definition of the composite source model.

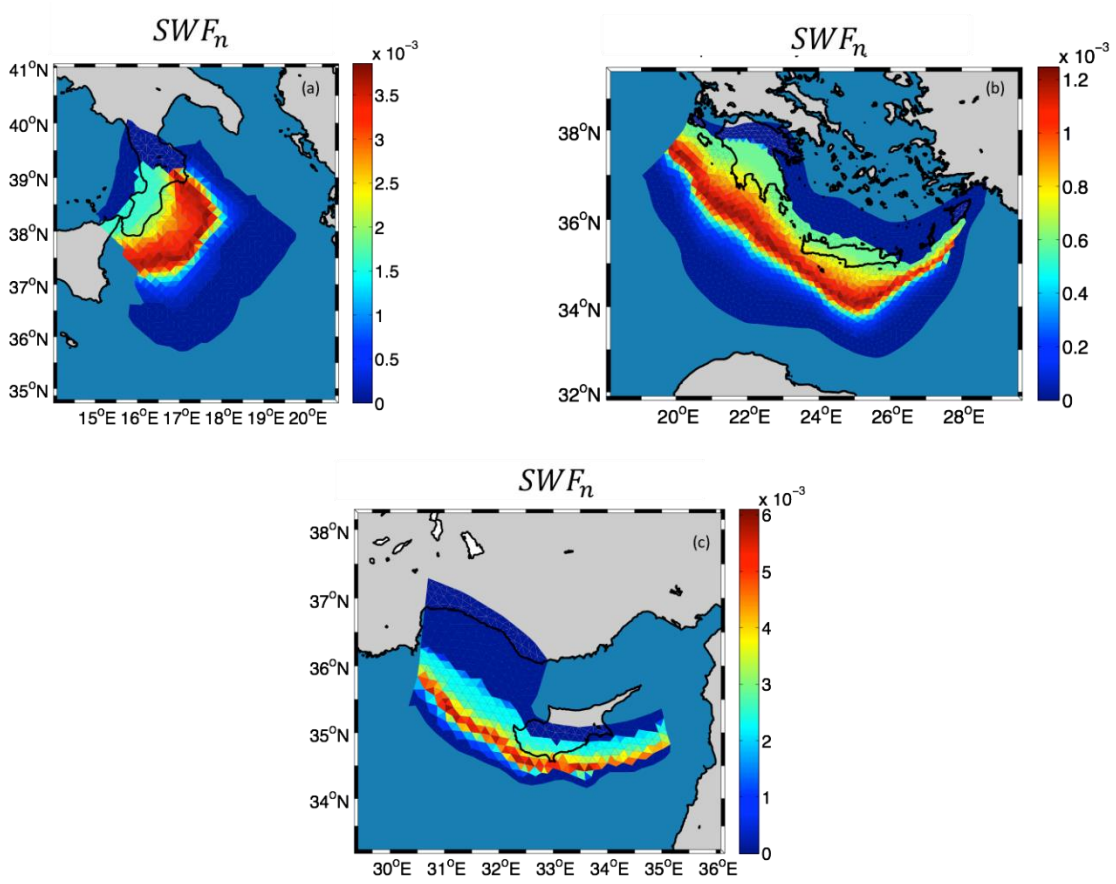

FIGURE 1.20: The SWFs for the three subduction zones.

In FIGURE 1.21, some examples of the different type of slip distribution are shown. For lower magnitudes ($\boldsymbol{M_w < 8.6}$), and for homogeneous classes the slip is computed as: $\boldsymbol{\delta u = \frac{M}{[\mu(33GPa)]\cdot A}}$, where $\boldsymbol{A}$ is the measure of the surface where the slip is defined. This slip value is imposed as uniform over all the selected area and assigned to all the cells (see FIGURE 1.21a) Instead, for variable rigidity case, once a scenario is extracted, the restriction to the scenario of the $\boldsymbol{SWF_n}$ is used to modulate the slip (FIGURE 1.21b). We thus obtain a non-uniform slip distribution with a slip amplification in the zone where the restriction to the $\boldsymbol{SWF_n}$ is maximum. The absolute values of the slip within each cell are constrained by the definition of the seismic moment.

These choices are necessary because for small size earthquakes we do not have enough resolution in the definition of k^{-2} slip distributions.

For larger magnitudes, the composite k^{-2} slip distributions are computed as previously described. Two examples of k^{-2} slip distributions for high magnitude respectively within the homogeneous and variable rigidity/coupling class are shown in FIGURES 1.21c and 1.21d. The shallow slip amplification due to the $\boldsymbol{SWF_n}$ is clearly visible for high magnitudes.

Due to the random choices made in the definition of the k^{-2} slip distributions, many different seismic scenarios can be defined for each of the extracted areas. To explore this variability, we extract 5 different scenarios for each area.

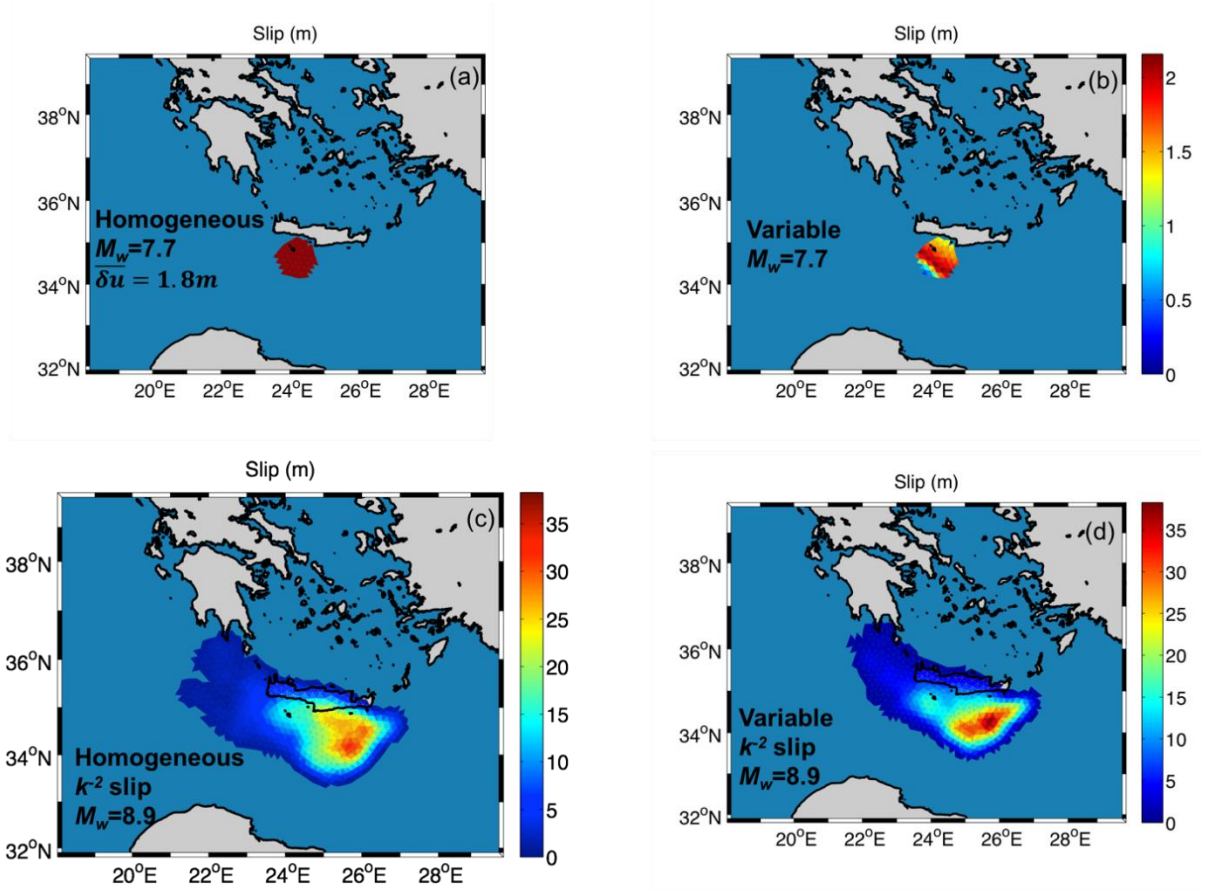

FIGURE 1.21: Example of slip distributions. (a) Low magnitude, homogenous case. (b) Low magnitude, variable case. (c) k^{-2} slip distribution for high magnitude and homogeneous case. (d) k^{-2} slip distribution for high magnitude and variable case.

When a possible shallow slip amplification is included in the model, it must be imposed that in the long-term slip accumulations is nearly uniform over the fault plane. We therefore defined the average slip over all the defined scenario as follows:

$$\widehat{\boldsymbol{\delta}}_{\boldsymbol{n}} = \sum_{M_{w_{min}}}^{M_{w_{max}}} \sum_{i=1}^{N(M_w)} \boldsymbol{\delta}_{\boldsymbol{ni}} \cdot \boldsymbol{P}(\boldsymbol{M_w}) \cdot \boldsymbol{P}(\boldsymbol{Sc_i}|\boldsymbol{M_w})$$

The sum is performed over all the magnitude bins and, within each bin, over all the $\boldsymbol{N(M_w)}$ scenarios at that magnitude with $\boldsymbol{\delta_{ni}}$ being the slip within the $\boldsymbol{n}$-th cell due to the $\boldsymbol{i}$-th scenario having magnitude $\boldsymbol{M_w}$. To average the slip over long term, this has to be modulated by the probability of occurrence of an event within a defined magnitude bin $\boldsymbol{P(M_w)}$ and by the probability $\boldsymbol{P(Sc_i|M_w)}$ of each scenario $\boldsymbol{Sc_i}$ conditioned to the magnitude $\boldsymbol{M_w}$; while $\boldsymbol{P(M_w)}$ is computed from the Gutenberg-Richter law defined for the specific subduction zone the first attempt is to define all the scenarios, at fixed magnitude, as uniformly distributed, that is $\boldsymbol{P(S_i|M_w)} = \frac{\boldsymbol{1}}{\boldsymbol{N(M_w)}}$ $\forall \boldsymbol{i}$.

The obtained average slip is a proxy of the total slip over long term, given that the probability of occurrence of all the scenarios is proportional to their annual rates. Therefore, this choice ensures a depth independent long-term slip over the subduction when the stack is performed over the set of the seismic scenarios deriving from the homogeneous rigidity and coupling hypothesis.

Nevertheless, it generates, as expected, an accumulation of the long-term slip when the variable rigidity/coupling set of scenarios is considered.

Since the amplification of the slip linearly increases with the decreasing rigidity, we quite satisfactorily balanced the long-term slip by imposing a $\boldsymbol{P(S_i|M_w)}$ that linearly increases with the average rigidity of the ruptured area of $\boldsymbol{i}$-th scenario.

As a result of Levels 1 and 2, the total set of scenarios to be modeled for PS and SPS, $\{\sigma_k\}^{(PS/SPS)}$, is composed by all combinations of regions R_i, magnitudes M_j, centers $\{x_c, y_c\}$ and all the sampled slip distributions $\vec{s}$. The corresponding mean annual rate is computed then as:

$$\lambda\left(\sigma_k^{(PS/SPS)}\right) = \lambda^{(PS/SPS)}(R_i, M_j, x_c, y_c, \vec{s}) = \lambda_i^{(PS/SPS)}(M_j)\ \Pr_i(x_c, y_c|M_j)\ \Pr_i(\vec{s}\,|x_c y_c, A, M_j)\ .$$

1.6 Level 2b - Variability of BS/SBS earthquakes of a given magnitude within a given region

This Level includes the two possible BS-like parameterizations, that is to say BS or SBS (FIGURE 1.1a). This includes all regions treated as BS and the structures modeled as SBS because are not well constrained for being treated as PS (only the Cadiz subduction zone). The dominant faulting mechanism and the spatial distribution of earthquakes are not pre-determined. They both vary within the volume defined by a set of cells on a regular 3D grid. Coordinates of the fault centers are distributed along the nodes of the regular grid. Similarly to the PS/SPS case, the correspondence of a BS earthquake to a particular region is controlled by the position of its geometrical center. Ruptures are modeled as single rectangular planar faults with uniform slip distribution, taking the average values from scaling relations. We model the variability of all the parameters listed in SECTION 1.1 and FIGURE 1.1a: location, depth, strike, dip, rake, and average slip, identifying all individual sources.

This Level also includes the Cadiz subduction treated as SBS, since the parameterizations are similar. However, as described in SECTION 1.1, the rake is fixed, dip and strike have more limited variability, and depth is extended to deeper values.

The BS/SBS analysis is subdivided into the 3 sub-Levels that stack on Level 1, that are:

- sub-level 2b.1 - spatial distribution of earthquakes
- sub-level 2b.2 - depth distribution of earthquakes
- sub-level 2b.3 - focal mechanisms

The results of Elicitation #1 indicated to limit the number of alternatives to be implemented (Doc_P1_S3). Therefore, we use a total of two alternatives exploring the epistemic uncertainty induced by BS catalogue definitions. Note also that, among the selected models, the one for sub-level 2b.3 (strike-dip-rake) is Bayesian, allowing for the quantification of the inherent epistemic uncertainty (see discussion in SECTION 1.3.4).

For what concerns SBS, all probability distributions are set as uniform over the considered variability, in analogy with the with the PS/SPS case discussed at Level 2a. More specifically, the spatial probability distribution (sub-level 2b.1) is uniform (they are all equiprobable) over a subset of 10 grid points within the region, as reported in FIGURE 1.16. The depth range for sub-level 2b.2 is much larger than for BS (used for modelling crustal faults), as discussed in SECTION 1.3.7, and all these

depths are also assumed equiprobable. A uniform distribution is considered also for focal mechanisms (sub-level 2b.3), for which a very limited variability is foreseen (with only four cases: two strikes, two dips, one rake, see SECTION 1.1.4).

The total set of scenarios to be modeled for the Special Background Seismicity $\{\sigma_k\}^{(SBS)}$ is composed by all combinations of regions R_i, magnitudes M_j, positions $\{x, y\}$, depths d and focal mechanisms $\{strike, dip, rake\}$. The corresponding mean annual rate is then computed as in FIGURE 1.1a, that is:

$$\lambda\left(\sigma_k^{(SBS)}\right) = \lambda^{(SBS)}\left(R_i, M_j, x, y, d, strike, dip, rake\right) = \lambda_i^{(PS)}\left(M_j\right) Pr_i(x, y) Pr_i\left(d \middle| M_j, x, y\right) Pr_i(strike, dip, rake\ |x, y)$$

where $Pr_i(x, y) = 1/10$ in the 10 allowed positions (and 0 otherwise) and $\Pr_i(strike, dip, rake|x, y) = 1/4$ for the 4 allowed faulting mechanisms (and 0 otherwise).

More specific probabilistic models are instead applied for BS.

At sub-level 2b.1 - spatial distribution of earthquakes - given an earthquake of a given magnitude in a given tectonic region, the geometrical center of a fault may be at different positions. The area covered by the region is thus discretized by a regular 2D grid (FIGURE 1.14). The assessment consists of quantifying the conditional probability $Pr_i(x, y)$ for each potential rupture center $\{x, y\}$ within region R_i. Note that, differently from PS/SPS, this quantification is assumed to be independent from the magnitude value, which is consequently omitted from the notation.

To compute the BS spatial distribution, we use the smoothed seismicity approach (Frankel, 1995). To increase the number of seismic events to be considered, we adopt the approach of Hiemer et al. (2014) who introduce a correction to consider the variability of the completeness magnitude in the spatial smoothing. In this way, we can use longer time intervals of the catalogue adopting an increasing magnitude of completeness going back in time. The analysis is based on BS-only complete declustered catalog (ISC in the Atlantic and EMEC in the Mediterranean), as defined in SECTION 1.3. The BS-only catalogues are considered as emerging from the 2 alternative cut-off distances considered at Level 0 (SECTION 1.3 and FIGURE 1.1b).

We adopted the fixed spatial kernel strategy. This means that the kernels (that are related to the probability density function, PDF, associated to the earthquakes) has a constant dimension, for all the events.

The functional form for the kernel for the j-th earthquake e_j in the i-th position of the spatial cell $\overrightarrow{x_i}$ is at it follows:

$$K(\overrightarrow{x_i}, e_j) = \frac{c}{\left(R_{ij}^2 + d^2\right)^{3/2}} \frac{10^{b(M_{c,j} - M_{cmin})}}{T_j}$$

Where c is a normalization constant for the spatial part of the kernel and it is set so that $\sum_i K(\overrightarrow{x_i}, e_j) = 1$, R_{ij} is the distance between the earthquake e_j and the spatial cell $\overrightarrow{x_i}$, d is a the smoothing distance, b is the b-value of the frequency-magnitude distribution that we set to 1, $M_{c,j}$

and T_j are the completeness magnitude and the relative time length referred to the earthquake e_j, and M_{cmin} is the minimum completeness magnitude for the catalog.

For each earthquake, the kernel is evaluated at the center of all the cells that compose the grid, instead of considering the integral over the cell's area. This approximation can lead to an underestimation of the real rate in the cells if the smoothing distance d is quite smaller than the cell dimension. Following Hiemer et al. (2014), who used the same SHEEC-EMEC catalogue, the optimal value for the fixed kernel smoothing distance d is 10 km. In our application, the average dimension of the cell edge is about 25 km.

To correct this potential approximation, we slightly modulate the fixed smoothing distance for the cells close to the earthquake. To do that, we adopt as kernel distance the distance between the earthquake and the second nearest cell center. If the earthquake falls near the cell center, the smoothing distance increase up to about 25 km, whereas if the earthquake falls between two cell centers the smoothing distance decrease up to about 12 km (FIGURE 1.22).

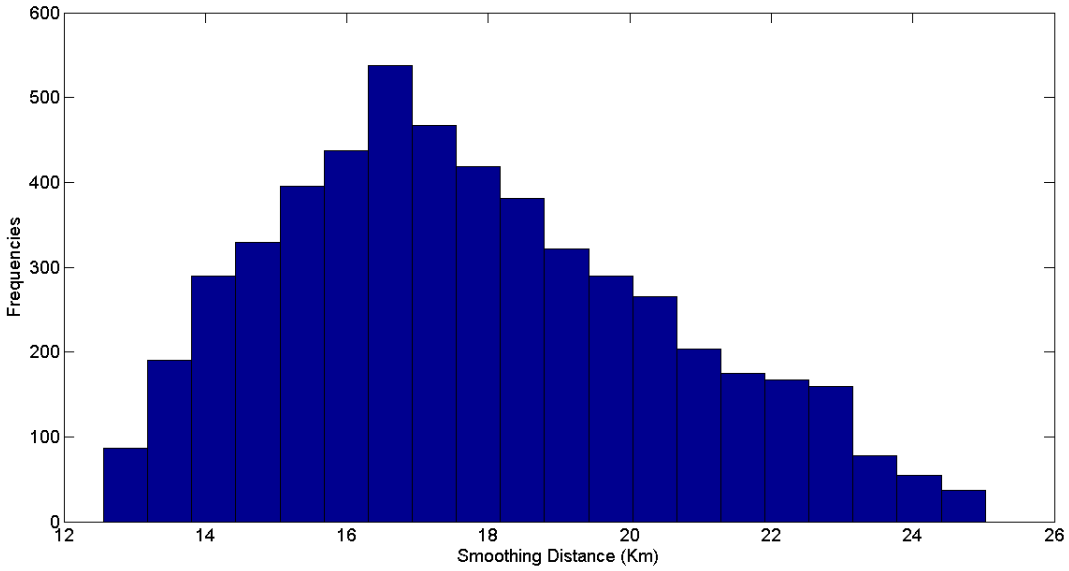

FIGURE 1.22: distribution of the smoothing distances, that varies, according to our method, with the distance between earthquakes and cell centers.

The impact on this modulation in the spatial distribution of the kernel is reported in FIGURES 1.23 and 1.24. Note that while both approximations hold for all the far cells, the use of the standard methods determines an underestimation of the kernel function. Adopting our correction, we have an overestimation only in the cell to which the earthquake belongs, and less biased results for all the other cells.

To further check if our method gives robust results, we perform a statistical prospective S-test against independent data. More details are reported in Doc_P2_S5.

At sub-level 2b.2 - depth distribution - given an earthquake of a given magnitude in a given region at a given grid cell, the focal depth is addressed, according to the discretization presented in SECTION 1.3.7 (see FIGURE 1.15 and TABLE 1.7). A uniform distribution for depths is assumed. The column of crust identified by $\{x, y\}$ is thus discretized by depth levels. The assessment consists of quantifying in

each region R_i the conditional probability of these different depth levels $\Pr_i(d|M_j, x, y)$ conditioned to magnitude M_j and geographical position $\{x, y\}$.

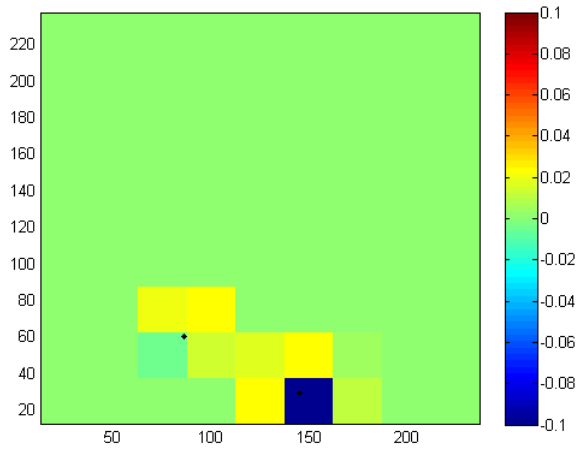

FIGURE 1.23: difference between the real and the approximated spatial kernel for cell dimension of 25 km and smoothing distance of 10 km. Colors show the difference between PDFs, the black dots are simulated earthquakes: looking at the lower event we can see that if the earthquake falls near the cell center, we have an underestimation of the rate.

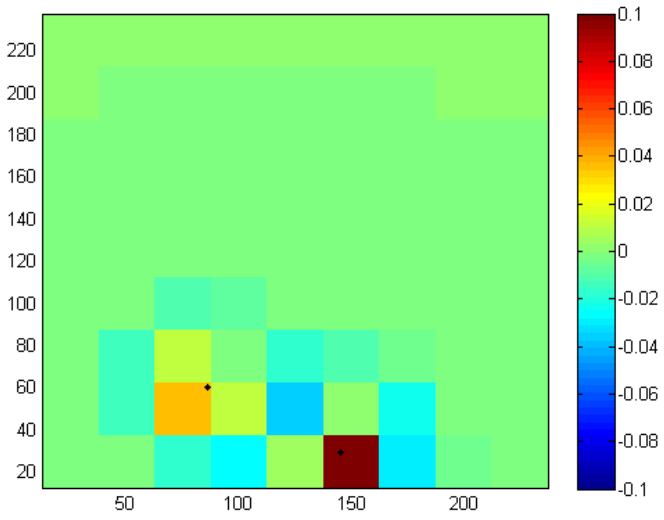

FIGURE 1.24: difference between the real and the approximated spatial kernel for cell dimension of 25 km and smoothing distance of 10 km, using our method. Colors show the difference between PDFs, the black dots are simulated earthquakes: looking at the lower event we can see that now the underestimation is disappeared, and we have an overestimation, which is preferable since the event is falling right in the cell.

At sub-level 2b.3 - focal mechanisms -given an earthquake of a given magnitude in a given region at a given cell and depth, various faulting mechanisms are possible. Here we analyze probabilities of different strike/dip/rake combinations for each cell. Note that these probabilities are not uniform but, instead, their expected PDF's are derived according to past seismicity and known faults. The joint conditional probability $\Pr_i(\text{strike}, \text{dip}, \text{rake}|x, y)$ is quantified in each cell $\{x, y\}$. A Bayesian

method like the one adopted in Selva et al. (2016) is implemented. In each region an informative prior model based on the worldwide data discussed in SECTION 1.3.9. This prior is built in the form of a Dirichlet distribution for all angle combinations following the procedure discussed in Selva et al. (2010), in which the prior is set by updating a pseudo maximum ignorance hyper-prior with global/general data. In practice, the resulting prior Dirichlet distribution has average equal to 1 plus the counts reported in TABLE 1.10 and normalized to 1 (by summing 1 to each cell we avoid setting prior distributions identically equal to 0). The Dirichlet's equivalent sample size is set to 10 (meaning that the prior is completely forgot whenever we have >> 10 data in the likelihood, while it influences the posterior when we have smaller datasets). The likelihood is modelled as a multinomial distribution based on the focal mechanism catalogue available. We considered the BS-only non-declustered entire (without considering completeness) catalogue, that is the global CMT in the Atlantic and the regional CMT in the Mediterranean (as defined in SECTION 1.3.3). Both focal planes are assumed equiprobable and included into the uncertainty quantification by reporting 1/2 datum for both solutions, as in Selva and Sandri (2013). The BS-only catalogues are considered as emerging from the 2 alternative cut-off distances considered at Level 0.

The obtained regional posterior is then used as prior in each cell. If faults are present in the fault catalogue in each cell, this prior is combined to a strongly informative prior distribution based on local faults. In this case, a Dirichlet distribution is set by forcing an average equal to the fault strike, dip, and rake, with an equivalent sample size of 100 (ten times stronger than the regional prior). If more than one faults are present in one cell, all the mechanisms are considered, weighting for their respective moment rate.

Note that this quantification is assumed to be independent from magnitude and depth, which are consequently omitted from the notation.

The total set of scenarios to be modeled for BS $\{\sigma_k\}^{(BS/SBS)}$ is composed by all combinations of regions R_i, magnitudes M_j, positions $\{x, y\}$, depths d and focal mechanisms $\{strike, dip, rake\}$. The corresponding mean annual rate is then computed as in FIGURE 1.1a as:

$$\lambda\left(\sigma_k^{(BS/SBS)}\right) = \lambda^{(BS/SBS)}\left(R_i, M_j, x, y, d, strike, dip, rake\right) = \lambda_i^{(BS/SBS)}\left(M_j\right) \Pr_i(x, y) \Pr_i(d|M_j, x, y) \Pr_i(strike, dip, rake|x, y).$$

2 STEP 2 - TSUNAMI GENERATION & MODELING IN DEEP WATER

The standard way of estimating the tsunami intensity on the coast (e.g., run-up) and producing inundation maps is to apply depth averaged nonlinear shallow water (NLSW) numerical models that include drying-wetting schemes for the simulation of the tsunami inundation phase. However, direct simulation of coastal inundation using nonlinear shallow-water theory is nowadays not yet generally affordable in case of PTHA studies operating at the regional scale and with millions of seismic scenarios. For this reason, we separate tsunami modeling in two stages at STEPS 2 and 3.

At STEP 2, we deal with deterministic numerical simulation of large-scale processes of tsunami generation and deep-water propagation. We here apply specific approximations, since offshore tsunami propagation can be reasonably well approximated using relatively coarse grids with modelling schemes assuming linearity of the tsunami with respect to coseismic displacement at the source. Hence, this STEP is relatively affordable from the computational point of view, and the publicly available digital elevation models are generally considered accurate enough for deep sea tsunami modelling purposes.

The local processes of coastal shoaling and inundation are modelled at STEP 3 (CHAPTER 3). These processes are to a large extent inherently nonlinear and their realistic direct simulation would require fine grid resolution meaning unaffordable computational costs (within current project scope) as well as availability of high-precision topo-bathymetric models not currently available for the majority of the coastline. Instead of using deterministic numerical models, we then developed a stochastic modelling approach on purpose, which considers these limitations. STEP 2 provides then the input to STEP 3 for this modelling, which consists of tsunami mareograms at offshore Points of Interest (PoIs).

Hence, the goals of STEP 2 are, in particular:

1. the numerical (deterministic) simulation of the sea floor displacement corresponding to each of the individual earthquake scenarios $\{\sigma_k\}$ defined at STEP 1;

2. the numerical (deterministic) simulation of the corresponding tsunami generation and propagation from each source up to each offshore Point of Interest (POI), resulting in the mareograms $\{M(\sigma_k, POI)\}$; out of which parametric lookup tables $\{(max_t, T, \mp)[M(\sigma_k, POI)]\}$ of wave amplitude maxima max_t, wave periods T, and polarities $\mp$ can be derived for the later use at STEP 3.

2.1 Levels at STEP 2

At STEP 2 we have defined 4 Levels (0-3):

- Level 0 (input data): Crustal elastic model; topo-bathymetric datasets and digital elevation models; Points of Interest (POIs).
- Level 1: Co-seismic displacement model.
- Level 2: Tsunami generation model.
- Level 3: Tsunami propagation (in deep water) model.

Level 0 is used for treating the databases which are relevant for this STEP.

Levels 1-3 in STEP 2 is the sequence composing the tsunami modeling from generation of the tsunami due to the sea floor displacement, to tsunami propagation in deep water up to the offshore POIs.

These Levels are described in detail below.

Following the indications from the first elicitation of the Panel of Experts, no alternatives were implemented at STEP 2, since the uncertainties at this STEP are thought to have a limited influence on the final model uncertainty. Accordingly, the descriptions at STEP 2 are much shorter than at previous STEP 1.

However

1) as described in the following SUBSECTIONS, some common simplifications are here adopted, which are nevertheless sources of uncertainty in the final results. They are: Okada-like faults in a homogeneous half space; Kaijura-type filtering of the sea floor displacement; Green's functions approach (linear combinations, to limit the computational burden). Only the uncertainties introduced by the Green's functions approach are here addressed and later, at STEP 3 (described in SECTION 3), propagated onto the final results.

2) Some Levels within this STEP contain some elements which are more critical than others. For example, at Level 0, the importance of possibly adopting a different digital elevation model used for tsunami simulations was pointed out. However, human and computational resources for repeating these simulations for another topo-bathymetric dataset were unaffordable. A comparison of the model adopted with the one suggested is anyway reported with the responses to the Reviewers.

2.2 Level 0 - Crustal elastic model; topo-bathymetric datasets and digital elevation models; POIs

At this Level, we treat the choice of:

- the crustal model employed for calculation of the co-seismic surface displacement;
- the topo-bathymetric database, and the preparation of the digital elevation model on a grid used for subsequent tsunami numerical modeling;
- the POIs used as locations for output calculation from numerical simulations, also used as nominal locations for conditional probabilities and for NEAMTHM18 results afterwards at STEPS 3 and 4.

The adopted crustal model for coseismic displacement calculations is an elastically homogeneous Poisson solid. The geometry is that of an infinite half-space, which is the setting used in all the Okada (e.g. Okada, 1992) and Okada-like algorithms described in the following. All the faults are buried, or they cut the surface of this homogeneous half space. The adopted shear modulus (rigidity) is generally 33 GPa; however, for a given slip value, the specific value of the shear modulus does not influence the Okada coseismic displacement in case of a Poisson's solid.

The topo-bathymetry generally employed is SRTM30+. It has a resolution of 30 arc seconds (~ 900 meter). However, SRTM30+ is improved in the NE Atlantic region with local data in the NE Atlantic in the Gulf of Cadiz (Zitellini et al., 2009; see also FIGURE 2.1), using DEMs available from the ASTARTE

project (www.astarte-project.eu). Conversely, in the Black Sea, SRTM15+ resampled to 30 arc seconds is used. Both SRTM datasets are available at http://topex.ucsd.edu/WWW_html/srtm30_plus.html.

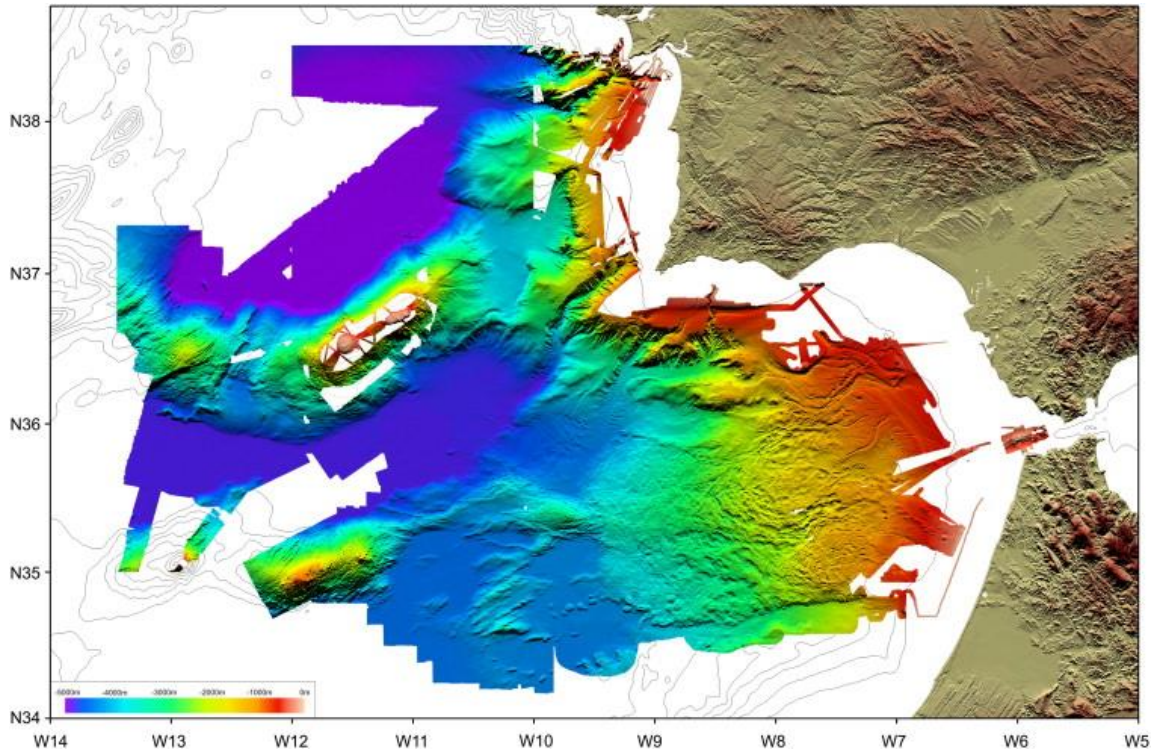

FIGURE 2.1 --- Multibeam compilation data used in the NE Atlantic region. Modified after Zitellini et al. (2009).

The Points Of Interest (POIs) used to output tsunami simulations and subsequently the tsunami hazard quantities are derived from the topo-bathymetric models. We set our POIs to lie along the 50 meters isobath around the whole NEAM region with a spacing of roughly 20 km from each other (FIGURE 2.2). Actually, the POI depths feature some variability which is related to the approximations made during the extraction of the 50 m depth contour from regularly gridded data with the GMT algorithms (Wessel et al., 2013). We limit this variability between 40-100-meter depths. The POIs that do not fall in the prescribed range 40-100 m were discarded for the subsequent analyses. Hence, the distance between two adjacent POIs can be larger than 20 km at places, due to the removal of POIs after this sanity check. This occurred mainly in area with very steep coasts. Due to the depth variability, we can moreover think of the POIs as often only nominally lying on the 50 m isobath.

The choice of a ~20 km spacing between subsequent POIs is a compromise between getting a dense enough coverage and the need for containing computational cost and disk space occupancy. The distance of 20 km is in the same order of magnitude of the discretization step applied for the position of the seismic sources (approximately 25 km, see SECTION 1.3.7 and FIGURE 1.14).

Similarly, the choice of the 50 m isobaths can be regarded as the result of a compromise between two contrasting needs: preserving linearity of the tsunami propagation, on one hand, and being close enough to a coastline, on the other hand. Linearity should be in principle guaranteed as long as

tsunami amplitude, which increases progressively during shoaling towards the coast, remains much smaller than sea depth.

Linearity is in fact needed because of the enormously large number of seismic scenarios accounted for in the PTHA study – about 50 million – along with the vastness of the region under investigation. Hence, individual tsunami propagation scenarios cannot be all computed in a direct way, which would require much larger computational resources. Instead, we employ the method of Green's functions and evaluate off-shore POIs mareograms by linear superposition of precomputed virtual POI tsunami time-series from unit sources. As described in what follows, also the duration of simulations and the size of computational domains, as well as the spatial and temporal resolution of the calculation grids, were optimized seeking for a reasonable compromise. Overall, we needed to find an affordable trade-off between the required source coverage and practical feasibility (limited computational time/resources). It must be noted though that, there are several locations where the offshore POIs cannot really be associated to the coast behind which is too distant. This is true for example for the southern part of the North Sea, or, though at a smaller scale, for the northern Adriatic Sea or for the western coast of Tunisia in the Mediterranean Sea. Given the vastness of the study region, it was out of reach to apply special treatments for these situations, and care should then be applied when using the results at the local level.

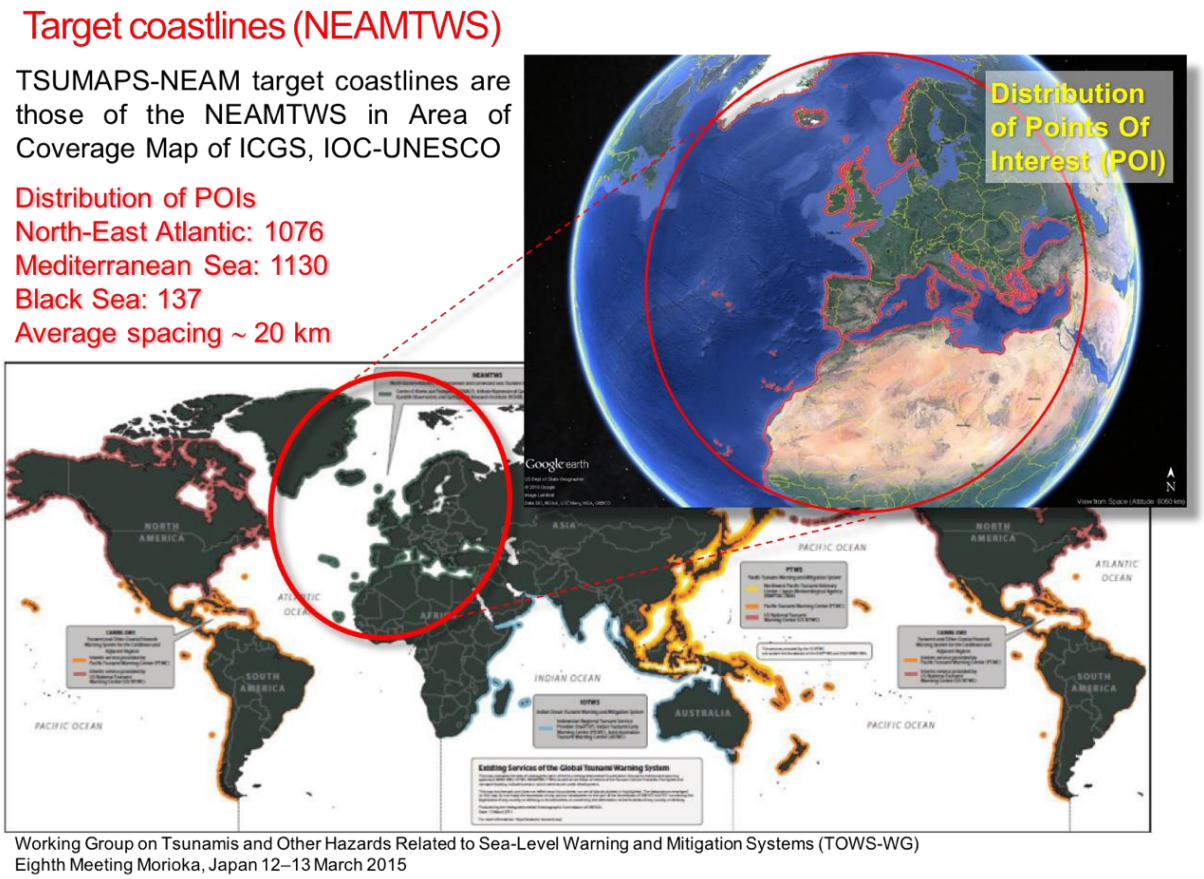

FIGURE 2.2: Distribution of Points of Interest (POIs) in the NEAM region.

2.3 Level 1 – Co-seismic displacement model

The sea-floor co-seismic displacement is modeled at STEP 2 for each earthquake scenario $\{\sigma_k\}$ defined by the ET (event tree) at STEP1.

In the case of BS (Background Seismicity, see SECTION 1.1), each earthquake scenario corresponds to a single rupture characterized by a set of parameters including location, geometry (fault size and orientation in space), slip direction and amount. The co-seismic displacement associated to BS is modelled with 'Okada faults' (Okada, 1992) according to these parameters.

This applies also to SBS (Special Background Seismicity, see SECTION 1.1), and to the lower magnitudes of the SPS (Special Predominant Seismicity, see SECTION 1.1), which are parameterized in the same way of the BS (see SECTION 1.1, and the description of Level 2b of STEP 1 in SECTION 1.6).

The lower magnitude earthquakes on SPS (Gloria fault, normal and transform faults in the central section of Mid-Atlantic Ridge, closer to the Azores, FIGURE 1.13), are treated as well with BS-like subfaults, that is with individual faults of different size for each magnitude sharing the same centers, in this case as much as possible along the SPS structure (see the definition at the beginning of SECTION 1.1, and the description of Level 2a of STEP 1 in SECTION 1.5).

Resulting sea-surface deformation from BS, SBS, and lower magnitude SPS is then projected onto the Gaussian tsunami unit sources as described in SECTION 2.5.

Conversely, the higher SPS magnitudes are modelled using planar rectangular faults divided into subfaults (see FIGURE 1.7). Here, tsunami unit sources are directly related to the unit slip at the subfaults and the uniform slip value coefficient for each subfault is obtained from a scaling relation. These quite common simplifications, made to save computational time, are considered appropriate because these structures are distant or very distant from (most of) the target coast lines.

In case of PS (Predominant Seismicity, see SECTION 1.1), rupture scenarios incorporate co-seismic slip distributed with either uniform or variable amplitude and direction across multiple fault patches (subfaults), aligned along non-planar plate boundaries (see SECTION 1.5).

For PS sources relatively close to the coastlines (the ones in the Mediterranean, see SECTION 1.3.4 and FIGURE 1.12), sufficiently 'short-wavelength' slip heterogeneity needs to be modelled. We recall from STEP 1 that for Hellenic, Cyprus and Calabrian Arcs, in the Mediterranean Sea, the PS ruptures are modelled using non-planar triangular meshes (with typical edge length of about 15 km); hence, this relatively small triangles allow modelling heterogeneous stochastic slip distribution.

For the Caribbean Arc, the triangles honor the subduction geometry; however, given its relative distance from NEAM coastlines, heterogeneous slip is not used. For the distant Mid Atlantic Ridge, rectangular subfaults were used.

Either triangular (Hellenic, Cyprus, Calabrian and Caribbean Arcs), or quadrilateral (Mid-Ocean Ridge and Gloria Fault) PS subfaults were treated as well Okada subfaults, and the total seafloor deformation was computed as a superposition of either equal contributions from these individual patches, or different contributions when the heterogeneous slip is used. In case of triangular patches constituting a finite-element mesh, a special version of the "Okada's" algorithm (Meade, 2007) is

used. The resulting sea-surface deformation from all these sources is then either used as initial condition for tsunami generation in numerical simulation or, like for the BS, only for the PS in the Mediterranean, projected onto the Gaussian tsunami unit sources as described in the next SECTION.

More specifically, in all cases, the vertical component of the sea-floor displacement is used as input for Level 2, where the tsunami generation is treated. The vertical component of the sea-floor displacement is sampled on a regular 30 arc-second grid automatically approximately centered on the rupture. Since Okada's analytical solution is prone to produce very long 'tails' of low-amplitude surface displacement, for practical reasons, we restricted the deformation area to vertical displacements larger than 1 cm.

2.4 Level 2 - Tsunami generation model

At this Level, tsunami initial conditions at the surface are derived starting from the seafloor vertical deformation obtained at the previous Level.

The water column works as an effective low-pass filter for the co-seismic deformation of the sea-floor (e.g., Nosov and Kolesov, 2011). The filtering effect strongly increases with depth and, thus, should not be neglected for modeling of small- and medium-size earthquakes at the subduction zones as well as for rupture models with heterogeneous slip.

In order to account for the attenuation of the short wavelengths through the water column, we apply a two-dimensional filter of the form 1/cosh(kH) (Kajiura, 1963) to the static vertical sea-floor deformation field calculated at Level 1. Here *k* is the wavenumber and *H* is the effective water depth taken as the average above the 4 fault corners. This filter is realized through forward and backward Fast Fourier transforms with high-pass filtering applied to the Fourier image in between. Because of the requirement of the constant water depth, this approach has a clear drawback in case of large ruptures stretching over highly-variable bathymetry. Recently, Nosov and Kolesov (2011) suggested a more sophisticated but also more precise filtering algorithm which is not restricted to the effective uniform water depth but, instead, can be applied above arbitrary complex bathymetry. This algorithm is, however, much more time consuming, so we had no possibility to employ it within the limited time of the TSUMAPS-NEAM project.

Moreover, this filtering was not applied to all sources treated as rectangular subfaults, that is all the relatively shallow sources of the Gloria fault and of the Mid-Atlantic Ridge, and the Caribbean Arc.

2.5 Level 3 - Tsunami propagation (in deep water) model

At this Level, we simulate tsunami mareograms $\{M(\sigma_k, POI)\}$ at the off-shore (ca. 50 m depth) POIs, according to the initial conditions evaluated at the previous Level for all the considered earthquake scenarios $\{\sigma_k\}$. These offshore time-series are also further analyzed to derive the principal wave characteristics – maximum amplitude, period, and polarity – that are the necessary input for the subsequent processing at STEP3 "Shoaling and Inundation" (CHAPTER 3).

Two types of tsunami Green's functions are here used to obtain from linear combinations the mareograms $\{M(\sigma_k, POI)\}$ for different sources belonging to the $\{\sigma_k\}$ set in the different zones under consideration. The first type of tsunami Green's functions is that associated to Gaussian shaped sea level elevation unit sources. The second type is the more usual one considering unit slip at elementary subfaults. The reason for this choice is once again merely practical: Gaussian tsunami

database pre-existed the project and it was then used as it was; in some cases, the resources allowed to extend it; in some other cases, it was less computationally expensive to adopt the subfault approach, for example for distant sources not requiring for modelling of low earthquake magnitude and size.

For BS, SBS and PS scenarios in the Mediterranean, we use a new approach with Gaussian-shaped elementary sources distributed directly at the sea surface (Molinari et al., 2016). Based on arbitrary initial sea surface displacement, the database allows the fast calculation of full waveforms at POIs (distributed along the 50 m isobaths) by means of linear superposition. A computationally inexpensive procedure is set to estimate the weights for the linear superposition based on the preservation of potential energy of the initial elevation field.

Note that, in contrast to the more common tectonic elementary subfaults technique, these sea-surface Gaussian elementary sources are fully independent of any presumed earthquake focal mechanism. Once computed, their Green's functions allow simulation of tsunami propagation for arbitrary tectonic sources or even for an arbitrary displacement of the sea surface, which would allow in principle to use these same tsunami simulations for non-seismic sources. This property of the sources is important because in the BS seismicity approach, for example, different faulting mechanism are always possible in the same cell, and then it is convenient, also in terms of computational coast, to have mechanism-free tsunami unit sources.

These Gaussian-shaped elementary sources are uniformly distributed at the sea surface along the whole area of possible near-field co-seismic deformation (the whole Mediterranean and Black Sea, as well as pre-coastal European NE Atlantic domain: see the blue region in FIGURE 2.3). That is, the blue areas include the source zones but cover a wider area around them which includes the spatial extension of the co-seismic fields which each source is capable to generate. We recall that BS sources within the stable oceanic regions of the Atlantic Sea, to the north and to the south of the area covered by Gaussian unit sources and to the west of the mid-Atlantic spreading ridge, are ignored (see SECTION 1.3.4 and FIGURE 1.7). This choice is supported by the observation that the seismicity of plate interiors, including both oceanic and continental stable regions, accounts for less than 4% of all global seismicity (Kagan et al., 2010). More in general, BS occurring within all far-distant areas in relation to the Atlantic coasts is neglected, assuming that it has a very little impact on hazard. As a result, we selected a buffer within 200 km from the coasts, as the presence of Gaussians is necessary in the near field due to the higher sensitivity to earthquake mechanism and to tsunamis generated by smaller earthquakes.

The coverage is also somehow limited toward north, also because the overall seismicity rates along the NE Atlantic European coasts decrease from south to north. However, some exceptions do exist. One exception is around Iceland, which being in the near-field from the seismic sources should have been covered with BS (hence elementary sources) due to the lack of resources.

Note also that some very shallow waters in the Black Sea (depth < 50 m) host neither Gaussian nor seismic sources. A very local hazard assessment would possibly require a more detailed treatment of tsunami sources. For this and other zones, such as the northern Adriatic, where the water is quite shallow as well, linearity assumption may in fact fail. These issues of involving linearity assumption breach in shallow waters is somehow the same which determines, such as in the North Sea (FIGURE 2.2), a great distance of the POIs from the coast lines.

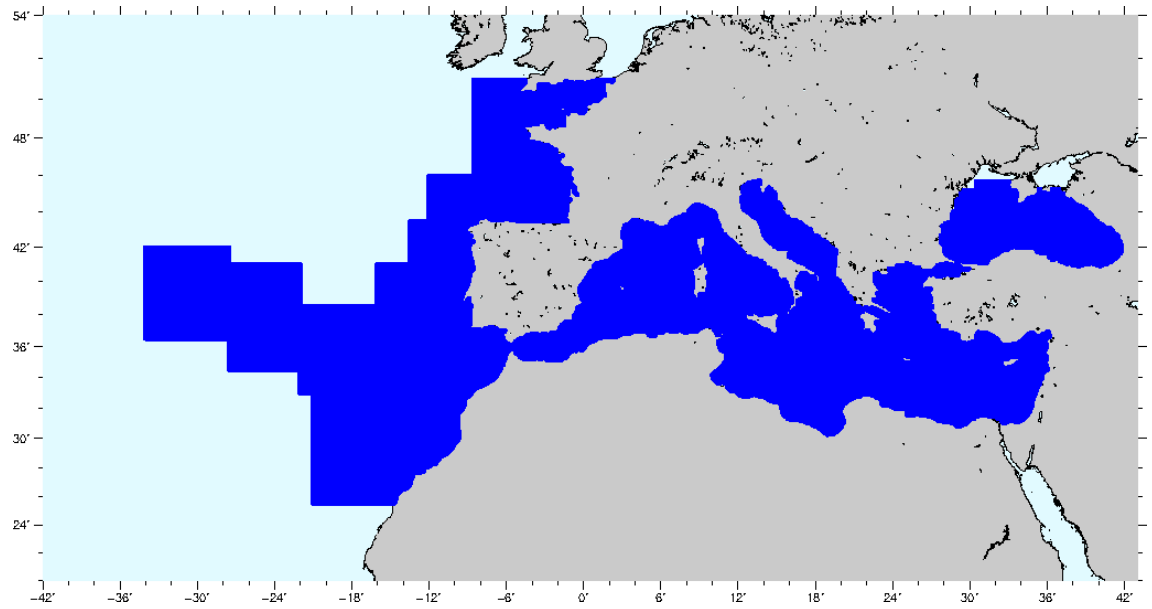

FIGURE 2.3: Gaussian sources coverage is indicated by the dark blue color superimposed to the light blue.

All the mentioned limitations have been set mainly because of the project temporal and financial limitations, so that the maximum homogeneous coverage has been focused on areas with relatively higher seismicity. However, they may introduce some local biases that should be carefully evaluated for more local applications (from sub-regional/national to sub-national/local levels).

The size (~20 km base width) and spacing (~7 km) of elementary sources are illustrated by FIGURE 2.4. Molinari et al. (2016) showed that these spatial dimensions are fine enough to satisfactorily reproduce the initial sea level displacement generated by M ≥ 6.0 earthquakes.

To limit the computational and the storage resources, the mareograms associated to each Guassian elementary source is limited to a given simulation spatio-temporal domain. Spatial and temporal extensions of the simulation domain generally depend on the maximum earthquake magnitude that needs to be simulated at each location. The largest domains are those associated to the biggest magnitudes, since their tsunamis reach to larger distances, and/or to the distant sources.

The Gaussians in the Mediterranean, with a simulation temporal domain of 8 hours and a spatial domain enclosing the entire Mediterranean from Gibraltar Strait (with a small buffer in the Atlantic) to Eastern Mediterranean and to Aegean and Marmara Seas, were already available at the beginning of TSUMAPS-NEAM Project from the database of Molinari et al. (2016). For all other domains, the extensions have been optimized to save computational resources by means of preliminary simulations performed at the beginning of the project as described in the next paragraphs.

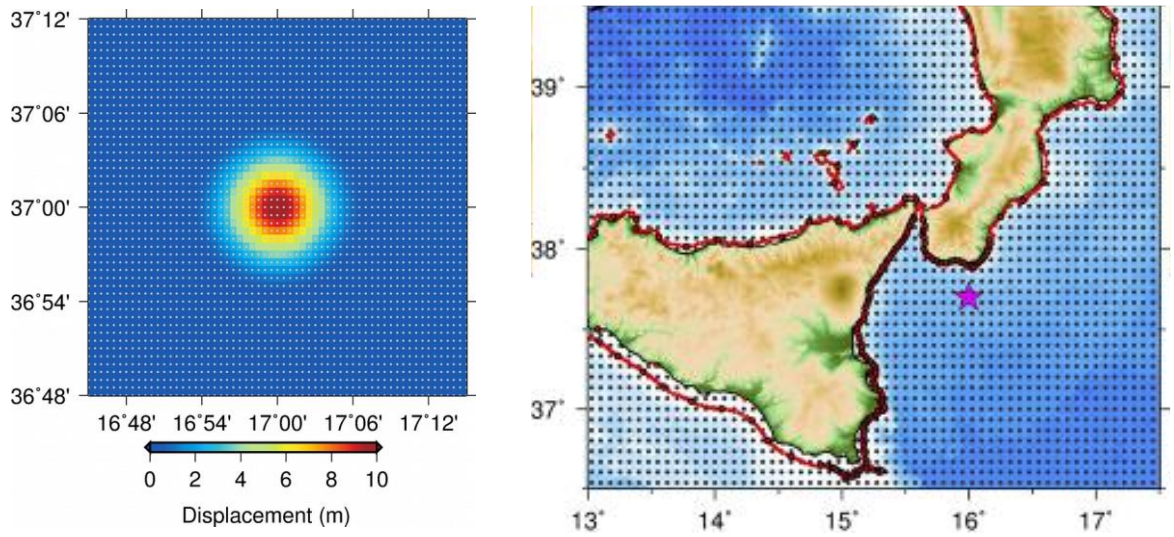

FIGURE 2.4: Unit source size and spacing. Modified after Molinari et al. (2016).

FIGURE 2.5 shows the NE Atlantic Gaussian source zones. Very large simulation domains have been used only for Gaussians around the Cadiz subduction (region R1), which includes very large magnitudes (see "Geometry, spatial discretization and tectonic data for BS and SBS (Cadiz subduction) sources", in SECTION 1.1). Anywhere else in the Atlantic, Gaussians are used only to treat smaller events in the BS (maximum modelled earthquake magnitudes up to M7.5, see SECTIONS 1.3.1 and 1.3.5), whereas the bigger earthquakes (up to M9) out of region R1 are included as PS/SPS simulated directly with subfaults (see SECTION 1.4). The duration of the simulations was decided accordingly, that is in order to propagate all the significant tsunami waves to the POIs.

More specifically, for each source zone (R1-R9 in FIGURE 2.5), we chose some strategic points (generally the region corners) as fault centers for simulating "extreme scenario" events with maximum magnitude 9 for R1 and 7.5 for the others, vertical dip, strike 0, 45, 90, 135 and rake 90, -90. We modelled in total 21 source points and 168 different mechanisms. We analyzed the propagation patterns (maxima of the maxima over all simulations taken together) to infer the minimum required simulation domain for each source zone. FIGURE 2.6 shows some examples for R1, R7 and R8. As the scenarios are "extreme" (very conservative), we opted for a minimum threshold of 0.5 m to define the simulation domain. For each source zone, we also computed tsunami travel times starting from the perimeter of the source zone rectangles to establish the optimal simulation length.

It turned out that for source zone R1 almost the full NEAM domain is required. Conversely, for the others, a significant reduction of the simulation domain is achieved.

In conclusion, for the Gaussians, the durations are: in the Mediterranean, 8 hours; in the Black Sea, 4 hours; in the Atlantic, 15 hours for the larger grid (R1 of FIGURE 2.6, top) and 8 hours for the smaller grids (all the others, R2-R9).

The more classical Green's functions based on subfaults with unit slip were adopted for the Predominant Seismicity and the Special PS (PS/SPS, see SECTION 1.1) scenarios in the Atlantic Ocean (earthquakes along the Caribbean Arc, Mid-Atlantic Ridge, and Gloria Fault Zone). They took initial

displacements directly from Level 1. These displacements were copied to the sea surface as tsunami initial conditions.

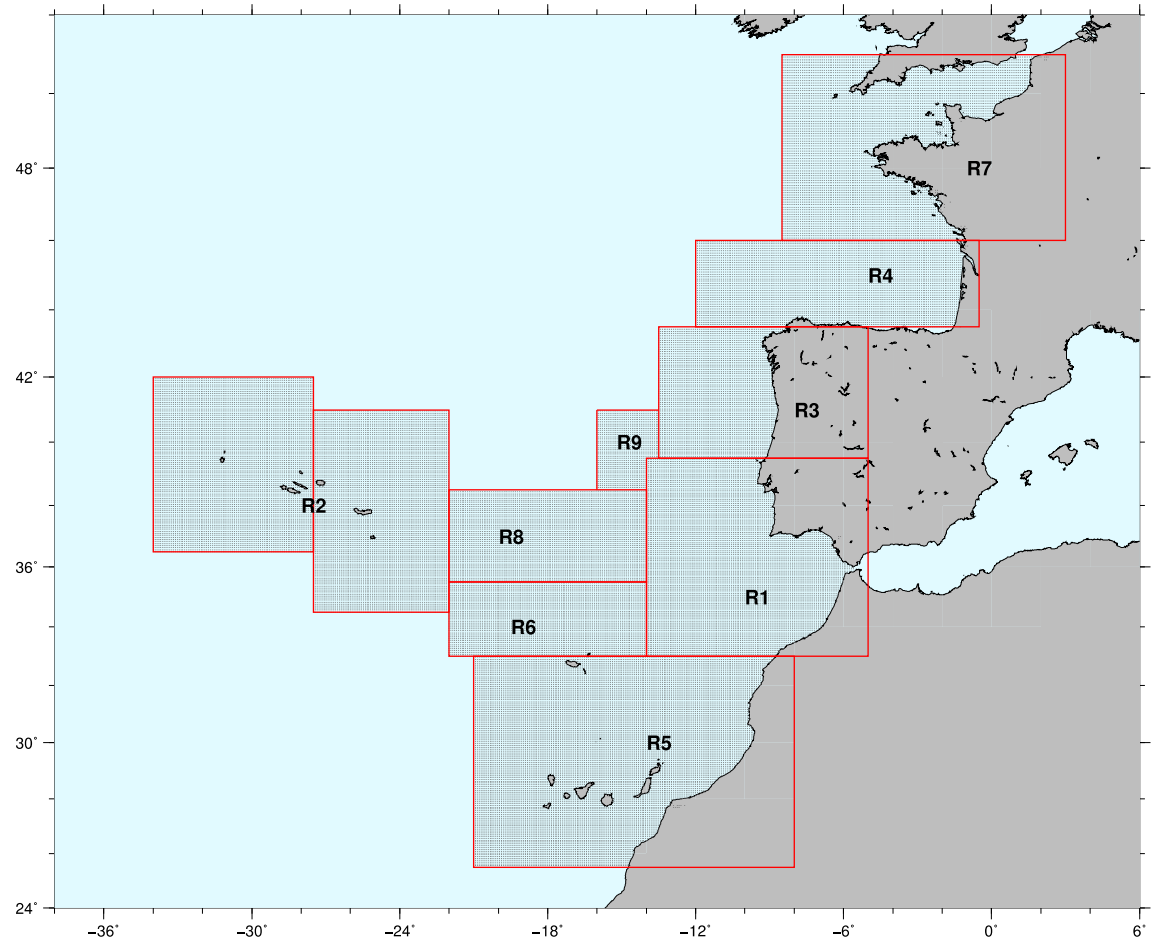

FIGURE 2.5: North-eastern Atlantic Gaussian source zones. The numbers indicate the priority (R1 is the one with the highest priority) attributed during the project to the completion of the simulations in each source zone. The computational resources initially allocated were in fact rather limited and subject to some degree of unpredictability. AN ISCRA class C project at CINECA (https://www.cineca.it/) provided in the end more than expected HPC resources which allowed for the completion up to R9.

The simulation spatial domains used for modelling the tsunamis generated by these subfaults are shown in FIGURE 2.7. Three sub-groups have been identified, with slightly different spatial extensions. The temporal domain for all of them is set to 16 hours. The extent of the domain and the duration of the simulations are chosen in a way that is completely analogous to what was just described for the Gaussians in the NE Atlantic.

The spatial and the temporal domains for all unit sources (both Gaussians and subfaults) are reported in TABLE 2.1.

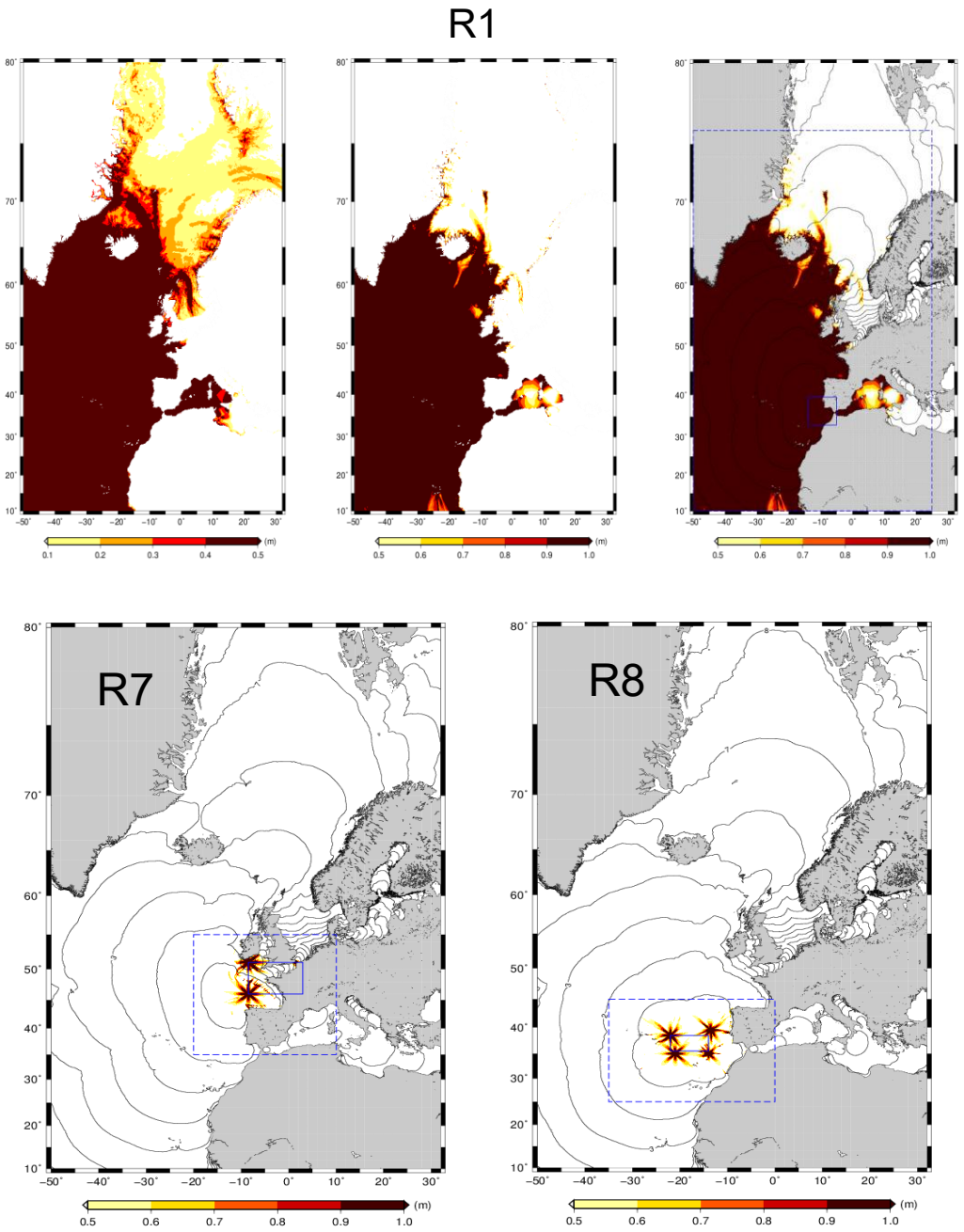

FIGURE 2.6: Examples of the "extreme scenario" results (maxima of the maxima over all simulations, all with maximum magnitude) used for setting the simulation domains for Gaussian unit sources in the NE Atlantic. The colormaps depicting the maxima of the maxima are saturated to different lower (0.1 or 0.5 m) or upper (0.5 or 1 m) to help in visually assessing the extent of the simulation domain. The chosen simulation domains are the dashed blue line rectangles; the solid blue rectangles enclose the source regions R1, R7 and R8; the tsunami travel times are represented by the black contours. The signature of the "rotating" sources combined all together are evident for R7-8 domains looking like little fireworks or Rapunzel's flowers.

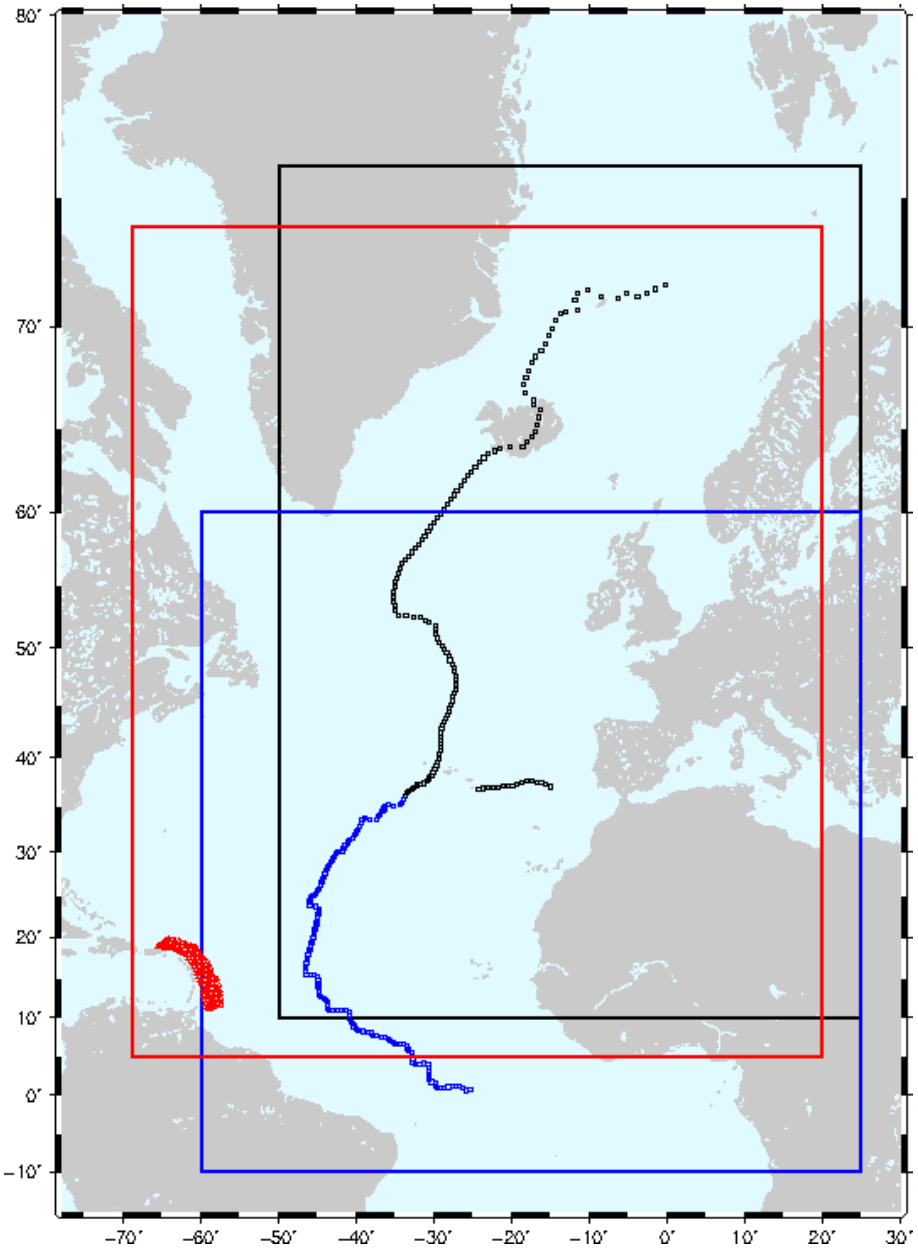

FIGURE 2.7: Computational domains for PS and SPS direct rectangular and triangular subfault tsunami modelling. Colors of the different source zones correspond to the colors of the simulation domains used for modelling their tsunamis.

Either subfault or Gaussian pre-computed tsunami Green's functions were simulated with the Tsunami-HySEA non-linear shallow water (NLSW) GPU-optimised code developed by the EDANYA Group of the Applied Mathematics Department of University of Malaga, Spain (https://edanya.uma.es/) (e.g., de la Asunción et al., 2013). The code has been benchmarked during several NTHMP (http://nws.weather.gov/nthmp/) benchmarking workshops (Macìas et al., 2016; 2017). Open boundary and drying-wetting schemes at the coast are used as boundary conditions. The spatial resolution of the simulation grid is 30 arc seconds. The time-step is automatically adapted by Tsunami-HySEA to match the Courant–Friedrichs–Lewy (CFL) condition for the deepest point in the simulation grid. Simulations for Gaussians in the Mediterranean, the Black Sea, some in the NEA and all the direct subfault simulations, were run on the AURIGA cluster at INGV, which is

composed of 12 TESLA K20 NVIDIA GPUs (4 nodes each with 3 GPUs). All the others simulations (that is most of the Gaussians in the NEA region, see FIGURE 2.5) were run on a subset of the GALILEO cluster at CINECA (https://www.cineca.it/), which allowed us, through an ISCRA class C project, to exploit 160 TESLA K40 NVIDIA GPUs. The GPU time is very heterogeneous depending on the specific simulation, ranging from less than 150 GPS seconds (50 seconds on 3 GPUs) for the relatively small Black Sea where the simulations are also relatively short, to 15 GPU hours for simulating 16 propagation hours on the big domain R1. We needed approximately 200k GPU hours for completing all the simulations.

TABLE 2.1: Domain size, grid size, and simulated time for all the considered sources. Mediterranean, Black-Sea and regions R1-R9 refer to Gaussian sources; Caribbean, Mid-Atlantic Ridge and Gloria Fault (bottom three lines), are parameters for subfaults.

Region	Simulation Domain	Grid Size	Simulated time
Mediterranean	-10/36.5/30/46	5581x1921	8h
Black Sea	26/42/40/47.5	1920x900	4h
R1	-50/25/10/76	9000x7920	15h
R2w	-50/0/25/55	6000x3600	8h
R2e	-35/0/25/55	4200x3600	8h
R3	-25/5/30/55	3600x3000	8h
R4	-25/5/35/55	3600x2400	8h
R5	-30/0/15/40	9000x7920	8h
R6	-30/0/20/45	6000x3600	8h
R7	-20/10/35/55	4200x3600	8h
R8	-35/0/25/45	3600x3000	8h
R9	-25/5/30/55	3600x3000	8h
Caribbean Subduction (subfaults)	-69/20/5/74	10681x8281	16h
Mid-Atlantic Ridge (subfaults)	-50/25/10/76 -60/25/-10/60	1920x900 10201x8401	16h
Gloria Fault (subfaults)	-50/25/10/76	1920x900	16h

In both cases, that is for direct subfault simulations or for Gaussians, virtual mareograms (Green's functions) are precomputed and stored for all possible combinations of elementary sources and off-shore Points-Of-Interest (POIs). The time series are saved each 30 seconds. The POIs are in total 2344 (1130 in the Mediterranean Sea, 1076 in the North-eastern Atlantic, 137 in the Black Sea). For each POI, we have about 120000 time series, each corresponding to a tsunami source, for a total of roughly 30 Tera Bytes of data storage.

The elementary mareograms (Green's functions) computed both for the Gaussians and for the subfaults at each POI were linearly combined to approximate the desired source according to STEP 1 and to previous Levels 1 (for the subfaults) or 1 and 2 (for the Gaussians) at STEP 2 which define the initial sea level elevation for tsunami simulations.

Simple linear combinations according to local slip values were performed for the elementary tsunamis generated by the subfaults. Conversely, for the Gaussians, we use an algorithm for sea level displacement reconstruction and unit sources linear combination coefficient determination starting from an arbitrary fault, as described in detail by Molinari et al. (2016). Some examples of the performance of this approach are given in FIGURE 2.8 for different earthquake magnitudes and mechanisms.

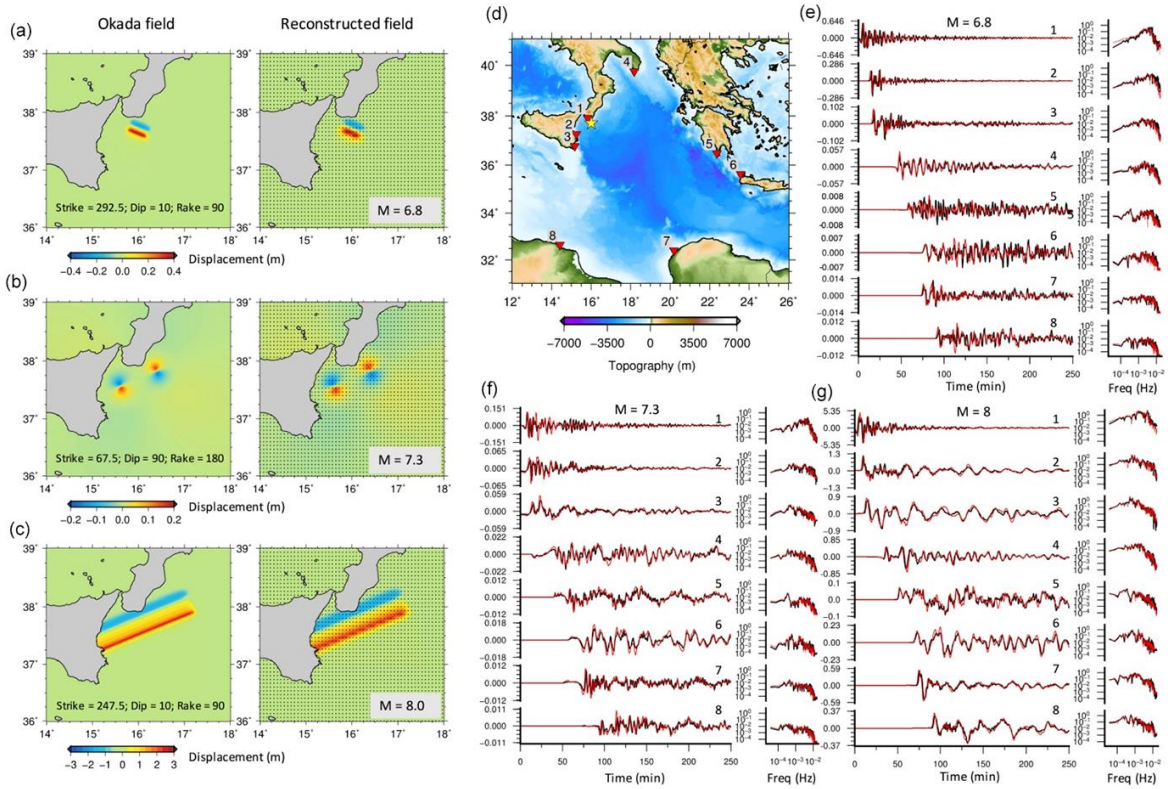

FIGURE 2.8: (a-c) Three examples of original initial conditions with different faulting parameters and earthquake magnitudes (left panels) and their reconstruction (right panels) obtained through the linear combination of the Gaussian-shaped sources. (d) Tsunami receivers (red triangles) and epicenters (yellow star) of scenarios in (a)–(c). (e–g) Comparison between directly simulated (black lines) and linearly combined waveforms and frequency spectra, corresponding to the scenarios in (a)–(c). Modified after Molinari et al. (2016).

More specifically, the reconstruction starts with the sea level displacement calculated at Level 2 by Kajiura's filtering of the sea floor displacement calculated at Level 1 (SECTION 2.3). This algorithm is then based on the preservation of the potential energy of the initial displacement and includes two corrections. The first one is related to the distortion with latitude, and the second one is related to the imperfect orthogonality of the Gaussian functions whose effect on the linear combinations become non-negligible for sea level elevations 'cropped' by the presence of land overlapping with the Gaussians when they are near to coastlines. Further details can be found in Molinari et al. (2016). Full tsunami waveforms at the off-shore positions (POIs distributed along the 50 m isobaths) are in this way evaluated by means of linear superposition of the elementary sources.

The uncertainty associated to this procedure for linear combinations of the Gaussians was estimated by Molinari et al. (2016) by comparing, at different sites and for the different source locations, the tsunamis directly simulated from the seismic initial condition to those obtained by linearly combining the Green's functions generated with the Gaussians. The found weak non-linearity of tsunami evolution affects the reconstruction of the waveforms and of their maxima by introducing an almost unbiased (centered at zero) error distribution of relatively modest extent. The overall errors are illustrated in FIGURE 2.9. Some further details can be found in Molinari et al. (2016). This epistemic uncertainty is propagated to STEP 3 (see SECTION 3.4).

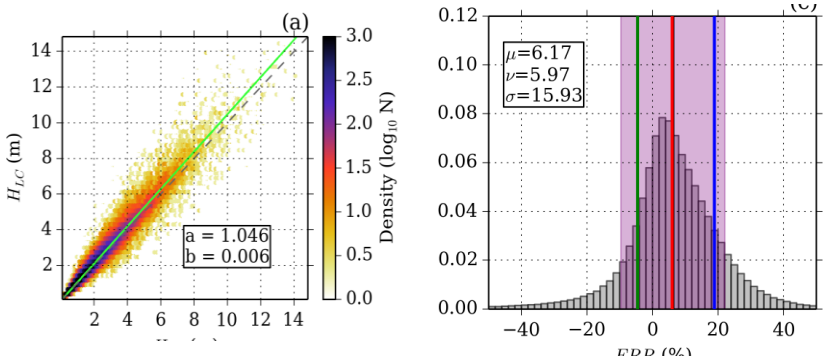

FIGURE 2.9: Misfit between the waveforms obtained using latitude/crop correction and potential energy preservation for the linear combinations, and the waveforms resulting from direct simulations, for all magnitudes and mechanisms. In the top panel, scatter plots are those between tsunami maxima from Linear Combinations (LC) and numerically simulated (NS). In the bottom plot, percentage error with respect to NS. Modified after Molinari et al. (2016).

The last activity done within Level 3 of STEP 2 is the post-processing of the mareograms $\{M(\sigma_k, POI)\}$, obtained via linear combinations. The post-processing phase is necessary to obtain the main wave characteristics that are needed for applying the amplification factors at STEP 3 (see CHAPTER 3). These characteristics include: (1) wave maximum positive amplitude, (2) polarity of the arrival preceding that maximum and (3) dominant wave period. Whereas $max_t[M(\sigma_k, POI)]$, the maximum amplitude over time can be read directly from the mareogram, dominant wave period and polarity need special treatment due to the usual high-frequency noise present at mareograms. We employ the LOWESS (locally weighted scatterplot smoothing) non-parametric filtering technique to get rid of the noise (Barbosa et al., 2004), and then derive wave polarity and dominant period by analyzing the amplitudes and positions of the two minima around the selected maximum (see FIGURE 2.10). Time-difference between the two minima gives us the half-period $T_P/2$. Incident wave preceding the maximum is declared to have negative polarity in case of negative amplitude of the left-hand minimum is larger than 25% of the maximum (note- we work with the filtered mareogram). These values are stored in lookup tables for subsequent use.

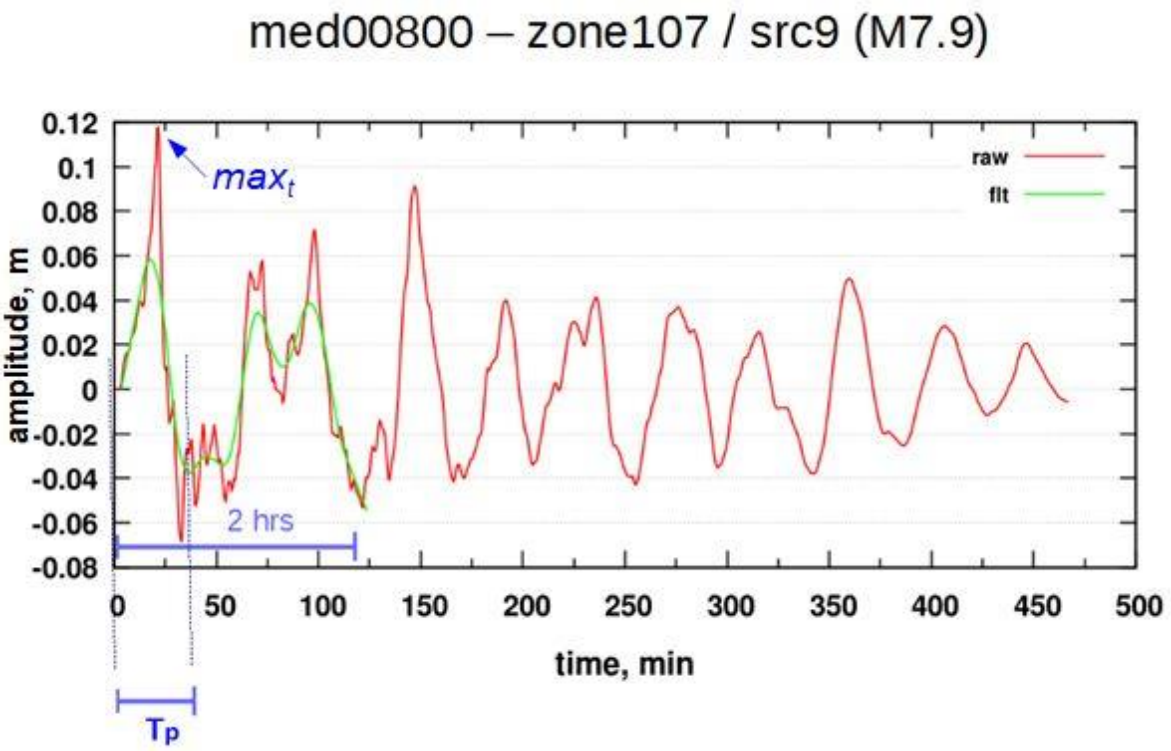

FIGURE 2.10: Principles of the mareogram post-processing analysis for derivation of main wave characteristics required for the "offshore-to-onshore" transformation at STEP 3: maximum wave amplitude, dominant wave period and polarity.

Concluding this CHAPTER, we can explicitly mention again approximations and exceptions we had to accept in order to limit the computational costs associated with the tsunami simulations. Some of these exceptions are based on geophysical constraints discussed at STEP 1 (SECTION 1.3). We recall that: (1) we didn't cover stable oceanic regions with Gaussians, assuming that their seismicity is low enough; (2) for most of the Gaussians in the Atlantic, we didn't extend enough the computational domains to allow distant propagation of the magnitudes higher than 7.5, assuming that their probability is low out of the PS sources; (3) for distant PS sources, we didn't use sub-faults small enough in order to simulate small magnitudes, instead, we assumed that tsunamis associated with these magnitudes would not significantly affect distant NEAM coastlines; (4) for some PS sources in the Atlantic, we used rectangular sub-faults instead of triangular meshes over 3D geometry, assuming that detailed geometries of distant sources were less important; (5) we considered everywhere M6 as the lowest tsunamigenic magnitude.

STEP 2 ends up with full waveform mareograms $\{M(\sigma_k, POI)\}$ and associated principal wave characteristics (amplitude maximum, dominant period and polarity) recorded at all POIs due to every individual earthquake scenario $\{\sigma_k\}$ defined at STEP 1. The principal wave characteristics are stored in corresponding tables $\{(max_t, T, \mp)[M(\sigma_k, POI)]\}$ of maxima max_t, periods T, and polarities $\mp$ to be used at STEP 3.

3 STEP 3 - SHOALING AND INUNDATION

The aim of STEP 3 is the evaluation of the propagation of the tsunami intensity at the coast starting from the mareograms computed off-shore at each POI. Our main metric to express tsunami intensity on the coast is Maximum Inundation Height (MIH). It is the maximum water height reached during the whole inundation process; or, in other words, the maximum height of the envelope of the tsunami waves at all times (see FIGURE 3.1). MIH is measured with respect to the mean sea level.

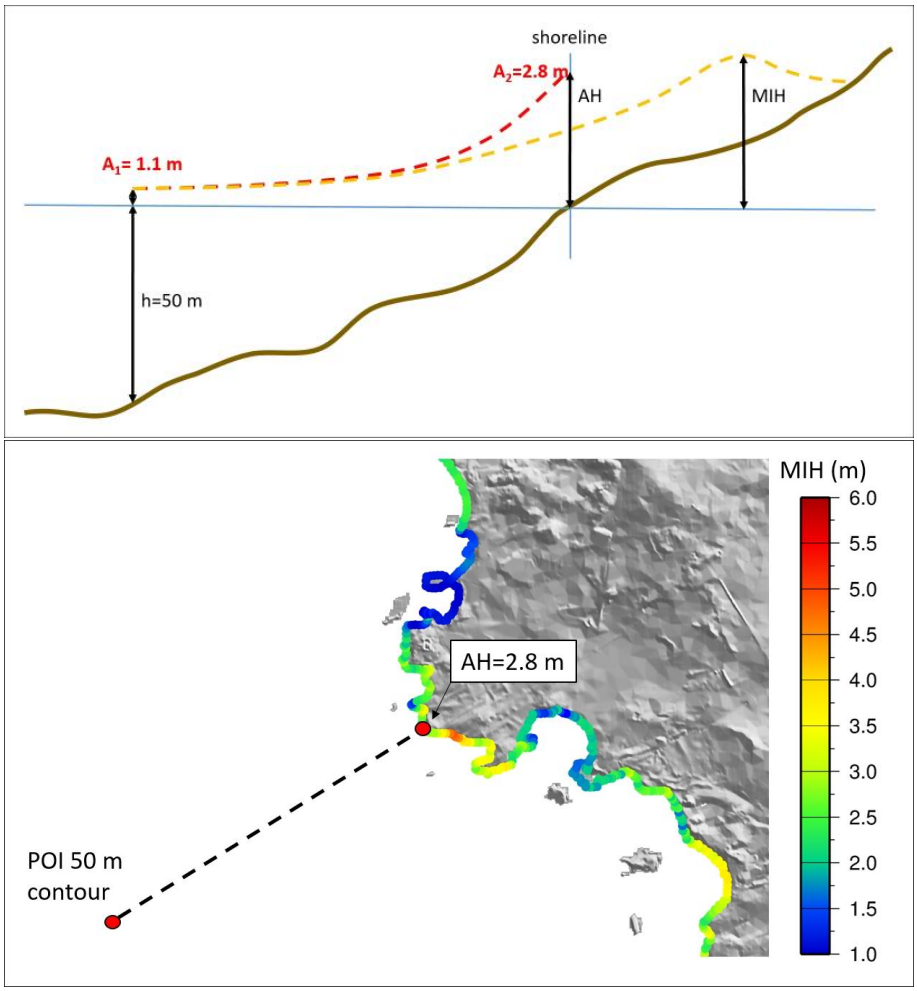

FIGURE 3.1: (Top panel) Schematic representation of MIH and of its estimator, the Amplified Height AH, obtained with the amplification factors. More details in the text. (Bottom panel) Sketch of the lateral MIH variability behind a given POI. Figure modified after Glimsdal et al. (2019).

To account for the uncertainty in this estimation, this evaluation is made by quantifying the hazard curve conditional upon the occurrence of each of the scenario (defined in STEP 1 and propagated offshore in STEP 2), and the relative uncertainty. The conditional hazard curve is the probability of exceedance (PoE) for different thresholds MIH_{th} of the tsunami intensity MIH in all the coastal areas corresponding to the offshore POIs, given the occurrence of the scenario σ_k.

In what follows, we adopt for this conditional PoE the notation $P(> MIH_{th}|\sigma_k)_{POI}$. $P(> MIH_{th}|\sigma_k)_{POI}$ is combined at STEP 4 with the rates $\lambda(\sigma_k)$ for completing the SPTHA.

MIH is suitable for a regional, initial screening assessment type such as the one in this project. The regional approach is primarily meant as an initial screening needed for comparing different areas and / or locating areas that are particularly hazardous. We stress that locally, e.g. for assessing detailed hazard or risk for a given harbor or city, this approach might be not directly applicable, and regional hazard should rather be used as an input for guiding higher-resolution numerical inundation models and higher-resolution inundation hazard (e.g. Lorito et al., 2015).

Hence, this is the STEP in which modelling of the tsunami both at shallow depths, between the POI and the coastline, and of tsunami inundation, as quantified by MIH, is performed.

To evaluate $P(> MIH_{th}|\sigma_k)_{POI}$, we start from the mareograms $\{M(\sigma_k, POI)\}$ at the off-shore POIs computed at the last Level 3 of the previous STEP 2 (SECTION 2.5). The maximum tsunami amplitude $max_t[M(\sigma_k, POI)]$ at the POI (for example A1 in FIGURE 3.1) is translated into an estimator of MIH (for example A2 in FIGURE 3.1) through approximated 1D local amplification factors (e.g. Løvholt et al., 2012, Davies et al., 2018). The amplification factors depend on several properties of the incident offshore tsunami wave at the POI, namely the dominant period and polarity (previously stored in lookup tables), but also on the characteristics of local bathymetry. We here developed specific amplification factors using local bathymetric transects at each POI for the NEAM region (Glimsdal et al., 2019).

Due to the way in which the uncertainty is estimated by Glimsdal et al. (2019), which we here follow, $P(> MIH_{th}|\sigma_k)_{POI}$ refers to the inundation over a transect approximately perpendicular to the coastline, which starts from a random coastal point on the stretch of coast behind the POI. $P(> MIH_{th}|\sigma_k)_{POI}$ hence describes the lateral MIH variability over the considered stretch of coast (see for example bottom panel of FIGURE 3.1).

The (epistemic) uncertainties stemming from the approximations described above, as well as those related to linear combinations described at STEP 2, are propagated onto the final results in the form of alternative estimations of $P(> MIH_{th}|\sigma_k)_{POI}$ (distributions of $P(> MIH_{th}|\sigma_k)_{POI}$ curves).

We also derive a hazard metric alternative to MIH, obtained by amplification of the mareograms $\{M(\sigma_k, POI)\}$ with the Green's law.

Summarising, the goals of STEP 3 are then:

1. deterministic modelling of the coastal tsunami impact at all POIs as evaluated at STEP 2, corresponding in turn to the scenarios $\{\sigma_k\}$ defined at STEP 1

    a. with approximated amplification factors $AF(T, \mp, POI)$ lookup tables, for each of the mareograms $\{M(\sigma_k, POI)\}$;

    b. and through Green's law;

2. assessment of the variability along the coast of the tsunami intensity in the form of conditional hazard curves $P(> MIH_{th}|\sigma_k)_{POI}$;

3. assessment of the associated uncertainties (including uncertainties originated from linear combinations at STEP 2), estimated through alternative implementations of the conditional hazard curves $\{P(> MIH_{th}|\sigma_k)_{POI}\}$.

3.1 Levels at STEP 3

At STEP 3 we have defined 3 Levels (0-2):

- Level 0 (input data): Topo-bathymetric datasets and digital elevation models; bathymetric transects; amplification factors;
- Level 1: Amplification and inundation model, including lateral variability;
- Level 2: Uncertainty modeling for tsunami hazard metrics (including uncertainties from linear combinations of tsunami elementary sources at STEP 2).

As for the previous STEPS, Level 0 is used for collecting and treating the databases which are relevant for this STEP.

Level 1 deals with the "deterministic" approximated estimation of shoreline/on-shore tsunami hazard intensity, through amplification of the tsunamis modelled in relatively deep-waters at Level 3 of STEP 2 (SECTION 2.5), and the along-coast variability of the tsunami intensity.

Level 2 deals with modeling of the uncertainty introduced at Level 1, combined with the uncertainty stemming from tsunami unit sources linear combinations at STEP2. In other words, at Level 3 we quantify the uncertainty associated with our modeling approach.

These Levels are described in more details below.

The adoption of alternative datasets as well as alternative modelling approaches to the approximation of inundation at STEP 3 were recommended by the Panel of Experts.

Alternatives were recommended for: the topo-bathymetric datasets and digital elevation models employed; for the amplification and inundation model and the associated uncertainty.

While we share this view, some of these alternatives were unaffordable within the project resources. For example, it was not possible to adopt alternative topo-bathymetric datasets, nor to directly simulate coastal inundation on a fine-resolved grid all over the target area.

However, following these indications, we subsequently further developed the approach to uncertainty quantification for MIH, resulting in the method presented by Glimsdal et al. (2019). This allowed to combine the treatment of the epistemic uncertainty stemming from the Green's function approach (described in SECTION 2.5) with the epistemic uncertainty derived from the approximated amplification factor method.

We also adopted also the largely employed Green's law amplification as an additional, alternative hazard intensity (e.g., Kamigaichi et al. 2011). Note that using the Green's law is not an alternative modelling approach in the strict sense, since this is probably an estimation of a different tsunami hazard intensity metric, not an alternative approach to the estimation of the same metric. However, this allowed to define a sanity check on NEAMTHM18 results, comparing them with what we would have obtained adopting an alternative amplification scheme. The results of this sanity check are presented in Doc_P2_S5.

Application of both MIH from amplification factors method and of Green's law do not require large computational effort and / or very-high grid resolution for the offshore input simulations.

Remark #1.

1) *The uncertainty estimation based on detailed inundation simulations presented at Level 3 later in this STEP will be performed for MIH only, not for Green's law amplification.*
2) *The adopted approach is probably sufficient for the Project purpose of homogeneous regional screening of the coastal hazard and for prioritization of more detailed local studies. The results from Green's law are available upon request and are shown in several sensitivity / disaggregation tests.*
3) *for more local scale hazard analysis, we recommend developing at least a local set of amplification factors, or the use of other amplification methods based on different approximations depending on the target application (e.g. Kriebel et al., 2017; Gailler, 2018), or on the selective use of high-resolution hydrodynamic simulations (e.g. Lorito et al., 2015).*

Remark #2.

In the previous version of the NEAMTHM18, also tides in the Atlantic were considered. However, we did not have the resources to fully address neither some issues related to the probabilistic treatment of the tides, nor some issues related to the communication of such a quantity to end users, as we had to focus on some other issues along the whole chain. As a result, for coastal places within the NEAM region where the tides are significant, the hazard intensity provided by the NEAMTHM18 should be considered as occurring above the current tidal level.

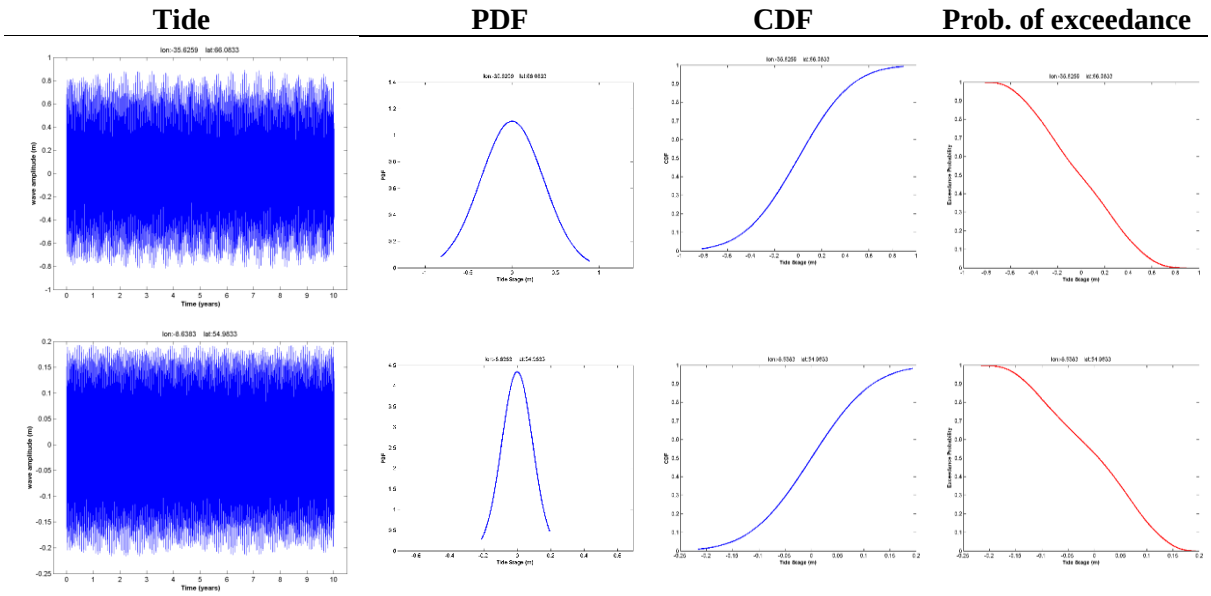

FIGURE 3.2: Results from the TMD model. At left the predicted tide for a period of 10 years, and the corresponding PDF, CDF, and the probability of exceedance.

Our tide predictions for the Atlantic are nevertheless available upon request. The tide prediction was accomplished with the Tide Model Driver (TMD) developed by Egbert and Erofeeva (2002; https://www.esr.org/ptm_index.html). The original Atlantic Ocean inverse tide model presents a grid resolution of 1/12º. In our study, we used a bathymetry grid of higher resolution (1/120º). This bathymetry grid file was then converted to OTIS file (the format required for the TMD model). At each POI of the NE Atlantic, the tidal signal was predicted for a 10-year period, starting from 2017/01/01 at 00h00min00sec, and considering a sampling interval of 10 min. As an output of the

TMD model, each POI has its corresponding predicted tide time series. Using these outputs, the probability density function (PDF), the cumulative density function (CDF) and the probability of exceedance were derived at each POI of the NE Atlantic. In FIGURE 3.2 we show examples of calculations for 2 POIs, and the corresponding prediction of tide signal, PDF, CDF, and probability of exceedance.

3.2 Level 0 - Topo-bathymetric datasets and digital elevation models; bathymetric transects; amplification factors

Here we treat the choice of the digital elevation model (DEM) on a grid (the topo-bathymetric grid). This level also deals with: the extraction from the DEM of the local 1D bathymetric profiles; and of the amplification factors, determined in correspondence of these bathymetric profiles.

The SRTM15+ bathymetric model (15 arc seconds spatial resolution, http://topex.ucsd.edu) was used as basis for extracting the profiles, within both the Mediterranean Sea and the Black Sea. For the North East Atlantic the SRTM30+ (30 arc seconds spatial resolution), improved with local data in Portugal (Zitellini et al, 2009), was used. The latter is the same already used at STEP 2. Hence, we do not repeat here the description already developed in SECTION 2.2.

The method of 1D amplification factors relates the near-shore surface elevations at the offshore POIs to the maximum shoreline water levels. The surface elevation at the shoreline then acts as an approximation for the maximum inundation height or run-up height. The basic principles of the 1D method are described by Løvholt et al. (2012) and Løvholt et al. (2015). It makes use of linear wave theory, and for non-breaking plane waves the amplification factor method should then theoretically yield the exact run-up.

To obtain the amplification factors, wave propagation is simulated along bathymetric profiles, using 1D LSW model from the deep sea all the way to the shoreline. The incident wave is a sinusoidal pulse, with leading peak or leading trough. Combined with results from offshore tsunami simulations, it can be used to estimate the mean or median tsunami run-up or maximum inundation height at a coastal location. However, the Løvholt et al. (2012; 2015) version of the method used a set of idealized bilinear profiles as a basis for the computation of the amplification factors. Then, the profile best matching the real profile was searched and the corresponding amplification factor used for hazard calculations. Moreover, their approach didn't attempt to estimate the amplification factor uncertainties.

We here employ a new and improved version of this amplification method. In the present study, local profiles normal to the coastline, describing the coastal water depth were extracted directly from the local bathymetry. Hence, the new amplification factor method takes into account shoaling on the local bathymetry rather than on some generic idealised profiles. The amplification factors are extracted for several profiles in correspondence of each POI; however, the factor eventually applied to estimate the amplification experienced by the single tsunami scenario, for the specific stretch of coast, is the median of those obtained for each profile in front of that stretch. As discussed later, the local amplification factor method is expected to replicate the median tsunami inundation height more accurately than the previous method using idealized profiles.

This new version of the method was partly developed within the ASTARTE EU project (http://www.astarte-project.eu/). Some details are then described in the ASTARTE Deliverable

D8.39, SECTION 3.2. The methodology has been completed and further developed afterwards in the TSUMAPS-NEAM project and published by Glimsdal et al. (2019), also accounting for the results of the first elicitation and the review. The full set of bathymetric profiles for the whole NEAM region, and the full set of amplification factors, have been then completed within this project. FIGURE 3.3 shows in map view all the profiles that we extracted within the Mediterranean, the Black Sea, and the North East Atlantic. In total, 149 profiles were extracted for the Black Sea, 935 for the Mediterranean Sea, and 1158 for the North East Atlantic region.

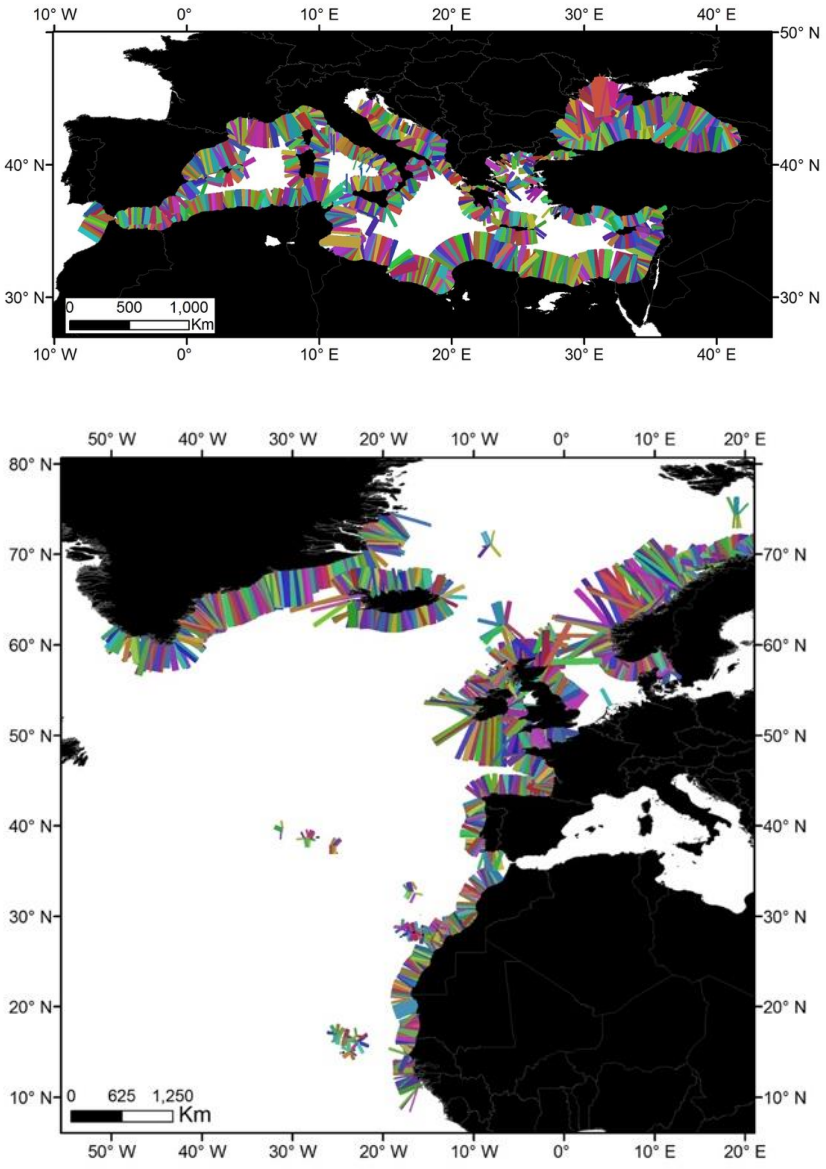

FIGURE 3.3: Map of transects for the analysis of the amplification factors in the NEAM region.

The procedure to acquire the bathymetric profiles begins with extracting onshore points along a 50 m depth isobath with an initial separation distance of ~2 km. A nearest neighbor algorithm is then used to select coastal points roughly each 20 km, by identifying correspondence between coastline points and the offshore POIs. These identified shoreline points were then applied to define a piecewise linear shoreline contour. A set of 40 transects spaced at about 1 km and perpendicular to

this contour line where then created (i.e. 20 km to each side of the onshore hazard points, see FIGURE 3.4). Some examples of the profiles we extracted are shown in FIGURE 3.5.

All profiles that intersected islands were deleted in order to avoid positive values (i.e., land). Profiles with anomalous orientation with respect to the shoreline were then identified and manually corrected.

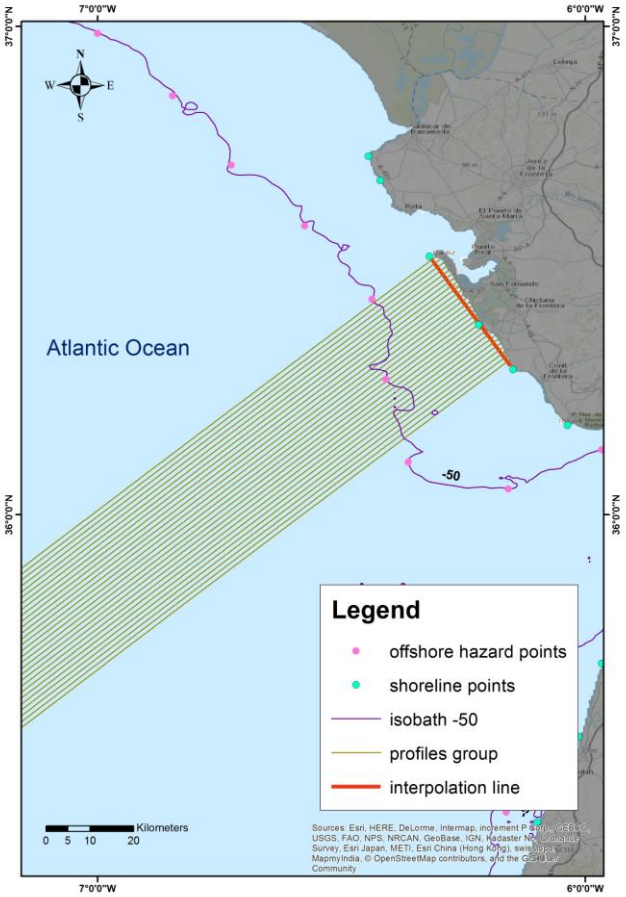

FIGURE 3.4: Correspondence between POIs, transects and onshore hazard points. Figure modified after Glimsdal et al. (2019).

However, we could not straightforwardly apply the above procedure in areas characterized by complex non-planar shorelines with many islands, such as the Aegean islands, deep and narrow bays (e.g., fjords) and the Croatian islands. Therefore, in these areas, some POIs were left out without transects in the automatic procedure and transect positions were drawn manually.

For amplification factor calculations, we subjectively selected seven profiles out of the 40 profiles previously extracted for each POI, considered enough representative of the overall visually observed variability. The subjective selection was done for the sake of saving computational resources.

Following Løvholt et al (2012), a 1D LSW model, solved over a staggered Arakawa C-grid with variable spacing, was used for the amplification factor production runs. The resolution of the grid depends on the wave period and the water depth and is tuned to give a constant Courant number = 0.9 over the entire domain. The Courant number is here defined as the local linear shallow water wave velocity times the numerical grid step times the inverse of the time step.

We here used incident waves with both leading peak (positive polarity) and leading trough (negative polarity), and wave periods ranging from 120-3600s. For waves with period larger than 600 s, the grid size ranges from about 300 m in the deepest part of the domain (water depth of 2000 m) down to 7 m at 1 m depth; for a wave period shorter than 300 s, the grid resolution varies from 80 m to about 2 m, respectively. The grid spacing is not refined further in water depths less than 1 m. The resolution applied in the simulations are justified by convergence tests. At the shoreline, we have applied a no-flux boundary condition, and the waves are fed into the model from the offshore boundary.

To calculate the amplification factors, an initial wave of 1 m amplitude, shaped as a single period sinusoidal wave pulse, is fed over the deep-water boundary of the model. This is done for all profiles. Maximum surface elevations are extracted. The amplification factor is computed as the ratio of the amplitude from the LSW simulation at 50 m depth and its height at the shoreline (0 m depth), i.e. A1 and A2 in upper panel of FIGURE 3.1. We use the median value of the seven amplification factors, corresponding to the seven subjectively chosen profiles, to avoid unrealistic alongshore fluctuations. Examples of amplification factors and related median values as a function of the incident wave periods are shown in the lower panels of FIGURE 3.5.

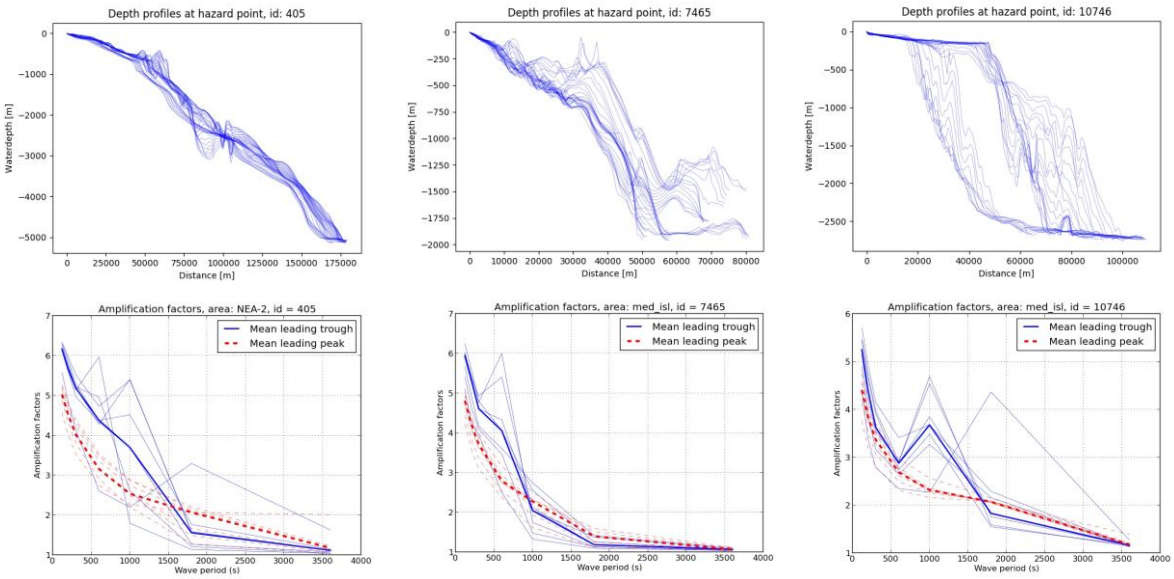

FIGURE 3.5: Some examples of depth profiles in correspondence of different POIs (top panels) and of amplification factors (bottom panels), plotted versus the wave periods. Modified after Glimsdal et al. (2019).

Amplification factor values, for all combinations of wave polarities and wave periods, are stored in lookup tables $AF(T, \mp, POI)$. As an example, amplification factors for both leading peak and trough polarity, and for two wave periods of 1000 and 1800s are depicted in FIGURE 3.6.

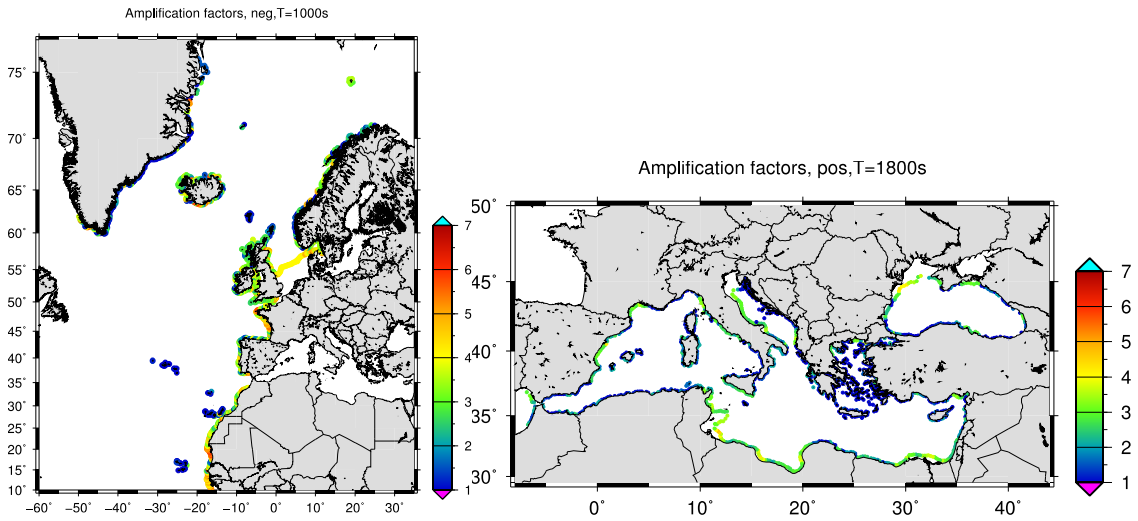

FIGURE 3.6: Two examples of amplification factor distribution in the NE Atlantic and in the Mediterranean and Black Seas, for different polarities and periods.

Two versions of the factors were produced, one set using the raw amplification factors values, and one set of factors smoothed along the shoreline with a median filter (using a filter length of five points). The median filtering was performed as an additional measure to avoid artificially short amplification fluctuations along the shoreline (see an example for the Black Sea in FIGURE 3.7).

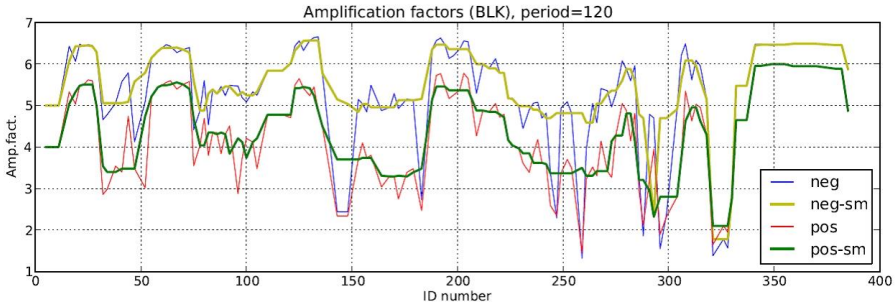

FIGURE 3.7: Median-smoothed and un-smoothed amplification factors for a wave period of 120s and for both negative and positive polarity of the leading wave, along the coasts of the Black Sea. Modified after Glimsdal et al. (2019).

More details on the amplification factors can be found in Glimsdal et al. (2019).

3.3 Level 1 – Amplification and inundation model

We stress once again that this project dealt with a homogeneous hazard assessment over a very big region, and we took into account a very large number of seismic scenarios $\{\sigma_k\}$. This would make the computational coast of direct numerical modelling unaffordable, even by applying some recently proposed techniques for its reduction (e.g. Lorito et al., 2015). Moreover, sufficiently detailed, precise and accurate near shore and coastal digital elevation models, homogeneously covering the whole domain of interest for TSUMAPS-NEAM, do not exist.

Hence, we needed a different approach than "brute force" numerical simulations. We developed a rather novel approach to stochastic inundation modelling (Glimsdal et al., 2019). This approach is meant to assess the conditional PoE curves $P(> MIH_{th}|\sigma_k)_{POI}$ versus different values of the

threshold $\mathrm{MIH_{th}}$, describing the statistical variability of MIH along the shore (see for example FIGURE 3.1), rather than to numerically simulate the "exact" $\mathrm{MIH}(\mathbf{x}, \mathrm{M}(\sigma_\mathrm{k}, \mathrm{POI}))$ at different locations $\mathbf{x}$ within the inundation zone.

Following Choi et al. (2002) and Davies et al. (2018), in Glimsdal et al. (2019) the alongshore variability is modelled as a log-normal distribution, that is:

$$\mathrm{P}(> \mathrm{MIH_{th}}|\sigma_\mathrm{k})_\mathrm{POI} = 1 - \Phi\left(\frac{ln\mathrm{MIH_{th}} - \mu_k}{\beta_k}\right),$$

where Φ is the cumulative distribution function of the standard normal distribution. This is the distribution of the MIH values in the direction approximately perpendicular to the coastline behind the POI. It then describes the lateral MIH variability (e.g. as in the bottom panel of FIGURE 3.1) found on the coastal area behind the POI through searching for MIH on many coastal transects, parallel to each other and perpendicular to the coastline.

The curve $\mathrm{P}(> \mathrm{MIH_{th}}|\sigma_\mathrm{k})_\mathrm{POI}$, as a function of MIH, can be interpreted as the hazard curve of one randomly selected point within the stretch of coastline near to the target POI, conditional to the occurrence of the k-th tsunami scenario σ_k. This uncertainty is hereinafter treated as aleatory uncertainty through these conditional hazard curves. The epistemic uncertainty on the evaluation of the PoE curves is discussed at Level 2 (SECTION 3.4).

The parameters of the log-normal distribution are different for different scenarios and POIs. In particular, for the k-th tsunami scenario in the area corresponding to the j-th POI, we indicated these parameters with μ_{kj} and β_{kj}.

The MIH obtained with the amplification factor derived at Level 0 (SECTION 3.2) approximates the median value of the log-normal distribution of MIH values that the k-th tsunami scenario σ_k causes in stripes of land perpendicular to the coast and located around the j-th POI (and its projection to the coast and inland). In the previous SECTION, we have seen that this deterministic amplification depends on both the characteristics of local bathymetry (coastal slope configuration) and on the characteristics of the specific tsunami scenario (dominant period and wave polarity), as numerically simulated in a single offshore POI. To compute this amplification, the first input are the parameters of the mareograms $\{M(\sigma_k, POI)\}$, that is the maximum water elevation and the corresponding period polarity of the leading wave, which were stored in look-up tables $\{(max_t, T, \mp)[M(\sigma_k, POI)]\}$ at the end of STEP 2. The second input are the amplification factors at all POIs, which were stored as well in look-up tables $AF(T, \mp, POI)$ versus different values of the polarity and period. To obtain the MIH, the two types of look-up tables are used jointly for each earthquake-generated tsunami scenario $\{M(\sigma_k, POI)\}$ and for each POI. The correct amplification factor is thus retrieved and applied to the maximum positive wave amplitude, resulting in our primary tsunami impact metric MIH. By doing that, we linearly interpolated the amplification factors between tabulated wave periods.

Multiplying the amplification factor to the $max_t[M(\sigma_k, POI)]$ of a tsunami simulated in a POI, we obtain an approximate MIH for the nearby coast due to the considered individual tsunami scenario. In the following, for the k-th tsunami scenario in the j-th POI, we indicate $max_t[M(\sigma_k, POI)]$ with ζ_{kj}, and the corresponding amplified value of MIH:

$$MIH[M(\sigma_k, POI)] = AF[(max_t, T, \mp)[M(\sigma_k, [(max_t, T, \mp)[M(\sigma_k, POI)]],$$

with $MIH_{kj} = A_{kj} * \zeta_{kj}$.

Summarizing, the log-normal median $e^{\mu_{kj}}$ may be well approximated by $MIH_{kj} = A_{kj} * \zeta_{kj}$. The amplification factor A_{kj} and the scenario's ζ_{kj} depend on both the POI and the tsunami scenario, and can be estimated by knowing the local coastal slope configuration and with a linear simulation of the tsunami scenario in deep sea to reproduce the tsunami time history at the j-th POI ζ_{kj}.

The log-normal parameter β_{kj} depends, further than on the characteristic of the specific tsunami scenario, also very strongly on the local configuration of the coast around the j-th POI and can be estimated with NLSW simulations of the k-th tsunami scenario in the j-th location. An alternative approach would be correlating the variance to the intrinsic variability of MIH alongshore, for example considering the records coming from past tsunamis (Davies et al., 2018). Here, to estimate reasonable β_{kj}, we performed a set of NLSW simulations for a sample of locations and scenarios. Based on these simulations, we quantify the uncertainty on both the parameters of the log-normal distribution. The whole procedure is briefly described in the next SECTION and in more detail in Glimsdal et al. (2019).

We finally recall that local coastal tsunami impact is here expressed by one primary or another alternative hazard intensity metric. Our primary metric is the MIH. An alternative metric is the one obtained via amplification through the Green's law, quite commonly adopted, e.g. like in Kamigaichi et al. (2011). The Green's law is a relation defining the ratio between the offshore value H_D at a given depth D and the amplified value H_d after shoaling to a certain reference depth d, that is $H_d = H_D \sqrt[4]{D/d}$. We fix as customary this reference depth d to 1m. D is the depth of the POIs. In this way, if a POI lies at a depth of 50m, the amplification obtained via Green's law is for example ~2.66 time the maximum elevation provided by the mareogram.

3.4 Level 2 - Uncertainty modeling for tsunami hazard metrics

Here we model, at all POIs and for each scenario considered by the earthquake model, the parameters of the conditional PoE $\mathrm{P}(> \mathrm{MIH_{th}}|\sigma_\mathrm{k})_\mathrm{POI}$ for a discrete set of predefined hazard intensity thresholds, quantifying the uncertainty inherent to our amplification model discussed in SECTION 3.3. The PoE and the relative uncertainty will be subsequently used at STEP 4 for hazard assessment (CHAPTER 4). In other words, we here quantify and sample, for their subsequent use, the distributions describing the aleatory and the epistemic uncertainty associated with tsunami modeling.

The PoE is meant to describe the uncertainty stemming from the alongshore variability of the tsunami intensity MIH. The epistemic uncertainty related to the PoE should account for the uncertainty inherent to the approximated amplification factor method, as well as for uncertainties which may arise at the previous STEPs due to different model approximations and non-modeled effects (see e.g. Davies et al., 2018). As anticipated, we limit ourselves to including the uncertainty associated to the linear combinations, estimated at Level 3 of STEP 2 (SECTION 2.5). We establish a common uncertainty propagation framework for both MIH/amplification factors and for linear combination uncertainties. While doing this, we assume that the two are not correlated. At both levels, the foundation of the uncertainty quantification is the comparison with ad-hoc much more

accurate 2D NLSW numerical simulations, in which the specific approximations were removed (linear combinations and amplification factors).

Here, we briefly present the main aspects of the methodology followed for assessing uncertainties related to the approximated amplification factor method (more details can be found in Glimsdal et al., 2019), and its combination with the one arising from linear combinations of Gaussian unit sources.

To quantify the epistemic uncertainty related to the PoE, we compare the amplification model described in SECTION 3.3 and the results of local high-resolution 2D NLSW numerical inundation models.

The employed NLSW model is Tsunami-HySEA (de la Asunción et al. 2013; Macías et al. 2017), already introduced and used at STEP 2 for offshore tsunami simulation. Being the code properly benchmarked, we consider it a suitable reference model towards the less accurate 1D amplification factor approach. We consider six test sites for which a suitable and sufficiently detailed DEM existed, mostly from the ASTARTE project (http://www.astarte-project.eu/). The test sites are: one in the Atlantic Ocean, namely Sines, Portugal; the remainder in the Mediterranean, namely Colonia Sant Jordi (Mallorca) and SE Iberia in Spain, Siracusa and the Catania plain in Italy, and Heraklion on the island of Crete in Greece (Fig. 3.8). All offshore tsunami simulations are conducted on regular grids derived by downsampling SRTM15+ to a spatial resolution of 30 arc seconds. The NLSW models additionally use nested grids to simulate detailed local inundation at test sites. The resolution of the finest grid is about 10 m at all locations. The Manning-friction is set to $n = 0.03$ in all simulations.

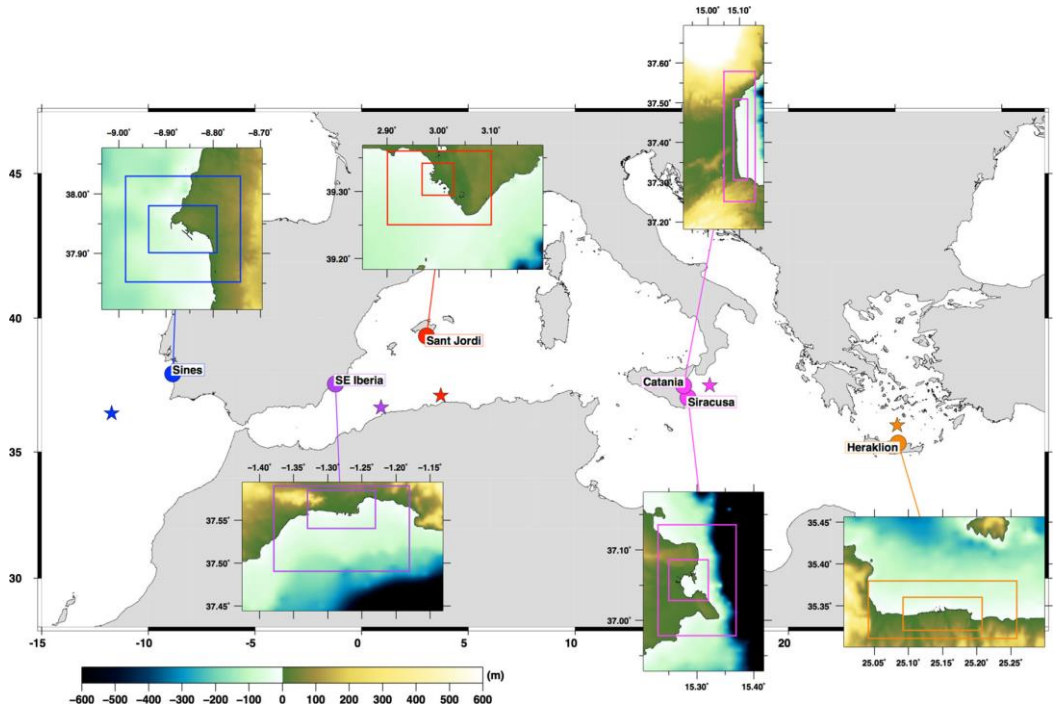

FIGURE 3.8: The test sites, indicated by the filled circles, with the progressively higher-resolution computational grids shown in the insets, which scale down to 10m in the inner grid at all sites; the geometrical centres of the modelled earthquake, indicated by the stars, of the same color of the filled circles where their tsunamis are modelled. Modified after Glimsdal et al. (2019).

For each test site, we use 96 earthquake sources with varying magnitude, strike, dip, and rake in order to explore a variety of situations, which determine a significant variability of the wave period and wave polarity. In particular, we use six different moment magnitudes (7.1, 7.5, 8.1, 8.5, 8.8, 9.0), four strike angles (22.5, 112.5, 202.5, 292.5), and four pairs of dip/rake angles (10/ 90, 30/90, 50/270, 70/270). Empirical earthquake relations (Strasser et al., 2010) are then employed to define the slip and fault size for each earthquake source.

For each considered test site and source scenario, we compare the "deterministic" MIH, obtained with the amplification factor look-up tables previously stored, with the numerically simulated MIH on the high-resolution grid. The details of MIH extraction from simulations and of the comparisons can be found in Glimsdal et al. (2019).

From all the MIH values obtained for a given site, it is possible to build and empirical cumulative distribution function which is then fitted to a log-normal distribution. The results show that the log-normal distribution reasonably well represents the alongshore variability of the tsunami intensity (Glimsdal et al., 2019). Consequently, here we try to evaluate our capability of quantifying the parameters of these distributions.

In FIGURE 3.9, we compare the normalized bias, defined as the relative difference between the log-normal median e^{μ} and the amplified maximum height (the "deterministic" MIH) found for the amplification factor method, with the analogous quantity determined by applying the Green's law instead of the amplification factor. It is evident that the Green's law provides a stronger and more strongly positively skewed bias. This demonstrates that the "deterministic" MIH represents a good estimator of the median of the log-normal distribution, while Green's laws provide biased values. More details on this and other analyses are provided by Glimsdal et al. (2019).

The bias from various model runs represents just one component of the variability among the different simulations. In addition to the variability of the bias, the tsunami inundation height does vary spatially across each site. This variability is related only to the properties of the NLSW simulations at the site, which are hopefully consistent with the natural variability, and not to the method as a predictor of the median in itself. Among other things, this variability may be related to the 2D character of the inundation which gives rise to phenomena such as refraction and focusing. It is also related to the period, polarity and specific site.

Consider that the uncertainties we estimate here are in a sense "global", since we are combining all together the results from comparison over a large number of simulations spanning the source parameter space (location, size, mechanism, etc. of the earthquakes) and different locations (different POIs and test sites for inundation with different local characteristics). Glimsdal et al. (2019) analysed a bit further the different sources of uncertainty by dividing them into period, polarity, and site. The first two are more closely related to the source characteristics. The most important differences seem to be related with specific site characteristics. Of course, it is not achievable to separate the bias and the variability from each possible location in a regional analysis, for the very same reasons which made us work with approximated methods. Consequently, provided that we are considering a large enough range of conditions / sites, it is possible that merging uncertainties from different sites increases (overestimates) the overall MIH uncertainty in a PTHA analysis. However, taking the root mean square of the different σ (bias uncertainty, mean local uncertainty, and standard error, with the latter being the larger contributor) as an estimation of the "global"

variability of compound distribution, for all the model runs we arrive at a value of 0.55 due to the inundation process. It is noted that Davies et al. (2018) found an overall uncertainty of $\sigma = 0.92$ when comparing single scenario results with observations from past events (Glimsdal et al. 2019).

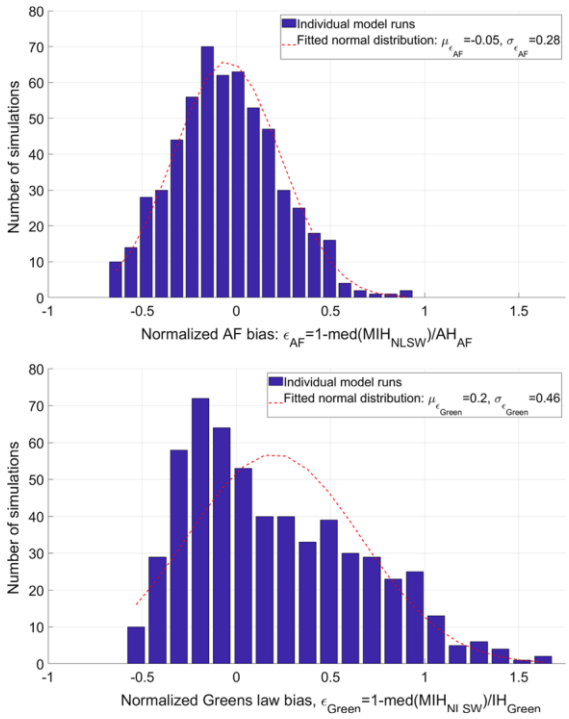

FIGURE 3.9: Comparison of the normalized bias obtained for all model runs for the amplification factors (upper panel) to that obtained for the Green's law. Figure modified after Glimsdal et al. (2019).

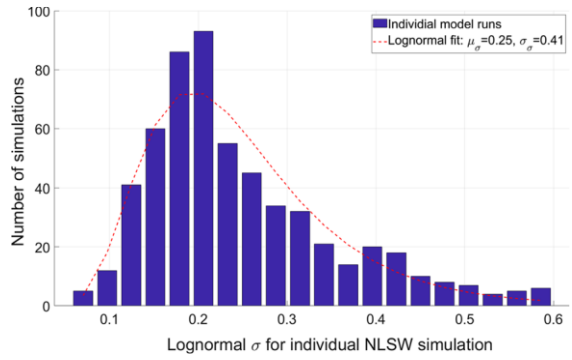

FIGURE 3.10: Variability distribution over all model runs. Figure modified after Glimsdal et al. (2019).

For the purpose of tsunami hazard, a large number of POIs is defined, each POI representing an entire stretch of the nearby coastline. As discussed in SECTION 3.3, we assume that this coast is reasonably close to the POI, and that, for each tsunami scenario, the distribution of MIH in this part of the coast is again well represented by a lognormal distribution, with median evaluated adopting the approximated amplification factor corresponding to the local coastal slope and the

approximated characteristics of the tsunami scenario (which was not previously individually simulated).

As demonstrated above, there is a certain degree of epistemic uncertainty regarding its parameters that should be adopted for any given POI. Indeed, all these parameters, would be in principle well known only for the locations in which we have the NLSW simulations, which clearly is not the case. Conversely, we have in fact introduced some further approximations, already described in this and in the previous SECTIONS.

For the large number of POIs that any regional hazard quantification considers, the parameters μ_{kj} and β_{kj} can be estimated from the available general information. More specifically:

- the amplification factor A_{kj} for a set of different tsunami scenarios has been approximated as described in SECTION 3.3; that is, the offshore 1D simulations have not been conducted for the exact scenario under consideration but for a reasonably wide range of scenarios used to form the lookup tables.

- the mareograms and the local maxima ζ_{kj} were approximated as combination of unit sources.

- given the large number of POIs and the lack of accurate local topographic and bathymetric data, the estimation of the parameters μ_{kj} and β_{kj} was made as explained at the beginning of this SECTION for a limited number of test sites and for a limited number of tsunamis.

Therefore, while it can perhaps be assumed that the amplification factor A_{kj} is reasonably well known for all POIs, the uncertainty on the applicable ζ_{kj}, μ_{kj}, and β_{kj} must be considered.

Concerning ζ_{kj}, we recur to the distribution of the relative error of the Gaussian approximation, that is of $\epsilon_{kj} = (z_{kj} - \zeta_{kj})/\zeta_{kj}$, as evaluated in Molinari et al. (2016), which we already reported in SECTION 2.5 (see FIGURE 2.9, right panel). This distribution is obtained using a very large number of simulations over a quite large range of tsunami intensities (up to > 10 m), and we may assume that it may reasonably approximate the uncertainty on ζ_{kj} for all tsunami scenarios in POIs. For what it concerns b_{ij} and σ_{ij}, we use the parameters from the distributions already presented in this SECTION and shown in FIGURES 3.9 and 3.10. From this equation, we may obtain ζ_{kj} as a function of z_{kj} and the uncertainty parameter ϵ_{kj}, that is $\zeta_{kj} = z_{kj}/(\epsilon_{kj} + 1)$.

For what it concerns μ_{kj}, we have seen that the effective median of the log-normal distribution may be slightly biased for different locations and tsunami scenarios (FIGURE 3.9). To account for this uncertainty, we have to account for the normalized bias $b_{kj} = \frac{A_{kj}\zeta_{kj} - e^{\mu_{kj}}}{e^{\mu_{kj}}}$ (see Eq. 2 in Glimsdal et al., 2019), distributed as reported in FIGURE 3.9. From this equation, we may obtain μ_{ij} as a function of $A_{kj}\zeta_{kj}$ and the normalized bias b_{kj}, that is $\mu_{kj} = exp\left[A_{kj}\zeta_{kj}/(b_{kj} + 1)\right]$.

Finally, for the parameter β_{kj}, we can use the distribution already presented in this SECTION and shown in FIGURE 3.10, that exactly represent the variability of this parameters for different locations and different tsunami scenarios.

To propagate this epistemic uncertainty for the k-th tsunami σ_{kj}, scenario at the j-th POI, we adopt a Monte Carlo simulation scheme. We take as input the applicable A_{kj} and z_{kj} obtained from the simulation of the k-th tsunami scenario based on the combination of the Gaussian unit sources for the *j*-th POI. Then, for each POI and each tsunami scenario, we sample i) the correction ϵ^* from $f(\epsilon_{kj})$ of FIGURE 2.9; and ii) the parameters b^* from $f(b_{kj})$ and FIGURE 3.9; and β^* from $f(\beta_{kj})$ of FIGURE 3.10. For each sampled $\{\epsilon^*, b^*, \beta^*\}$, we can estimate the consequent conditional hazard curve of equation (1) as:

$$P(MIH > MIH_{th}|\sigma_k)_{POI_j} = 1 - \Phi\left(\frac{\ln MIH - \ln\left[A_{kj}z_{kj}/[(1+\epsilon^*)(1+b^*)]\right]}{\beta^*}\right)$$
$$= 1 - \Phi\left(\frac{\ln MIH - \ln\left[MIH_{kj}/[(1+\epsilon^*)(1+b^*)]\right]}{\beta^*}\right)$$

where we set $MIH_{kj} = A_{kj}z_{kj}$ as the best guess reference *MIH* from the modelled *k*-th scenario σ_k in the *j*-th POI. This is the PoE we were looking for as a result of STEP 3.

Actually, we repeat 1000 times this procedure, to obtain 1000 alternative conditional hazard curves for the *k*-th scenario in the *j*-th POI. The variability of the results in this distribution of curves represent the sampled epistemic uncertainty in the conditional hazard curves to be applied for each tsunami scenario and each POI.

To increase the computational efficiency of this estimation, since $\{\epsilon^*, b^*, \sigma^*\}$ do not depend on the selected POI or tsunami scenario, the conditional hazard curves are pre-computed for a discrete number (50 predefined thresholds) of MIH_{ij} values, to be subsequently applied to the different scenarios and POIs.

In FIGURE 3.11, we report one example of the obtained epistemic uncertainty for a $MIH_{ij} \cong 5\,m$. This example shows that, given a scenario with this amplified value, the best guess for the frequency of exceedance of $MIH_{th} = 10\,m$ at one randomly selected point along the coastline is less than 10%.

We conclude SECTION 3.4 with some methodological remarks.

The numerical simulations are here done in the 2D vertically-averaged NLSW, which is still an approximation. For example, 3D free surface Navier-Stokes models, which probably not only in terms of computational cost are clearly out of reach, would be in principle more accurate. Yet, numerical simulations are not the reality, and cannot be considered as a replacement for observations. However, tsunami run-up data are generally not sufficient for hazard purposes. This is the reason why it is customary to recur to modelling of source recurrence combined with tsunami numerical simulations, which is the so-called computational approach to PTHA (e.g. Geist and Parsons, 2006).

The issue for uncertainties at the inundation stage is analogous and possibly even more challenging than that related to tsunami occurrence, generation and propagation at open sea (see e.g. discussion in Grezio et al., 2017). It is in fact almost never the case that run-ups observed at a single location sample densely enough events of various intensities and are distributed over a sufficiently

long-time span. We nevertheless mention that there have been attempts to estimate uncertainty from observed runup data (e.g. Davies et al., 2018). The latter study made a kind of ergodic assumption, since the uncertainty was estimated by combining together observations for multiple events and for the entire Pacific Ocean; it is possible that such an approach introduces itself an uncertainty overestimation. Moreover, Davies et al. (2017) implicitly include uncertainty from heterogeneous slip distributions, which is here explicitly treated at least for some subduction zones and uses the method of the amplification factors based on the cruder approximation of the idealized profiles.

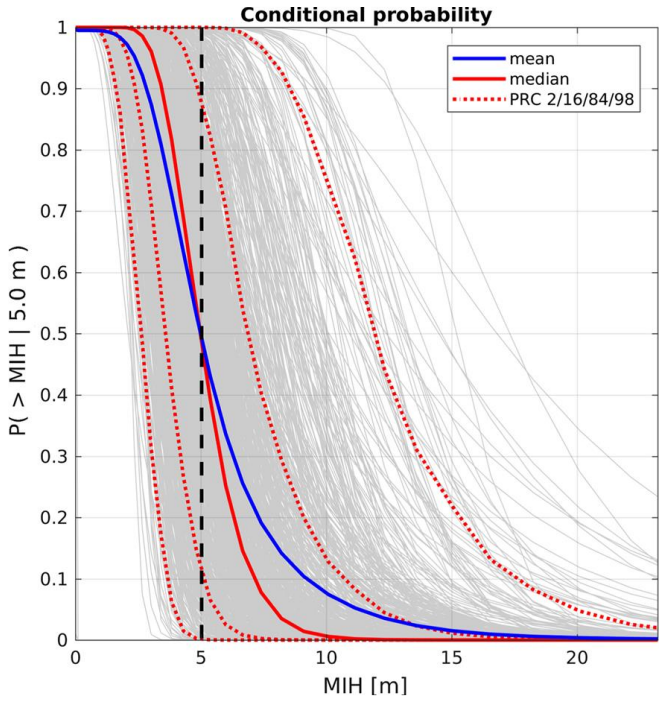

FIGURE 3.11: Conditional hazard curves for a $MIH_{ij} \cong 10\ m$. In light gray, we report the N=1000 sampled alterative curves; in red, we report different statistics of the epistemic uncertainty (mean value as thick red line, 2nd,16th, 50th (median), 84th and 98th percentiles as dashed lines). Modified after Glimsdal et al. (2019).

Although not feasible with the project resources, it is certainly advisable to further assess in the future the uncertainty introduced by simplified source modelling. A similar approach based on comparison with more sophisticated modelling could be envisaged for the source/generation modelling stage. More sophisticated – and obviously more time consuming – techniques, exist which could replace Okada static initial conditions in homogeneous media, such as 3D-FEM, time-dependent initial conditions, 3D potential theory (e.g. Nosov and Kolesov, 2011). The uncertainty stemming from a simplified modelling of the earthquake source and the tsunami generation are nevertheless in principle included in the approach by Davies et al. (2018); note that in this case though the source effect is not separated from the propagation and inundation effects and this is to be taken into account along with the limitation just discussed. Qualitative 'safety' factors could be discussed for other effects not considered in our approach, such as the various discretizations used at all levels; then, these PDFs can be sampled and the uncertainty on the PoE curve assessed.

4 STEP 4 - HAZARD AGGREGATION & UNCERTAINTY QUANTIFICATION

At STEP 4 we have defined 4 Levels (0-3). The main aim of STEP 4 is the quantification of the NEAMTHM18 and of its uncertainty.

The NEAMTHM18 is expressed through the hazard curves at all POIs, that is the exceedance probability within a given time window (here fixed at $50\ yr$) for different MIH intensity thresholds MIH_{th}, that is:

$$P(> MIH_{th}, 50\ \mathrm{yr})_{POI}$$

This is obtained by aggregating the conditional PoE $P(> MIH_{th}|\sigma_k)_{POI}$ (from STEP 3) with the mean annual rates $\lambda(\sigma_k)$ of each individual scenario σ_k (from STEP 1).

The uncertainty of the NEAMTHM18 is quantified with an ensemble modelling technique accounting for alternative models and uncertainty propagation from previous STEPS and providing as a result families of hazard curves and their statistics (mean model, different percentiles). The NEAMTHM18 uncertainty is assessed through an ensemble modelling technique (Selva et al., 2016), which considers relative weights assigned to the alternative scientifically acceptable models here considered.

Differently from Logic Tree applications, the ensemble modelling does not require a probabilistic interpretation of weights (Marzocchi et al., 2015). Alternatives are assumed to represent an unbiased sample of the epistemic uncertainty, in which weights simply measure the representativeness of each alternative within the sample. This implies, for example, that the alternatives at all STEPs and Levels do not require to be Mutually Exclusive and Collectively Exhaustive (MECE).

This STEP includes also all the post-processing of hazard curves, including the production of hazard and probability maps, the hazard disaggregation, as well as some comparisons with observations.

The results of STEP 4 are then the final NEAMTHM18 results (the results of the TSUMAPS-NEAM hazard model). To avoid duplications, in this document we discuss only the methodological details, while the NEAMTHM18 results themselves are discussed in Doc_P2_S5_Results.

Summarising, the goals of STEP 4 are then:

1. probabilistic hazard model of the coastal tsunami impact expressed through the exceedance probability in $50\ yr$ $\{P(> MIH_{th}, 50\ \mathrm{yr})_{POI}\}$ versus different MIH intensity thresholds MIH_{th}; this is obtained by aggregating all scenario annual rates $\{\lambda(\sigma_k)\}$ from STEP 1 with the conditional PoE $\{P(> MIH_{tr}|\sigma_k)\}$ from STEP 3;

2. assessment of the model uncertainties expressed through distributions of hazard curves $\{P(> MIH_{th}, 50\ \mathrm{yr})_{POI}\}$ and their statistics; hazard and probability maps; disaggregation products.

4.1 Levels at STEP 4

At STEP 4 we have defined four Levels (0-3):

- Level 0 (input data):Weight assessment based on the elicitation of experts, and tsunami DB;

- Level 1: Combination of STEPS 1-3;
- Level 2: Quantification of uncertainty;
- Level 3: Comparison/test with tsunami records & disaggregation.

More specifically, Level 0 deals with definition of the weights for the alternative models (via expert elicitation), as well as the collection of the available past tsunami data.

Level 1 deals with the aggregation of the results of all the previous STEPs, performed once for each model in a subset sampling, according to the weights of the alternatives, all the considered individual alternative models (each single model is defined as one of the possible chains of alternatives considered at each STEP and Level). The results are produced in terms of PoE for different pre-defined hazard intensity thresholds at all POIs, conditional to each specific combination of alternative models.

Level 2 deals with the concrete uncertainty estimation, producing unconditional hazard curve ensembles (distributions of hazard curves conditional to the specific model) that characterize the NEAMTHM18 uncertainty.

Level 3 deals with the production of all the post-processing products enabling a deeper evaluation of the NEAMTHM18 results and their comparison with observations. This included the production of hazard and probability maps, the hazard disaggregation, and a first attempt of comparison between hazard results and observed tsunamis. Within the specific project constraints, we did not have the opportunity for a more organic and quantitative statistical comparison between NEAMTHM18 results and past tsunami data, which is left for future projects.

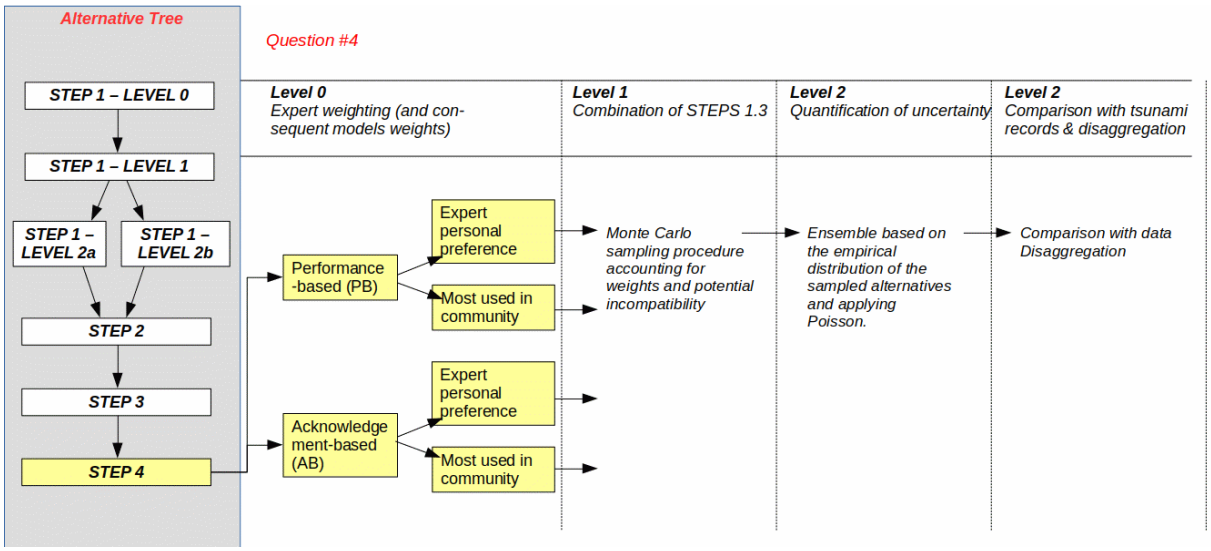

FIGURE 4.1: Alternative implementations at level 0 of STEP 4, as described in SECTIONS 4.1 and 4.2.

Coherently with the results of the first elicitation, we implemented 2 alternative methods at Level 0, concerning the weighting of the experts, and 2 alternative criteria to define preference for the different alternative models, as graphically reported in FIGURE 4.1. All these alternatives are dealt with within the elicitation procedure.

The details about the quantifications required at all the levels of STEP 4 are reported in the next SUBSECTIONS.

4.2 Level 0 – Weights of alternatives and tsunami DB

The relative credibility of alternative implementations at all STEPs and levels is quantified by means of weights (Bommer and Scherbaum, 2008). Therefore, the assessment consists of the quantification of $\mathrm{w}_{\mathrm{mnl}}$ where m represents a given alternative model of STEP n and Level l.

The weights must be assigned to all the different available models at each STEP and each Level of the SPTHA model. Their subjective character has been formally managed with a quantification process based on a structured elicitation experiment with the Pool of Experts (PoE). The details of this elicitation are reported in Doc_P2_S4. In the following, we summarize only the main points.

As in PHASE 1, the elicitation experiment was based on a structured questionnaire provided to the Pool of Experts (PoE). The second elicitation experiment is based on the same prioritization method adopted in the first experiment (Analytical Hierarchical Process - AHP procedure; Saaty 1980), with several modifications mainly introduced to account for the requirements of the first elicitation that suggested alternatives (or sensitivity tests) for the quantification of weights of the experts and of models. The analytic hierarchy process (AHP) is a structured technique for organizing and analyzing complex decisions, ending up with a ranking of alternatives based on pairwise comparisons. Given the interpretation of weights within the ensemble model, which are not interpreted as probabilities, we adopted the AHP scores as weights at each STEP and each Level of the hazard model.

To introduce alternative weights for the models, we defined 2 distinct criteria for the comparison of the alternative models:

- Criterion 1: Expert's personal preference
- Criterion 2: Most used in the community according to expert's best knowledge

This differs from the first elicitation, where only one criterion expressing the personal opinion was present. The two criteria adopted here express two different ways of thinking of the prioritization among the models, and the expert is asked to isolate his/her personal opinion from the community opinion. Following the AHP procedure, these two criteria are not equally considered, but they are prioritized by the same panel of experts through a specific question.

Based on the above two criteria, for each expert and each set of alternatives, the AHP method provides in output only one set of weights $w_i^{(e)}$, expressing the priority for each expert *e* of the different alternatives available at STEP *m* and Level *l*.

Adopting an Aggregation of Individual Judgments (AIJ) strategy (Forman and Peniwati, 1998), the opinions of the different experts are merged by analyzing the statistics of the results, to obtain the set of weights expressed by the panel. The panel's weights may be obtained by taking, for each alternative *i*, the mean weight over the experts, that is the geometric mean $w_i = \left(\prod_{e=1}^{N}(w_i^{(e)})^{w_e}\right)^{1/\sum_{e=1}^{N} w_e}$, where *N* is the number of experts in the pool, and w_e are the weights of the experts themselves.

For addressing the latter, we adopted two different methods in the first elicitation: the Performance-based weights (PW) and Acknowledgement-based weights (AW). A third weighting scheme (equal weights) is instead used to check the consistency of the results, as well as to set the preference of the pool of experts between PW and AW. This defines two set of weights for the experts which are $w_{e,PW}$. and $w_{e,AW}$.

Entering the two expert weighting schemes (PW and AW) into the AIJ procedure described above, we obtained two independent set of weights for the models. These two sets must be merged.

TABLE 4.1: Weights of the alternative models implemented for the ensemble.

STEP/LEVEL - Question	Alternative models	Ensemble weight
STEP 1 – Level 0 Question 1	Cut-off distance of 5 km around the PS sources	0.39
	Cut-off distance of 10 km around the PS sources	0.61
STEP 1 – Level 1 Question 2a	The mean annual rates rates for PS and BS are quantified jointly	0.44
	The mean annual rates rates for PS and BS are quantified independently	0.56
STEP 1 – Level 1 Question 2b	The tapered distribution (with probability > 0 for all magnitudes) with the parameter β (equivalent to the b-value) set to 2/3 (equivalent to b-value = 1), independently from data.	0.30
	The tapered distribution (with probability > 0 for all magnitudes) with the parameter β (equivalent to the b-value) set from data.	0.31
	The truncated distribution (with probability = 0 for all M > M_{max}) with the parameter β (equivalent to the b-value) set from data.	0.19
	The truncated distribution (with probability = 0 for all M > M_{max}) with the parameter β (equivalent to the b-value) set to 2/3 (equivalent to b-value = 1), independently from data.	0.20
STEP 1 – Level 2 Question 3a	Scaling relations from Strasser et al. (2010).	0.55
	Scaling relations from Murotani et al. (2013).	0.45
STEP 1 – Level 2 Question 3b	Co-seismic slip is not allowed or allowed to happen at shallow depths under the accretionary wedge.	0.34
	Co-seismic slip can happen at shallow depths under the accretionary wedge.	0.66
STEP 1 – Level 2 Question 3c	Rigidity is uniform with depth (PREM).	0.35
	Rigidity varies with depth according to Geist and Bilek (2001).	0.65
STEP 4 – Level 0 Question 4	Performance-based weights (PB)	0.57
	Acknowledgement-based weights (AB)	0.43
STEP 4 – Level 0 Question 0	Criterion 1: Expert's personal preference	0.64
	Criterion 2: Most used in the community according to expert's best knowledge	0.36

Hence, we asked the experts to prioritize also these two last alternative weighting schemes. We found that the AHP scores (considering equal weights for experts) resulted w_{PW} = 0.57 and and w_{AW} = 0.43. To avoid further nesting of epistemic levels (with alternative weights for the alternative models within the alternative tree), we preferred to merge these two sets into one overall reference set of weights (note that the sampling procedure described in SECTION 4.1 is independent from this choice).

The merged (and final) set of weights for the alternative models have been obtained by considering the weighted mean of the results obtained from PW and AW. The merged weights, for each STEP and level, are reported in TABLE 4.1. We tested that, in the sampling procedure defined at STEP 4 - Level 1 (SECTION 4.1), this procedure is equivalent to defining two alternatives within an alternative tree.

More details about the second expert elicitation experiment and its results can be found in Doc_P2_S4.

For the comparison between past tsunamis and the hazard results, we considered the Euro-Mediterranean Tsunami Catalogue (Maramai et al. 2014; http://roma2.rm.ingv.it/en/facilities/data_bases/52/euro-mediterranean_tsunami_catalogue).

4.3 Level 1 - Combination of STEPS 1 to 3

The contributions of all sources to the hazard at each POI are aggregated, considering the mean annual rate of each source (STEP 1), the generation and propagation in deep water of the consequent tsunami (STEP 2) and its inundation (STEP 3). The assessment consists of quantifying the hazard curves in terms of probability of exceedance within the considered exposure time of $50\ yr$ and different hazard intensity thresholds.

The hazard curve is first expressed in terms of mean annual rate of exceedance of MIH_{th} at each POI (defined at STEP 2), for a predefined set of MIH_{th} values (as defined at STEP 3). This curve is computed combining the mean annual rates $\lambda(\sigma_k)$ of each potential generating seismic scenario σ_k (from STEP 1) and the probability that this scenario lead to exceeding a given MIH_{th} (from STEPs 2 and 3), that is:

$$\lambda(> MIH_{th}, 1yr)_{POI} = \\ = \sum_i \lambda(\sigma_i)\, P(> MIH_{th}|\sigma_i)_{POI} = \sum_j \sum_k \lambda\left(\sigma_k^{(Type_j)}\right)\, P\left(> MIH_{th}\middle|\sigma_k^{(Type_j)}\right)_{POI}$$

where $\mathrm{Type_j}$ cover all seismicity types described in STEP 1 (BS and PS types, including SBS and SPS subtypes, see SECTION 2.1; and SECTIONS 2.5-2.6 for their rate evaluation), and $\mathrm{P}\left(> MIH_{th}\middle|\sigma_{\mathrm{k}}^{(\mathrm{Type_j})}\right)_{POI}$ is one hazard curve at one POI, conditional to the k-th scenario sampled from the epistemic uncertainty on the log-normal parameters, as described in STEP 3 – Level 3 (see SECTION 3.4).

Each curve expressed above as mean annual rate of exceedance versus the different thresholds MIH_{th}, can be converted into a hazard curve (PoE versus MIH_{th}) considering the exposure time of 50 years and assuming that the tsunamigenic earthquakes follow a Poissonian arrival time process.

Hence, the probability of observing at a given POI at least one exceedance of the tsunami intensity threshold MIH_{th} in 50 years can be written as:

$$P(> MIH_{th}, 50\ \mathrm{yr})_{POI} = 1 - \exp(-\lambda(> MIH_{th})_{POI} \cdot 50)$$

The quantification of $\lambda(> MIH_{th})_{POI}$ and hence of $P(> MIH_{th}, 50\ \mathrm{yr})_{POI}$ is performed over a pre-defined set of 50 MIH thresholds, as discussed in STEP 3 – Level 3 (see SECTION 3.4).

It might be convenient to consider that PoE in a given exposure time ΔT can be converted into average recurrence periods ARP using the formula $ARP = \frac{\Delta T}{\mathrm{abs}(\ln(1-P(>MIH_{th},\Delta T)_{POI}))}$, which, for example, for a PoE of 2% in $50\ yr$ gives $ARP = \sim 2475\ yr$, sometimes used in coastal planning against tsunamis, and, for a PoE of 10% in $50\ yr$ gives $ARP = \sim 475\ yr$, often used for civil seismic building code definition.

These quantities could be in theory computed for all the combinations of alternative models of all STEPs and Levels from 1-3, as well as for all possible realizations of the parameters of the Bayesian model at STEP 1 Lev 1, and STEP 1 Lev 2b. To bound the computational effort, a Monte Carlo sampling procedure is here adopted (similarly to Selva et al., 2016). At each STEP and level, potential alternatives are sampled proportionally to their weights (the larger the weight, the higher the chance to sample for the corresponding model). Recall that model weights emerge from Level 0 at this STEP. If one Bayesian model is sampled, a randomly selected single realization of the model's parameters is considered.

In doing this, potential incompatibility among models are accounted for. For example, if a 10 km cut-off for the PS/BS-only catalogue is sampled at STEP 1 Level 0, for coherence only this option is considered in all the following levels. To allow for that, weights are sampled starting from STEP 1 – Level 0 through STEP 3 – Level 3, running first levels and then STEPs. At each sampling step, only the alternative implementations which are compatible with the already sampled models at previous STEPs and Levels are considered, re-normalizing the weights. Once a complete chain of models is sampled from all potential alternatives at all levels and STEPs, one realization of $\lambda(> MIH_{th})_{POI}$ is computed.

A total of 1000 chains of models are sampled according to the model weights, obtaining a sample of 1000 alternative $\lambda(> MIH_{th})_{POI}$, subsequently converted into a sample of 1000 alternative hazard curves $P(> MIH_{th}, 50\ \mathrm{yr})_{POI}$ at each POI.

4.4 Level 2 - Quantification of uncertainty

All the alternative implementations at Level 1 are used in input to the ensemble modeling procedure to produce, for each target point, an ensemble distribution that quantifies both aleatory and epistemic uncertainty.

The set of 1000 alternative $P(> MIH_{th}, 50\ \mathrm{yr})_{POI}$ is treated as an unbiased sample of epistemically alternative hazard curves. The corresponding parent distribution represents the ensemble distribution quantifying simultaneously aleatory and epistemic uncertainties (Marzocchi et al. 2015). This distribution coincides with the community distribution for hazard curves (SSHAC 1997; Bommer 2012).

Given the relatively large size of the sample of alternative models (1000 samples), we produced the ensemble distribution as an empirical distribution emerging from the sample itself, that is without fitting any predefined parametric distribution. So at Level 2 we basically derive statistics from the sampled empirical distributions of hazard curves. This is the simplest possible choice. It does not explicitly deal neither with the problem of potential non unimodality of the ensemble distribution (potentially emerging from separated families of hazard curves), nor with the possibility of tails going outside the range defined by the input sample (about both these issues, see discussions in Marzocchi et al., 2015). However, given the relatively large size of the sample (1000) and considering that in output we provide both mean and median curves and we restrict the epistemic statistics up to 98th and down to 2nd percentiles, we argue that this should not have any important practical implication.

The ensemble hazard curves are reported considering mean, median, and percentiles 2, 16, 84 and 98. Probability are considered robust in the range $1x10^{-3}\ to\ 1$ (equivalent to $ARP\ < \sim 50{,}000\ yr$). Results for probabilities smaller than $5x10^{-4}\ in\ 50\ yr$ (equivalent to $ARP > \sim 100{,}000\ yr$) are not considered sufficiently enough well constrained, for example due to the time span covered by the used seismic catalogues, thus they are omitted from the final results.

Hazard maps have been produced for Average Return Periods of 500, 1,000, 2,500, 5,000 and 10,000 years, for the mean and the 16th and 84th percentiles. Probability maps have been computed for MIH of 1, 2, 5, 10 and 20 m. In both cases, maps have been calculated by linear interpolation between the two closest points in the hazard curves.

As discussed in Doc_P2_S3, the hazard curves for all defined POIs are saved in XML files for each statistic, in a format similar (but not identical) to the Natural hazards' Risk Markup Language (NRML) defined by GEM/OpenQuake (https://www.globalquakemodel.org/; GEM, 2018). All these files represent the input for the Interactive Hazard Curve Tool reported in the TSUMAPS-NEAM project website. Curves and maps are freely and seamlessly accessible through the Internet (http://www.tsumaps-neam.eu/). More details can be found in Doc_P2_S5.

4.5 Level 3 - Comparison/test with tsunami records and disaggregation

The results of Levels 1-2 are post-processed for production of secondary results. The main goal of this section is to introduce post-processing operations that can translate the complex probabilistic results into some more “readable” products, potentially comparable with real data. The proposed post-processing analyses are of two types: explicit forecasts and disaggregation.

The goal of the forecasts is to process hazard results so that they may be used as input for statistical tests against real data. Hazard disaggregation instead allows for individuating the source scenarios that are more influent on the hazard in a given location, considering both their tsunamigenic capability and their frequency of occurrence. For any given hazard level and any given location, disaggregation allows for understanding what the most influential sources on different bases are, such as magnitude range, distance, tectonic region, seismicity type, and so on. This type of results is not only clearly readable and interpretable (thus, allowing for example the comparison with our a priori ideas), but also it is very useful in practice, providing for example an objective prioritization of sources based on their importance in producing a given hazard in a given location.

The comparison between the NEAMTHM18 results and the tsunami data available may be regarded as one final sanity check, following the comparisons to past data of all the components of the probabilistic seismic model (see Sanity Checks in Doc_P2_S5). This final comparison is nevertheless not very straightforward since the NEAMTHM18 results are expressed in terms of mean MIH, that is typically not recorded for past tsunamis (since almost impossible to be measured in the field). Moreover, MIH represents a tsunami hazard intensity averaged over a coastal sector (see discussion in STEP 3 Level 3, in SECTION 3.4), while real data usually report the known maximum of the maxima over an area hit by a tsunami in the past.

Considering the results of the NLSW simulations used to constrain the uncertainty distribution of STEP 3 – Level 3 (SECTION 3.4, Glimsdal et al., 2019), we can estimate an approximated general relationship between the MIH and the run-up. To do this, we divided each of the coastal stretches where the NLSW simulations were performed into stripes of land perpendicular to the coast, and we estimated from the results of each NLSW simulation the ratio between the maximum (among the stripes) run-up and the mean MIH. The aggregated results for all simulated earthquakes and all test sites are reported in FIGURE 4.2.

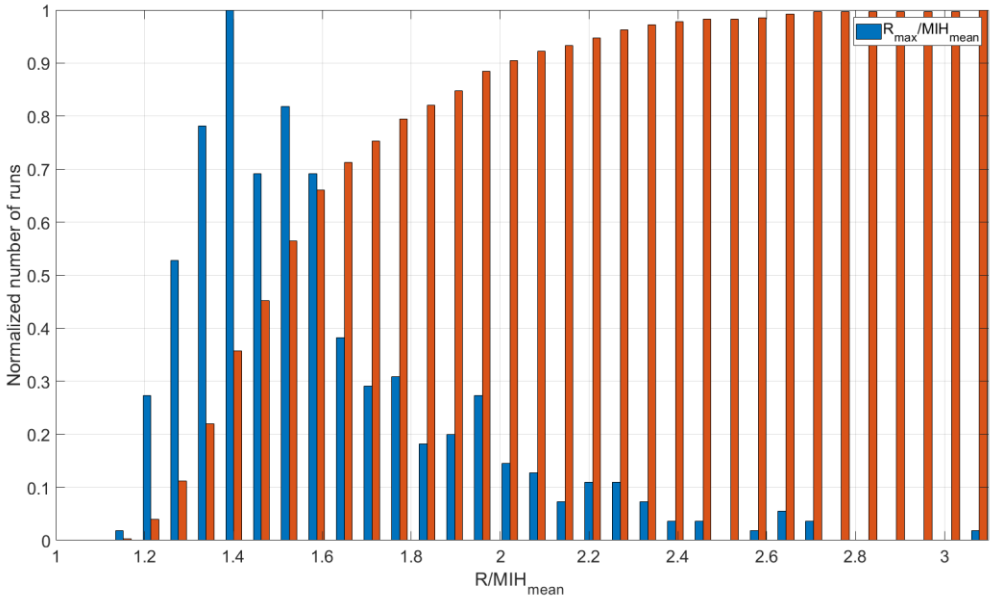

FIGURE 4.2: Empirical probability density function (blue) and empirical cumulative density function (red) of the ratio between the maximum run-up and the mean MIH.

The results reported in FIGURE 4.2 show that the maximum run-up over a sector of the coast may be even (slightly) larger than 3 times the mean MIH, due to the lateral variability of the tsunami intensity.

To compare the NEAMTHM18 with past data, we must anyway at least qualitatively account for these aspects. An apparently quite safe simplified conversion suitable for a qualitative comparison between the MIH and the maximum run-up can be obtained by multiplying the MIH values from the NEAMTHM18 by a factor of 3. A “safe” conversion is here required since we have also to consider potential instabilities in the tails of the distributions, given the still limited number of case studies considered in Glimsdal et al. (2019). Including more coastal sites and more cases in the analysis with

respect to Glimsdal et al. (2019) may indeed lead to a larger variability. The study, used also here at STEP 3, had in fact the purpose to estimate the MIH uncertainty, not the run-up.

Despite there might be relevant methods for building empirical hazard curves directly from tsunami data (e.g. Geist & Parsons, 2016), in this specific case there are also other important issues that may limit even the possibility for an immediate comparison between hazard results and past data. First, in this area of the world the data are quite scarce and the records typically incomplete (e.g. for a given single site), due to the relative rarity of tsunami events and given the difficult preservation of paleotsunami data. In addition, completeness analysis is not available. Moreover, historical data are often expressed only in terms of a tsunami intensity scale (e.g., the Sieberg-Ambraseys intensity scale, Ambraseys, 1962) that is only loosely connected to a quantitative tsunami intensity measure (like run-up or maximum inundation distance). This makes the comparison of data with hazard models rather critical and, at the very least, quite uncertain. Also, in the case of data expressed in terms of quantitative intensity measures, often the only intensity measure in the considered catalogue that can be used for comparisons with MIH is the maximum known run-up, which – if coming from an earthquake-generated tsunami – should be smaller than, or equal to the maximum MIH. Moreover, we have often available, for a given event, only the largest record at a single site, rather than a distribution of records spanning different sites, is reported as a quantitative tsunami intensity.

All these issues, along with the limited time frame and budget in the project, limited by far our possibility for a systematic comparison between the hazard results and past tsunami data. This would have required specific resources to post-process and re-elaborate tsunami data, in order to enable a meaningful comparison. This is left to future projects.

Regardless, we made two examples of possible comparison, to be then considered as preliminary. One example is based on the fact that, if one considers a relatively small and closed basin, all the tsunami intensity recorded in this basin may be assumed as experienced in many target points. To this end, we considered the case of the Marmara Sea, for which several historical events are known (at least, in the area of Istanbul). In this area, the Euro-Mediterranean Tsunami Catalogue (Maramai et al., 2014) reports several historical tsunamis, most of them have intensity 2 o 3 and no quantitative estimation of run-up. To enlarge as much as possible the data, we may compare the smallest MIH considered (MIH = 0.5, corresponding to maximum local run-ups up to 1.5 m). From the definition of tsunami intensity (Ambraseys, 1962), a reasonable minimum intensity threshold to make this comparison is intensity 4 or 5. Given the limited extension of the Marmara Sea, we can assume that all the largest tsunamis (derived from the intensity) are all observed at least in one point, potentially the one with the largest hazard in the area. The results of this comparison are discussed in Doc_P2_S5, along with the other sanity checks.

Another important sanity check can be made by comparing a reference hazard map with the quantitative observations in a given area. Given that one potential use of tsunami hazard results is the definition of evacuation areas for tsunami warnings. In New Zealand (MCDEM, 2016) and Italy (DCDPC, 2018), a reference hazard maps to this end has been established by decision makers as the one corresponding to an average return period of 2500 years at the 84^{th} percentile of the epistemic uncertainty. Also in this case, we should consider the lateral variability of the tsunami intensity, for example multiplying the tsunami intensity MIH to a factor 3, to compare with local maximum run-

up. In this case, the comparison is made in Italy, where the selected hazard map is being used as reference for tsunami warning, and a relatively large number of historical events with an explicit estimation of the quantitative tsunami intensity (11 records reporting the maximum tsunami intensity per event, provided in terms of run-up and/or inundation length) are available, also due to its central position in the Mediterranean Sea. The results of this comparison are discussed in Doc_P2_S5, along with the other sanity checks.

Disaggregation analyses have been performed in 42 POIs, spread over the Black Sea, the Mediterranean Sea and the Atlantic Ocean (see the map in Doc_P2_S5, FIGURE 2.3). Disaggregation has been performed for seismicity class (BS/PS), tectonic region, magnitude, and fault location. Only for BS/PS, we quantified the effect of epistemic uncertainty in disaggregation, while in all the other cases the disaggregation has been computed only the mean hazard. For BS/PS, tectonic regions, and several magnitudes, it has been extended to all the available tsunami intensities. For all the other magnitudes, is computed for MIH = 1.11, 5.373 and 12.314 m, while for fault location only to MIH = 1.11 and 5.373 m. All the results are reported in Doc_P2_S5 and its appendices.

In all cases, the disaggregation has been computed as in Selva et al. (2016). For example, the disaggregation for seismicity class is made evaluating the probability that the exceedance of a given intensity at the site is caused by a given seismicity class through the Bayes' rule, that is

$$P(\mathrm{PS}|>MIH_{th})_{POI}=\frac{\sum_{\sigma_i\in PS}\lambda(\sigma_i)\,P(>MIH_{th}|\sigma_i)_{POI}}{\sum_{\forall i}\lambda(\sigma_i)\,P(>MIH_{th}|\sigma_i)_{POI}}$$

Epistemic uncertainty is evaluated repeating this quantification for all the 1000 samples produced at STEP 3 – Level 1 (SECTION 3.3) and quantifying each time the statistics of this set. The other disaggregation analyses have been produced by using analogous formulae, where the numerator is restricted according to the quantity for which disaggregation is performed. In order to cumulate the effect of spatial PS and BS in spatial disaggregation, this is performed by subdividing the source space with equal hexagons, with a dimension on approximately 50 km, twice the cell dimension of BS. To each hexagon, we consider all the included PS sources and all BS cell centers (allowing for their accumulation at the source level).

More details about the disaggregation procedure and its results are reported in Doc_P2_S5.

References

Alasset, P., Hébert, H., Maouche, S., Calbini, V. and Meghraoui, M. (2006), The tsunami induced by the 2003 Zemmouri earthquake (MW= 6.9, Algeria): modelling and results. Geophysical Journal International, 166: 213-226. doi:10.1111/j.1365-246X.2006.02912.x.

Ambraseys, N.N. (1962) Data for the investigation of the seismic sea-waves in the Eastern Mediterranean. Bulletin of the Seismological Society of America; 52 (4): 895–913.

Bakırcı T., Yoshizawa K., Özer M. F. (2012). Three-dimensional S-wave structure of the upper mantle beneath Turkey from surface wave tomography, Geophysical Journal International, 190(2), 1058–1076, https://doi.org/10.1111/j.1365-246X.2012.05526.x.

Barbosa, S. M., Fernandes, M. J., Silva, M. E. (2004). Nonlinear sea level trends from European tide gauge records. Annales Geophysicae, 22, 1465–1472.

Basili, R., M. M. Tiberti, V. Kastelic, F. Romano, A. Piatanesi, J. Selva, S. Lorito (2013a). Integrating geologic fault data into tsunami hazard studies, Nat. Hazards Earth Syst. Sci., 13(4), 1025-1050, doi: 10.5194/nhess-13-1025-2013.

Basili R., Kastelic V., Demircioglu M. B., Garcia Moreno D., Nemser E. S., Petricca P., Sboras S. P., Besana-Ostman G. M., Cabral J., Camelbeeck T., Caputo R., Danciu L., Domac H., Fonseca J., García-Mayordomo J., Giardini D., Glavatovic B., Gulen L., Ince Y., Pavlides S., Sesetyan K., Tarabusi G., Tiberti M. M., Utkucu M., Valensise G., Vanneste K., Vilanova S., Wössner J. (2013b). The European Database of Seismogenic Faults (EDSF) compiled in the framework of the Project SHARE. *http://diss.rm.ingv.it/share-edsf/*, doi: 10.6092/INGV.IT-SHARE-EDSF.

Basili R, Volpe M, Maesano FE, Tiberti MM, Lorito S, Romano F, Tonini R (2017). Influence of seismogenic source geometrical accuracy on PTHA: a test case for the Calabrian subduction interface, Geophysical Research Abstracts, Vol. 19, EGU2017-18872-1, EGU General Assembly 2017.

Basili, R., and M. M. Tiberti (2016). New statistics of earthquake-fault dip angles. Paper ESC2016-447, presented at the 35th General Assembly of the European Seismological Commission, Trieste, 4-10 September 2016.

Berryman K., Wallace L., Hayes G., Bird P., Wang K., Basili R., Lay T., Pagani M., Stein R., Sagiya T., Rubin C., Barreintos S., Kreemer C., Litchfield N., Stirling M., Gledhill K., Haller K., Costa C. (2015). The GEM Faulted Earth Subduction Interface Characterisation Project, Version 2.0, April 2015, GEM Faulted Earth Project, available from http://www.nexus.globalquakemodel.org/gem-faulted-earth/posts.

Bilek S. L. & Lay T. (1999). Rigidity variations with depth along interpolate megathrust faults in subduction zones. Nature, 400, 443-446. https://doi.org/10.1038/22739.

Bird, P. (2003) An updated digital model of plate boundaries, Geochem Geophys Geosys 4(3), 1027, doi:10.1029/2001GC000252.

Blaser, L., Krüger, F., Ohrnberger, M., Scherbaum, F., 2010. Scaling relations of earthquake source parameter estimates with special focus on subduction environment. Bulletin of the Seismological Society of America 100, 2914-2926, doi: 10.1785/0120100111.

Bommer, J.J. (2012). Challenges of Building Logic Trees for Probabilistic Seismic Hazard Analysis, EARTHQUAKE SPECTRA, Vol: 28, 1723-1735, ISSN: 8755-2930.

Bommer, J.J., Scherbaum, F. (2008). The use and misuse of logic trees in Probabilistic Seismic Hazard Analysis, Earthq. Spectra, 24, 997–1009.

Boyd, O. S. (2012). Including foreshocks and aftershocks in time-independent probabilistic seismic-hazard analyses, Bull. Seismol.Soc. Am. 102, 909–917.

Burridge, R., (1973). Admissible Speeds for Plane-Strain Self-Similar Shear Cracks With Friction but Lacking Cohesion, *Geophysical Journal International* Vol. 35(4): 439–455. doi: 10.1111/j.1365-246X.1973.tb00608.x.

Carafa, M.M.C., Kastelic, V., Bird, P., Maesano, F.E. & Valensise, G., 2018. A "geodetic" gap in the Calabrian Arc: evidence for a locked subduction megathrust? Geophys. Res. Lett., 45(4), 1794–1804.

Campbell KW (1982), Bayesian analysis of extreme earthquake occurrences. Part I. Probabilistic hazard model, Bulletin of the Seismological Society of America, Vol. 72, No. 5, pp. 1689-1705, October 1982

Choi, B.H., Pelinovsky, E., Ryabov, I., Hong, S.J. (2002). Distribution Functions of Tsunami Wave Heights. Natural Hazards, 25(1), doi: 10.1023/A:1013379705323.

Christophersen, A., Berryman, K., Litchfield, N. (2015) The GEM Faulted Earth Project, Version 1.0, April 2015, GEM Faulted Earth Project, doi: 10.13117/GEM.GEGD.TR2015.02.

Collettini, C. & Sibson, R.H. (2001). Normal faults, normal friction?, Geology, 29, 927-930.

Cornell C (1968): Engineering seismic risk analysis, Bull. Seismol. Soc. Am. 58:1583–1606.

Davies G, Griffin J, Løvholt F, Glymsdal S, Harbitz C, Thio HK, Lorito S, Basili R, Selva J, Geist E, Baptista MA (2018). A global probabilistic tsunami hazard assessment from earthquake sources. From: Scourse, E. M., Chapman, N. A., Tappin, D. R. & Wallis, S. R. (eds) Tsunamis: Geology, Hazards and Risks. Geological Society, London, Special Publications, 456, https://doi.org/10.1144/SP456.5.

DCDPC (Decreto del Capo Dipartimento della Protezione Civile) 2018, Indicazioni alla Componenti ed alle Strutture operative del Servizio nazionale di protezione civile per l'aggiornamento delle pianificazioni di protezione civile per il rischio maremoto, Presidenza del Consiglio dei Ministri – Dipartimento della Protezione Civile, Reportorio n 3976 del 10/10/2018

de la Asunción, M., Castro, M. J., Fernández-Nieto, E. D., Mantas, J. M., Ortega Acosta, S., and González Vida, J. M. (2013). Efficient GPU implementation of a two waves TVD-WAF method for the two-dimensional one layer shallow water system on structured meshes, Comput. Fluids, 80, 441–452.

Delavaud E., Cotton F., Akkar S., Scherbaum F., Danciu L., Beauval C., Drouet S., Douglas J., Basili R., Sandikkaya M., Segou M., Faccioli E., Theodoulidis N. (2012). Toward a ground-motion logic tree for probabilistic seismic hazard assessment in Europe. Journal of Seismology, 16(3), 451-473, doi: 10.1007/s10950-012-9281-z.

Di Giacomo, D., E.R. Engdahl and D.A. Storchak (2018). The ISC-GEM Earthquake Catalogue (1904–2014): status after the Extension Project, Earth Syst. Sci. Data, 10, 1877-1899, doi: 10.5194/essd-10-1877-2018.

DISS Working Group (2018). Database of Individual Seismogenic Sources (DISS), Version 3.2.1: A compilation of potential sources for earthquakes larger than M 5.5 in Italy and surrounding areas. http://diss.rm.ingv.it/diss/, Istituto Nazionale di Geofisica e Vulcanologia; DOI:10.6092/INGV.IT-DISS3.2.1.

Duarte, J.C., Rosas, F.M., Terrinha, P., Schellart, W.P., Boutelier, D., Gutscher, M-A., Ribeiro A. (2013). Are subduction zones invading the Atlantic? Evidence from the southwest Iberia margin. Geology, 41 (8): 839–842. doi: https://doi.org/10.1130/G34100.1.

Dziewonski, A.M., T.A. Chou, and J.H. Woodhouse (1981). Determination of earthquake source parameters from waveform data for studies of global and regional seismicity, Journal of Geophysical Research, 86(B4), 2825, doi: 10.1029/JB086iB04p02825.

Dziewonski, A.M. & Anderson, D.L. (1981). Preliminary reference Earth model. *Physics of the Earth and Planetary Interiors*, 25 (4), 297–356. https://doi.org/10.1016/0031-9201(81)90046-7.

Egbert, G.D., and S.Y. Erofeeva, 2002: Efficient inverse modeling of barotropic ocean tides, J. Atmos. Oceanic Technol., 19(2), 183-204.

Ekström, G., M. Nettles, and A.M. Dziewoński (2012). The global CMT project 2004–2010: Centroid-moment tensors for 13,017 earthquakes, Physics of the Earth and Planetary Interiors, 200-201, 1-9, doi:10.1016/j.pepi.2012.04.002.

Gailler A, Hébert H, Schindelé F, Reymond D (2018) Coastal amplification laws for the french tsunami warning center: Numerical modeling and fast estimate of tsunami wave heights along the French riviera. Pure and Applied Geophysics 175(4):1429–1444, DOI 10.1007/s00024-017-1713-9, URL https: //doi.org/10.1007/s00024-017-1713-9

Geist E. L. & Bilek S. L. (2001). Effect of depth-dependent shear modulus on tsunami generation along subduction zones. *Geophysical Research Letters, 28 (7),* 1315-1318. https://doi.org/10.1029/2000GL012385.

Geist, E. & Parsons, T., 2006. Probabilistic analysis of tsunami hazards, *Nat. Hazards,* 37, 277–314.

Eshelby, J. The determination of the elastic field of an ellipsoidal inclusion and related problems. Proc. Roy. Soc. London, Series A 241, 376–396. doi: 10.1098/rspa.1957.0133 (1957).

Field Edward H., Ramon J. Arrowsmith, Glenn P. Biasi, Peter Bird, Timothy E. Dawson, Karen R. Felzer, David D. Jackson, Kaj M. Johnson, Thomas H. Jordan, Christopher Madden, Andrew J. Michael, Kevin R. Milner, Morgan T. Page, Tom Parsons, Peter M. Powers, Bruce E. Shaw, Wayne R. Thatcher, Ray J. Weldon, Yuehua Zeng; Uniform California Earthquake Rupture Forecast, Version 3 (UCERF3)—The Time-Independent Model. Bulletin of the Seismological Society of America; 104 (3): 1122–1180. doi: 10.1785/0120130164.

Forman, E. & Peniwati, K. (1998). Aggregating individual judgments and priorities with the analytic hierarchy process. European Journal of Operational Research, 108(1), 165-169.

Frankel, A. (1995). Mapping seismic hazard in the central and eastern United States. Seismological Research Letters, 66(4), 8-21.

Ganas, A., and Parsons, T. (2009). Three-dimensional model of Hellenic Arc deformation and origin of the Cretan uplift. Journal of Geophysical Research: Solid Earth, 114(B6), 10.1029/2008JB005599.

Gardner, J. K., and L. Knopoff (1974). Is the sequence of earthquakes in Southern California, with aftershocks removed, Poissonian? Bulletin of the Seismological Society of America; 64 (5): 1363–1367.

Geist, E. L. and Parsons, T. (2006). Probabilistic Analysis of Tsunami Hazards, Nat. Hazards, 37, 277–314, doi:10.1007/s11069-005-4646z.

Geist, E.L., and Parsons, T., 2016, Reconstruction of far-field tsunami amplitude distributions from earthquake sources: Pure and Applied Geophysics, v. 173, p. 3703-3717, doi:10.1007/s00024-00016-01288-x.

GEM (2018). The OpenQuake-engine User Manual. Global Earthquake Model (GEM) OpenQuake Manual for Engine version 3.2.0. doi: 10.13117/GEM.OPENQUAKE.MAN.ENGINE.3.2.0, 189 pages.

Giardini D., J. Woessner, L. Danciu, H. Crowley, F. Cotton, G. Gruenthal, R. Pinho, G. Valensise, S. Akkar, R. Arvidsson, R. Basili, T. Cameelbeck, A. Campos-Costa, J. Douglas, M.B. Demircioglu, M. Erdik, J. Fonseca, B. Glavatovic, C. Lindholm, K. Makropoulos, F. Meletti, R. Musson, K. Pitilakis, K. Sesetyan, D. Stromeyer, M. Stucchi, A. Rovida (2013). Seismic Hazard Harmonization in Europe (SHARE): Online Data Resource, doi: 10.12686/SED-00000001-SHARE.

Glimsdal, S., Løvholt, F., Harbitz, C.B., Romano, F., Lorito, S., Orefice, S., Brizuela, B., Selva, J., Hoechner, A., Volpe, M., Babeyko, A., Tonini, R., Wronna, M., Omira, R. (2019). A New Approximate Method for Quantifying Tsunami Maximum Inundation Height Probability. Pure Appl. Geophys, https://doi.org/10.1007/s00024-019-02091-w.

González, F. I., E. L. Geist B. Jaffe U. Kânoğlu H. Mofjeld C. E. Synolakis V. V. Titov D. Arcas D. Bellomo D. Carlton T. Horning J. Johnson J. Newman T. Parsons R. Peters C. Peterson G. Priest A. Venturato J. Weber F. Wong A. Yalciner (2009), Probabilistic tsunami hazard assessment at Seaside, Oregon, for near- and far-field seismic sources, J. Geophys. Res., 114, C11023, doi:10.1029/2008JC005132.

Grezio, A., Babeyko, A., Baptista, M. A., Behrens, J., Costa, A., Davies, G., et al. (2017). Probabilistic Tsunami Hazard Analysis: Multiple sources and global applications. Reviews of Geophysics, 55, 1158–1198. https://doi.org/10.1002/2017RG000579

Grünthal G. and R. Wahlström (2012). The European-Mediterranean Earthquake Catalogue (EMEC) for the last millennium. Journal of Seismology, 16, 535-570, doi 10.1007/s10950-012-9302-y.

Gutscher, M.A., Malod, J., Rehault, J.P., Contrucci, I., Klingelhoefer, F., Mendes-Victor, L., and Spakman, W. (2002). Evidence for active subduction beneath Gibraltar. Geology, v. 30, p. 1071–1074.

Hanks, T.C., Bakun, W.H., 2008. M-logA Observations for Recent Large Earthquakes. Bulletin of the Seismological Society of America 98, 490-494, doi: 10.1785/0120070174.

Hayes G.P., G.L. Moore, D.E. Portner, M. Hearne, H. Flamme, M. Furtney, G.M. Smoczyk (2018). Slab2, a comprehensive subduction zone geometry model. Science, 10.1126/science.aat4723.

Hayes, G. (2018). Slab2 - A Comprehensive Subduction Zone Geometry Model: U.S. Geological Survey data release, https://doi.org/10.5066/F7PV6JNV.

Heinrich P., Schindele F., & Guibourg S. (1998). Modeling of the February 1996 Peruvian tsunami. *Geophysical Reasearch Letters, 25,* 2687-2690. https://doi.org/10.1029/98GL01780.

Herrero A, Murphy S, Lorito S, Romano F, Volpe M (2017). The influence of complex fault geometry and slip of large subduction earthquakes on tsunami generation, Geophysical Research Abstracts Vol. 19, EGU2017-14724-1, EGU General Assembly 2017.

Herrero A., S Murphy (2018). Self-similar slip distributions on irregular shaped faults, Geophysical Journal International, 213(3), 2060–2070, https://doi.org/10.1093/gji/ggy104

Herrero, A. & Bernard, P. A Kinematic Self-Similar Rupture Process for Earthquakes (1994). Bull. Seismol. Soc. Am. 84(No. 4), 1216–1228.

Hiemer, S., J. Woessner, R. Basili, L. Danciu, D. Giardini, and S. Wiemer (2014), A smoothed stochastic earthquake rate model considering seismicity and fault moment release for Europe, Geophys. J. Int., 198, 1159-1172, doi:10.1093/gji/ggu186.

Howell A., Jackson J., Copley A., McKenzie D., Nissen E. (2017). Subduction and vertical coastal motions in the eastern Mediterranean, Geophysical Journal International, 211(1), 593–620, https://doi.org/10.1093/gji/ggx307.

Ichinose, G.A., 2006. Moment Tensor and Rupture Model for the 1949 Olympia, Washington, Earthquake and Scaling Relations for Cascadia and Global Intraslab Earthquakes. Bulletin of the Seismological Society of America 96, 1029-1037, doi: 10.1785/0120050132.

Iervolino, I., M. Giorgio, and B. Polidoro (2012). Probabilistic seismic haz-ard analysis for seismic sequences, in Vienna Congress on RecentAdvances in Earthquake Engineering and Structural Dynamics2013, C. Adam, R. Heuer, W. Lenhardt, and C. Schranz (Editors),28–30 August 2013, Vienna, Austria, Paper No. 66

ISC - International Seismological Centre (2016), On-line Bulletin, http://www.isc.ac.uk, Internatl. Seismol. Cent., Thatcham, United Kingdom.

Kagan, Y. Y. (2002a). Seismic moment distribution revisited: I. Statistical results, Geophys. J. Int., 148, 520–541, doi:10.1046/j.1365-246x.2002.01594.x.

Kagan, Y. Y. (2002b). Seismic moment distribution revisited: II. Moment conservation principle, Geophys. J. Int., 149, 731–754, doi:10.1046/j.1365-246X.2002.01671.x.

Kagan, Y.Y., Bird, P., Jackson, D.D. (2010) Earthquake Patterns in Diverse Tectonic Zones of the Globe, Pure Appl. Geophys., 167(6), 721-741, doi:10.1007/s00024-010-0075-3.

Kajiura, K. (1963). The leading wave of a tsunami, Bull. Earthquake Res. Inst. Univ., Tokyo, 41, 535–571.

Kamigaichi O., "Tsunami Forecasting and Warning," Encyclopedia of Complexity and System Science, Springer., pp. 9592-9618, 2009. https://doi.org/10.1007/978-1-4419-7695-6

Keller M., Pasanisi A., Marcilhac M., Yalamas T., Secanell R., and Senfaute G. (2014), A Bayesian Methodology Applied to the Estimation of Earthquake Recurrence Parameters for Seismic Hazard Assessment, Qual. Reliab. Engng. Int., 30, 921–933, doi: 10.1002/qre.1735

Kriebel D. L., Lynett P. J., Cox D. T., Petroff C. M., Robertson I. N. and Chock G. Y. K.; 2017: *Energy method for approximating energy overland tsunami flows*. J. Waterway, Port, Coastal, Ocean Eng., 143(5), DOI 10.1061/(ASCE)WW.1943-5460.0000393.

Laske, G., G. Masters., Z. Ma, and M. Pasyanos (2013), Update on CRUST1.0 - A 1-degree Global Model of Earth's Crust, Geophys. Res. Abstracts, 15, Abstract EGU2013-2658.

Laigle, M., Sachpazi, M., & Hirn, A. (2004). Variation of seismic coupling with slab detachment and upper plate structure along the western Hellenic subduction zone. Tectonophysics, 391(1-4), 85-95, 10.1016/j.tecto.2004.07.009.

Lay, T., Kanamori, H., Ammon, C.J., Koper, K.D., Hutko, A.R., Ye, L., Yue, H., Rushing, T.M., 2012. Depth-varying rupture properties of subduction zone megathrust faults. J. Geophys. Res. 117, B04311. http://dx.doi.org/10.1029/2011JB009133.

Leonard, M., 2010. Earthquake Fault Scaling: Self-Consistent Relating of Rupture Length, Width, Average Displacement, and Moment Release. Bulletin of the Seismological Society of America 100, 1971-1988, doi: doi: 10.1785/0120090189.

Leonard, M., 2014. Self-Consistent Earthquake Fault-Scaling Relations: Update and Extension to Stable Continental Strike-Slip Faults. Bulletin of the Seismological Society of America, doi: 10.1785/0120140087.

Lorito, S., Selva J., Basili R., Romano, F., Tiberti, M. M.,and Piatanesi, A (2015). Probabilistic Hazard for Seismically-Induced Tsunamis: Accuracy and Feasibility of Inundation Maps, Geophys. J. Int., 200, 574–588.

Løvholt F, Glimsdal S, Harbitz CB, Zamora N, Nadim F, Peduzzi P, Dao H, Smebye H (2012) Tsunami hazard and exposure on the global scale. Earth- Science Reviews 110(1):58 73, DOI https://doi.org/10.1016/j.earscirev. 2011.10.002

Løvholt, F., Griffin, J., & Salgado-Gálvez, M. (2015). Tsunami Hazard and Risk Assessment on the Global Scale (pp. 1–34). Berlin, Heidelberg: Springer Berlin Heidelberg. https://doi.org/ 10.1007/978-3-642-27737-5_642-1.

Macías, J., Mercado, A., González-Vida, J. M., Ortega, S., & Castro, M. J. (2016). Comparison and computational performance of Tsunami-HySEA and MOST models for LANTEX 2013 scenario: Impact assessment on Puerto Rico coasts. Pure and Applied Geophysics, 173(12), 3973–3997. doi: 10.1007/s00024-016-1387-8.

Macías, J., Castro, M. J., Ortega, S., Escalante, C., & González-Vida, J. M. (2017). Performance benchmarking of tsunami-HySEA model for NTHMP's inundation mapping activities. Pure and Applied Geophysics. doi: 10.1007/s00024-017-1583-1.

Maesano, F. E., Tiberti, M. M., and Basili, R., 2017, The Calabrian Arc: three-dimensional modelling of the subduction interface: Sci Rep, v. 7, no. 1, doi:10.1038/s41598-017-09074-8.

Mai P. M. & Thingbaijam K. K. S. (2014). SRCMOD: An online database of finte fault-fault rupture models. Seismological Research Letters, 85(6), 1348-1357. https://doi.org/10.1785/0220140077.

Maramai A., Brizuela B., Graziani L. (2014). The Euro-Mediterranean Tsunami Catalogue, Annals of Geophysics, 57, 4, S0435; doi:10.4401/ag-6437.

Marzocchi W., Taroni, M., Selva, J., 2015. Accounting for epistemic uncertainty in PSHA: logic tree and ensemble modeling. Bulletin of the Seismological Society of America, 105(4), 2151-2159.

MCDEM (2016) - Tsunami Evacuation Zones- Director's Guideline for Civil Defence Emergency Management Groups [DGL 08/16] February 2016 . ISBN 978-0-478-43515-3. Published by the Ministry of Civil Defence & Emergency Management – New Zealand

Meade, B. J. (2007), Algorithms for the calculation of exact displacements, strains, and stresses for triangular dislocation elements in a uniform elastic half space, Comput. Geosci., 33, 1064–1075, doi:10.1016/j.cageo.2006.12.00.

Molinari I, Tonini R, Lorito S, Piatanesi A, Romano F, Melini D, Hoechner A, Gonzàlez Vida JM, Maciás J, Castro MJ, de la Asunción M (2016). Fast evaluation of tsunami scenarios: uncertainty assessment for a Mediterranean Sea database, Nat. Hazards Earth Syst. Sci., 16, 2593-2602, doi: 10.5194/nhess16-2593-2016.

Murotani, S., Miyake, H., Koketsu, K., 2008. Scaling of characterized slip models for plate-boundary earthquakes. Earth Planets Space 60, 987-991.

Murotani, S., Satake, K., Fujii, Y., 2013. Scaling relations of seismic moment, rupture area, average slip, and asperity size forM~9 subduction-zone earthquakes. Geophysical Research Letters 40, 5070-5074, doi: 10.1002/grl.50976.

Murphy, S. et al. (2016) Shallow slip amplification and enhanced tsunami hazard unravelled by dynamic simulations of mega-thrust earthquakes. Sci. Rep. 6, 35007; doi: 10.1038/srep35007.

Nijholt N., Govers R., Wortel R. (2018). On the forces that drive and resist deformation of the south-central Mediterranean: a mechanical model study, Geophysical Journal International, 214(2), 876–894, https://doi.org/10.1093/gji/ggy144.

Nosov, M.A. & Kolesov, S.V. (2011). Optimal Initial Conditions for Simulation of Seismotectonic Tsunamis, Pure Appl. Geophys. 168: 1223, doi: 10.1007/s00024-010-0226-6.

Novotni, M. & Klein, R. Computing geodesic distances on triangular meshes. The 10-th International Conference in Central Europe on Computer Graphics, Visualization and Computer Vision 2002 (WSCG 2002).

Okada, Y. (1992). Internal deformation due to shear and tensile faults in a half-space, Bull. Seismol. Soc. Am., 82, 1018–1040.

Pondrelli S. and Salimbeni S. (2015). Regional Moment Tensor Review: An Example from the European Mediterranean Region. In Encyclopedia of Earthquake Engineering (pp. 1-15), http://link.springer.com/referenceworkentry/10.1007/978-3-642-36197-5_301-1, Springer Berlin Heidelberg.

Power, W., Wang, X., Lane, E., Gillibrand, P. (2013). A Probabilistic Tsunami Hazard Study of the Auckland Region, Part I: Propagation Modelling and Tsunami Hazard Assessment at the Shoreline. Pure Appl. Geophys. 170: 1621. https://doi.org/10.1007/s00024-012-0543-z

Romanowicz, B., Ruff, L.J., 2002. On moment-length scaling of large strike slip earthquakes and the strength of faults. Geophysical Research Letters 29, 45-41-45-44, doi: 10.1029/2001GL014479.

Ruiz, J. A., Baumont, D., Bernard, P. & Berge-Thierry, C. Modelling directivity of strong ground motion with a fractal, k− 2, kinematic source model. Geophys. J. Int. 186, 226–244, doi: 10.1111/j.1365- 246X.2011.05000.x (2011).

Saaty, T.L., 1980. The Analytic Hierarchy Process: Planning, Priority Setting, Resource Allocation, ISBN 0-07-054371-2, McGraw-Hill.

Sachpazi, M., Laigle, M., Charalampakis, M., Diaz, J., Kissling, E., Gesret, A., Becel, A., Flueh, E., Miles, P., and Hirn, A. (2016). Segmented Hellenic slab rollback driving Aegean deformation and seismicity. Geophysical Research Letters, 43(2), 651-658, doi: 10.1002/2015GL066818.

Salaün G., Pedersen H.A., Paul A., Farra V., Karabulut H., Hatzfeld D., Papazachos C., Childs D.M., Pequegnat C., and SIMBAAD Team (2012). High-resolution surface wave tomography beneath the Aegean-Anatolia region: constraints on upper-mantle structure, Geophysical Journal International, 190(1), 406–420, https://doi.org/10.1111/j.1365-246X.2012.05483.x.

Satake K. (1995). Linear and nonlinear computation of the 1992 Nicaragua earthquake tsunami, *Pure and Applied Geophysics, 144,* 455-470. https://doi.org/10.1007/BF00874378.

Scala A, Lorito S, Romano F, Murphy S, Selva J, Basili R, Babeyko A, Herrero A, Hoechner A, Løvholt F, Maesano FE, Perfetti P, Tiberti MM, Tonini R, Volpe M, Davies G, Festa G, Power W, Piatanesi A (2019) Effect of shallow slip amplification uncertainty on probabilistic tsunami hazard analysis in subduction zones: use of long-term balanced stochastic slip models, submitted

Sellier N.C., Loncke L., Vendeville B.C., Mascle J., Zitter T., Woodside J., Loubrieu B. (2013a). Post-Messinian evolution of the Florence Ridge area (Western Cyprus Arc), Part I: Morphostructural analysis,Tectonophysics, 591, https://doi.org/10.1016/j.tecto.2012.04.001.

Sellier N.C., Vendeville B.C., Loncke L. (2013b). Post-Messinian evolution of the Florence Rise area (Western Cyprus Arc) Part II: Experimental modeling, Tectonophysics, 591, 143-151, https://doi.org/10.1016/j.tecto.2011.07.003.

Selva J, Marzocchi W (2004), Focal parameters, depth estimation and plane selection of the worldwide shallow seismicity with Ms >= 7.0 for the period 1900-1976. G-cubed, 5, Q05005, doi:10.1029/2003GC000669.

Selva J, Costa A, Marzocchi W, Sandri L (2010), BET_VH: exploring the influence of natural uncertainties on long-term hazard from tephra fallout at Campi Flegrei (Italy) , Bull. Volcanol. 72(6): 705-716.

Selva J, Sandri L (2013), Probabilistic Seismic Hazard Assessment: Combining Cornell-like approaches and data at sites through Bayesian inference , Bull. Seism. Soc. Am., 103(3):1709-1722, DOI: 10.1785/0120120091

Selva J., Tonini R., Molinari I., Tiberti M.M., Romano F., Grezio A., Melini D., Piatanesi A., Basili R., Lorito S. (2016). Quantification of source uncertainties in Seismic Probabilistic Tsunami Hazard Analysis (SPTHA). Geophys. J. Int., 205, 1780-1803, doi:10.1093/gji/ggw107.

Shaw B., Jackson J. (2010). Earthquake mechanisms and active tectonics of the Hellenic subduction zone, Geophysical Journal International, 181(2), 966–984, https://doi.org/10.1111/j.1365-246X.2010.04551.x.

Sibson, R.H. & Xie, G. (1998). Dip Range for Intracontinental Reverse Fault Ruptures: Truth Not Stranger than Friction?, Bulletin of the Seismological Society of America, 88, 1014-1022.

Skarlatoudis, A.A., Somerville, P.G., Thio, H.K., 2016. Source-Scaling Relations of Interface Subduction Earthquakes for Strong Ground Motion and Tsunami Simulation. Bulletin of the Seismological Society of America 106, 1652-1662, doi: 10.1785/0120150320.

Sodoudi, F., Brüstle, A., Meier, T., Kind, R., Friederich, W., and Egelados Working Group. (2015). Receiver function images of the Hellenic subduction zone and comparison to microseismicity. Solid Earth, 6(1), 135-151, doi:10.5194/se-6-135-2015.

Sørensen, M. B., Spada, M., Babeyko, A., Wiemer, S., and Grünthal, G. (2012). Probabilistic tsunami hazard in the Mediterranean Sea, J. Geophys. Res., 117, B01305, doi:10.1029/2010JB008169.

SSHAC (Senior Seismic Hazard Analysis Committe), 1997. Recommendations for probabilistic seismic hazard analysis: Guidance on uncertainty and use of experts, U.S. Nuclear Regulatory Commission Report NUREG/CR-6372.

Storchak, D.A., D. Di Giacomo, I. Bondár, E. R. Engdahl, J. Harris, W.H.K. Lee, A. Villaseñor and P. Bormann, 2013. Public Release of the ISC-GEM Global Instrumental Earthquake Catalogue (1900-2009). Seism. Res. Lett., 84, 5, 810-815, doi: 10.1785/0220130034.

Storchak, D.A., D. Di Giacomo, E.R. Engdahl, J. Harris, I. Bondár, W.H.K. Lee, P. Bormann and A. Villaseñor (2015). The ISC-GEM Global Instrumental Earthquake Catalogue (1900-2009): Introduction, Phys. Earth Planet. Int., 239, 48-63, doi: 10.1016/j.pepi.2014.06.009.

Strasser, F.O., Arango, M.C., Bommer, J.J., 2010. Scaling of the source dimensions of interface and intraslab subduction-zone earthquakes with moment magnitude. Seismological Research Letters 81, 941-950, doi: 10.1785/gssrl.81.6.941.

Stucchi, M., A. Rovida, A.A. Gomez Capera, P. Alexandre, T. Camelbeeck, M.B. Demircioglu, P. Gasperini , V. Kouskouna, R.M.W. Musson, M. Radulian, K. Sesetyan, S. Vilanova, D. Baumont, H. Bungum, D. Faeh, W. Lenhardt, K. Makropoulos, J.M. Martinez Solares, O. Scotti, M. Zivcic, P. Albini, J. Batllo, C. Papaioannou, R. Tatevossian, M. Locati, C. Meletti, D. Viganò and D. Giardini (2012). The SHARE European Earthquake Catalogue (SHEEC) 1000-1899. Journal of Seismology, doi 10.1007/s10950-012-9335-2.

Tanioka Y., & Satake K. (1996b). Fault Parameters of the 1896 Sanriku Tsunami Earthquake Estimated from Tsunami Numerical Modeling. *Geophysical Research Letters 23,* pp. 1549-1552. https://doi.org/10.1029/96GL01479.

Tonini, R., Maesano, F. E., Tiberti, M. M., Romano, F., Scala, A., Lorito, S., Volpe, M., Basili, R. (2017). How much does geometry of seismic sources matter in tsunami modeling? A sensitivity analysis for the Calabrian subduction interface. Abstract NH23A-1948 presented at 2017 Fall Meeting, AGU, New Orleans, Louis., 11-15 Dec.

USNRC (U.S. Nuclear Regulatory Commission), 1997. Recommendations for probabilistic seismic hazard analysis: Guidance on uncertainty and use of experts, prepared by the SSHAC (Senior Seismic Hazard Analysis Committe - RJ Budnitz (Chairman), G Apostolakis, DM Boore, LS Cluff, KJ Coppersmith, CA Cornell, PA. Morris), NUREG/CR-6372.

USNRC (U.S. Nuclear Regulatory Commission), 2012. Practical Implementation Guidelines for SSHAC Level 3 and 4 Hazard Studies, Prepared by AM Kammerer & JP Ake, NRC Project Manager: R Rivera-Lugo, NUREG-2117.

USNRC (U.S. Nuclear Regulatory Commission), 2018. Updated Implementation Guidelines for SSHAC Hazard Studies, Prepared by JP Ake, C. Munson, J. Stamatakos, M. Juckett, K. Coppersmith, J. Bommer, NUREG-2117.

Vernant P., Reilinger R., McClusky S. (2014). Geodetic evidence for low coupling on the Hellenic subduction plate interface, Earth and Planetary Science Letters, 385, 122-129, https://doi.org/10.1016/j.epsl.2013.10.018.

Weichert DH. (1980) Estimation of the earthquake recurrence parameters for unequal observation periods for different magnitudes. Bulletin of the Seismological Society of America; 70:1337–1356.

Wessel, P., Smith,W.H.F., Scharroo, R., Luis, J.F. &Wobbe, F. (2013).Generic mapping tools: improved version released, EOSTrans. Am. Geophys. Un., 94, 409–410.

Wiemer, S. (2001). A software package to analyse seismicity: ZMAP. Seismol. Res. Lett., 72, 3, 373-382.

Woessner J., Danciu L., Giardini D., Crowley H., Cotton F., Grünthal G., Valensise G., Arvidsson R., Basili R., Demircioglu M., Hiemer S., Meletti C., Musson R.W., Rovida A., Sesetyan K., Stucchi M., and the SHARE consortium. (2015). The 2013 European Seismic Hazard Model - Key Components and Results. Bulletin of Earthquake Engineering, 13, 3553-3596, doi: 10.1007/s10518-015-9795-1.

Woessner J., S. Wiemer (2005). Assessing the Quality of Earthquake Catalogues: Estimating the Magnitude of Completeness and Its Uncertainty. Bulletin of the Seismological Society of America, 95(2), 684-698, doi: 10.1785/0120040007.

Zheng, Y. H., Anderson, J. G. & Yu, G. A (1994) Composite Source Model for Computing Realistic Synthetic Strong Ground Motions. Geophys. Res. Lett 21, 725–728, doi: 10.1029/94GL00367.

Zitellini N, Gracia E, Matias L, Terrinha P, Abreu M, DeAlteriis G, Hen- riet J, Danobeitia J, Masson D, Mulder T, Ramella R, Somoza L, Diez S (2009) The quest for the Africa-Eurasia plate boundary west of the Strait of Gibraltar. Earth and Planetary Science Letters 280(1):13 50, doi: https://doi.org/10.1016/j.epsl.2008.12.005.

Probabilistic TSUnami Hazard MAPS
for the NEAM Region (TSUMAPS-NEAM)
ECHO/SUB/2015/718568/PREV26

PHASE II – STAGE 3: Data and Codes

Author: **TSUMAPS-NEAM Technical Integrator (TI) team**

Date: **22 March 2019**

Version: **1.0**

Table of Contents

Executive Summary

This document lists and describes the datasets and the computational procedures adopted in the Phase 2 of the TSUMAPS-NEAM Project (see Doc_P2_S1_Implementation for details on the implementation workflow). There are two main types of input data: 1) the publicly available data retrieved from a trusted source, and 2) the data specifically composed for the project. As regards type 1), we provide here the link to the original source that is usually accompanied by relevant documentation. As regards type 2), we here provide a technical description of the data files with enough details so that a competent user could reuse them.

To guarantee the reproducibility of the NEAMTHM18, all the files mentioned here are stored in a private repository and supplied upon request. The codes are also preserved in a computational platform that can be accessed upon request and subject to having obtained the necessary credentials.

Overall, this document must be considered as a work in progress because files and codes described here can be modified to improve the potential of their usage.

This page is intentionally left blank.

1) Input Data (Level 0) at all STEPs

In this Section we provide a technical description of the main input files that document the NEAMTHM18 and that complement the scientific description and usage details given in other documents. Specifically, we consider here only the files that constitute the Level 0 of each STEP, as summarized below. This section should be considered as a work in progress, as both the file formats and their description may be modified either to enhance their usage or to improve their clarity or even to extend their potential for uses also outside the TSUMAPS-NEAM project main scopes. A copy of all the original files here described is stored private repository for verification and reproducibility of the results. They can be made available upon request.

STEP 1: Level 0 (input data):

- Tectonic regionalization model.
- Seismic datasets (earthquake catalogs including de-clustering and completeness).
- Fault datasets (including focal mechanisms).
- Assignment of sources to seismicity modeling types.
- Earthquake magnitude discretization.
- Empirical earthquake scaling relations.
- Discretization of the fault and earthquake parameters for the different sources assigned to the different seismicity modeling types.
- Attribution ("separation") of the observed seismicity in each region to each seismicity modeling type.

STEP 2: Level 0 (input data):

- Crustal elastic model;
- topo-bathymetric datasets and digital elevation models;
- Points of Interest (POIs).

STEP 3: Level 0 (input data):

- Topo-bathymetric datasets and digital elevation models;
- bathymetric transects;
- amplification factors.

STEP 4: Level 0 (input data):

- Weight assessment based on the elicitation of experts;
- tsunami DB.

In general, there are two main types of input data: 1) the publicly available data retrieved from a trusted source, and 2) the data specifically composed for the project. As regards type 1), we cannot redistribute these data and provide here only the link to the original source. We also recall to carefully consider the license for reusing these data. In this case, the reader is redirected to that source for obtaining detailed technical information. As regards type 2), we here provide a description of the data file names and internal formatting. In most cases, these are tabulated ASCII

files which we describe to a level of detail that allows the user to write a script for correctly parsing and reusing the included information. Occasionally, and especially for more complex formatting, we provide a snippet of the actual file. The description may be simpler for files that are not directly used for the hazard calculations but that are necessary to document actual input files.

To guarantee the reproducibility of the NEAMTHM18, all the files mentioned here are stored in a private repository and supplied upon request.

1.1) STEP 1:

1.1.1) Tectonic regionalization model

This Section illustrates the formats of the regionalization files. In these files all geographic coordinates are given as Lat/Lon, positive N/E, Datum WGS84.

File Regions_Tectonics_Geo_HDF5.txt: geographic information about the tectonic regionalization; only the coordinates of the polygons are provided.

Column	Variable	Delimiter	Value	Description
1	String	":"	ID	Region unique identifier
2	String	","	Name	Region name
n>2	Float	"," + "EOR"	Lon Lat	Longitude and Latitude coordinate pairs of all polygon vertexes

File Regions_Tectonics_Settings_HDF5.txt format: codes and names of the tectonic settings in the regionalization.

Column	Variable	Delimiter	Value	Description
1	String	":"	ID	Region unique identifier
2	Integer	","	Tectonic_Code	Code of the tectonic setting
3	String	"EOR"	Tectonic_Setting	Name of the tectonic setting

File Regions_Tectonics_FSL_HDF5.txt: Association between the codes of the tectonic settings and the fault scaling laws to use in each region.

Column	Variable	Delimiter	Value	Description
1	String	":"	ID	Region unique identifier
2	Integer	","	FSL_TectoCode	Code of the tectonic setting for the Fault Scaling Laws
3	String	"EOR"	FSL_LawCode	Code of the Fault Scaling Law

File Regions_Completeness_Geo_HDF5.txt: geographic information about the regionalization for the completeness analysis; the coordinates of the polygons are provided along with the acronym of the catalog used in the completeness analysis.

Column	Variable	Delimiter	Value	Description
1	String	":"	ID	Region for Completeness unique identifier
2	String	","	Name	Region name
3	String	","	Catalog	Acronym of earthquake catalog used for the completeness analysis
n>3	Float	"," + "EOR"	Lon Lat	Longitude and Latitude coordinate pairs of all polygon vertexes

File Regions_Completeness_Values_HDF5.txt: values of the completeness for magnitude classes associated to the regions for the analysis and the used catalog.

Column	Variable	Delimiter	Value	Description
1	String	":"	ID	Region for Completeness unique identifier
2	String	","	Name	Region name
3	String	","	Catalog	Acronym of earthquake catalog used for the completeness analysis
4	Integer	","	M35	Year of completeness in the magnitude bin (Mw > 3.5), NaN = -1
5	Integer	","	M40	Year of completeness in the magnitude bin (Mw > 4.0), NaN = -1
6	Integer	","	M45	Year of completeness in the magnitude bin (Mw > 4.5), NaN = -1
7	Integer	","	M50	Year of completeness in the magnitude bin (Mw > 5.0), NaN = -1
8	Integer	","	M55	Year of completeness in the magnitude bin (Mw > 5.5), NaN = -1
9	Integer	","	M60	Year of completeness in the magnitude bin (Mw > 6.0), NaN = -1
10	Integer	","	M65	Year of completeness in the magnitude bin (Mw > 6.5), NaN = -1
11	Integer	","	M70	Year of completeness in the magnitude bin (Mw > 7.0), NaN = -1
12	Integer	","	M75	Year of completeness in the magnitude bin (Mw > 7.5), NaN = -1
13	Integer	"EOR"	M80	Year of completeness in the magnitude bin (Mw > 8.0), NaN = -1

File Regions_Tectonics_Completeness_Values_HDF5.txt: values of the completeness for magnitude classes associated to the tectonic regions and the used catalog.

Column	Variable	Delimiter	Value	Description
1	String	":"	ID	Region unique identifier
2	String	","	Catalog	Acronym of earthquake catalog used for the completeness analysis
3	String	","	ID	Region for Completeness unique identifier
4	Integer	","	M35	Year of completeness in the magnitude bin (Mw > 3.5), NaN = -1
5	Integer	","	M40	Year of completeness in the magnitude bin (Mw > 4.0), NaN = -1
6	Integer	","	M45	Year of completeness in the magnitude bin (Mw > 4.5), NaN = -1
7	Integer	","	M50	Year of completeness in the magnitude bin (Mw > 5.0), NaN = -1
8	Integer	","	M55	Year of completeness in the magnitude bin (Mw > 5.5), NaN = -1
9	Integer	","	M60	Year of completeness in the magnitude bin (Mw > 6.0), NaN = -1
10	Integer	","	M65	Year of completeness in the magnitude bin (Mw > 6.5), NaN = -1
11	Integer	","	M70	Year of completeness in the magnitude bin (Mw > 7.0), NaN = -1
12	Integer	","	M75	Year of completeness in the magnitude bin (Mw > 7.5), NaN = -1
13	Integer	"EOR"	M80	Year of completeness in the magnitude bin (Mw > 8.0), NaN = -1

1.1.2) Seismic datasets

These are the sources for earthquake catalogs.

- EMEC-SHEEC
  - hhttps://www.gfz-potsdam.de/en/section/seismic-hazard-and-risk-dynamics/data-products-services/emec-earthquake-catalogue/ttps://www.gfz-potsdam.de/emec/
  - https://www.emidius.eu/SHEEC/
- ISC http://www.isc.ac.uk/

1.1.3) Fault datasets

These are the sources the fault data, including focal mechanisms (GCMT, RCMT), crustal faults (EDSF, DISS, ASTARTE, PB2002), and subduction zones (EDSF, SLAB2).

- GCMT https://www.globalcmt.org/
- RCMT http://rcmt2.bo.ingv.it/index.html
- EDSF http://www.seismofaults.eu/
- DISS http://www.seismofaults.eu/
- ASTARTE http://www.astarte-project.eu/index.php/deliverables.html
- PB2002 http://peterbird.name/oldFTP/PB2002/
- SLAB2 https://www.sciencebase.gov/catalog/item/5aa1b00ee4b0b1c392e86467

1.1.4) Assignment of sources to seismicity modeling types

This file determines which sources have been modeled as Background Seismicity (BS), Predominant Seismicity (PS), Special PS (SPS), and Special BS (SBS).

File Regions_Tectonics_BSPS_HDF5.txt: association between the regions of the tectonic regionalization and the four modeling types, either alone or in combination (five cases, plus the not-assigned case; see Doc_P2_S1, Section 1.3.4).

Column	Variable	Delimiter	Value	Description
1	String	":"	ID	Region unique identifier
2	Integer	"EOR"	BSPSCode	Code of the BSPS assignment: 1 = BS, 2 = PS, 3 = BS+SBS, 4 = BS+SPS, 5 = BS+PS, 0 = Not assigned.

1.1.5) Earthquake magnitude discretization.

This information is the same as Table 1.2 in Doc_P2_S1.

1.1.6) Empirical earthquake scaling relations.

This information is the same as that provided in the papers by Leonard (2014), Strasser et al. (2010), and Murotani et al. (2013).

1.1.7) Discretization of the fault and earthquake parameters

These files provide the geometric and kinematic discretization of the different sources assigned to the different seismicity modeling types.

Discretization of BS and SBS

Files Grid025_CNTR_HDF5.txt and Grid025_REDUCEDCNTR_HDF5.txt: geographic information about the grid; only the coordinates of the cell centers are provided. File Grid025_REDUCEDCNTR_HDF5.txt contains a reduced set of centers for the actual implementation. All other files contain info on the entire grid. Properties of grid cells can be transferred to the reduced set through their unique IDs.

Column	Variable	Delimiter	Value	Description
1	String	":"	ID	Cell unique identifier
2	Float	"EOR"	Lon Lat	Longitude and Latitude of cell center

File Grid025_QUAD_HDF5.txt: geographic information about the grid; only the coordinates of the cell corners are provided.

Column	Variable	Delimiter	Value	Description
1	String	":"	ID	Cell unique identifier

2	Float	","	LatUL	Latitude of cell upper-left corner
3	Float	","	LonUL	Longitude of cell upper-left corner
4	Float	","	LatUR	Latitude of cell upper-right corner
5	Float	","	LonUR	Longitude of cell upper-right corner
6	Float	","	LatLR	Latitude of cell lower-right corner
7	Float	","	LonLR	Longitude of cell lower-right corner
8	Float	","	LatLL	Latitude of cell lower-left corner
9	Float	"EOR"	LonLL	Longitude of cell lower-left corner

File Grid025_FAULTS_HDF5.txt: Fault kinematics in each cell of the grid obtained from the crustal fault datasets (EDSF, DISS, ASTARTE). The kinematic values are given by strike, dip, rake. To deal with the possible presence of multiple faults in the same cell, the kinematic values are associated to a weight derived from the relative moment rate expressed by the portion of all the faults the falls within each grid cell.

Column	Variable	Delimiter	Value	Description
1	String	":"	ID	Cell unique identifier
2	Integer	","	NValues	Number (N) of fault kinematics values to follow in 3
3	String	"," & "EOR"	Kinematics	N quadruplets of Strike-Dip-Rake-Weight separated by blanks

Discretization of PS and SPS

This section illustrates the formats of the files used for the three-dimensional discretization of the PS and SPS sources, of either subduction or crustal type. In these files all geographic coordinates are given as Lat/Lon, positive N/E, Datum WGS84. The subduction interfaces are composed by triangular meshes, whereas crustal sources are composed by combinations of rectangles. Since the combination of rectangular elements for crustal sources is dependent from the modeled earthquake magnitude, the corresponding files are called “scenarios” and contain the full set of parameters to simulate the earthquake rupture.

Files CaA_tsumaps_mesh.inp, HeA_tsumaps_mesh.inp, CyA_tsumaps_mesh.inp, and CrA_tsumaps_mesh.inp provide the mesh geometry of subduction interfaces. They are composed of two main data sections: the first section provides the collocation of triangle nodes; the second section provides the association between nodes and triangular elements. The two sections are preceded by an unspecified number of heading lines and followed by Unspecified number of trailing lines. The two data sections can be identified by the keyword: *NODE and the Keyword: *ELEMENT.

Section *NODES

Column	Variable	Delimiter	Value	Description
1	Integer	“blk”	ID	Identifier of mesh nodes.
2-3	Float	"blk"	Lon Lat	Longitude and latitude of mesh nodes, in decimal degrees.
4	Float	"EOR"	Depth	Depth of mesh nodes, below sea level, in meters.

Section *ELEMENT

Column	Variable	Delimiter	Value	Description
1	Integer	“blk”	ID	Identifier of mesh element (triangle).

2-4	Integer	"blk, EOR"	ID	Identifier of mesh nodes that compose the element (triangle).

Snippet

```
….
*NODE, NSET=ALLNODES
       1,    1.62830727750938E+01,    3.98362107284888E+01,    -3.096829E+04
       2,    1.60665989430604E+01,    3.99030028605239E+01,    -3.697633E+04
       3,    1.61974141941471E+01,    3.97950511328749E+01,    -3.295673E+04
       4,    1.63253557262817E+01,    3.97079144861906E+01,    -2.906385E+04
….
*ELEMENT, TYPE=STRI3, ELSET=EB1
       1,       1,       2,       3
       2,       4,       1,       3
….
```

Files CaA_tsumaps_attributes.txt, HeA_tsumaps_attributes.txt, CyA_tsumaps_attributes.txt, and CrA_tsumaps_attributes.txt provide the necessary attributes of all nodes. The node position (coordinates) are the same as in the mesh geometry files.

Column	Variable	Delimiter	Value	Description
1-2	Float	"blk"	Lon Lat	Longitude and latitude of mesh nodes, in decimal degrees.
3	Float	"blk"	Depth	Depth of mesh nodes, below sea level, in meters.
4-6	Float	"blk"	Kinematics	Strike, dip, and rake of mesh nodes, in degrees, following the right-hand rule.
7	Float	"EOR"	Elevation	Top-bathymetric elevation of the Earth's surface in correspondence of the mesh nodes, in meters.

Snippet:

```
16.28307278 39.83621073 -30968.29 17.47 188.93 69.82183439 933
16.06659894 39.90300286 -36976.33 18.01 184.01 65.12616994 1355
16.19741419 39.79505113 -32956.73 17.96 183.9 65.01338152 360
```

Files CaA_Nucl, CaA_Prop, HeA_Nucl, HeA_Prop, CyA_Nucl, CyA_Prop provide the geometry of nucleation and propagation polygons.

Column	Variable	Delimiter	Value	Description
1-2	Float	"blk"	Lon Lat	Longitude and latitude of polygon nodes, in decimal degrees.

Snippet

```
  15.26494   38.10693
  15.26532   37.99374
  15.47622   37.84667
```

Files MidAtlanticNN_Scenarios.txt, MidAtlanticSS_Scenarios.txt, and GloriaFault_Scenarios.txt provide the location, geometry and parameters of crustal faults modelled as PS or SPS.

Column	Variable	Delimiter	Value	Description
1	String	":"	ID	Scenario unique identifier
2	Float	","	Lon Lat	Longitude and Latitude of scenario center

3	String	","	ID	Region unique identifier
4	Float	","	Mw	Moment magnitude of the scenario
5	Float	","	M0	Seismic Moment of the scenario
6	Integer	","	Subfaults	Number of subfaults for the scenario
7	Float	","	Area*	Total area of subfaults of the scenario
8	Float	","	Slip*	Average seismic slip of the scenario
9	String	"EOR"	IDs	Unique identifiers of subfaults involved in the scenario (= tsunami model ID)

* Notice: this is the area resulting from the sum of subfaults, the slip is derived from seismic moment and area using rigidity of 33 GPa consistently with Leonard (2014) fault scaling laws.

Snippet

```
W01487N6994:-14.867  69.938,W01908N7103W01380N6733,7.928,9.93e+20,5,9000,3.34,N00101
N00102 N00103 N00104 N00105
W01525N6958:-15.252  69.584,W01908N7103W01380N6733,7.928,9.93e+20,5,9000,3.34,N00102
N00103 N00104 N00105 N00106
W01565N6923:-15.653  69.234,W01908N7103W01380N6733,7.928,9.93e+20,5,9000,3.34,N00103
N00104 N00105 N00106 N00107
```

1.1.8) Separation of the observed seismicity within the seismicity modeling types.

There are two datasets.

The first dataset is formed by four files. There are eleven columns in each file. The first ten columns are data about the earthquake: location date, time, and magnitude. The eleventh column indicate if the earthquake belongs to PS or BS source modeling type.

The file names are as follows:

1. BSPS_separation_EMEC_5km.dat
2. BSPS_separation_EMEC_10km.dat
3. BSPS_separation_ISC_5km.dat
4. BSPS_separation_ISC_10km.dat

The file name contains the name of the earthquake catalog and the PS/BS separation distance (5 km or 10 km).

Column	Variable	Delimiter	Value	Description
1	Float	"tab"	Lon	Longitude of the earthquake epicenter
2	Float	"tab"	Lat	Latitude of the earthquake epicenter
3	Float	"tab"	Year	Date of the earthquake, calendar year
4	Float	"tab"	Month	Date of the earthquake, month, NaN if absent
5	Float	"tab"	Day	Date of the earthquake, day, NaN if absent
6	Float	"tab"	Magnitude	Moment magnitude (Mw)
7	Float	"tab"	Depth	Hypocenter depth in km
8	Float	"tab"	Hour	Time of the earthquake, hour, NaN if absent
9	Float	"tab"	Minute	Time of the earthquake, minute, NaN if absent
10	Float	"tab"	Second	Time of the earthquake, second, NaN if absent
11	Float	"EOR"	BS/PS	Positive, 10.000000 = PS; Negative, -10.000000 = BS

The second dataset is formed by four files. There are 17 columns in each file. The first ten columns are data about the earthquake: location date, time, and magnitude. The following six columns are the angles of the nodal planes. The 17th column indicate if the earthquake belongs to PS or BS source modeling type.

The file names are as follows:

5. BSPS_separation_GCMT_5km.dat
6. BSPS_separation_GCMT_10km.dat
7. BSPS_separation_RCMT_5km.dat
8. BSPS_separation_RCMT_10km.dat

The file name contains the name of the focal mechanism catalog and the PS/BS separation distance (5 km or 10 km).

Column	Variable	Delimiter	Value	Description
1	Float	"tab"	Lon	Longitude of the earthquake epicenter
2	Float	"tab"	Lat	Latitude of the earthquake epicenter
3	Float	"tab"	Year	Date of the earthquake, calendar year
4	Float	"tab"	Month	Date of the earthquake, month, NaN if absent
5	Float	"tab"	Day	Date of the earthquake, day, NaN if absent
6	Float	"tab"	Magnitude	Moment magnitude (Mw)
7	Float	"tab"	Depth	Hypocenter depth in km
8	Float	"tab"	Hour	Time of the earthquake, hour, NaN if absent
9	Float	"tab"	Minute	Time of the earthquake, minute, NaN if absent
10	Float	"tab"	Second	Time of the earthquake, second, NaN if absent
11	Float	"tab"	Strike1	Strike of first nodal plane, in degrees
12	Float	"tab"	Dipè1	Dip of first nodal plane, in degrees
13	Float	"tab"	Rake1	Rake of first nodal plane, in degrees
14	Float	"tab"	Strike2	Strike of second nodal plane, in degrees
15	Float	"tab"	Dip2	Dip of second nodal plane, in degrees
16	Float	"tab"	Rake2	Rake of second nodal plane, in degrees
17	Float	"EOR"	BS/PS	Positive, 10.000000 = PS; Negative, -10.000000 = BS

1.2) STEP 2:

1.2.1) Crustal elastic model

- CRUST 1.0 https://igppweb.ucsd.edu/~gabi/crust1.html

1.2.2) Topo-bathymetric datasets and digital elevation models

- ETOPO1 https://www.ngdc.noaa.gov/mgg/global/
- SRTM 30+ and SRTM 15+ http://topex.ucsd.edu/WWW_html/srtm30_plus.html
- Zitellini et al. (2009), Appendix A, https://doi.org/10.1016/j.epsl.2008.12.005 or direct download from https://ars.els-cdn.com/content/image/1-s2.0-S0012821X0800753X-mmc1.zip

1.2.3) Points of Interest (POIs)

File tsumaps_all_poi.txt format:

Column	Variable	Delimiter	Value	Description

1	String	"blk"	ID	POI unique identifier
2	Integer	"blk"	Code	Code North-eastern Atlantic = 0; other Seas = 1.
3-4	Float	"blk"	Lon Lat	Longitude and latitude of POI, in decimal degrees.
5	Float	"EOR"	Depth	Depth of POI, below sea level, in meters.

1.3) STEP 3:

1.3.1) Topo-bathymetric datasets and digital elevation models

They are the same as those listed in STEP 2 (Section 1.2.2)

1.3.2) Bathymetric transects

This is a package of GIS files in the ESRI shapefile format. Like many standard GIS files, the shapefile is composed by a suite of files with the same name and different extensions, namely ".shp", "sbx", "sbn", "dbf", "prj". (see ESRI 1998, ESRI Shapefile Technical Description downloadable from https://support.esri.com/en/white-paper/279).

In each shapefile there is a set of profiles. Each profile corresponds to a polyline composed by a variable number of almost equally-spaced nodes. The profile elevation is sampled from the bathymetry datasets (Section 1.3.1) at each of these nodes. These files are named after the POI unique identifier to connect each profile set to a single POI and set of amplification factors (see Sections 1.2.3 and 1.3.3).

1.3.3) Amplification factors

File poi_AF_sm.lst format:

Column	Variable	Delimiter	Value	Description
1	String	"tab"	ID	POI unique identifier
2	String	"tab"	lead	Polarity of leading wave: "neg" for negative.
3-9	Float	"tab"	120, 200, 300, 600, 1000, 1800, 3600	Wave period (T) in seconds
10	String	"tab"	lead	Polarity of leading wave: "pos" for positive.
11-17	Float	"tab, EOR"	120, 200, 300, 600, 1000, 1800, 3600	Wave period (T) in seconds

1.4) STEP 4:

1.4.1) Weight assessment based on the elicitation of experts

There are 27 files, each file addressing the weights of a different alternative of the event tree. The list of file names follows below.

1. TSUMAPS_weights_BS-1_Magnitude.txt #1
2. TSUMAPS_weights_BS-2_Position.txt #1
3. TSUMAPS_weights_BS-3_Depth.txt #2
4. TSUMAPS_weights_BS-4_FocalMechanism.txt #1
5. TSUMAPS_weights_BS-5_Area.txt #2
6. TSUMAPS_weights_BS-6_Slip.txt #2

7. TSUMAPS_weights_PS-1_Magnitude.txt #1
8. TSUMAPS_weights_PS-2_PositionArea.txt #1
9. TSUMAPS_weights_PS-3_Slip.txt #2
10. TSUMAPS_weights_PSMar-1_Magnitude.txt #1
11. TSUMAPS_weights_PSMar-2_PositionArea.txt #2
12. TSUMAPS_weights_PSMar-3_Slip.txt #2
13. TSUMAPS_weights_PSSlip-1_Magnitude.txt #1
14. TSUMAPS_weights_PSSlip-2_PositionArea.txt #1
15. TSUMAPS_weights_PSSlip-3_Slip.txt #2
16. TSUMAPS_weights_SBS-1_Magnitude.txt #1
17. TSUMAPS_weights_SBS-2_Position.txt #2
18. TSUMAPS_weights_SBS-3_Depth.txt #2
19. TSUMAPS_weights_SBS-4_FocalMechanism.txt #2
20. TSUMAPS_weights_SBS-5_Area.txt #2
21. TSUMAPS_weights_SBS-6_Slip.txt #2
22. TSUMAPS_weights_SPS-1_Magnitude.txt #1
23. TSUMAPS_weights_SPS-2_Position.txt #2
24. TSUMAPS_weights_SPS-3_Depth.txt #2
25. TSUMAPS_weights_SPS-4_FocalMechanism.txt #2
26. TSUMAPS_weights_SPS-5_Area.txt #2
27. TSUMAPS_weights_SPS-6_Slip.txt #2

They are all ASCII files but are written in two different formats.

Ten of these files (identified by #1) have two rows, each row dedicated to the weights relative to the BS/PS separation (see Section 1.1.8) of 5 km and 10 km. Each row starts with a label that identifies the separation model, followed by a series of space-delimited numbers, in scientific notation. Each number is the weight of an event-tree branch.

Snippet

```
PS05km: 5.2364e-05  5.2364e-05  5.2364e-05 …
PS10km: 8.3497e-05  8.3497e-05  8.3497e-05 …
```

The remaining 17 files (identified by #2) are used to assign the same weight, equal to 1, to all branches of the event tree. The has only one row containing a label followed by the number 1.

Snippet

```
ALL: 1
```

1.4.2) Tsunami DB

- Euro-Mediterranean Tsunami Catalogue
  http://roma2.rm.ingv.it/en/facilities/data_bases/52/euro-mediterranean_tsunami_catalogue

2) Codes

In this section, the most relevant codes, tools and software used or developed in the frame of TSUMAPS-NEAM project are listed and briefly described and/or referenced. This section should be considered as a work in progress because changes to the organization of the codes may be modified to improve their ease of use, particularly in view of successive potential uses, even outside the project scopes.

2.1) Directory Structure

2.1.1) Project configuration

The main configuration file is the INI file located at TSUMAPS/project_def.txt. Configuration is parsed using the configobj [1] Python module and it defines most of the relevant aspect of the the modeled domain, including:

- the adopted regionalization;
- the metrics to compute the hazard;
- the implemented seismicity classes;
- the structure of the event trees used for each seismicity class;
- the discretization, the data and probability dependencies for each level of the event trees;
- the points of interest list;
- the alternatives discretization models to use building the event trees;
- the random seed used when computing the probabilistic ensembles.

It worth noticing that six different seismicity classes and event trees are defined here: this is due to different treatment of initial conditions and elementary sources linear combinations, particularly among PS/PSSlip/PSMar/SPS classes, as documented later.

2.1.2) Program sources and binaries

Directory structure

```
TSUMAPS
├── bin
├── data
│   └── [...]
├── results
│   └── [...]
└── src
    ├── PySPTHA
    └── [...]
```

The executable programs are collected in bin/ while the the PySPTHA library is located under the src/PySPTHA directory, with its own directory structure to host the Python package necessary virtual environment (python_tsumaps.env) and files. The Python script we use to manage the data and compute the hazard are in src/PySPTHA/bin directory and the conda virtual environment has to be created and activated to successfully execute them.

2.1.3) Data

Directory structure

```
TSUMAPS
```

```
├── bin
├── data
│   ├── discretizations
│   ├── catalogues
│   │   ├── faults
│   │   ├── earthquakes
│   │   │   └── completeness
│   │   ├── focalmechanisms
│   │   ├── topobathymetric
│   │   └── tsunamis
│   ├── faults
│   ├── forecastpoints
│   ├── gf
│   ├── GGF
│   ├── metrics
│   │   └── uncertainty
│   ├── models
│   │   └── weights
│   └── regionalizations
├── results
│   └── [...]
└── src
    └── [...]
```

The data directory is where all the data necessary to compute scenarios, annual rates, probabilities, metrics and final hazard is located. In this context we define 'Data' as everything that is not computed by the programs documented here, including:

- catalogues:
- discretizations: all files describing the discretization defined for all trees' levels are collected here;
- forecastpoints: the list of the points of interest, containing names and coordinates,
- GF: Green's Functions, a method to model tsunami scenarios by linear combinations of unit sources
- GGF: Gaussians Green's Functions, a set of elementary sources with a 2D Gaussian shape used to model tsunami scenarios using the GF approach;
- metrics: defined thresholds, metrics discretization and relative uncertainty;
- models: model weights to use during probabilistic ensembles;
- regionalizations: the regionalizations of domain area.

2.1.4) Project final and intermediate results

Directory structure

```
TSUMAPS
├── bin
├── data
│   └── [...]
├── results
│   ├── event_trees
│   │   └── frequencies_trees
│   ├── step1
│   │   ├── longterm
│   │   ├── initial_conditions
│   │   └── scenarios
```

```
│   ├── step2
│   ├── step3
│   │   ├── mih
│   │   └── poi_cond_unc_indexes
│   └── step4
│       ├── poi_hc
│       └── hazard_curves
└── src
    └── [...]
```

In results/ are collected all the output produced by computation steps. While in subsequent sections the output formats will be described in detail, it is important to note here the event_trees/ directory that contain all the HDF5 files, one per region per seismicity class. These files are used by PySPTHA as local databases to store probabilities and MIH values. This intermediary step is necessary because of the size of scenarios lists (~10^7 scenarios) and resulting file size and memory footprint of the running code.

2.1.5) Execution workflow

The general workflow is summarized in the schema of FIGURE 2.1 and it is detailed in the following Chapters. Note that codes do not have one-to-one correspondence with the STEPs defined in the project workflow and that this document will follow closely the code, to serve as a guide to reproducibility of the obtained results.

2.2) Probabilistic source model

2.2.1) Input

(A) Regionalization

```
<reg_id>:<reg_name>:<seis_class1>,..,<seis_classN>:<vert1>,..,<vertN>
```

Snippet

```
E01964N3926E02184N3685: Kefalonia Lefkada: 1, 2: 19.64 37.6611,...
E01598N4052E01840N3892: Calabrian Arc North: 1: 16.258 40.5105,...
W02533N3777W00789N3522: Gloria: 1, 5, 6: -25.3306 36.8887,...
```

In the regionalization file, like a .csv file, each line defines a single region element. Two fields separators are defined: ':' is used between the fields, while ',' is used to list elements within a field. The defined fields are:

- <reg_id>: an alphanumeric unique id used to identify each region, obtained concatenating the coordinates of zone edges (west-north-east-south). During steps 2 and 3 is also used a numeric id (see Section 1) to ease referring to a zone;
- <reg_name>: a mnemonic name with no restrictions;
- <seis_class$_1$>,..,<seis_class$_N$> : the id list of seismicity classes modeled in the region;
- <vert$_1$>,..,<vert$_N$> : the vertex list for the region shape (list of lon lat coordinates)

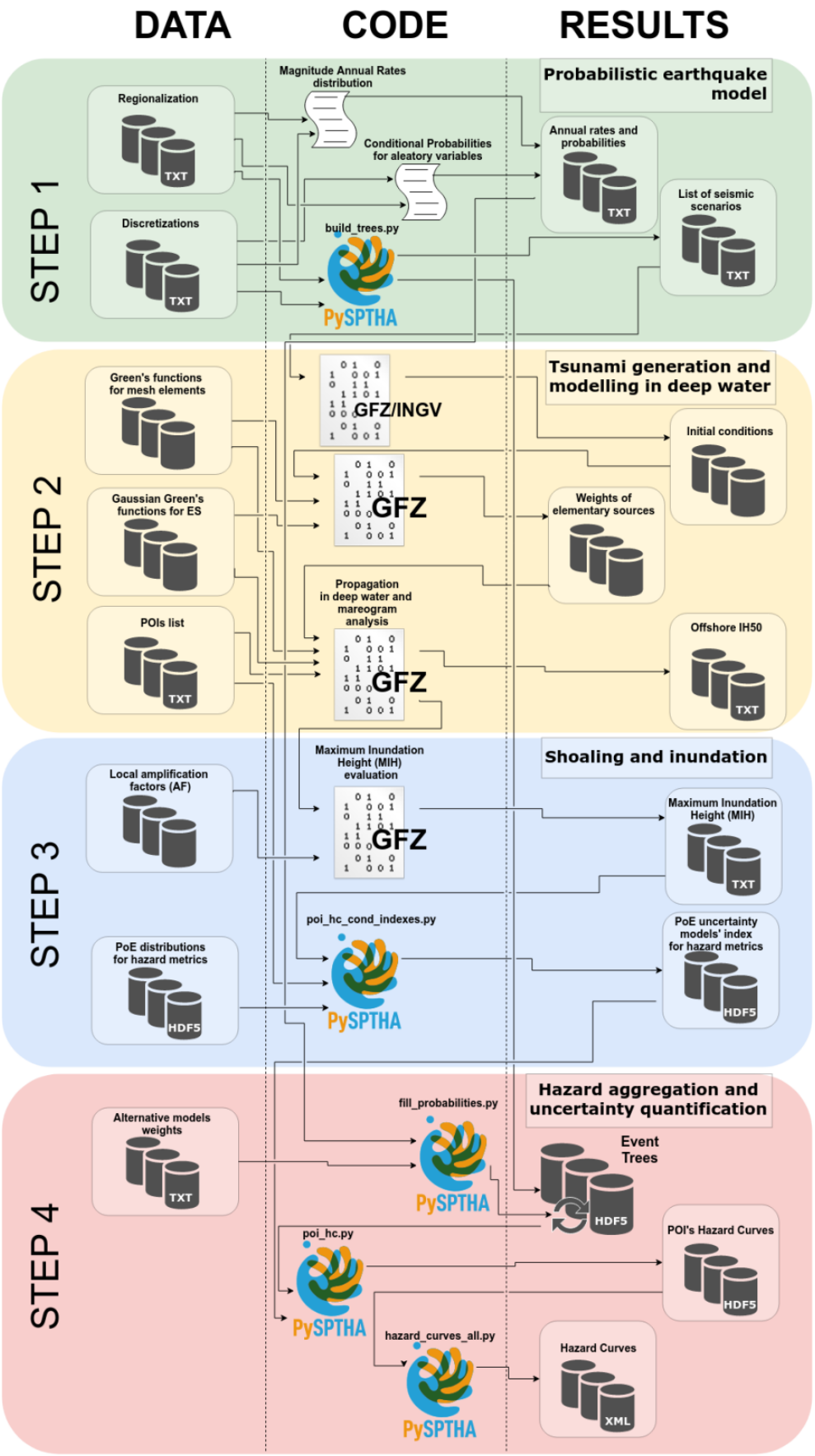

FIGURE 2.1: Workflow of the hazard computation platform.

(B) Discretizations

A discretization file is created in the TSUMAPS/data/discretizations for every Event Tree level defined in project configuration. Different formats can be used according to possible combinations of DiscretizationDependencies, Alternatives (if applicable) and variable length parameters (e.g. mesh's elements slip values). The separators are defined as following:

- ":" between element's label and values;
- "_" to separate different id in element's label;
- "," to separate different discretizations steps;
- "[]" to group alternatives in step definition;
- "|" to separate among alternatives;
- "()" to group list elements in values definitions;
- " " to separate values for different variables.

Some examples are provided below:

- No dependencies/no alternatives

Discretization file for BS-2_Position.txt:

```
E00667N4007: 6.67277 40.0754
E00820N3692: 8.20317 36.9278
E02216N3040: 22.1607 30.4077
```

- Dependencies / no alternatives

Discretization file for BS-3_Depth.txt (multiple steps per line):

```
M732_W00441N5154: 1.00, 7.62, 14.23, 20.85
M754_W00441N5154: 1.00, 9.13, 17.25
M774_W00441N5154: 1.00, 10.79
```

Discretization file for BS-4_Area.txt (single step per line):

```
E01470N3877E01631N3641_M600_S022D70R090: 100.876 11.370
E01470N3877E01631N3641_M600_S022D70R180: 88.263 12.525
```

- Dependencies / Alternatives

Discretization file for PS-2_PositionArea.txt (multiple alternatives and lists):

```
M600_E01516N3813: 15.16 38.13 [10.78 15.95 (269 270)|…|… ]
M600_E01520N3807: 15.20 38.07 [10.789 15.959 (270 274)|…|… ] M600_E01526N3816:
15.26 38.16 [10.789 15.959 (877 272)|…|… ] M600_E01530N3804: 15.30 38.04 [10.789
15.959 (274 271 272)|…|… ]
```

2.2.2) Code

(C) Annual Rates (Level 1 of Event Trees: BS-1, PS-1, SBS-1)

Workflow:

1. *MainMCMC_Model_1.m, MainMCMC_Model_2.m, MainMCMC_Model_3.m, MainMCMC_Model_4.m (Generation of Annual Rates for Bayesian Models)*
2. *BSPSseparation.m (Generation of Bayesian probability for separating BS and PS in regions)*
3. *freqmagPostproc.m (Generation of Annual rates for Davies' models and postprocessing, preparing input for PyPTHA)*

Name: MainMCMC_Model_1.m, MainMCMC_Model_2.m, MainMCMC_Model_3.m, MainMCMC_Model_4.m

Short description: These scripts implement the Bayesian estimation of the parameters for the total frequency-magnitude distribution in each region, before the potential separation between PS, BS and SBS. Models 1 to 4 are respectively: Tapered Pareto and beta from data; Tapered Pareto and beta set to 2/3; Truncated Pareto and beta from data; Truncated Pareto and beta set to 2/3 (see Technical documents for more details). The programs read the seismic catalogs, fit the Bayesian models, and provide in output 1000 samples of model's parameters for each region.

Parallelization: none

Input: Seismic catalogs; regionalization and discretizations.

Output: 1 text file per region, containing 1000 alternative model's parameters. The output files are in the same folder of the script.

Position in file system: subfolder of `TSUMAPS/src/Step1_Lev1-BSPS_freqMag`: regFreq_weichart/Mod1_50_compl, regFreq_weichart/Mod2_50_compl, regFreq_weichart/Mod3_50_compl, regFreq_weichart/Mod4_50_compl

Programming language: Matlab

Name: BSPSseparation.m

Short description: It implements a Bayesian model to sample the potential models for separating BS from PS/SBS. The model is equal for all the regions, but the input parameters differ. In each region, the model is run 2 times, adopting two alternative input catalogs, for 5km and 10km buffers (see Technical documents for more details). *Parallelization:* none

Input: Seismic catalogs; regionalization and discretizations.

Output: 1 file containing the magnitude levels for the computation and 1 text file per region containing 1000 alternative probabilities for BS/PS-SBS separation; the results are in subfolders output_03-Nov-2017/5km and output_03-Nov-2017/10km, for the two alternative buffer choices.

Position in file system: subfolder of TSUMAPS/src/Step1_Lev1-BSPS_freqMag : BSPSseparation/BSPSseparation.m

Programming language: Matlab

Name: freqmagPostproc.m

Short description: It reads the output of models (Davies' and Bayesian models and BSPSseparation.m) and it prepares the input for the PySPTHA for Level 1 of the event trees of all the seismicity types. In parallel, it prepares the ground for the sanity checks (figures and input for N-test).

Parallelization: none

Input: regionalization and discretizations; output of MainMCMC_Model_1.m, MainMCMC_Model_2.m, MainMCMC_Model_3.m, MainMCMC_Model_4.m, BSPSseparation.m; parametric information for Davies's models (daviesParChr.mat and daviesParTru.mat, prepared by readIndependentPar.m).

Output: annual rates output file of Section 2.3.1 (one text file per region and seismicity type); png figures with annual rates in each region, compared with input data; text files for N-test (sanity check). All the output files are in subfolder output_final_revised_MagIntResampled.

Position in file system: TSUMAPS/src/Step1_Lev1-BSPS_freqMag

Programming language: Matlab

(D) Probabilities

Probability models are required at all the levels of all event trees, except for level 1 (for which, annual rates are computed, see Section 2.2.2). In the following, the different scripts used at the different levels are reported in subparagraphs.

Spatial probability of BS (Level 2 of BS Event Tree)

Workflow:

1. *ScriptAdaptiveGlobal.m (Generation of Smoothed seismicity Models)*
2. *postProc.m (Postprocessing, preparing input for PyPTHA)*

Name: ScriptAdaptiveGlobal.m

Short description: It reads the catalogs for BS seismicity, and it implements a smoothed seismicity models with adaptive kernel, set as in SHARE. See Technical documents for more details.

Parallelization: none

Input: regionalization and discretizations; grid extending the spatial discretization of BS in order to completely cover all the regions (not only where tsunamis are generated at STEP 2).

Output: AdaptiveSmoothing_BS_5km.txt and AdaptiveSmoothing_BS_10km.txt, containing coordinates of the grid points and the computed rate of the smoothed seismicity. The output is in the same folder of the script.

Position in file system: TSUMAPS/src/Step1_Lev2-BS_xy

Programming language: Matlab

Name: postProc.m

Short description: It reads the output of postProc.m and it prepares the input for the PySPTHA for Level 2 of the event trees of BS type.

Parallelization: none

Input: regionalization and discretizations; output of postProc.m.

Output: probability output file of Section 2.3.1 (one text file per region, only where BS is present); png figures with annual rates and not selected grid points. The output is in the folder output_final.

Position in file system: TSUMAPS/src/Step1_Lev2-BS_xy

Programming language: Matlab

Fault mechanism probability of BS (Level 4 of BS Event Tree)

Name: anglesProb.m

Short description: It implements the Bayesian model for strike, dip and rake angles, to be applied to BS seismicity. The prior is based on global data (internal input) for each tectonic regime, and on RCMT and GCMT (RCMT in the Mediterranean and GCMT in the Atlantic, same division of seismicity catalogs EMEC/ISC) in each region. The likelihood is based on the faults in each cell of the grid. See Technical documents for more details. It prepares the input for the PySPTHA for Level 4 of the event trees of BS type, and for few other sanity checks.

Parallelization: none

Input: regionalization and discretizations; focal mechanism and fault catalogs.

Output: probability output file of Section 2.3.1 (one text file per region, only where BS is present); text files for sanity checks. The output is in the folder TSUMAPS/results/step1/longterm/BS-4_FocalMechanism/.

Position in file system: TSUMAPS/src/Step1_Lev4-BS_angles

Programming language: Matlab

Depth probability of BS (Level 3 of BS Event Tree), area/spatial probability of PS seismicity (Level 2 of PS Event Tree) and slip distribution of PS seismicity (Level 3 of PS Event Tree).

If the probability of the value of a parameter is depending just on aleatory variability, Jupyter notebooks are used to generate probability files according the defined discretizations. For example, this is the case for depth values in background seismicity (BS-3_Depth) or positions along the defined unmodeled faults (SBS-2_Position). Slip distribution (PS-3_Slip) is somehow a particular case: the conditional probability stored in this file is always 1 and in case more than one distribution is defined in discretization files (e.g. stochastic slip distributions for high magnitude in the Mediterranean arcs) a uniform distribution is then created by fill_probabilities.py when populating HDF5 files probabilities.

The file creation is done mainly interactively using the notebooks stored in TSUMAPS/src/PySPTHA/examples/ and named after the respective seismicity class (e.g. SBS_discr_probs_misc.ipynb)

(E) PySPTHA: build_trees.py

Name: build_trees.py

Short description: This program reads all the discretization files relevant to a specific region and seismicity class, combining them to obtain the resultant Event Trees. Usually an instance of this program is run for every seismicity class / region, to parallelize and great improvement to program performance.

Parallelization: per (seismicity class,region) pair.

Input: Regionalization, discretizations and TSUMAPS configuration file.

Output: one HDF5 file and list of scenarios per (seismicity class, region) pair.

Position in file system: TSUMAPS/src/PySPTHA/bin

Programming language: Python3

(F) Initial conditions code

We have different procedures depending on the class of seismicity.

BS/SBS/SPS classes:

For these seismicity classes there is no a specific code producing explicit outputs with the tsunami initial condition, but there is some function based on Okada (1992) elastic dislocation model and Kajiura (1963) filtering theory implemented in the suite of codes described in weights and linear combination sections.

PS class:

Workflow:

1. *k223d.f90 (Selection of triangular elements of the mesh involved in each rupture and calculation of slip on each of them)*
2. *make_init_cond_ps.py (Computation of tsunami initial condition by combining contribution of slip on each mesh's triangular element and application of Kajura's filter)*

Name: k223d.f90

Short description: Reads the mesh discretization for the subduction zones referred to as Predominant Seismicity (PS). For each magnitude range and for each sub-class (different scaling laws, shallow propagation yes/no) it selects the triangular elements involved in the scenario. It then computes k^{-2} slip distributions based on the pre-imposed rigidity profile.

Parallelization: for each magnitude/sub-class

Input: mesh discretization for the Mediterranean PS

Output: vtk files containing the slip distributions for all the used scenario for the Mediterranean PS

Position in file system: TSUMAPS/src

Programming language: Fortran90

Name: make_init_cond_ps.py

Short description: Reads mesh characteristics and attributes, reads the slip produced by each scenario and sum their contribution. Then applies the Kajura's filters to simulates the physical attenuation of the short wavelengths through the water column and save a NetCDF files containing the tsunami initial condition.

Parallelization: for each earthquake/rupture (using the script run_ps_init_cond.sh)

Input: Mesh of the PS source, mesh's attributes and slip distribution for each mesh element.

Output: NetCDF containing water displacement at origin time

Position in file system: TSUMAPS/src/

Programming language: Python3

PSMar/PSSlip

N/A since elementary sources are propagated and directly linearly combined without using the procedure which reproduces the tsunami initial conditions used with GGF.

2.2.3) Output

(G) Annual rates / Probabilities

Annual rates are used at Level 1 of the event trees, while probabilities are used in all the other levels. Annual rates and probabilities files' format is similar to the one defined for discretizations, with labels and values, but simplified due to the absence of alternatives and lists support.

The files are created per region in a subdir of TSUMAPS/results/step1/longterm named after the Event Tree level. Probability values are in variable number according to used alternative models (and models types):

The separators are defined as following:

- ":" between discretization step label and probabilities;
- "_" to separate different id in steps' label;
- "," to separate different model types;
- " " to separate between models' probabilities.

Some examples are provided below:

- Annual rates (Level 1) file for E01548N3896E01854N3659_PS-1_Magnitude:

```
M600:0.00086497 … ,0.00165890 …
M650:0.00037156 … ,0.00054977 …
M680:0.00024346 … ,0.00030587 …
M707:0.00015526 … ,0.00016842 …
```

- Probabilities (Level > 1) file for W00129N4390E00919N3644_BS-3_Depth:

```
M600_E01492N3850_D166: 0.142857
M600_E01492N3850_D198: 0.142857
M650_E01492N3850_D010: 0.250000
```

(H) Scenarios lists

Scenarios lists are located under TSUMAPS/results/step1/scenarios/ in directories named after the seismicity class in exam. Two files for every relevant region:

- Indexing files (TSUMAPS_indexing_<seisclass>_<reg_id>) establishing a correspondence between the scenario's long id derived from event Tree with a short numeric id used in step2-3 computation. E.g.:

```
# scenario_id: zone_index seismicity_type_index scenario_index
E00197N5793E02760N4372-BS-M600_E00951N4771_D010_S022D10R270_A056_S06: 43 1 1
E00197N5793E02760N4372-BS-M600_E00951N4771_D010_S022D30R090_A056_S06: 43 1 2
E00197N5793E02760N4372-BS-M600_E00951N4771_D010_S022D30R270_A056_S06: 43 1 3
```

- Parameters files (TSUMAPS_parameters_t<seisclass_idx>_z<reg_idx>) establishing a correspondence among the scenario's short id and the parameters whose describe the scenario, e.g.:

```
# scenario_id: mag lon lat depth strike dip rake area length slip
43 1 1 :  6.0 9.51678 47.7196 1.00 22.5 10 90 56.467 10.181 0.675
43 1 2 :  6.0 9.51678 47.7196 1.00 22.5 30 -90 56.467 10.181 0.6755
43 1 3 :  6.0 9.51678 47.7196 1.00 22.5 30 90 56.467 10.181 0.675
```

(I) HDF5 Structure

HDF5 files are used as local hierarchical databases to store scenarios' annual rates and probabilities (and their alternative quantifications due to epistemic uncertainty), avoiding data replication. One file is defined for each modeled [seismicity-class, region] pair and the internal structure depends on the event tree structure described in the project configuration.

Ideally every single .hdf5 contains all the metadata needed to reconstruct the modeled scenarios, the region, the seismicity class, etc. The following attributes are stored in the root node of every tree:

- etree_version: a version number to keep track of possible development;
- levels: space separated list of levels as named in configuration file;
- project_name: 'TSUMAPS' in this case;
- region_id: the semantic id of the region;
- region_idx: the numeric short id of the region;
- region_name: the mnemonic free text name of the region;
- region_polygon: the polygon of the region (well-known text format, WKT);

- seismicity_type: the abbreviation of seismicity class;
- seismicity_type_idx: the short numeric id of the seismicity clas.

For all levels, every discretization step is stored as a 'group' and its parameters values as attributes of the node. Eg. in the BS-2_Position level, two attributes are defined, longitude and latitude.

Two more attributes are defined for every node in the trees and they are filled during the step4:

- probabilities containing the frequency or the conditioned probability sample of the node;
- probability_model_types: containing indexes of all sampled models and used to ensure that different model types are not mixed when computing scenarios annual rates.

Taking advantage of the hierarchical structure of the tree, it is possible to read all the parameters describing a specific scenario by navigating the corresponding branch in the .hdf5 file and to compute the annual rates by multiplying the probabilities array encountered along the branch path from the root to the selected leaf.

(J) Initial conditions

BS/SBS/SPS classes:

No explicit output is produced by procedures which calculate the tsunami initial conditions

PS class:

NetCDF matrix containing a regular grid with longitude (decimal degrees), latitude (decimal degrees) and water displacement (in meters).

PSMar/PSSlip

N/A since elementary sources are propagated and directly linearly combined without using the procedure which reproduces the tsunami initial conditions used with GGF.

2.2.4) Sanity checks

Sanity check reports are (currently) located in: @Dropbox/TSUMAPS_Phase2_reporting/.

(K) Seismic rates

Statistical tests checking the consistency of the seismic source model applied in TSUMAPS with observations were performed performing (retrospective) N- and S-tests on input data, as well as on independent data. Other visual sanity tests were performed directly on the figures produced by the codes, as discussed in Sections 2.3.1 and 2.3.3. The code for N-Test can be found in a subfolder of the Annual Rates codes of Section 2.3.1, in subfolder SanityChecks/. The code for S-Test can be found in a subfolder of the Annual Rates codes of Section 2.3.2.1, in subfolder SanityChecks/.

The results are reported in the technical document of sanity checks currently located in: @Dropbox/TSUMAPS_Phase2_reporting/ DocSan/DocSan_2018_R2/DocSanSeisMod.

(L) Seismicity mechanism

A visualization and comparison of the TSUMAPS seismicity mechanism assumptions is made in: @Dropbox/TSUMAPS_Phase2_reporting/DocSan/DocSan_2018_R2/DocSanMech.

2.3) Propagation in deep water and amplification

In the TSUMAPS-NEAM computations of deep-water propagation was organized in three different ways depending on the type of a source zone:

1. *background seismicity (BS, SBS, and SPS types) – implementing single-fault uniform-slip Okada model combined with pre-computed propagation Green's functions for elementary Gaussian-shaped surface sources;*
2. *predominant seismicity (PS type) – implementing distributed slip along curved plate-boundary interfaces together with the same Green's functions for Gaussian-shaped sources;*
3. *predominant seismicity in the far field (PSSlip and PSMar types) – classical Green's functions approach – implementing distributed slip along the set of bured elementary faults together with pre-computed tsunami Green's functions pre-computed for each of the elementary faults.*

This Chapter describes the organization of computations for the most common cases encompassing >90% of all computations, namely, the case of 'background sesimicity' (BS): type (1) from the listing above. Processing differences/alternatives, specific for the two other seismicity types, will be explicitly highlighted.

Simulation of tsunami generation, propagation in deep water and coastal amplification in case of background seismicity (BS) is implemented in a deterministic way and is organized according to the following algorithmic chain (FIGURE 2.2):

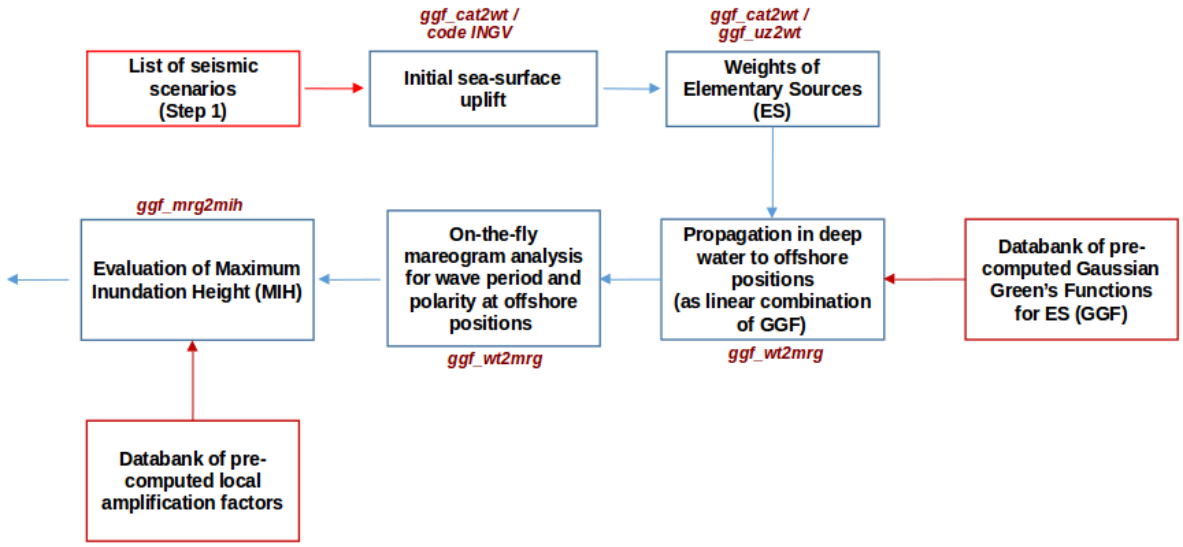

FIGURE 2.2: Workflow and codes for STEP 2 and STEP 3 related to Gaussian combination and the deep-water propagation (excluding the uncertainty treatment level of STEP 3).

Individual earthquake scenarios listed by their parameters at the end of STEP 1 are pipelined to the (1) computation of the initial sea-surface uplift, then to the (2) mapping of the uplift onto the pre-computed Gaussians followed by (3) their linear combination resulting in the offshore mareogram

POI position and, finally, to the (4) on-the-fly mareogram analysis for main wave characteristics and (5) derivation of the MIH (maximum inundation height).

2.3.1) Input

Following components constitute the input of the BS-processing deterministic chain.

(M) List of seismic scenarios from STEP 1

Scenarios to be processed are organized in files representing individual seismic zones and having notation like that:

- *TSUMAPS_parameters_t1_z025.txt*

where *t1* stands for the seismicity type 1 (=BS) and *z025* means seismic zone number 25 (here: North Anatolia).

This file has the following format:

```
# Scenarios parameters TSUMAPS, source zone North Anatolia, id
E02302N4161E04479N3793, seismicity type BS
# File creation time: Thu Mar 01 01:48:30 UTC 2018
#
# scenario_id: magnitude longitude latitude depth strike dip rake area length slip
#
25 1 1 :  6.0 23.2217 39.4009 1.00 22.5 10 90 100.87622972487786 11.37074295344586
0.378135296733672
25 1 2 :  6.0 23.2217 39.4009 1.00 22.5 30 -90 100.87622972487786 11.37074295344586
0.378135296733672
25 1 3 :  6.0 23.2217 39.4009 1.00 22.5 30 90 100.87622972487786 11.37074295344586
0.378135296733672
```

Here *scenario_id* is represented by a triplet consisting of zone index (25), seismicity type index (1) and sequential number of a scenario (1,2,3,…..). These three numbers form a unique scenarioID to be used in the subsequent computations and database storage. Fault parameters constitute a classical set of the Okada's rupture parameters and will be directly used for the modeling of the initial uplift.

Catalogs for zones of predominant seismicity (PS, PSslip, PSmar) represented by slip distributed along buried patches (tri- or quadri-lateral) have slightly different format:

```
# Scenarios parameters TSUMAPS, source zone Paphos, id E03177N3588E03306N3420,
seismicity type PS
# File creation time: Fri Oct 27 10:34:09 UTC 2017
#
# scenario_id: magnitude longitude latitude length width mesh_elements  slip_type
slip_distrs
#
36 2 1 :   6.0 32.06334 34.61787 10.277 15.202 [245, 564]   UNIFORM [0.18358,
0.18358]
36 2 2 :   6.0 32.08426 34.54918 10.277 15.202 [574, 245]   UNIFORM [0.20608,
0.20608]
```

Here, the slip distribution is given together with corresponding ID's of elementary faults (=patches).

(N) Gaussian Green's functions

Gaussian Green's Functions (GGF) consists in a set of NetCDF files storing pre-computed sea level time histories at several points of interest (POI, sampled at about 10 km each other along the 50 m depth isobath) using a Gaussian-shaped unit source as tsunami initial condition. Tsunami simulations for each unit source has been propagated for 8 hours, using HySea, a GPU code (De la Asuncion et al., 2013) that solves nonlinear shallow water equations on a computational grid with a spatial resolution of 30 arc-sec. NetCDF files are organized in a three-dimensional matrix containing: the number of Gaussian unit sources, the number of POI, the number of time steps. Details on the GGF dataset features and performances can be found in Molinari et al. (2016).

(O) 'Classical' tsunami Green's functions for far-field sources

For far-field zones (Caribbean and Mid-Atlantic ridge), mareograms at POIs were calculated using the 'classical' tsunami Green's function approach, namely, by pre-computing of wave propagation from bured elementary faults (=patches) loaded with unit slip and subsequent superposition of these "patches Green's functions" in accord with the implied scenario slip distribution.

The patches Green's functions were precomputed for all the "patch/POI" pairs and stored in a way similar to the Gaussian Green's functions described above.

(P) Lists of Points Of Interest (POI)

Files listing POIs have the following format:

```
# name  longitude  latitude  ID  depth
5      -16.385840   10.191670    12443  -50.751343
11     -16.458330   10.358330    12449  -50.000168
13     -16.558330   10.462500    12451  -48.499916
```

Here the first field called '*name*' won't be used, it is kept due to historical reasons. POIs ID will be generated from the integer number within the 4th column preceeded by the prefix of the geographical domain (specified within the chain configuration file '*ggf.cfg*', see Codes section)

(Q) Local amplification factors

Individual amplification factors for each POI are presented in the following format:

```
# ID      lead  120   200   300   600  1000  1800  3600 lead  120   200   300   600
1000  1800  3600
nea12438      neg    4.77   4.68   2.61   1.29   1.08   1.03   1.01   pos    3.40
       2.84   2.40   1.34   1.11   1.03   1.01
nea12443      neg    6.46   6.46   6.32   5.66   4.74   3.48   1.90   pos    5.84
       5.65   5.38   4.75   4.15   3.50   2.80
nea12449      neg    6.46   6.46   6.32   5.66   5.30   3.48   1.90   pos    5.84
       5.65   5.38   4.75   4.15   3.50   2.80
```

where numbers present offshore wave amplitude multiplication factors referred to the 50 meters depth for 7 wave periods (in seconds) and 2 incident wave polarities. The factors will be linearly interpolated to the actual wave period estimated during on-the-fly mareogram analysis (see Codes section).

(R) 3D Triangular mesh (seismicity type PS only)

Well-known seismogenic structures are modeled by meshing the slabs using triangular elements. Each element is described by: corner coordinates, strike, dip, rake, overlaying water depth (negative if inland).

The 3D meshes are built up by Cubit (https://cubit.sandia.gov/; Casarotti et al., 2008), a powerful mesher tool suite from Sandia National Laboratories, and are stored using the Abaqus file format (.inp), which is an ASCII file with two sections: the first part contains an ordered list of the nodes of the mesh, with the corresponding coordinates; the second part contains the connectivity matrix of each triangular element, in terms of element number followed by node numbers forming the element . This file is coupled with a second ASCII file containing the other features at each node: strike, dip, rake, water depth. Each line corresponds to a node of the mesh ordered as in the .inp file.

Snippet of the mesh .inp file for Hellenic Arc PS

```
*HEADING
**
********************************** P A R T S **********************************
*PART, NAME=Part-Default
**
********************************** N O D E S **********************************
*NODE, NSET=ALLNODES
       1,    1.91905367164497E+01,    3.67608155835915E+01,    -1.0000000E+04
       2,    1.93109884140337E+01,    3.68759238484866E+01,    -9.0637600E+03
       …
       …
       …
    1639,    2.24757976240805E+01,    3.60626495410863E+01,    -2.0136870E+04
    1640,    2.23804148944738E+01,    3.59664860554189E+01,    -1.8216600E+04
**
********************************** E L E M E N T S ****************************
*ELEMENT, TYPE=STRI3, ELSET=EB1
       1,       1,       2,       3
       2,       4,       5,       6
       ...
       …
       …
    3104,    1627,    1637,    1631
**
```

Snippet of a mesh attributes .txt file for Hellenic Arc PS

```
X Y Z dip strike rake topo
19.19053672 36.76081558 -10000 3.243702 162.461472 -47.5842782 -3444.77
19.31098841 36.87592385 -9063.76 2.577673 162.479187 -47.5497009 -3421.25
```

(S) Bathymetric mesh

Bathymetry data is used to translate the co-seismic sea-bottom displacement into the corresponding tsunami initial conditions at the sea surface. This translation is necessary because the water column effectively acts as a low-pass filter for the bottom deformation (see Doc_P2_S1 for more information). We retrieve the depth of the filtering water column from the same bathymetry model as used to populate the Gaussian's propagation databank (SRTM30+).

2.3.2) Codes

The codes listed and explained below share several common datasets (e.g., pre-computed Gaussian Green's functions, or POI-database), that is why it was suitable to create a common configuration file containing full definitions for deterministic step. This file is usually called '*ggf.cfg*' and has a well self-explained structure. We do not paste it into the current document due to its relatively large size and easily understandable structure.

Codes listed below usually have embedded help which will be displayed in case of program start without any or with wrong command-line arguments.

(T) Preparation steps

ggf_prepare:
This routine takes the project config file '*ggf.cfg*' as a single input parameter and generates:

- list of POIs with their offsets within the Gaussians databases ('poi.lst');
- list of elementary Gaussians with their offsets within the databases ('*gs.lst*');
- a caching database containing indexed information about local density of the Gaussians non-regular grid with local weighting factor ('gs_cache.db')

ggf_prefetch:
This routine will read the original Gaussians netCDF's and re-organize them 'by POIs'.

In the original Gaussian netCDF databases information is stored 'by sources' - in the process of database creation, POI mareograms are being added source-after-source. Thus, mareograms corresponding to a single POI are distributed through the huge dataset in a non-contiguous way. For a tera-byte size dataset, such a distributed data storage may result in a slow data access when picking mareograms for a given POI. Note, we usually perform hazard analysis in a POI-based way. To speed up deterministic computations, *ggf_prefetch* routine fetches GS-mareograms into individual POI-files named like:

ggf.med03512.idx and ggf.med03512.db

where *med03512* stands for the POI ID, and the database file (*.db) contains their mareogram time series for all registered Gaussians sources stored sequentially as 4-byte floats whereas the indexing file (*.idx) saves their absolute offsets for the fast access.

There are three additional useful routines.

ggf_check_nc:
Performs some basic sanity checks for the original Gaussian netCDF including:

- if mareogram is an oscillating function, not just a constant;
- number of zero-crossings;
- number of maxima;
- number of minima;
- reliability of wave amplitudes (not too large values).

Parameter thresholds are to be given in configuration file called '*ggf_check_prefetched.cfg*'.

ggf_check_prefetched:
Similar checks but with POI-wise prefetched Gaussian datafiles.

ggf_extract_gf:
Extracts a single GF-mareogram for a given Gaussian/POI pair out of original netCDF.

(U) Computing initial sea surface uplift followed by weights of elementary sources

As mentioned in the Methods document, tsunami propagation from all the seismic sources except that in the far-field (Mid-Atlantic Ridge and Caribbean) was simulated by a linear combination of pre-computed Gaussian-shaped surface elementary sources. Weights for such a linear combination were retrieved by 'fitting' of the Gaussians into actual initial sea-surface dislocation profile. The latter was computed in two steps: (1) running a co-seismic deformation model according to source parameters derived at STEP 1 and (2) applying the Kajiura-like filtering to account for the damping effect of the water column.

Depending on the seismicity type, co-seismic deformation modeling took part in two different but merging branches. For seismic sources represented by a single Okada-type fault (seismicity types: BS, SBS, and SPS), computation of the co-seismic bottom deformation, water column filtering and derivation of Gaussians' weights was accomplished in one single run of the routine named '*ggf_cat2wt*'.

ggf_cat2wt:
Reads seismic catalog (list of seismic scenarios represented by their 'Okada'-parameters, see the section *Input-A* above) and computes weights for Gaussians. Computed weights are then stored in a binary library of weights (usually organized by seismic zones and seismicity types). Each record in such a library contains a set of non-zero GS-weights per seismic scenario.

Typical notation for a weights-library is like that:

wt.z017.t1.db
where prefix 'wt' stays for the type of dataset (here- weights), 'z017' stays for the seismic zone number 17, and 't1' for the seismicity type 1 (here- BS).

This routine reads configuration file '*ggf_cat2wt.cfg*' containing 4 parameters: (1) path to the main configuration file '*ggf.cfg*'; (2) path to the bathymetry to calculate water filtering effect; (3) threshold for minimal vertical deformation (to restrict area around the fault to reasonable size, note- Okada's model solution gives a very broad area of almost negligible deformation which, if included, would heavily increase the number of affected Gaussians and, hence, simulation time and storage volume), (4) grid resolution for computing of initial deformation.

For seismic scenarios of the Mediterranean predominant seismicity (PS-sources attributed to the main subduction zones), co-seismic bottom deformation due to the distributed slip at the curved 3-D plate interface (see section *Input-E* above) and subsequent Kajiura-like filtering were computed in a separate branch using INGV original Python modules developed in the PySPTHA framework. Resulting sea surface deformation was stored in a netCDF file – one file per seismic scenario – and then passed to the routine called '*ggf_uz2wt*'.

ggf_uz2wt:

Reads initial sea-surface deformation from a netCDF file and computes weights for Gaussians. This routine is essentially a reduced version of the previous tool without modeling of elastic deformation and water column filtering.

Like the previous tool, this routine expects to read a config file called '*ggf_uz2wt.cfg*' containing 3 parameters: (1) path to the main configuration file '*ggf.cfg*'; (2) path to where to find netCDF grids with initial uplifts; (3) threshold for minimal vertical deformation.

There is an additional useful routine:

ggf_lib_wt:
Performs different actions with binary weights library:

- provides basic information about the library and its contents;
- lists seismic scenarios whose weights are stored in the library;
- runs a small sanity check for the library;
- extracts weights for given srcID;
- deletes scenarios according to the list.

(V) Linear combination/Propagation and mareogram analysis

As soon as the tsunami initial conditions for seismic scenarios are converted into the weights of the participating Gaussians, resulting mareogram at any off-shore POI can be calculated by simple linear superposition of the precomputed Gaussian-to-POI mareograms.

ggf_wt2mrg:
For a given weight library and POI, this routine computes mareograms for all the scenarios within the library, one-by-one, using linear combinations of the precomputed GS-to-POI time series. Resulting mareogram time series will not be stored but, instead, dynamically analyzed to retrieve principal wave characteristics: first arrival, maximum amplitude, dominant wave period and polarity. See the *Methods* document regarding analysis technique. These wave characteristics are needed for the offshore-to-onshore projection and will be saved to a binary library, one file per POI, named like:

mrg.blk00027.db
here prefix 'mrg' stays for the type of dataset (here- mareogram information), 'blk00027' stays for the POI name.

This routine reads configuration file '*ggf_wt2mrg.cfg*' containing 3 parameters: (1) path to the main configuration file '*ggf.cfg*'; (2) threshold to output offshore wave height (to save disk space and store only scenarios triggering non-negligible wave heights at given POI); (3) parameter for the LOWESS filter.

Additional routine called:

ggf_wt2mrg_debug:
does not process the entire weights library but, instead, extracts weights and compute a mareogram for a single given seismic scenario and POI. The resulting mareogram time series will be printed out, together with its filtered version and principal wave characteristics derived out of wave analysis.

Like the weights' library, there is a (mareogram analysis products) library inspection and check routine:

ggf_lib_mrg:
This tool:

- provides basic information about the library and its contents;
- lists seismic scenarios whose mareogram analysis products are stored in the library;
- runs a small sanity check for the library.

(W) Propagation in case of far-field sources

The above described way of processing makes use of the Gaussian-shaped surface elementary sources. This way of deterministic computations applies to the seismicity types BS, PS, SBS, SPS and encompasses more than 99% off all the seismic scenarios. However, besides these, near-field, sources treated by means of Gaussians, we also included in our SPTHA analysis far-field sources at the Caribbean subduction zone and Mid-Atlantic Ridge. Tsunami generation and propagation along these sources was modeled in line with common Green's function approach, namely, by pre-computing wave propagation from buried elementary faults loaded with unit slip and subsequent superposition of these tsunami Green's functions according to the implied scenario slip distribution.

For these zones and seismicity types (PSslip and PSMar), seismic scenario files created at STEP 1 already contain information on corresponding slip distribution. A routine called:

ggf_slip2mrg:
loops through seismic scenario catalog with slip distributions and computes final POI offshore time-series by linear superposition of the "elementary fault / POI" pairwise Green's functions. After the time-series is build, processing – wave analysis and output – is the same as described above by '*ggf_wt2mrg*'. Also, configuration file '*ggf_slip2mrg.cfg*' has the same content as '*ggf_wt2mrg.cfg*'.

(X) Coastal amplification and estimation of MIH

Final stage of the deterministic wave height computations is off- to on-shore projection by means of the method of local amplification factors (see the *Methods* documents as well).

Processing at this stage is POI-wise: binary datasets with off-shore wave characteristics ('*mrg.poiID.db*') will be read and processed scenario-by-scenario. Specific wave-period and wave-polarity dependent POI amplification factor will be estimated by linear interpolation between wave periods stored in the lookup table. The amplified wave height – MIH: Maximum Inundation Height – will then be written together with the corresponding scenario IDs into the text file. Additionally, Green's law extrapolation as well as raw offshore wave height will be written in separate text files.

This processing is accomplished by the routine called:

ggf_mrg2mih:
This routine takes a mareogram database as the only input parameter and reads the configuration file '*ggf_mrg2mih.cfg*' containing path to the main configuration file '*ggf.cfg*', threshold to output MIH values and the three output flags: for MIH, for Green's law and for offshore wave heights.

The format of output files, which are essentially results of the deterministic chain, is described below.

2.3.3) Output

(Y) MIH file format

MIH (Maximum Inundation Height) files are organized by POIs and have names like:

mih.af.blk00027.db
here prefix '*mih*' stays for the type of dataset, '*af*' stays for the method of amplifications factors. Alternatively, these could be '*gl*' for Green's law, or '*os*' for off-shore wave heights (however, the last two cases, strictly speaking, should not be prefixed with 'mih'). '*blk00027*' stays for the POI name.

These files are simple ASCII text files containing records each having four columns:

1. source zone integer index;
2. source type integer index;
3. source number (within this zone and type);
4. wave height (either MIH, or GL, or OS).

Thus, each file contains deterministic wave heights for all relevant seismic sources at given POI.

Example dataset for the POI nea05221, seismic zone 106, seismicity type 6 and wave metric GL (file called '*mih.gl.nea05221.db*'):

```
106 6 79 0.0803648
106 6 80 0.0872359
106 6 81 0.0847917
```

2.3.4) Sanity checks

Sanity check reports are (currently) located in: @Dropbox/TSUMAPS_Phase2_reporting/.

(Z) Tsunami Elementary Sources

See report 'DocSanES' on Dropbox.

(AA) Deterministic tsunami results

See report 'DocSanScen' on Dropbox.

(BB) Amplification factors

See reports 'Doc_SanChecks_2' section 8 and 'Doc_SanChecks' section 4 on Dropbox.

2.4) Uncertainty on hazard metrics

2.4.1) Input

The distribution of the uncertainty due to the use of linear combination of Gaussian (instead of direct modelling the tsunami) comes from Molinari et al. (2016), and the Distribution of bias and dispersion comes from the NLSW simulations of Glimsdal et al. (2019).

2.4.2) Code

(CC) MIH/Runup distribution

Here we describe the workflow which was applied in order to compute the conditional probabilities used for treatment of the uncertainty of the Gaussian's linear combination and the amplification factor method. It is based on J. Selva's original Matlab codes, modified by A. Hoechner for computational ease and modified to correct a definition misunderstanding in sampleLognPar.m (line 86).

Inputs: the lin. comb. uncertainty compilation in folder STEP3_1A_GAUSS (provided by R. Tonini INGV), the amp. fact. uncertainty compilation in folder STEP3_1B_AMPLM (provided by F. Lovholt NGI).

Location: The codes are currently on: TSUMAPS/src/Tide_LinComb_AmpFact_Uncertainty

First, run (with Octave):

- setup.m which generates files:
- MIHinputs: discretization of input MIH (251 steps from 0.01…100 m exp. distrib.)
- thresholds: discr. of output cond prob (51 steps from 0.01…100 m exp. distrib.)
- nsampleEU: nr of samples for epistemic uncertainty
- all_poi _t0 _t1 (loads TSUMAPS_POI.txt)
- and calls:
- sampleLognPar (Gaussians lin comb and amp. fact. uncertainty sampling)

For computation execute (using Linux):

- run_t0.bat which executes run_t0.m under Octave

on same or different computers for saving time, each launches several Octave instances.

Output:

Folders: poe_tide_0

Containing files: <poi_id>_af.hdf5 (amp. fact.), <poi_id>_gl.hdf5 (Green's law)

having overall size of 350GB uncompressed and 170GB compressed

Located on: TSUMAPS/data/metrics/uncertainty

The above files are then used for the next computational steps for hazard calculation by P. Perfetti's codes.

(DD) PySPTHA poi_hc_cond_indexes.py

Name: poi_hc_cond_indexes.py

Short description: This program associates an exceedance probability distribution to every MIH threshold defined in every (POI, scenario) pair for all metrics, regions and seismicity classes. It introduces a workflow optimization that has not correspondence in the TSUMAPS schema, referring

to precomputed samples indexes instead of copying every time the whole dataset, to avoid excessive data replication and to speed up computation. Along the index is stored a random seed to permute the sample on later step of hazard computation.

Parallelization: per (POI, metric) pair.

Input: POI list, MIH for all POIs and scenarios, project configuration.

Output: per (POI,metric) HDF5 file.

Position in file system: TSUMAPS/src/PySPTHA/bin

Programming language: Python3

2.4.3) Output

(EE) POI MIH distribution per scenario

HDF5 file are used to store indexes and random seeds and are located the TSUMAPS/results/step3/poi_cond_unc_indexes/ directory. The hierarchical structure of these files is exploited to organize data, in this order, by metric name, seismicity class class, region and scenario (<metric>/<seisclass>/<reg_id>/<scen_id>) using the short numerical indexes to easily refer to the MIH data from step3. Thus, by example, the pair stored in the leaf reachable by the path af/1/43/3 correspond to the uncertainty sample for the scenario E00197N5793E02760N4372-BS-M600_E00951N4771_D010_S022D30R270_A000056_S006 as defined in the proper scenario list TSUMAPS/results/step1/scenarios/BS/TSUMAPS_indexing_BS_E00197N5793E02760N4372.txt

2.4.4) Sanity checks

Some sanity checks regarding uncertainty treatment are described in Document:

@Dropbox:/TSUMAPS_Phase2_reporting/DocSan/DocSan_2018_R2/Doc_SanChecks_2.docx

Some Matlab scripts used for the sanity checks are located on: @MyCloud/TaskB/Tide_LinComb_AmpFact_Uncertainty:

- show_histo.m: for histograms comparing NLSW, AmpFact, Green's law
- load_stat.m: to import mean and percentiles PoE for all POI
- show_stat.m: to plot PoE for all POI
- check_for_nan.m: checks for erroneous NaN
- check.m: plots PoE for selected POI

2.5) Hazard computation

2.5.1) Input

(FF) Annual rates/Probabilities

One text file located under TSUMAPS/results/step1/longterm and formatted as described in "Probabilistic source model/Output", is expected per every valid (seismicity class, event tree level, region) tuple.

(GG) Models' weights

Models weights files are used to associate a weight to every model used to build the probabilistic ensemble ad thus must be coherent with the annual rates/probabilities files.

The files, one for every (seismicity class, event tree level), are in the directory TSUMAPS/data/models/weights and they must:

- contain as many lines as the model types defined in the correspondent event tree level's section in project configuration;
- for each line they must have as many space separated values as the rates/probabilities that are provided for this model type in the relevant annual rates/probabilities file.

Some examples are provided below:

- BS-1_Magnitude
    - Project configuration

      ProbabilityModelTypes = PS05km, PS10km
    - Models' weights

PS05km: [8320 space separated values]
PS10km: [8320 space separated values]
    - Annual rates for a specific discretization step in a region

M600: [8320 values], [8320 values]
- BS-2_Position
    - Project configuration

      ProbabilityModelTypes = PS05km, PS10km
    - Models' weights

PS05km: 0.38542
PS10km: 0.61458
    - Probabilities for a specific discretization step in a region

```
E03997N3917:0.011067,0.011067
```

- BS-3_Depth
    - Project configuration

      ProbabilityModelTypes =
    - Models' weights

      ALL: 1
    - Probabilities for a specific discretization step in a region

```
M600_E03997N3917_D010: 0.083333
```

2.5.2) Code

(HH) Models weights code

Workflow:

1. *AHP_setAndRun.m.m (Run elicitations)*

2. *weightModels.m (Postprocessing, preparing input for PySPTHA)*

Name: AHP_setAndRun.m

Short description: It implements the AHP elicitation procedure. This procedure is implemented in Phase 1 and Phase 2. The weights of the models are quantified in elicitation 2. The script is in two subfolders, relative to the two elicitations. Essentially, this script set the main variables, read the answers to questionnaires and the weights of the experts, and perform a standard AHP with common scripts.

Parallelization: none

Input: experts' answers and weights.

Output: A txt file containing the weights and the prioritization for each questionnaire; png figures for visual checks of the results. The output is in subfolders, named AHP_run_output_20180316 for both elicitations #1 and #2 (in their respective folders).

Position in file system: TSUMAPS/src/Step4/elicitations/AHP_Phase1_matlab and Step4/elicitations/AHP_Phase2_matlab

Programming language: Matlab

Name: weightModels.m

Short description: It prepares the input for the PySPTHA for models' weights (STEP 4). The output of elicitation #2 is set by hangs within the script. The Davies' weights are cut&paste from the spreadsheet file davies_weights_revised.ods.

Parallelization: none

Input: regionalization and discretizations; output of postProc.m.

Output: models' weight files of Section 5.1.2 (one text file per Event Tree level for all seismicity types: BS, PS, SBS); 1 text file for sanity checks. The output is in the folder weightsMod_revised.

Position in file system: TSUMAPS/src/Step4

Programming language: Matlab

(II) PySPHTA fill_probabilities.py

Name: fill_probabilities.py

Short description: In order to use exploit the hierarchical format of HDF5 files, this program is defined to sample the annual rates and probabilities, according to the model weights defined, normalizing where necessary and updating every event trees' node. After an error-less execution of this script, every scenario's absolute rate can be obtained navigating the corresponding branch in the HDF5 file and multiplying the probabilities array along the path.

Parallelization: per (seismicity class, region) pair.

Input: Event Trees' HDF5 files, annual rates and probabilities, models' weights.

Output: Event Trees' HDF5 files.

Position in file system: TSUMAPS/src/PySPTHA/bin

Programming language: Python3

(JJ) PySPHTA poi_hc.py

Name: poi_hc.py

Short description: This script is intended to compute hazard from the metric values sampling and the absolute rates computed by the previous fill_probabilities.py step. For every (POI, metric) all the pre-computed probabilities of exceedance distributions indexed by the POI's HDF5 indexes files are multiplied by the absolute rate and then added to obtain a total sample for the global hazard curve of every (POI, metric) pair.

Parallelization: per (POI, metric) pair.

Input: Event Trees' HDF5 files updated with probabilities and annual rates, POI uncertainty indexes' HDF5 files.

Output: one HDF5 file per (POi, metric) pair containing the global hazard curve and the independent contribution for every seismicity class. If a dedicate flag is activated (--update_marginals) also the disaggregated hazard for each event-tree node is stored.

Position in file system: TSUMAPS/src/PySPTHA/bin

Programming language: Python3

(KK) PySPTHA hazard_curves_all.py

Name: hazard_curves_all.py

Short description: In order to visualize all POIs hazard on the online tool, an XML file containing the hazard curve for every POI is needed. This tool is used to compute and list together all the POIs' PoE, given the chosen statistic (mean, median or percentile). Every single POI hazard curve is read from the corresponding HDF5 file and concatenated in the global hazard XML file.

Parallelization: none.

Input: POIs' HDF5 files containing hazard curves.

Output: one hazard XML file per (metric, statistic).

Position in file system: TSUMAPS/src/PySPTHA/bin

Programming language: Python3

2.5.3) Output

(LL) POI hazard curves HDF5

POI hazard curves files, one per (POI, metric) pair, are in the directory TSUMAPS/results/step4/poi_hc/. Two slightly different format are defined, depending on the use of the update_marginals flag:

- without marginals (*_frequencies.hdf5 files) only total annual rates and single seismicity classes contributions are stored in frequencies datasets, along with the used_models to be able to isolate different models contributions;

Snippet of the file structure:

```
/af                                                                    Group
/af/1                                                                  Group
/af/1/frequencies                                        Dataset     {1000,      51}
/af/2                                                                  Group
/af/2/frequencies        Dataset {1000, 51}
```

- with marginals (*_frequencies_marginals.hdf5 files), in addition to previous data, for every seismicity class and level, all discretization steps are listed in the HDF5 tree and for each of them all defined scenarios absolute hazard are summed, to keep track of their contribution in the global hazard.

Snippet of the file structure:

```
/af/1/regions/1/marginals Group
/af/1/regions/1/marginals/BS-1_Magnitude Group
/af/1/regions/1/marginals/BS-1_Magnitude/M707 Group
/af/1/regions/1/marginals/BS-1_Magnitude/M707/frequencies
                                              Dataset          {1000,          51}
/af/1/regions/1/marginals/BS-2_Position/E01488N3827 Group
/af/1/regions/1/marginals/BS-2_Position/E01488N3827
                           /frequencies Dataset {1000, 51}
```

(MM) XML Hazard curves

The hazard curves for all defined POIs are saved in one XML file for each (metric, statistic) pair, in a format similar (not identical) to the Natural hazards' Risk Markup Language (NRML) defined by GEM/OpenQuake (https://www.globalquakemodel.org/). After a preamble containing the metadata necessary to identify the right context for the data, one <HCNode> XML tag is defined for every POI and its child <poE> contains the hazard curve values for every threshold defined. Although XML files could be exported for arbitrary return period and statistic, the choice has been to use 50 years as return period and 02, 16, 84, 98, median and mean as statistics.

An example is provided below:

```
<?xml version="1.0" ?>
<hazardResult>
  <file_version date="20180212_161710"/>
  <tsunami tsunamiName="TSUMAPS"/>
  <hazardModel Model="ALL">AF</hazardModel>
  <timeterm deltaT="50yr"/>
  <hazardCurveField percentileValue="84" statistics="percentile">
    <IML IMT="MIH">0.01 0.11 [...] 91.11 100.00</IML>
    <HCNode>
      <site>
```

```
        <gmlPoint>
          <gmlpos>45.421 31.736</gmlpos>
        </gmlPoint>
      </site>
      <hazardCurve>
        <poE>0.035675 0.01937 [...] 2.034794555072494e-12</poE>
      </hazardCurve>
    </HCNode>
    <HCNode>
     [...]
    </HCNode>
    [...]
    </HCNode>
  </hazardCurveField>
</hazardResult>
```

2.5.4) Sanity checks

We check the consistency of the sampled models, as sampled by PySPTHA and the input weights, evaluated independently from the results of section as computed by the scripts of Section 5.2.1. Other visual sanity tests were performed directly on the figures produced by the codes, as discussed in Section 5.2.1. The code can be found in a subfolder of the script weightModels.m of Section 5.2.1, in subfolder sanityWeights/. The results are reported in the technical document of sanity checks.

2.6) Models weights code

2.6.1) 2.6.1) Input

XML files from 2.5.3B.

2.6.2) 2.6.2) Code

Name: POIS_hazard_disaggregation.ipynb

Short description: Given a POI label, the notebook analyzes and plot marginal probability distribution using the disaggregation techniques.

Several static images are produced, including per seisclass/region/magnitude/position hazard disaggregation.

Parallelization: per POI.

Input: POI label, used metric name, POI's HDF5 files containing hazard curves with marginal data aggregation.

Output: compiled notebook results as HTML/PDF file.

Position in file system: TSUMAPS/src/PySPTHA/notebooks

Programming language: Jupyter Python3 Notebook

References

Casarotti, E., M. Stupazzini, S. J. Lee, D. Komatitsch, A. Piersanti, and J. Tromp (2008), CUBIT and Seismic Wave Propagation Based Upon the Spectral-element Method: An Advanced unstructured Mesher for Complex 3D Geological Media, in *Proceedings of the 16th International Meshing Roundtable*, M. L. Brewer and D. Marcum (Editors), Springer, New York. (session 5B) pp. 579--597, doi: 10.1007/978-3-540-75103-8_32.

de la Asunción, M., Castro, M. J., Fernández-Nieto, E. D., Man- tas, J. M., Ortega Acosta, S.,González Vida, J. M. (2013) Efficient GPU implementation of a two waves TVD-WAF method for the two-dimensional one layer shallow water system on structured meshes, Comput. Fluids, 80, 441–452

Glimsdal, S., Løvholt, F., Harbitz, C.B., Romano, F., Lorito, S., Orefice, S., Brizuela, B., Selva, J., Hoechner, A., Volpe, M., Babeyko, A., Tonini, R., Wronna, M., Omira, R. (2019). A New Approximate Method for Quantifying Tsunami Maximum Inundation Height Probability. Pure Appl. Geophys, https://doi.org/10.1007/s00024-019-02091-w.

Kajiura, K. (1963). The leading wave of a tsunami, Bull. Earthquake Res. Inst. Univ., Tokyo, 41, 535–571.

Leonard, M., 2014. Self-Consistent Earthquake Fault-Scaling Relations: Update and Extension to Stable Continental Strike-Slip Faults. Bulletin of the Seismological Society of America, doi: 10.1785/0120140087.

Molinari I, Tonini R, Lorito S, Piatanesi A, Romano F, Melini D, Hoechner A, Gonzàlez Vida JM, Maciás J, Castro MJ, de la Asunción M (2016). Fast evaluation of tsunami scenarios: uncertainty assessment for a Mediterranean Sea database, Nat. Hazards Earth Syst. Sci., 16, 2593-2602, doi: 10.5194/nhess16-2593-2016.

Murotani, S., Satake, K., Fujii, Y., 2013. Scaling relations of seismic moment, rupture area, average slip, and asperity size forM~9 subduction-zone earthquakes. Geophysical Research Letters 40, 5070-5074, doi: 10.1002/grl.50976.

Okada, Y. (1992). Internal deformation due to shear and tensile faults in a half-space, Bull. Seismol. Soc. Am., 82, 1018–1040.

Strasser, F.O., Arango, M.C., Bommer, J.J., 2010. Scaling of the source dimensions of interface and intraslab subduction-zone earthquakes with moment magnitude. Seismological Research Letters 81, 941-950, doi: 10.1785/gssrl.81.6.941.

Zitellini N, Gracia E, Matias L, Terrinha P, Abreu M, DeAlteriis G, Hen- riet J, Danobeitia J, Masson D, Mulder T, Ramella R, Somoza L, Diez S (2009) The quest for the Africa-Eurasia plate boundary west of the Strait of Gibraltar. Earth and Planetary Science Letters 280(1):13 50, doi: https://doi.org/10.1016/j.epsl.2008.12.005.

Probabilistic TSUnami Hazard MAPS
for the NEAM Region (TSUMAPS-NEAM)
ECHO/SUB/2015/718568/PREV26

PHASE II – STAGE 4: Elicitation Experiment

Author: TSUMAPS-NEAM Technical Integrator (TI) team

Date: 22 March 2019

Version: 1.2

Table of Contents

This page is intentionally left blank.

Executive Summary

In this document, we report the second elicitation experiment of the Pool of Experts (PoE). Based on the results of the first elicitation experiment and on the review, a final list of alternative implementations at the different STEPs/LEVELs has been established by the Technical Integrator (TI) and implemented into the SPTHA. This second elicitation experiment is organized to assign to each of the alternatives a weight indicating the (subjective) credibility that each model has in the technical community. This was achieved by asking the experts to compare pairs of alternative modelling implementations and to assign them a relative degree of preference. The quantitative results of the elicitation will support the TI team in quantifying these weights.

In ***Section 1***, we introduce the rationale and the selected method for the elicitation.

In ***Section 2***, we discuss the elicitation results.

To complete the information of the present document, we attach the questionnaire used for the elicitation experiment as Appendix 1 (document DocP2S4_Appendix1_Questionnaire).

This page is intentionally left blank.

1. Elicitation

1.1 Elicitation preparation

As foreseen in the final implementation plan (see Doc P2_S1), the second elicitation of the Panel of Experts (PoE) in PHASE 2 is focused on quantifying the credibility of the different models through a weight. The trees, for each of the model STEPs, of the implemented alternatives to be weighted are reported in Doc_P2_S1. The selection of the alternatives is based on the results of Elicitation #1 (Doc_P1_S3) and the revision of the Internal Reviewers (IR) team.

In agreement with the first elicitation of the PoE (Doc_P1_S3), also for this second elicitation we considered Performance-based (PW) and Acknowledgement-based weights (AW) as 2 alternative expert-weighting schemes. As a sensitivity test, the consistency of the results is checked against the equal weights scheme.

As in PHASE 1, the elicitation is based on a structured questionnaire provided to the TSUMAPS-NEAM Pool of Experts (PoE). The same elicitation scheme is performed at all the levels of all the STEPs for which alternatives are available. Note that this includes STEP 4, which is the STEP where the weights are concretely applied to combine the alternative models into the final hazard estimation. Here, also the weighting methods, that is performance-based and acknowledgement-based, are considered as alternatives to be weighted themselves.

The quantification is based on an Analytical Hierarchical Process (AHP) procedure (Saaty 1980), which is the same method adopted in PHASE 1 (pre-assessment) – STAGE 3, as described in detail in Doc_P1_S3_Elicitation. Here, in PHASE 2, a slightly more sophisticated implementation of AHP is adopted. Indeed, we implemented AHP adopting two criteria (personal preference and preference in the community according to expert's best knowledge), instead of using just one single criterion (personal preference) as in PHASE 1. This has implications in both the formulation of the questionnaire (also criteria are compared, and for alternatives, all questions are duplicated for all criteria) and in the analysis of the results (the results of single criteria are merged).

As 2 alternative expert weights (PW and AW) will be implemented, we will have also two alternative quantifications of model scores. Therefore, one further question is added to the questionnaire to weight also these two alternatives (PW against AW). The weight obtained (adopting, only in this case, equal weighting for experts) is used to produce a weighted average of the normalized PW and AW scores, obtained by the implementing AHP with PW and AW, respectively. The final model weights in input to SPTHA are then assumed equal to these normalized average scores, without any further elaboration.

1.2 Elicitation method

Several structured elicitation methods with prioritization purpose are described in scientific literature (e.g., Morgan 2014). We use one procedure that is named Analytic Hierarchy Process (AHP). AHP was originally developed by Saaty (1980); it is a multi-criteria decision-making method that is suitable for complex problems. The hierarchy process breaks down the complex decisions into a series of pairwise comparisons, synthesizes the results, and then helps to take into account both subjective and objective aspects of the decision. Additionally, the process incorporates a useful technique for checking the consistency of the expert judgments, thus reducing the bias in the process of decision making.

The process works by decomposing the decision-making problem into a hierarchy of evaluation criteria and alternative options. In general, the structure of the method consists of an overall goal, a group of options or alternatives for reaching the goal, and a group of factors or criteria that relate the alternatives to the goal.

Here, we have implemented both "criteria" and "alternatives". Specifically, we first compute a score for each criterion, then we compute the score for each alternative, in both cases through the experts' pairwise comparisons of criteria and of models with respect to each criterion under consideration. Finally, the results for the different criteria are combined accounting for their relative scores.

The relative importance of one criterion/model over the others is usually expressed with numeric rating from one (equally important) to nine (extremely important) (Saaty 1980) and can be collected into a matrix; the scores are the components of the normalized principal eigenvector of this matrix (Saaty and Hu 1998). Here, we adopted the numeric translation reported in **Table 1 – Column 4 ("Weights of models")**, which was presented to the experts and reported in the introduction of the questionnaire. This scale is judged to be closer to the common way of thinking of hazard/risk analysts. However, the results are tested for robustness against the classical linear rating 1 to 9 of Saaty (1980), as reported in **Table 1 – Column 5 ("Standard AHP weights")**. The test showed that the variability introduced by these different scales is inside the inter-expert variability, leading to consistent prioritizations (even if to different weight values).

Some inconsistencies may arise when many pairwise comparisons are performed (Harker and Vargas 1987), which is typically measured by the Consistency Ratio (CR) (Saaty 1980). A perfectly consistent judgement by experts should always be zero, i.e. CR = 0, but inconsistencies are tolerated if CR < 0.1 (Saaty 1980). However, it has been suggested to relax this cutoff value up to 0.3 depending on the number of criteria and the kind of project (Goepel 2013).

One important issue in AHP is aggregation of judgements when many experts are involved. Different approaches can be employed to aggregate their individual or group opinions (Forman and Peniwati, 1998), depending on the level of the aggregation and mathematical method used for the aggregation. As for the level of aggregation, the most popular methods consist of either aggregating individual judgments regarding each set of pairwise comparisons to produce an aggregate hierarchy (Aggregation of Individual Judgments - AIJ) or synthesizing each of the individual hierarchies and aggregating the resulting priorities (Aggregation of Individual Priorities – AIP). As for the mathematics of the aggregation, both weighted geometric and arithmetic means are commonly used as aggregation method, considering equal or subjective weights on experts (Goepel, 2013; Forman and Peniwati, 1998; Zio, 1996). However, to preserve the consistency of prioritizations, while for AIP both geometric and arithmetic may be used, for AIJ the geometric mean must be used (Forman and Peniwati, 1998).

In this application, we select the aggregation of individual judgments (AIJ), in order to analyze and visualize both individual and group prioritizations. As already anticipated, both Performance-based (PW) and Acknowledgement-based weights (AW) are used, weighting their relative importance with a pairwise comparison included into the Questionnaire for the PoE. The score, only in this case, is obtained equally weighting the results. To analyze the uncertainty on the results (resulting from the variability of opinions within the PoE), we take the ensemble distribution of individual priorities of all

experts and, to estimate the group central tendency, we consider the weighted geometric means, following Goepel (2013) and Forman and Peniwati (1998).

We note that the procedure described above implies that each expert had to answer a rather complicated questionnaire, with a relatively large number of questions to answer and tables to fill. Of course, this may have confused some of the expert. However, we note that AHP foresees a check of the consistency of the answers of each expert in each question, and in this elicitation experiment significant inconsistencies have never been observed.

1.3 Questionnaire

The questionnaire sent to the experts can be found in ***Appendix A***. The questionnaire is structured into a short introduction followed by 5 questions. Question #0 is focused on prioritizing the criteria to be used for the comparison. We considered 2 possible criteria to compare the models:

- Criterion 1: Expert's personal preference
- Criterion 2: Most used in the community according to expert's best knowledge

Questions #1 through #4 are then dedicated to prioritizing the alternative models at the different STEPs of the analysis. Questions #2 and #3 had 2 and 3 sub-questions, respectively. For each of these 7 questions, 2 comparison tables were present (1 for each criterion), leading to a total of 15 tables to be filled by the experts. All these tables had only 2 alternatives to be compared, except for Question 2b, for which we had 4 alternatives.

Table 1: Fundamental scale of absolute numbers.

Intensity of Importance	**Definition**	**Explanation**	**Weights as used in elicitation**	***Standard AHP weights***
1	Equal importance	Two steps/levels/sublevels contribute equally to the objective	0.5-0.5	*0.5-0.5 (x1)*
3	Moderate preference	Experience and judgment slightly favor one step/level/sublevel over another	0.6-0.4 (x1.5)	*0.75-0.25 (x3)*
5	Strong preference	Experience and judgment strongly favor one step/level/sublevel over another	0.75-0.25 (x3)	*0.83-0.17 (x5)*
7	Very strong preference	A step/level/sublevel is favored very strongly over another; its dominance demonstrated in practice	0.95-0.05 (x19)	*0.86-0.14 (x7)*
9	Extreme preference	Overwhelming evidence favoring one step/level/sublevel over another	0.99-0.01 (x99)	*0.90-0.10 (x9)*

2. Results

2.1 Analysis of the results

The questionnaire was sent to the Pool of Experts (PoE) members (15 experts). We received answers from 13 experts. Each questionnaire included five questions (0 to 4). Question 0 was about the 2 criteria for comparison and had only one comparison table (since only one criterion is used to compare criteria, as in standard AHP). For all the other questions, 2 separate comparison tables were provided, one for each criterion (PW and AW). Out of the 15 prioritization tables, only in 3 cases we had more than 2 pairwise comparisons that may potentially lead to inconsistency. However, no large inconsistencies (> 0.1) were found in the 13 completed questionnaires.

The results are used to quantify the weights of the alternative models. The following procedure has been adopted:

1. We normalized to 1 the AHP scores obtained in Question 4 (Expert weights method) adopting the equal weight scheme for experts. In this way, we obtained 2 weights w_{PB} and w_{AB}, relating to the performance-based and the acknowledgement-based weighting schemes, respectively.
2. We normalized to 1 the AHP scores obtained in all the other questions (Questions 1 to 3) adopting both the performance-based and the acknowledgement-based weighting schemes. In this way, we obtained 2 sets of weights for all the models.
3. The final set of weights for the models was obtained as the weighted (arithmetic) mean of the 2 sets of weights obtained by the performance-based and the acknowledgement-based weighting schemes, using as weights for the mean w_{PB} and w_{AB}.

2.2 Specific results

From the results of ***Question 0,*** reported in **Figure 1**, the PoE had to select between Criterion 1 defined "Expert's personal" (C1_Pers hereinafter) and Criterion 2 defined "Most used in the community according to expert's best knowledge" (C2_Used hereinafter). The PoE has shown a clear preference for adopting as leading criterion the personal opinion of the experts about one model, more than its acknowledgement within the technical community. The results are coherent for all weighting schemes, with w_{PB} = 0.63 and w_{AB} = 0.65 for C1, and w_{PB} = 0.37 and and w_{AB} = 0.35 for C2.

Following the logic described above in Section 2.1, we present the quantification of the weights w_{PB} and w_{AB} from ***Question 4*** (Expert weights method), and then the results from the other questions. The results are reported in **Figure 2**. Concerning the weighting schemes to be adopted for the experts, the PoE showed a slight preference for the performance-based scheme over the acknowledgement-based scheme, independently from the weighting scheme adopted to evaluate this. Adopting a neutral weighting scheme (equal weights), we have w_{PB} = 0.57 and and w_{AB} = 0.43. The performance-based weighting scheme is strongly preferred under C1_Pers, while the results are less clear under C2_Used.

The results of **Question #1**, reported in **Figure 3**, are relative to STEP 1 – Level 0. In particular, the experts were asked to report their preference in using a buffer of either 5 or 10 km around the known fault interface to separate BS from PS seismicity in the seismic catalogs. The PoE clearly

preferred the 10 km option, for all weighting methods and criteria. The combined weights of the two options are 0.39 and 0.61 for 5 and 10 km, respectively.

The results of **Question #2** are relative to STEP 1 – Level 1. In particular, the experts were asked to report their preference for the magnitude-frequency models for the earthquake in each region. At this Level, we have a quite large number of alternative models (a total of 6), thus we separate the comparison of these alternative models in 2 questions: Q2a and Q2b. In Q2a, we consider two alternatives: either rates for PS and BS are quantified jointly, or independently. In Q2b, we enter into the details of the joint quantification of the regional magnitude-frequency (MF) distributions, by considering 4 alternative implementations. No questions have been asked for the separate quantification, since this quantification is based on Davies et al. (2017), from which also the model weights will be adopted.

The results for Q2a, reported in **Figure 4**, show that the PoE clearly preferred the separate quantification for BS and PS, for all weighting methods and criteria. The combined weights of the two options are 0.44 and 0.56 for joint and separate quantifications, respectively.

The results for Q2b, reported in **Figure 5**, show that the PoE tends to prefer the Tapered distribution compared to the Truncated distribution and minor differences between b-value computed from data than set to 1. Minor differences are observed when the alternative criteria and weighting schemes for the experts are adopted, with a smaller weight to the case “Tapered & β from data” in one case (criterion C1_Pers and performance-based weights). The combined weights of the four options are 0.30, 0.31, 0.19, and 0.20 for “Tapered & β = 2/3”, “Tapered & β from data”, “Truncated & β from data” and “Truncated & β = 2/3” respectively.

The results of **Question #3** are relative to STEP 1 – Level 2a. In particular, the experts were asked to report their preference for the models regarding Predominant Seismicity (PS) branch. Also at this Level, we separate the comparison of the alternative models in 3 questions: Q3a, Q3b, and Q3c. In Q3a, we consider two alternatives for the earthquake scaling law: either the Murotani et al. (2013) or the Strasser et al. (2010) scaling law is used. In Q3b, we consider two alternatives for the updip extension of the seismogenic zone: co-seismic slip is not allowed or allowed to happen at shallow depths under the accretionary wedge. In Q3c, we consider two alternatives regarding the possibility of using or not depth-dependent rigidity, as a model for explaining the observed depth-dependence of normalized earthquake duration.

The results for Q3a, reported in **Figure 6**, show that the PoE clearly preferred the Strasser model as scaling relation for PS, for all weighting methods and criteria. The combined weights of the two options are 0.55 and 0.45 for Strasser and Murotani, respectively.

The results for Q3b, reported in **Figure 7**, show that the PoE clearly preferred the modelling strategy that allows slip at shallow depths under the accretionary wedge, for all weighting methods and criteria. The combined weights of the two options are 0.34 and 0.66 for not-allowing and allowing this slip, respectively.

The results for Q3c, reported in **Figure 8**, show that the PoE clearly preferred the modelling strategy with depth-dependent rigidity, for all weighting methods and criteria. This preference results

stronger for criterion C1_Pers. The combined weights of the two options are 0.35 and 0.65 for uniform and depth-dependent rigidity, respectively.

The results for the obtained weights for the ensemble's alternatives are summarized in **Table 1**.

Table 1: Weights of the alternative models implemented for the ensemble, resulting from the elicitation.

STEP/LEVEL - Question	**Alternative models**	**Ensemble weight**
STEP 1 – Level 0 Question 1	Cut-off distance of 5 km around the PS sources	0.39
	Cut-off distance of 10 km around the PS sources	0.61
STEP 1 – Level 1 Question 2a	The mean annual rates rates for PS and BS are quantified jointly	0.44
	The mean annual rates rates for PS and BS are quantified independently	0.56
STEP 1 – Level 1 Question 2b	The tapered distribution (with probability > 0 for all magnitudes) with the parameter β (equivalent to the b-value) set to 2/3 (equivalent to b-value = 1), independently from data.	0.30
	The tapered distribution (with probability > 0 for all magnitudes) with the parameter β (equivalent to the b-value) set from data.	0.31
	The truncated distribution (with probability = 0 for all $M > M_{max}$) with the parameter β (equivalent to the b-value) set from data.	0.19
	The truncated distribution (with probability = 0 for all $M > M_{max}$) with the parameter β (equivalent to the b-value) set to 2/3 (equivalent to b-value = 1), independently from data.	0.20
STEP 1 – Level 2 Question 3a	Scaling laws from Strasser et al. (2010).	0.55
	Scaling laws from Murotani et al. (2013).	0.45
STEP 1 – Level 2 Question 3b	Co-seismic slip is not allowed or allowed to happen at shallow depths under the accretionary wedge.	0.34
	Co-seismic slip is allowed to happen at shallow depths under the accretionary wedge.	0.66
STEP 1 – Level 2 Question 3c	Rigidity is uniform with depth (PREM).	0.35
	Rigidity varies with depth according to Geist and Bilek 2001.	0.65
STEP 4 – Level 0 Question 4	Performance-based weights (PB)	0.57
	Acknowledgement-based weights (AB)	0.43

Figure 1: Results of Question 0, regarding the criteria to be adopted. Two options were available: "Expert's personal preference" ("Pref" in Figure), and "Most used in the community according to expert's best knowledge" ("Used" in Figure). The different panels report: (first row) the empirical cumulative distribution showing the variability among the experts, adopting the different weighting schemes in each column; (second row) the results of AHP scores and relative uncertainty, adopting the different weighting schemes in each column; (third row – left column) the inconsistency CI for each expert; (third row – right column) the different weights.

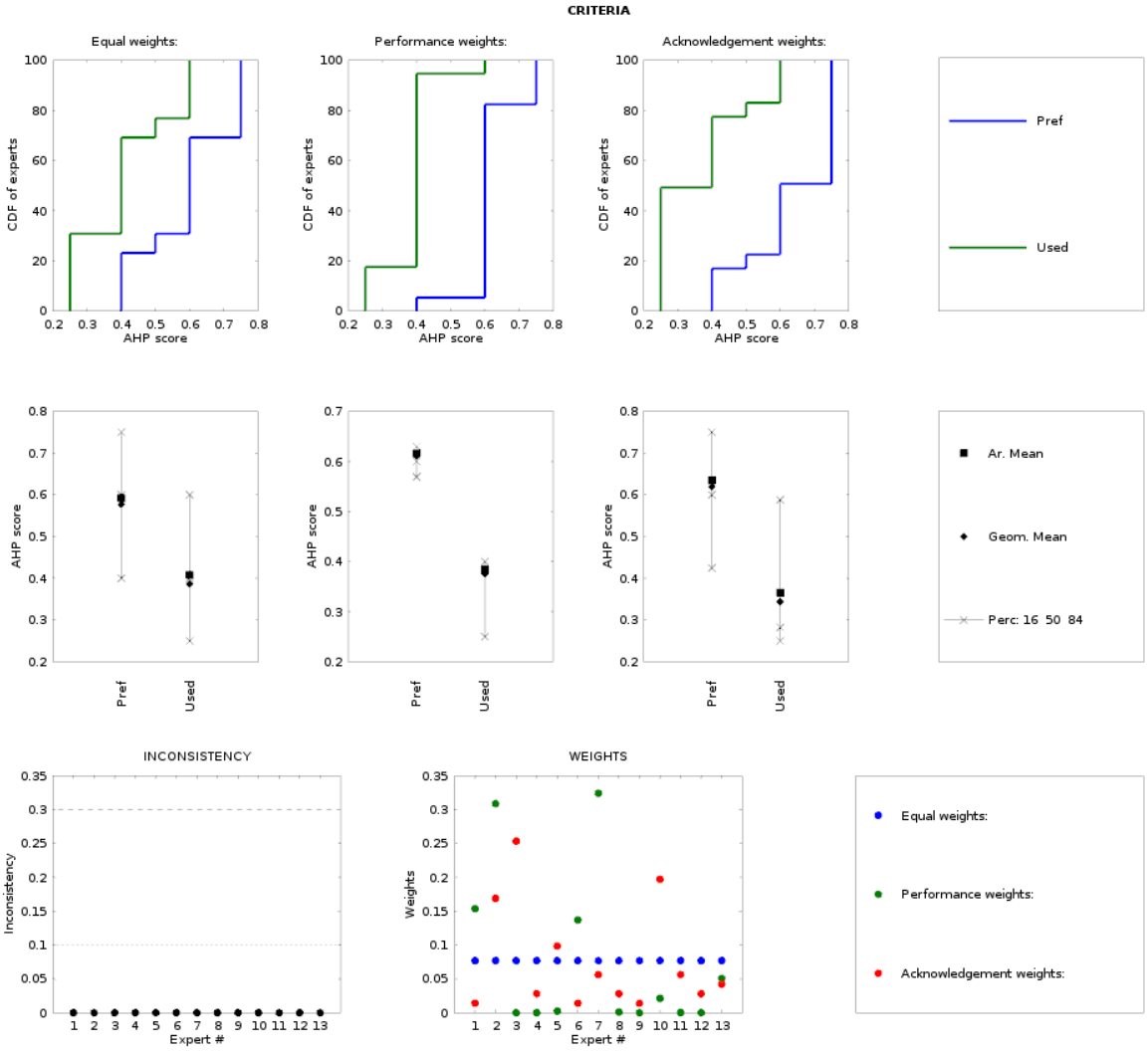

Figure 2: Results of Question 4, regarding the criteria to be adopted. Two options were available: "Acknowledgement-based weighting scheme" ("Acknowl." in Figure), and "Performance-based weighting scheme" ("Perform." in Figure). The different panels report: (first row) the empirical cumulative distribution showing the variability among the experts, adopting the different weighting schemes in each column; (second row) the results of AHP scores and relative uncertainty, adopting the different weighting schemes in each column; (third row – left column) the inconsistency CI for each expert; (third row – right column) the different weights.

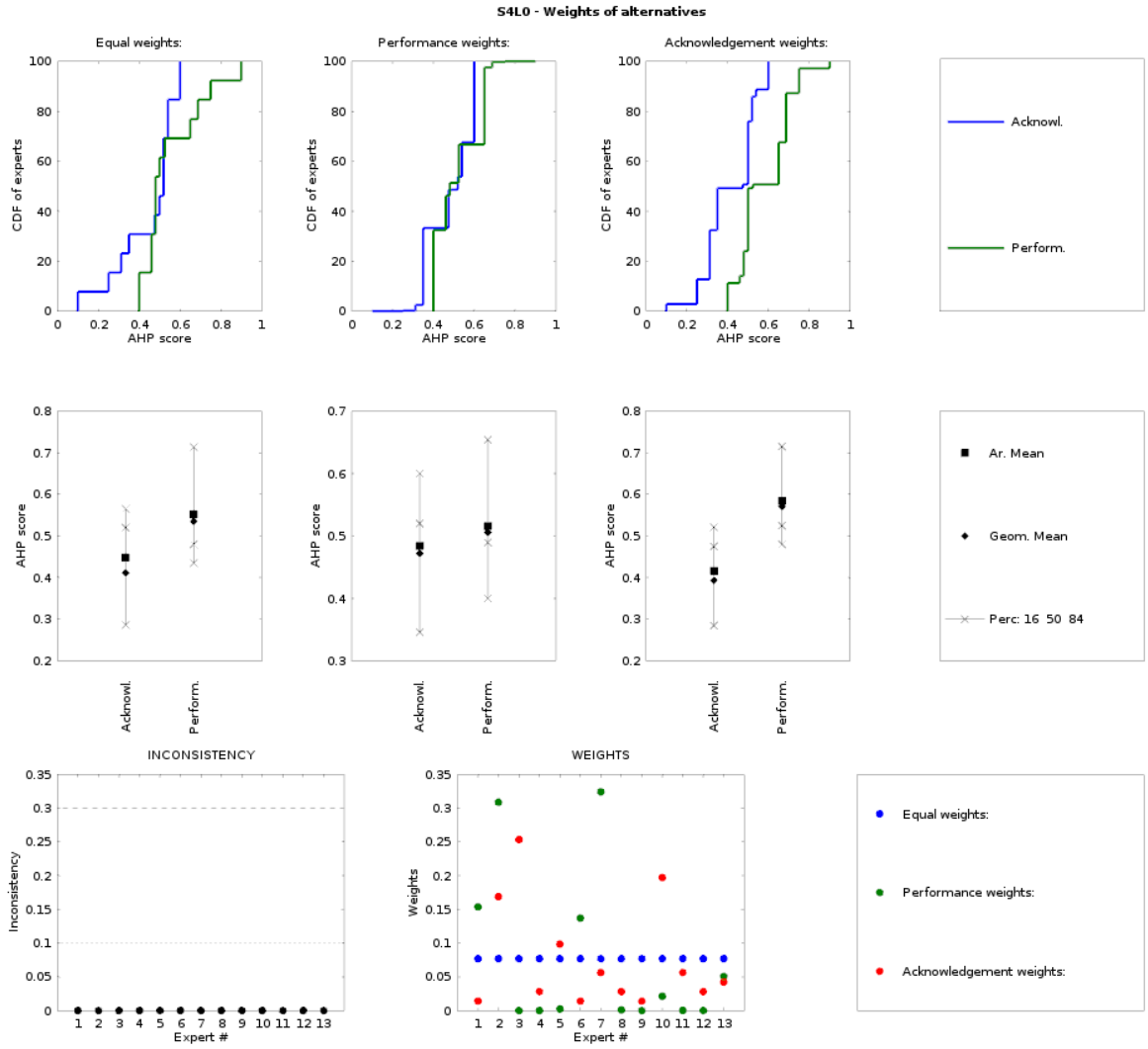

Figure 3: Results of Question 1, regarding the separation between PS and BS events in catalogs. Two options were available: “Cut-off distance of 5 km around the PS sources” (“Buffer 5 km” in Figure), and “Cut-off distance of 10 km around the PS sources” (“Buffer 10 km” in Figure). The different panels report: (first row) the empirical cumulative distribution showing the variability among the experts, adopting the different weighting schemes in each column; (second row) the results of AHP scores and relative uncertainty, adopting the different weighting schemes in each column; (third row – left column) the inconsistency CI for each expert; (third row – right column) the different weights.

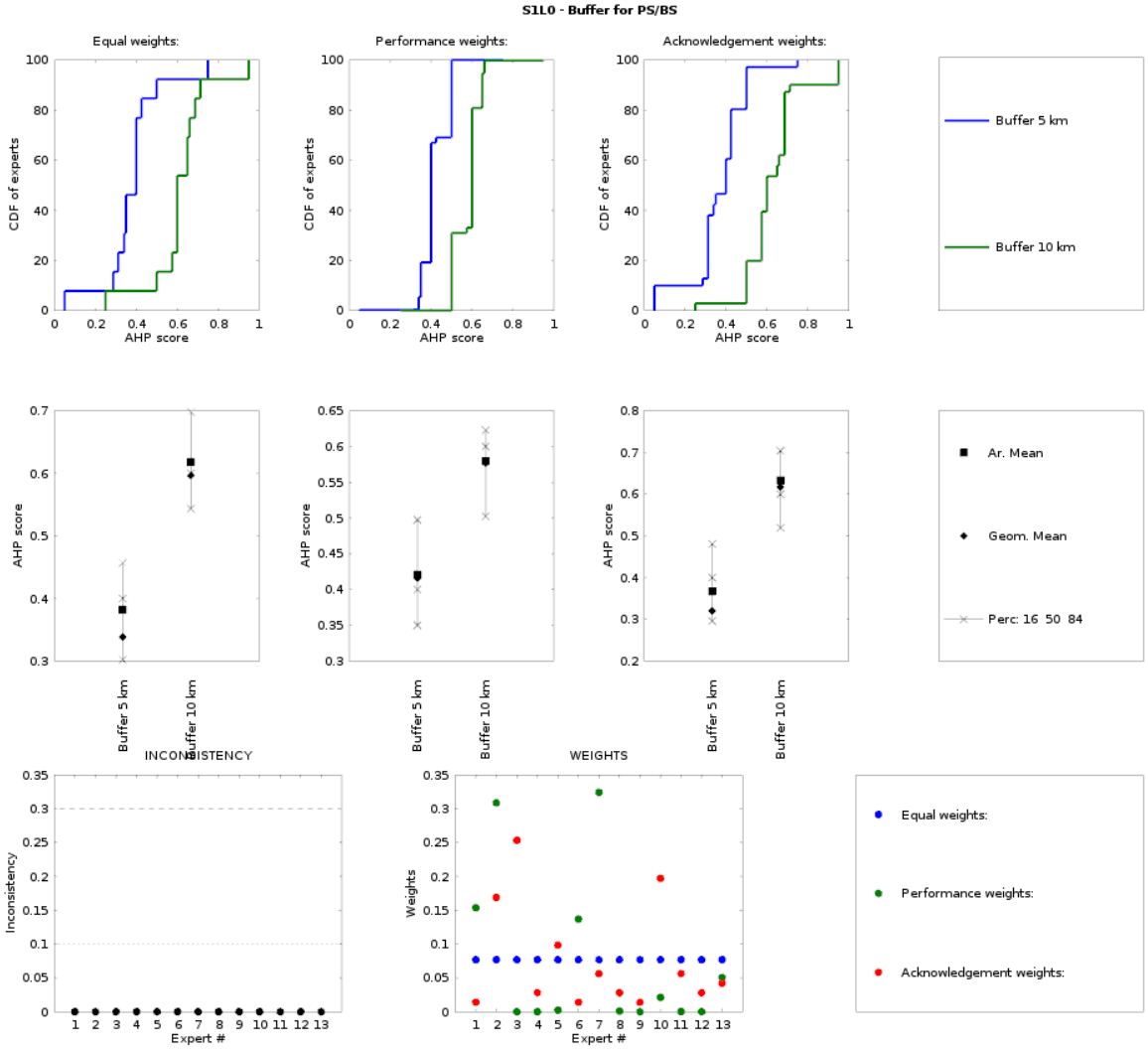

Figure 4: Results of Question 2 – Q2a, regarding the independent/joint quantification of the frequency-magnitude distribution for PS and BS. Two options were available: "The mean annual rates rates for PS and BS are quantified jointly" ("Joint" in Figure), and "The mean annual rates rates for PS and BS are quantified independently" ("Indep" in Figure). The different panels report: (first row) the empirical cumulative distribution showing the variability among the experts, adopting the different weighting schemes in each column; (second row) the results of AHP scores and relative uncertainty, adopting the different weighting schemes in each column; (third row – left column) the inconsistency CI for each expert; (third row – right column) the different weights.

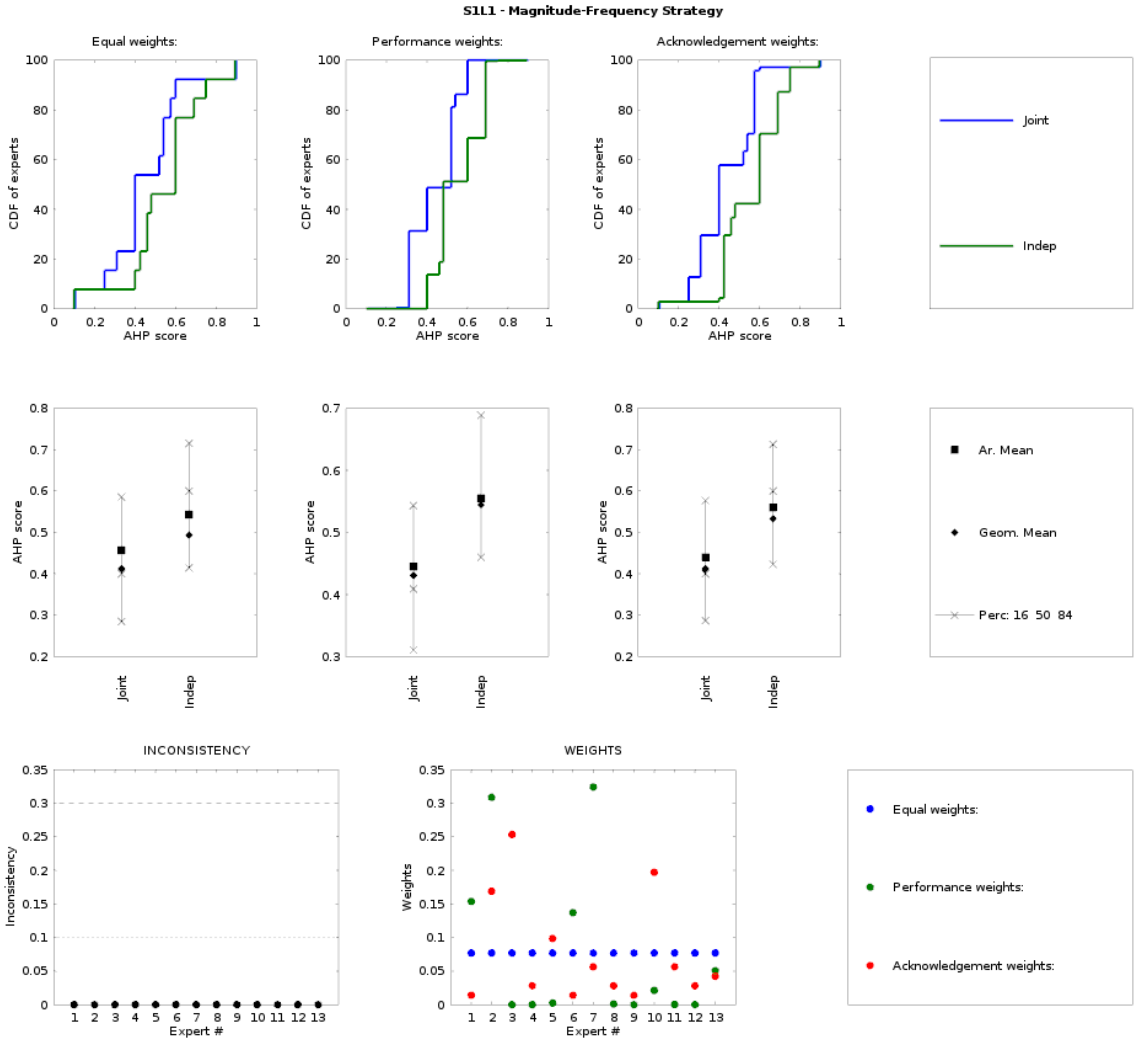

Figure 5: Results of Question 2 – Q2a, regarding the shape of the frequency-magnitude in case of joint quantification distribution for PS and BS. Four options were available: "Tapered & β = 2/3" ("Tapered+b=1" in Figure), "Tapered & β from data" ("Tapered" in Figure), "Truncated & β from data" ("Trunc" in Figure), and "Truncated & β = 2/3" ("Trunc+b=1" in Figure). The different panels report: (first row) the empirical cumulative distribution showing the variability among the experts, adopting the different weighting schemes in each column; (second row) the results of AHP scores and relative uncertainty, adopting the different weighting schemes in each column; (third row – left column) the inconsistency CI for each expert; (third row – right column) the different weights.

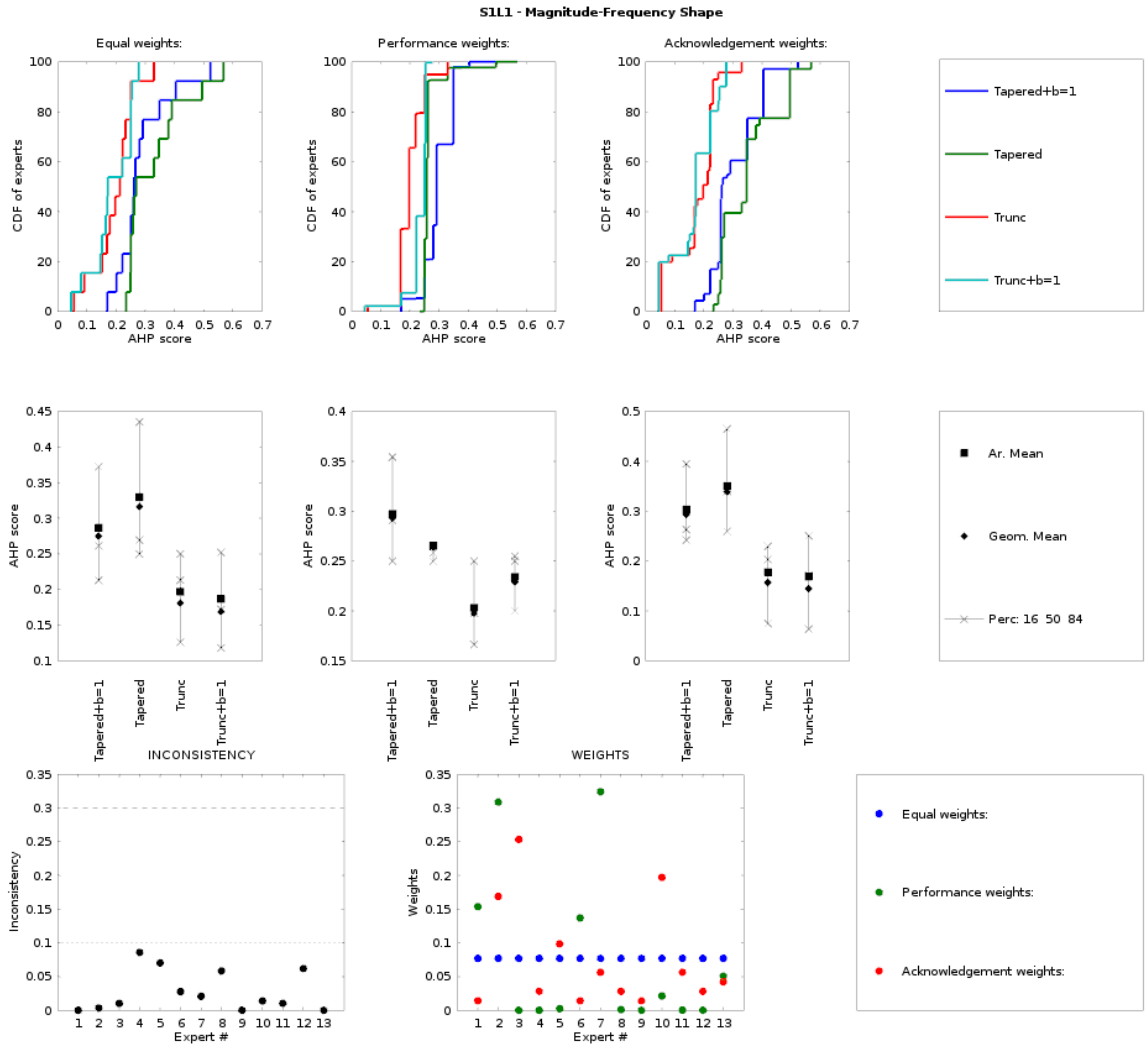

Figure 6: Results of Question 3 – Q3a, regarding the earthquake scaling law to be adopted for PS seismicity. Two options were available: "Scaling laws from Strasser et al. (2010)" ("Strasser" in Figure), and "Scaling laws from Murotani et al. (2013)" ("Murotani" in Figure). The different panels report: (first row) the empirical cumulative distribution showing the variability among the experts, adopting the different weighting schemes in each column; (second row) the results of AHP scores and relative uncertainty, adopting the different weighting schemes in each column; (third row – left column) the inconsistency CI for each expert; (third row – right column) the different weights.

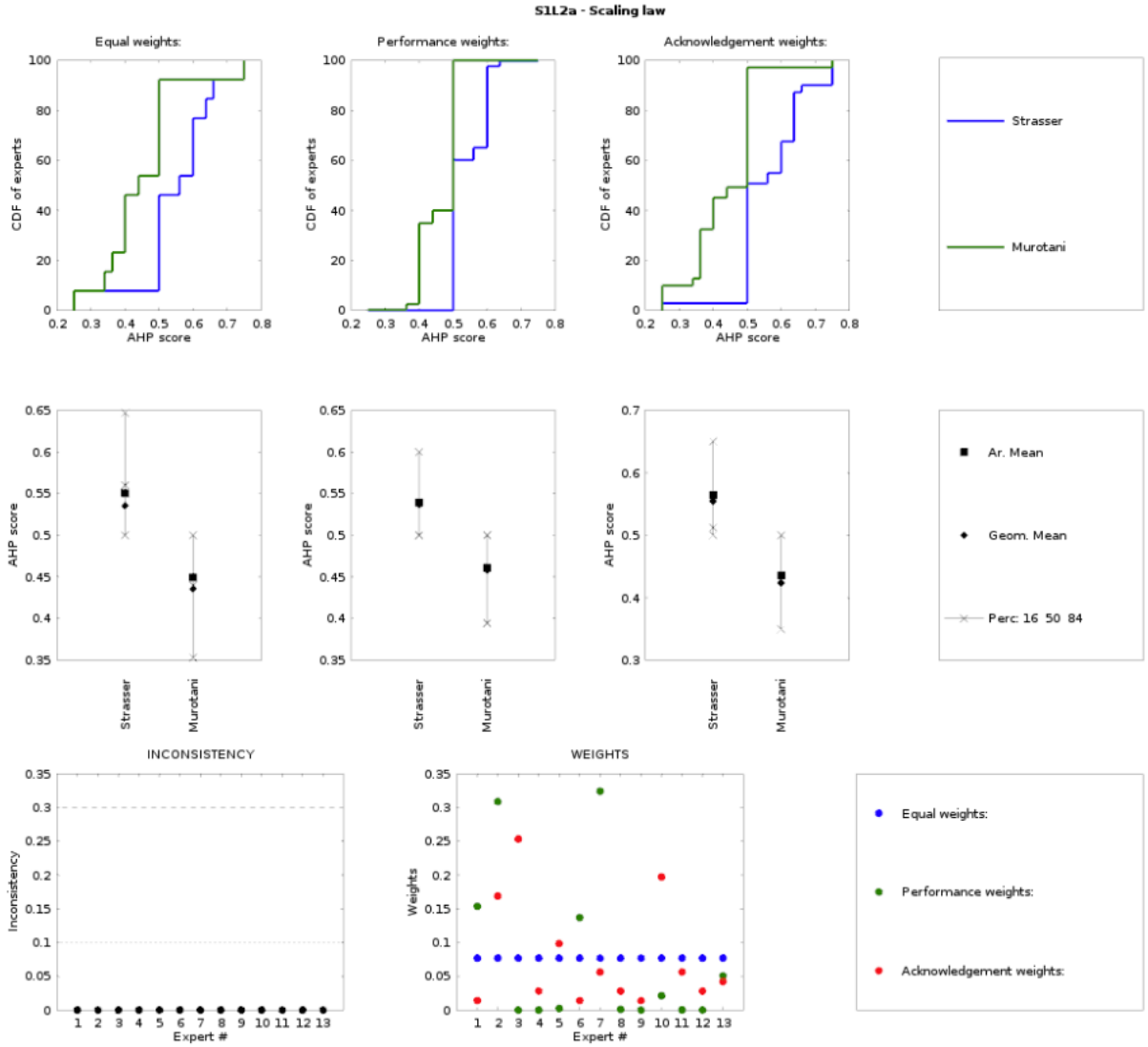

Figure 7: Results of Question 3 – Q3b, regarding the seismogenic depth for PS seismicity in subduction interfaces. Two options were available: "Co-seismic slip is not allowed or allowed to happen at shallow depths under the accretionary wedge" ("Nucl." in Figure), and "Co-seismic slip is allowed to happen at shallow depths under the accretionary wedge" ("Nucl+Prop" in Figure). The different panels report: (first row) the empirical cumulative distribution showing the variability among the experts, adopting the different weighting schemes in each column; (second row) the results of AHP scores and relative uncertainty, adopting the different weighting schemes in each column; (third row – left column) the inconsistency CI for each expert; (third row – right column) the different weights.

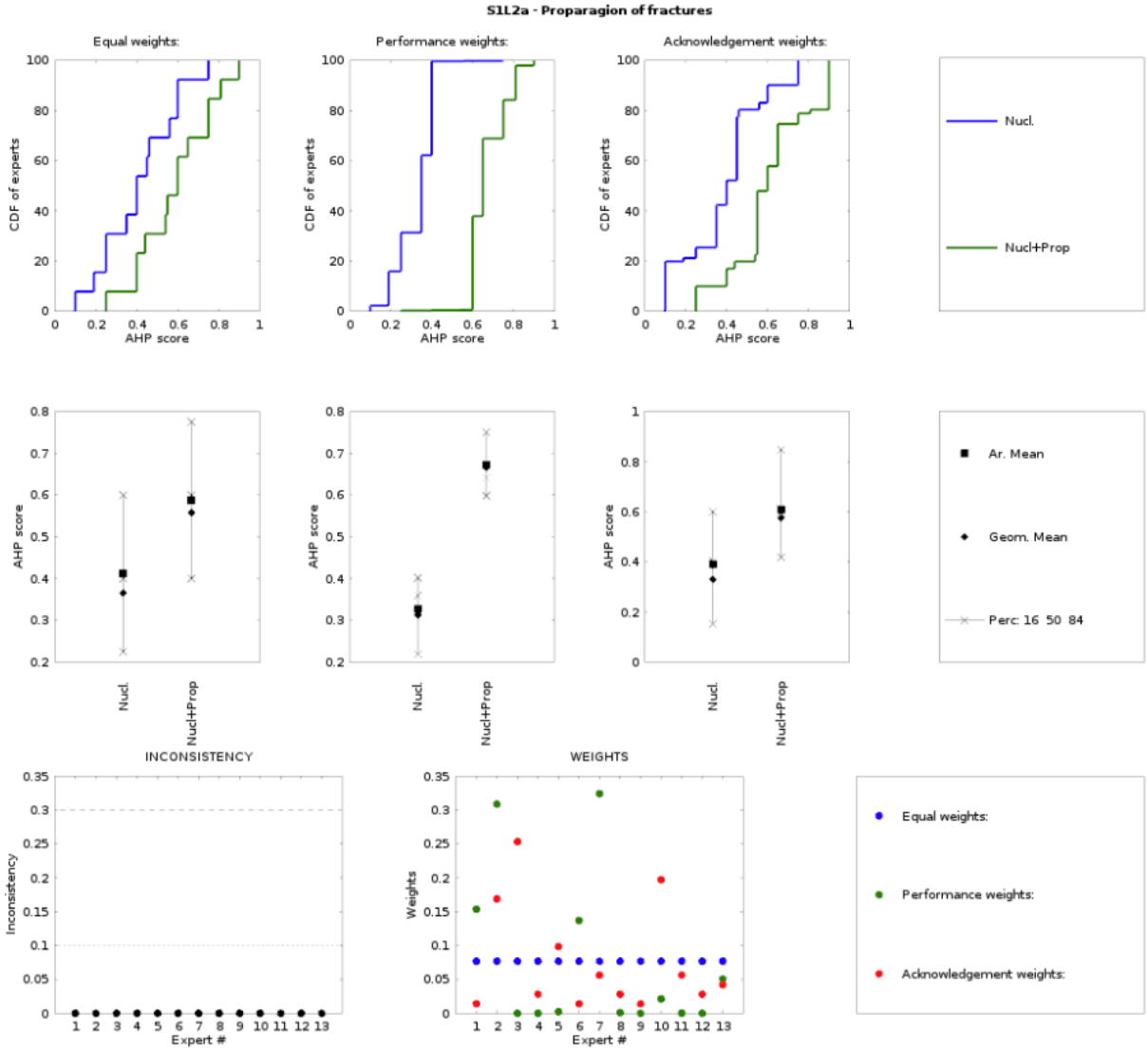

Figure 8: Results of Question 3 – Q3c, regarding the possibility of using or not depth-dependent rigidity. Two options were available: "Rigidity is uniform with depth (PREM)." ("Uniform" in Figure), and "Rigidity varies with depth according to Geist and Bilek 2001." ("Depth-dep" in Figure). The different panels report: (first row) the empirical cumulative distribution showing the variability among the experts, adopting the different weighting schemes in each column; (second row) the results of AHP scores and relative uncertainty, adopting the different weighting schemes in each column; (third row – left column) the inconsistency CI for each expert; (third row – right column) the different weights.

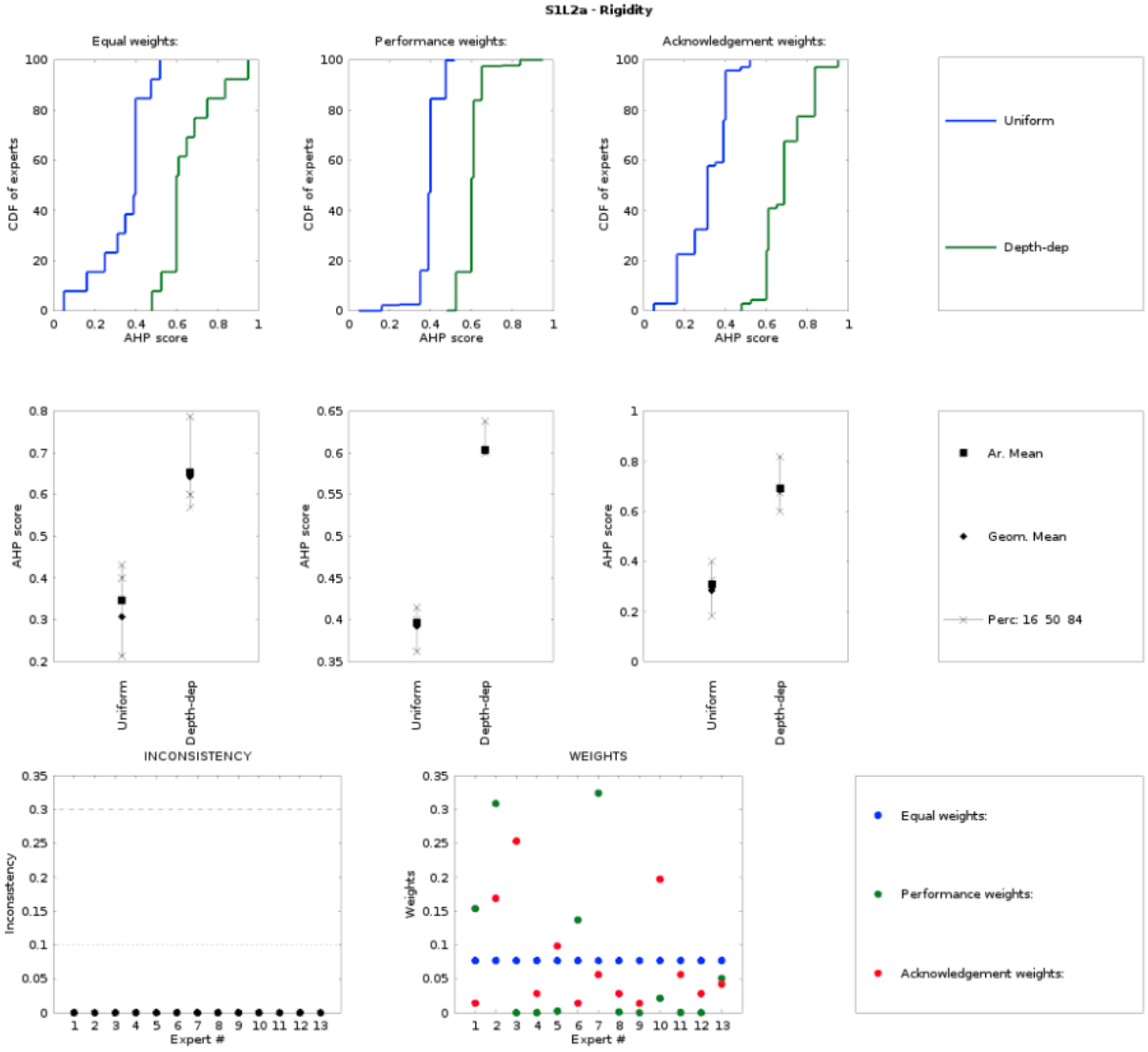

References

Davies, G., Griffin J., Løvholt F., Glimsdal S., Harbitz C., Thio H.K., Lorito S., Basili R., Selva J., Geist E., Baptista M.A. (2017) A global probabilistic tsunami hazard assessment from earthquake sources, Geological Society, London, Special Publications, 456, 23 February 2017, https://doi.org/10.1144/SP456.5.

Forman, E. & Peniwati, K. (1998). Aggregating individual judgments and priorities with the analytic hierarchy process. European Journal of Operational Research, 108(1), 165-169.

Geist, E.L. & Bilek S.L. (2001), Effect of depth-dependent shear modulus on tsunami generation along subduction zones, Geophys. Res. Lett., 28, 7, 1315-1318, https://doi.org/10.1029/2000GL012385.

Goepel, K.D. (2013), IMPLEMENTING THE ANALYTIC HIERARCHY PROCESS AS A STANDARD METHOD FOR MULTI-CRITERIA DECISION MAKING IN CORPORATE ENTERPRISES – A NEW AHP EXCEL TEMPLATE WITH MULTIPLE INPUTS, Proceedings of the International Symposium on the Analytic Hierarchy Process 2013.

Harker, P. & Vargas L. (1987), The Theory of Ratio Scale Estimation: Saaty's Analytic Hierarchy Process. Management Science. 33(11), 1383–1403.

Morgan, M.G. (2014). Use (and abuse) of expert elicitation in support of decision making for public policy, Proc. Nat. Acad. Sci. 111(20); 7176-7184, DOI:10.1073/pnas.1319946111

Murotani, S., Satake K., & Fujii Y. (2013), Scaling relations of seismic moment, rupture area, average slip, and asperity size for Mw~ 9 subduction zone earthquakes, Geophys. Res. Lett., 40, 5070–5074, doi:10.1002/grl.50976.

Saaty, T.L. (1980), The Analytic Hierarchy Process: Planning, Priority Setting, Resource Allocation, ISBN 0-07-054371-2, McGraw-Hill.

Saaty, T.L., Hu G. (1998), Ranking by Eigenvector Versus Other Methods in the Analytic Hierarchy Process, Appl. Math. Lett. Vol. 11, No. 4, pp. 121-125, 1998.

Strasser, F.O., Arango M.C., & Bommer J.J. (2010), Scaling of the source dimensions of interface and intraslab subduction-zone earthquakes with moment magnitude, Seismol. Res. Lett., 81, 941–950.

Zio E. (1996), On the use of the analytic hierarchy process in the aggregation of expert judgments, Reliability Engineering & System Safety, Volume 53 (2), 127-138, ISSN 0951-8320.

Probabilistic TSUnami Hazard MAPS
for the NEAM Region (TSUMAPS-NEAM)
ECHO/SUB/2015/718568/PREV26

PHASE II – STAGE 5: Results

Author: **TSUMAPS-NEAM Technical Integrator (TI) team**

Date: **12 September 2019**

Version: **2.1**

Table of Contents

Executive Summary

This document illustrates the NEAM Tsunami Hazard Model 2018 (hereinafter referred to as "NEAMTHM18"), as well as the results of the main tests performed to check the NEAMTHM18 consistency and robustness.

The first Chapter addresses the NEAMTHM18 in terms of hazard curves and derived maps. It also briefly illustrates few by-products derived from the NEAMTHM18 construction. The main results are discussed through sample navigation of the hazard curves and maps, simple statistics of the hazard geographic distribution, and a frank presentation of the main limitations of the NEAMTHM18. The possible uses of the NEAMTHM18 are illustrated by two potential use cases. One describes how it is possible to move from the long-term hazard to evacuation maps to be used in tsunami early warning systems. The other addresses how such a wide regional hazard model can be used to set priorities in local hazard assessments and risk analysis. Finally, the users are guided in how to use the graphic user interface with which they can navigate the hazard and probability maps, inspect hazard curves of individual point of interests, and download data. These results can be accessed at http://www.tsumaps-neam.eu/, under the "PTHA" menu.

The second Chapter addresses the quality of the NEAMTHM18 through four different analyses. Sanity checks carried out to verify the correctness of the automatic implementations; disaggregation to reveal "what is due to what" by linking hazard intensities to their causative sources; sensitivity to test the consequences of critical choices that were necessarily made during the implementation phase; and few checks against data on past tsunami.

This page is intentionally left blank.

1) Hazard model results: NEAMTHM18

The hazard model is the main result of the TSUMAPS-NEAM project. These results are constituted by hazard curves (Section 1.1) and hazard and probability maps (Section 1.2). In addition, there are several by-products (Section 1.3) which are intermediate results obtained in the process of calculating the hazard. The hazard model is disseminated online through the dedicated webpage http://www.tsumaps-neam.eu/neamthm18/, which is the landing page associated with the Digital Object Identifier (DOI) to be minted by INGV through DataCite (https://datacite.org/). The DOI is persistently associated to the present version of the hazard model, i.e. NEAMTHM18. In the case an update of the hazard model is deemed necessary, it would take a new DOI, but the present model will remain online to guarantee the reproducibility of any study of experiment that may have been carried out in the meanwhile. Conversely, the by-products are considered as a work in progress. A copy of all of them will be permanently stored in the INGV servers and made available upon request for verification and reproducibility of the NEAMTHM18. Their dissemination will depend on the availability of resources to put them in a form suitable for distribution outside INGV.

1.1) Hazard curves

The hazard curves available at http://www.tsumaps-neam.eu/neamthm18/ epitomize the main result of all calculations. Hence, they are the principal product of the NEAMTHM18. All other results are either intermediate results used to derive hazard curves or are derived from hazard curves (including hazard maps). The hazard curves express the probability of exceedance versus different values of a "hazard intensity threshold", during a given period, called the "exposure time." The probability of exceedance is always a number between 0 and 1. Probability and frequency of an event in time are linked together so that each probability value corresponds to a so-called average return period (ARP), which is the average time span between two consecutive events of the same intensity.

In TSUMAPS-NEAM, the adopted exposure time is 50 years, whereas the adopted hazard intensity measure (or metric) is the tsunami Maximum Inundation Height (MIH) evaluated at a point of interest (POI), which is representative of the stretch of coast behind the POI itself. A single MIH value (at a single POI) represents an estimate of the mean value along the coast, as the actual MIH values vary laterally along the coast behind the POI. Based on our methodological analysis, we can say that local maxima of the actual MIH (and maximum run-up) values along the coast are expected not to exceed 3-4 the mean MIH estimated at POI. More details on MIH and its lateral variability can be found in *Doc_P2_S1*, CHAPTER 3 and Section 4.5.

We recall that the NEAMTHM18 deals with earthquake-generated tsunamis, and that it is a time-independent hazard model, as the earthquake occurrence is modelled as a Poisson process.

To represent the uncertainty of the NEAMTHM18 several curves are shown in a single plot, corresponding to different percentiles of the hazard curve distribution spanning the NEAMTHM18 uncertainty (**Figure 1.1**).

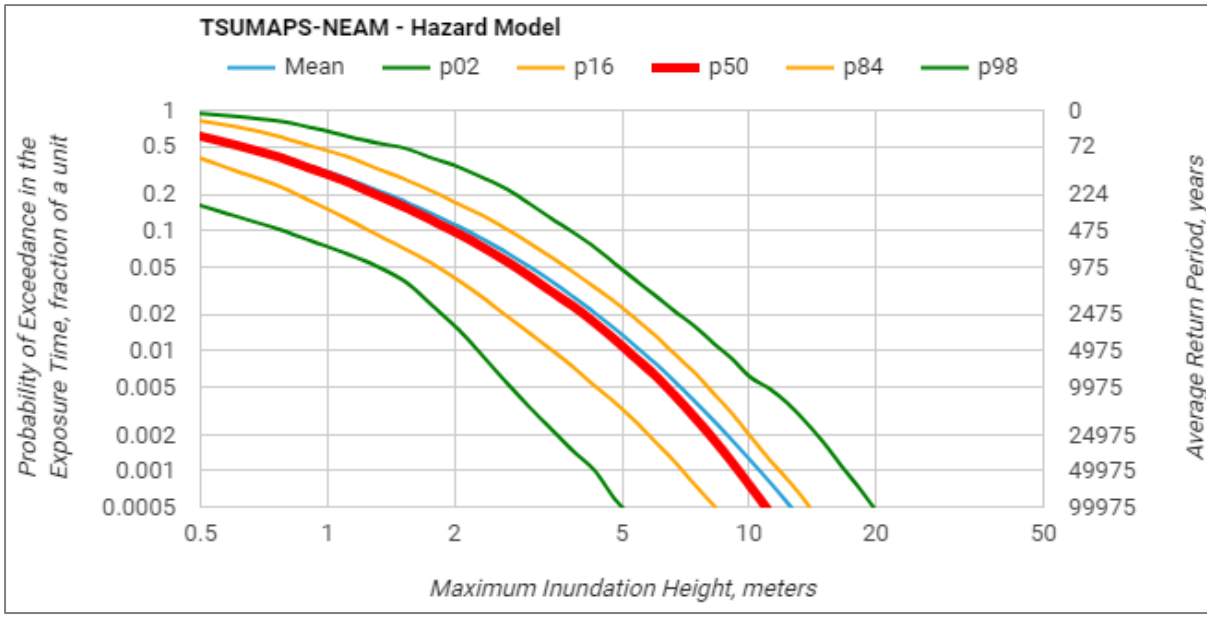

Figure 1.1 Example of a plot of a hazard curve distribution at a POI, expressed through different percentiles spanning the uncertainty of the NEAMTHM18.

The NEAMTHM18 results can be summarized as follows:

- We calculated **Hazard curves** at **2,343 POIs** (North-Eastern Atlantic: 1,076; Mediterranean Sea: 1,130; Black Sea: 137) at an average **spacing of ~20 km**.
- For each curve, we provide values for the **mean, 2nd, 16th, 50th, 84th, and 98th** percentiles of the whole ensemble of models that represent the epistemic uncertainty on the hazard.

1.2) Hazard and probability maps

Hazard and probability maps available at http://www.tsumaps-neam.eu/neamthm18/ are derived from hazard curves. On such maps, each POI is assigned a color value according to the value of hazard intensity or probability of exceedance, respectively (**Figure 1.2**).

To make a hazard map, we extract the MIH corresponding to a chosen design probability (left-hand y-axis of a hazard curve in **Figure 1.1**), or, equivalently, to a given ARP (right-hand y-axis of a hazard curves in **Figure 1.1**), for each POI. POI's colors on this map scale according to the MIH measured in meters. Engineers and other hazard specialists generally use this type of maps.

To make a probability map, we extract the probability of exceedance in 50 years corresponding to a chosen value of MIH (x-axis of a hazard curve) for each POI. POI's colors on the probability map scale according to the probability expressed by a number between 0 and 1. This type of maps is more useful to communicate the hazard to administrators, decision makers, and to the general public.

Based on the scheme illustrated above, we put together the following portfolio of maps:

- **Probability maps** for **MIH 1, 2, 5, 10, 20** meters;
- **Hazard maps** for **ARP of 500, 1000, 2500, 5000, 10000** years.

For each map, we prepared three different map views including the **mean, and the 16th and 84th** percentiles of the epistemic uncertainty.

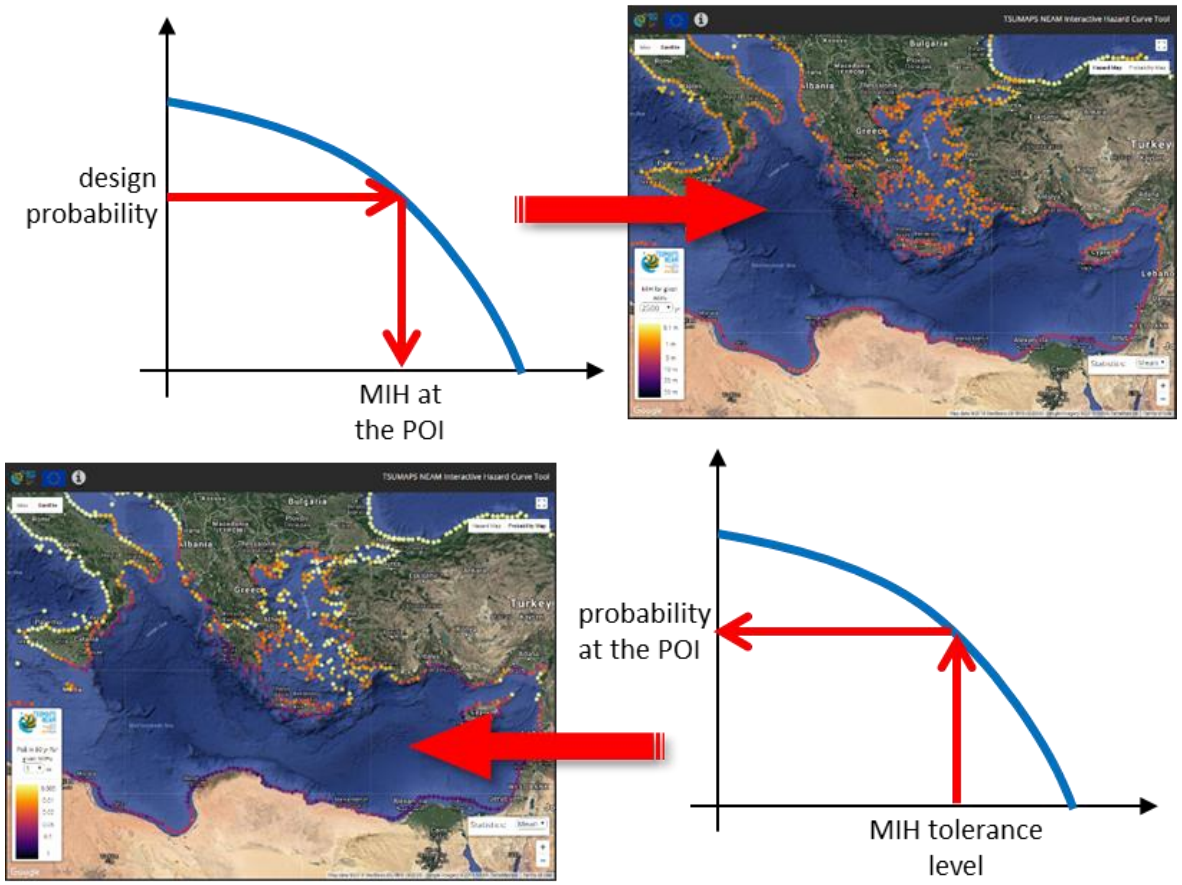

Figure 1.2 Top: Hazard map, i.e. values of MIH in meters at each POI, obtained by cutting hazard curves at a given probability of exceedance in 50 years. Bottom: Probability map, i.e. probability of exceedance in 50 years, obtained by cutting hazard curves at a given MIH value.

All these hazard curves and maps are accessible through the Internet. User can explore and download these data through a specially designed interactive tool (see Section 1.6). As an example, **Figure 1.3** shows default views presented by the interactive tool on the corresponding website.

1.3) By-products

All the final and intermediate project's results are available for future research. Some intermediate results of potential interest and relevance for other applications are listed below.

- Database of earthquake scenarios and relative mean annual rates included into the NEAMTHM18. The source area covers all the Mediterranean, Marmara, and Black sea, as well as a large area in the northern Atlantic Ocean, including the Mid-Atlantic Ridge (north of the equator) and the Caribbean arc. More details are reported in *Doc_P2_S1.*

- Database of pre-calculated tsunami scenarios for more than 120,000 elementary Gaussian sources (ca. 30 Tb of data) covering an area of ca. $6x10^6$ km^2. This database allows reproducing of arbitrary tsunami scenarios by means of linear combination of the Gaussian-shaped elementary sources distributed directly over the sea surface (Molinari et al., 2016).

The source area covers all the Mediterranean, Marmara, and Black sea, as well as a large area in the northern Atlantic Ocean. More details are reported in *Doc_P2_S1.*

- Database of local amplification factors calculated following the model proposed by Glimsdal et al. (2019). Amplification factors are evaluated for different incoming wave periods and polarities along the large set of local bathymetric profiles offshore target areas in the NEAM region. They can be applied to simulate the coastal impact (in terms of MIH) of any tsunami hitting the target area. Amplification factors have been evaluated for all the adopted POIs, covering all the NEAM region. More details can be found in *Doc_P2_S1*.

- Hazard calculation platform: the platform allows the automatic quantification of SPTHA with alternative hazard models in the form of ensemble models. The model can be customized in terms of discretization, probabilistic models, propagation models, amplification models, treatment of alternative implementations, etc. More details can be found in *Doc_P2_S3.*

A more detailed description of these results can be found in the other technical documents and are published or will be included into manuscripts to be submitted for publication on scientific journals. They are also available upon request to the project coordination (http://www.tsumaps-neam.eu/contact-us/).

1.4) Selected examples

Tsunami waves can travel long distances without dispersing too much energy. Therefore, relatively-high hazard can even affect places that are relatively far from the earthquake source that generated the tsunami.

This is the case of the Caribbean subduction zone that contributes to the tsunami hazard of European and African coastlines in the Atlantic Ocean. Within the Mediterranean Sea, seismic sources are always much closer to most of the coastlines than in the Atlantic Ocean. Nonetheless, tsunami hazard can be high also in zones that are known for not hosting significant seismic sources. For example, although Libya and Egypt do not host hazardous seismic sources, probability maps show that their coastlines are more likely to be affected by tsunami than the coastlines of southern Italy, Greece, Turkey, and Cyprus – regions located closer to the subduction zones hosting the largest seismic sources in the entire NEAM region. In other words, differently from other types of earthquake-related hazards, both local and distant sources contribute to earthquake-generated tsunami hazard. This means that although the closeness to seismic sources is certainly a good proxy for relatively high tsunami hazard, the farness from seismic sources is not necessarily a proxy for low tsunami hazard.

An added value of a region-wide hazard map is that the hazard of different and even very distant places can be compared at a glance. It is often convenient to start from the map view. One can then dig into the more complete hazard curves starting from the maps. As an example, the probability of exceeding an MIH of 5 meters in northern Libya is 25 times larger than in southern Sicily (**Figure 1.4**).

Also places that are as far apart as Ireland and the Black Sea can be compared (**Figure 1.5**). Ireland can be affected by tsunamis from earthquake sources as distant as the Caribbean subduction, whereas the Black Sea, an almost closed basin, can be affected by local earthquake sources only.

Such comparisons are possible only because tsunami hazard was computed all at once and in a consistent manner everywhere in the NEAM region.

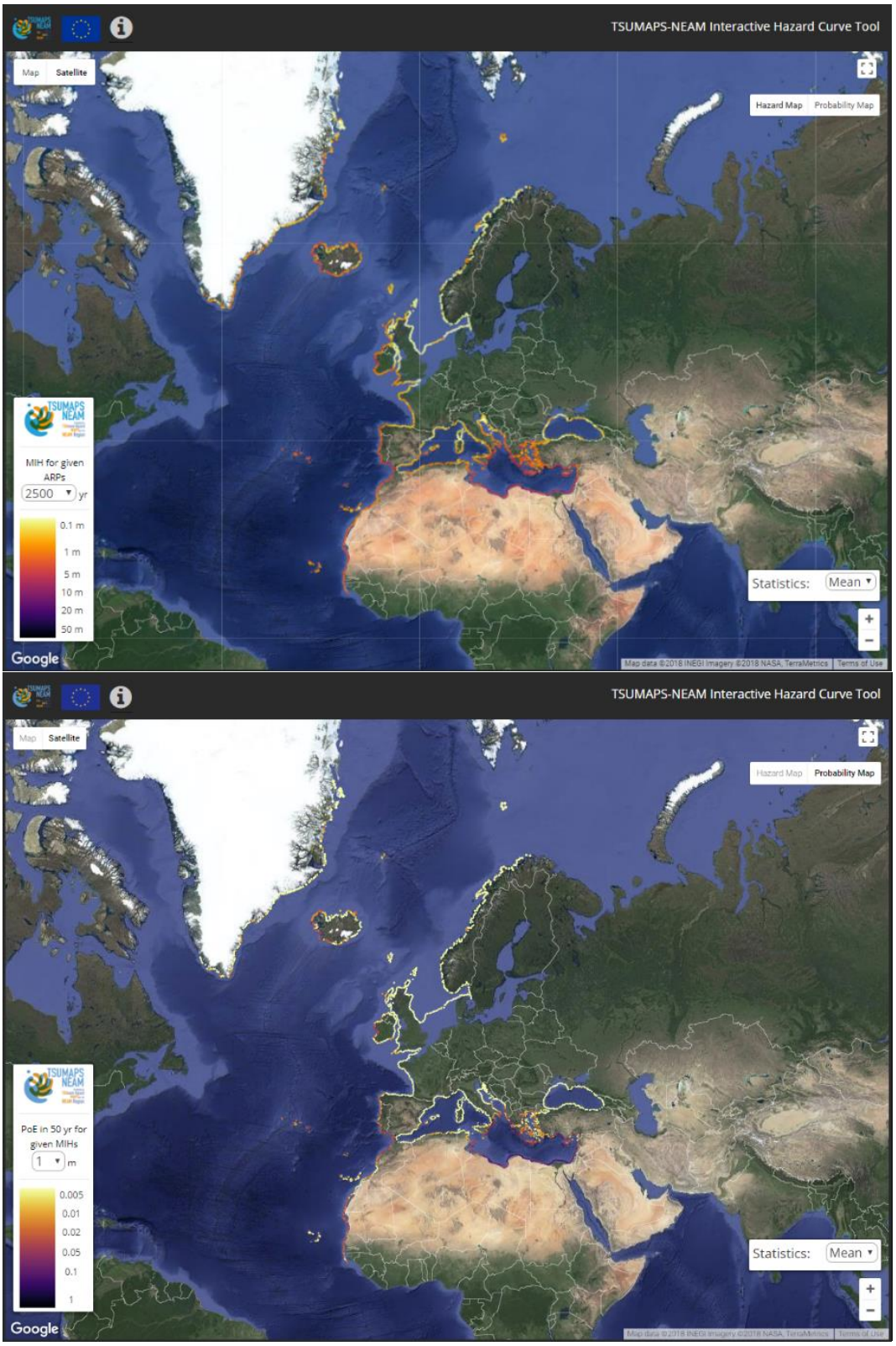

Figure 1.3 Default view for hazard, ARP = 2500 yr (top) and probability, MIH = 1 m (bottom) maps of the NEAM region.

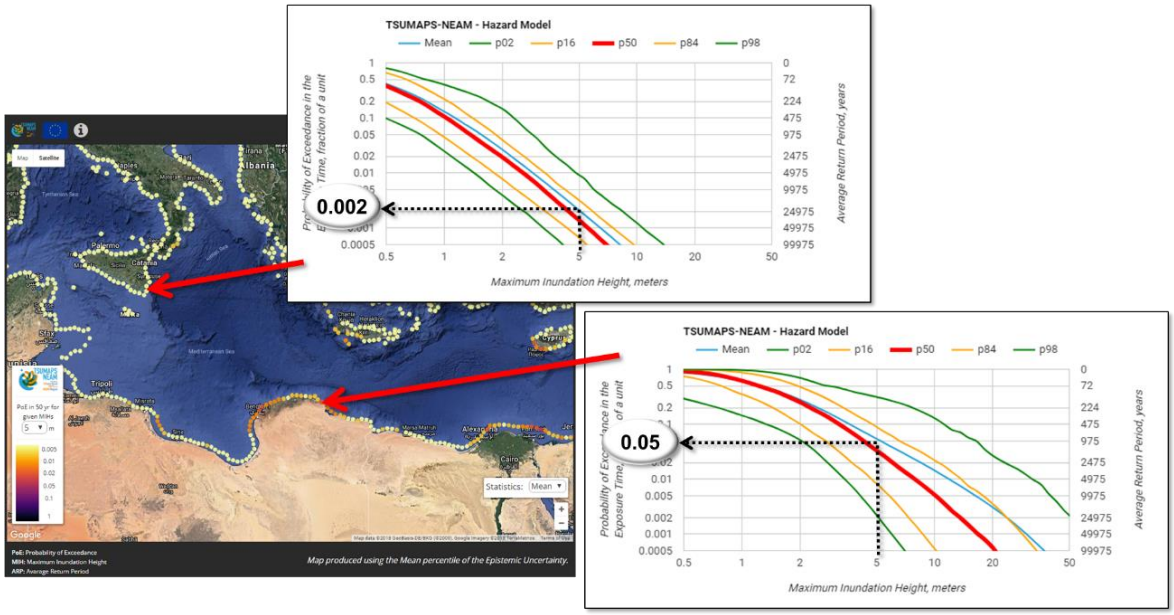

Figure 1.4 Comparison of the probability of exceeding an MIH of 5 meters at two sample localities.

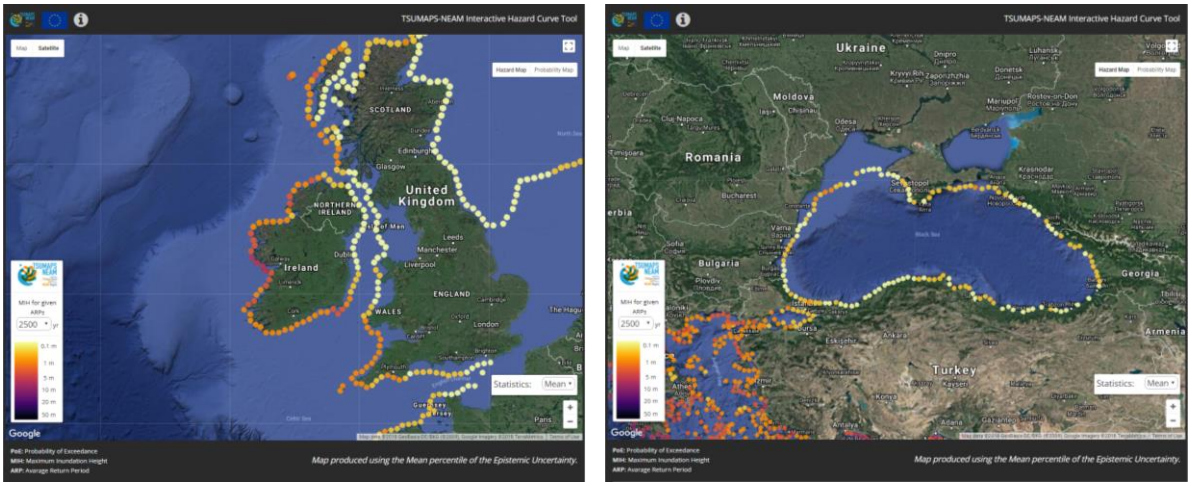

Figure 1.5 Close-up views of two distant locations within the NEAM region. Compare the differences between the western coast of Ireland (left) and the Black Sea (right). Both views are hazard maps showing the MIH that can be exceeded with an ARP of 2500 years.

In general, catastrophic events, such as those that can produce MIHs larger than several meters, are rare but not impossible. The highest tsunami hazard of the NEAM region is to be found in the central-eastern Mediterranean, where long stretches of the coastline can exceed an MIH of 5 m with significant probability values, and in the region of the Gulf of Cadiz (**Figure 1.6**). In the latter, much of the hazard is driven by the Cadiz subduction zone and surroundings.

On the one hand, considering an ARP of 2,500 years, altogether the cases of MIH larger than 5 m remain within the 1% of the entire NEAM region. On the other hand, over 30% of NEAM coastlines correspond to an MIH larger than 1 meter, whose local fluctuations may lead to a run-up of several meters (**Figure 1.7**, Left).

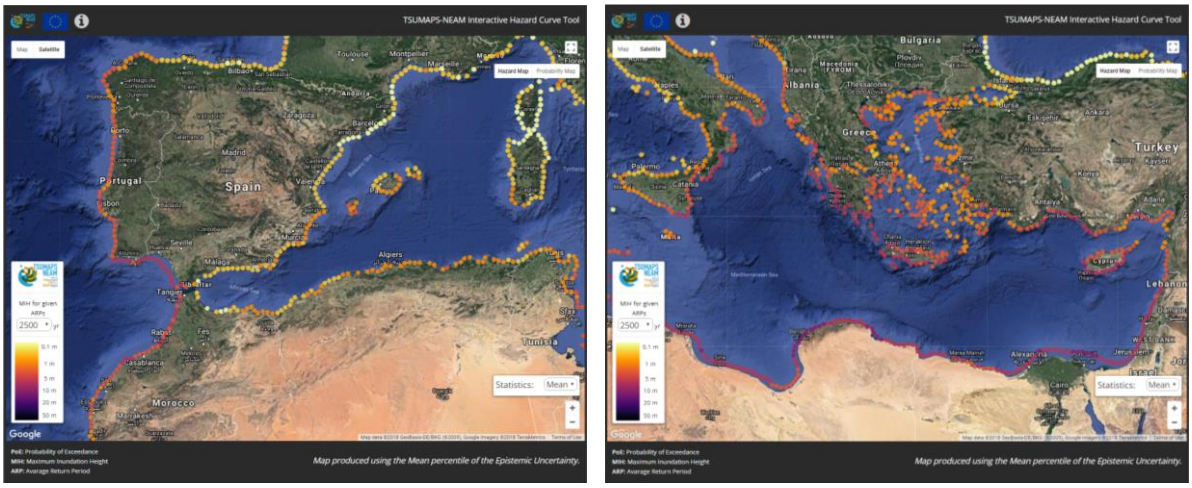

Figure 1.6 Close-up views of the coastlines with the highest hazard of the NEAM region. The Gulf of Cadiz (left) and the eastern Mediterranean (right). Both views are hazard maps showing the MIH that can be exceeded with an ARP of 2500 years.

The NEAM region is very large and includes coasts facing zones of relatively low seismicity. If we repeat the analysis for the Mediterranean only, we indeed find a larger incidence of destructive events (**Figure 1.7**, Right).

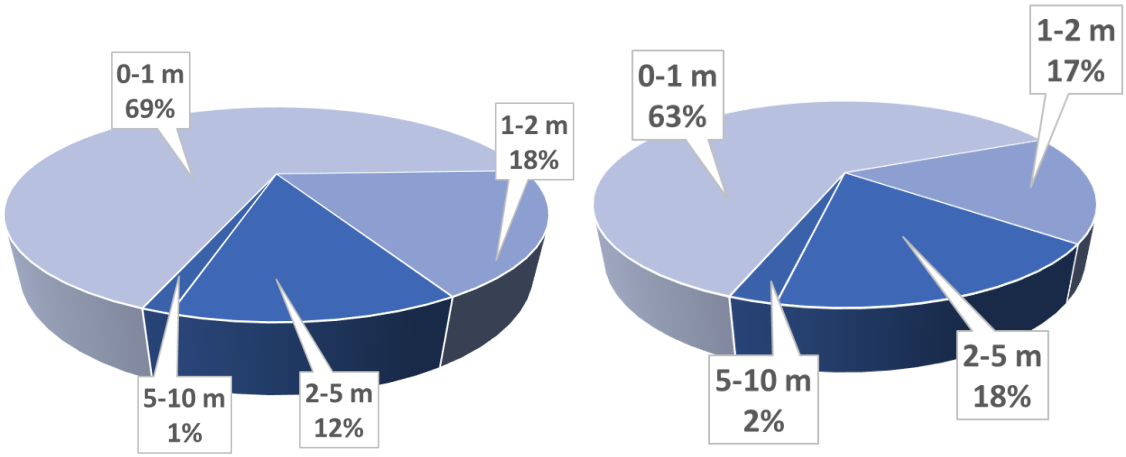

Figure 1.7 Left: Pie chart showing the percentage of NEAM coastlines that corresponds to different tsunami intensities MIHs for an ARP of 2500 yr. Notice that this percentage decreases with increasing MIH because larger events are rarer than smaller events. Right: Same as left but for the Mediterranean only.

1.5) Remarks, and Limitations of the hazard model

We make in this paragraph some general remarks concerning the NEAMTHM18. Through them, we want also to stress that the NEAMTHM18 results have several limitations.

We start with noting that the NEAMTHM18 shares the same limitations as any other hazard model. A probabilistic hazard model attempts to predict future hazard at a location. However, a model cannot ever be an exact representation of the reality or predict the future hazard precisely, also due to limited scientific understanding and lack of data. Indeed, even if two places have the same mean hazard, the actual hazard can be very different for different percentiles of the epistemic uncertainty.

The spreading of the hazard curves at every POI conveys in fact the information about the uncertainty that affects these estimates. For example, one of the results of the hazard model is the ARP of a given MIH being exceeded at some location. The longer the ARP, the scarcer the observations for building and for testing (and eventually falsifying) the model. This fact is generally expressed by a greater dispersion of the NEAMTHM18 percentiles around the mean ARP.

The growing of uncertainty for increasing ARP and in general uncertainties of tsunami hazard models are strongly related to the fact that tsunamis are rather low-frequency (but possibly high-impact) events. Therefore, tsunami hazard models, in comparison with hazard models for more frequent phenomena, have typically even scarcer observations to be based on and for calibration, perhaps with the Pacific Ocean making an exception (e.g. Geist & Parsons, 2016). For this reason, following a common and almost standard practice (Geist and Lynett, 2014; Grezio et al., 2017), the NEAMTHM18 was built by modelling earthquake probability and tsunami generation and impact from these earthquakes, rather than building it directly from available tsunami data, which is an almost impossible task.

Tsunami data, such as long records of a measured run-up at a specific coastal site, are even scarcer in the NEAM region than in other regions characterized by more frequent (large) earthquakes, as it may be the case for Chile, for example.

In any case, all the above-mentioned circumstances ask for caution when using hazard results for practical applications, particularly for long ARPs.

The NEAMTHM18 is the result of a project that, likewise any other project, relies on finite material and human resources. We strived for an optimal trade-off between feasibility and depth of the analysis. However, some further analyses, the collection of new data, and general improvements may be achieved in future updated versions. For example, the impact on hazard results of the uncertainty of the bathymetric model used for tsunami propagation was not fully assessed, because this task was out of reach for the project. Only a qualitative check of the differences in the results of some scenarios performed with a different bathymetric model was performed. This circumstance and other issues are reported in the documentation, including some other points raised by the reviewers which could not be addressed for practical reasons.

We also wish to clearly point out that our regional-scale model cannot substitute the in-depth analysis at sub-regional (national) and local levels. Being a regional model, its resolution and spatial completeness are limited. Its primary purpose, and consequently usage, is that of a screening tool for prioritizing further higher-resolution hazard and risk assessments at a more local scale. Local models require in fact very detailed calculations over coastal areas, and higher-resolution local data. Moreover, as mentioned above, a MIH of 1 m at some POI may indicate 3-4 m of maximum local run-up. This is another reason why a region-wide hazard assessment cannot replace detailed local hazard assessments.

If the local scale is considered in any practical application based on the regional model, great caution is needed, and it must be understood that very large uncertainty would characterize this application. These uncertainties are necessarily larger than those stemming from specific local high-resolution model.

Nevertheless, a regional hazard may provide informative input to decision-making as well as local studies. The next section will describe a couple of potential use-cases. They are just examples, however. Any further application reusing hazard data for risk-management applications and decision making is not necessarily straightforward. We recommend to always rely on the work done by hazard and risk specialists.

1.6) Potential Use-Cases

Establishing a regional long-term probabilistic tsunami hazard assessment for seismic sources is the first step to be undertaken for starting local and more detailed hazard and risk assessments and then risk management. Coastal regulation and planning, building code definition, and safety of critical infrastructures all depend on these actions. The main advantage of the probabilistic approach in comparison with classical scenario-based methods is that it allows engineers to perform spatially-homogeneous quantitative risk-analysis, and decision-makers to base their choices on quantitative cost-benefit analysis and comparative studies between different areas, allowing for rational and ethical decisions.

1.6.1) From Long-Term Hazard to Evacuation Maps for Tsunami Early Warning

People can become aware of an impending tsunami by warnings issued by a National Authority or by observing natural signs, such as strong and unusually long shaking, receding sea, roars from offshore. In both cases, it is crucial though that people know in advance the possible escape routes toward higher ground.

In the absence of a probabilistic tsunami hazard map, the local authorities usually follow the experts' advice coming from the scientific community. This behavior sometimes leads to the decision of setting the limit of the tsunami hazard zone at a distance from the coast that corresponds to a certain topographic height or to a maximum tsunami run-up. These distances may be spatially very inhomogeneous because they hardly contemplate all the possible scenarios or because they may refer to scenarios with very different ARPs. Using probabilistic tsunami hazard maps can help to make this decision less subjectively. The inundation distance corresponding to a design probability or ARP, potentially considering uncertainty for increasing safety, can be extrapolated with approximated methods from the MIH provided by the NEAMTHM18. For example, one can consider the relationship between MIH and maximum run-up discussed in Section 3.5 of *Doc_P2_S1* and various approaches to consider wave energy dissipation on large inundation distances. This type of approach is being followed in New Zealand (MCDEM, 2016). The Italian Civil Protection has also followed this approach for establishing the national guidelines for the local planning against tsunamis (DCDPC, 2018).

1.6.2) Setting priorities for Local Probabilistic Inundation Maps in Hazard and Risk Analyses

Local hazard analyses can be expensive and time-consuming and should then be standardized and prioritized, for example, to start working on the areas with the largest hazard. Standardization can be based on the comparison with a common regional analysis. A prioritization based on the selection of an ARP suitable for a specific application (e.g., an ARP of 2,500 years is being proposed for building codes by civil engineers in the USA) can help the work of decision makers. The priority assessment can be done by comparing the regional-scale hazard at different locations for that

specific ARP. Other aspects to take into consideration are the locally exposed coastal population or the infrastructures, thus basing the prioritization also on risk elements.

Local tsunami hazard analysis (**Figure 1.8**) requires the use of state-of-the-art high-performance computing, provided that high-resolution digital elevation models be available for nearshore and onshore areas. To limit the computational cost, the analysts may need to select a limited number of high-resolution inundation scenarios (e.g., Lorito et al., 2015; Volpe et al., 2019), for which regional hazards may provide a first screening. The relevant scenarios for the site under examination can be selected using NEAMTHM18 results, and then perform detailed simulations without compromising the results of the analysis.

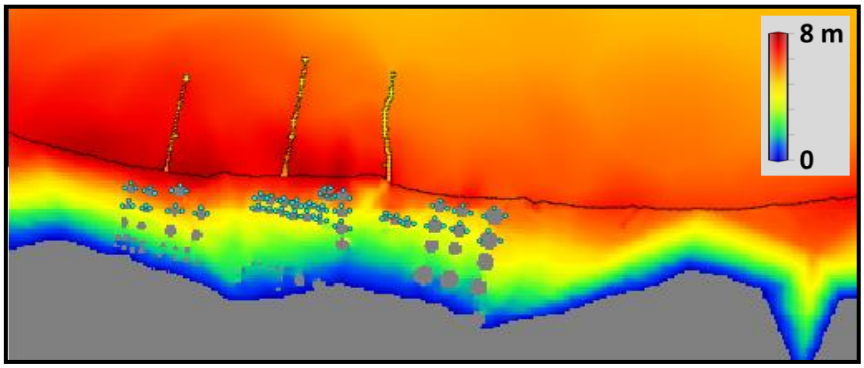

Figure 1.8 Example of a high-resolution tsunami inundation map showing the maximum wave height in the Milazzo Port, southern Italy, for a nearby magnitude 8 earthquake.

1.7) Interactive Tool

The NEAMTHM18 results (curves and maps) are freely and seamlessly accessible through the Internet (http://www.tsumaps-neam.eu/), in particular through its "Interactive Hazard Curve Tool" that can be found in PTHA section. Through this tool, all the results can be visualized, and the main results downloaded. No authorization, no login, no special permission is required to navigate and download these data. Only a web browser and an internet connection are needed.

There are two main layouts for the tool (**Figure 1.9**). One is a mapper that displays a geographic base map where hazard and probability maps are overlain; the other is a pop-up window that displays a graph with hazard curves.

There are 30 different hazard displays in this mapper. Five views for different ARPs (500, 1000, 2500, 5000, and 10000 years), and five views for different MIHs (1, 2, 5, 10, and 20 m). For each map, there are three views (mean, 16th, and 84th percentiles) to explore the uncertainty of the reported values. All these displays can be rendered with different backgrounds and zoom levels for enhancing the user's navigation experience.

The POI can be queried by a simple mouse-click that triggers the display of the hazard curve graph. Mouse-hovering on the curves changes the pointer into a crosshair to visually connect the axes of the plot and a balloon that shows the exact values of the curve. The filters on the left-hand side of the pop-up window turn on and off hazard curves of different percentiles. Two links on the left-hand side of the pop-up window start the download of the hazard curve data or an image of the hazard plot.

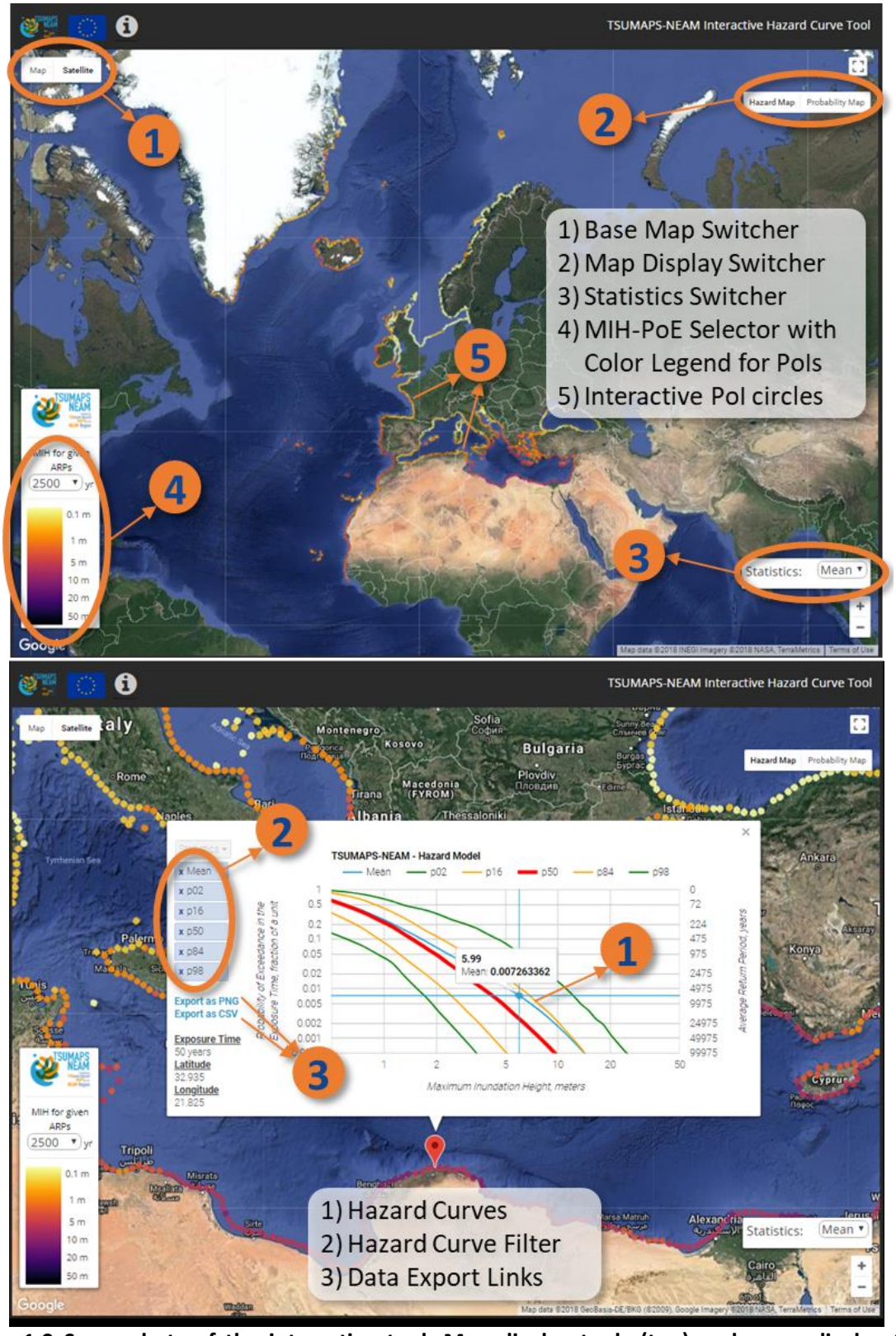

Figure 1.9 Screenshots of the interactive tool. Map display tools (top) and curve display tools (bottom).

2) Tests and checks on intermediate and final results

The results are produced throughout a long chain of analyses, sometimes well rooted in the literature, sometimes more innovative. This chain is extensively described in *Doc_P2_S1.* To perform these analyses, several codes were produced and then implemented in the project computational platform. Different authors wrote these codes in different programming languages. These analyses were then run mostly automatically, to ensure the use of up-to-date versions and the required homogeneousness over the very large source and target areas here considered.

The impact of specific modeling choices, assumptions, discretization, as well as of errors and bugs, is sometimes hidden, not determining unreasonable results nor effects that can attract the attention of the authors at first sight.

To make as sure as possible that the results correspond to the intention of the authors and to decrease the possibility of unwanted behaviors, a series of in-depth analyses were performed, which can be subdivided into four categories:

1. **Sanity checks**: to verify that all automatic implementations provided results consistent with what expected and with their input data, mainly to identify potential errors and bugs in implementations. Some of these checks have been implemented in the early stages of the project (as described in earlier versions of the documentation), eventually updated here. Others are on the final results.
2. **Disaggregation**: to deepen into the hazard results, unveiling "what is due to what" and quantifying the probabilistic link between specific hazard intensities with their potential causative sources. Disaggregation results depend on both tsunami propagation (modelling) and on probability of occurrence of individual scenarios.
3. **Sensitivity**: to explicitly test the consequence of some of the methodological choices, especially if innovative. Many of these sensitivity tests were proposed in the project's implementation plan, as an outcome of the first elicitation of the Pool of Experts and the suggestions emerged during project meetings and the review of the Internal Review panel.
4. **Checks against past tsunamis:** to compare the available tsunami record with the hazard results. This task has been developed only in the very last part of the project, and it has been limited by lack of time and resources, as well as by other more technical issues. This task should be better defined and developed in future projects.

2.1) Sanity checks

Sanity checks are specifically focused on identifying potential bugs and/or unwanted results, such as the disagreement with input data. Many specific tests were performed while developing codes. Here, we list only the most important, that is those which compare the results of multiple codes and/or analyze steps that are particularly relevant (e.g., annual rates for sources). All these tests implied development of specific codes. Sanity checks can be subdivided into two main classes: one class regarding deterministic tsunami modeling and another regarding probabilistic modeling.

Checks on deterministic tsunami results: millions of individual earthquake and tsunami scenarios are used to compute probabilistic hazard results. Within the long chain producing such scenarios, we performed the following tests:

- **POIs and Regions**: POIs were defined automatically. The definition and position of the Point of Interests have been checked for consistency with the expected depth (50 m), retaining only the POIs located at depths between 40-100m.
- **Tectonic Regions**: Tectonic regions were compared with available seismicity data, to avoid unwanted spurious effects at the borders due for example to epicentral uncertainty. Some tectonic regions were reshaped (mostly at outer boundaries) to be more adapted to the available seismic catalogs or completeness zonation; some zones could be removed altogether since they were far from any water.
- **Tsunami Elementary Sources**: One of the project's innovations is the adoption of the Gaussian-shaped elementary tsunami sources (ES) approach for hazard assessment. Checks of the ES comprise an assessment of their suitability related to spacing, extension, and resolution (ES propagation), their integrity, and the linear combination scheme. Several sets of ES were produced: for the Mediterranean, the Black Sea, and the Atlantic. Information and figures on checks for all basins (BLK, MED, NEA) and the full set of POIs can be found in ***Appendix 1***.
- **The integrity of scenarios**: Checks are mainly focused on verifying the integrity of BS/PS scenarios, from ES to tsunami wave evaluation offshore and its amplification. A short description of the 'deterministic production chain' and its sanity checks are given in ***Appendix 2***.
- **Mareogram period and polarity extraction**: the period-and-polarity extraction algorithm is checked for stability of the results, which is achieved in virtually all cases; an estimate of the quantities is always given (***Repository 1***).

Checks on the Probabilistic seismic model*:* Given the very large extension of the source area, probabilistic models have been produced automatically. Therefore, in addition to standard tests of the codes' authors, we implemented some further independent tests. These tests are mainly based on the check of the consistency of the outputs with the input, performed by codes developed independently from the ones used for quantifying the probabilistic models.

- **Magnitude and spatial distribution**: The consistency of the results of probabilistic models have been tested through standardized statistical tests checking the consistency of the probabilistic models of seismic sources and their input data, in terms of number and spatial distribution of earthquakes (N- and S-tests; Zechar et al., 2010). When possible, also independent data have been used. The tests have been applied in different sub-regions and with different input dataset, as illustrated in more details in ***Appendix 3***. In **Figure 2.1**, as an example, we report the result of N-test for the entire source region and for magnitude larger than 7.0. The input data and data from Pacheco and Sykes (1992), which are a subset of the entire period, from a different catalogue, contain a number of events in each magnitude interval that is compatible with what forecasted by the seismic source models. In the magnitude of interest for tsunamis (larger than 6.5), the results are compatible for all datasets and sub-areas.
- **Background seismicity mechanism**: The NEAMTHM18 has two basic types of seismicity: One is the Predominant Seismicity (PS) for the large subduction earthquakes. It involves 3D fault geometry and may have a heterogeneous slip. All other seismicity is modeled as Background Seismicity (BS), which is defined as probability density function over different earthquake

mechanisms for geographical cells. An attempt to verify these PDF against available data and past studies was made in the document in ***Appendix 4***.

- **Elicitation code**: the processing of experts' answers has been performed in parallel by two codes, developed independently, providing identical results.
- **Ensemble sampling**: The ensemble model was generated by 1000 samples of the alternatives tree, accounting for the weights of the alternative provided by the elicitation results. We verified the consistency of the weights with the sampled models in the 1000 samples, as reported in the document in ***Appendix 5***.
- **Conditional hazard curves**: Randomly sampled conditional hazard curves for all POIs have been visually inspected, as reported in **Figure 2.2**. In addition, we performed a sensitivity test (Section 2.3) comparing these curves with the ones that would have been obtained adopting a more classical Green's law amplification.

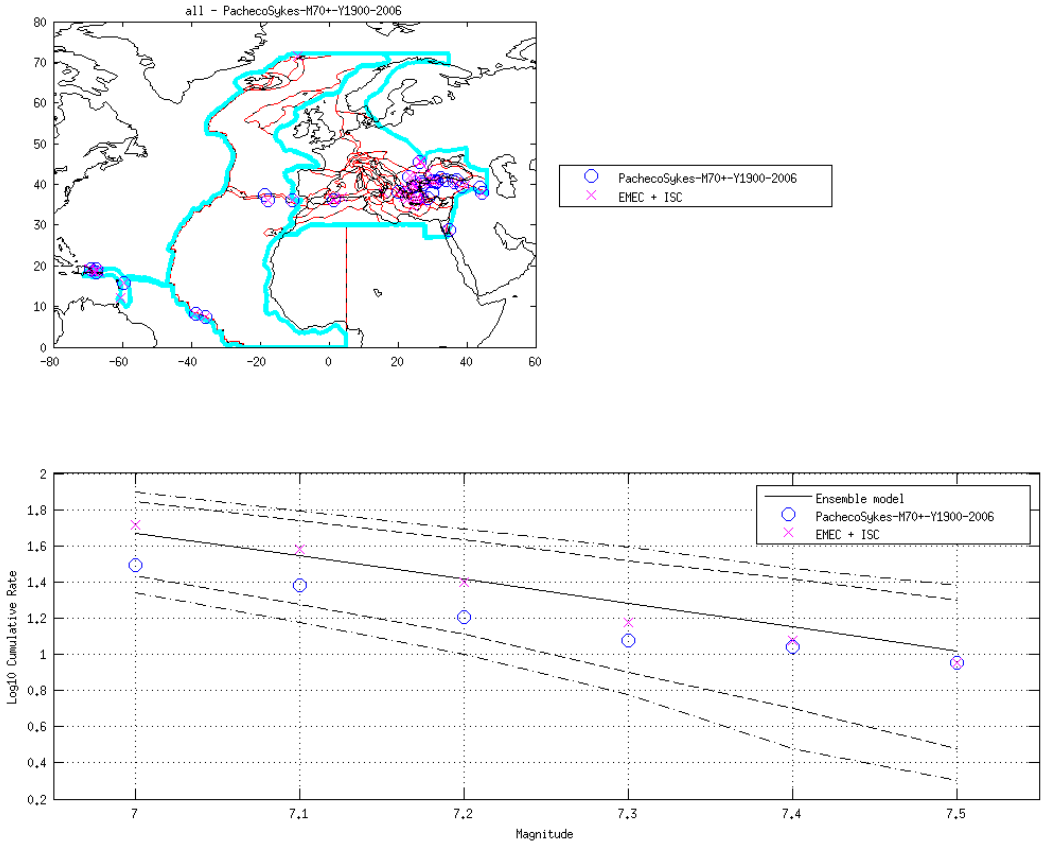

Figure 2.1 N-test results for the entire source region. Pink crosses are the input data (EMEC and ISC for Mediterranean and Atlantic, respectively), for which different completeness periods are considered for the different magnitudes and areas. Blue circles are Pacheco and Sykes (1992) catalog (from 1900 to 2006), with completeness magnitude Mw 7.0. The different black lines indicate the rates forecasted by the source model, along with their confidence intervals (0.95 and 0.99), compared with the observed ones. Similar tests have been produced for sub-regions (Atlantic and Mediterranean) for both Pacheco and Sykes (1992) catalog and global CMT catalog (completeness magnitude Mw 5.5).

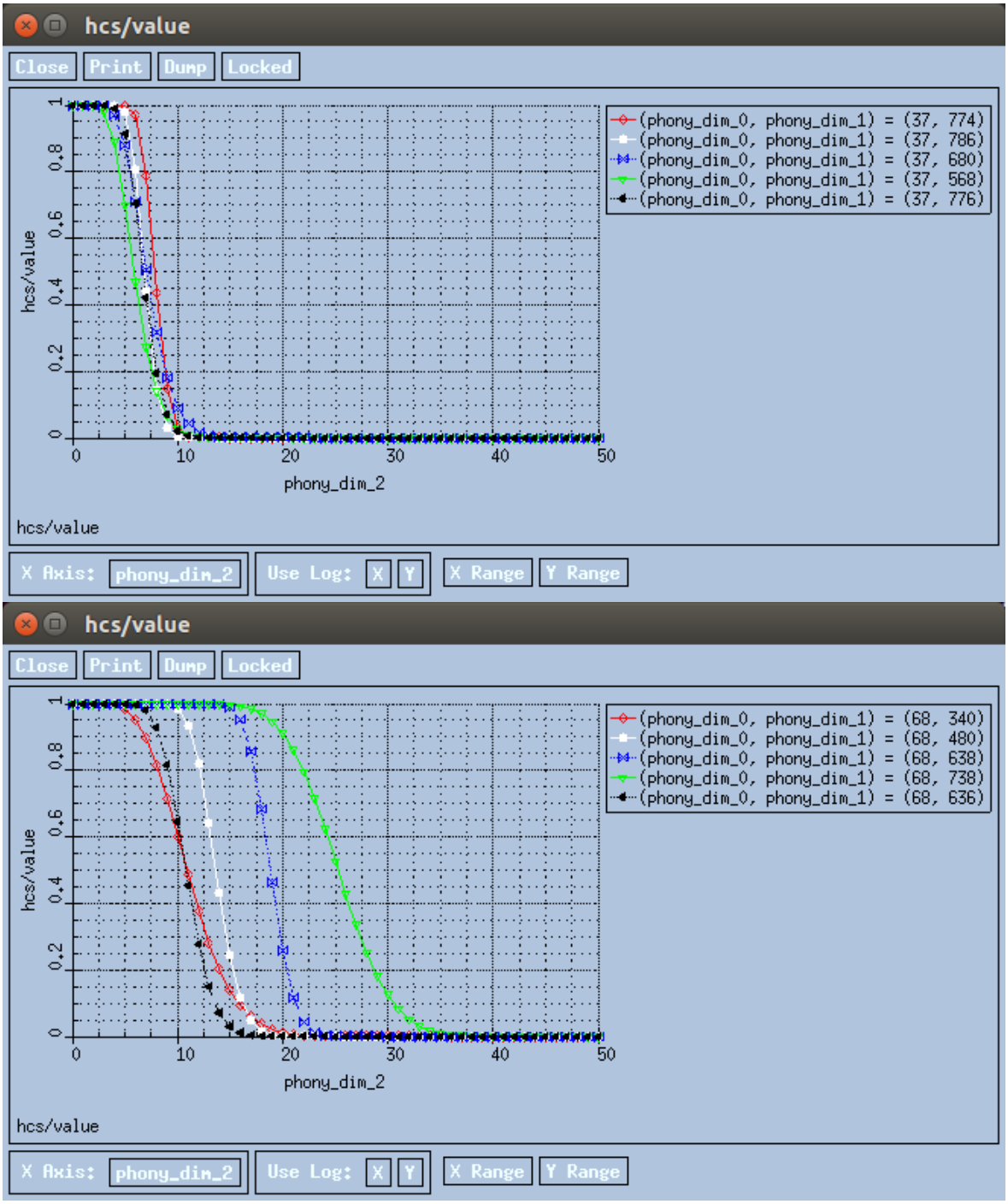

Figure 2.2 Example of visual inspection of alternative conditional hazard curves (conditioned upon the occurrence of a given scenario).

2.2) Disaggregation results

Disaggregation allows deepening into the hazard results, trying to identify the main sources for specific target hazards (Bazzurro and Cornell, 1999; for SPTHA, Selva et al., 2016). This allows quantifying the relative importance of different source areas, or magnitudes, or whatever parameter in input to the hazard, as a function of specific hazard levels in one POI.

A standard set of disaggregation analyses has been performed for 42 POIs spread over the Black Sea, the Mediterranean Sea and the Atlantic Ocean, as reported in **Figure 2.3**.

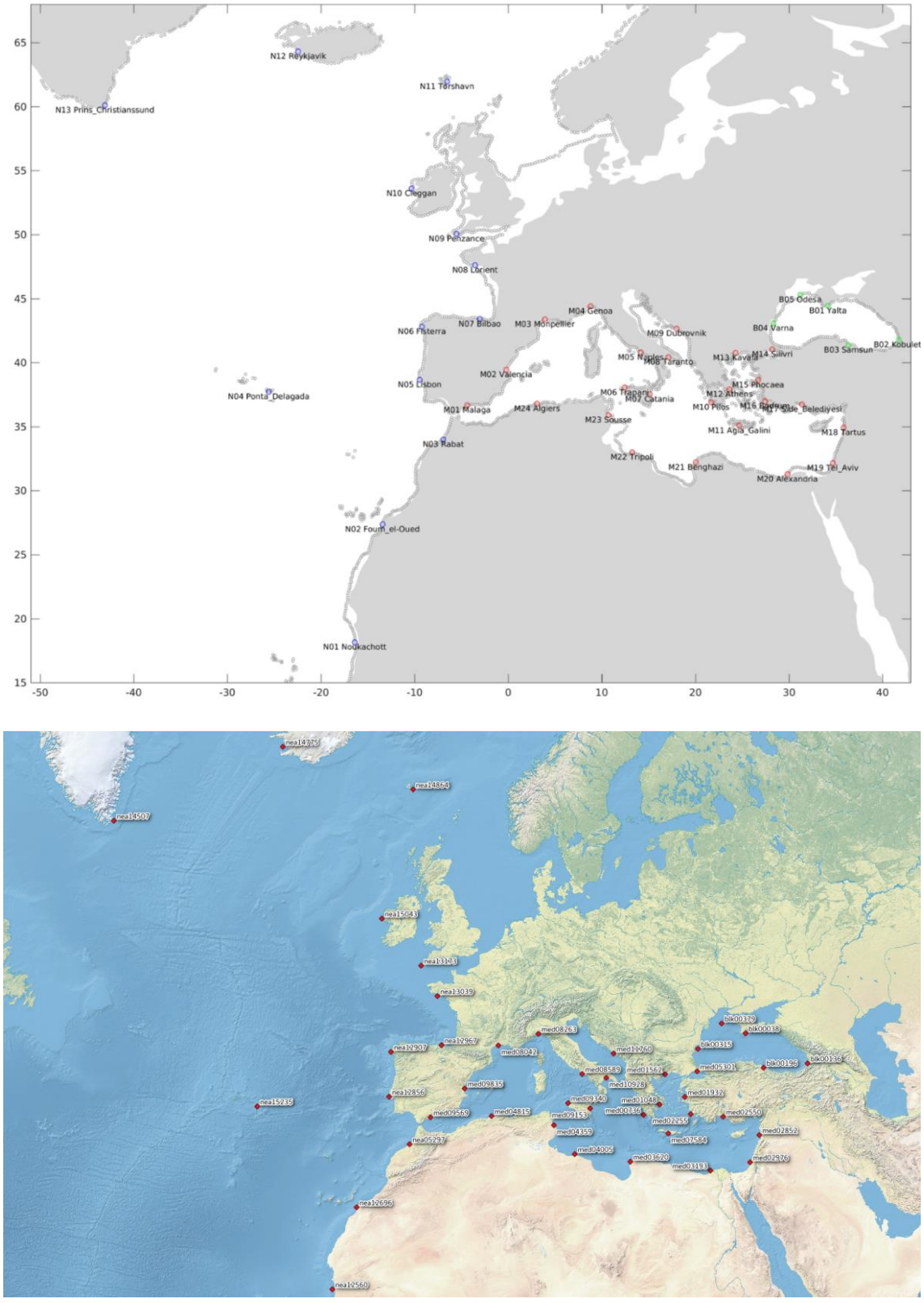

Figure 2.3 Location of the 42 Points of Interest (POI) in which the disaggregation results are provided (names above, codes below).

The following disaggregation analyses were produced in each of these POIs:

- **Seismicity Class**: we computed the relative importance of PS and BS sources as a function of the tsunami intensity, that is Pr(PS|MIH>x) and Pr(BS|MIH>x), reporting also the impact of epistemic uncertainty in this evaluation. An example of this figure is reported in **Figure 2.4A**.
- **Tectonic Region**: we computed the relative importance of the different tectonic regions in each POI, that is Pr(Region|MIH>x). We produced three plots, either separating the contribution of BS and PS or evaluating them jointly. These plots have been produced only for the mean of the epistemic uncertainty. An example of this figure is reported in **Figure 2.4B**.
- **Magnitude**: we computed the relative importance of different magnitudes, that is Pr(M|MIH>x). For each POI, we prepared 2 plots reporting the mean of the epistemic uncertainty only. In the first plot, we report Pr(M|MIH>x) as a function of x for several magnitude levels. In the second plot, we report Pr(M|MIH>x) as a function of M for x = 1.11, 5.373 and 12.314 m. An example of this figure is reported in **Figure 2.4C**.
- **Fault location**: we computed the relative importance of different fault locations, that is Pr(lon,lat|MIH>x), where lon, lat are the coordinates of the geometrical center of the faults. An example of this map is reported in **Figure 2.4D**. The maps are produced for the mean of the epistemic uncertainty for x = 1.11 and 5.373 m.

The figures for all the selected POIs of Figure 2.3 are reported in ***Repository 2***.

2.3) Sensitivity tests

Several sensitivity tests were described in the preliminary documentation of the NEAMTHM18, as well as proposed at various project's meetings. Some other sensitivity tests were suggested by the PoE (Pool of Experts), as an outcome of the first elicitation. Sensitivity was planned mainly as an analysis in support of some decisions, such as the choice of implementing or not implementing an alternative model or fixing a magnitude threshold for tsunami modelling.

Some tests that were discussed or proposed during the implementation plan of the NEAMTHM18 (*Doc_P1_S4*); some are still mentioned in *Doc_P2_S1*). Such tests were either suggested by the PoE through the first elicitation (*Doc_P1_S3)* or proposed by the project partners (*Doc_P1_S4 or Doc_P2_S1*). Some others were also suggested during the review process (*Doc_P2_S1*).

Hereinafter, we report the list of the main sensitivity tests performed, considering available resources, as a result of this discussion.

a. **Inclusion/exclusion of PS sources**: the disaggregation results have partially overcome this sensitivity (discussed in Section 2.2 of *Doc_P2_S1*), since we have quantitatively evaluated the influence of PS sources at different levels of the hazard and in different areas. Inclusion of further PS sources was not addressed, mainly for the lack of suitable very-well constrained fault models.
b. **PS geometry and mechanism**: the single scenario results obtained with 3D geometries have been tested against progressive simplifications of the fault geometry for the Mediterranean subduction zones (Tonini et al., 2017, ***Appendix 6***). The results show that geometrical complexities are relevant and their inclusion for the Mediterranean subductions was appropriate.

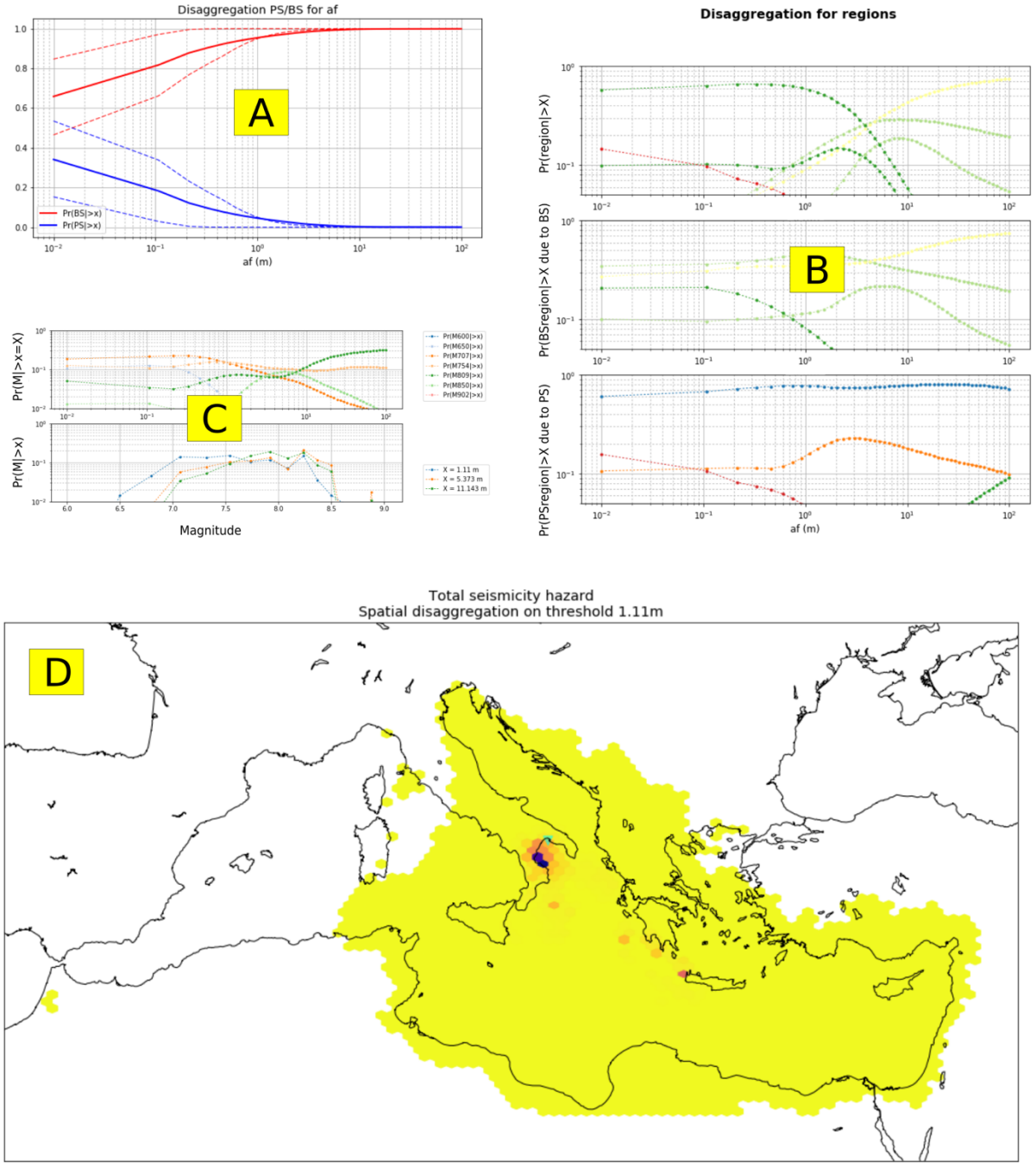

Figure 2.4 Example of the figures produced for the disaggregation in all the POIs reported in Figure 2.3.

c. **Consistency of Bayesian models with standard models:** we visually compared the observed rates (from the catalogs) and the ones modeled with all modeling approaches (including the Bayesian one). All these comparisons are collected in ***Repository 3***. All comparisons are repeated twice, for the two implemented buffers that were adopted to separate BS and PS in the catalogs of past events. The comparison is made considering both jointly or separately the BS and PS contributions (in the regions in which both are present). **Figure 2.5** shows an example of such comparisons. Note that this visual comparison, made for each tectonic

region, provides further details to the results of the N-test (discussed in Section 2.1) that produces a quantitative statistical comparison at much larger scale as regional and sub-regional levels.

d. **Unmodeled magnitudes (large magnitudes)**: some of the input seismicity models do not have any upper limit for magnitudes. This test was foreseen in the implementation plan. Indeed, tsunami modeling has an upper limit due to physical reasons. More specifically, the limit is imposed by the local thickness of the crust for BS and by the size of the 3D fault for the PS. To test the consistency of these assumptions, we extracted from our seismicity model the mean annual rate of the unmodeled sources, to check whether they can be negligible. The results for BS are reported in **Figure 2.6.** BS has very low mean annual rates for the un-modeled magnitudes (M > 8.1551) in each cell of the BS grid, always < 10^{-6} yr^{-1}. The only exception is in the Azores area, in which probably the volcano-tectonic activity is not well modeled by unbounded frequency-size distribution. The results for PS are reported in **Figure 2.7**, where we also report the maximum modeled earthquakes in each region. Here, we generally have larger mean annual rates. However, we have to account that this time (differently from BS) the annual rates are the total of the region (and not for one specific location). For the Mediterranean faults, we generally have a low mean annual rate (mostly < 10^{-5} yr^{-1}, always < 10^{-4} yr^{-1}), compatible with the range of validity of the hazard curves (< 10^{-5} yr^{-1}). We have also to note that in the Mediterranean the main subduction interfaces are split over multiple regions, and we can see that in the central part of the faults (where the largest magnitudes have their centers) the mean annual rates are smaller (< 10^{-6} yr^{-1}), while larger rates always occur in peripheral areas. This occurrence corresponds to the fact that large magnitude events are foreseen only if the center of their hypothetical fault fit in the region. This implies that large magnitudes are not included in peripheral regions, thus they are not modeled. In the future, more attention should be probably paid to this border problems, possibly introducing buffers in the fault areas. In the Atlantic, we have generally higher mean annual rates for unmodeled seismicity, especially in the mid-Atlantic ridge. Note that values are lower (< 10^{-4} yr^{-1}) where the ridge is closer to inhabited areas (Azores and Iceland). This generally large values may indicate that the total area (and consequently the maximum magnitude) foreseen in each fault is probably too small. We must note that, in these areas, unbounded magnitude-frequency distributions may be not adequate in describing the seismicity rates of large magnitudes. This shows that more attention should be paid in the future also to the seismicity distribution in these predominant faults. A special mention should be given to the Gloria fault, for which a very large maximum magnitude (when foreseen) is given in the literature and other previous hazard assessments (e.g., ESHM13 from the EU project SHARE). This large magnitude does not match the size of the known Gloria fault, whereas it would better fit in the near region of the Cadiz subduction zone. Therefore, only in this area we allowed for very large magnitudes (up to 9.1) to happen through the SBS type (see Doc_P2_S1). We didn't deal with the possibility for multi-fault and/or compound ruptures as for example in the UCERF3 model (Field et al., 2017).

e. **Unmodeled magnitudes (small magnitudes)**: the disaggregation results have overcome this sensitivity analysis (discussed Section 2.2), where we quantitatively evaluated the influence of the minimum magnitude influencing the hazard at the POI. In general, the contribution of the minimum magnitudes (in all the sources where the background seismicity is modeled, M=6.0) is negligible. The only exceptions are in the northernmost part of the Atlantic

(Iceland and Faroe Islands), where the minimum modeled magnitude (M = 7.3203 from the mid-Atlantic ridge, while no background seismicity is modeled) still is contributing to the hazard of 1.11 m. These areas have a relatively low hazard and a potentially significant (but not evaluated) contribution from volcanic sources. More attention to these areas should be given in future assessments.

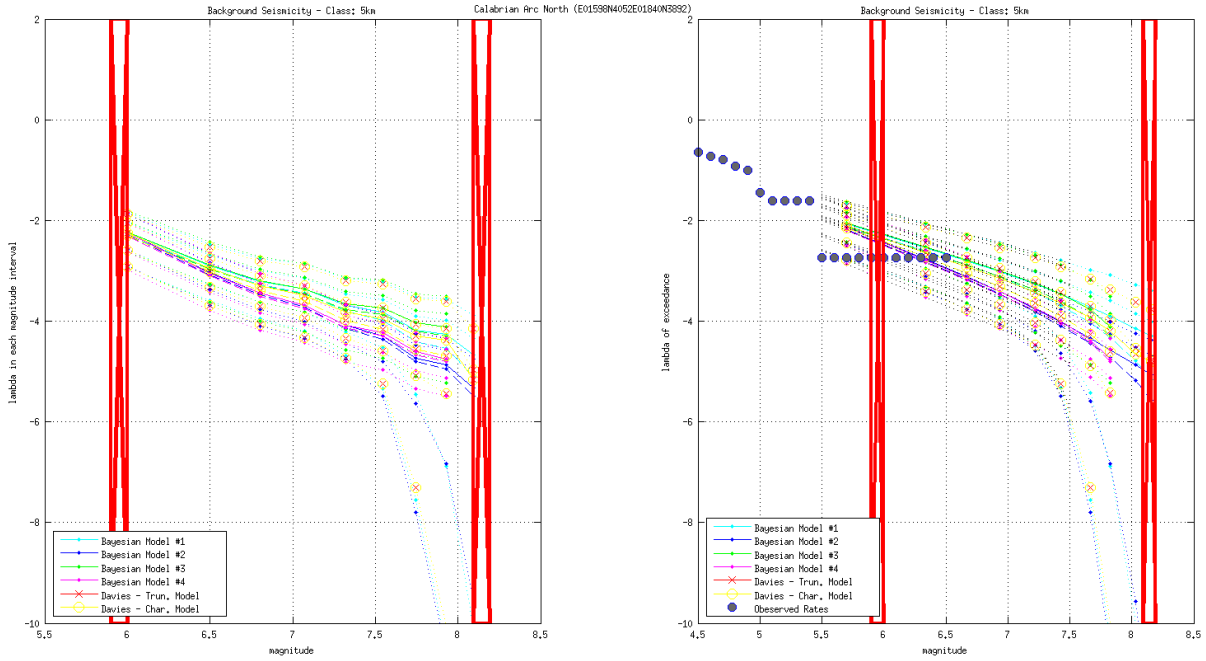

Figure 2.5 Example of the figures reported in Repository 3. Magnitude-frequency relationships are reported both decumulated (left panel) and cumulated (right panel). Dots represent the empirical cumulative distribution from the catalog. Different colors represent different models (alternatives for the epistemic uncertainty). The areas of the plot deleted in red represent the ranges of magnitudes which are not modeled, either because below the minimum magnitude modeled, or because considered not physically possible (sensitivity check d. is foreseen for this seismicity).

f. **MIH with uncertainty quantification against Green's law**: a systematic visual comparison was performed between the hazard curves obtained by adopting the method based on amplification factors, with uncertainty quantification, and the ones obtained by the standard Green's law amplification. The comparison is made in each of the NEAMTHM18 POIs. In **Figure 2.8A**, we report the summary statistics for all POIs of this difference for different tsunami intensity (panel A) and an example of comparison for POI in the Black sea (panel B). We can note that there is not a systematic bias (being all statistics approximately centered on 0), but also significant differences are observed. Several figures were produced in each POI. As reported in **Figure 2.8B,** for each POI we report the position of the POI, the hazard curves with amplifications and with Green's law (including the epistemic uncertainty confidence interval), and the difference between their mean models as a function of the tsunami intensity. These figures for all POIs are reported in ***Repository 4***.

g. **The consistency of the results against the equal weights assumption in elicitations**: we systematically compared the results of the elicitation adopting the 2 defined weighting schemes (based on performance or acknowledgment). The comparisons are reported in *Doc_P1_S3* (first elicitation) and *Doc_P2_S4* (second elicitation).

h. **Unimodality of ensemble models**: we did not implement this test. We note that being the ensemble model based on the empirical distribution of input alternative models (See *Doc_P2_S1*), potential multi-modality can be tracked.

Note that only a few of the planned tests have not been implemented, mainly due to the timing constraint of the project. We suggest considering performing these tests in future hazard quantifications.

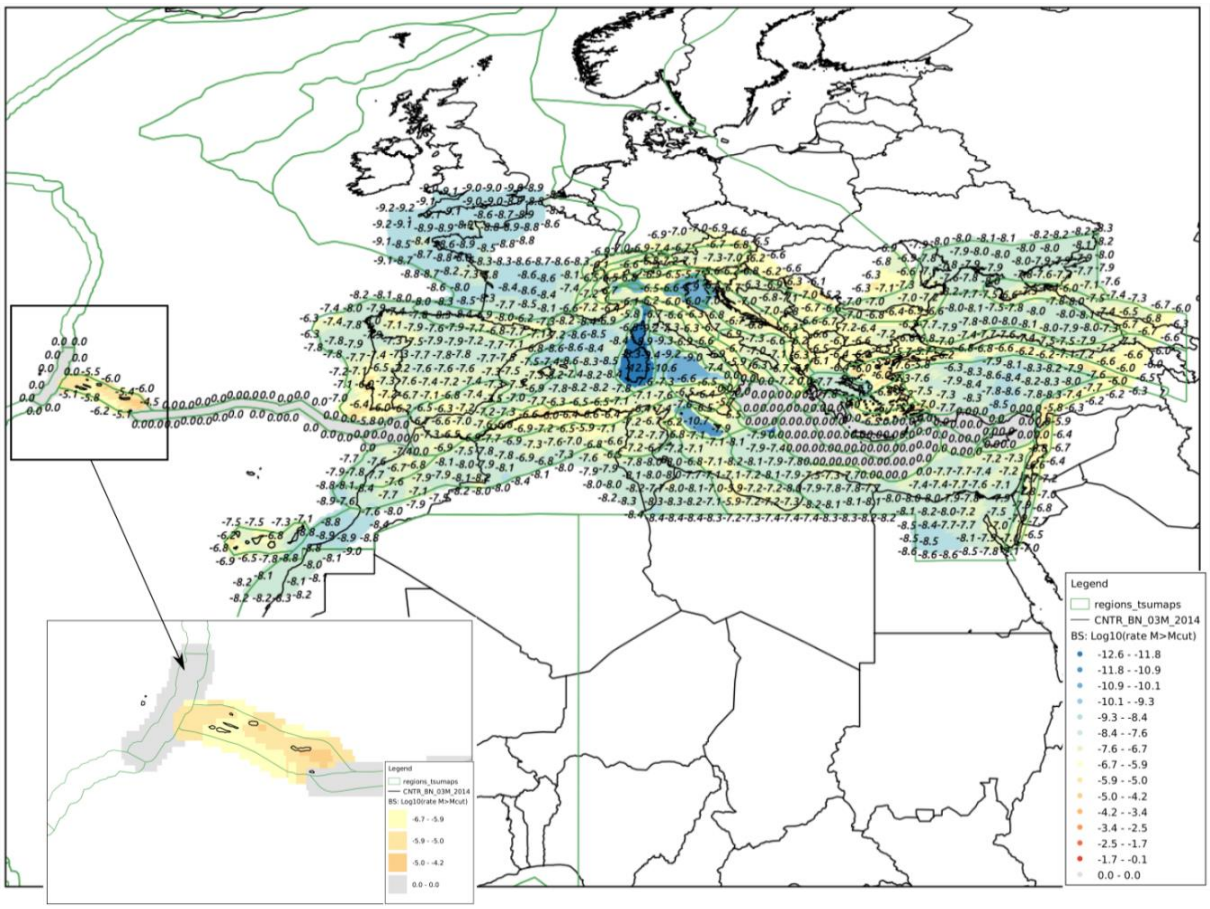

Figure 2.6 Mean annual rates of the non-modeled BS seismicity in each cell (mostly, M > 8.1551). In the regions where PS is also modeled, this means the annual rate is identically 0 since larger magnitudes are assumed to potentially occur only on the PS faults. The numbers indicate the Log_{10}(mean annual rate), expressed in yr^{-1}.

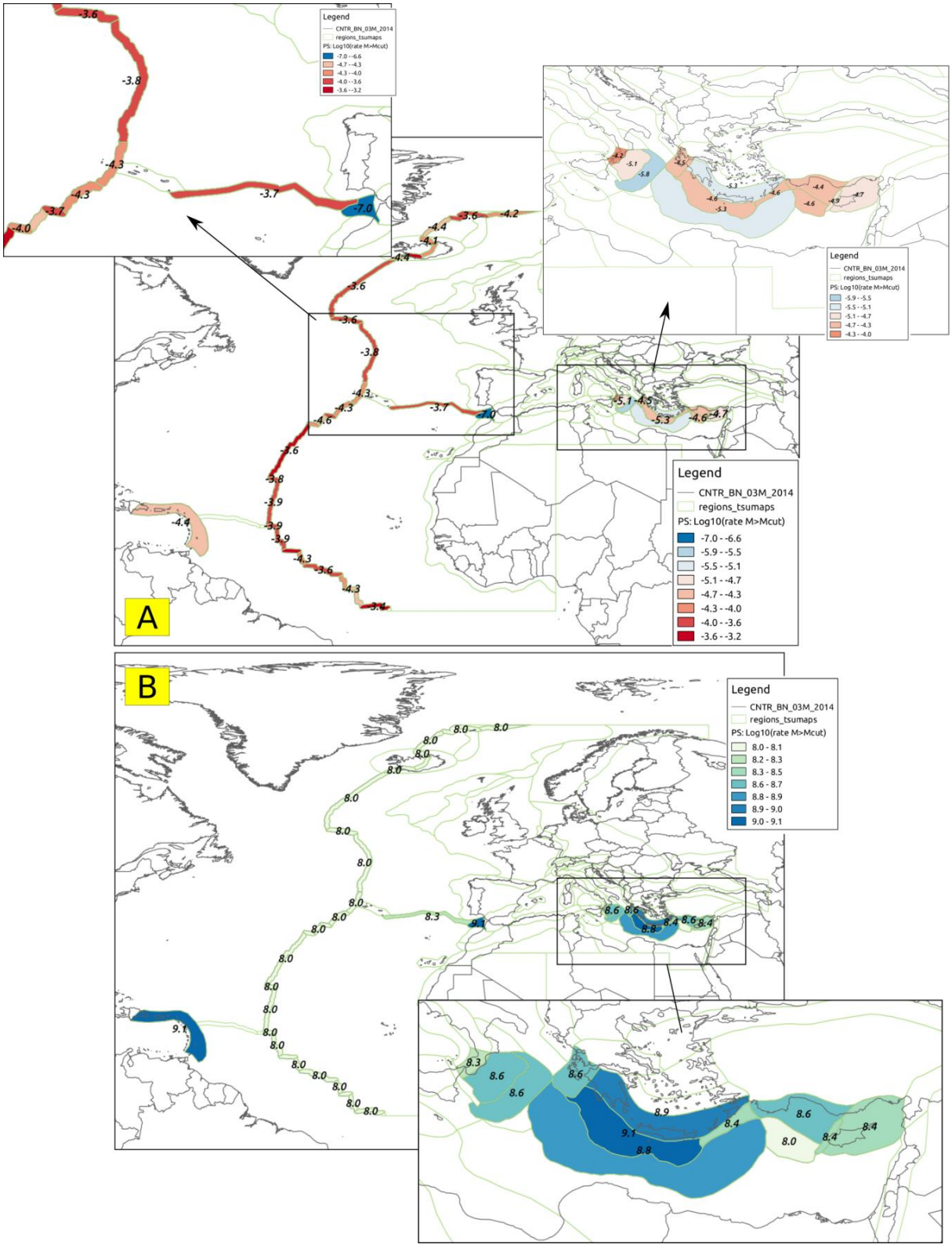

Figure 2.7 A) Mean annual rates of the non-modeled PS seismicity in each tectonic region. The numbers indicate the Log_{10}(mean annual rate), expressed in yr^{-1}. B) Maximum magnitude modeled in each region.

A)

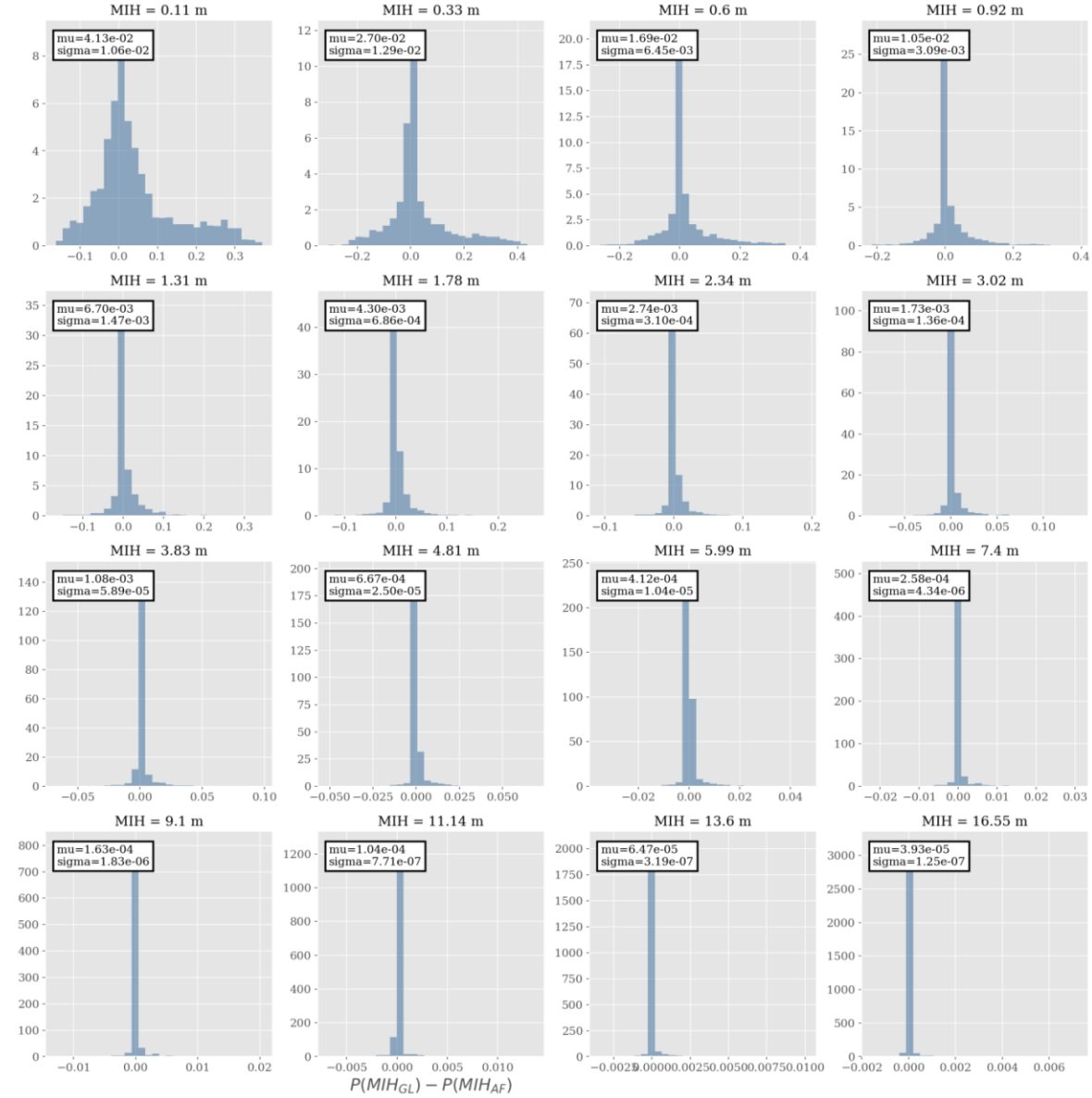

B)

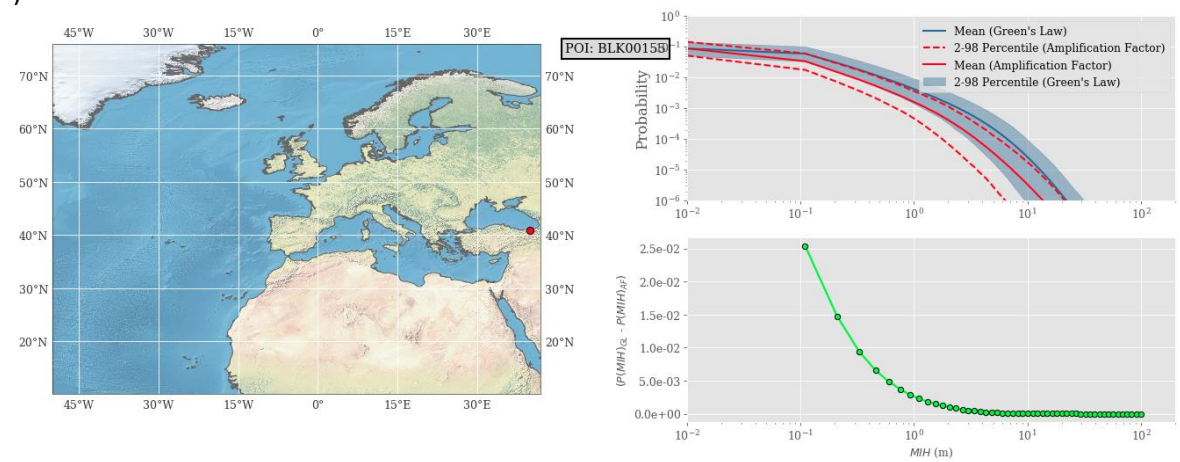

Figure 2.8 A) Summary statistics for all POIs of this difference for different tsunami intensity. B) example of comparison in in POI in the Black sea.

2.4) Checks against past tsunamis

An important class of sanity checks is represented by the comparison between past tsunami data and the hazard results. Even if tsunami data are obtained independently from the seismic and the geodetic inputs used in the tsunami hazard model, they still refer to the same seismic events that are present in the seismological databases (which should be true at least for the entries in the tsunami catalogues which are generated by earthquakes). Therefore, even if tsunami and seismic data are produced and maintained separately and independently, they cannot be considered as independent. Consequently, even the results of formal statistical tests comparing hazard results and tsunami data should be considered as sanity checks, and do not correspond to an effective statistical 'validation' (or not falsification).

The selection of the comparison tests is discussed in Doc_P2_S1. This selection has been strongly limited by i) the very limited time available, ii) the need of using external databases, not prepared to this end, and iii) the difficulty imposed by the conversion between NEAMTHM18 tsunami intensity and the intensity metrics available in past tsunami catalogs. Moreover, quantitative testing is difficult since the data are sparse and scarce, and because the source of the tsunami (e.g. earthquake, landslide, or a combination) is sometimes doubtful.

Hereinafter, we report two comparisons between NEAMTHM18 results and past data. These tests do not attempt to be exhaustive, nor statistically significant, and they should be considered just as examples of comparison.

We stress that, however, in our opinion, this kind of tasks should be significantly deepened in future hazard analyses, both developing specific, standardized, and statistically robust methods for the comparison, and collecting/reorganizing/post-processing past tsunami databases according to the needs of these established methods.

a. **Marmara Sea test**: The reference historical catalog (Euro-Mediterranean Tsunami Catalogue, Maramai et al., 2014) is organized per source (reporting only the maximum observed tsunami intensity for each event) and it is not searchable per site. To partially overcome this problem, we selected the Marmara Sea area since it is a relatively close and small sea that experienced tsunamis in the past. The historical catalog reports several historical tsunamis in this area, as shown in **Figure 2.9A**. We assumed 4 or 5 as reasonable intensity threshold to be considered to compare with the occurrence of our minimum MIH (0.5 m, corresponding to local run-ups up to 1.5/2.5 m). This limits the events in the catalog to 5 or 2 events (for intensities 4 and 5, respectively) in approximately 1500 years in the whole Marmara Sea, with 3 or 1 events in its central part (closer to Istanbul). The choice of the POI to be selected for the comparison is not trivial. Indeed, we are looking at tsunamis in a relatively large area instead of in one point, and the curves in the different points cannot be considered statistically independent. Given the relatively small scale of the Marmara Sea, the simplest choice is to assume that all the largest events are all observed at least in one point, potentially the one with the largest hazard. Looking at the NEAMTHM18 results, we have quite a large variability in the hazard curves in the area, and the curve with larger probabilities seems to be right north of the 1343 event, as reported in **Figure 2.9B**. Let's assume that at least in this area all the events have been observed. Here, the overcoming of MIH 0.5 m has a mean probability of approximately 0.04 in 50 yr (with epistemic uncertainty

in the range 0.03-0.05), corresponding to an average return period in the range 1000-1500 years. For the tsunami record, there is not a completeness quantification. The oldest observation in the area dates to 447. Assuming a Poisson process, the probability of observing more than 0, 1, 2, 3, 4 and 5 events in 1500 and 2000 years is reported in **Figure 2.9C**. It can be observed that, considering also the epistemic uncertainty, the probability of exceeding 4/5 observations in 1500/2000 years is not negligible (> 0.01). Considering the limitations of the method for the comparison (among the others, all events are assumed to be observed in one point and there is not a clear correspondence between MIH and observed intensities), the observation of 2 to 5 tsunamis in all the Marmara Sea (and 1 to 3 in its central part) in 1500 years seems to be compatible with the hazard model.

b. **Italian coasts**: a reference tsunami intensity derived from the tsunami hazard is often adopted for planning evacuation in case of tsunami warning. For example, in New Zealand (MCDEM, 2016) and Italy (DCDPC, 2018), it has been chosen to plan for a reference hazard intensity corresponding to an average return period of 2500 years and the 84th percentile of the epistemic uncertainty. To check the robustness of this kind of choices, we compared the quantitative tsunami intensities reported in the historical catalog with the tsunami intensity computed in our model, considering the MIH for ARP of 2,500 years at the 84th percentile. According to what discussed in Doc_P2_S1, the MIH has been here multiplied by a factor 3 to account for the potential difference between mean and peak intensity along the coast lines, which is also consistent with the recommendations contained in DCDPC (2018). We may expect that most of the historical observations, mainly concentrated in the last 4 centuries, do not overcome significantly these reference values. Given the central position of Italy in the Mediterranean and given that this threshold has been applied in Italy for operational purposes, we limited the comparison to the Italian coasts. In Italy, the reference hazard intensity from the NEAMTHM18 is generally rather small, even after the multiplication by the factor 3 (**Figure 2.10A**). Most POIs (about 60%) with intensity less than 2 m, 80% with less than 5 m, and 90% with less than 8 m. The historical catalog (Euro-Mediterranean Tsunami Catalogue, Maramai et al., 2014) contains a certain amount of data, but only few of them have a quantitative estimation of the tsunami intensity, in terms of either run-up or inundation distance. In **Figure 2.10B**, we report all the observations related to tsunamis of earthquake origin occurred after 1624 (for which the catalog seems reasonably complete), with EMTC reliability greater or equal than 3 and reporting values of observed run-up and inundation that were classified as Q1. The intensity of each Q1 observation reported refers to the global effects produced by the triggering tsunami, therefore we report only 1 maximum per event. The catalog contains only 11 such observations, reported in 5 zooming zones. The comparison between the hazard results and these records is reported in **Figures 2.11** and **2.12**, for the 5 zooming zones. Considering that we expect a maximum of 200 m of inundation per 1 m of maximum run-up (in flat plains, Fraser and Power, 2013; MCDEM, 2016; DCDPC, 2018), we generally found that historical maxima tend to be comparable with the reference hazard values. There are few exceptions that may potentially be related to very unlikely events, as well as due to uncertainty in the historical data (e.g., 1905 Calabria earthquake, see also Piatanesi and Tinti, 2002) or possible local amplifications related to seismically induced (e.g., 1908 Messina) or volcanic (e.g., 1916 Stromboli) landslides.

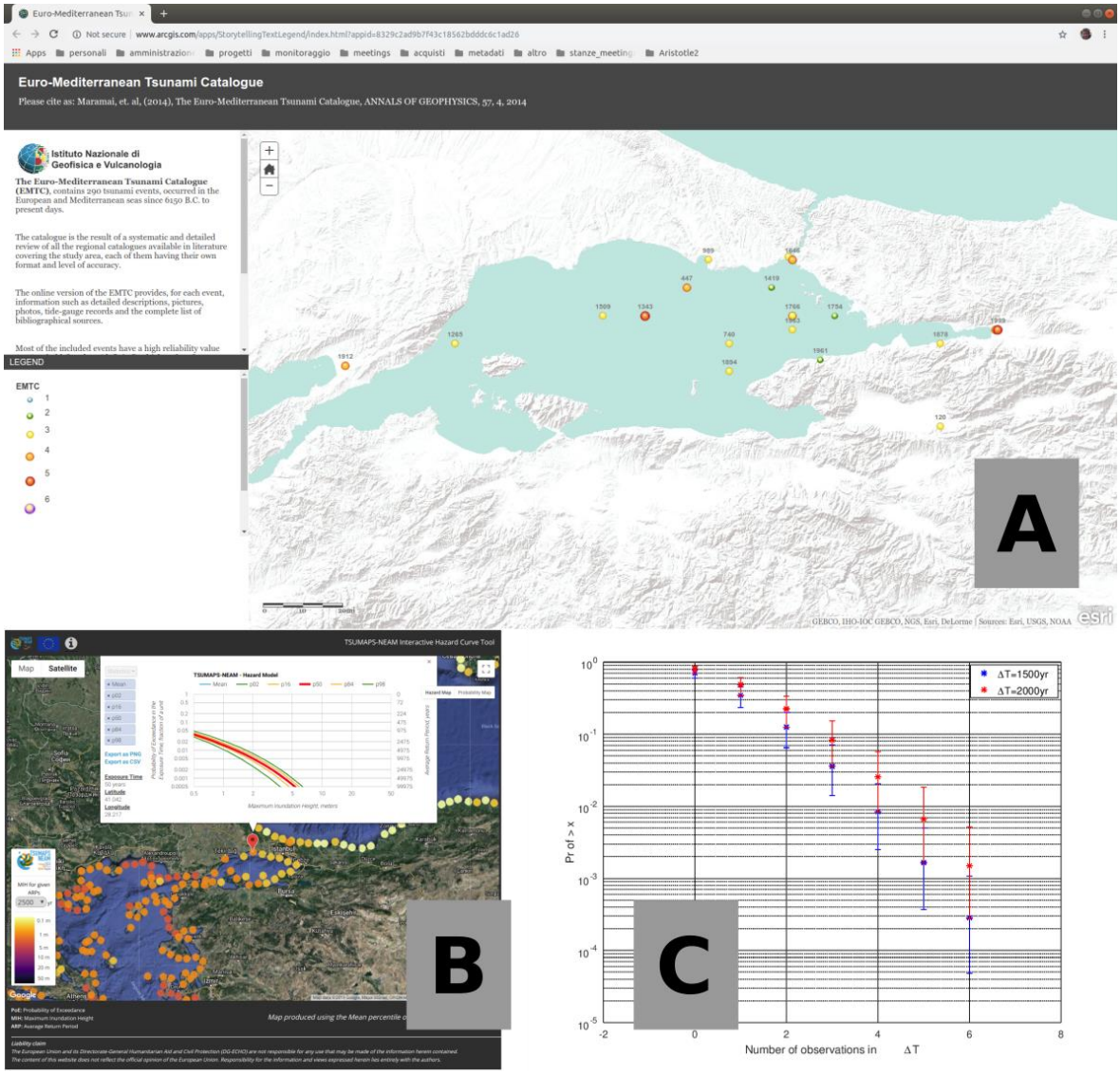

Figure 2.9: A) Historical tsunami in the reference Euro-Mediterranean Tsunami Catalogue (Maramai et al., 2014) in the area of the Marmara Sea. B) Reference hazard curve in central Marmara Sea from the NEAMTHM18 (see text for more details in the POI selection). C) Evaluation of multiple observations of MIH > 0.5 m in 1500 and 2000 years in the selected POI (see text for more details).

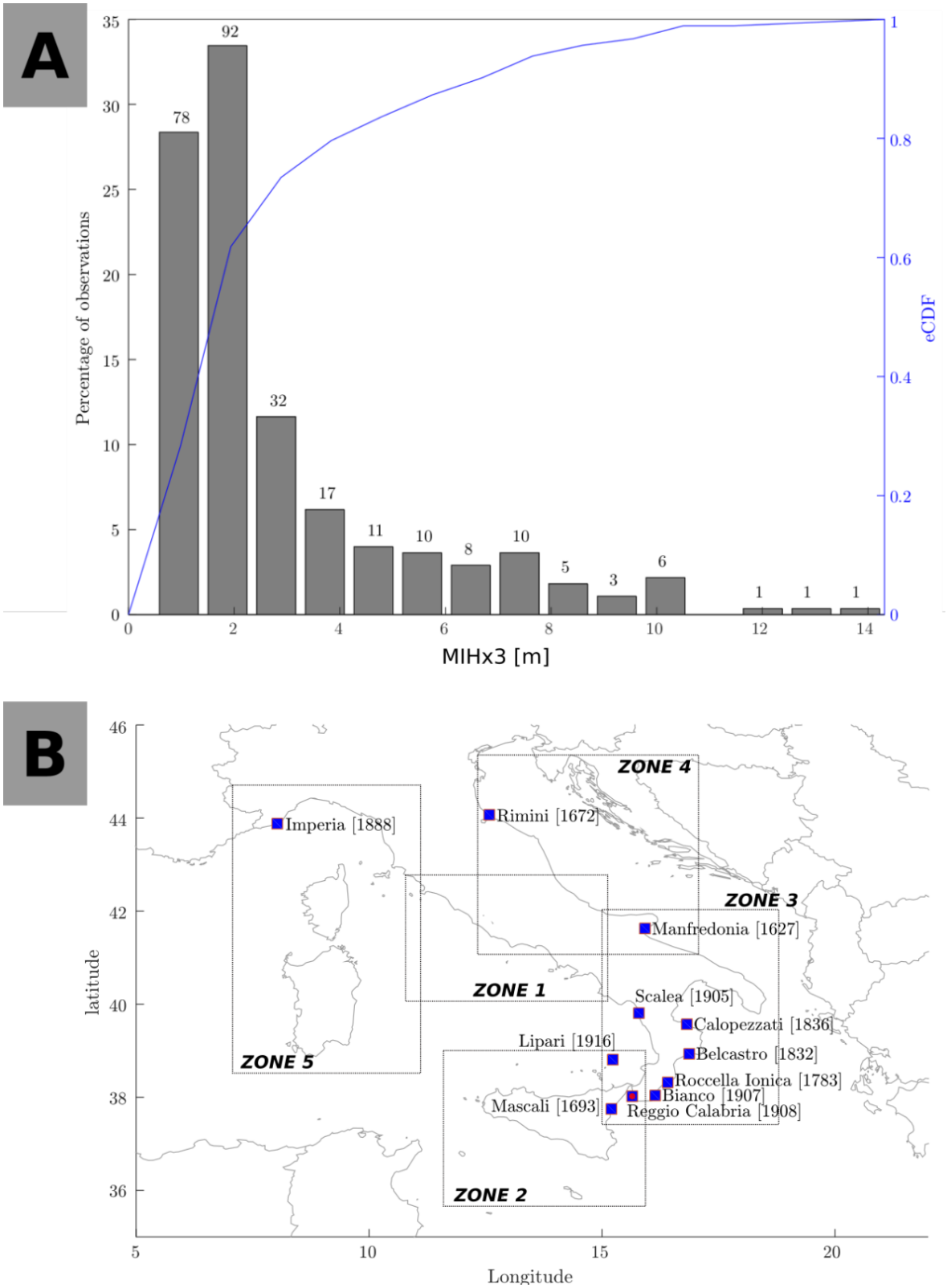

Figure 2.10: A) Cumulative distribution of the MIHx3 in all the POIs in Italy. B) Observations in the catalog and zones for the comparison between observations and hazard results.

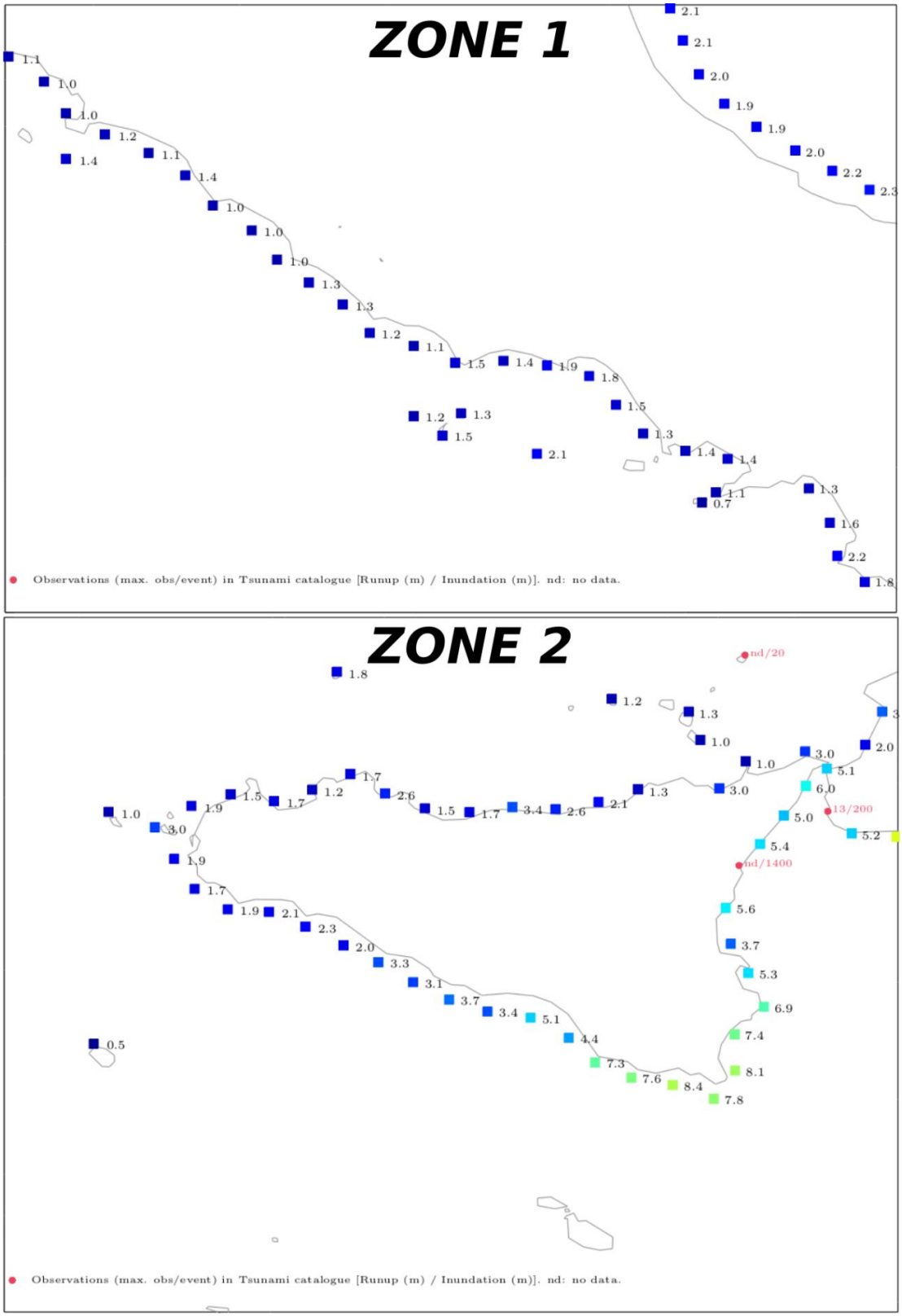

Figure 2.11: Detailed comparison between the available observations (run-up / inundation length) and the hazard results expressed in terms of 3xMIH relative to the 84th percentiles of the 2,500 yr Average Return Period, in Zones 1 and 2.

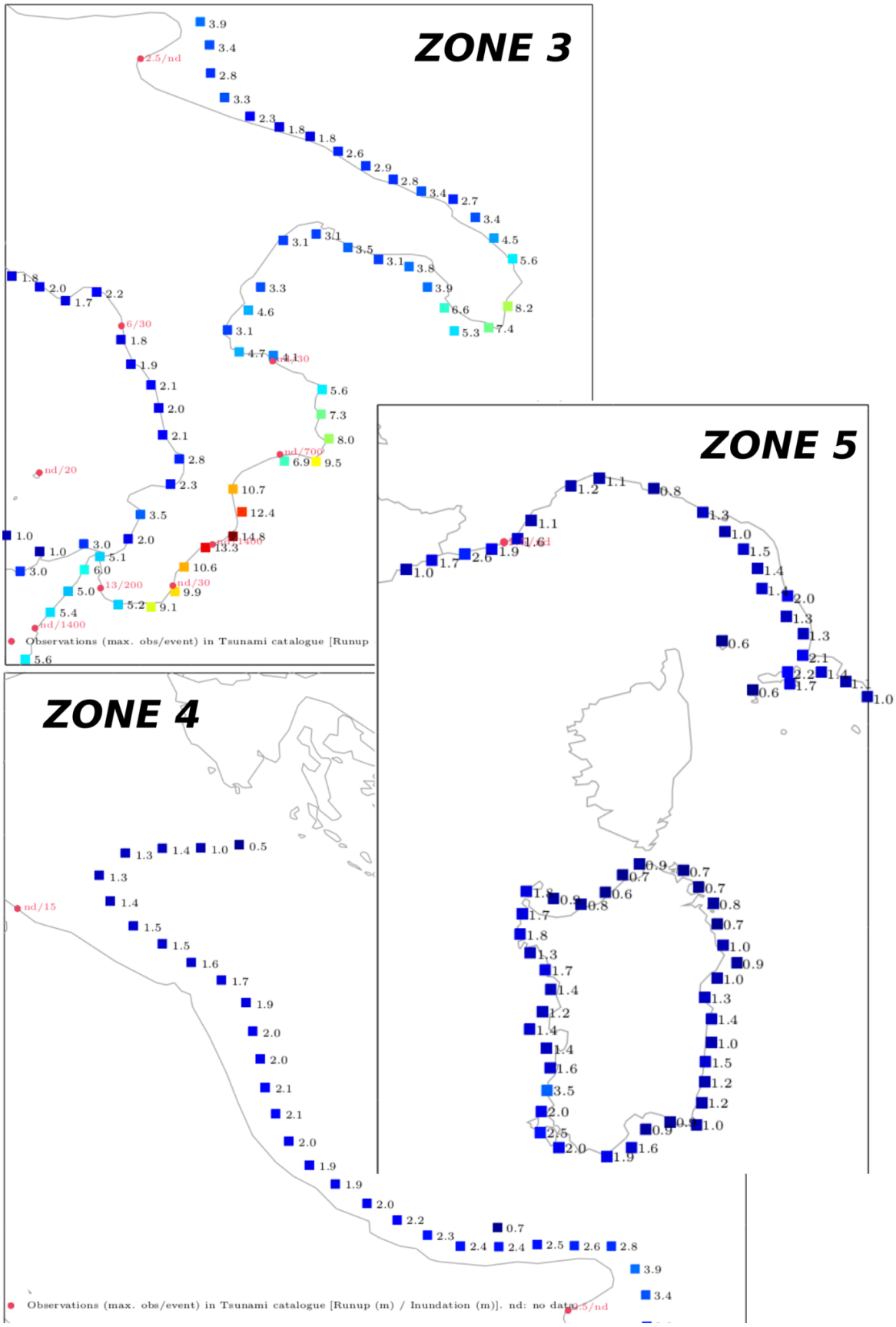

Figure 2.12: Same as Figure 2.111, but in Zones 3, 4, and 5.

References

Bazzurro P, Cornell C (1999). Disaggregation of seismic hazard, Bull. Seismol. Soc. Am., 89(2), 501–520.

DCDPC (Decreto del Capo Dipartimento della Protezione Civile) 2018, Indicazioni alla Componenti ed alle Strutture operative del Servizio nazionale di protezione civile per l'aggiornamento delle pianificazioni di protezione civile per il rischio maremoto, Presidenza del Consiglio dei Ministri – Dipartimento della Protezione Civile, Reportorio n 3976 del 10/10/2018

Field, E. H., Jordan, T. H., Page, M. T., Milner, K. R., Shaw, B. E., Dawson, T. E., Biasi, G. P., Parsons, T., Hardebeck, J. L., & Michael, A. J. (2017). A synoptic view of the third uniform California earthquake rupture forecast (UCERF3). *Seismological Research Letters*, 88, 5, 1259–1267, doi:10.1785/0220170045.

Fraser SA, Power WL (2013). Validation of a GIS-based attenuation rule for indicative tsunami evacuation zone mapping. GNS Science Report 2013/02. Lower Hutt. 21 p.

Geist EL, Lynett P J (2014) Source processes for the probabilistic assessment of tsunami hazards, Oceanography, 27, 86–93.

Geist, E.L., and Parsons, T., 2016, Reconstruction of far-field tsunami amplitude distributions from earthquake sources: Pure and Applied Geophysics, v. 173, p. 3703-3717, doi:10.1007/s00024-00016-01288-x.

Glimsdal, S., Løvholt, F., Harbitz, C.B., Romano, F., Lorito, S., Orefice, S., Brizuela, B., Selva, J., Hoechner, A., Volpe, M., Babeyko, A., Tonini, R., Wronna, M., Omira, R. (2019). A New Approximate Method for Quantifying Tsunami Maximum Inundation Height Probability. Pure Appl. Geophys, https://doi.org/10.1007/s00024-019-02091-w.

Grezio A, Babeyko A, Baptista MA, Behrens J, Costa A, Davies G, Geist EL, Glimsdal S, González FI, Griffin J, Harbitz CB, LeVeque RJ, Lorito S, Løvholt F, Omira R, Mueller C, Paris R, Parsons T, Polet J, Power W, Selva J, Sørensen M, Thio HK (2017). Probabilistic Tsunami Hazard Analysis: Multiple sources and global applications. Reviews of Geophysics, 55. https://doi.org/10.1002/2017RG000579.

Lorito S, Selva J, Basili R, Romano F, Tiberti MM, Piatanesi A (2015). Probabilistic Hazard for Seismically-Induced Tsunamis: Accuracy and Feasibility of Inundation Maps, Geophys. J. Int., 200, 574–588.

Maramai A., Brizuela B., Graziani L. (2014). The Euro-Mediterranean Tsunami Catalogue, Annals of Geophysics, 57, 4, S0435; doi:10.4401/ag-6437.

MCDEM (2016) - Tsunami Evacuation Zones- Director's Guideline for Civil Defence Emergency Management Groups [DGL 08/16] February 2016. ISBN 978-0-478-43515-3. Published by the Ministry of Civil Defence & Emergency Management – New Zealand

Molinari I, Tonini R, Lorito S, Piatanesi A, Romano F, Melini D, Hoechner A, Gonzàlez Vida JM, Maciás J, Castro MJ, de la Asunción M (2016). Fast evaluation of tsunami scenarios: uncertainty

assessment for a Mediterranean Sea database, Nat. Hazards Earth Syst. Sci., 16, 2593-2602, doi: 10.5194/nhess16-2593-2016.

Pacheco, J. F., and L. R. Sykes (1992), Seismic moment catalog of large shallow earthquakes, 1900 to 1989, Bull. Seismol. Soc. Am., 82, 1306 – 1349.

Piatanesi, A. and Tinti, S. (2002), Numerical modeling of the September 8, 1905 Calabrian (southern Italy) tsunami. Geophys. Journ. Intern., Vol. 150, No. 1, pp. 271-284.

Selva J, Tonini R, Molinari I, Tiberti MM, Romano F, Grezio A, Melini D, Piatanesi A, Basili R, Lorito S (2016) Quantification of source uncertainties in Seismic Probabilis- tic Tsunami Hazard Analysis (SPTHA), Geophys. J. Int., 205, 1780–1803, doi:10.1093/gji/ggw107.

Tonini, R., Maesano, F. E., Tiberti, M. M., Romano, F., Scala, A., Lorito, S., Volpe, M., Basili, R. (2017). How much does geometry of seismic sources matter in tsunami modeling? A sensitivity analysis for the Calabrian subduction interface. Abstract NH23A-1948 presented at 2017 Fall Meeting, AGU, New Orleans, Louis., 11-15 Dec.

Volpe, M., Lorito, S., Selva, J., Tonini, R., Romano, F., and Brizuela, B.: From regional to local SPTHA: efficient computation of probabilistic tsunami inundation maps addressing near-field sources, Nat. Hazards Earth Syst. Sci., 19, 455-469, https://doi.org/10.5194/nhess-19-455-2019, 2019.

Zechar, D., Gerstenberger, David, M.C., Rhoades, A. (2010), Likelihood-Based Tests for Evaluating Space–Rate–Magnitude Earthquake Forecasts. Bulletin of the Seismological Society of America; 100 (3): 1184–1195. doi: https://doi.org/10.1785/0120090192.

Summary of the Internal Review Process Phase 2: TSUMAPS-NEAM Project

The TSUMAPS-NEAM project has implemented a voluntary internal review process that consists of two stages. In the first review stage, reviewers were asked reviewers were asked to express opinions regarding the project processes and methods, as described in the Preliminary Assessment Plan documents and its appendices. This report summarizes the second review stage, wherein reviewers were asked to express their opinions on the final project implementation, results, assessment of sensitivity of results to inputs, tools, and documentation.

Specifically, reviewers were asked to submit a numerical rating from 0-5 (5 being the highest rating) on the following questions:

RQ1. Using a scale of 0-5, how do you rate the clarity of the provided documentation for judging the hazard model implementation?

RQ2. Using a scale of 0-5, how do you rate the clarity of the provided documentation for judging the hazard model results?

RQ3. Using a scale of 0-5, how do you rate the capability of the method to capture and quantify model uncertainty?

RQ4. Using a scale of 0-5, how do you rate the quality of the sensitivity analyses and sanity checks to assess the robustness of the results?

RQ5. Using a scale of 0-5, how do you rate the readability of the hazard model through the online interactive tool?

RQ6. Using a scale of 0-5, how do you rate the usefulness of the hazard model with respect to Disaster Risk Reduction practice?

Reviewers were given the opportunity to add specific suggestions and comments to accompany their responses, and also to give unlimited general comments. Received Stage-2 reviews from the internal review panel are listed in the table below:

Name	Affiliation
Mauro Dolce & Daniela Di Bucci	Italian Civil Protection Department (DPC), Italy
Eric Geist	United States Geological Survey (USGS), Pacific Coastal and Marine Science Center, USA
Marco Pagani	Global Earthquake Model (GEM) Foundation, Italy
Alessandro Amato	Istituto Nazionale di Geofisica e Vulcanologia, INGV, National Earthquake Centre, Italy
Andrey Zaytsev	Russian Academy of Sciences (RAS), Special Research Bureau for Automation of Marine Researches, Russia
Jose Manuel Gonzalez Vida	Universidad de Málaga (UMA), Dpto. Matemática Aplicada, Spain

The numerical scoring was very positive with all scores assessed at 4 or above. No significant trend is identified across the six questions. From 6 scorers, the mean values for each question were:

RQ1	4.8
RG2	4.4
RQ3	4.6
RQ4	4.8
RQ5	4.8
RQ6	4.5

This scoring is interpreted as support for the implementation of, and results from the TSUMAPS-NEAM project and documentation. However, there were some specific comments/recommendations raised that might be considered currently, or in future versions/implementations.

RQ1: Clarity of the provided documentation for judging the hazard model implementation

Reviewers generally found the TSUMAPS-NEAM project documentation to be thorough, clear and well structured. In addition, reviewers noted that project strengths and weaknesses were clearly identified. While agreeing with that overall view, two reviewers made several specific suggestions /recommendations for improved clarity in the documentation, changes to

mathematical notation, as well as some potential citations that would strengthen some of the points made. They also noted some typos and other small mistakes.

RQ2: Clarity of the provided documentation for judging the hazard model results

Reviewers generally found that the documentation was very detailed, well-illustrated, and allowed for clear judgement of the hazard model. Major assumptions and limitations are clearly identified. Reviewers appreciated the documented efforts to verify all code, and reproducibility of the hazard results.

A few specific comments of note include a suggestion to mention that unmodeled earthquakes in the hazard model may include multisegment, or compound ruptures, and some continued difficulty understanding the differences between predominant and background seismicity.

RQ3: Capability of the method to capture and quantify model uncertainty

While it is probably impossible to account for every uncertainty inherent in a probabilistic hazard assessment, the reviewers generally expressed confidence that a strong effort was made to assess uncertainties. However, some areas where uncertainties may not be completely assessed are noted by the reviewers, including:

• Magnitude-area and magnitude-slip relationships

• Uncertainty estimates at the inundation stage might be improved by using numerical models

•Alternatives to dislocation sources for earthquakes, including for example, dynamic solutions.

•Nonlinearity at some deep-water sites

RQ4: Quality of the sensitivity analyses and sanity checks to assess the robustness of the results

Generally, the reviewers acknowledge a thorough sensitivity analysis and "sanity checks". Some limitations are pointed out, including that by necessity, the input and testing data are linked by the same historical catalogs. Additionally, one reviewer suggests a broader analysis by simultaneously varying not only input data to the propagation codes, but also some of the variables inherent to the codes themselves.

RQ5: Readability of the hazard model through the online interactive tool

Reviewers were unanimously enthusiastic about the interactive mapping and hazard curve tools, finding them informative, and easy to use. A few specific notes were made after experimenting with the tools as:

•Although the curves are shown as continuous, not all the values along them can be selected.

•Only 3 percentiles are available under the "Statistics" pull-down menu (missing 2nd and 98th percentiles.)

• Areas where linearity hypothesis for deep water is invalid might need to be marked in the interactive tools.

•Suggestion to change nomenclature: "hazard map" to "intensity map".

RQ6: Usefulness of the hazard model with respect to Disaster Risk Reduction practice

An important measure of the usefulness of the hazard model comes from the Italian National Civil Protection Department, who state that, "While waiting for a national S-PTHA,

whose realization is currently ongoing supported by our Department, we decided to adopt the results provided by TSUMAPS to implement the system and the new contingency plans."

Additionally, reviewers point out that using probabilistic tools for tsunami early warning is an emergent application that needs clear communication to hazard managers and the public. A further application is suggested that the model and its results could be applied in a quantitative risk analysis.

General Comments:

Several specific recommendations were made by the reviewers, mostly in the context of future applications and developments:

•A reviewer suggests comparisons between TSUMAPS-NEAM and the SHARE model.

•A reviewer suggests applying the TSUMAPS-NEAM source model into a probabilistic seismic hazard assessment (PSHA), though this would need to be somehow combined with terrestrial sources.

•It is suggested that the authors of TSUMAPS-NEAM provide their own list of future areas of improvement and directions for further investigations, based on their relevant experience on the project.

•A question is raised about the consistency of TSUMAPS-NEAM with other published work, for example:

Sorensen M.B., Spada M., Babeyko A., Wiemer S., Grünthal G. Probabilistic tsunamihazard in the Mediterranean Sea. J. Geophysical Research, 2012, vol. 117, B01305.

• Two reviewers suggested in a future regional PTHA that tsunami sources such as landslides, slumps, volcanic activity, etc. be included.

•A reviewer suggests that in a future edition of TSUMAPS-NEAM when more computational resources and time are available, shallower areas such as the southern part of the North Sea, the northern Adriatic Sea, and the western coast of Tunisia in the Mediterranean Sea could be also specifically treated.

•A reviewer asks if there will be a public release of the source codes used in TSUMAPS-NEAM

Final Recommendations:

In my opinion, the results and their uncertainties are well documented, and the user applications are easy to use, and provide useful information. My suggested priorities from the stage-2 reviewer comments are (1) to make the suggested changes/additions in the documentation for improved clarity, and (2) to comment on some apparently unaddressed sources of uncertainty repeated here as:

• Magnitude-area and magnitude-slip relationships

• Uncertainty estimates at the inundation stage might be improved by using numerical models

•Alternatives to dislocation sources for earthquakes, including for example, dynamic solutions.

•Nonlinearity at some deep-water sites.

Many of the reviewers' ideas for future improvements and additions are interesting. It might be nice to have some commentary on future research and improvements, but I don't think it is necessary.

Contacts

INGV
Istituto Nazionale di Geofisica e Vulcanologia
Via di Vigna Murata, 605, 00143, Roma, Italy

http://www.tsumaps-neam.eu